UNIVERSIDADE DE LISBOA

FACULDADE DE CIÊNCIAS

Ciências
ULisboa

Geomorphological framework control on beach dynamics

Doutoramento em Geologia
Geologia Económica e do Ambiente

Tanya Mendes Silveira

Tese orientada por:
Professor Doutor César Augusto Canelhas Freire de Andrade
Dr Norbert P. Psuty

Documento especialmente elaborado para a obtenção do grau de doutor

2017

UNIVERSIDADE DE LISBOA

FACULDADE DE CIÊNCIAS

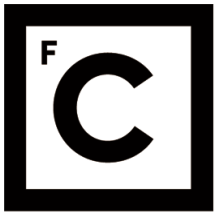

Ciências
ULisboa

Geomorphological framework control on beach dynamics

Doutoramento em Geologia
Geologia Económica e do Ambiente

Tanya Mendes Silveira

Tese orientada por:
Doutor César Augusto Canelhas Freire de Andrade
Dr. Norbert P. Psuty

Júri:
Presidente:
- Doutora Maria da Conceição Pombo de Freitas

Vogais:
- Doutor Paulo Renato Enes Baganha Baptista
- Doutor Óscar Manuel Fernandes Cerveira Ferreira
- Doutor César Augusto Canelhas Freire de Andrade
- Doutora Maria da Conceição Pombo de Freitas
- Doutor Rui Pires de Matos Taborda

Documento especialmente elaborado para a obtenção do grau de doutor

Fundação para a Ciência e Tecnologia, Bolsa de Doutoramento SFRH/BD/72555/2010

2017

dedicated to Sara and Isabel ♡

Abstract

Beaches occur when sediment is available and where accommodation space exists for the sediments to settle and accumulate. Beaches that occur within one coastal cell share the same oceanographic forcing climate, essentially related to waves and tides, and the same distribution and intensity of sources and sinks of sediment. However, contrasting beach forms and dynamics are frequent along the same coastal cell, leading to the questioning of what other factors are controlling beach morphodynamics.

Conceptual models have been developed and are very useful in describing and classifying beaches according to the characteristics of the incoming waves and beach sediments or morphology. Still, several studies suggest that site-specific characteristics, such as the geology, geomorphology or even the human-induced framework of beaches, can play a determinant role in beach systems' behavior and evolution. However, the majority of studies focusing on the role of geomorphological framework on beach dynamics, address cases sharing the same general characteristics.

This thesis focused on how the geomorphological framework interacts with the available coastal sediments and controls the subaerial beach configuration and responses. It investigates a myriad of beach geomorphological conditions along a high-energy coastal stretch that is under the influence of the same general deepwater wave regime. By comparing the morphodynamic response of adjacent constrained and unconstrained, platform and no-platform beaches, exposed to the same offshore forcing conditions, the present work provides new insights on the role of the geomorphological settings on beach dynamics.

The central hypothesis of this study was formulated as follows: *the geomorphological constraints and the local settings of beaches are the primary drivers for the varying temporal and spatial groupings of morphological responses*. In order to verify this, work was carried out at the seasonal scale, under modal process-response conditions, and over a two and a half year period, along 14 selected beach sites representative of a 200 km coastal stretch. The study was divided in three major components: 1) geomorphological framework; 2) beach response; and 3) hydrodynamic forcing.

Geomorphological framework was analyzed in terms of planform geometry and description of physical boundaries, and type of nearshore and backshore features present at each study site. Beach response investigation relied upon regular field sampling planned to ensure accurate and representative data collection on subaerial beach

morphology and sediments. A total of 52 beach profiles were monitored quarterly along the study area. The hydrodynamic forcing description included characterization of the deepwater and nearshore wave regimes at each study site and made use of numerical modelling of wave propagation. In addition, total water levels were computed for each site. The overall results were further explored to derive metrics and investigate and detect spatial organizations related to the geomorphological settings.

The geomorphological framework analysis attests to the high variability of settings in which the studied beaches occur. These include several combinations between nearshore and backshore type of features, physical boundaries and subsequent wave obliquities and degrees of indentation. Beach response was analyzed in terms of geoindicators, which were used to evaluate and describe the study sites' seasonal behavior. Results show that the magnitude of seasonal change between study sites varied considerably, in relative as well as absolute terms, especially regarding the morphological geoindicators. The hydrodynamic forcing included the analysis of a 36-year time series, used to describe the typical modal and storm regimes, and of a two and a half years subset, synoptic of the sediment and morphological field surveys. Results show that the study period was appropriate to characterize the modal process-response conditions, descriptive of a period with no extreme events. They also highlight the differences between sites exposed to higher and lower waves and total water level regimes.

The exploratory analyses of the data showed no linear relationship between forcing, controlling and response variables. However, it put in evidence the existence of clusters of beaches sharing similarities in types of boundaries. Beaches with rocky platforms experienced low volumetric variation, consistently lower than beaches with no rocky platform. In addition, within the no-platform beaches, those with the higher degree of embaymentization, varied the most.

A conceptual model of the subaerial beach dynamics as a function of the geomorphological framework is put forth, in which the magnitude of beach variation is controlled by: 1) the presence of a rocky platform; and 2) in no-platform beaches, by the degree of embayment and its impact on beach circulation.

It is suggested that the presence of a permanent and rigid obstacle in the surf zone, such as a rocky platform, limits the range of broken wave characteristics reaching the subaerial beach, and thus the amount of volumetric variation. On the other hand, beaches characterized by a mobile substrate (no-platform beaches) can present a variety of morphological features in the surf zone, and are expected to allow for a wider range of

broken wave conditions and subsequent effects on the subaerial beach, including higher volumetric changes.

Within the no-platform beaches, subaerial volume variations increase with the degree of embaymentization. Unconstrained beaches have open lateral boundaries, and therefore see their cross-shore morphology and volume vary mostly with the cross-shore sediment exchanges, that are expected to be small under modal conditions. The constrained beaches (with higher degree of embaymentization) on the other hand, are bounded laterally and therefore are prone to beach rotation processes (and subsequent higher volume variation) promoted by longshore sediment transport that occurs under modal conditions.

The conceptual model herein proposed departs from existing morphodynamic models that apply only to unconstrained beaches. It incorporates both unconstrained and constrained beaches and relates the constraining boundaries (both lateral and vertical) to the beach subaerial dynamics. It provides a first description on how the geomorphological framework controls subaerial beach dynamics, and hopefully can be developed and evaluated further.

Resumo

As praias formam-se onde existe espaço de acomodação e sedimento disponível para se depositar e acumular. As praias que ocorrem na mesma célula sedimentar partilham do mesmo forçamento oceanográfico, essencialmente relacionado com as ondas e marés, e da mesma distribuição e magnitude de fontes e sumidouros de sedimentos. No entanto, é frequente encontrar praias com formas e dinâmicas contrastantes ao longo da mesma célula sedimentar, sugerindo a existência de outros fatores controladores da morfodinâmica das praias.

Os modelos conceptuais existentes são muito úteis na descrição e classificação de praias, agrupando-as, de uma forma generalista, de acordo com as características da agitação, e do sistema (morfologia e sedimentos). Ainda assim, são vários os estudos que sugerem que as características específicas locais, como a geologia, a geomorfologia ou mesmo a presença de estruturas de engenharia, podem desempenhar um papel determinante no comportamento e na evolução dos sistemas de praia. No entanto, a maioria dos trabalhos que estudam a influência do contexto geomorfológico na dinâmica das praias, abordam casos de estudo que partilham das mesmas características locais.

Este trabalho procurou avaliar de que forma o contexto geomorfológico interage com os sedimentos disponíveis e condiciona a configuração e dinâmica da praia subaérea. Foi avaliado um número considerável de praias com diferentes contextos geomorfológicos, localizadas ao longo de um troço litoral de alta energia, e sob a influência do mesmo regime de agitação ao largo. A comparação entre praias adjacentes, encaixadas e abertas, com e sem plataforma rochosa, e expostas às mesmas condições de forçamento oceanográfico, corresponde a uma abordagem nova que pode ajudar a melhor compreender o papel do contexto geomorfológico na dinâmica das praias.

A hipótese central deste estudo foi formulada da seguinte forma: *o contexto geomorfológico e configuração local das praias são os principais fatores condicionantes dos diferentes agrupamentos espaciais e temporais que se observam nas respostas morfológicas das praias*. Para testar esta hipótese, o estudo foi efetuado à escala sazonal, em condições modais de processo-resposta, e ao longo de dois anos e meio, em 14 praias selecionadas, representativas de um troço costeiro de 200 km. O estudo foi dividido em três componentes principais: 1) contexto geomorfológico; 2) resposta da praia; e 3) forçamento hidrodinâmico.

O contexto geomorfológico foi analisado em termos da geometria plana da praia e descrição dos seus limites físicos, e tipo de estruturas presentes na alta e baixa praia em cada local de estudo. A descrição da resposta da praia baseou-se em campanhas de campo com levantamentos da morfologia e recolha de sedimentos, feitas com caráter regular, de acordo com protocolos estabelecidos para o efeito. Um total de 52 perfis de praia foram monitorizados trimestralmente ao longo da área de estudo. A descrição do forçamento hidrodinâmico incluiu a caracterização dos regimes de agitação em águas profundas e agitação local, e recorreu a modelação numérica para a propagação das ondas. Adicionalmente, calcularam-se os níveis totais de água para cada local. Os resultados das várias componentes foram analisados conjuntamente e explorados por forma a detetar organizações espaciais das praias relacionadas com o contexto geomorfológico.

Da análise do contexto geomorfológico resulta a descrição da variabilidade das configurações locais nas quais as praias estudadas ocorrem. Estas incluem várias combinações entre os tipos de estruturas presentes na alta e baixa praia, configuração dos limites físicos e, consequentes obliquidades das ondas e graus de indentação. A resposta da praia foi analisada em termos de geoindicadores que foram utilizados para avaliar e descrever o comportamento sazonal dos locais de estudo. Os resultados mostram que a magnitude da variação sazonal varia consideravelmente entre os locais de estudo, em termos relativos e absolutos, especialmente no que diz respeito aos geoindicadores morfológicos. O forçamento hidrodinâmico incluiu a análise de uma série temporal de 36 anos, usada para descrever os regimes típicos de tempestades e modais, e de um subconjunto de dois anos e meio, sinótico das campanhas de campo. Os resultados indicam que o período de estudo foi apropriado para caracterizar as condições modais de processo-resposta, num período sem ocorrência de eventos extremos. Os dados revelaram ainda as diferenças entre os locais mais expostos e mais abrigados da agitação.

A análise exploratória dos dados não apresentou quaisquer relações lineares entre as variáveis de forçamento, condicionantes e de resposta. No entanto, evidenciou a existência de agrupamentos de praias com semelhanças no tipo de limites físicos. Praias com plataformas rochosas apresentaram valores de variação volumétrica reduzidos, consistentemente inferiores aos das praias sem plataforma rochosa. Adicionalmente, entre as praias sem plataforma, aquelas com maior grau de indentação, variaram mais.

É apresentado um modelo conceptual da dinâmica da praia subaérea, em função do contexto geomorfológico, em que a magnitude da variação volumétrica da praia é

controlada por: 1) a presença de uma plataforma rochosa; e 2) em praias sem plataforma, pelo grau de indentação e o seu impacto na circulação da praia.

Sugere-se que a presença de um obstáculo permanente e rígido na zona de espalho, como uma plataforma rochosa, limita a amplitude das características das ondas quebradas que atingem a praia subaérea e, portanto, a magnitude das variações volumétricas induzidas. Por outro lado, as praias caracterizadas por um substrato móvel (praias sem plataforma) podem apresentar uma maior variedade de estruturas e características morfológicas na zona de espalho, permitindo uma maior gama de condições de ondas quebradas e subsequentes efeitos na praia subaérea, incluindo maiores variações volumétricas.

Nas praias sem plataforma, as variações volumétricas aumentam com o grau de indentação e o seu impacto na circulação da praia. As praias consideradas abertas, sem limites laterais, vêem a sua morfologia e volume variar principalmente com as trocas transversais de sedimentos, que se estimam de reduzida magnitude em condições modais. As praias encaixadas (com maior grau de indentação), por outro lado, são delimitadas lateralmente e, portanto, são propensas a processos de rotação de praia (e subsequente maior variação volumétrica) promovidos pelos processos de transporte longilitoral de sedimentos que ocorrem sob condições modais.

O modelo conceptual proposto no âmbito deste trabalho parte dos modelos morfodinâmicos existentes, e procura incluir praias com fronteiras e limites físicos com impacto na circulação da praia. O modelo inclui praias abertas e encaixadas, e relaciona os limites físicos (tanto laterais quanto verticais) com a dinâmica da praia subaérea. O presente trabalho procura descrever de que forma o contexto geomorfológico condiciona a dinâmica da praia subaérea e, espero, apresenta um ponto de partida para futuros trabalhos nesta temática.

Acknowledgments

The present work was made possible thanks to the support from the Fundação para a Ciência e Tecnologia through grant SFRH/BD/72555/2010; and the Administração da Região Hidrográfica do Tejo, I.P., at present Agência Portuguesa do Ambiente, I.P., through the CISML project, reference: QREN/POVT-12-0233-FCOES-000034, funded by the QREN/POVT national program. The work benefited from the facilities and equipment of the Instituto Don Luiz and the department of Geology of the Faculty of Sciences of the University of Lisbon.

Most importantly, I was fortunate to have the support of my advisors, who have been my mentors well before the PhD endeavor and encouraged me to go forward. I am grateful to Professor César Andrade for the always intense work and brainstorm sessions, PhD related or not, from which I learned so much. I am grateful to Dr. Norb Psuty, for giving me the opportunity to work alongside him in exciting projects in the US, providing me with two of the most productive years of my early career as a coastal scientist.

Professor Rui Taborda was fundamental to the successful development of this work. His endless enthusiasm for scientific research and problem solving is contagious and inspiring. I deeply appreciate his knowledgeable guidance and presence throughout.

Working in a university environment means working with inspiring people that are pursuing knowledge and most importantly, promoting and stimulating scientific education. I co-worked with students, researchers, technicians and professors that were always, always available to help. They helped carry out field surveys and data processing, shared their time and knowledge, provided encouragement, and helped search for ways to solve problems, discussing them with enthusiasm, as if they were their own. This was an invaluable and enriching experience that translated into a steep, but rewarding, learning curve. My sincere gratitude to all.

Finally, the emotional support was essential and I was fortunate to have the best at home.

- Acknowledgements -

Table of contents

List of tables

Chapter 3. Methods

Chapter 4. Results

Chapter 5. Analysis and Discussion

List of figures

Chapter 2. Study Area

Chapter 3. Methods

Chapter 4. Results

Chapter 5. Analysis and Discussion

Chapter 1. Introduction

The scope of the thesis and the motivation that led to its development is presented, and a comprehensive state of knowledge on the subject is made through reporting of the previous research. Lastly, the objective of the thesis and outline of the manuscript is presented.

1.1 Motivation and scope of the thesis

It's a matter of scale. The most common way of handling and classifying the coast for research or management purposes is to define coastal stretches of similar characteristics, or limited by well-defined physical boundaries. This is normally done at the regional scale, considering alongshore components on the order of tens or hundreds of kilometers, and is helpful in defining coastal cells wherein sediment is mobilized, transported and deposited along pathways. Beaches occur when sediment is available and where accommodation space exists for the sediments to settle and accumulate, and beaches that occur within one coastal cell share the same (oceanographic) forcing climate, essentially related to waves and tides, and the same distribution and intensity of sources and sinks of sediment.

When one increases the scale of observation, the irregular characteristics of the coast become obvious, and the contiguous segments of coast can be very different, even though they are part of the same broad coastal cell. The coastal features can change from continuous long beaches to pocket beaches, or from beaches with underlying platforms to rocky cliffs, within a short distance, on the order of tens to hundreds of meters. And even between morphologically similar segments, such as two enclosed beaches, the morphodynamic behavior is often different. One beach might vary considerably between summer and winter whereas another, close by, might be surprisingly stable, with modest changes through time.

The wide range of beaches of different shapes and materials that occur around the world in different environments and geomorphological settings are well documented and most coastal scientists, or even non-scientists, are aware that beaches have combinations of similarities and differences that are both generic and site-specific. Moreover, there is a pattern of temporal variability of the morphological response of beaches that is based on seasonal contrasts that have patterns of re-occurrence, responding to the changes of the incident wave regime.

But, for the same regional settings, for the same general sediment sources and sinks, and for the same offshore wave regime, why do beaches occur only in specific places and have different form and behavior? Contrasting beach forms and occurrences are especially evident along crenulated coasts, where beaches constrained by physical boundaries exist, and in these cases, availability of accommodation space for the beach to develop seems to be the principal controlling factor. Also, at local scales, the nearshore wave regime is often site-specific, and the existing sediment sources and sinks are normally unevenly

distributed along the coast. All of these aspects are controlled by the *geomorphological framework* of the system, herein used to describe the three-dimensional settings, including geological and anthropogenic features where the waves and sediments interact to form a beach. Two major reference textbooks on beach dynamics, written 40 years apart, refer, in their own terms, to the geomorphological framework and its role in the beach morphodynamics:

> In King (1959): "*The character of the foundation on which this incoherent beach material rests is also relevant to the study of the beach. Its gradient, height in relation to mean sea level and its permeability are important, while its resistance to erosion is significant in the general rate of development of the coastline*."

> In Short (1999): "*Beaches are dynamic sedimentary systems which require a number of boundary conditions and external inputs. While waves and sediment are essential for beach formation, a sub-surface boundary or base is required for the beach to rest on. The three-dimensional morphology of this surface or 'accommodation space' is critical to the formation and maintenance of the beach."*

Despite the myriad of beach forms and settings, conceptual models have been developed to describe beach morphology and dynamics and are very useful in classifying beaches with the same general morphological configuration (e.g. Wright and Short, 1984; Masselink and Short, 1993; Silvester and Hsu, 1993). The most important factor these and other authors have found to determine beach differentiation is the nearshore and local wave regime. Therefore, beach classification generally focuses on the nearshore and foreshore description and seldom addresses and explains the backshore and subaerial portion of the beach. This is however, the most important part of the beach system for coastal management: for estimation of beach recreation area and associated uses, and for erosion and overwash-related risk assessment and beach nourishment planning. These applications are the reasons that motivate the implementation of monitoring programs undertaken by coastal management authorities that use these data to inform strategic studies, plan management intervention, or check compliance with environmental requirements. This was the case for the Portuguese Environment Agency District Administration (Administração de Região Hidrográfica - ARH, Agência Portuguesa do Ambiente – APA, I.P.) in the area covered by the Tagus River Basin. A 2.5 year project was developed to monitor beaches along a 200 km-long coastal stretch, and the first step was to select the study sites to conduct the analysis and achieve the program's objective. Fourteen sites were selected based on the agency's needs for dimensional data on specific

beaches (areas of special concern), but also, and importantly, based on their representativeness of the overall study area. The assumption that beaches had different physical constraints and settings, and therefore were morphologically different and responded differently, was a logical component of the project design, but, it also became the basis for a hypothesis that, albeit intuitive, should be pursued.

The present work was developed in the frame of the APA's monitoring program, taking advantage of the exceptionally extensive study area and amount of collected data, and was set up to determine to what degree the geomorphological framework controls beach dynamics within the same regional area.

1.2 Previous research

The research literature on beaches and their process-response mechanism is extensive and widespread, covering diverse environments and settings, from low-lying extensive beach-dune systems, to small enclosed pocket beaches. The current state of knowledge on beach morphology and sediment dynamics is such, that variability of these systems in space and time, in response to the major forcing factors, is fairly well described. In fact, a number of models are widely used to predict beach evolution and are being applied to coastal erosion and risk management (e.g. Larson et al., 2004; Ferreira et al., 2006; Silva and Coelho, 2007; Davidson and Turner, 2009; Mather et al., 2011).

Most of these models, however, suggest that site-specific characteristics, such as the geology, geomorphology or even the human-induced framework, can play a determinant role in the system's behavior and evolution (Jackson and Nordstrom, 1992; Riggs et al., 1995; Larson et al., 2002; Jackson and Cooper, 2009; Loureiro et al., 2009; Psuty et al., 2016). Furthermore, some of the widely-used parameters to describe and classify beach equilibrium and morphodynamic state have sometimes been found to be inapplicable to some beaches (Pilkey et al., 1993; Thieler et al., 1995; Klein and Menezes, 2001; Loureiro et al., 2013), suggesting that other controls, such as the inherited geological framework, are more important determinants of beach morphology than contemporary dynamics (Jackson et al., 2005). Overall, controls are important at the local and regional scale of coastal processes and impose constraints on the sediment transport pathways (Larson et al., 2002). Coastal change is not merely a response to the hydrodynamic conditions, but rather it is a reaction to these driving physical agents as they interact with an often restrictive and inherited geological framework (Harris et al., 2005).

Site-specific controlling factors are especially important along crenulated coasts, where natural headlands, rocky platforms and coastal cliffs add complexity to the shoreline and beach configuration. Jackson and Cooper (2009) presented a conceptual model in which beaches that co-exist along a coastal stretch may vary in morphological response due to differing lateral and submerged geological constraints. The authors suggest a classification based on the control that geology imposes to the beach profile volumes: Unconstrained; Semi-constrained; and Highly constrained beaches. This is however based on qualitative observations and the authors stress the need for further studies comparing the morphodynamic behavior of adjacent constrained and unconstrained beaches exposed to similar forcing conditions.

Studies that focus on some dimension of the geomorphological framework and that conclude about the importance of the characteristics that bound the beach-system emerged in the 1970s. Particularly, studies that focused on the shoreface and mapping of the sea-floor geology and morphology provided description on earlier morphologies, such as pre-existing low-relief headlands, valleys, and ancient drainage systems (e.g. Demarest et al., 1981). The influence of inherited nearshore geologic framework on modern beach dynamics was demonstrated by several authors, especially on shoreline change patterns along coastal barrier systems (e.g. Belknap and Kraft, 1985; Riggs et al., 1995; Thieler et al., 1995; Cleary et al., 1996; Schwab et al., 2000; Honeycutt and Krantz, 2003; McNinch, 2004; Browder and McNinch, 2006; Schupp et al., 2006; Valvo et al. 2006; Khalil and Finkl, 2007; Backstrom et al., 2009; Lentz and Hapke, 2011; Cooper et al., 2012).

Beaches between two closely-located lateral boundaries often develop a curve-shaped shoreline and are referred to as headland bay beaches. Early it was realized that there was a correspondence between the beach planform and the incoming wave patterns and an extensive bibliography exists on the subject (e.g. Krumbein, 1944; Silvester, 1960; Yasso, 1965; Hsu et al., 1987; Silvester and Hsu, 1997; Short and Masselink, 1999; Klein et al., 2002; Ojeda and Guillén, 2008; Bowman et al. 2009; Pinto et al., 2009; Short, 2010; Silveira et al., 2010; Thomas et al., 2010; Daly et al., 2011; Gama et al., 2011; Harley et al., 2011; Thomas et al., 2012; Bowman et al., 2014). Recently, Bowman et al. (2014) studied twenty-three pocket beaches encompassing the crenulated coast of Elba Island, in Italy, and proposed a logarithmic bay-shape classification tool to estimate the dimensional depth of embayments. Studies have generally focused on beach shape and planform and their equilibrium configuration, yet some authors have also highlighted the importance

of the geomorphological framework in their morphodynamics (Klein and Menezes, 2001; Loureiro et al., 2009, 2012; Dubois et al., 2011).

Some studies focused on the effect of shore-perpendicular features that constitute lateral boundaries to the beach-system, and how these function as obstacles to longshore sediment transport (e.g. Jackson and Nordstrom, 1992; Badiei et al., 1994; Riggs et al., 1995; Loureiro et al., 2012). Several authors have studied the impact of these boundaries on the littoral drift and associated sediment budget, and consequently beach behavior and shoreline change (Short and Masselink, 1999; Smith, 2001; Ribeiro et al., 2014; Ribeiro, 2017).

The influence of underlying hard bottoms, such as rocky platforms, on beach dynamics, has received less consideration on such studies, although these features border many of the existing cliffed shorelines (Bird, 2000). Hard bottoms are non-erodible features that extend across the intertidal zone, that may consist of any type of rocky material or reef and exist in a wide range of environments (Larson and Kraus, 2000). Beaches that lie above these features are generally called platform beaches or perched beaches and these may be robust and permanent, or consist of a thin sheet of sand that intermittently gets transported offshore. Only recently, studies have started to focus on the effect of rocky platforms on beach dynamics dealing with storm response or sea level rise (e.g. Larson and Kraus, 2000; Trenhaile, 2004, 2016; Muñoz-Perez and Medina, 2010; Gallop, 2011, 2012; Marshall and Stephenson, 2011; Jeanson et al., 2013; Kennedy and Milkins, 2014; Taborda and Ribeiro, 2015). The main conclusions of these studies point to the influence of the platform gradient and the availability of sediment in the system on beach dynamics.

The most evident effect of the geomorphological constraints described above is the hampering of the incoming ocean wave energy, and a vast literature exists on the topic of sheltered beaches. Hegge et al. (1996) conducted a study of Southern Australia sheltered sandy beaches, many of them in embayments or fronted by reefs, and proposed a classification based on morphology and sediment characteristics that include the low-energy beach types. Other studies on sheltered beaches determined the effect of site specific controls on beach dynamics and their prevailing influence over wave regime (e.g. Jackson and Nordstrom, 1992; Masselink and Pattiaratchi, 2001; Aleman et al., 2015).

Other impacts, such as stream discharge and human-induced changes on coastal dynamics, have also been reported (Carrasco et al., 2012; Pranzini et al., 2013).

In general, studies on beaches that are somehow constrained indicate that, unlike open beaches where the process-response models can be fairly well explained by the wave and sediment characteristics, the behavior of these beaches is greatly influenced by the regional and site-specific physical constraints. These constraints operate in such a way that they probably function outside the bounds of existing morphodynamic models, as put forth by Jackson and Cooper (2009). The same limitation is valid for sea level rise impact tools that are generally developed for open coast sandy beaches with a doubtful applicability to beaches that develop on shore platforms (Taborda and Ribeiro, 2015).

From the above bibliography, only some of the recent studies deal with the comparison of morphological dynamics between beaches with varying degree of constraints. Klein et al. (2002) studied short-term beach rotation processes, monthly and during 2 years, along three beaches with different lengths, degrees of curvature, and levels of exposure to the incident waves. The authors' conclusions led to a vast list of factors influencing morphological changes along headland bay beaches: beach planform and indentation ratios, presence of rip currents and submerged bars, shoreline length, and beach type.

The study by Anfuso et al. (2003) covered 14 km of sandy beaches along the southwest coast of Spain, and monitored 12 profiles monthly during 2 years. The analysis revealed an irregular longshore variation of morphodynamic beach states that the authors interpret to be a result of the presence of local rocky shoals. Besides the dissipative and low-reflective types of beaches, the authors identified a third type as rocky-shore platform beaches that recorded smaller variations.

Short (2006, 2016) conducted a review of the systematic investigation of Australian beaches conducted from 1986 onwards, and of the beach models that resulted from this investigation. The author accounts for the relative relevance of waves, tides and sediment, together with geological control, in determining the type of beaches that occur along that extensive coastline. He added to the beach state classification of the process-based models (wave-dominated - Wright and Short, 1984; tide-modified - Masselink and Short, 1993; and tide dominated - Short, 2006) two additional beach states to account for geologically-controlled beaches: reflective beaches with rock flats and reflective beaches with coral reef flats.

Short and Masselink (1999) and Short (2010) put forth an embayment scaling parameter to account for the degree of embaymentization on beach dynamics. These authors list the following as the major impacts of the geological inheritance: 1) greater wave attenuation and lower breaker waves resulting in lower energy beach types; 2) greater wave

refraction, resulting in beaches that are more arcuate along the crenulated coast; 3) creation of topographically-controlled rips and megarips; and 4) interruption of longshore sand transport inducing beach rotation.

Muñoz-Perez and Medina (2010) conducted intensive topo-bathymetric surveying during 5 years at a beach in the southern coast of Spain with varying alongshore characteristics: one profile crossed a zone of rocky flat outcrop (reef) and another profile crossed a sand-rich area. Results show that the reef-flat profile showed the steeper slope, smaller sand volume mobilized and slower accretion rate, compared to the non-protected profile. The authors suggest that the difference in beach morphological behavior is the result of the attenuation of the wave energy promoted by the reef flat.

Gallop et al. (2011, 2012) found different responses for beach profiles that were fronted by rocky outcrops or reefs compared to those that were fronted by sandy substrate. However, the short period of analysis (1 week) and number of profiles (3 along a distance under 1 km) lessens the representability of the results.

Gama et al. (2011) carried out seasonal surveys during a 2-year period along five embayed sandy beaches on the rocky coast of southwest Portugal. The authors analyzed beach planform configuration, wave climate, sediment grain size, volume changes, and morphologic and morphodynamic parameters. They concluded that the main factors controlling the beach morphodynamic state (according to the model by Wright and Short, 1984) were the geological inheritance, the indention ratio, distance between headlands and the available sedimentary sources.

Scott et al. (2011) assessed the applicability of the traditional beach classification models (Wright and Short, 1984; and Masselink and Short, 1993) to the coast of England and Wales using a data-set on morphological, sedimentological and hydrodynamic characteristics, as well as local environmental settings on 92 beaches. They differentiated 9 beach types, and found that the morphodynamic parameters were effective in discriminating them. They also suggested that the presence of three-dimensional bar-rip morphology in intermediate beaches was controlled by wave power. The authors used time-averaged parameters that disregarded the variability in wave/tide/sediment conditions that drives beach change. Furthermore, geological or geomorphological controls were not accounted for in the classification methodology.

Thomas et al. (2012) assessed beach profile response to external forcing along two adjacent embayed beaches, but with different backshore features, in West Wales. Beach

profiles and sediments were collected annually during an 8-year period, along with hydrodynamic parameters. The authors suggested that the differences between the two beaches' response to the same forcing climate were related with the geological and physical constraints, but did not explore the results further.

Loureiro et al. (2012) conducted a 2-year study on 6 embayed beaches with varying levels of exposure to wave action and various degrees of geological control, in the rocky southwestern and southern coast Portugal. The authors demonstrated that natural geological boundaries constrained the morphological behavior of embayed beaches. Both lateral and vertical boundaries interfere with beach and nearshore dynamics by restraining longshore sediment transport and causing beach rotation, topographically-controlled rip circulation, and limited profile fluctuation. A conceptual framework describing boundary effects on embayed beaches was proposed.

In a different geographical and geological setting, Jeanson et al. (2013) carried out four field experiments to assess and compare the wave attenuation process promoted by a barrier reef and its implications on morphological changes of three pocket beaches. They found that beach morphological changes driven by the residual wave energy following reef attenuation were strongly affected by the degree of beach embayment. The low bay-indented beaches were characterized by longshore sediment mobility that, according to this study, provided a rare example of inferred rotation of reef-fronted beaches.

Kennedy and Milkins (2015) conducted topographical surveys along 48 profiles in two study areas in microtidal coastal Australia, allowing a range of platform morphologies to be investigated. The authors studied the morphological boundary conditions of beach accumulation and change and concluded that, in addition to sediment supply, sandy platform beaches in microtidal settings can be considered to be width- and elevation-limited rather than slope-limited as found in mesotidal to macrotidal environments.

Karunarathna et al. (2016) used statistical techniques to analyze and compare cross-shore morphodynamic behavior of four beaches with different regional morphological settings, wave climate and sediment characteristics. The authors focused on the cross-shore component of beach-profile data and found that the time-changes in profile shape relate to sediment characteristics across the profile.

From the existing literature, one can define three major ways that the geomorphological framework is expected to influence the forcing mechanisms and the beach response, form and dynamics:

- By affecting the incoming waves, and influencing the nearshore time and space distribution of wave parameters;
- By controlling the available space for the beach to migrate and expand, both spatially and vertically; and
- By controlling the sediment inputs and outputs of the system.

The majority of these studies focused on beaches with the same general characteristics. The present work provides new insights to the control of the geomorphological settings by comparing the morphodynamic response of adjacent constrained and unconstrained, platform and no-platform beaches, exposed to the same offshore forcing conditions.

1.3 Objectives and outline of the thesis

The observations and literature review led to questioning about the role of the geomorphological framework on beach dynamics and gave rise to the following hypothesis:

Geomorphological constraints and the local settings of beaches are the primary drivers for the varying temporal and spatial groupings of morphological responses.

That is, the geomorphological framework interacts with the available coastal sediments and incoming waves, and controls the beach configuration and responses. But how and to what extent? To test this hypothesis, three objectives were established:

1) Evaluate the magnitude and patterns of beach dynamics for modal seasonal conditions along a coastal segment with contrasting geomorphological settings;
2) Characterize waves and total water levels and their alongshore variation, departing from the same deepwater conditions;
3) Detect and interpret any existing spatial organization of beach response related to the geomorphological settings.

In order to achieve these goals, fourteen study sites, located along the same regional coastal stretch were monitored quarterly, over two and a half years. The following assumptions (see Chapter 2. Study area and Chapter 4. Results, for description of some of

these statements) provided this investigation the frame of reference that guided the methodology and interpretation of results:

- The study sites are representative of the coast's landforms in which small to large beaches occur, with varying length, indentation and exposure to the incident waves;
- The study sites are under the influence of the same general off-shore wave regime;
- The study area is located along a coastal reach with a balanced sediment budget for the study period;
- Quarterly surveys are appropriate to detect beach morphological and sedimentary variations at the seasonal scale;
- Beach dynamics can be described using the characteristics of the subaerial portion of the beach, extending between mean sea level and the landward limit of the beach;
- The two and a half years monitoring program during which there was no extreme event is appropriate to characterize the modal process-response conditions.

Hereupon, the study was conducted in three main components:

1) Geomorphological framework: analyzed in terms of planform geometry and description of the physical boundaries, and type of nearshore and backshore features present at each study site;

2) Beach response: included regular field sampling planned to ensure accurate and representative data collection on beach morphology and sediments. A total of 52 beach profiles were monitored quarterly along the study area;

3) Hydrodynamic forcing: characterization of the nearshore wave climate at each study site was done through numerical modelling of wave propagation for a 36-year time series, and total water levels were estimated for each site.

Data generated for each of the three components were analyzed collectively, and exploratory analyses were performed to integrate the above results and to relate the oceanographical forcing and other physical controls, and beach response.

A thorough description of the data acquisition and analyses methods is presented in Chapter 3. Results of the three components of investigation are included in Chapter 4, and the combined analysis and discussion of the results is presented in Chapter 5. Chapter

6 holds the concluding remarks of this study. A preceding evaluation of the study area, based on the bibliography and observation, is described in Chapter 2.

Chapter 2. Study Area

The present chapter describes the study area and selected study sites and provides a summarized description of the geology and geomorphological setting, coastal processes and landforms, as well as the recent historical shoreline change.

2.1. Study sites

The study area covers 200 km of coastline in the central west coast of mainland Portugal (Figure 2.1). Looking the north Atlantic, this high-energy coast presents a myriad of coastal landforms controlled and shaped by natural and anthropogenic processes. It comprises the coastal stretch between Marinha Grande and Cabo Espichel.

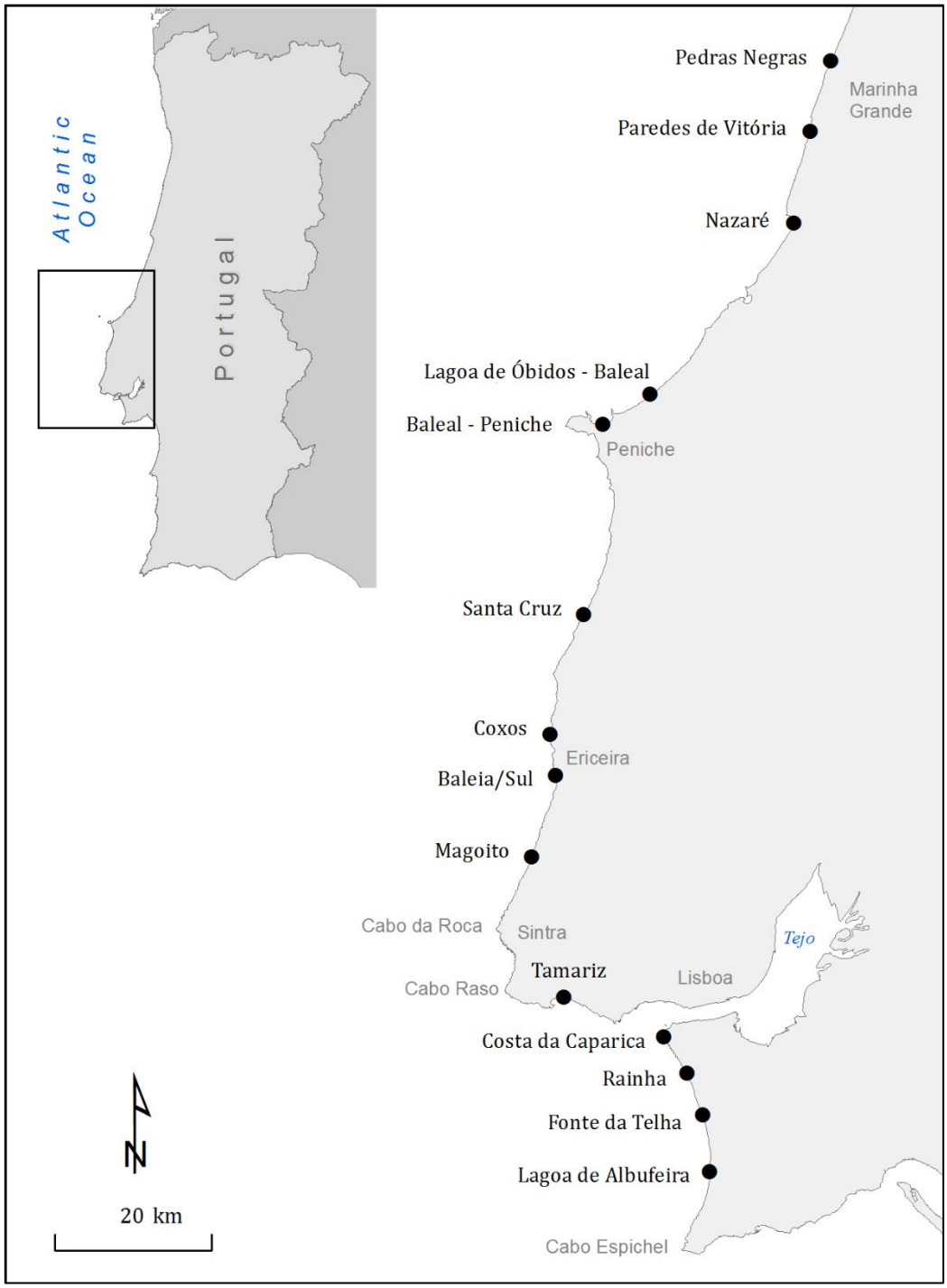

Figure 2.1. Study area and identification of the 14 selected study sites.

The coastline is predominantly rocky, with cliffs cut in meso-cenozoic formations, and characterized by constrained beaches limited by physical boundaries, with varying length, curvature and exposure to the incident waves. The southern and northernmost sectors of the study area, however, exhibit characteristics of open-coast continuous, or unconstrained beaches with well-developed dune systems. A number of urban beaches exist along this coast, adjacent to densely occupied coastal land, in some cases protected by hard structures. A number of beaches have been subject to beach nourishment and others to beach scrapping activities.

Fourteen coastal segments were selected as study sites (Figure 2.1), comprising a total of 33 beaches along the study area. The sites are considered representative of larger segments, covering a wide range of geological, geomorphological, hydrodynamic, and land occupation settings. A short presentation of each site is provided, and further description is made in subsequent chapters. Each of the study sites name has an abbreviation (in brackets) that is used throughout the text for convenience.

Study site 1 | Pedras Negras [PN]

Pedras Negras is the northernmost study site and is located along an open-coast segment, just north of São Pedro de Moel village. The beach is backed by a robust vegetated dune field that represents the seaward section of an extensive natural and protected area of pinewood (*Mata Nacional de Leiria*) (Figure 2.2). Although unoccupied with permanent structures, the beach is used for recreational purposes and the backshore is the location of elevated boardwalks and a parking lot.

Study site 2 | Paredes de Vitória [PV]

Paredes de Vitoria is a relatively extensive beach (about 1800 m) that developed at the mouth of the Ribeira de Paredes stream valley, and the adjacent village. The central area of the site, next to the stream, is backed by an artificial dune field stabilized with palisades, and boardwalks. Away from the central area, the beach is free of any human intervention, and high cliffs with small dunes at the base comprise the backshore (Figure 2.3).

Figure 1. General view of Pedras Negras: aerial photograph looking east showing the dune field backing the beach, where boardwalks and parking lots exist. Source: SIARL, 2011.

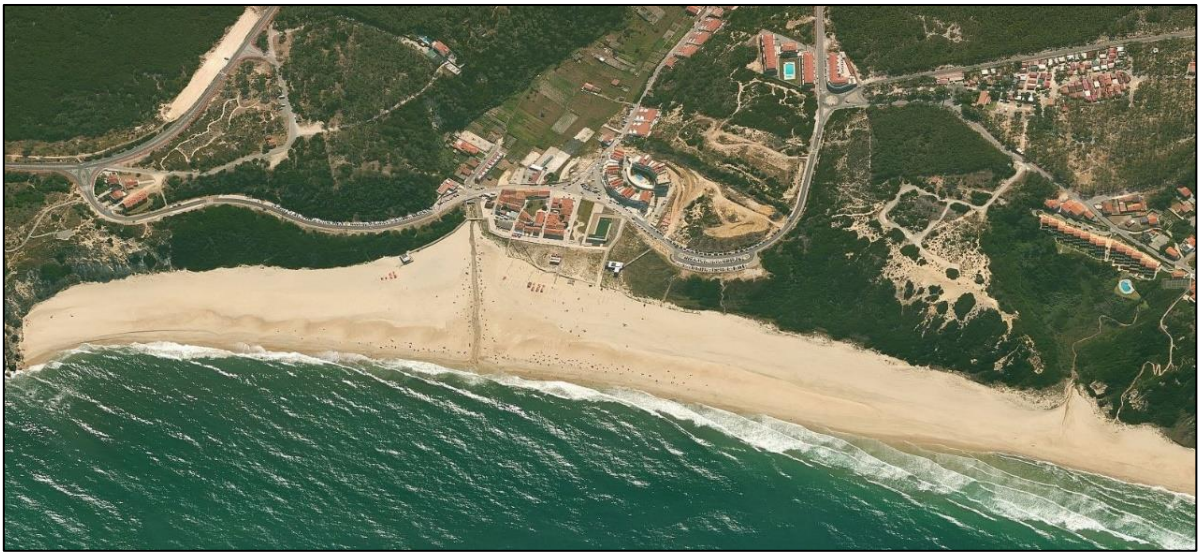

Figure 2.2. Aerial view of Paredes de Vitória study site, showing the location of the Ribeira de Paredes crossing the beach. Source: Bing Maps, unknown date.

Study site 3 | Nazaré [NZ]

The urban beach of Nazaré fronts a fishing village that developed along the sloping margin of a Holocene coastal plain. A concrete seawall extends along the total length of the beach and serves as protection to the village that expanded over the former dune field, and a jetty in the southern end of the study site provides the stabilization of the

Alcoa river mouth and shelter to the fishing harbor (Figure 2.4). To the north, the promontory of Sítio da Nazaré, rises 50 m above MSL and provides for some shelter from the NW prevailing waves, especially to the northernmost part of the Nazaré beach.

Figure 2.4. View of Nazaré study site, looking south towards the Alcoa river jetties and harbor entrance. The beach is backed by a seawall. Photo taken on March 7, 2011.

Study site 4 | Lagoa de Óbidos - Baleal [LOB]

The Lagoa de Óbidos – Baleal study site corresponds mostly to a high-relief cliffed coastal stretch about 10 km long that extends from the Lagoa de Óbidos mouth to Baleal. The cliffs are locally interrupted by streams and valleys that provide the access routes for beach users, and for each beach concession there is a different beach designation. The study site was monitored at Rei do Cortiço, Praia d'El Rei, Almagreira, and Baleal beaches (Figure 2.5). The latter is the extreme southern end of this site and unlike the rest of the monitored beaches, is located on a sandy tombolo and is surrounded by the more intense human development of Baleal village.

Figure 3. Ground photos of the beaches of Lagoa de Óbidos-Baleal study site, from north to south: A –Rei do Cortiço; B –Praia D'El Rei; C –Almagreira; and D –Baleal. The latter corresponds to the north-facing margin of the Baleal tombolo.

Study site 5 | Baleal - Peniche [BP]

The Baleal-Peniche study site, similar to the LOB study site, is a coastal stretch of continuous beach that includes several concessionary units, and therefore different beach designations. The 4 km of shoreline extends from Baleal tombolo to Peniche village, in a bay-shaped outline backed in its central section by a large dune field (Figure 2.6). The beaches have been left fairly natural and the dune field is only locally interrupted where the main access paths are located.

Figure 2.6. General view of the embayment between Baleal and Peniche, looking south. The curved beach is backed by a field of dunes most of its length. Photo taken March 15, 2013.

Study site 6 | Santa Cruz [SC]

Santa Cruz study site extends for about 4.4 km between two promontories. The beach is limited landward by high-relief rocky cliffs in its northern region. The central and southernmost sectors of the study site front the village of Santa Cruz and are characterized by the presence of hard structures and other anthropogenic features related to beach activities (Figure 2.7).

Study site 7 | Coxos [CX]

Coxos is the smallest of all the study sites with only 100 m of beach length, representing one of the typical pocket beaches that occur along the study area (Figure 2.8). It is located along the Ericeira coast, known for its powerful surfing waves and steep rocky cliffs that at Coxos reach 30 m in elevation.

Study site 8 | Baleia/Sul [BS]

Baleia/Sul, similar to Coxos, is located on the Ericeira coast, but in the center of the village, where most of the buildings and services are located (Figure 2.9). The urban character of this particular beach has led to the complete armoring of the backbeach boundary and the beach is further bounded by groins and a seawall.

Figure 47. Santa Cruz study site: A – northernmost sector backed by high cliffs; and the more urban areas, B – central sector and C – southernmost sector, backed by structures.

Figure 2.8. Aerial photo of Coxos beach. Source: SIARL, 2007.

Figure 2.9. Aerial photo of Baleia/Sul beach in Ericeira, from October 2010, looking east (Photo by C. Andrade).

Study site 9 | Magoito [MG]

Magoito beach develops along the energetic and remote coastline of the Sintra mountain range, south of the Magoito Fort promontory (Figure 2.10). It is limited by high-relief cliffs and developed around the Mata River mouth and valley. The beach extends for about 600 m as a thin layer of sand covering the underlying rocky substrate. The northern section is where beach access is made and where all human activities and associated development exist.

Study site 10 | Tamariz [TM]

Tamariz is an urban beach located in the greater Lisbon area, along the Estoril coast (Figure 2.11). The beach is bounded by hard structures, including a seawall and one groin, as well as a variety of infrastructure that supports the intense beach use and activities all year round. The general orientation of the shoreline, east-west, makes this a particularly sheltered area from the energetic Atlantic Ocean wave regime.

Figure 2.10. Aerial view of Magoito beach, looking south and showing the Sintra mountain range in the background. Source: SIARL, 2007.

Figure 2.11. Aerial view of Tamariz beach, looking northeast, showing the intense urban background. Source: Google Earth, 2004.

Study site 11 | Costa da Caparica [CC]

Costa da Caparica includes a number of urban beaches located along the coastal plain that lies south of the Tejo river, and that serves as the main coastal recreation setting for the greater Lisbon area (Figure 2.12). The area has long been used as a primary location for beach recreational use, leading to intense urban development over the former dune field and very close to the shoreline. A groin field and seawall protect the urban front and serve as a promenade for beach users.

Figure 2.12. Costa da Caparica study site. A - Aerial view overlooking the several beaches in the southeast direction, and showing the intense urban surrounding and groin field. Source: Google Earth, 2015, and B – ground photograph of one of the groin field beaches limited by a seawall.

Study site 12 | Rainha [RA]

Rainha is one of the many recreational beaches that exists along the sandy low-lying coastal stretch that extends southward from the Tejo river. South of the Caparica groin field, beaches are maintained in a somewhat natural condition, and the foredune still persists despite the localized access routes that connect parking lots and some infrastructure to the beach (Figure 2.13).

Figure 2.13. Aerial view of Rainha beach, looking east. Source: Google Earth, 2015.

Study site 13 | Fonte da Telha [FT]

Fonte da Telha is located farther south from Rainha, along the same sandy coastal stretch. But, unlike Rainha, this site has been intensely and disorderly developed, resulting in an ill-planned coastal settlement with severe impact on the dune field and land cover (Figure 2.14).

Study site 14 | Lagoa de Albufeira [LA]

The southernmost of the study sites is located near the Lagoa de Albufeira lagoon. The beach area monitored in this study site is located somewhat to the south of the lagoon, where the barrier merges with the sand beach at the base of the soft cliffs that characterize the remaining length of the coastal stretch extending southwards to Cabo Espichel (Figure 2.15).

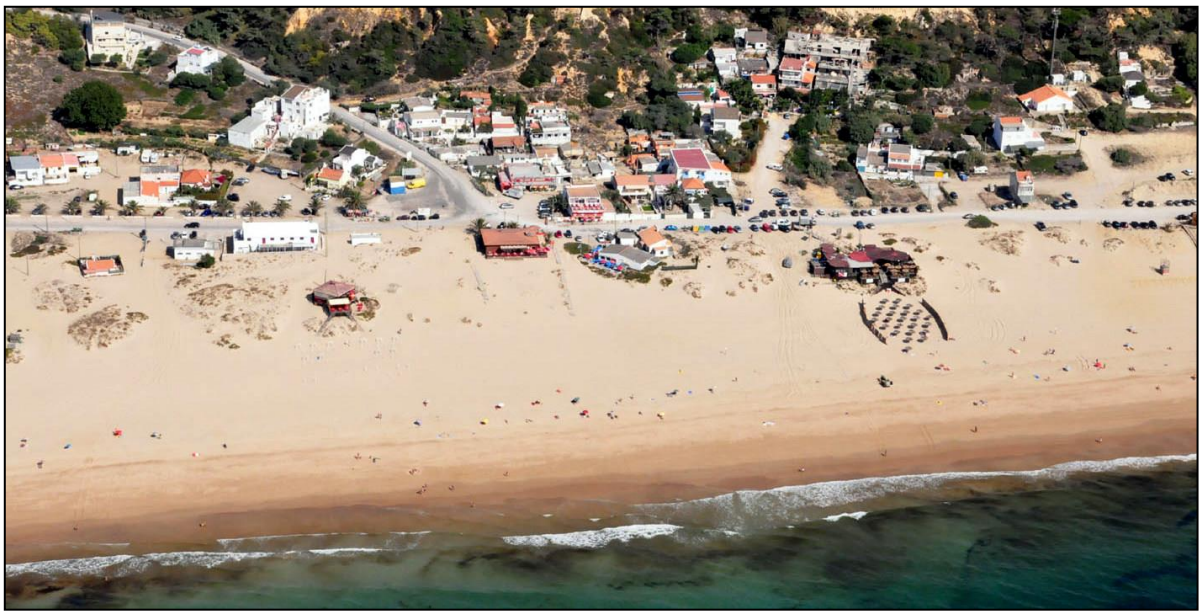

Figure 2.14. Aerial view of Fonte da Telha, looking east; showing the disorderly settlement at the shoreline. Source: Google Earth, 2009.

Figure 2.15. Aerial view of Lagoa de Albufeira study site, looking northeast; showing the barrier and lagoonal system in the background and the monitored beach in the cliff section in the foreground. Source: SIARL, 2008.

2.2. Geology and Geomorphology

2.2.1. Geologic Setting

Coastal features along the study area developed as a result of the Holocene transgression, under a rapid sea-level rise, being stabilized and reshaped over the last 5000-6000 calendar years, when sea level has remained fairly stable (Dias et al., 2000). Since then, evolution of coastal landforms is mostly due to the sediment balances occurring within the existing littoral cells (see section 2.2.2.3). Beaches are mostly composed of sand with occasional occurrences of coarser material associated with local stream and river discharge.

The geology of the Portuguese central west coast comprises mainly rocks of sedimentary origin. Cliffs are mostly carved into Mesozoic dolomite, marls, limestone and sandstone. Locally, in the Sintra region and coastal section extending to the west of Lisbon, there are occurrences of igneous formations, such as granites, syenites and basalts from the Sintra Igneous Complex and the Lisbon Volcanic Complex. Cenozoic formations correspond mainly to the recent beach, dune and alluvial sand deposits and, to a lesser extent, Miocene and Pliocene sandstones along two coastal stretches: north of the Nazaré and Caparica-Espichel segments.

2.2.2. Coastal Processes

2.2.2.1. Waves

The study area is exposed to the high-energy wave regime generated in the North Atlantic. It is considered a severe climate, with winter storms commonly generating deep-water maximum significant wave heights (H_s) greater than 7 m (Costa and Esteves, 2009). Extreme storms can reach easily maximum significant wave heights on the order of 9.0 m and higher, and last for several days. The recent 2013/2014 winter Christina storm, for example, reached a maximum wave height of 14.9 m, and maximum wave period (T_{max}) of 28.1 s, measured at the Sines buoy (Diogo et al., 2014). These storm events are typically approaching from the WNW.

Deep-water significant wave height and mean wave period have annual averages of about 2 m and 6.7 s, respectively, and peak wave period (T_p) lies most frequently between 9 and 13 s, associated with waves coming from NW (Costa and Esteves, 2009). Seasonality is reflected

in the wave characteristics: small waves (H_s < 2 m and T_p < 11 s) characterize the summer months (April to September), whereas higher waves characterize the winter months (November through February) (Andrade et al., 2013b).

2.2.2.2. Water Levels

The astronomical tide is semidiurnal, with an average period of 12h 25min, resulting in two high tides and two low tides per day. The study area is characterized by a mesotidal regime, with an average amplitude of the astronomical tide on the order of 2.10 m, reaching a maximum elevation of 4.30 m in Lisbon and 3.99 in Cascais (data from Antunes, 2007). The surge phenomenon associated with storms has a small contribution to the overall water levels reaching a maximum of 0.6 m, measured at Cascais tide gauge (Andrade et al., 2006; Antunes et al., 2013).

2.2.2.3. Littoral Cells

Beaches, from their subaerial expression to their submarine limit, are part of a sand-sharing system in which the sediment moves freely between the various sources and sinks along the coast. It is the balance between the various inputs (sources) and outputs (sinks) of sediment that determines if a system is in sedimentary deficit or gain that in turn is reflected in the morphological response of the system's beaches.

These sand sharing systems are defined in terms of littoral cells, with well-defined geographical boundaries. According to Inman (2003): "a littoral cell is a coastal compartment that contains a complete cycle of sedimentation including sources, transport paths, and sinks". Sediment paths follow the general littoral drift that in this case is predominantly directed towards south because of the prevailing NW wave regime and the general N-S alignment of the Portuguese west coast.

The study sites are included in four different littoral cells, described in Santos et al. (2014) (Figure 2.16). The first two study sites, Pedras Negras and Paredes de Vitória are part of littoral cell 1c that extends between Cabo Mondego and Nazaré. Most of this coastal stretch is composed of low lying beaches and dune systems with an approximate orientation NNE-SSW, locally disrupted by a section of coastal cliffs enclosing embayed beaches. Santos et al. (2014) estimate that the northern section of this cell started an erosive process to counter the sediment deficit imposed by the coastal hard structures of

the Mondego harbor and related dredging operations to the north. However, the southern section, where the study sites are located, is considered to be in a stable area, where the potential sediment transport is effectively transferred along the cell, with inputs matching the outputs. The sediment is finally lost to the Nazaré submarine canyon that represents the cell's downdrift boundary.

Littoral cell 2 extends from the Nazaré promontory to Peniche. The general orientation of this coastal stretch is normal to the mean wave direction, and therefore there is no meaningful nor prevailing net littoral drift. Santos et al. (2014) consider that the volume of sediment entering the system is equal to the volume of sediment leaving. Moreover, sediment inputs are of small magnitude (c. $10^4 m^3$/year) derived mainly from fluvial discharge and cliff erosion. Study sites Nazaré, Lagoa de Óbidos-Baleal, and Baleal-Peniche are included in this cell.

Littoral cell 3 is mainly characterized by a rocky cliffed coast, with several pocket and embayed beaches developing at the mouths of small rivers and streams, or downdrift of rocky promontories. Sediment input is small and limited to discharge from a few streams and erosion of rocky cliffs that contribute very little sediment to the potential littoral drift (c. $10^4 m^3$/year) (Santos et al., 2014; Ribeiro, 2017). Sediment is finally captured by the Guincho dune system, south of Cabo da Roca, and intermittently bypasses Cabo Raso by wind transport. This sand eventually reaches the cliffed coast extending to the south and east of Cabo Raso, where it is re-distributed by littoral drift. The work by Ribeiro (2017) corroborates that sediment sources balance the sinks and that this coastal stretch is in equilibrium. The study sites of Santa Cruz, Coxos, Baleia/Sul and Magoito are part of this littoral cell.

Littoral cell 4 extends from Cabo Raso to Cabo Espichel, surrounding the estuary of Tejo river. Sediment pathways are dependent of the river inlet and ebb delta and can be circuitous and hard to define, but in general, net littoral drift converges in the ebb delta (Taborda and Andrade, 2014).

The northern margin, where Tamariz study site is included, is mainly characterized by rocky low-relief cliffs and small pocket beaches, and the shoreline is heavily intervened with hard stabilization structures. This segment has a general W-E orientation and is therefore sheltered from the prevailing NW wave regime. Santos et al. (2014) admit that sediment transport is small and that the occurring beaches correspond to stable and closed systems.

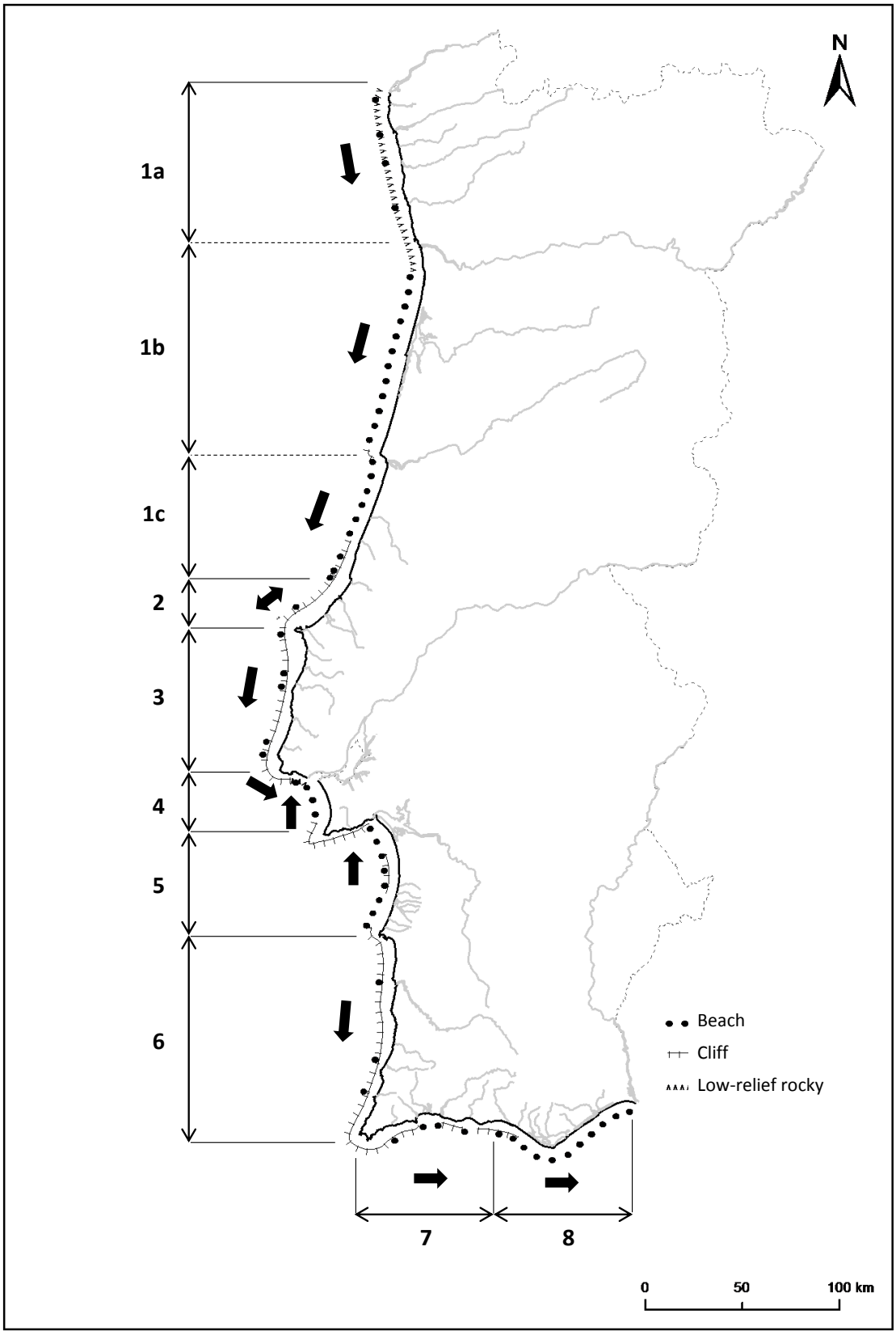

Figure 2. 16. Littoral cells of mainland Portugal and direction of net littoral drift. The study area is included in cells 1c to 4 (modified from Santos et al., 2014).

South of the Tejo estuary, the coast exhibits a long and continuous beach, gently arcing, that extends southwards ca. 23 km until the high-relief rocky cliffs of Cape Espichel. Study sites Rainha, Fonte da Telha and Lagoa de Albufeira are located along this coastal stretch. The northern section of this segment – Costa da Caparica study site – has been severely modified by coastal structures, groins and a seawall, that were built to hold the shoreline when severe erosion started to threat the local human settlement in the 1950s. This erosive trend persists and is mostly caused by the intense dredging and sediment extraction from the inlet for navigation purposes (Taborda and Andrade, 2014). The input of sediment eroded from the soft cliffs in the south is considered insufficient to counter this deficit. Recently however, sediment dredged from the inlet channel has been used to nourish these beaches, and has helped to stabilize the shoreline.

2.2.3. Coastal Landforms

There are 192 beaches along the study area, representing ca. 50% of its total length. Coastal cliffs are the most frequent backshore feature, corresponding to 62% of the coastline, whereas dunes and structures make up the remaining coastline, in equal percentage (Marques et al., 2013). These settings result in a majority of constrained beaches, of varying size, bounded by cliffs and headlands. In the absence of a consensual terminology regarding this kind of beach, herein we designate as pocket beaches features with length up to 10^2 m, and wider features as embayed beach. Where there are no beaches, the sea contacts directly with the cliff or structure, or there is a rocky shore platform making the transition to these features. Figure 2.17 presents the geomorphological classification of the coast according to the foreshore and backshore domains along the study area, as defined by Marques et al. (2013).

Large dune fields occur only in the northernmost and southernmost littoral cells adjacent to exceptionally longer stretches of beach (North of São Pedro de Moel, and south of Tejo river). In addition, there are localized areas where dune fields occur along sheltered embayments in the study area: between Baleal and Peniche, and between Peniche and Consolação, for example.

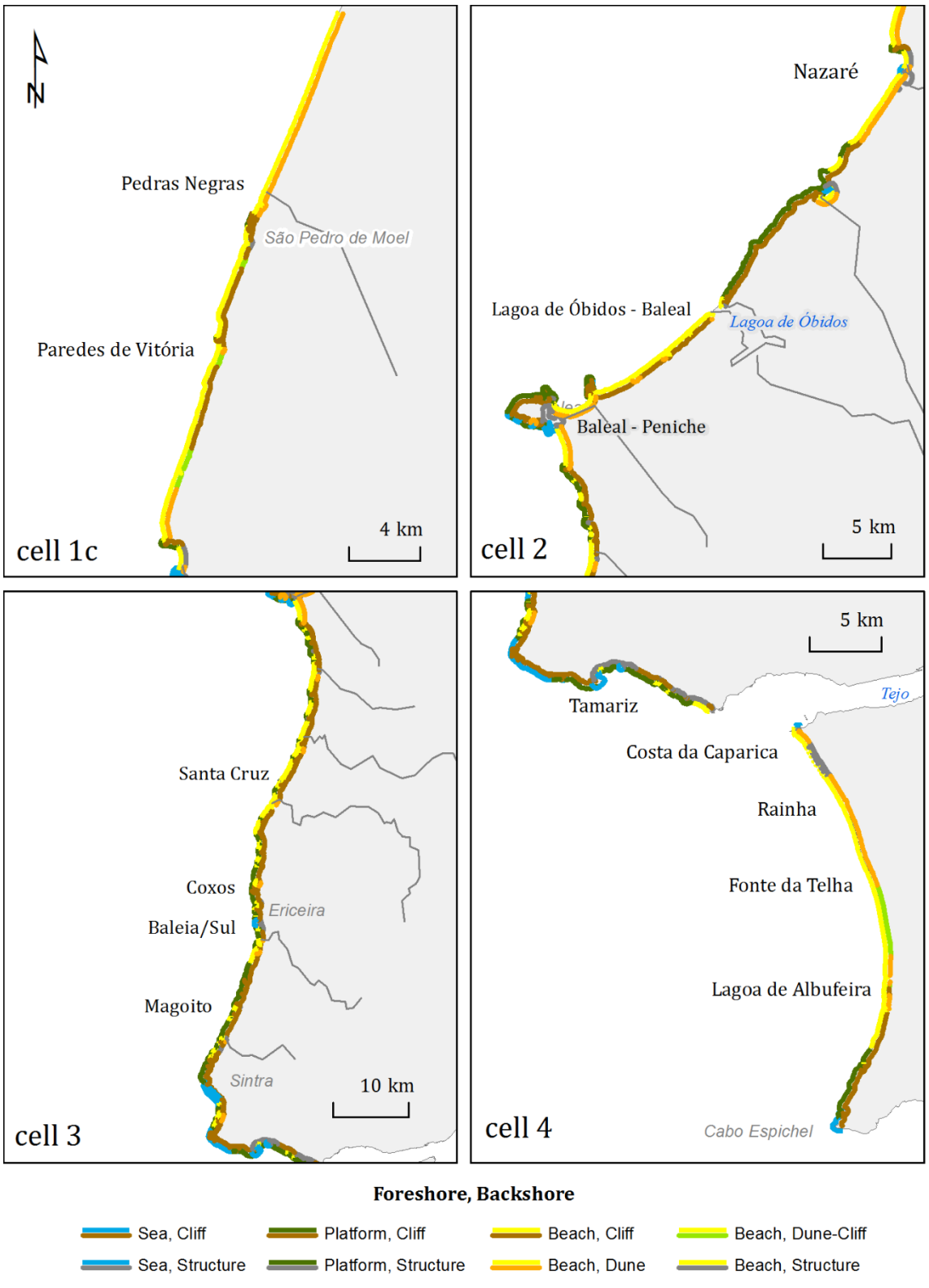

Figure 2.17. Geomorphological classification of the foreshore and backshore domains along the study area, presented by coastal cells 1c to 4 (Adapted from Marques et al., 2013).

Two major water bodies interrupt the shoreline – Lagoa de Óbidos and Tejo. The former is a coastal lagoon and its inlet and beach at the ocean margin of the barrier is wave-dominated and therefore has little interference on the shoreline outline. The latter is a tectonic type of estuary and creates a large ebb delta that interferes with the coastal processes of cell 4. In addition, minor streams drain to the study area, most of them intermittent, and occurring in association with small beaches that develop in the associated valleys. These and smaller water bodies (eg. Lagoa de Albufeira) occur along the study area but with no major impact on the features at the shoreline.

2.2.4. Influence of Human Activities

The study area includes the capital city of Lisbon and surrounding communities, and therefore is one of the most developed parts of the country. As a result, human perturbations to the natural system are evident, and the coast is not an exception. As stated previously, structures make up ca. 19% of the coastline, and include mainly groins, jetties and seawalls.

Most of these engineered structures resulted in growth of beaches on their updrift side. In most cases, the effect of the structures is localized, mostly because sediments are concentrated in small and closed beaches, with no alongshore connection.

In Costa da Caparica, in the southernmost littoral cell, however, structures that were built to avoid further shoreline retreat and erosion, were only temporally effective and beaches continue to erode. To counter this trend, further soft interventions have been regularly adopted, such as beach nourishment (Pinto et al., 2015).

Cliff stabilization is another common practice along the study area, in locations of high human occupation, such as recreational beaches and seaside promenades. These include the installation of mesh systems, retaining walls or application of concrete.

Another form of human interference in the coastal system is through the construction of dams, drainage control, and increase of impervious soils that led to the reduction of sediment supply to the coast. Moreover, intensive dredging of sand bodies related to the Tagus inlet, as a source of construction material and for enhancement of navigation activities, had further impacts, particularly on the Costa da Caparica beaches (Santos et al., 2014).

2.3. Historical Shoreline Change

The study area incorporates a myriad of coastal landforms and therefore there isn't one single method to analyze shoreline change along the variety of features along the entire coast. Extensive work has been done using aerial digital photogrammetry to detect cliff retreat events covering several decades (since 1943/7) along the study area rocky coastline (e.g. Marques, 2009; Penacho, 2012; Marques et al., 2013; Matildes, 2016). Cliffs are inherently erosional coastal forms, and the study area is essentially characterized by sea cliffs with low retreat rates, typically lower than 0.1 m/year. In the Lagoa de Óbidos – Baleal stretch, however, retreat can reach 0.4 m/year.

Silva et al. (2013a and 2013b) and Lira et al. (2016) focused on the low-lying sandy coastline and derived shoreline change analysis using aerial photography dating back to 1958. In these works, the uncertainty affecting coastline change rate was calculated as ±0.2 m/year. The following description is based on these authors' data.

The low-lying areas of the northernmost section of the study site, corresponding to cell 1c, had a tendency of stability or accretion (Figure 2.18). The shoreline in the area of the Pedras Negras study site had an average shoreline change rate of ca. +0.35 m/year. The localized beach of Paredes de Vitória was mostly stable with an average rate of +0.05 m/year (well below the measure of uncertainty). North of the Nazaré promontory (the downdrift end of the littoral cell), average rates attained ca. +0.9 m/year, with a local maximum of +1.4 m/year.

The low-lying sandy shoreline segments north and south of Peniche had alternate periods of shoreline retreat and advance, resulting in a very low average annual retreat rate (within the measure of uncertainty of the method), between -0.11 and -0.18 m/year, between 1958 and 2010.

The low and sandy coastline between Caparica and Cabo Espichel, in cell 4, had distinct patterns of shoreline change along the coastal segment. São João da Caparica had the higher magnitudes of change, with an average rate of ca. -4 m/year that corresponded to a 215 m shoreline retreat between 1958 and present, but more significant during the 1958 -1980 period. The recent beach nourishment interventions were able to counter this erosive trend and, for the period between 2005 and 2010, the rate of change was +0.2 m/year. South of Costa da Caparica, and to Fonte da Telha, the coastline had annual average rates of shoreline change of ca. +0.56 m/year. South of Fonte da Telha the

shoreline position was mostly constant or accreting with average annual variation rates between +0.19 and +0.40 m/year along the coastal stretch.

The comparison of historical ground photographs, from the beginning of the 20th Century, and recent photographs taken to recreate the view of the older ones, was done by Ribeiro (2017) in the coastal stretch between Peniche and cape Raso and by Carapuço (2016) in the coast of Cascais (between cape Roca and Carcavelos). Both authors found that there were no significant changes in the beach area and general configuration during the span of 100 years.

In general, the literature review suggests shoreline meta-stability of the study area for the most recent decade.

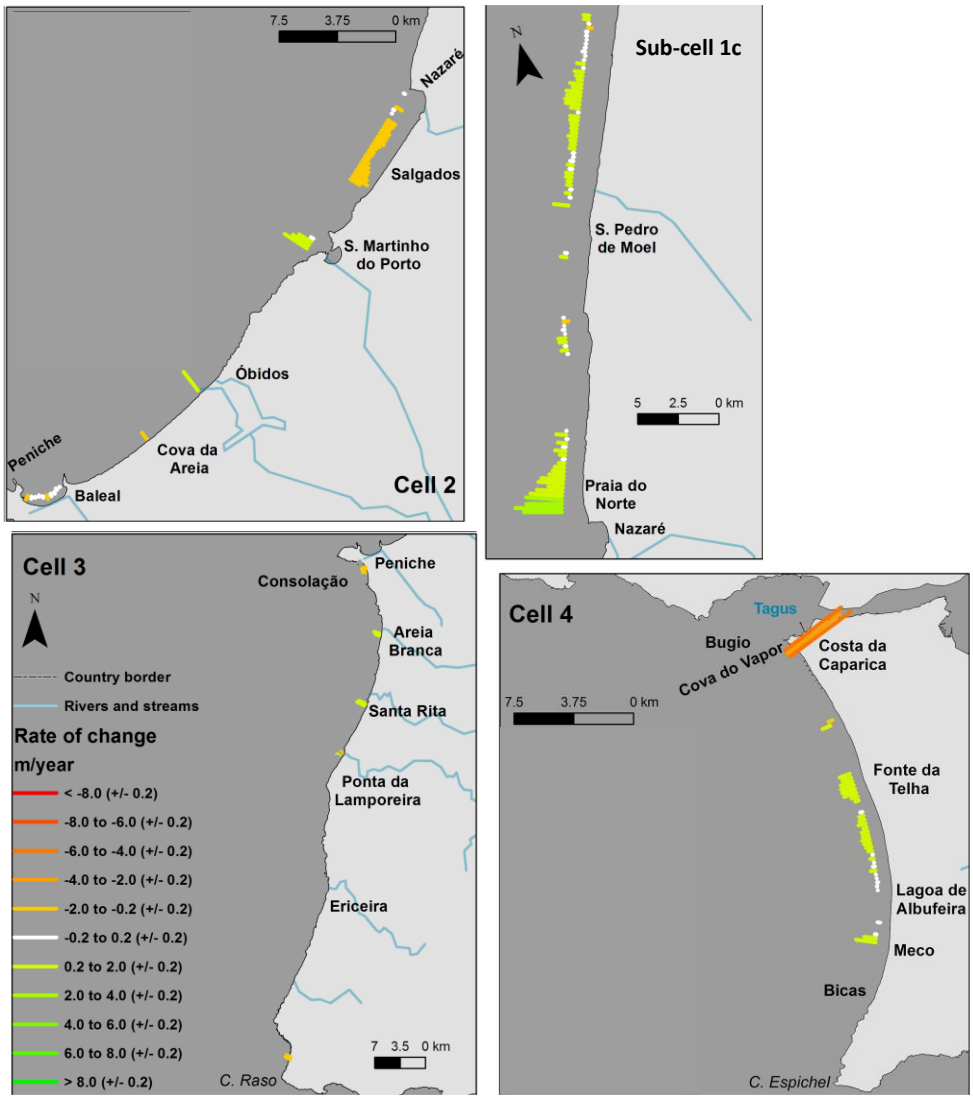

Figure 2.18. Shoreline change rates (m/year) for the low-lying sandy coastline (cells 1c to 4), for the period between 1958 and 2010 (Adapted from Lira et al., 2016).

Chapter 3. Methods

This chapter describes the approaches selected to test the hypothesis pursued in this thesis, including the data gathering, analysis, and evaluation. It includes four sub-chapters: 3.1 - the methods used in the description of the geomorphological framework; 3.2 - characterization of the beach morphology and sediment analyses; 3.3 - the hydrodynamic forcing modeling and assessment; and 3.4 - the methods applied in the exploratory analysis of the data.

3.1. Geomorphological framework

The geomorphological framework of each study site was analyzed in terms of planform geometry and description of the physical boundaries, and type of nearshore and backshore features. The analysis included the use of several different sources that portray the geomorphological characteristics, including aerial photography, orthoimagery and oblique photography of the coast, from several years, as well as LiDAR data (Table 3.1). Also, the photographs taken at the time of each survey (described in Subchapter 3.2) were evaluated to assess the consistency of the characteristics of the subaerial beach through time.

Table 3.1. Datasets used in the analysis and description of the geomorphological framework for each study site.

Source	Type of data	Date
Direção-Geral do Território	Orthoimagery	2005/2008/2010/2014
	LiDAR	2011
Agência Portuguesa do Ambiente - SIARL	Oblique aerial photography	2007/2008/2009/2011/2012
Faculdade de Ciências da Universidade de Lisboa	Oblique aerial photography	2010
Google Earth	Satellite and aerial imagery	2001 - 2017

The geological description made use of the results of the project *Criação e Implementação de um Sistema de Monitorização do Litoral,* specifically, the output files and report of the characterization of the geology of the coastal zone (Marques et al., 2013).

3.1.1. Physical boundaries

Beach lateral boundaries were considered to be the locations of fixed morphological structures that restrict alongshore sediment transport, such as promontories or smaller headlands, or anthropogenic structures. For the purpose of this study, analysis focused on the identification of margins where there is no evidence of sediment transport under modal (non-storm) conditions. This means that rather than coastal cells as described by Santos et al. (2014), the study identifies beach systems, lengths of continuous sand, enclosed between two lateral boundaries. Figure 3.1 schematizes the hierarchy and definition of the terms herein used: study area, referring to the overall study sites; study site, referring to the selected areas for conducting the monitoring program; and beach systems, referring to the closed systems, laterally bounded.

Three criteria were used to define the beach system margins:

- Existence of a shoreline offset;
- No evidence of wave breaking seaward of the lateral boundary structure; and
- No evidence of sediment bypassing at low tide.

The backshore boundary of each beach system was classified as: dune, cliff or anthropogenic structure. The nearshore features were divided into: nearshore bars or rocky platform.

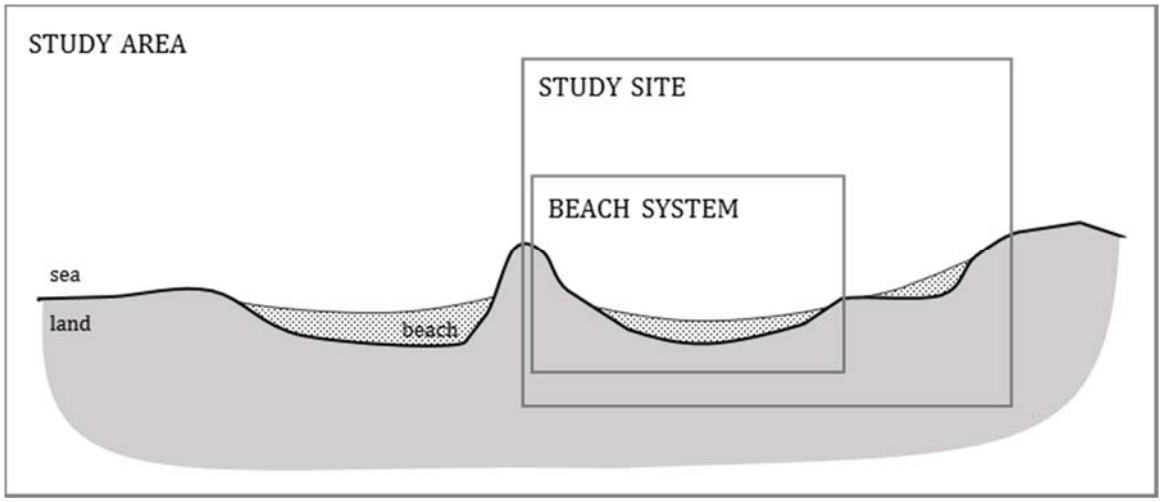

Figure 3.1. Definition of terms used to identify areas addressed in this study: study area; study site and beach system.

3.1.2. Planform geometry parameters

The planform geometry analysis was directed towards using parameters and relationships that could best quantify the entire range of beach configurations of the study area, by providing a degree of indentation, or in another perspective, the level of linearity of each beach. The method resorted to parameters that have been widely used in the literature, mostly related to the study of the stability of embayed beaches (e.g., Short and Masselink, 1999; Bowman et al., 2009) and uses the following notation:

C_l – Embayment width: linear distance between the seaward tips of the two lateral boundaries;

S_l – Embayment length: perimeter of the embayment, measured along the coastline, between the seaward tips of the two lateral boundaries;

a – Bay indentation: maximum bay depth taken as the maximum distance between C_l and S_l, features, measured normal to C_l; and

β – Wave obliquity: angle between dominant wave crest and headland alignment.

The parameters are schematized in Figure 3.2 and were measured on each beach system using ArcGis® tools and the toolbox Digital Shoreline Analysis System (Thieler et al., 2009). The latter was used to create the C_l-normal control lines spaced 10 m alongshore, along which distances were measured between C_l and S_l, to determine the bay indentation (a). The dominant wave direction was taken as the wave mean peak direction for the study period (305° - see table 4.5 in Chapter 4. Results).

From the above parameters, two criteria were used to estimate the degree of indentation for each study site:

a/C_l - Indentation Ratio (Hsu et al. 1989a,b); and

S_l/C_l - Indentation Index (Mastronuzzi et al., 1992).

Both parameters have been widely used in the bibliography, and are especially useful in the comparison between beach segments (e.g. Spagnolo et al. 2008; Bowman et al. 2009; Lasagna et al. 2011, Klein et al. 2002).

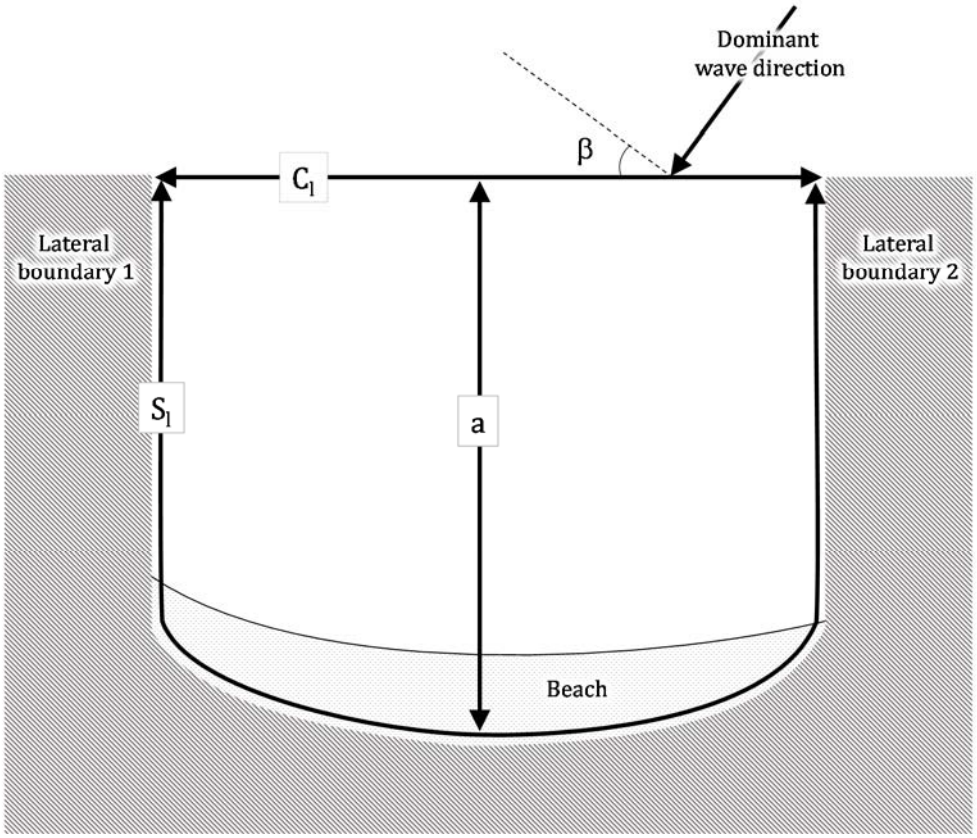

Figure 3.2. Planform geometry parameters used in the present study. C_l – Embayment width; S_l - Embayment length; a – Bay indentation; and β – Wave obliquity. Figure modified from Short and Masselink (1999).

3.2. Beach morphology and sediments

A monitoring program was designed and implemented along the selected study sites with the aim of quantifying the temporal and spatial variability of the beach characteristics within the study area, concurring to the goal of this work to determine the regional and local groupings and singularities between beaches.

3.2.1. Field data collection

Field sampling was planned to ensure that data collection would fit the objectives of this study. Topographic measures, sediment samples, and photographic records were acquired at each study site to provide a large database of beach morphological features and characteristics, at seasonal as well as annual scales.

The field and laboratory work benefited from the project carried out by the Faculty of Sciences for the Portuguese Environmental Agency (CISML project -*Criação e Implementação de um Sistema de Monitorização do Litoral abrangido pela área de jurisdição da ARH do Tejo*) described in Andrade et al. (2013a).

The monitoring program was carefully designed and extensive information was created pertaining to data collection, data quality check, and data storage procedures. The methods were established prior to the beginning of the field data collection and assured that surveying of such a vast study area could be secured by a varied team of surveyors, and thus guaranteed the construction of a consistent and coherent database.

3.2.1.1. Preparatory procedures and survey planning

Benchmarks

For each selected study site, a network of benchmarks was established to serve as reference points to aid in the topographic data collection. The location of benchmarks followed the criteria: 1) ease of access, 2) compatibility with the use of classic topography equipment (e.g. total station), 3) distance (far) from the reach or impact of waves and tides, roads, or activities that could risk their integrity, and, where possible, 4) corresponding to the landward starting point of a beach profile selected for monitoring. The composition of the benchmarks was selected to assure their stability and durability, and correspond to the following (Figure 3.3):

- Stainless steel mountaineering plugs inserted in concrete or rock;
- Steel nails inserted in wood or masonry;
- PVC pipes driven into the ground and filled with mortar;
- Wooden stakes driven into the ground;
- Pre-existing benchmarks from national institutions (e.g. Instituto Hidrográfico).

The coordinates and elevations of the benchmarks were measured using GNSS (Global Navigation Satellite System) equipment in static mode during at least 20 minutes, with post-processing. Coordinates were measured in the PT-TM06/ETRS89 (European Terrestrial Reference System of 1989/ Portuguese Transverse Mercator Projection of 2006) reference system according to the recommendations in the INSPIRE Directive

(Infrastructure for Spatial Information in the European Community). Elevation is relative to the Portuguese datum, the mean sea level (MSL) of Cascais, 1938.

Figure 3.3. Examples of benchmarks established along the study area: a) steel plug at Paredes de Vitória, b) nail on wooden stake at Almagreira, c) PVC pipe at Pedras Negras, and d) pre-existing IH benchmark at Pedras Negras.

Profile lines

Between one and three (only in two cases, five and seventeen) profile lines were established perpendicular to the general orientation of the shoreline at each selected site according to the following criteria:

- Representation of the local geomorphological units;
- Representation of areas of special concern;
- Evenly-spaced distribution;
- Ease of access;
- Pre-existing profile locations.

A total of 52 beach profiles were established along the studied coast and are presented for each study site in Figure 3.4.

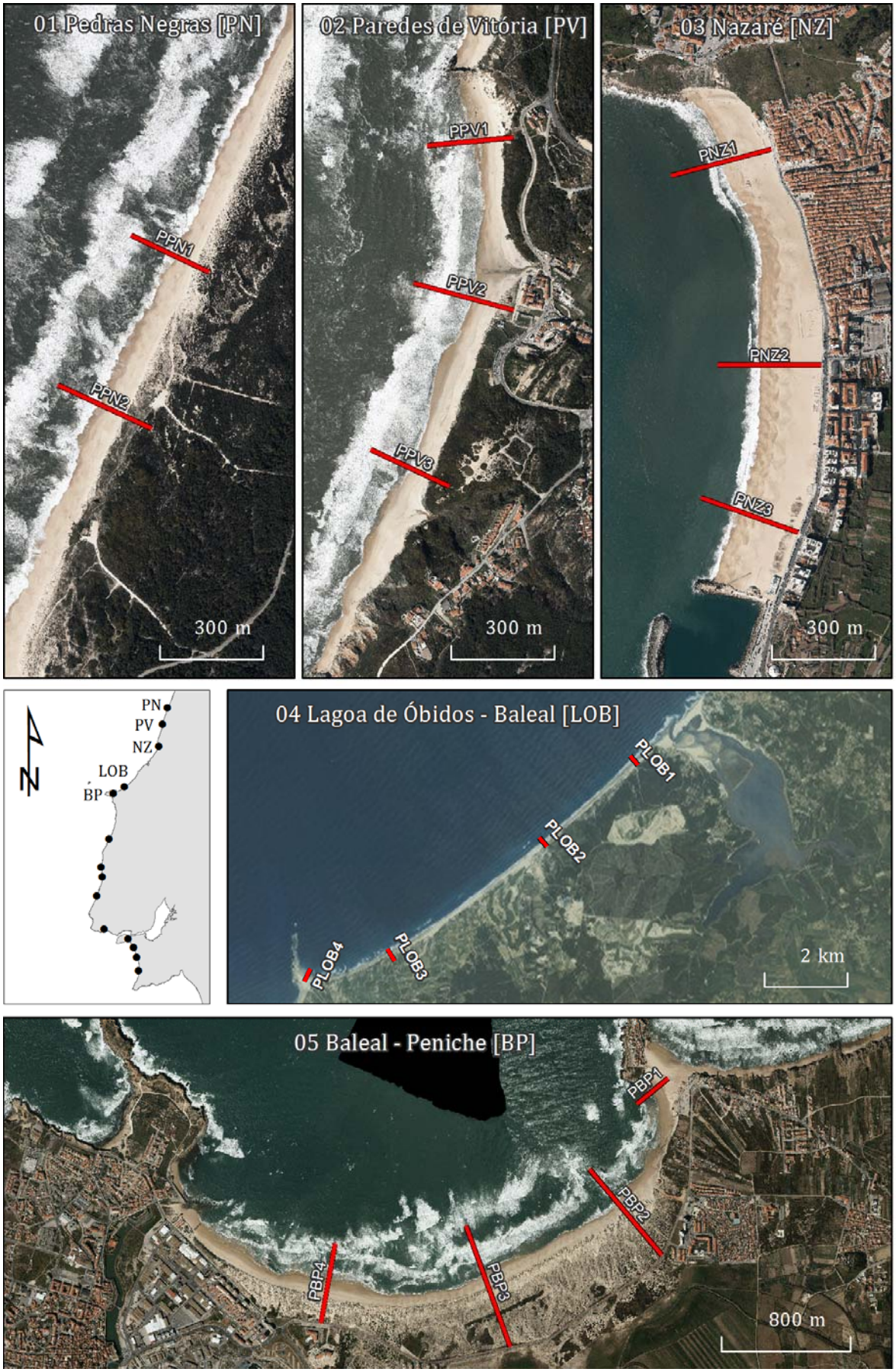

Figure 3.4. Location of the profile lines (in red) monitored at the study sites.

Figure 3.4 (continuation). Location of the profile lines (in red) monitored at the study sites.

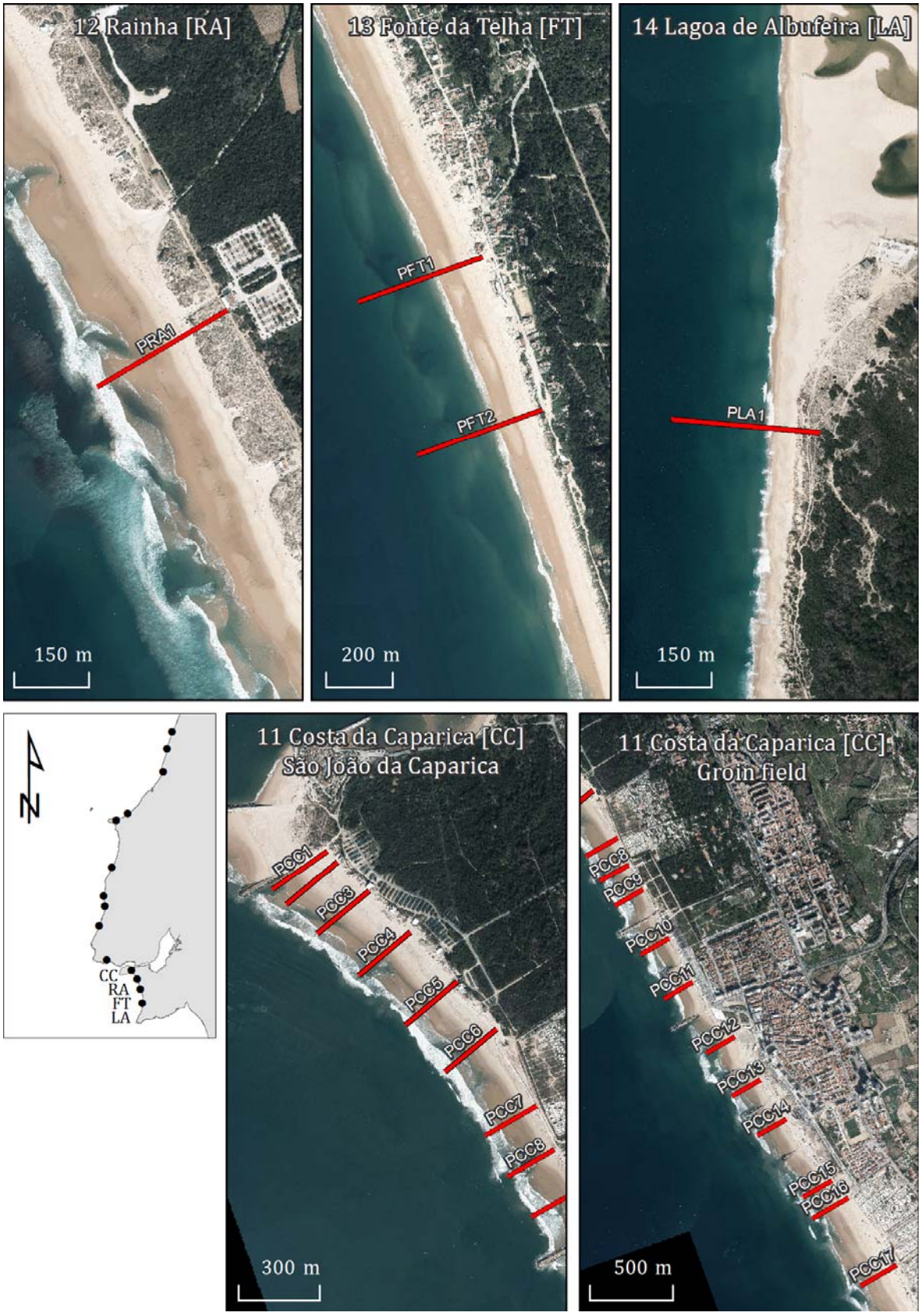

Figure 3.4 (continuation). Location of the profile lines (in red) monitored at the study sites.

Support files

Field booklets were created with cardfiles summarizing the information of the benchmarks and profile lines established at each site (an example of a benchmark cardfile prepared for the Nazaré beach is given on Figure 3.5). Each cardfile includes information on when and how the benchmark was established, who did the work, the benchmark's composition, coordinates, and elevation, as well as location maps and photographs. The position and direction of the beach profiles are also included. Two booklets were created: one pertaining to the beaches along the coast between Praia da Vieira (Marinha Grande) and São Julião da Barra (Cascais), north of Tagus river, and one pertaining to the beaches between Cova do Vapor (Almada) and Cabo Espichel (Sesimbra), south of the Tagus. The booklets are written in Portuguese to facilitate their wider and further use by other national researchers and surveyors, and are presented in Appendix A.

A nomenclature guide and a list of measurement codes were created and included in the field booklet to guarantee the standardization of the database. The booklet also contains instructions on deciphering and preparing beach codes and profiles lines, as well as on the naming of the fieldwork jobs and the codes describing the measurements of features.

A vector format file (.dbx) was created for each study site containing the benchmarks and profile lines. This file was imported into the field equipment mobile device to aid in positioning during fieldwork and to ascertain that points were always collected along the profile line, with minimum deviation.

Finally, a field form was created (also in Portuguese) to keep the records concerning each fieldwork job, such as the operator's name, date and time of data collection, equipment used, and any additional information that might be useful to the utilization and verification of the dataset (Figure 3.6).

Resources

The operational requirements for performing the monitoring program included field surveyors trained in GNSS equipment operation, and having a basic understanding of the coastal features being measured. At least two surveyors accomplished each field survey.

NAZARÉ - NZ	NZ3

Estabelecido por: GeoFCUL (Tanya Silveira e Pedro Costa) **Data:** 2011/02/02

Qualidade: Planimetria – I, Altimetria – I, Monumentação – I

Objectivo: Ponto de Referência + Cabeça de Perfil (PNZ3)

Descrição: Spit no lancil do paredão da praia; localizado entre dois cafés de praia, em frente à esquina norte do edifício "Dom Fuas", e a cerca de 200 m do esporão sul da Nazaré.

M	P	H
-80754.566	-8022.244	9.017

Sistema Coordenadas: PT-TM06 | Datum Vertical: NMM Cascais 1938 | medido em: 2011/02/02

Versão 1, Março 2011 20

Figure 3.5. Example of one page from the field booklet: cardfile with the information pertaining to the NZ3 benchmark.

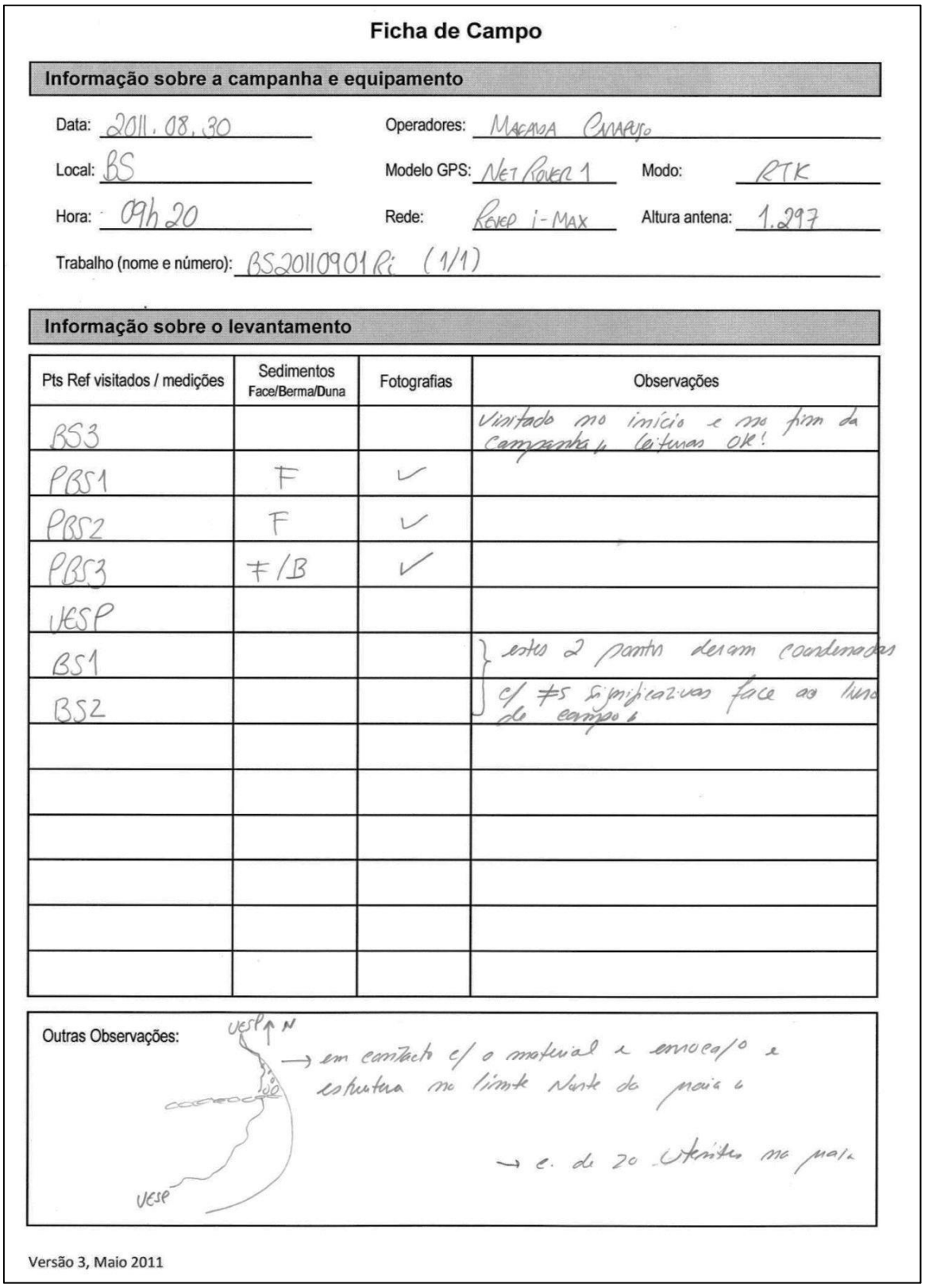

Ficha de Campo

Informação sobre a campanha e equipamento

Data: 2011.08.30 Operadores: MACIEL CARVALHO

Local: BS Modelo GPS: NET ROVER 1 Modo: RTK

Hora: 09h 20 Rede: ROVER i-MAX Altura antena: 1.297

Trabalho (nome e número): BS20110901Ri (1/1)

Informação sobre o levantamento

Pts Ref visitados / medições	Sedimentos Face/Berma/Duna	Fotografias	Observações
BS3			Visitado no início e no fim da campanha, leituras OK!
PBS1	F	✓	
PBS2	F	✓	
PBS3	F/B	✓	
VESP			
BS1			estes 2 pontos deram coordenadas c/ ≠5 significativos face ao usado em campo
BS2			

Outras Observações:

VESP N

→ em contacto c/ o material e enrocamento e estrutura no limite Norte da praia

→ c. de 20 utentes na praia

VESP

Versão 3, Maio 2011

Figure 3.6. Example of a completed field form.

The equipment used in the topographic data collection included GNSS roving receiver units (Leica Geosystems models GPS 900 and NetRover) (Figure 3.7) that operated in real-time, connected to one of the two national available internet-based corrections services: RENEP (Rede Nacional de Estações Permanentes) and SERVIR (Sistema de Estações de Referência GPS VIRtuais), operated by the Instituto Geográfico Português and Instituto Geográfico do Exército, respectively.

Additional field resources included a digital camera to record the aspect of the beach profile's major features and the overall aspect of the beach, or coastal site, as well as plastic bags and markers for sediment collection.

Figure 3.7. GNSS field equipment: backpacks with receiver antennas and hand-held receivers of Leica Geosystems GPS 900 mobile units.

Survey frequency and timing

Field surveys were conducted at least four times per year, in March, June, September, and December, and immediately after a storm event.

Beach configuration changes in response to variations of the waves' characteristics through the year (Figure 3.8). Sediment is transferred from the beach to the nearshore during high-energy events, typically in the winter, and returns to the subaerial part of the beach profile during calmer conditions, promoting volumetric recovery in low-energy periods, characteristic of the summer season. The March and September surveys

corresponded to the end of the winter and summer seasons, respectively, when beaches reach their greatest contrasting configuration. The June and December surveys helped to track the beaches' seasonal variation, as well as to evaluate rates of recovery. The post-storm surveys provided information on the magnitude of short-term variations of the beach in response to high energy events, such as beach erosion and maximum swash inland incursion. Whenever necessary, timing of the surveys was slightly changed to fit the equipment and/or surveyors availability.

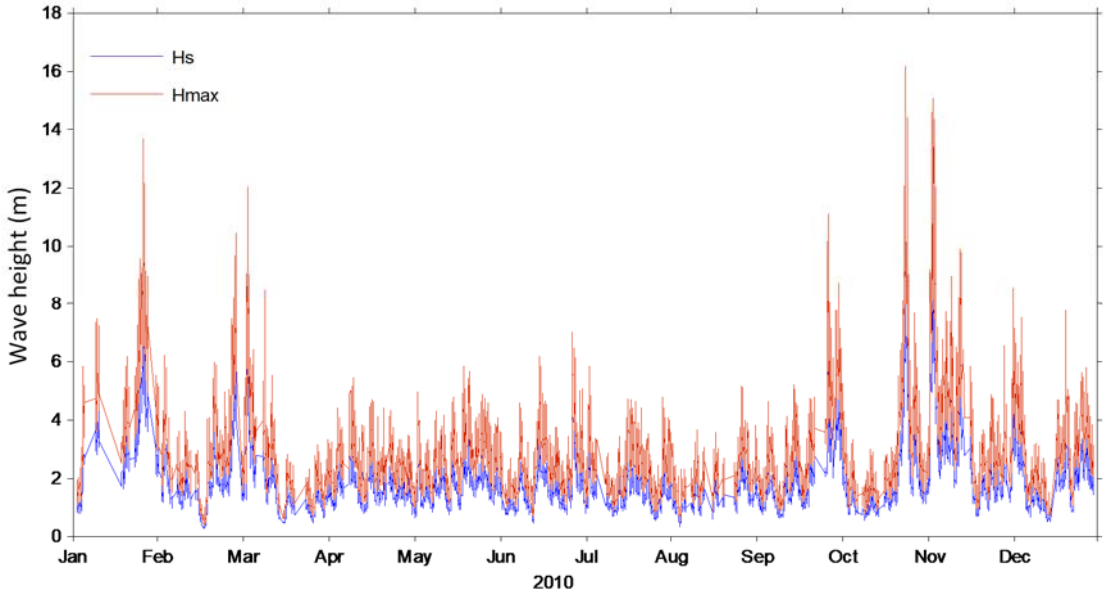

Figure 3.8. Wave height (significant-Hs and maximum-Hmax) record retrieved from the Instituto Hidrográfico Leixões buoy for 2010, showing the more energetic winter months (October to March), and the calmer conditions during summer (April to September).

Survey dates were selected based on the maximum tidal range, and therefore were performed during spring tides. Field data collection was conducted near low tide, assuring maximum exposure of the intertidal area of the beach profile, and maximum seaward data collection. A low tide maximum elevation was defined for surveys to take place, at -1 m (MSL), to ascertain that the surveyed areas were similar across all surveys.

The dates of the surveys are presented in Table 3.1. Between 10 and 11 surveys were carried out at each selected study site, totalizing 145 surveys conducted between March 2011 and June 2013. The January 2013 surveys correspond to post-storm assessment, conducted in the beaches that showed morphological impacts caused by the Gong storm

that crossed the Portugal mainland on 19 January 2013, impacting the Nazaré beach and all beaches in the stretch between Cova do Vapor and Cabo Espichel. The offshore wave buoy (Monican01 - CSA88/1 Estação Oceânica) recorded a maximum significant wave height of 12.71 m with 15.5 s associated wave peak period, and maximum wave height of 19.42 m with 14.9 s associated wave peak period, approaching from northwest (304-321º).

Table 3.1. Dates (dd/mm) of the surveys conducted between 2011 and 2013 at the study sites. Shaded records correspond to post-storm conditions.

	Study site													
	PN	PV	NZ	LOB	BP	SC	CX	BS	MG	TM	CC	RA	FT	LA
2011	07/03	06/03	07/03	08/03	23/03	24/03	22/03	22/03	05/03	09/03	19/03	27/03	20/03	20/03
	02/06	02/06	01/06	14/06	18/06	15/06	17/06	17/06	30/05	31/05	04/06	05/06	05/06	05/06
	15/09	15/09	13/09	27/09	29/09	03/09	26/09	01/09	31/08	30/08	11/09	02/09	02/09	02/09
	27/12	30/12	27/12	15/12	16/12	02/12	29/12	29/12	28/12	01/12	29/11	28/11	28/11	28/11
2012	25/03	25/03	22/03	26/03	13/03	21/03	08/03	08/03	09/03	07/03	12/03	11/03	10/03	10/03
	02/06	02/06	02/06	08/06	25/06	07/06	04/06	04/06	05/06	03/06	06/06	22/06	22/06	22/06
	20/09	20/09	20/09	21/09	19/09	18/09	01/09	01/09	31/08	30/08	04/09	17/09	17/09	17/09
	18/12	18/12	18/12	19/12	17/12	03/12	16/12	16/12	29/11	28/11	02/12	30/12	30/12	30/12
2013	-	-	23/01	-	-	-	-	-	-	-	21/01	21/01	21/01	21/01
	03/03	03/03	03/03	14/03	15/03	13/03	28/03	28/03	12/03	11/03	01/03	28/02	28/02	28/02
	26/06	26/06	24/06	27/06	25/06	12/06	20/06	20/06	21/06	07/06	11/06	24/06	24/06	24/06

3.2.1.2. Field survey procedures

Procedures in the field included a number of steps to ensure the quality of data collection, and to minimize post-processing.

Equipment set-up

The first step included setting up the GNSS equipment and making sure that the roving receiver unit was connected to the real-time correction service. The littoral zone is a particularly vulnerable area because of the lack of coverage from the reference stations

on the oceanside, and in some cases because of the proximity to coastal cliffs, seawalls, or dunes that obstruct part of the sky, and thus, some of the available satellites. A number of parameters were set prior to data collection:

- Coordinate system – PT-TM06/ETRS89;
- Automatic mode point measurement and storage while moving – by distance, at 1 m intervals;
- Point object measurement and storage in static mode – 10 positions;
- Point quality tolerance level – 0.05 m.

The vector file (.dbx) containing the benchmarks and profile lines' location was imported into the field equipment mobile controller. Codes were created according to the list pre-established in the field booklet, and each measured point was assigned with a code.

Data collection

After setting up of the GNSS unit, the following tasks were accomplished at each study site:

- Beach cross-shore survey, from the beach landward limit to a depth below MSL;
- Beach surface 3-dimensional topographic survey (at selected sites);
- Survey of the alongshore landward limit of the beach;
- Survey of the high-tide swash line;
- Sampling of the surface sediment layer from the beach face;
- Sampling of the surface sediment layer from the beach berm;
- Sampling of the surface sediment layer from the foredune;
- Photographic record of the beach cross-section location; and
- Photographic record of the general beach area.

During the survey, at least one local benchmark was visited and measured for on-site and post-processing validation and accuracy verification.

Beach profiles

Beach profile data collection was accomplished by setting the GNSS unit to record in automatic mode along the pre-established profile lines displayed on the controller's map screen (Figure 3.9). The scale bar was set to ≈10 m to improve the accuracy of the

measurements. Points were always measured between the upper limit of the beach (dune base, cliff base or structure contact) and the elevation of 0 m MSL. More points were usually measured below this elevation (down to -1 m). In the cases where dunes existed, measurements were extended landward of the dune toe, to the dune crest location or landward, whenever possible.

Figure 3.9. Automatic acquisition of points along the pre-established profile lines, as they are displayed in the GNSS equipment controller screen.

Beach 3-dimensional topography

In the Baleal-Peniche and São João da Caparica embayments, more detailed topographic surveys of the entire subaerial beach surface were accomplished in addition to the specific profile lines identified in the booklets. Surveys were usually completed by four surveyors by measuring points in automatic mode along shore-perpendicular lines that extended between the upper limit of the beach and MSL. The multiple profile lines were spaced about 30 m alongshore (example in Figure 3.10).

Figure 3.10. High-resolution survey of the Baleal-Peniche embayed beach (March 13, 2012). The black lines correspond to coordinate points spaced at 1 m intervals.

Landward limit of the beach

The landward limit of the beach was surveyed in automatic mode covering part or the whole alongshore extension, depending on the size and configuration of the beaches. Depending on the geomorphological setting and type of upper beach limit, the criteria used for identification of its location were as follows:

- Dune: seaward limit of the dune vegetation, and/or abrupt change in slope at the dune toe (Figure 3.11);
- Cliff: contact between the cliff face and the beach, or, in case significant cliff debris occurs, the seaward contour of the mass deposit (Figure 3.12);
- Structure: contact between the structure and the beach (Figure 3.13).

Figure 3.11. Field identification and survey of the landward limit of the beach when a dune is present (Lagoa de Albufeira, September 2, 2011).

Figure 3.12. Field identification and survey of the landward limit of the beach where a cliff is present (Paredes de Vitória, March 6, 2011).

Figure 3.13. Field identification and survey of the landward limit of the beach where a structure is present (Costa da Caparica, June 11, 2013).

High-tide swash line

Similar to the measurement of the landward limit of the beach, the high-tide swash line was surveyed in automatic mode covering part or the whole length of the beach, depending on its size and configuration. This line corresponded to the mark of the maximum incursion of the water left on the beach surface at the time of the high tide preceding the survey, and reflected the influence of both tide and waves. The criteria used to identify this line were as follows:

- Boundary between the wet and dry portions of the sand (Figure 3.14);
- Location where a myriad of debris, commonly shells, stems, algae and other organic and inorganic material, accumulated, sometimes forming a wrack or drift line (Figure 3.15);
- Boundary between the smooth surface evened out by the swash of the waves, and the more rugged portion of the upper beach affected by trampling and wind (Figure 3.16).

Figure 3.14. Swash line on the beach created by the high tide previous to the field survey. The boundary between the wet and dry sand is a clear indicator of the maximum level reached by the waters (Baleal, June 8, 2012).

Figure 3.15. Swash limit on the beach created during the high tide previous to the field survey and evidenced by a linear accumulation of debris (Rainha, March 11, 2012).

Figure 3.16. Swash limit on the beach created during the high tide previous to the field survey. The maximum reach of the water was well marked by the boundary between the smooth and more rugged beach surface (Baleia/Sul, June 4, 2012).

Sediments

Sediment samples were collected on the surface layer (Figure 3.17) at three locations along the beach profiles:

- Beach face, around MSL;
- Beach berm, at half width;
- Foredune (when present), on the seaward side;

Figure 3.17. Sediment sampling of the surface layer of the beach face (Baleia/Sul, June 17, 2011).

Photographs

At least two photographs were taken at each profile line to capture the general aspect of the upper beach features present. These photographs were always taken from the same perspective to make the records comparable: one photograph was taken ≈20 m away of the profile line and looking alongshore towards north (Figure 3.18a), and one photograph was taken approximately half way along the profile line looking towards the upper beach region (Figure 3.18b). A photograph capturing the general view of the overall study site was also taken whenever possible (Figure 3.19).

Figure 3.18. Photographs of beach profile PPN2, taken 18 December, 2012, at Pedras Negras. a) looking north towards the profile location, and b) looking towards the upper beach feature.

Figure 3.19. Panoramic view of Praia de Vitória de Paredes, showing the general aspect of the study site looking north, on June, 2011.

Survey completion

The following actions were undertaken in order to conclude each field survey:

- Field forms were filled out, one for each completed job;
- Raw GNSS data were downloaded and backup copies created;
- Photographs were downloaded, catalogued, and commented;
- Equipment was cleaned and batteries charged;
- Sediment samples were verified for correct labeling and stored.

3.2.1.3. Post-survey procedures

Post-survey procedures included quality check and data integrity verification: both were needed to ensure accurate and systematic processing of the data, as well as to provide information for creation of metadata. These steps assured that the data can be analyzed and processed by other users.

The GNSS raw data were at first analyzed using *Leica Geo Office*© software, and coordinates were transformed from the GPS world geographic coordinates to local rectangular ones. Data were then exported into text files and further analyzed in ArcGIS® software. The measurement points were filtered according to the following criteria:

- Measurement class → removal of "reference"; "control" and "estimated" points
- Planimetric and altimetric (3D) quality → removal of points tagged with > 0.05 m in point quality
- Measurement Codes → correction where needed
- General alignment with the pre-established profile lines → rejection of points collected at distance from profile line > 10 m
- Benchmark coordinates and elevation → survey points correction if differences in planimetry > 0.5 m and altimetry > 0.1 m
- Anomalous elevation → data removed

The filtered data were stored in text files and *shapefile* format, using designations that included the code of the beach and date of the survey. All the original, corrected, and processed data products were assembled and stored in a common database.

3.2.2. Beach morphology analysis

Beach seasonal behavior was described through the use of selected geoindicators (described below) extracted from the field data analysis. 2-dimensional metrics, cross-shore morphological parameters, were derived from the beach profiles, whereas a 3-dimensional analysis was applied to the beach surface where multiple profiles at 30 m intervals were collected. Seasonal and annual surveys provided for the tracking of beach modifications in response to the varying wave conditions, whereas the post-storm surveys recorded the lower energy beach morphodynamic response immediately following disturbances induced by high-energy wave forcing.

Analysis of the beach morphology data was performed on the surveyed subaerial beach, and was confined to the area between MSL and the landward limit of the beach as established in the field. In the study sites, the landward limit of the beach may correspond to the toe of foredunes, cliffs, or engineered structures. Carapuço et al. (2016) suggested that this limit is referred to as the coastline, whereas the shoreline refers to the physical interface of land and water. The present work follows this notation and makes use of the mean high water (MHW) level as the reference to define the shoreline (S_{MHW}) elevation and position at each survey (Figure 3.20). The average of the MHW levels between 2011 and 2013 (retrieved from the Instituto Hidrografico tide tables) provided S_{MHW}=1.05 m (MSL).

3.2.1.4. Beach profile

Beach profile data were processed through the use of MATLAB® programming routines that read the filtered text files, and associated codes. Feeding from a list of profile characteristics, such as the information on profile line starting point and direction, the measurement points collected in the field are first moved, shore-parallel, to the corresponding position along the established profile, creating a straight line. The program filters the data by date and profile code, according to the survey site. Distances relative to the profile starting point are calculated from the coordinates, and are used to plot the cross-section profiles of the beach for each date. The program calculates and returns measures of selected geoindicators, defined following the criteria proposed by Carapuço et al. (2016) (Figure 3.20):

- Beach volume, in m^3/m (per unit of length), measured above MSL, and limited by the coastline position;
- Beach width, in m, measured distance between the coastline and the shoreline position; and,
- Beach slope (β), calculated between the MSL contour and the shoreline position.

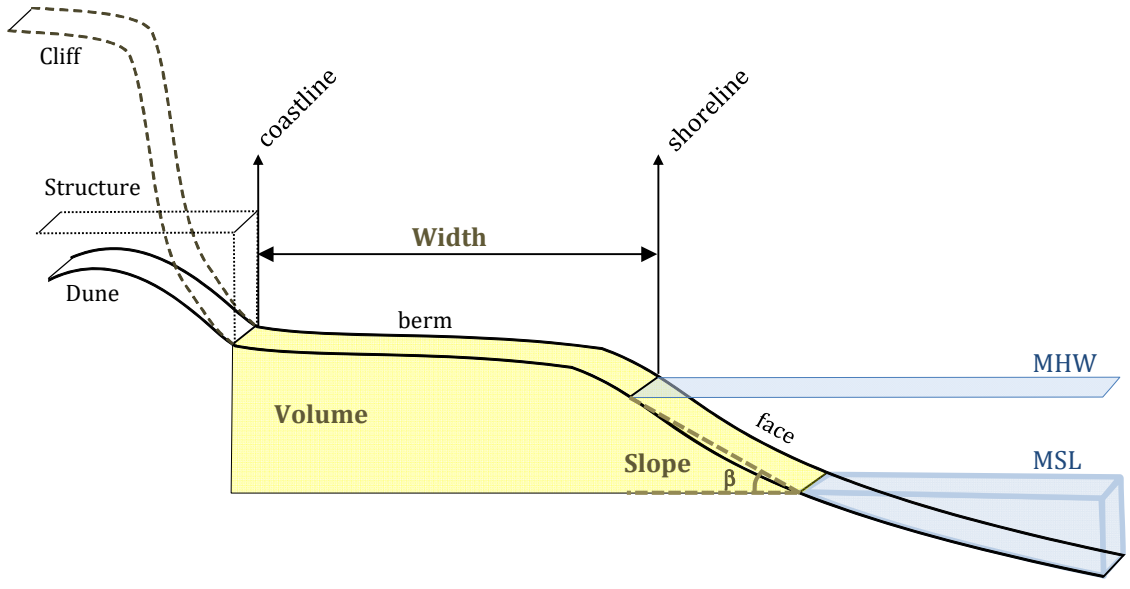

Figure 3.20. Representation of the measured geoindicators on a schematic beach profile: beach volume, beach width and beach slope. MSL – mean sea level; MHW – mean high water level.

To assure that the subaerial beach features' measurements were comparable through time during the study period, a constant coastline position, given as a relative distance from the profile benchmark, was defined for each beach profile. The constant coastline position was determined by looking at the entire series of beach cross-sections and beach landward limit surveys, and selecting its most consistent location. Whereas for the beach-cliff and beach-structure types of interface the identification of this line was straightforward, for the profiles that correspond to beach-dune morphology, this task was more difficult. Where the dune base migrated, the most seaward position was selected.

Beach slope was interpreted following the quantification and classification proposed by Short (1999). The author summarizes the characteristics that define the morphodynamic beach stages, and defines dissipative type of beaches as having slopes lower than 0.04 (2°), intermediate type of beaches between 0.04 and 0.11 (2° and 6°), and reflective type of beaches as presenting slopes typically higher than 0.07 (4°).

3.2.1.5. Beach 3-dimensional topography

The analysis of the high-resolution topography data was integrally done in ArcGIS® software. Digital elevation models (DEM) were created of each survey, for the two selected sites: the coastal stretch between Baleal and Peniche, and the stretch of São João da Caparica. At first, data were used to create a Triangular Irregular Network (TIN), with a 100 m maximum spacing between vertices, in order to confine the model to the surveyed area and limit the extent of interpolation. TINs were then exported to raster format using the Natural Neighbors interpolation method and setting the cell size to 0.5 m.

Raster format DEMs were analyzed and the following features and metrics were derived:

- MSL position;
- Beach volume (m^3), measured above MSL, and limited landward and laterally by an area common to all surveys;
- Difference in elevation models, computed through the difference between two DEMs, and for an area common to all surveys;
- Sediment budget (m^3), between successive surveys, computed from the difference in elevation models, providing total accretion volume (positive elevation change) and total erosion volume (negative elevation change). Because

survey measurements accuracy was set to 0.05 m, elevation changes smaller than 0.10 m were not used in the calculations, and this was considered as the uncertainty value.

Shoreline change analysis was performed using the MSL lines, with a 10 m spatial alongshore resolution, using the following ArcGIS® toolboxes: Digital Shoreline Analysis System (Thieler et al., 2009), and Shoreline Change Mapper (Psuty et al., 2010).

3.2.3. High-tide swash line

High-tide swash line measurements were taken as representative of the most landward reach of wave swash during the high-tide previous to the time of each survey. The position and elevation of these measurements were used to validate the computations of Total Water Levels reach upon the beach, using the model described in the following Subchapter (3.3.3. Total water levels).

3.2.4. Sediments

Sediment samples were subjected to laboratory analysis for determination of particle size distribution. The laboratory procedures include four stages:

1) Washing and oven-drying → Removal of salt, organic matter, and water from sediment sample
2) Disaggregation and splitting → Reduction of sample size to a 80-100 g representative subsample
3) Dry-sieving and weighing → Mechanical separation of grain size fractions using screens spaced at half-phi intervals
4) Data entry, analysis and archiving → Entry of weights into database, computation of statistical parameters of the grain size distribution and archiving of information.

Results from the grain size analysis were processed using the computer program *GRADISTAT* (Blott and Pye, 2001), and grain-size statistics were derived using the graphic method, following Folk and Ward (1957).

3.3. Hydrodynamic forcing

The hydrodynamic forcing was analyzed in terms of waves (both offshore and nearshore regime), tides, and their combined effect. A method was developed to estimate total water levels, including wave runup on the study sites, validated with local field data.

3.3.1. Waves

Numerical modeling was employed to simulate wave propagation from deep water towards the coast and characterize the nearshore wave regime along the study site. A 36-year time series of significant offshore wave data hindcast was used for a location in the ocean offshore mainland Portugal (see below). The model selected was SWAN - Simulating WAves Nearshore model (Booij et al., 1999), version 40.85, a third-generation model that applies to wind-generated surface gravity waves, developed by the Delft University of Technology. The SwanAuto toolbox (beta 1.0), developed by the GeoFCUL Coastal Processes team (http://disepla.fc.ul.pt/), was used to run SWAN in MATLAB®. The toolbox requires only one setup for a run in nesting mode, with multiple computational domains, and it is able to convert ArcGis® bathymetric grids (.ascii, for example) and several wave data file formats into SWAN-compatible formats.

The SWAN model was run in stationary mode and the computational domain was divided into a nested grid system (regional and local) to optimize the computational time. The setup followed the structure described in Figure 3.21. Wind-wave related processes (white-capping and quadruplets) were deactivated, and the model was used solely to propagate offshore-generated waves. The spectral domain was discretized with 31 frequency bins (distributed logarithmically between 0.04 and 1), with a directional spreading coefficient of 3 and uniform amplitude directional bins $\Delta\theta=10º$.

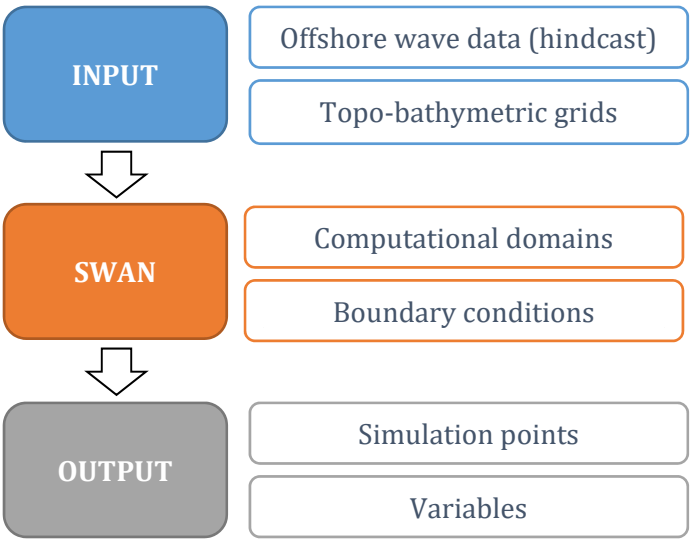

Figure 3.21. The SWAN model set-up for propagating waves from offshore to the study sites.

3.3.1.1. Offshore wave data

Deepwater wave data (significant wave height - Hs; peak period - Tp; and peak wave direction - θp) were retrieved from a hindcast time series (http://www.sonel.org) computed with the third-generation spectral wave model Wavewatch III (WW3) for a point off the study site's location [coordinates 40°N, 9.5°W] (hindcast node location on Figure 3.22), and forced with wind fields from the ERA-Interim dataset of global atmospheric reanalysis data (Dee et al., 2011). The wave model description is available from Bertin et al. (2013) and Dodet et al. (2010). The wave time series is a 3 hour interval, continuous record of wave characteristics, spanning the period from January 1, 1979 to 31 August 31, 2014.

3.3.1.2. Bathymetric grids

Topo-bathymetric grids were generated in ArcGis® with the best data available from different sources (Table 3.2). The Natural Neighbor interpolation method was used to generate the input grids: one regional grid with lower resolution (500 m), and 13 nested grids with higher resolution (50-100 m), covering the local or regional extent of the study sites (Table 3.3).

Table 3.2. Data used to generate the topo-bathymetric grids.

Source	Type of data	Geographical extent	Resolution
1. European Marine Observation and Data Network (EMODnet)	Bathymetry (sounding)	Offshore, beyond data from source 2	428 m
2. Instituto Hidrográfico (IH)	Bathymetry (sounding)	Nearshore – up to 40 km from the shoreline	250 m
3. Direção Geral do Território (DGT)	Topo-bathymetry (LiDAR)	Littoral zone - 1 km wide	2 m

3.3.1.3. Computational domains

The bathymetric grids were the base for generation of the computational grids, created in ArcGis® and exported as shapefiles to be directly read in SwanAuto. Figures 3.22 to 3.33 represent the bathymetric and computational grids used in the wave propagation model, as well as the location and designation of the simulation points.

3.3.1.4. Boundary conditions

The regional computational grid, G1, was forced along its open boundaries by the wave integral parameters – Hs, Tp and θp, given in the input file. Boundary conditions for the encased computational grids were defined by the coarser grids' (G1) outputs.

3.3.1.5. Output

Wave parameters (Hs in meters, Tp in seconds, and θp in degrees) were extracted at 29 simulation points, located at 15 m depth, positioned along the general direction of the beach profiles established and monitored at each study site (Table 3.3 and Figures 3.23 to 3.33). Two additional simulation points were established in the location where nearshore measurements exist, for validation purposes, as described in the next section.

Table 3.3. Information on the bathymetric and computational grids, and location of the simulation points used in the wave propagation model.

Grids			Simulation points (coords in m)		
ID	Geographical extent	Resolution (m)	Code	X	Y
G1	Regional	500	-	-	-
G2	Pedras Negras	100	wPPN1	-77307.18	14218.47
			wPPN2	-77390.56	13762.33
G3	Paredes de Vitória	50	wPPV1	-80106.75	4511.23
			wPPV2	-80138.34	4298.58
			wPPV3	-80209.88	4044.88
G4	Nazaré	50	wPNZ1	-81289.43	-7032.17
			wPNZ2	-81088.52	-7540.91
			wPNZ3	-81090.72	-7899.47
G5	Lagoa de Óbidos – Baleal (north)	50	wPLOB1	-96328.04	-26222.30
G6	Lagoa de Óbidos – Baleal (centre)	50	wPLOB2	-98523.85	-28178.31
G7	Lagoa de Óbidos – Baleal (south)	50	wPLOB3	-102188.25	-30730.46
			wPLOB4	-103421.46	-31145.33
G8	Baleal – Peniche	50	wPBP1	-104857.33	-31623.61
			wPBP2	-105289.85	-31873.48
			wPBP3	-105797.72	-31970.56
			wPBP4	-106397.53	-32270.84
G9	Santa Cruz	50	wPSC1	-107820.04	-56516.38
			wPSC2	-108120.55	-57172.33
			wPSC3	-108564.37	-57800.12
G10	Coxos	50	wPCX1	-112408.35	-72344.25
G11	Baleia/Sul	50	wPBS1	-112088.51	-78136.52
G12	Magoito	50	wPMG1	-115059.91	-88459.68
G13	Cascais bay (Tamariz)	100	wPTM1	-110754.27	-107683.07
G14	Caparica – Espichel (Costa da Caparica; Rainha; Fonte da Telha; Lagoa de Albufeira)	50	wPCC1	-97694.05	-114498.78
			wPCC2	-96343.55	-115295.64
			wPRA1	-95573.68	-116892.61
			wPFT1	-93399.16	-121592.96
			wPFT2	-93195.88	-122041.11
			wPLA1	-92400.90	-128689.52

3.3.1.6. Wave data analysis

The output wave data from the model were processed through the use of MATLAB® programming routines, and associated codes. Wave statistics were derived for all parameters, for the overall wave time series, as well as for the study period. Storm occurrences were identified and described. Storm events are herein defined as periods when offshore H_s remained consistently higher than 5 m (according to the storm threshold established by Costa and Esteves, 2009), including intervals of lower H_s, shorter than 24 h (as defined by Silva and Taborda, 2014).

To ensure the comparability with the general run-up formulations put forth by several authors, the simulated nearshore waves were reversed shoaled to deepwater using linear wave theory and the unrefracted wave height (H'_0) was used in the run-up calculations that use the offshore wave height.

The nearshore wave data were further analyzed to obtain the corresponding breaking wave for the study period. Bathymetry was assumed to be regular and parallel seaward of the nearshore simulation point (at 15 m depth), and the Snell law was used to derive the wave direction at breaking. Significant wave height at breaking was computed following the method by Larson et al. (2010).

3.3.1.7. Validation

The results from the propagation model were validated against wave measurements retrieved from two sources (Table 3.4):

1. ADCP (Acoustic Doppler Current Profiler) installed at Praia de Almagreira (Lagoa de Óbidos – Baleal stretch study site) by Instituto Hidrográfico; and
2. Wave buoy located at the Tagus outer estuary entrance (between Tamariz and Costa da Caparica study sites), property of APL (Administração do Porto de Lisboa).

The modeled and measured significant wave height, wave period, and wave direction parameters were compared for the period of data available, and error statistics were derived.

Table 3.4. Description of data used for validation of the wave propagation model.

Source	Designation	Coordinates (m)			Period of data
		X	Y	Z	
Porto de Lisboa (APL)	South channel buoy	-109278	-114962	-30	31/07/2005 – 31/12/2008
Instituto Hidrográfico (IH)	Praia de Almagreira	-101001	-29127	-28	01/01/2011 – 31/12/2011

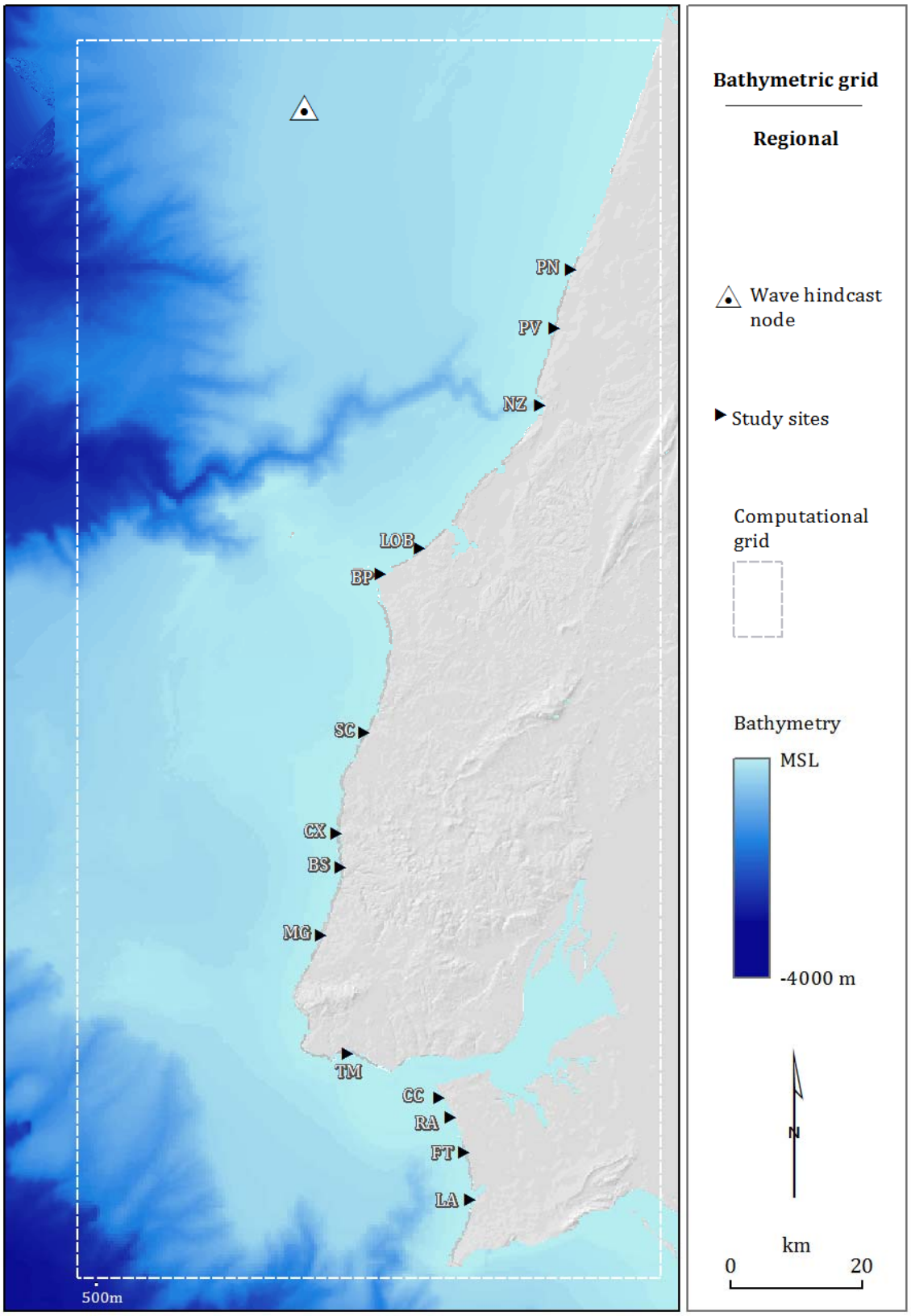

Figure 3.22. Regional bathymetric and computational grid used in the wave propagation model.

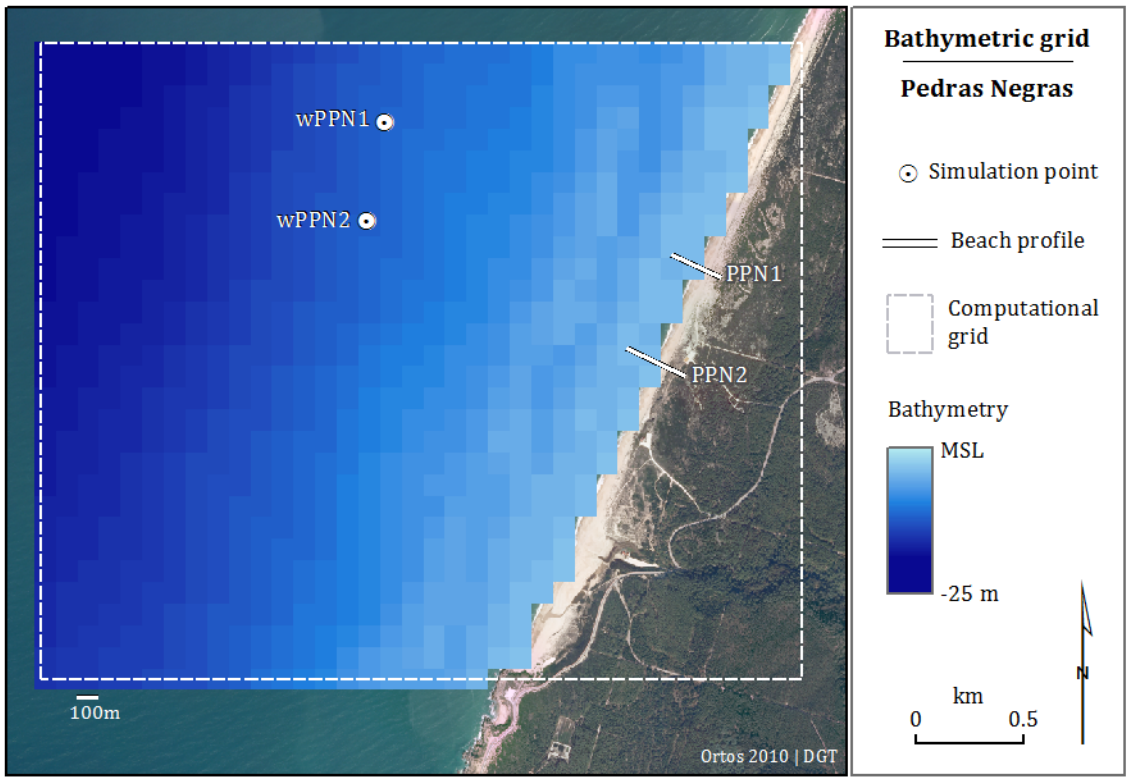

Figure 3.23. Local bathymetric and computational grid covering the Pedras Negras study site, used in the wave propagation model, and location of the simulation points.

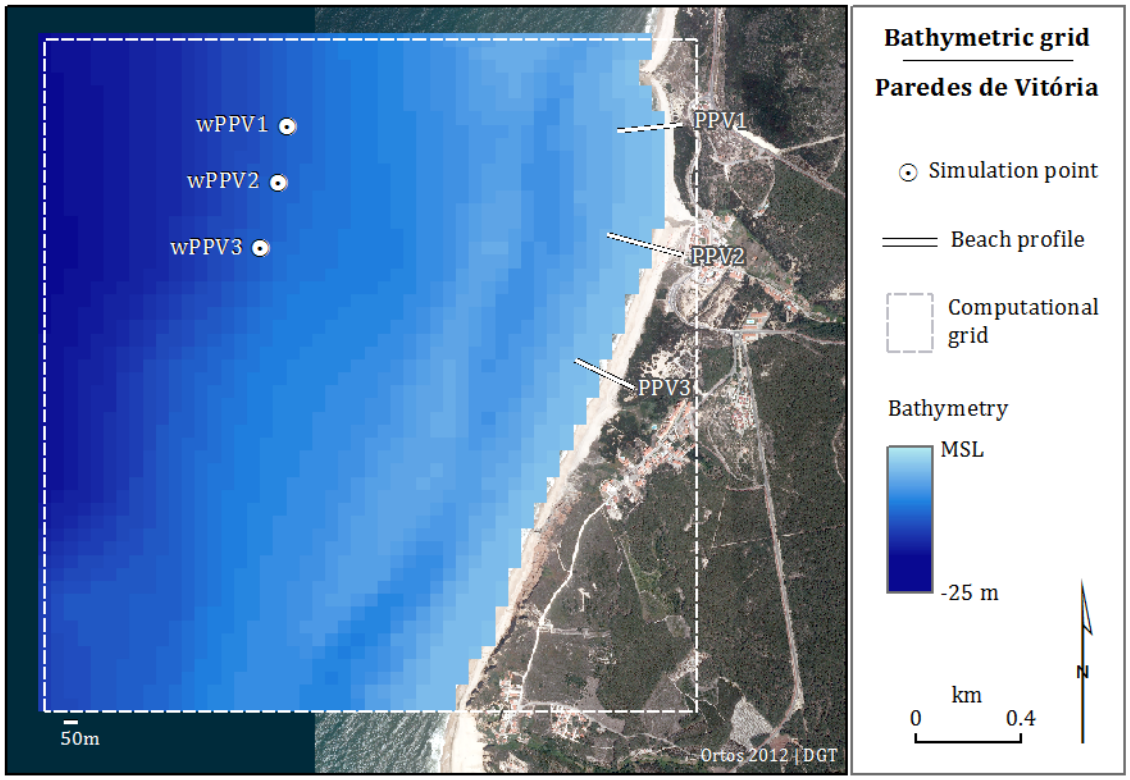

Figure 3.24. Local bathymetric and computational grid covering the Paredes de Vitória study site, used in the wave propagation model, and location of the simulation points.

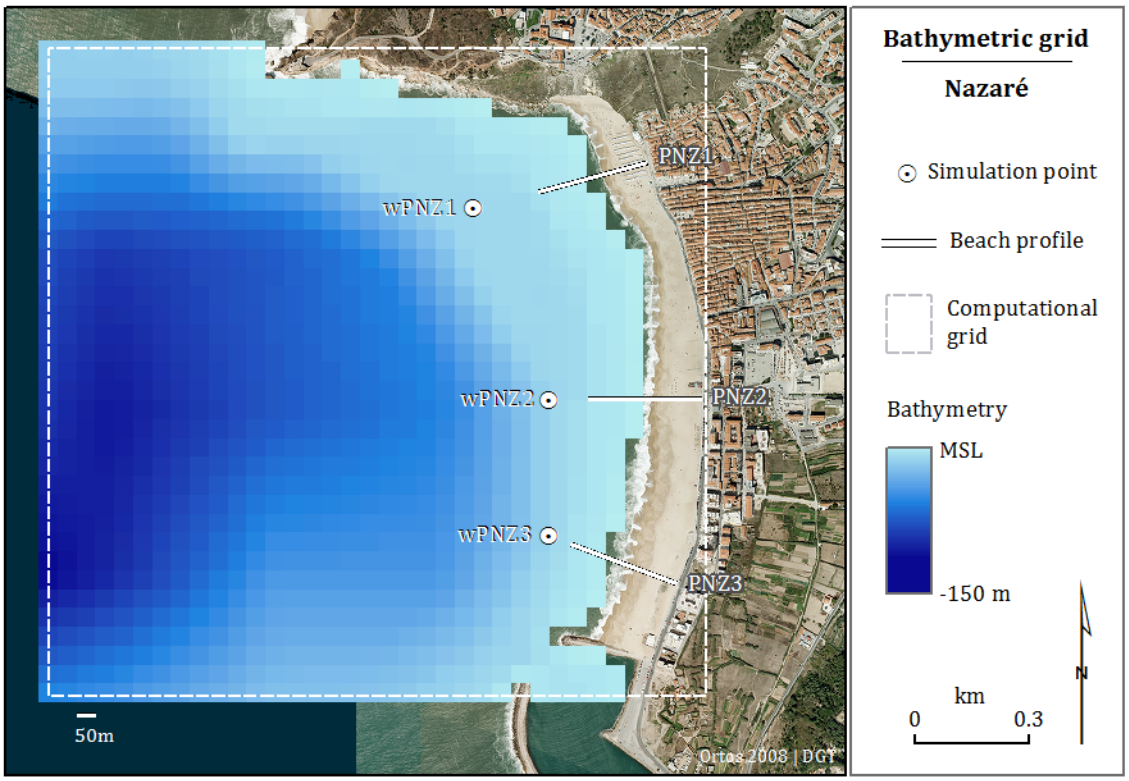

Figure 3.25. Local bathymetric and computational grid covering the Nazaré study site used in the wave propagation model, and location of the simulation points.

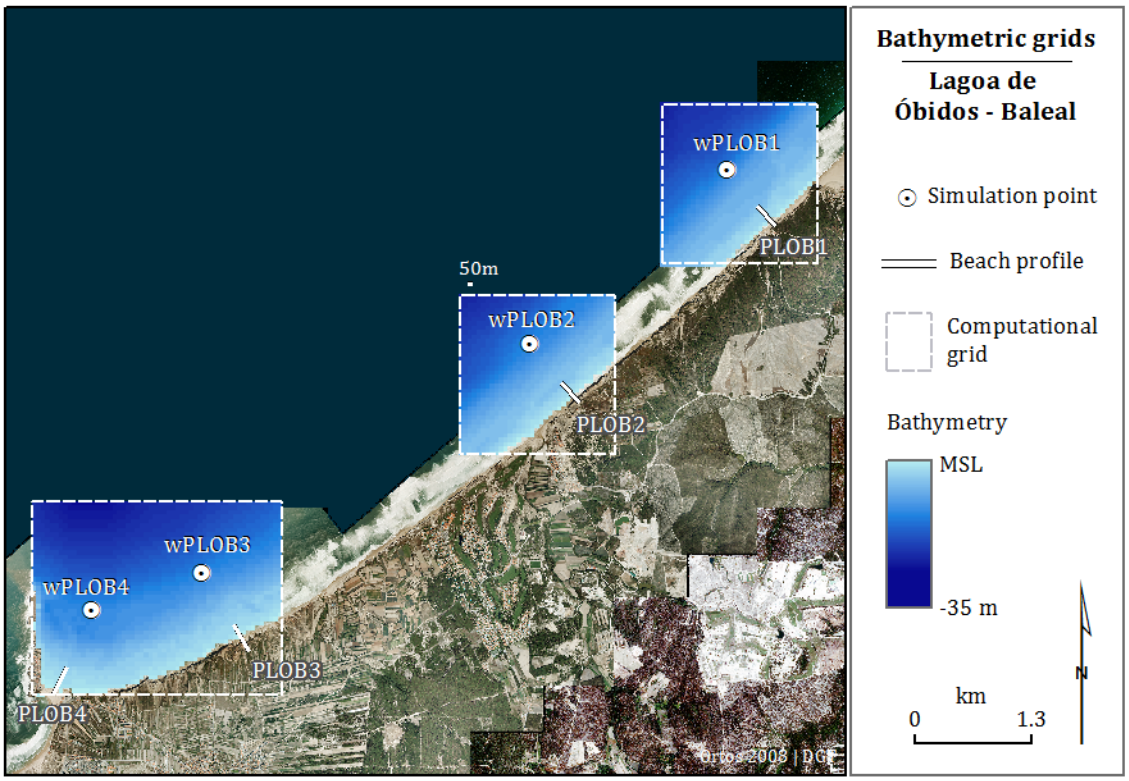

Figure 3.26. Local bathymetric and computational grids, for the Lagoa de Óbidos-Baleal study site used in the wave propagation model, and location of the simulation points.

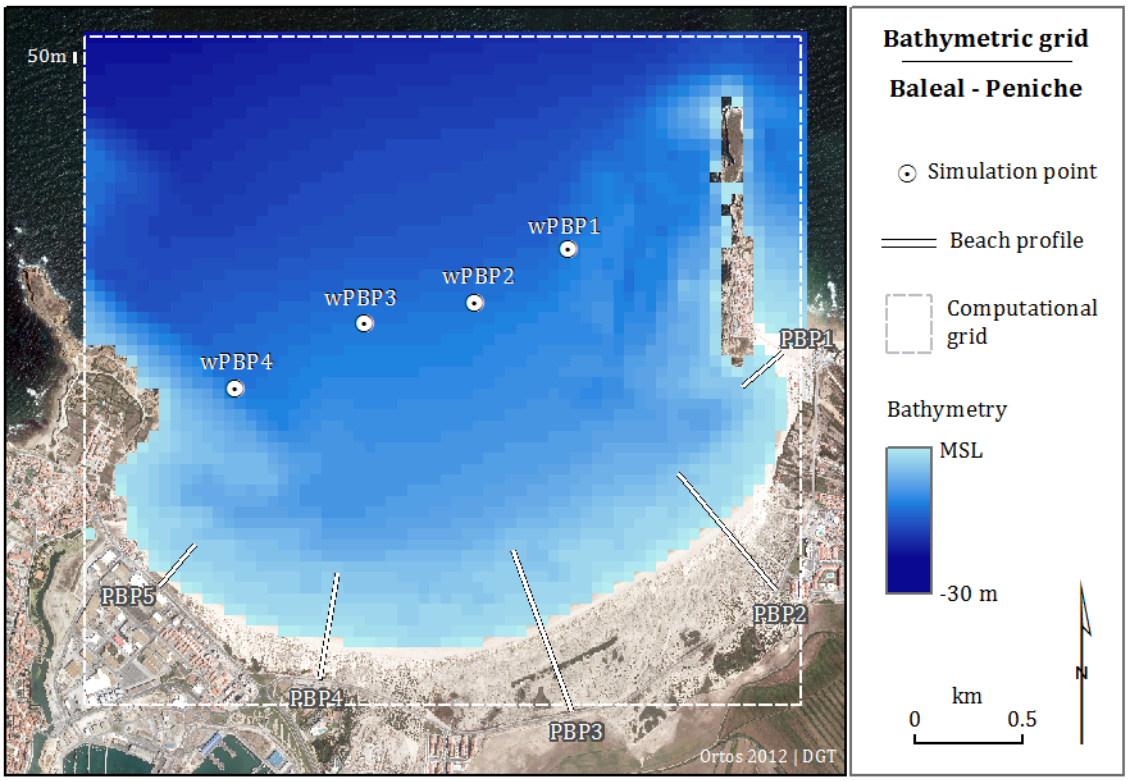

Figure 3.27. Local bathymetric and computational grid covering the Baleal-Peniche study site used in the wave propagation model, and location of the simulation points.

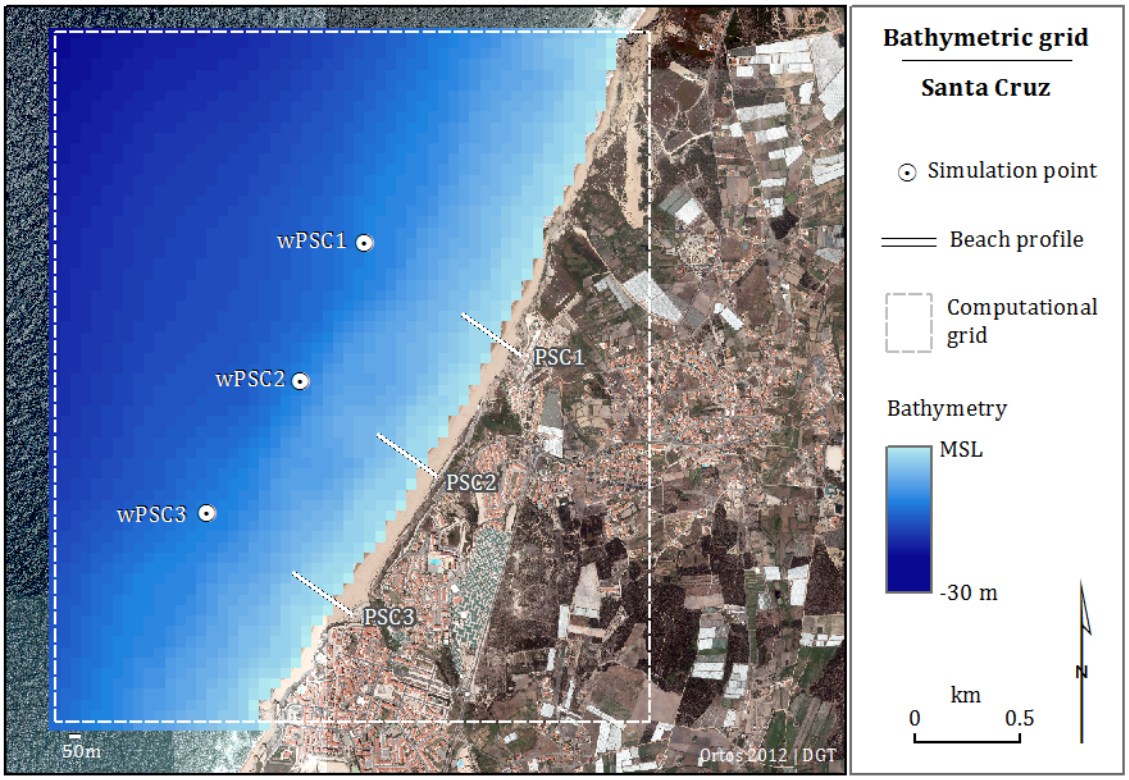

Figure 3.28. Local bathymetric and computational grid covering the Santa Cruz study site used in the wave propagation model, and location of the simulation points.

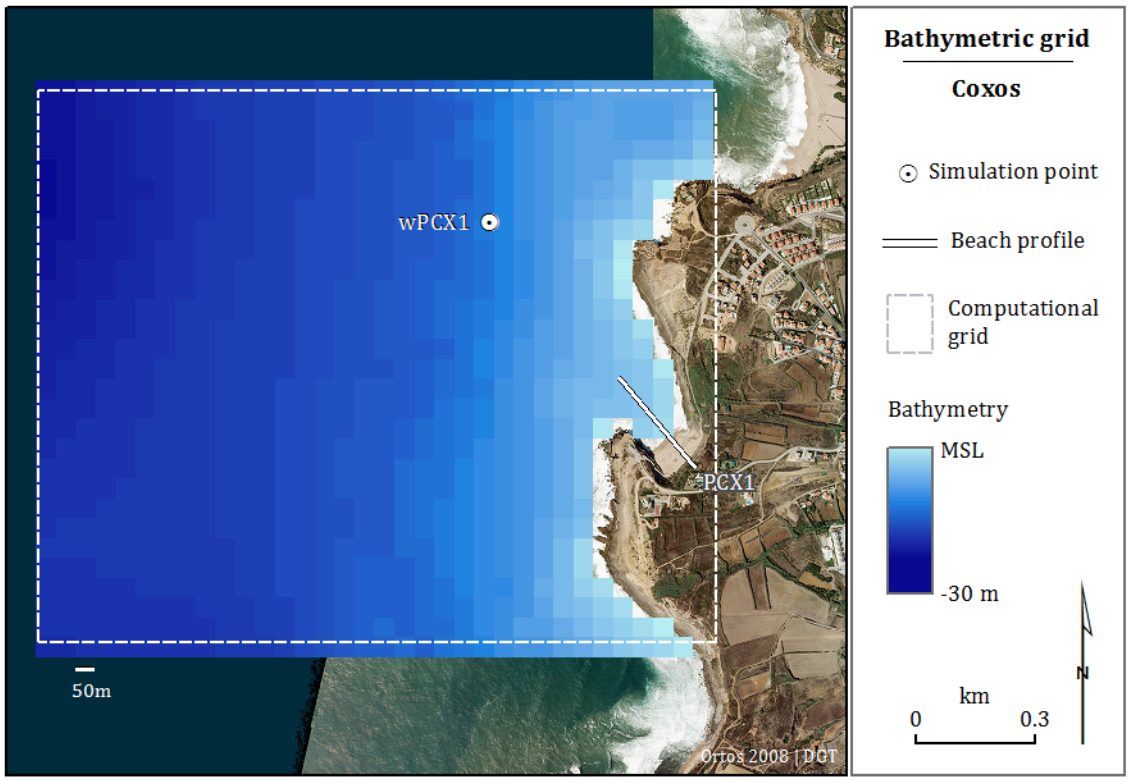

Figure 3.29. Local bathymetric and computational grid covering the Coxos study site used in the wave propagation model, and location of the simulation points.

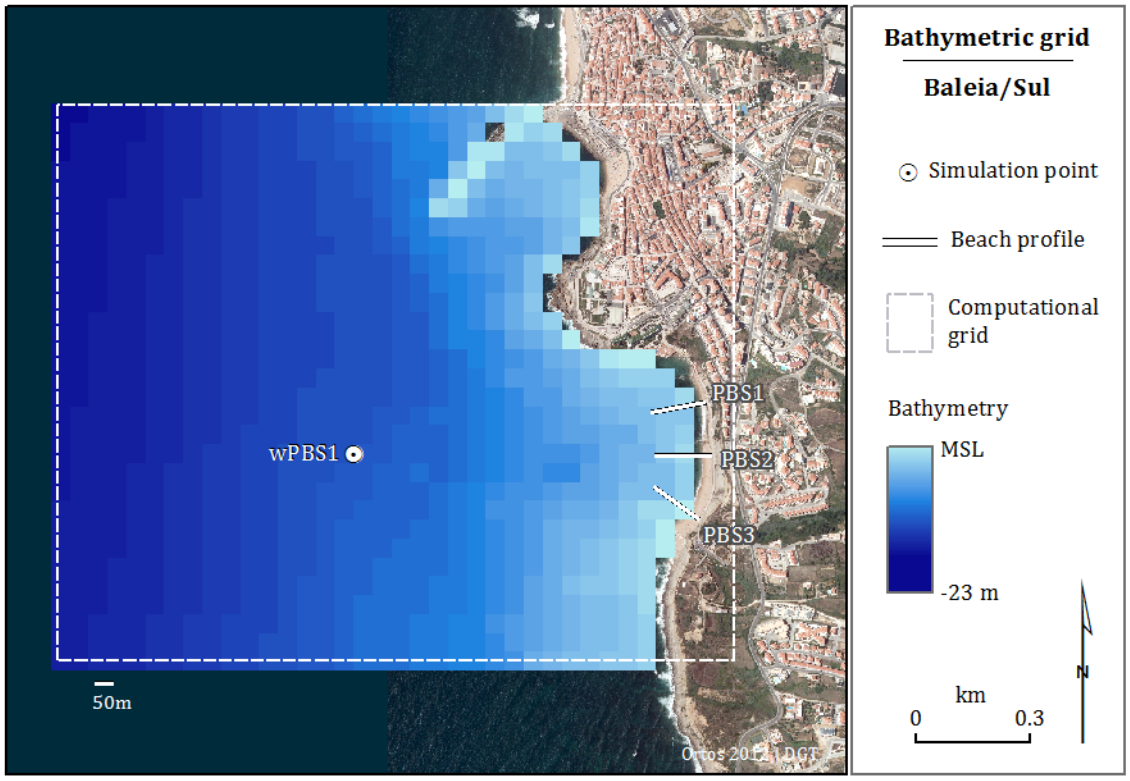

Figure 3.30. Local bathymetric and computational grid covering the Baleia/Sul study site used in the wave propagation model, and location of the simulation points.

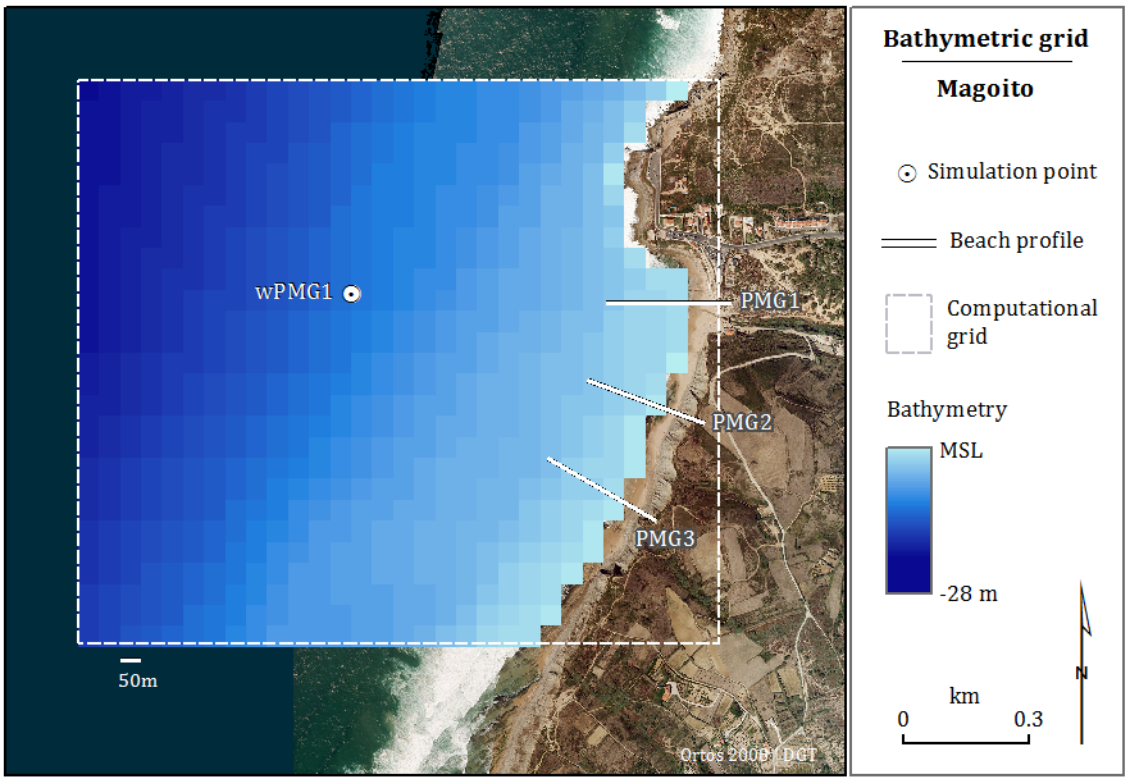

Figure 3.31. Local bathymetric and computational grid covering the Magoito study site used in the wave propagation model, and location of the simulation points.

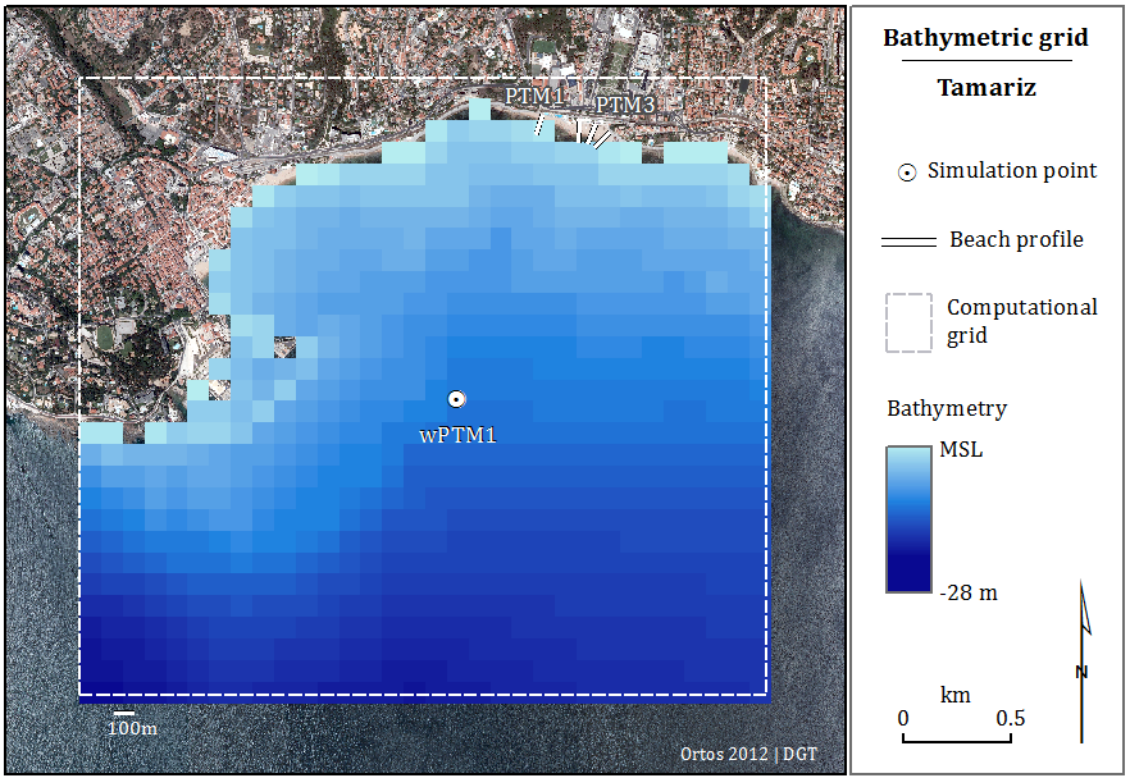

Figure 3.32. Local bathymetric and computational grid covering the Tamariz study site used in the wave propagation model, and location of the simulation points.

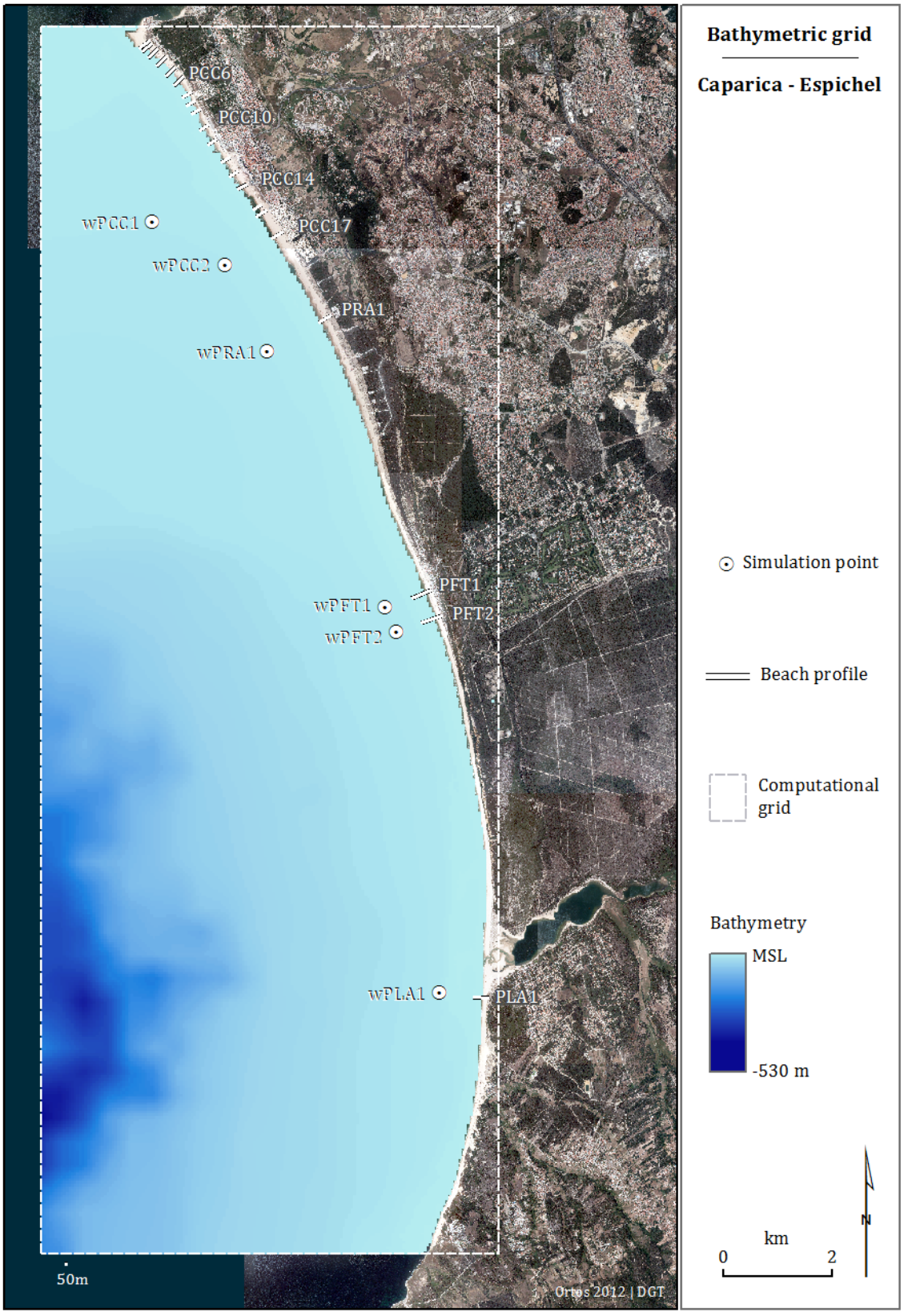

Figure 3.33. Local bathymetric and computational grid covering the Costa da Caparica, Rainha, Fonte da Telha, and Lagoa de Albufeira study sites used in the wave propagation model, and location of the simulation points.

3.3.2. Tides

Sea level data were retrieved from two data providers and corresponded to water level records from the Cascais tide gauge, located 30 km west of Lisbon. Despite some gaps, data consisted of an hourly record covering the period from 1979 to 2014, available from:

- British Oceanographic Data Centre (BODC) – from 1979/01/01 to 2005/12/31 and from 2008/11/06 to 2014/08/31
- Instituto Geográfico Português (IGP) – from 2007/10/04 to 2008/11/06

The sea surface levels recorded by the tide gauge corresponded to the sum of the vertical components associated with the astronomical tide and the non-tidal disturbances of meteorological source, including storm surge.

The largest tidal data gap corresponds to the period between January 2006 and October 2007. The UTide MATLAB® functions (Codiga, 2011) were used to compute the harmonic constituents of the tide, using a full year (1993) of hourly measured data, and derive the astronomical tide.

The measured (observed) and predicted (computed astronomical tide) records for the year of 1993 are plotted in Figure 3.34, along with the non-tidal residual calculated from the difference between the two datasets. Storm surge values - positive deviations from the astronomical tidal data - were within acceptable limits, mostly below 20 cm, not exceeding 30 cm, in agreement with the results of several works as synthesized in Andrade et. al (2002).

Gaps in the measured time-series were filled with data extracted from the astronomical tide predictions that did not include the non-tidal component. It is acknowledged that some of the gaps might correspond to times when the storm surge was more important, and in these cases, the total water levels might be underestimated. The largest gap corresponded to the period between January 2006 and October 2007. However, the relatively small contribution of the surge component, on the order of 0.1-0.2 m (Gama et al., 1994), to the overall sea level lessened the resulting underestimation of sea level during these periods. The complete sea level data-series was resampled in order to create a 3h interval dataset, synchronic of wave record (Figure 3.35).

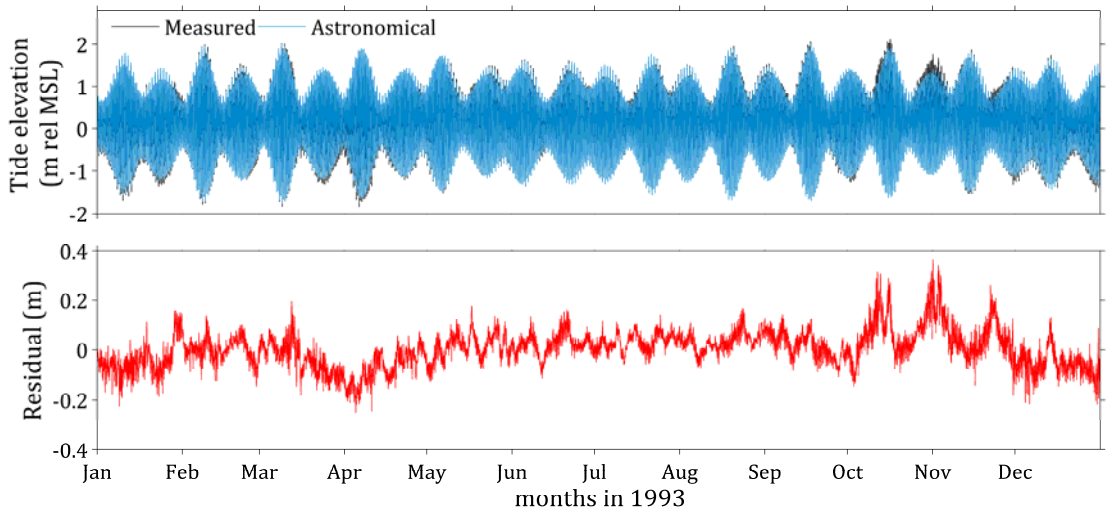

Figure 3.34. Measured water level and astronomical (computed from the tide harmonic constituents) tide elevations for 1993 at Cascais tide gauge (upper panel); and residual values (bottom panel), corresponding to the difference between the two datasets.

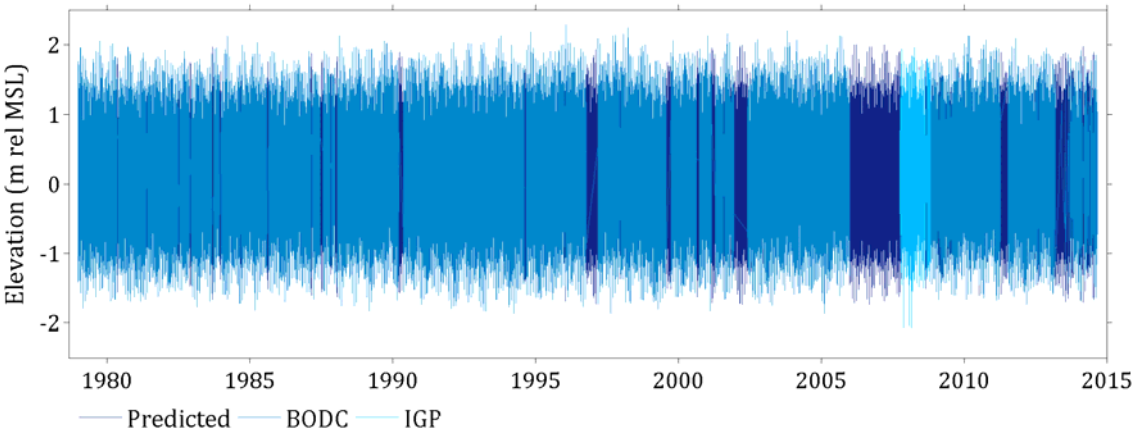

Figure 3.35. Tide data used in the present work, covering the period between 1979/01/01 and 2014/08/31. Sources of data correspond to IGP (light blue), BODC (blue) and the harmonic analysis (dark blue).

3.3.3. Total water levels

In the present work, total water level (TWL) is considered to be the sum of the following vertical components: 1) sea level (SL), determined by the sum of the astronomical tide (T) and the storm surge (S); and 2) wave runup (R), that included the setup induced by waves (η) and the uprush component of the wave swash (u) (Figure 3.36).

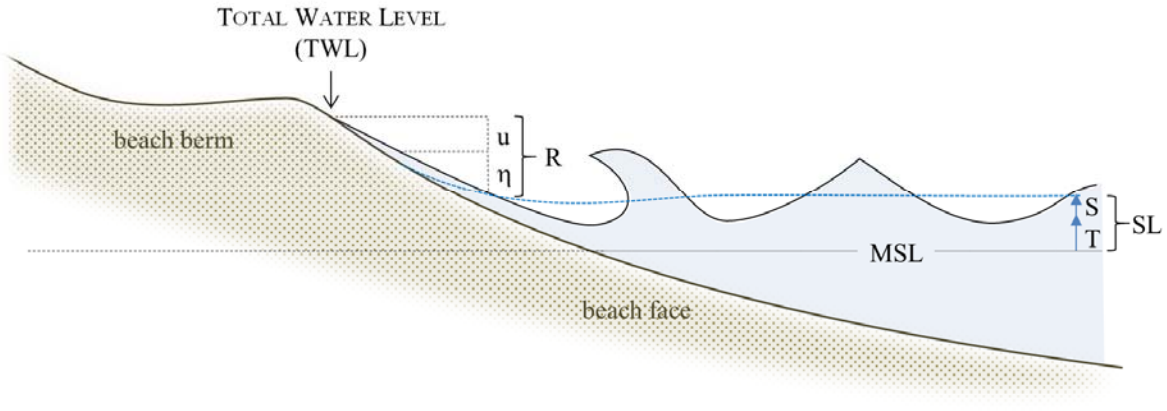

Figure 3.36. Illustration of a beach profile and components of the total water level (TWL): SL - sea level, T - astronomical tide, S – storm surge, R - wave runup, η - wave setup, and u - wave uprush.

Joint occurrences of sea level and runup were analyzed for the 36-year period of wave and tide data, and for the simulation points used in the wave propagation model, located along the study site. Assessment of the runup component required investigation of the most commonly used formulations and testing on the study sites, using the high-tide swash line surveys for validation. The procedure is described below.

3.3.3.1. Runup component

Studies on wave runup are numerous and date back to the 1950s. Teixeira (2014) provides a comprehensive listing of 60 formulas that can be found in the literature, including those applicable to beaches and structures, as well as to regular and irregular waves, and determined in either the field or laboratory settings. The number of formulations put forth by more than 30 authors for calculation of the maximum elevation reached by the wave runup process reveals the complexity involved in its description and full comprehension.

The available formulations typically include the characteristics of the incident waves and of the affected surface (beach, dune, cliff or structure). The more simple formulations relate runup to wave height alone, considering that higher waves promote higher runup levels (e.g., Guza and Thornton, 1982; CERC, 1995). Other formulations take into consideration the beach slope or include the surf similarity parameter, also known as the Irribarren number - ξ (Battjes, 1974):

$$\xi = \frac{\tan\beta}{\sqrt{H_0/L_0}} \qquad \text{Eq. 1}$$

where, tanβ is the beach slope, and H_0 and L_0 are the deepwater wave height and length, respectively. Several authors have tested and developed empirical solutions for runup estimation using the Irribarren number in association with the wave height, and a dimensionless empirical variable (k) that reflects the local conditions (e.g., Holman, 1986; Mase, 1989; Nielsen and Hanslow, 1991; Van der Meer and Stam, 1992; Grune and Wang, 2000):

$$R = k\, H\, \xi \qquad \text{Eq. 2}$$

Review of these works led to discriminating among three main types of solutions that considered runup to be dependent on one or more variables, and that were selected for testing the runup estimation in the present work (Table 3.5):

Table 3.5. Solutions used in the present work for testing wave runup.

#	Variables	Equation
1	$R = f(H, T, \beta)$	$R = H_0\, \xi = H_0 \tan\beta/(H_0/L_0)^{1/2}$
2	$R = f(H, T)$	$R = (H_0\, L_0)^{1/2}$
3	$R = f(H)$	$R = H_0$
4		$R = H_{10}$

Beach slope values were retrieved from the beach profiles analysis, and the offshore wave parameters (wave height and wave period) from the deepwater wave time series. One profile from each study site was selected to test the runup solutions.

Validation and solution selection

The field measurements of the high tide swash line were used to validate the runup estimation results and to select the best solution for computing the TWL time series for the overall study sites.

The field measurements were intended to survey the maximum excursion of the previous high tide water levels, but the task of identifying this line was sometimes difficult because of several human-induced factors masking this feature, such as trampling, and beach-cleaning machinery tracks. Only the surveys that provided an accurate identification and measurement of this line were used to compare with the predicted runup. Between 6 and 9 records were used for each site, adding to a total of 94.

The elevations measured in each field survey, at a 1 m resolution along the high-tide swash line in the study sites were filtered by location, and only the measurements within a 25 m distance from the selected profile location were used in the validation (Figure 3.37). The data obtained for this subset were averaged to produce a unique value of swash maximum elevation for each profile and survey date. In order to calculate the actual runup associated with this measurement, the sea level at the time of the high tide previous to the survey was subtracted from the measured elevation.

In order to simulate the conditions that produced the measured swash lines, runup was estimated with the wave parameters coincident with the high-tide previous to the survey.

Simple linear regression analysis was used to assess how well the model input parameters described the observed runup. The equation of best fit was derived (the y-intercept and slope values) and runup estimation with the fitted model was subsequently used to determine the following error statistics: r^2 (coefficient of determination), bias (mean error), rmse (root mean squared error) and nrmse (rmse normalized by the average of measured data).

The evaluation of the combined indicators of the accuracy of the runup estimation led to the choice of the method to be used in the TWL time series calculation. Analysis of the TWL and runup was performed with MATLAB® programming routines.

Figure 3.37. Maximum swash line position surveyed with RTK-GNSS equipment along the Nazaré study site on December 27, 2011, and measurements (in red) located within 25 m distance from the PNZ2 profile, selected for validation of the runup estimation results.

3.4. Exploratory Analysis

The acquired and analyzed data, regarding the geomorphological framework, beach morphology and sediments, and finally the hydrodynamic forcing, were combined and analyzed together. The data were applied to existing beach morphodynamic models and further analysis was made through simple regression analysis, cross-correlation between variables and multivariate analysis statistics.

The commonly used conceptual models that describe beach morphodynamic state were applied to the data. The model by Guza and Inman (1975) is one of the earliest of these models and describes the Surf Scaling Parameter - ε, as:

$$\varepsilon = \frac{a\sigma^2}{gT^2 \tan^2 \beta} \quad \text{Eq. 3}$$

where a is the wave amplitude, σ is the wave angular frequency (2π/T), and g is the acceleration due to gravity.

The model by Wright and Short (1984) applies to wave-dominated beaches and is one of the most used in the literature. It describes three main beach types (dissipative, intermediate and reflective) and the classification is based on the Dimensionless Fall Velocity parameter – Ω (following Gourlay, 1968), given by:

$$\Omega = \frac{H_b}{\omega_s T} \quad \text{Eq. 4}$$

where, ω_s is the sediment fall velocity, that in this case was calculated through the use of the formula put forth by Soulsby (1997):

$$\omega_s = \frac{\upsilon}{d}\left[(10.36^2 + 1.049 d_*^3)^{1/2} - 10.36\right] \quad \text{Eq. 5}$$

where, υ is the kinematic viscosity of water, d is the mean grain size, and d_* is the dimensionless grain size given by:

$$d_* = d\left[\frac{(s-1)g}{\upsilon^2}\right]^{1/3} \quad \text{Eq. 6}$$

where, s is the sediment relative density (quartz).

Short and Masselink (1999) put forth a parameter that relates the embayment configuration to the incident breaking wave conditions, by using the planform geometry parameters (C_l and S_l) and the incident wave characteristics to derive the Embayment Scaling Parameter – δ':

$$\delta' = \frac{S_l^2}{100 C_l H_b} \quad \text{Eq. 7}$$

According to the authors, the degree of embaymentization can be predicted using this parameter, such that:

For $\delta' > 19$ → normal beach circulation, as applies to typical unconstrained beaches. There is limited or no impact of headlands on the surf zone circulation.

For $\delta' = 8\text{-}19$ → transitional circulation. The influence of headlands on surf zone circulation increases, causing longshore currents flowing seaward against each lateral boundary.

For $\delta' < 8$ → cellular beach circulation. Lateral boundaries topography affects the surf zone circulation within the entire embayment, causing strong longshore currents.

The beach profile datasets were used to classify the study sites according to the conceptual framework proposed by Jackson and Cooper (2009): TYPE I (Unconstrained); TYPE II (Semi-constrained) and TYPE III (Highly constrained).

The dimensionless parameter put forth by Burvingt et al. (2017), the longshore variation index - LVI, was assessed to quantify the alongshore morphological variability in beach response:

$$\mathrm{LVI} = \frac{Q_{std}}{|Q_{mean}|+Q_{std}} \qquad \text{Eq. 3}$$

where, for each study site, $|Q_{mean}|$ is the absolute value of the mean of the profiles' volumetric change, and Q_{std} is the standard deviation of the profiles' volumetric change. LVI varies between 0 and 1 with higher values representing greater longshore variability in beach response.

The relationships between the sets of variables measured along the study sites were explored using a multivariate analysis technique - the Canonical Correspondence Analysis, CCA (ter Braak, 1986). The method distinguishes between predictor variables (in this case the geomorphological framework and hydrodynamic parameters) and the response data-sets (morphology and sediments). Originally, the method was created to analyze and interpret ecological data, such as occurrences or abundances of species, and their relation to data on environmental variables (ter Braak and Verdonschot, 1995), but has become widely used by other disciplines with similar process-response behavior.

Other statistical techniques (linear and non-linear) have been successfully used to analyze coastal field data and model medium to long-term behavior of coastal

morphology (Stokes et al., 2013; Larson et al., 2003; Southgate et al., 2003), and to explore their relationship with offshore forcing regimes (Kroon et al., 2008; Karunarathna et al., 2016), or geomorphological constraints (Loureiro et al., 2012).

The CCA analysis was conducted with the open-access statistics software package PAST (Hammer et al., 2001). In selecting the input datasets, parameters that were found redundant, and explanatory of the same measure, were eliminated and only one descriptive parameter was selected. This was the case of the degree of indentation (Indentation ratio vs Indentation Index) beach change (volume variation vs width variation) and wave height (offshore vs nearshore vs breaking wave height). Thus, the following variables were used (codes in square brackets are the notations used in the program):

Predictor variables:

1. S_l/C_l – Indentation Index [S/C]
2. β – wave obliquity [BETA]
3. T_p – mean wave period [T]
4. H_b – mean wave height at breaking [Hb]
5. TWL – mean total water levels [TWL]

Response variables:

1. Δ_{Vol} - Volume standard deviation [VOL]
2. Mz_{Face} – mean beach face sediment size [MzFace]
3. $\tan\beta$ – Beach face slope [SLOPE]

All study sites, including the two subdivisions that added two new locations to the data (see Subchapter 4.1 for explanation), totalized 16 observations that were used in the CCA analysis.

Chapter 4. Results

The present chapter describes the results obtained from the procedures of data gathering and analysis. Results are presented in three subchapters. In the first subchapter the description of the geomorphological framework of each beach is presented. The second subchapter presents the results on beach morphology and sediments. The third subchapter deals with the hydrodynamic characterization of the oceanographic forcing, including waves, tides and total water levels.

4.1 Geomorphological framework

The geomorphological framework of each study site is presented in terms of planform geometry and description of the physical boundaries, and type of nearshore and backshore features that are present and that constrain both the nearshore wave regime and the beach response.

Of the overall study sites, five are located along coastal stretches that exhibit a continuous and long sandy beach extending for at least 13 km (Pedras Negras, Lagoa de Óbidos - Baleal, Rainha, Fonte da Telha and Lagoa de Albufeira). Compared to the remaining sites that have lengths below 5 km, these may be regarded as unconstrained beaches. Still, physical boundaries exist, even though they occur at a different spatial scale when compared to the other sites. Therefore, planform geometry parameters were assessed for all study sites, including these, for the purpose of quantifying the degree of embayment and indentation, and inclusion of all data in the comparative and quantitative analysis.

Lateral boundaries were considered to define the beach systems where the study sites are included. In some cases, two or more study sites were part of the same beach system, and, on the other hand, some beach profiles monitored as being part of the same study site, were found to belong to different beach systems. An instance of two or more study sites being part of the same beach system, was along the Caparica - Espichel coastal stretch, characterized by a long and continuous beach. In this case, Lagoa de Albufeira, Fonte da Telha, Rainha and the profiles within the groin field in Costa da Caparica were considered to be part of the same beach system. In the study sites of Lagoa de Óbidos - Baleal and the northern part of Costa da Caparica, profiles were located in different beach systems and therefore were separated. As a result, two new locations were added to the data - BL (corresponding to Baleal beach, characterized by PLOB4 beach profile) and SJC (corresponding to São João da Caparica beach, characterized by PCC1 to PCC8 beach profiles).

4.1.1. Study sites

1 Pedras Negras

Pedras Negras beach system has a very low indentation index, because of the similarity between the embayment length (17.6 km) and embayment width (17 km) (Figure 4.1). Thus, Pedras Negras is regarded as a typical open and unconstrained beach. The northern

boundary corresponded to a small rocky headland that induced a displacement of about 200 m of the beach shoreline, in relation to the updrift (to the north) shoreline that fronts the village of Pedrógão. The southern boundary corresponds to the steep sloped rocky promontory of the São Pedro de Moel village, made of Jurassic limestones, and south of which small pocket beaches develop.

There is a small river - Rio Liz - draining to this coastal stretch in Praia da Vieira. The margins of the river channel at its seaward reach were contained and linearized with rubble walls that extend across the beach by two small jetties until the low tide contour line. However, there was no evidence of these artificial structures behaving as an obstacle to longshore sediment transport, and therefore they were not considered as a boundary.

Besides Praia da Vieira, that has a small seawall, the beach system is fairly continuous, backed by a large and well established vegetated dune that aligns parallel to the coastline and that at Pedras Negras attains 13 m in height. The nearshore exhibited shore-parallel sand bars that developed very close to shore. In the southernmost part of this beach system, a stream drains to the beach, but with no permanent connection with the sea.

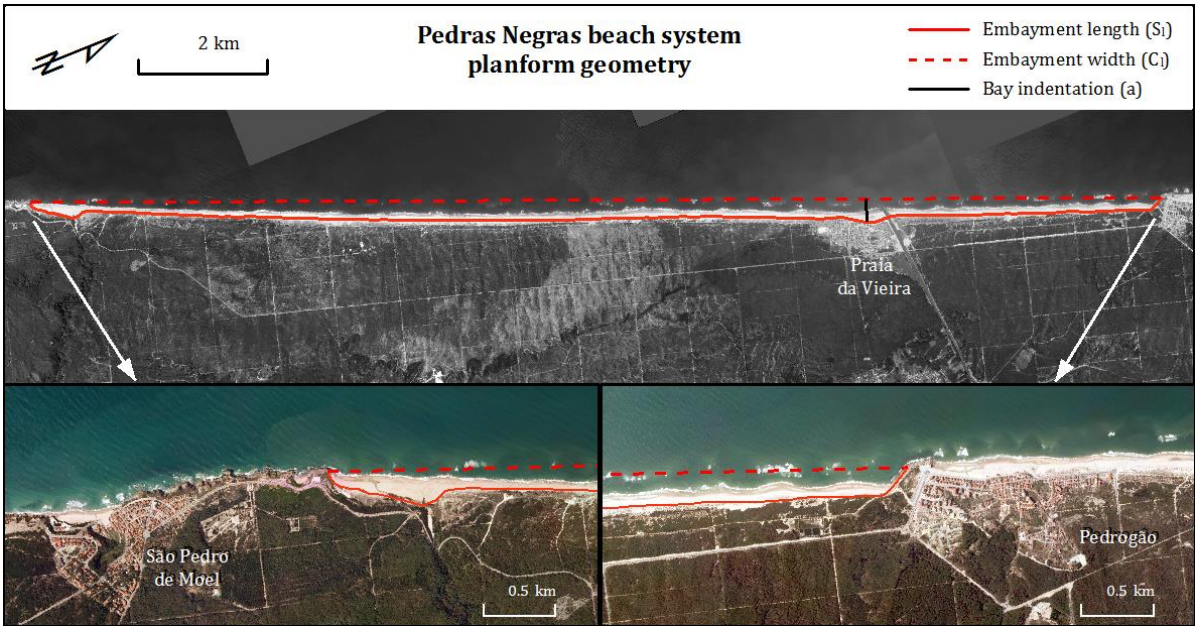

Figure 4.1. Planform geometry parameters for Pedras Negras beach system.

2 Paredes de Vitória

Paredes de Vitória develops at the mouth of the Ribeira de Paredes stream valley, bordered by high cliffs of mainly Pliocene sands, and to a lesser extent, in its southern section, of sandstone, silt- and claystone of Mesozoic age. The former are highly erodible formations and slope mass-waste deposits of sand are frequent at the base of the cliffs. This is especially frequent in the northernmost section where the beach is narrower and the waves easily reach its base. These are however of small dimensions and deliver an insignificant amount of sediment to the beach system.

South of the stream mouth location, and for almost 1 km, the back of the beach is covered by small vegetated dunes, that are artificially maintained through fences and elevated boardwalks in the more urban central section. River discharge is considered small and the very narrow channel that connects to sea wanders considerably.

Two promontories define the lateral boundaries of Paredes de Vitória beach system (Figure 4.2), that extends for almost 2 km. The nearshore is characterized by large sandbars that often weld onto the beach creating ridge and runnel type of morphology.

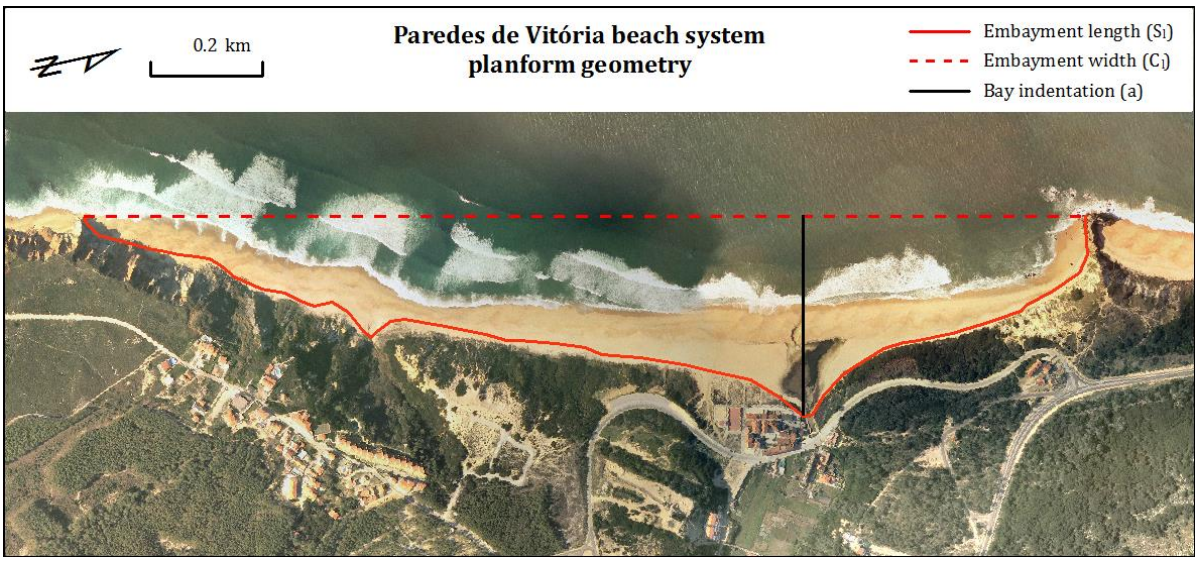

Figure 4.2. Planform geometry parameters for Paredes de Vitória beach system.

3 Nazaré

Nazaré corresponds to an embayed continuous beach (Figure 4.3) bounded landward by an alongshore seawall that stands c. 0.5 m above the beach berm. The south lateral

boundary corresponds to the north jetty of the fishery harbor, and the north lateral boundary is the rocky promontory known as Sítio da Nazaré. This promontory is essentially made of Cretaceous limestone and promotes a shoreline displacement of about 800 m between the updrift (north) and downdrift shorelines.

The nearshore is highly influenced by the presence of the submarine canyon of Nazaré whose head intersects the permanently submerged section of the beach profile landward of the 20 m depth contour line. A small dune field develops in the southernmost area, adjacent to the harbor jetty and extends for about 300 m alongshore.

The upper beach berm is frequently reshaped through anthropic action. Mechanical leveling and dune building done through beach scraping is conducted either for recreational purposes, or for protection against storms.

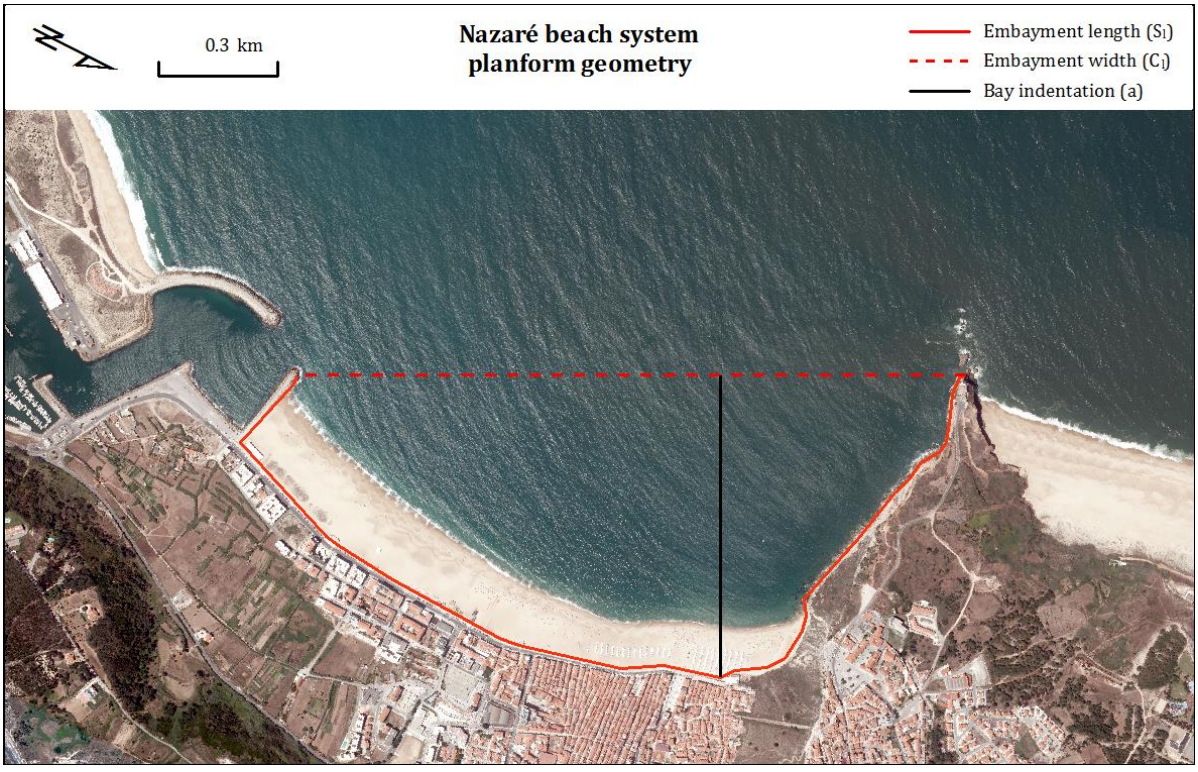

Figure 4.3. Planform geometry parameters for Nazaré beach system.

4a Lagoa de Óbidos - Baleal

The three northernmost profiles of the study site between Lagoa de Óbidos and Baleal (PLOB1 to PLOB3) are located in a beach segment that extends for c. 11 km between two

small headlands that define the lateral limits of a continuous strip of sand (Figure 4.4). This beach system is predominantly characterized by a narrow beach landward bounded by cliffs affecting Meso-Cenozoic sandstones. The cliffs vary in height throughout the segment, reaching almost 50 m, and are locally interrupted by small valleys of intermittent streams. Despite experiencing localized mass movements, the slope mass waste deposits are quickly washed away and it is estimated that the overall contribution has small significance in the beach sediment budget.

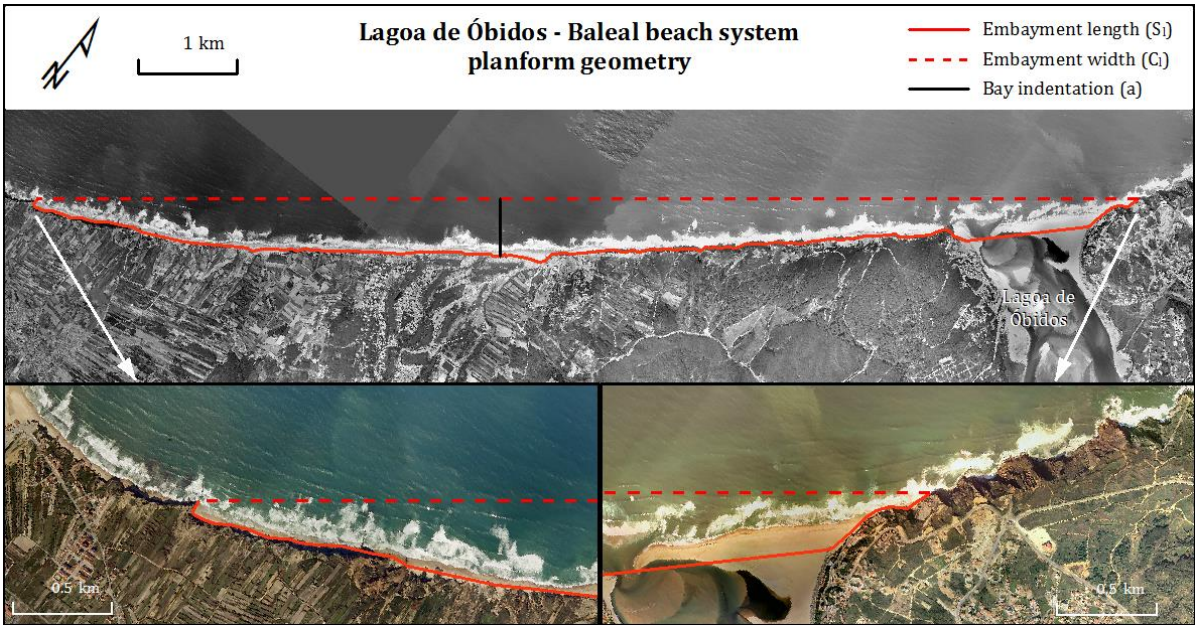

Figure 4.4. Planform geometry parameters for Lagoa de Óbidos -Baleal beach system.

In the northernmost section, Lagoa de Óbidos interrupts the cliffed coastline, and for a length of 1.5 km the coast is characterized by a welded sandy barrier that separates the coastal lagoon from the ocean. This flood-dominated system exhibits a highly wandering inlet and intense sedimentation inside the lagoon, indicating that little or no sediment is provided to the littoral drift. The nearshore is characterized by longshore bars that can attain several tens of meters in extension.

4b Baleal [BL]

The southernmost profile of the Lagoa de Óbidos - Baleal study site is located in a separate beach system that corresponds to the beach of Baleal (Figure 4.5). This too is laterally

limited by rocky headlands, consisting of Jurassic limestones in the western limit (Baleal), and clayey sandstone in the landward and eastern limit. Cliffs in this section are more irregular and lower in elevation than the cliffs farther to the north.

Part of this beach system creates the tombolo that developed between the mainland and the former island occupied by the village of Baleal, and in this section the landward boundary is the structure where the road was built to connect the two locations. The nearshore at this location is characterized by a rocky platform, often exposed at low tide.

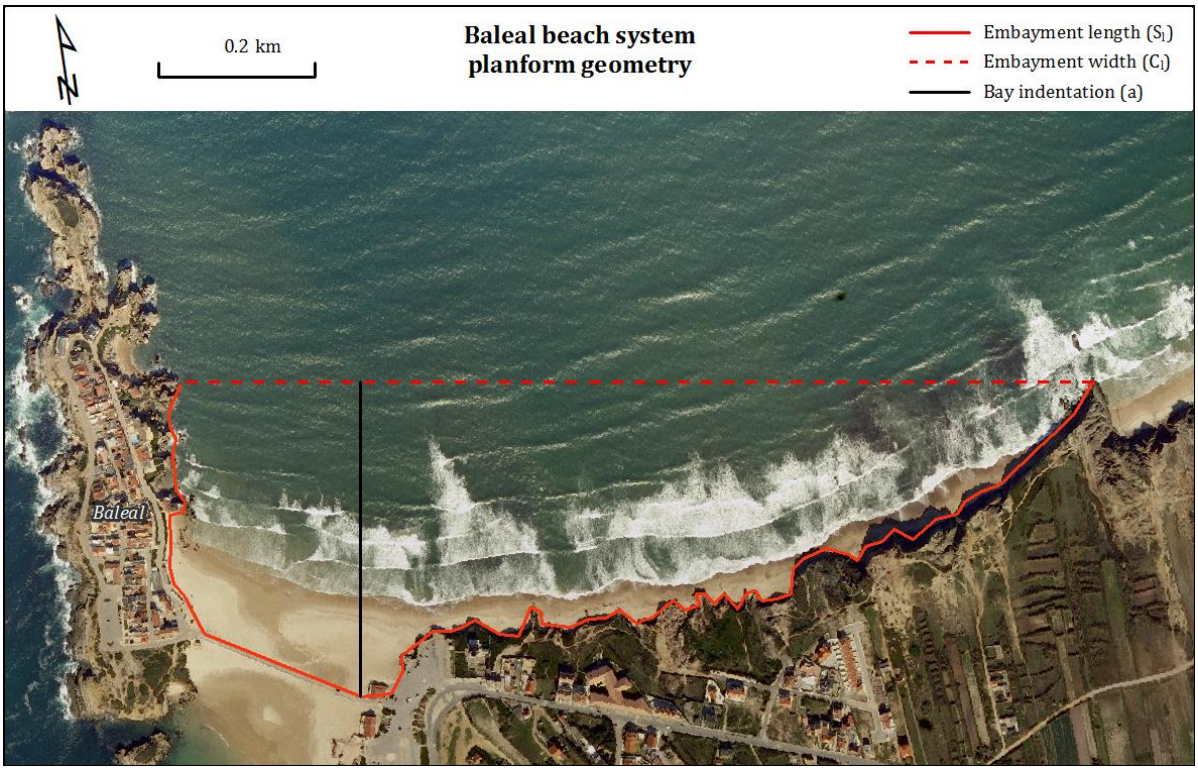

Figure 4.5. Planform geometry parameters for Baleal beach system.

5 Baleal - Peniche

Baleal-Peniche beach segment encompasses the arcuate-shaped beach that develops in the embayment between the Baleal tombolo and the village of Peniche, laterally bounded by rocky headlands (Figure 4.6). Cliffs at either end are made of resistant Jurassic limestone and marly limestone, and only a short segment of the beach is in contact with this formation at the easternmost end of the bay. Most of the embayment's backshore is characterized by a large dune field that is active and exchanges sediment with the beach.

The dunes at either end have been object of some human intervention (such as fences) in recreational and concessionary areas.

The beach develops over a rocky platform that is exposed at low tide at both ends of the bay. In the central part of the beach system, however, the platform is covered with sediment that develops bar and rip channel type of morphology according to Short's (1999) classification scheme.

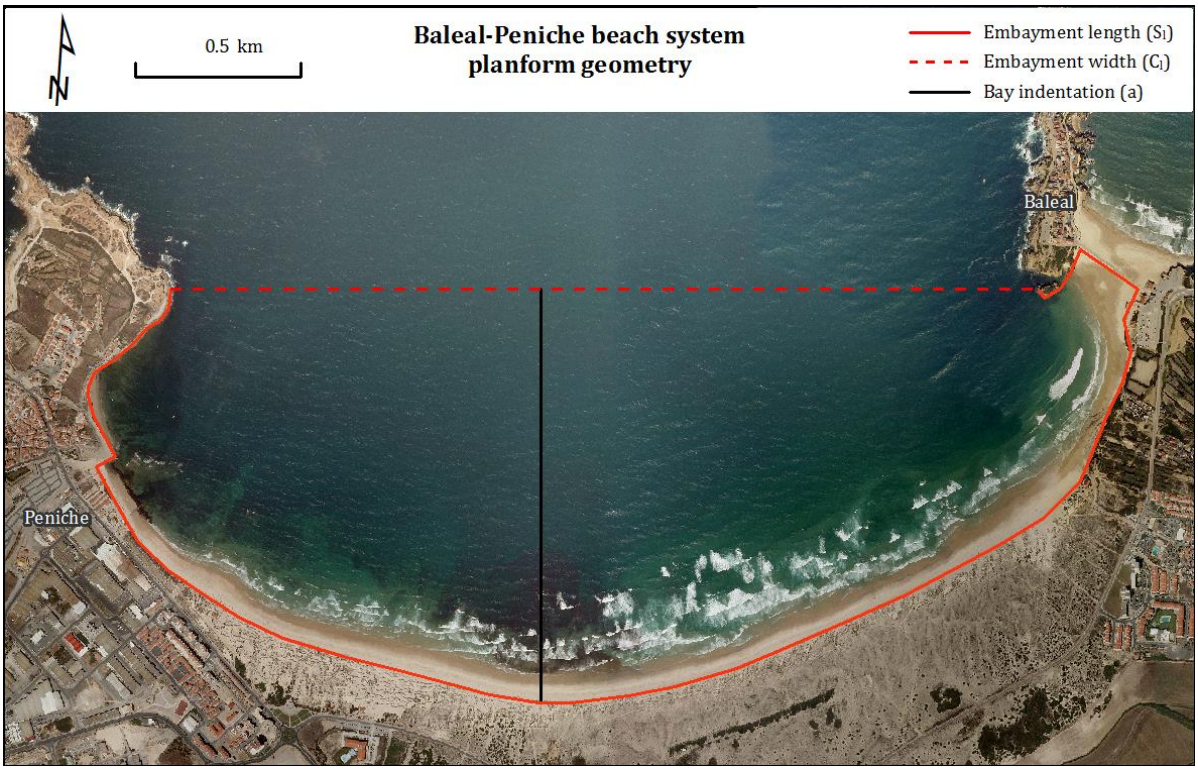

Figure 4.6. Planform geometry parameters for Baleal-Peniche beach system.

6 Santa Cruz

The beach system of Santa Cruz extends for about 3.6 km and is landward-bordered by cliffs affecting mainly Meso-Cenozoic sandstones, siltstones and marls, as well as limestones at the southernmost end. Small rocky headlands projecting seaward limit the longshore sediment transport and provide the lateral boundaries of this beach system (Figure 4.7). The beach serves the adjacent village as well as the surrounding populations and is therefore intensively used for recreational purposes. The central section backshore corresponds to stabilized dunes, and the southernmost section is bound by a seawall. In the concessionary areas the subaerial beach is sometimes artificially shaped by

mechanical means to create a levelled area for the summer season (Figure 4.8). Sandbars develop in the nearshore and often migrate inland welding onto the beach. However, in a limited area at the southernmost section, especially during the winter season, the underlying rocky formation may get exposed.

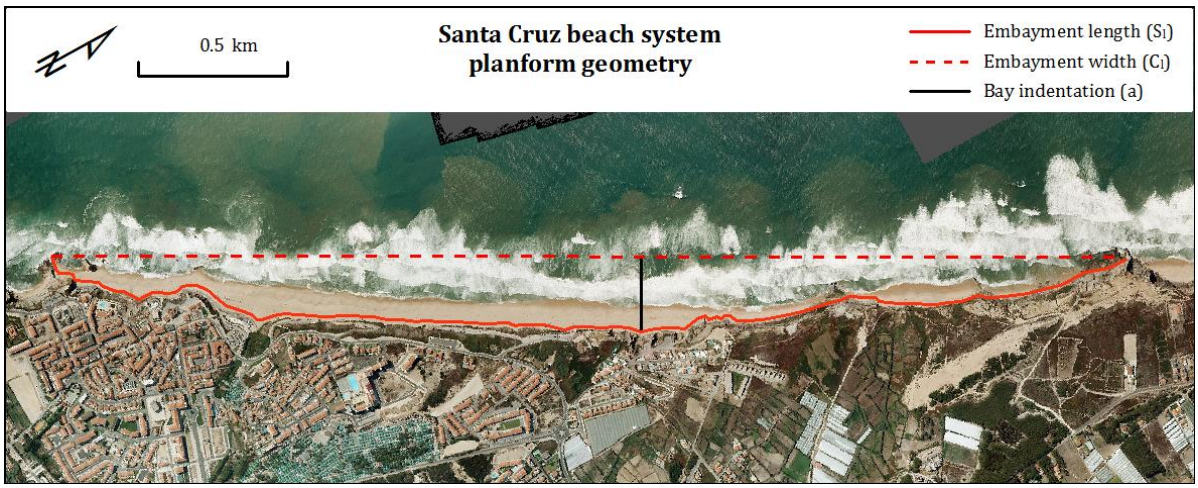

Figure 4.7. Planform geometry parameters for Santa Cruz beach system.

Figure 4.8. Some aspects of the interventions carried out on the beach of Santa Cruz, modeling the beach berm to optimize the bathing area: A - on June 15, 2011; and B - on June 12, 2013.

7 Coxos

Coxos is the smallest of all study sites and consists of a small pocket beach bounded by Cretaceous limestones forming steep cliffs and two rocky promontories (Figure 4.9). The offset between the tip of the northern headland and the coastline at the backbeach is just under 200 m. The northernmost promontory, gradually dips into a rocky platform. The landward bounding cliffs reach 30 m above MSL and show boulder deposits at the base. The beach accumulates over the rocky platform that gets exposed at low tide.

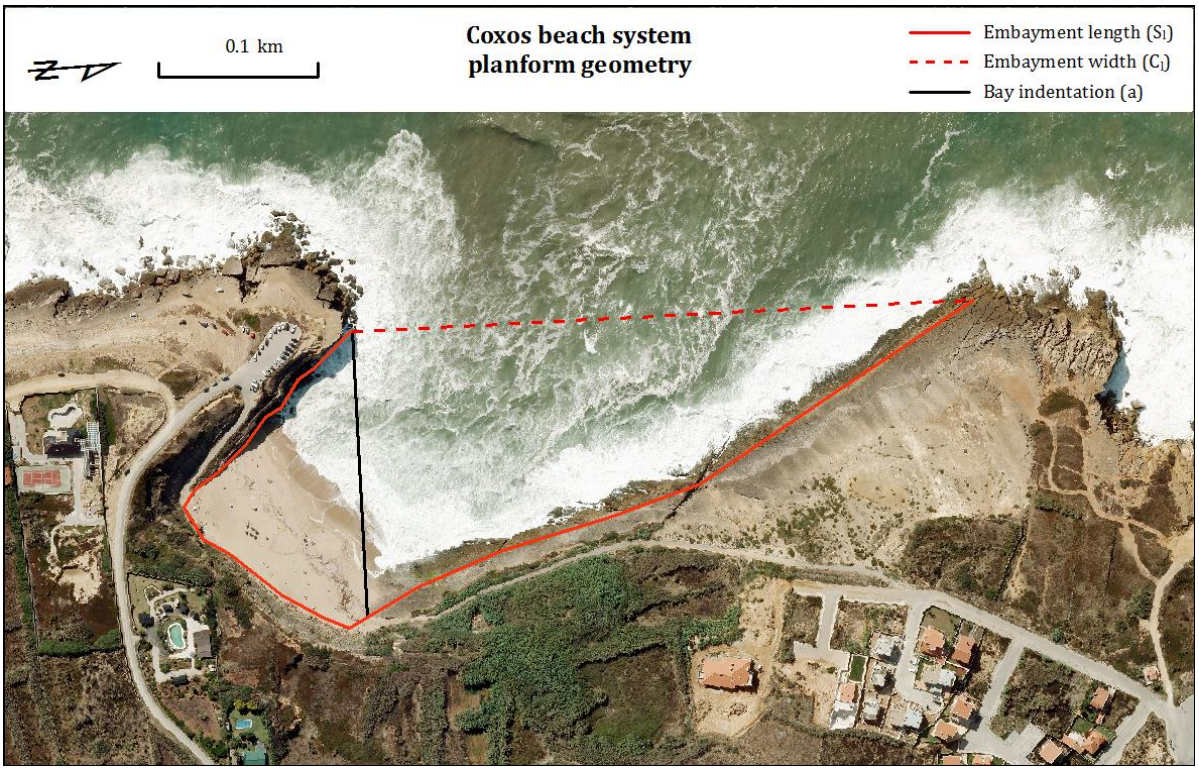

Figure 4.9. Planform geometry parameters for Coxos beach system.

8 Baleia/Sul

The Baleia/Sul beach corresponds to a 500 m long beach, bounded by coastal structures (Figure 4.10). Two groins establish the lateral limits of the beach. The southernmost groin is about 125 m long and the northernmost groin is actually the edge of a "swimming pool" and extends for 75 m seaward before joining the remaining structure that encloses the pool. In addition, a smaller groin exists along the beach, located halfway, however it is in a state of advanced degradation and is not an obstacle to longshore sediment transfer. The backshore corresponds to a seawall built at the base of a cliff and that stands between

1 and 2 m above the beach surface. The beach develops over a rocky platform that is exposed at low tide. This is an urban beach highly used for recreational purposes and, therefore, beach scraping activities take place before the summer season to increase the beach berm area (Figure 4.11).

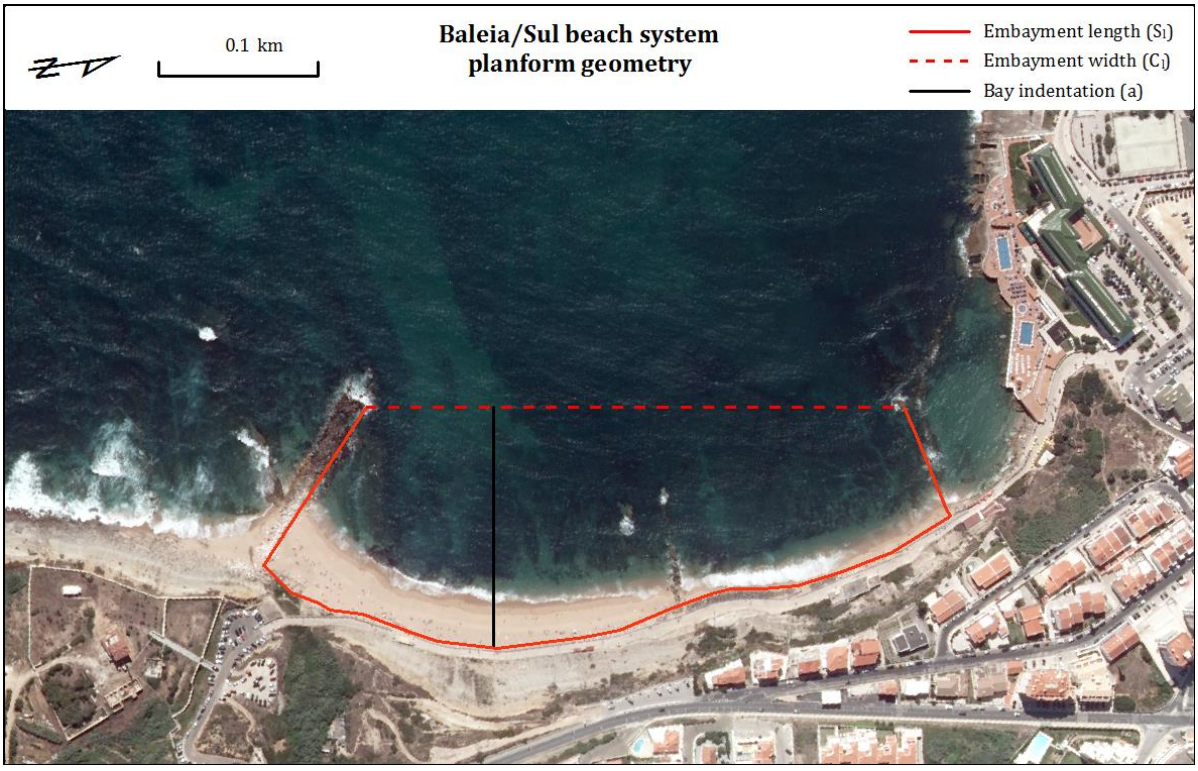

Figure 4.10. Planform geometry parameters for Baleia/Sul beach system.

Figure 4.11. Overview of the central sector of Baleia/Sul study site at the beginning of the summer season: A - construction of a subaerial berm through beach scraping on May 19, 2011; And B - reconstructed beach berm with installation of beach amenities, on June 20, 2013.

9 Magoito

Magoito beach system is bordered by the high cliffs of Cretaceous marl- and limestones that stand c. 60 m above MSL. The rocks cut by these cliffs create both the landward and lateral limits, as well as the substrate over which the beach develops. The beach extends from the rocky headland where the Magoito fort is located to the north, to about 800 m south, where a smaller rocky headland outcrops seaward (Figure 4.12). A small river – rio Mata, drains directly to the beach, c. 100 m south of the northern limit. It is an intermittent water course and there is no evidence that its discharge may be considered an important source for the beach system sediment budget.

The beach is composed by a layer of sand that rests on the rocky platform at the base of the cliffs, often removed and exposing the bedrock layers (Figure 4.13). During these periods the cliff base mass-waste deposits get exposed, as well as the fluvial deposits, consisting of larger pebbles at the mouth of river Mata.

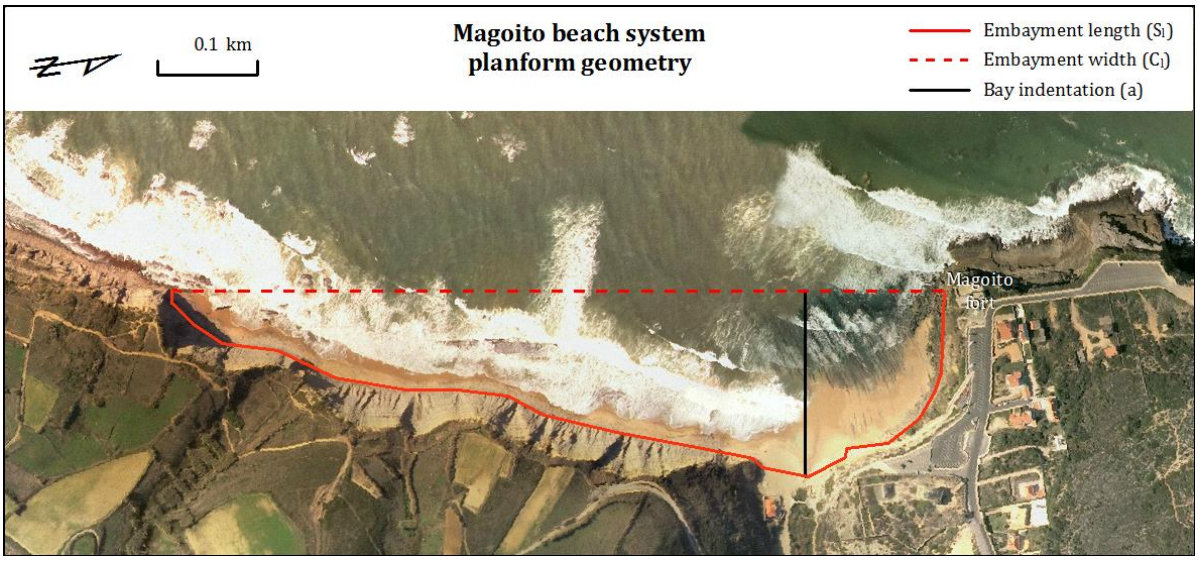

Figure 4.12. Planform geometry parameters for Magoito beach system.

Figure 4.13. General view of Magoito beach. Photographs taken looking towards southwest, showing two distinct configurations of the beach: A - on May 30, 2011, with the beach covering most of the rocky platform, forming a beach berm and developing beach crescents; and, B - on December 28, 2011, showing a very thin layer of sand, exposing much of the rocky shelf and cliff base deposits.

10 Tamariz

Tamariz is a beach surrounded by an urban environment (Figure 4.14). Groins create the lateral boundaries, the easternmost one being arcuate in shape and extending for 150 m, and the westernmost one, substantially smaller, extending only for 30 m. This latter groin is located in a section where the shoreline bends and imagery analysis indicates that it effectively confines the sediment to the Tamariz beach. The backshore is a seawall fronting a highly urbanized area. The beach develops over a rocky platform that gets exposed at low tide, especially in the west sector.

In order to improve the bathing area in the summer, the beach is subject to mechanical reshaping, to promote the reconstruction and flattening of the beach berm (especially in the easternmost sector).

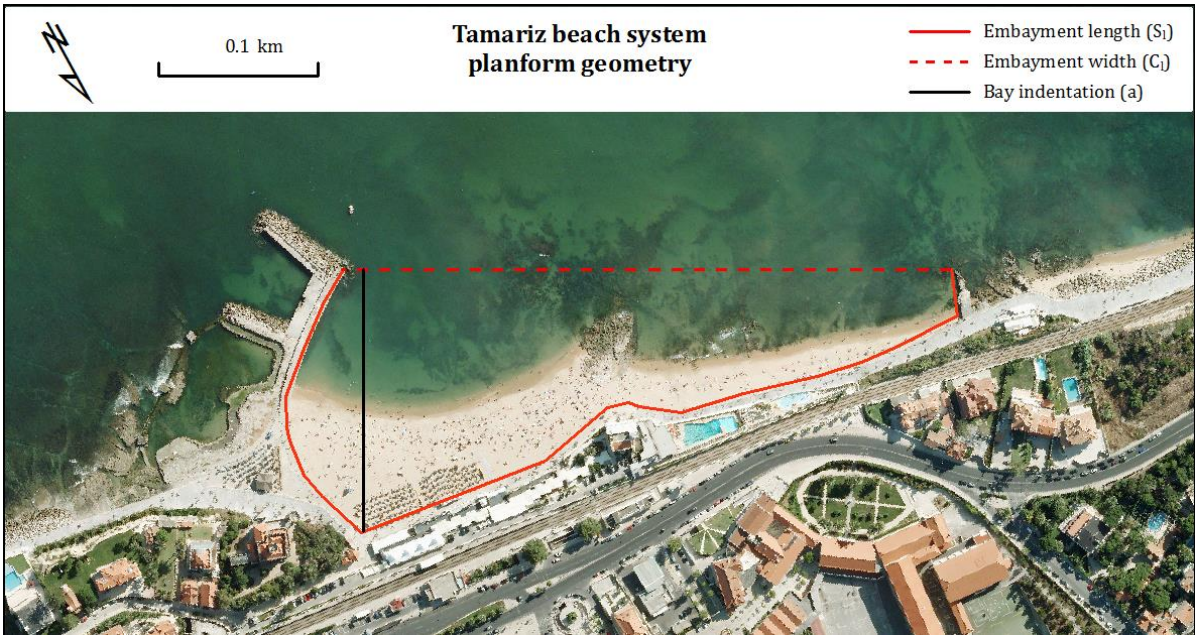

Figure 4.14. Planform geometry parameters for Tamariz beach system.

São João da Caparica (study site 11a)

São João da Caparica corresponds to the northernmost sector of Costa da Caparica study site. The beach extends for c. 1.7 km with an approximate southeast-northwest orientation, limited by two groins: the southern groin of Cova do Vapor to the northwest, about 360 m long; and a shorter groin to the southeast, about 250 m long, encompassing a smaller groin that confines a smaller beach – praia do Norte (Figure 4.15).

The backshore of the northern sector consists of a dune field that reaches elevations of 7 and 8 m (MSL), although it is much altered by human intervention, locally interrupted by beach accesses, and limited in its growth by numerous infrastructure and parking lots. The southern sector is characterized by a narrow beach, landward limited by a seawall that serves as protection for a camping site located a few tens of meters from the shoreline. The nearshore is characterized by the presence of longshore sand bars that often develop ridge and runnel type of morphology.

Given their recreational value, and the long-term erosional trend, these beaches have been subject to beach nourishment. The last intervention, prior to this study, occurred in 2009, and, despite not countering the erosional process because sediment is being brought from within the littoral cell (the Tejo inlet), it has been contributing to the resiliency and stability of these beaches in particular (Santos et al., 2014).

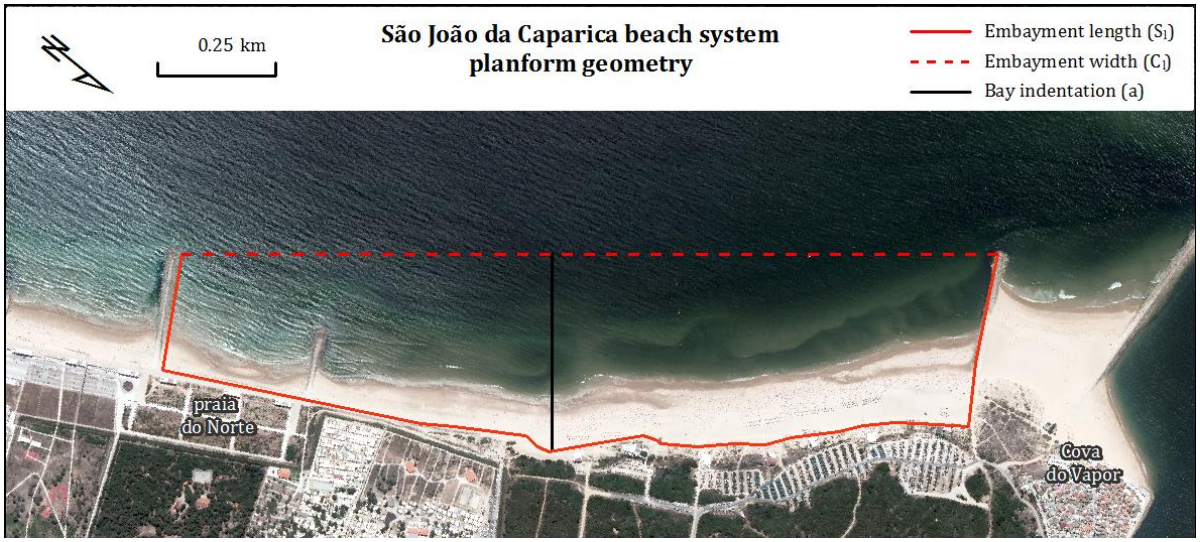

Figure 4.15. Planform geometry parameters for São João da Caparica beach system.

Caparica – Espichel (study sites 11b, 12, 13 and 14)

With the exception of São João da Caparica, the study sites located along the Caparica – Espichel coastal stretch - Lagoa de Albufeira, Fonte da Telha, Rainha and Costa da Caparica groin field beaches - share the same lateral boundaries and therefore were considered to be part of the same beach system (Figure 4.16). The northernmost lateral boundary corresponds to the southernmost longer groin that makes up the groin field of Costa da Caparica, c. 250 m in length. There was no evidence of sediment transport around this structure in modal wave conditions, and the groins located southward of this one show evidence of sediment bypassing. The southernmost boundary of the Caparica-Espichel beach system corresponds to the first rocky headland that extends seaward and provides the limit between the continuous strip of sand to the north and the pocket beaches that occur south of that location.

The Caparica-Espichel system is a large coastal embayment that extends for c. 22.5 km as a long strip of beach with no obstacles to the littoral drift and the nearshore is characterized by sand bars that locally weld onto the beach.

The backshore along this coastal stretch is very variable and therefore this feature will be described for each study site separately.

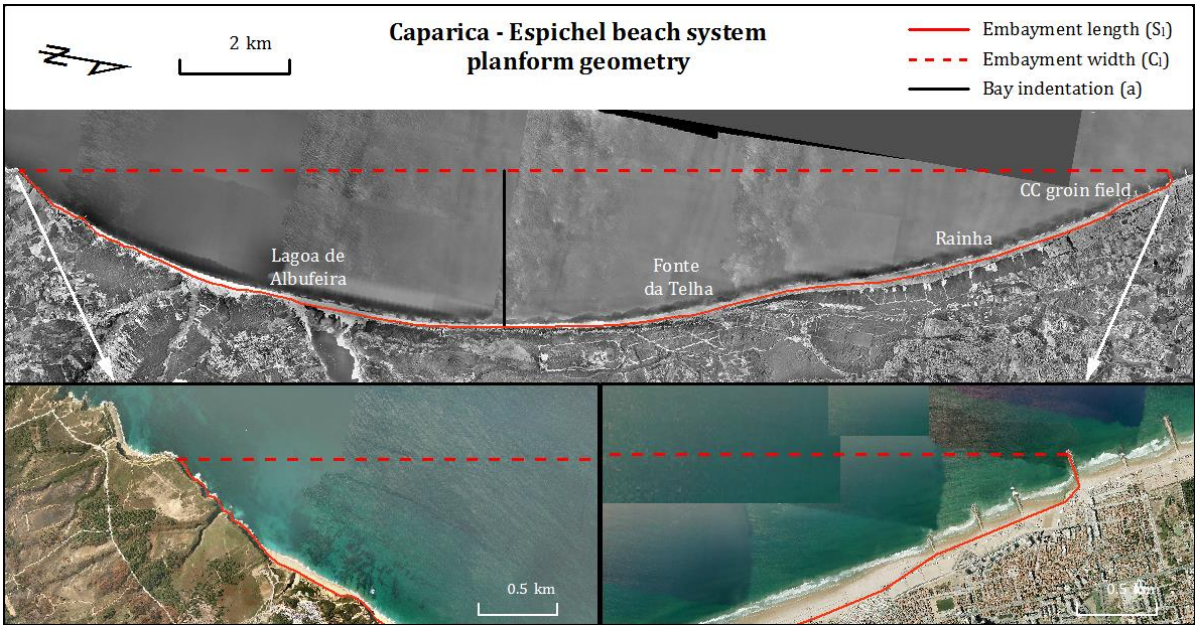

Figure 4.16. Planform geometry parameters for Caparica - Espichel beach system.

Costa da Caparica groin field (study site 11b)

The groin field section of Costa da Caparica study site, corresponds to the beaches that develop between groins and that are landward limited by the seawall that fronts the urban area.

Rainha (study site 12)

The backshore at Rainha study site is characterized by vegetated foredunes that develop parallel to the shoreline. They are however intersected by multiple paths and accesses and their evolution is highly constrained by the installation of recreational infrastructure and parking lots in their leeward side.

Fonte da Telha (study site 13)

At Fonte da Telha, the dunes that make up the backshore are even more altered and the area extending landward of the beach corresponds essentially to dump materials and earth landfill that occupied former dune areas and have been placed to make space for the infrastructures, as well as poorly-integrated beach access points and parking lots.

Lagoa de Albufeira (study site 14)

The beach monitored at the Lagoa de Albufeira study site is located south of the coastal lagoon's barrier inlet, in a coastal segment where the beach is in contact with a cliff affecting Cenozoic sandstones . Small embryo dune features develop at the base of the cliffs, probably fed by the highly erodible cliff sandy deposits.

4.1.2. Overall study area

The summary of the parameters that were used to describe the geomorphological framework for each study site is presented in table 4.1, including the measured values of planform geometry - embayment length (S_l), embayment width (C_l), and bay indentation (a), wave obliquity (β), and computed degree of embayment, expressed by the Indentation ratio (a/C_l) and Indentation index (S_l/C_l).

According to the classification proposed by Bowman et al. (2014) based on the indentation ratio, PN, LOB and SC are classified as having Extremely Low indentation. All the beaches included in the Caparica-Espichel segment, including SJC are in the category of beaches with Very Low indentation, along with PV and MG. All the other study sites are characterized as having Low indentation according to this classification.

Figure 4.17 provides a graphical visualization of the variation of these parameters along the study area. The beaches that have a rocky platform also have a smaller embayment width. The vertical dashed line in the left panel of Figure 4.17 marks the 1200 m threshold, and the lighter grey bars (C_l) for BL, CX, BS, MG and TM fall below this line. The only exception is BP study site that has an embayment width of 2619 m. Also, and contrary to the other platform beaches, BP study site presented nearshore bars in the central section of the embayment.

Another difference between platform beaches and no-platform beaches is that the former have higher degree of indentation. The panel on the right on Figure 4.17 shows the wave obliquity (β), indentation index (S_l/C_l) and Indentation ratio (a/C_l) as relative measures, given by the ratio between the study site value and the overall average (the vertical dashed line marks the 1 ratio). Platform beaches, except for MG, have indentation index (S_l/C_l) and Indentation ratio (a/C_l) (lighter grey bars) above average. Nazaré is an exception amongst the no-platform beaches showing a higher degree of indentation.

Table 4.1. Physical boundaries and planform geometry parameters for the study sites. Embayment length (S_l), embayment width (C_l), bay indentation (a), wave obliquity (β), indentation index (S_l/C_l) and Indentation ratio (a/C_l).

	Beach	Backshore	Nearshore	Lateral boundaries	S_l (m)	C_l (m)	a (m)	β	S_l/C_l	a/C_l
01	PN	dune	nearshore bars	headland	17673	17428	356	13.3	1.0	0.02
02	PV	cliff	nearshore bars	headland	2079	1801	357	22.5	1.2	0.20
03	NZ	structure	canyon	headland structure	2672	1688	759	61.9	1.6	0.45
04a	LOB	cliff	nearshore bars	headland	11681	11167	647	16.6	1.0	0.06
04b	BL	structure	rocky platform	headland	1676	1170	403	63.6	1.4	0.34
05	BP	dune	rocky platform + nearshore bars	headland	5133	2619	1248	51.0	2.0	0.48
06	SC	cliff + dune + structure	nearshore bars	headland	3825	3612	249	6.0	1.1	0.07
07	CX	cliff	rocky platform	headland	713	406	180	33.4	1.8	0.44
08	BS	structure	rocky platform	structure	674	345	151	26.9	2.0	0.44
09	MG	cliff	rocky platform	headland	977	802	187	26.4	1.2	0.23
10	TM	structure	rocky platform	structure	628	383	165	83.7	1.6	0.43
11a	SJC	dune+ structure	nearshore bars	structure	2377	1738	420	75.0	1.4	0.24
11b	CC	structure	nearshore bars	headland structure	22506	21031	2879	45.0	1.1	0.14
12	RA	dune								
13	FT	dune								
14	LA	cliff								
Average:					8758	7955	1040	41.3	1.34	0.25

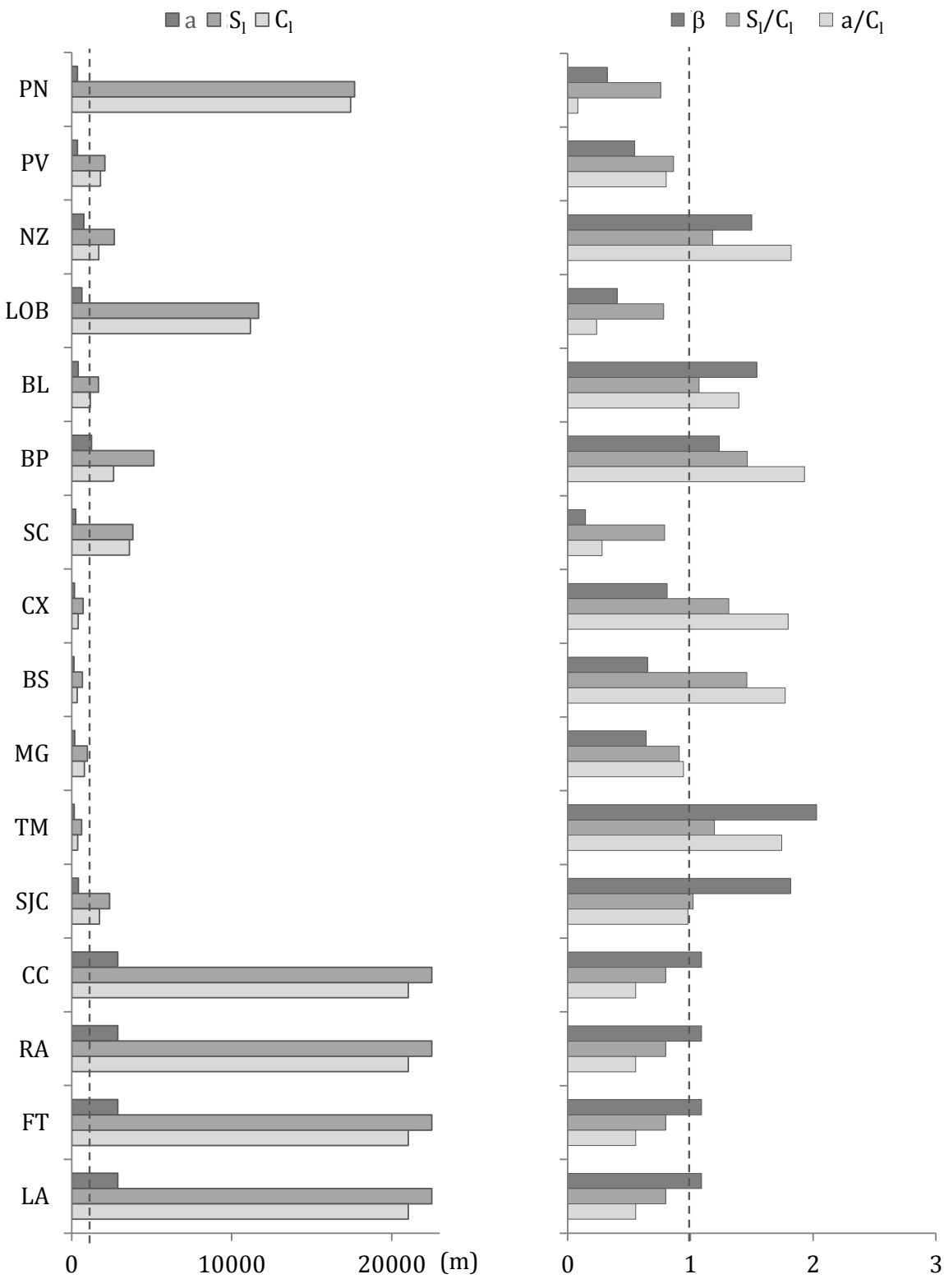

Figure 4.17. Planform geometry parameters along the study sites. Left panel shows the absolute values of embayment length (S_l), embayment width (C_l) and bay indentation (a); vertical dashed line marks the 1200 m threshold. Right panel shows wave obliquity (β), indentation index (S_l/C_l) and indentation ratio (a/C_l) as relative measures, given by the ratio between the study site value and the overall average (vertical dashed line marks the 1 ratio).

Figure 4.18 shows the plot of a/C_l versus S_l/C_l for all studied beaches. The high correlation between them (R^2=0.88) indicates that both are good descriptors of the variability of the beach planform geometry along the study area. However, considering that the study sites range between pocket beaches and open segments of beaches, the use of the bay indentation parameter (a) seems to be less meaningful in their comparison, because in longer beaches the embayment depth is expected to be fairly constant alongshore.

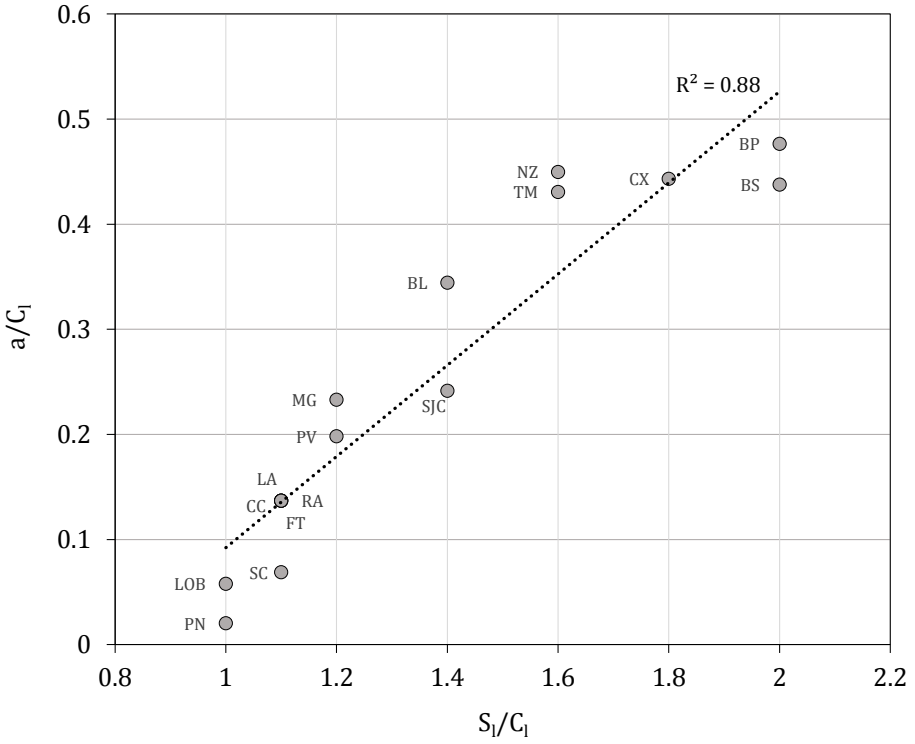

Figure 4.18. Relation between the two criteria used to assess the degree of embayment along the study sites.

The geomorphological framework can be very variable and the present study includes a large sample of beaches that reflects all types of boundary constraints that occur along the study area coast. Figure 4.19 depicts the study sites in terms of typology of beach systems, grouped by type of nearshore (XX axis) and backshore (YY axis) features. The diagram also portrays planform geometry, given by the indentation index, and wave obliquity. The former is represented by the size of the circles, and the latter is portrayed by color, according to legend. It shows that seven types of geomorphological frameworks (among the nine possible) are represented in the dataset, corresponding to several combinations between nearshore and backshore type of features.

Figure 4.19. Typology of beach systems of the study area, grouped by type of nearshore and backshore features. Planform geometry, given by the Indentation index, is proportional to the diameter of the markers. Colors indicate wave obliquity according to legend.

Again, it stands out from the diagram that the more indented beach systems are those that have an exposed rocky platform, regardless of the type of backshore features, or type of lateral boundaries. Conversely, all study sites that don't have a rocky platform and

exhibit nearshore sand bars have smaller values of Indentation Index, below 1.2, with the exception of SJC that has an Indentation Index of 1.4 (Figure 4.18 and Table 4.1). In the study area, platform beaches tend to occur along the more rocky and irregular parts of the coast, where there is small accommodation space, and beaches with sand bars typically occur along the open and unconstrained segments, where alongshore sediment transport through littoral drift encounters no obstacles. Moreover, the lower indentation beaches display smaller wave obliquity values, and therefore are more exposed to the dominant waves. The contrary is not necessarily true and the more indented beaches display a wide range of wave obliquity values. Figure 4.20 shows that there is no evidence of statistical correlation between these two parameters. But it does show that the lower wave obliquity values (< 22.5) are exclusive of the lower indentation (< 1.2) study sites.

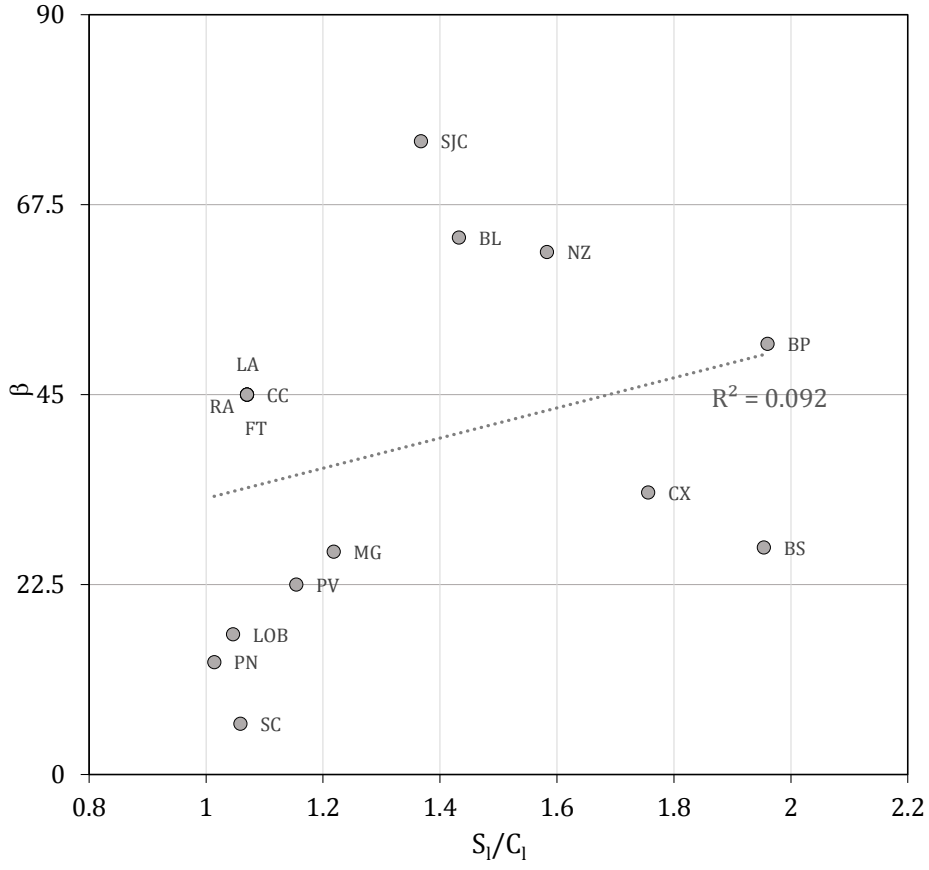

Figure 4.20. Correlation between the indentation index (S_l/C_l) and wave obliquity (β) along the study sites.

The parameters and relationships being defined and explored herein describe the geomorphological framework of the beaches of the study area, but probably apply elsewhere.

4.2 Beach morphology and sediments

Beach morphology was addressed in this study by analyzing beach profiles from which a number of geoindicators were extracted. Geoindicators were considered representative of the beach sampled by the profiles and further used to characterize and quantify aspects of the seasonal behavior of the beaches. The first subchapter presents the site-by-site analysis and the second subchapter portrays the alongshore distribution of the geoindicators along the overall study area.

Beach profiles are depicted as 2D (distance vs elevation) cross-sections, colored by date. The position of the limits used to calculate the geoindicators (volume, width and slope) are represented by lines on the graphic – Coastline; Shoreline (S_{MHW}) and Mean Sea Level (MSL). Two additional graphs depict the variation of the geoindicators through time. Sometimes the data didn't allow for the calculation of the geoindicators, and in these cases the marker is absent and there is a gap in the lines.

Figure 3.4 in Chapter 3. Methods, holds the location of the profile lines monitored at each study site, and might be helpful in the reading of this section of the results.

4.2.1. Study sites

1 Pedras Negras

The two beach profiles monitored at Pedras Negras are typically 50 m wide and contact with an active foredune that reaches 12 m and 14 m above MSL at PPN1 and PPN2, respectively (Figure 4.21 and 4.22). They exhibit very similar geometries with beach-face slope characteristic of intermediate-type beaches, ranging between 0.05 and 0.15. In general, profiles present a concave shape with a gently seaward sloping and ill-defined berm that at times can exhibit a more complex configuration, especially noticeable in PPN1. This configuration of a wider and more sub-horizontal berm usually occurs in March and June, following the winter period. Other than these cases, the beach profile surface changes moderately, and the differences between winter and summer surveys are small, and slightly more evident at PPN2.

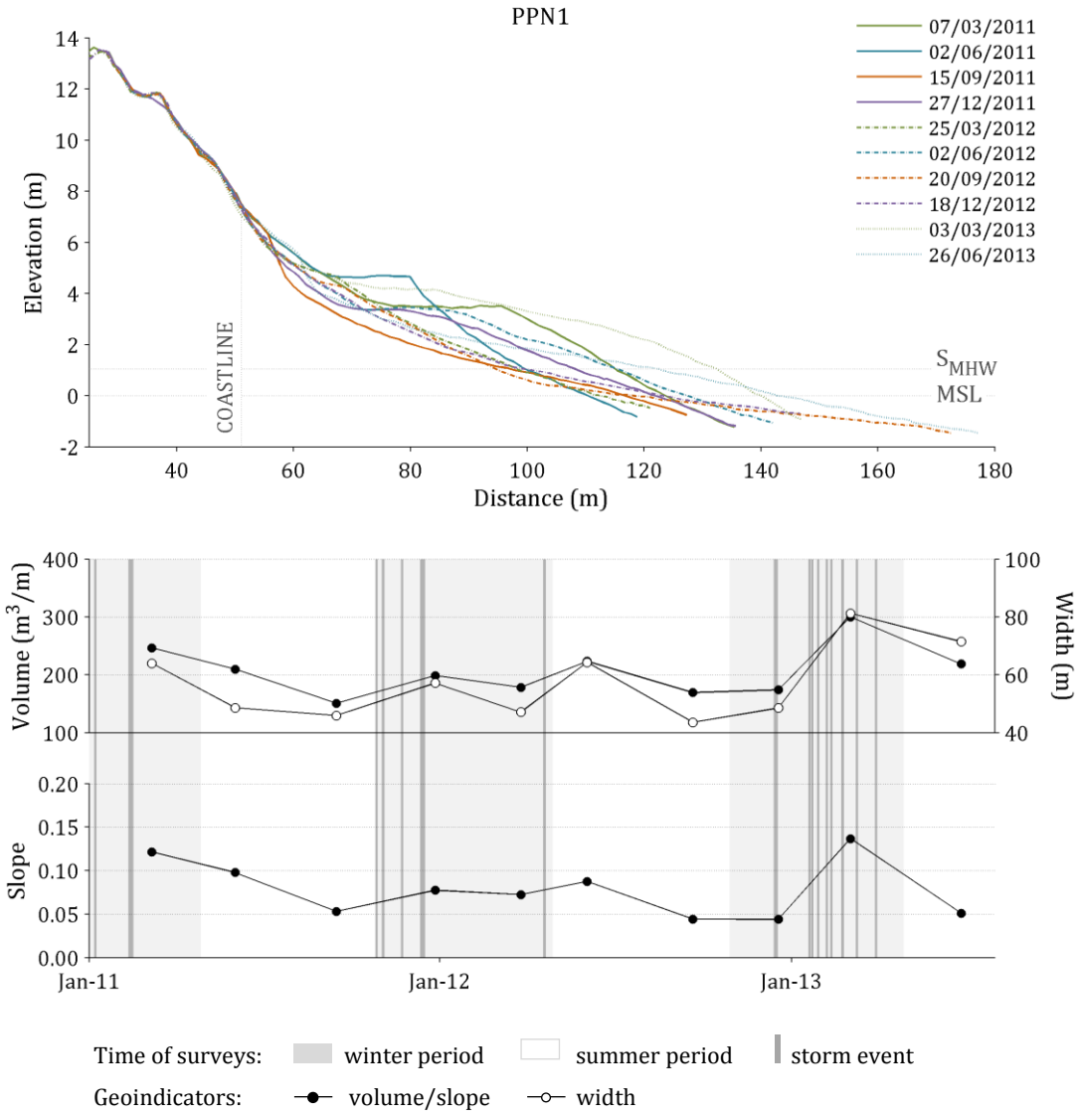

Figure 4.21. Beach profile PPN1 (Pedras Negras study site) and variation of beach geoindicators (volume, width and slope) for the period between March 2011 and June 2013.

Large beach cusps develop, especially during the periods of higher sediment accumulation, and scarps frequently form at the horn of the cusps, where the slope is steepest and in a non-equilibrium state with the incoming waves (Figure 4.23 A). On the other hand, the more frequent, gentle and concave shaped profile facilitate the incursion of wave swash, and high water levels typical of the winter season, easily reach the dune creating scarps that can reach 5 m in elevation (Figure 4.23 B).

The January 2013 winter storm promoted overwash along a 100 m long sector located between PPN1 and PPN2 (Figure 4.24), where the foredune crest lowers to 9 m above MSL. Due to poor GPS signal there are no beach profile surveys from this period to assess

the magnitude of change imposed by this storm, but field observations confirmed that wave swash reached the foredunes at PPN1 and PPN2. The next survey following the storm (March 2013) showed a robust beach with well-developed beach berm at both profiles, corresponding to the peak values for all geoindicators.

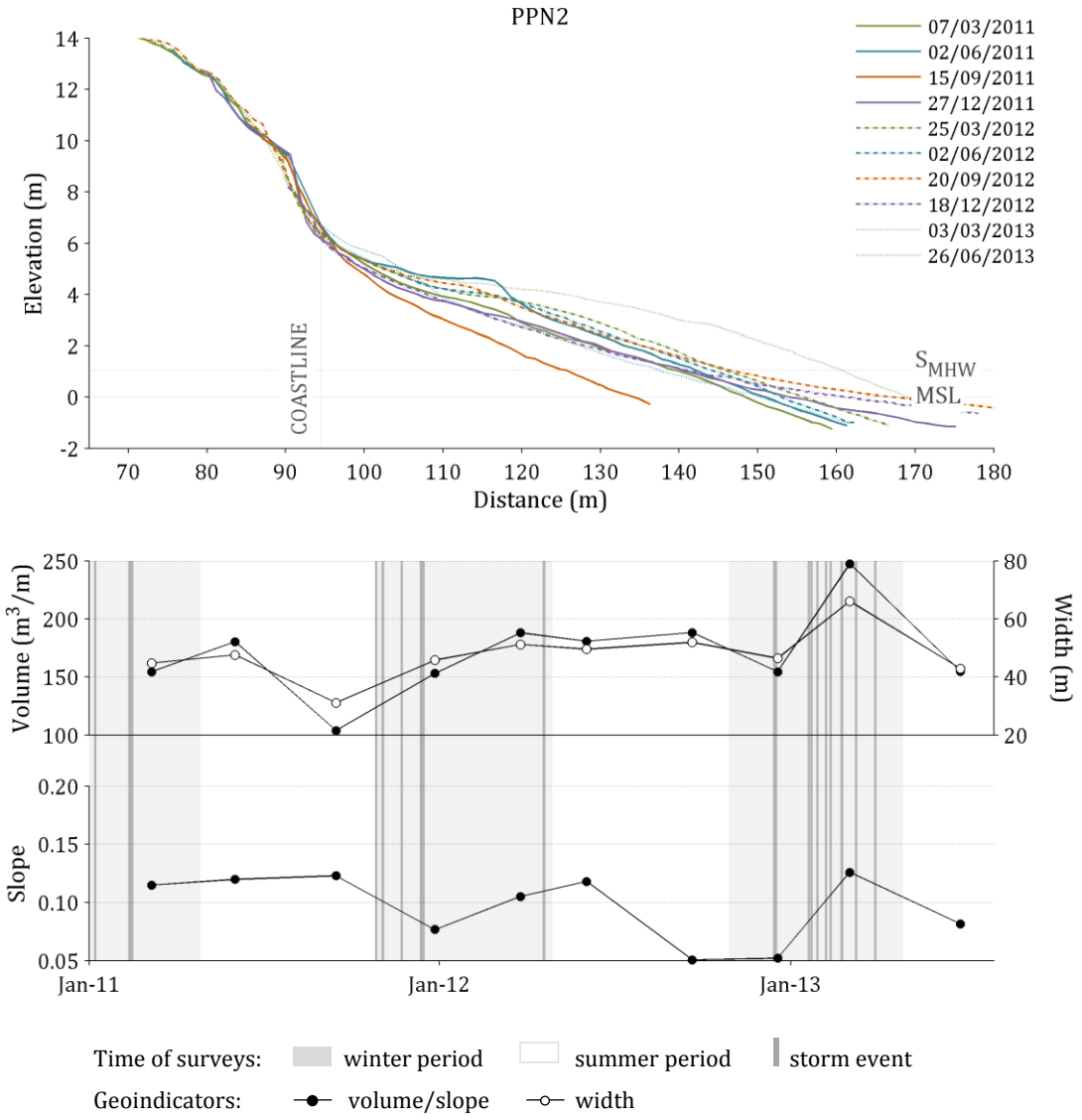

Figure 4.22. Beach profile PPN2 (Pedras Negras study site) and variation of beach geoindicators (volume, width and slope) for the period between March 2011 and June 2013.

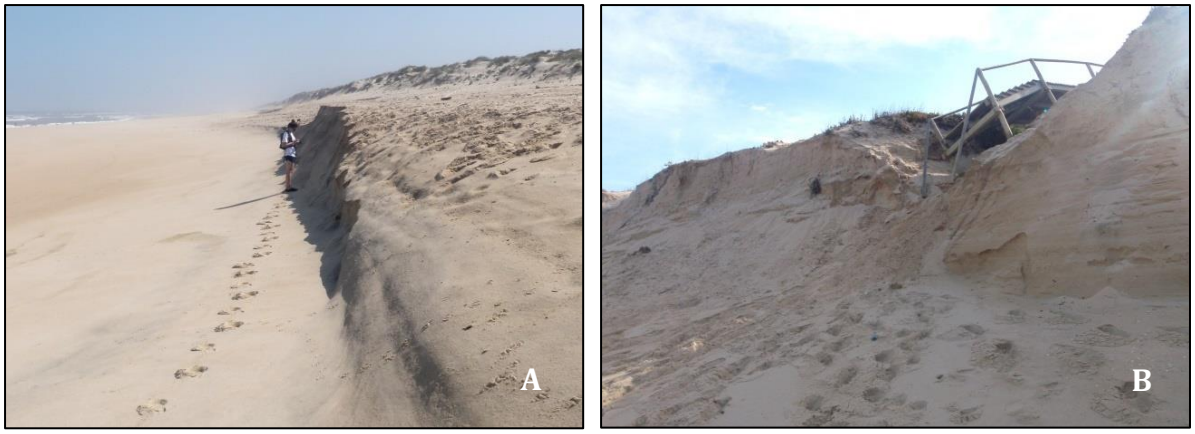

Figure 4.23. A) scarp at the horn of a beach cusp fronting PPN1 on June 26, 2013; and B) dune face scarp at PPN2, on March 7, 2011.

Figure 4.24. Pedras Negras study site. Photograph taken on January 23, 2013 following the Gong storm, and looking north towards PPN1 location. The footprint of the wave swash reach is visible along the seaward face of the foredune (far ground) and overwashing of a dune segment between PPN1 and PPN2 locations is shown in the foreground.

Sediments are characterized by medium to coarse sand on the beach face, varying by about 1 unit of ϕ between surveys (Figure 4.25). The dune sediments are more constant through time and correspond essentially to medium sand. Samples collected on the berm, whenever there was such feature, had an average diameter identical to that of the dune.

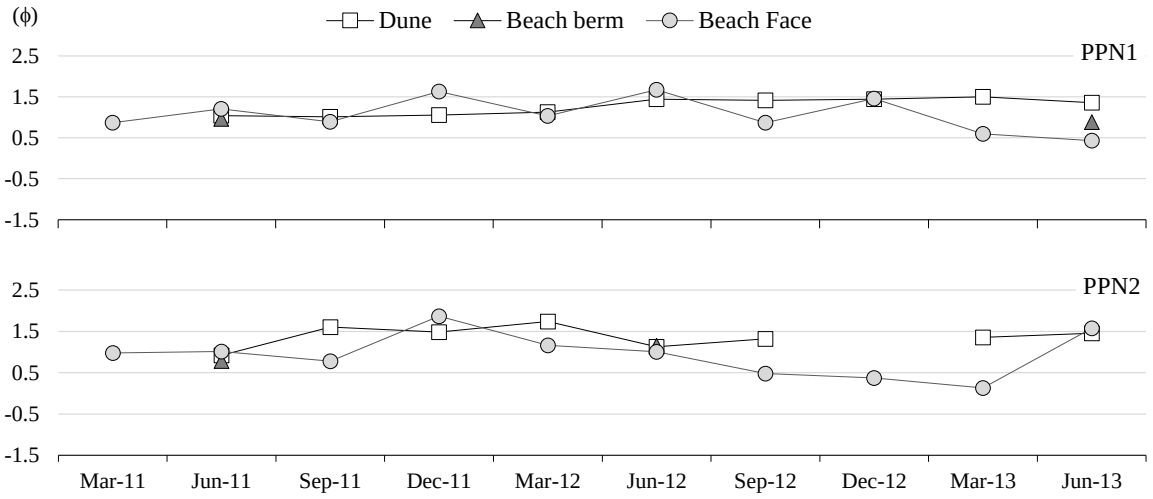

Figure 4.25. Variation of mean grain size for the period between March 2011 and June 2013, for samples taken at the beach face, beach berm and dune at Pedras Negras study site.

The pattern of change observable during the monitored period is that of a peak of sediment accumulation (given by the increase in volume and width) occurring at the end of each winter, indicating quick beach recovery following the more energetic winter season, through the onshore migration of the nearshore bars that exist along this coastal stretch (Figure 4.26) that eventually weld to the dune toe. Typically, by September, the beach profile attains a lower and more concave geometry, in-equilibrium with the relatively more energetic wave regime reaching this site.

Figure 4.26. Photograph taken on March 3, 2013 showing a large swash bar covered with coarser sediments (darker and seaward zone of the exposed beach) welding onto the upper beach, at Pedras Negras study site.

2 Paredes de Vitória

Paredes de Vitória is characterized by concave beach profiles, with beach face slopes characteristic of dissipative/intermediate beaches (Figures 4.27 to 4.29). Summer profiles are generally higher and wider, reaching 100 m and more in width with development of one or two berms. Winter profiles, on the other hand, are typically concave and featureless, characterized by lower surfaces, smaller volumes and widths.

The magnitude of seasonal variations is large, on the order of 100 m^3/m and greater, corresponding to 100% of variation relative to its mean volume in some cases.

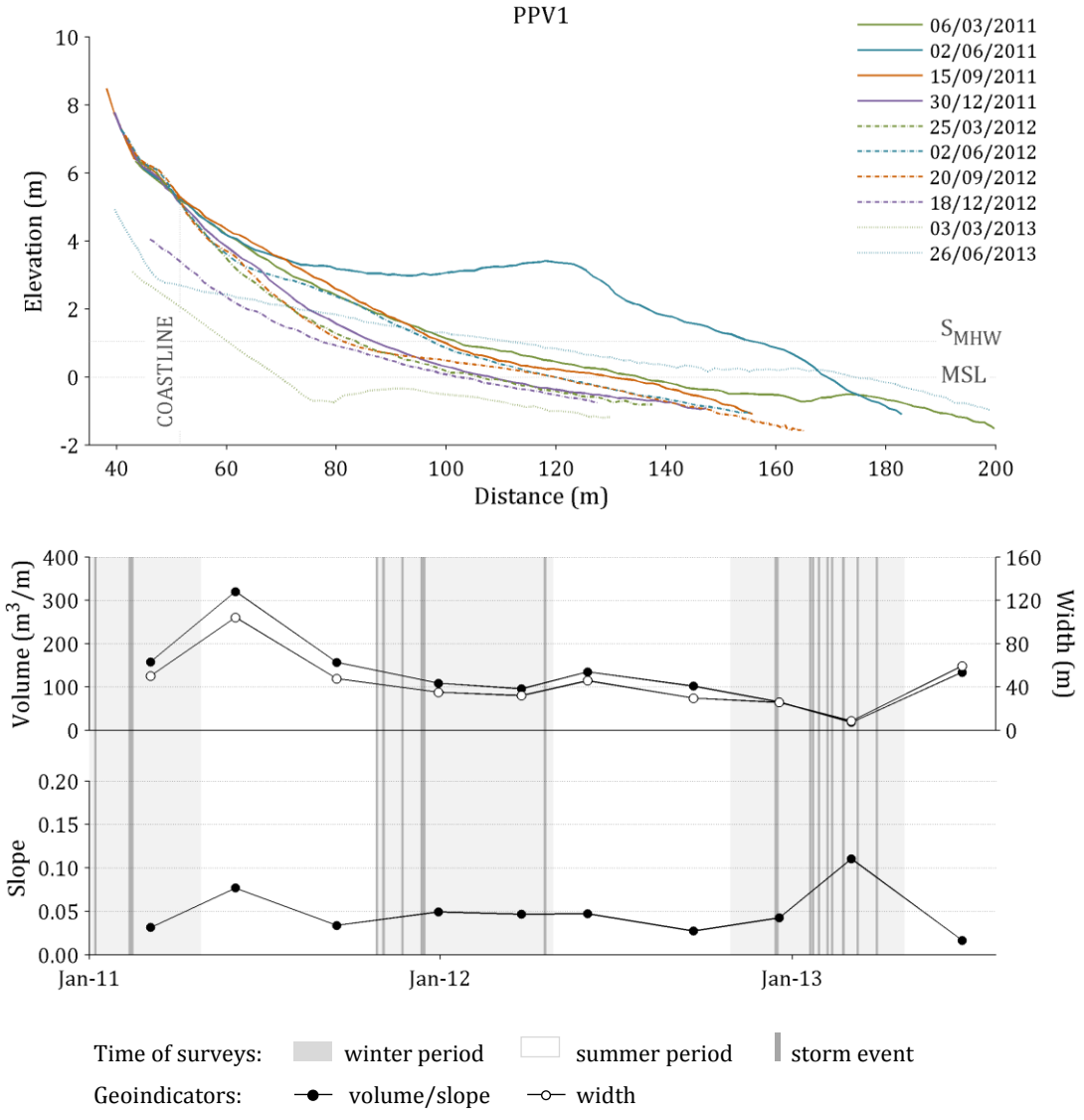

Figure 4.27. Beach profile PPV1 (Paredes de Vitória study site) and variation of beach geoindicators (volume, width and slope) for the period between March 2011 and June 2013.

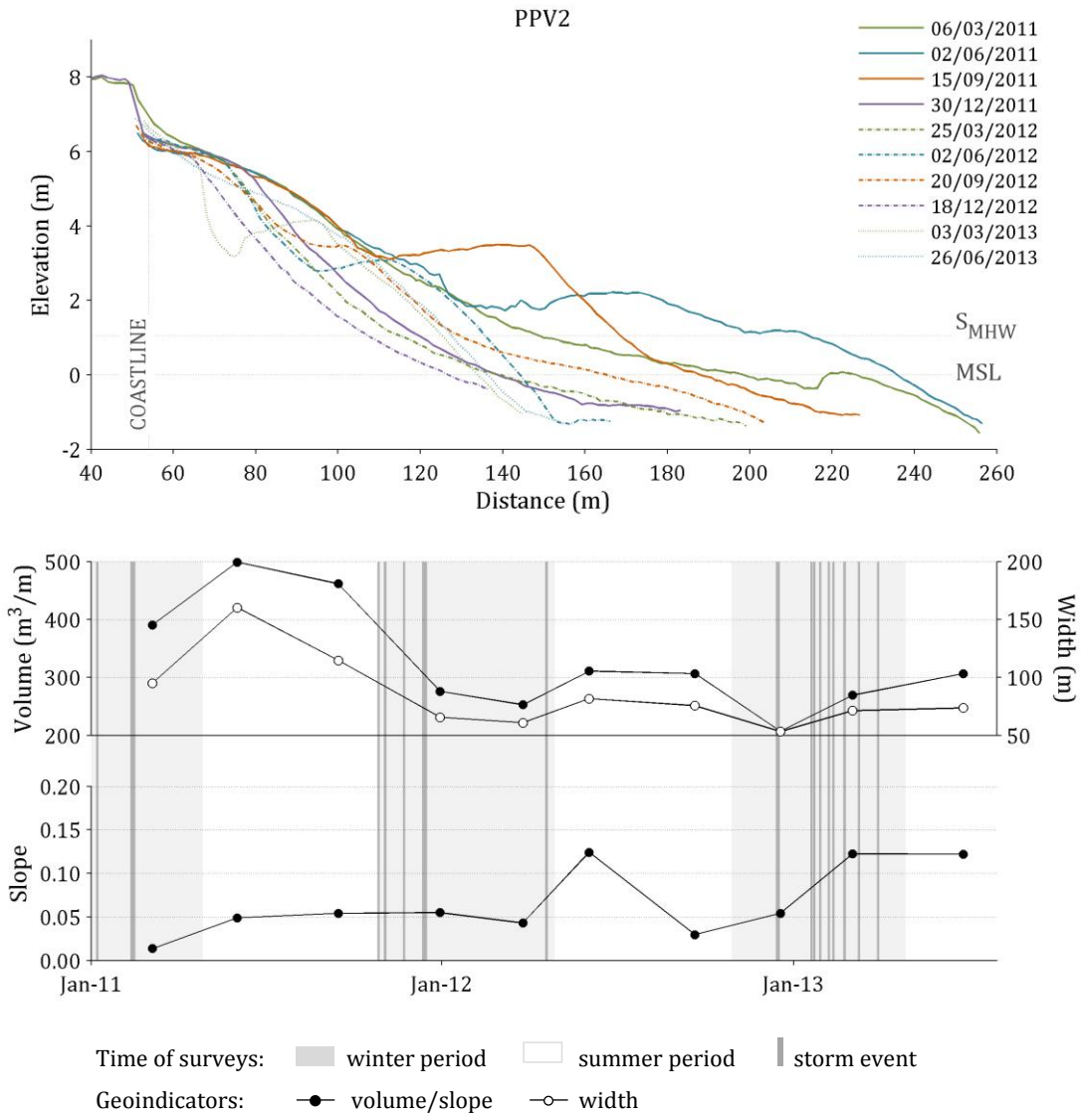

Figure 4.28. Beach profile PPV2 (Paredes de Vitória study site) and variation of beach geoindicators (volume, width and slope) for the period between March 2011 and June 2013.

Beach berm development is not synchronous in all profiles. There is a gradient of berm development between profiles that indicates longshore sediment transfer along the embayed beach, especially noticeable during the summer months, when sediment is brought onshore and the beach grows considerably. The early 2013 winter storm period promoted severe sediment loss in profile PPV1, leaving the subaerial section of the beach limited to a minimum volume and lowest width of the whole exposed beach (the lowest of the overall study period). The other two profiles had already suffered sediment loss and surface lowering in the previous months, particularly during the December 2012 storms, that had little effect on the other study sites, but promoted intense changes on the upper beach along Paredes de Vitória.

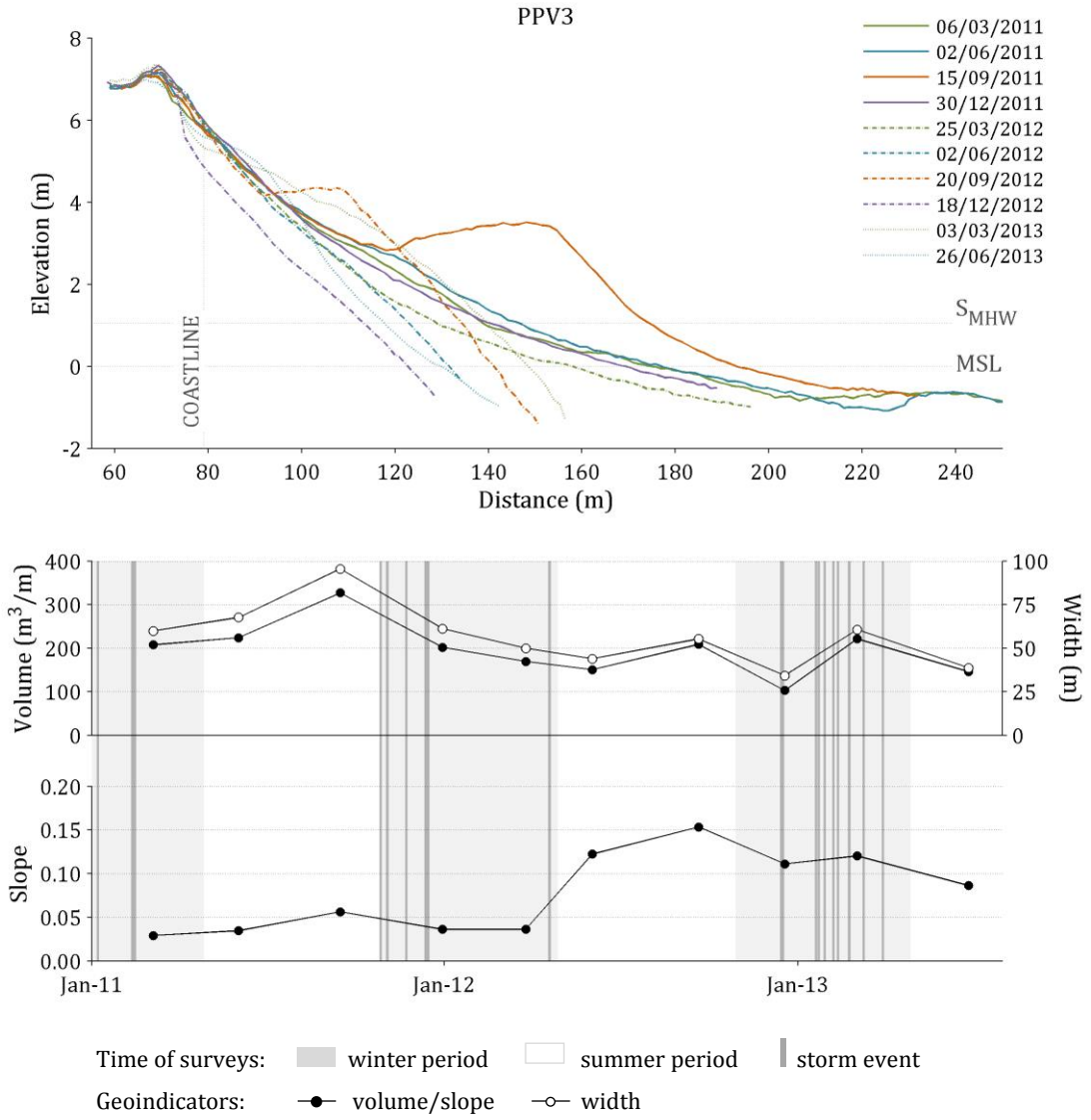

Figure 4.29. Beach profile PPV3 (Paredes de Vitória study site) and variation of beach geoindicators (volume, width and slope) for the period between March 2011 and June 2013.

Figure 4.30 shows some aspects of the scarps created in December 2012, in some cases resulting in damage to the beach infrastructure and access routes in the central part of Paredes de Vitória. Again, the recovery along the beach was not simultaneous, and by March 2013 the beach profiles showed very different configurations. The middle and southernmost profiles already showed signs of recovery through onshore migration and welding of nearshore bars (swash bars), whereas the northern sector (PPV1) only started to recover by June 2013.

Figure 4.30. Beach scarps formed along Paredes de Vitória upper beach area following the December 2012 storms. Central sector (PPV2) in panels A and B; northern sector (PPV1) in panel C; and southern sector (PPV3) in panel D.

The sediments of the beach face at Paredes de Vitória are variable in mean grain size, alternating between medium sand and coarse sand in the PPV1 profile, between medium sand and gravel in the PPV2 profile, and medium sand and very coarse sand in the PPV3 profile (Figure 4.31). In contrast, the sediments of the berm and dune correspond essentially to medium sand (slightly finer in the dune) at all three profiles, with rare exceptions of fine sand in the dune at PPV3 and coarse sand on the berm at PPV1 and PPV2 profiles. The presence of coarser sediments on the beach berm at the central profile (PPV2) may be associated with the proximity to the Ribeira de Paredes stream.

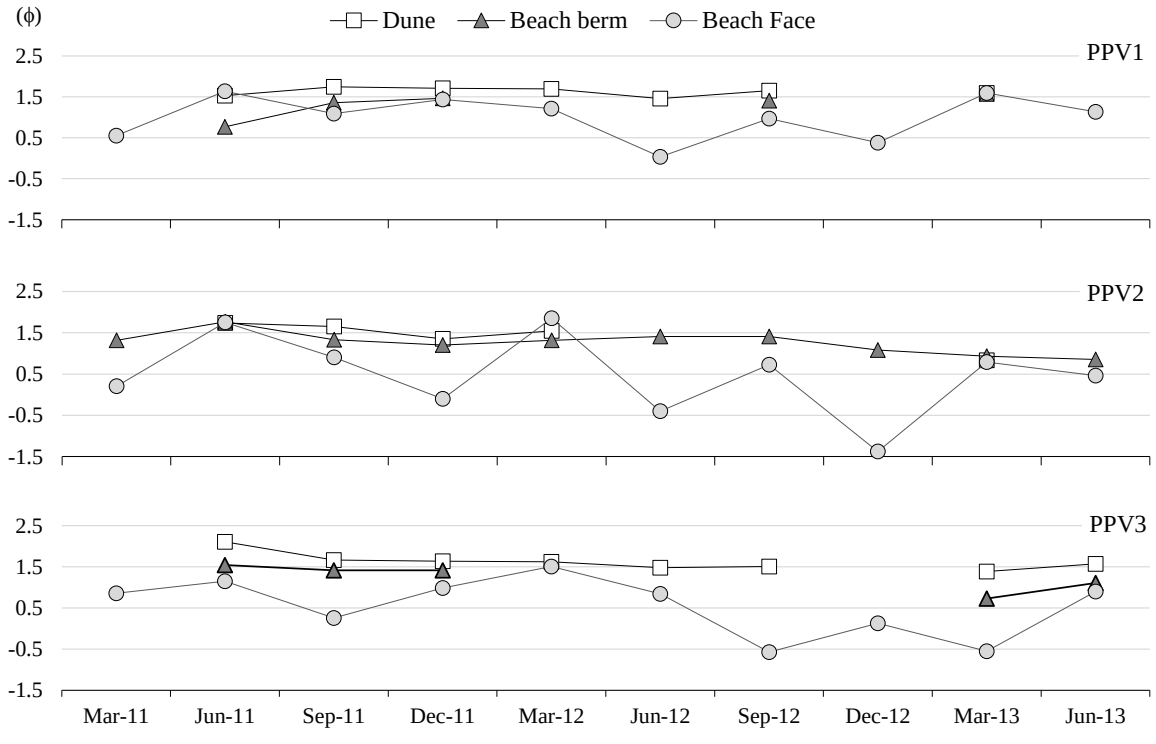

Figure 4.31. Variation of mean grain size for the period between March 2011 and June 2013, for samples taken at the beach face, beach berm and dune at Paredes de Vitória study site.

3 Nazaré

The beach at Nazaré is of reflective type, characterized by a steep beach face, with slopes ranging between 0.11 and 0.18, lowering to a minimum of 0.07 in a post-storm situation (Figures 4.32 to 4.34). Typically, two beach berms are present, reaching widths between 70 m and 140 m, and exhibiting a large beach cusp system of decameter amplitude, more prominent in the central and southern sectors of the bay. The landwardmost berm is a stable feature, and changes in this area are mainly induced by anthropic action, through mechanical leveling for recreational purposes. PNZ3, in the southernmost sector is an exception because of the existing small dune field that is left to grow naturally. This berm develops between 5.5 m elevation (relative to MSL) and 8 m where it contacts with the seawall. At the northermost sector of the bay (PNZ1) however, this berm develops at lower elevations, reaching a maximum of 6 m at the contact with the seawall. The second, seawardmost beach berm is more mobile and may be as low as 3.5 m (above MSL) at the berm crest.

The beach face is fairly constant in slope over time and advances seaward or retreats in tune with the growth or retreat of the beach berm. Maximum shift between consecutive surveys was of 10 m and a maximum of 20 m was measured throughout the overall study period. The exception is the early 2013 post-storm situation, wherein the shoreline migrated 30 m inland at all profiles.

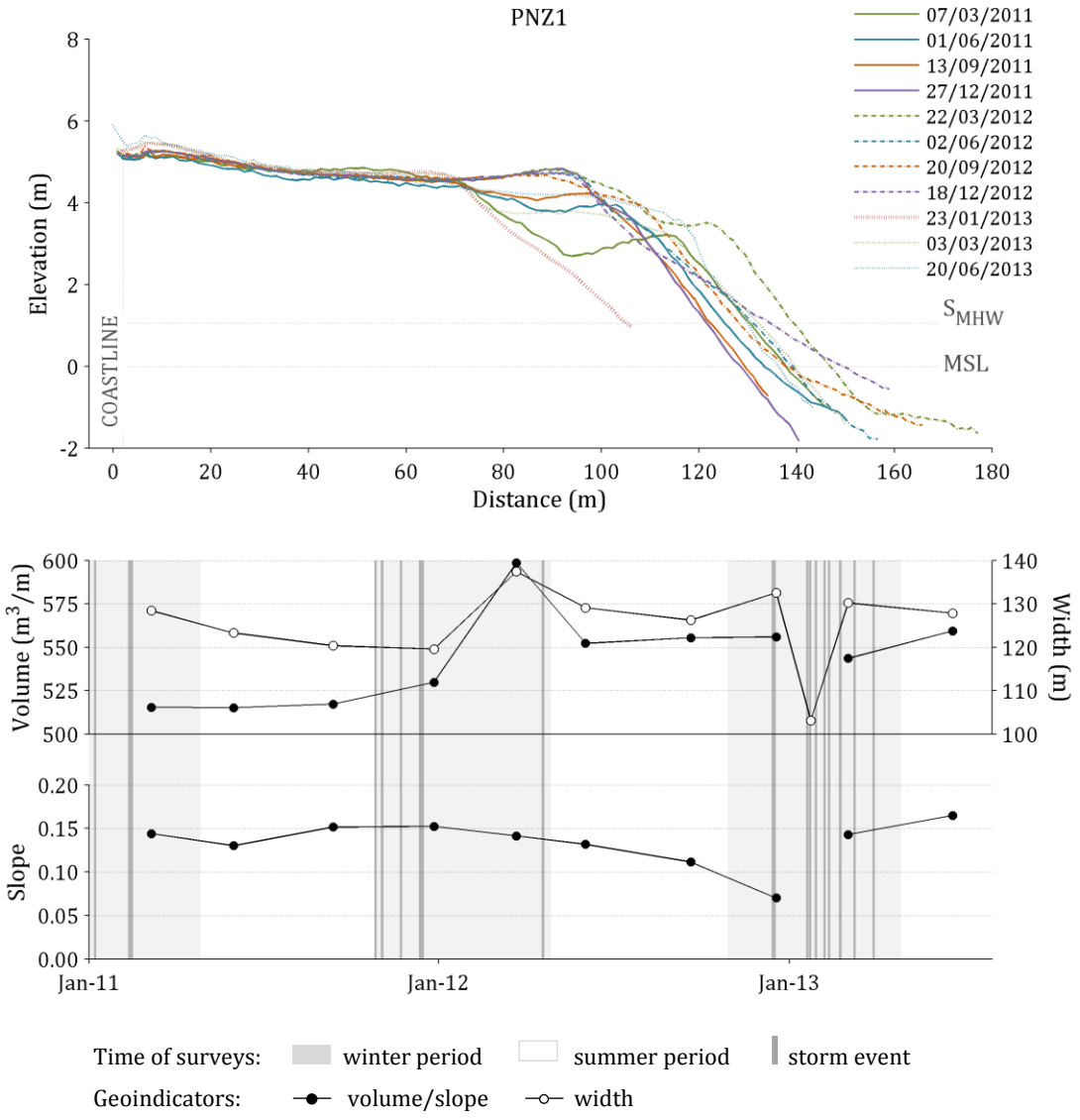

Figure 4.32. Beach profile PNZ1 (Nazaré study site) and variation of beach geoindicators (volume, width and slope) for the period between March 2011 and June 2013.

The early 2013 storm period, produced the lowest of all profile surfaces along the three monitored profiles. Furthermore, overtopping of the seawall occurred along the section between PNZ1 and PNZ2, resulting in beach sediment transport onto the seawall and adjacent road, and destruction of several beach equipment (Figure 4.35). By March 2013 the beach had recovered and the three profiles exhibited configurations similar to those previous to the storm.

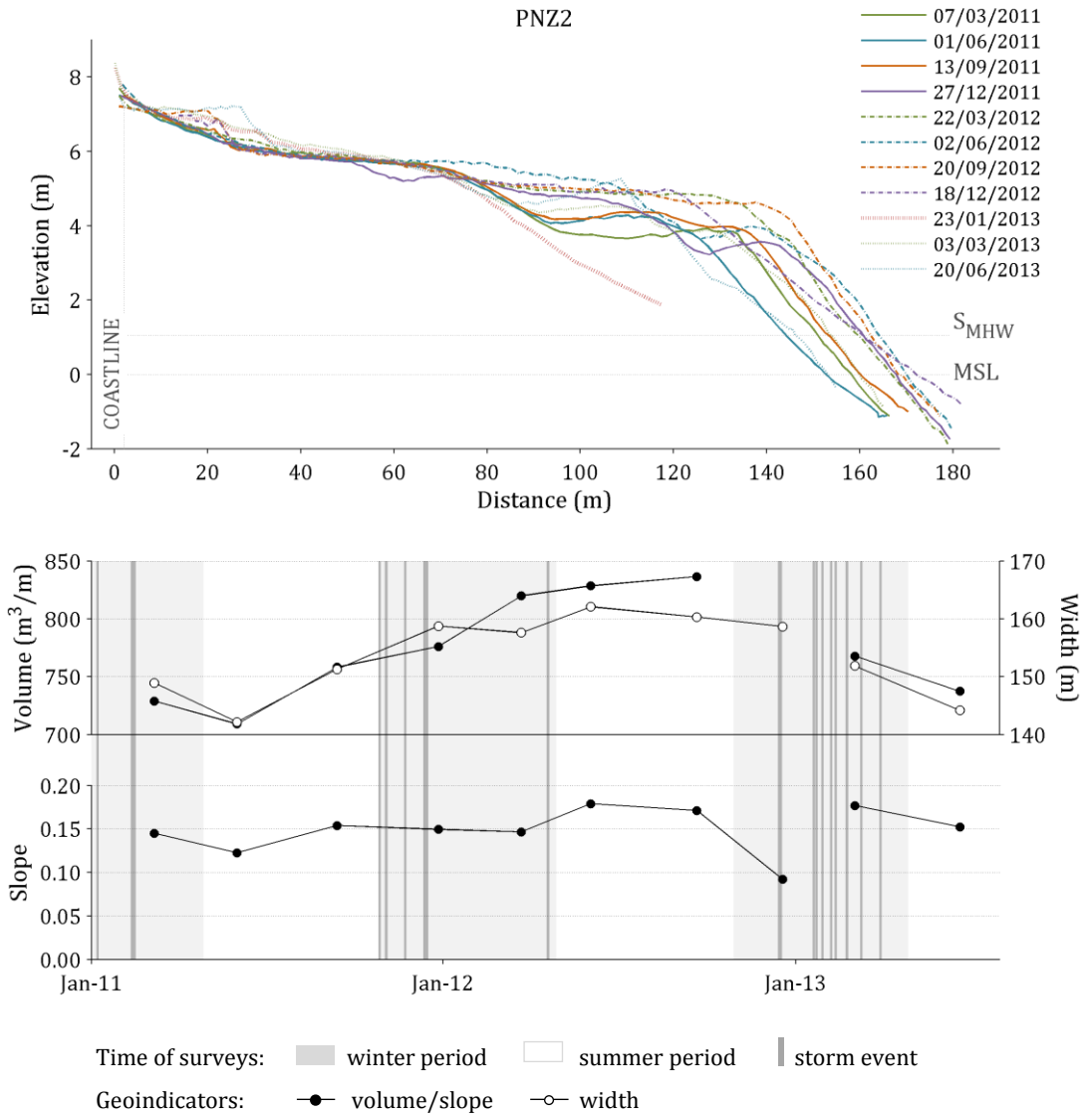

Figure 4.33. Beach profile PNZ2 (Nazaré study site) and variation of beach geoindicators (volume, width and slope) for the period between March 2011 and June 2013.

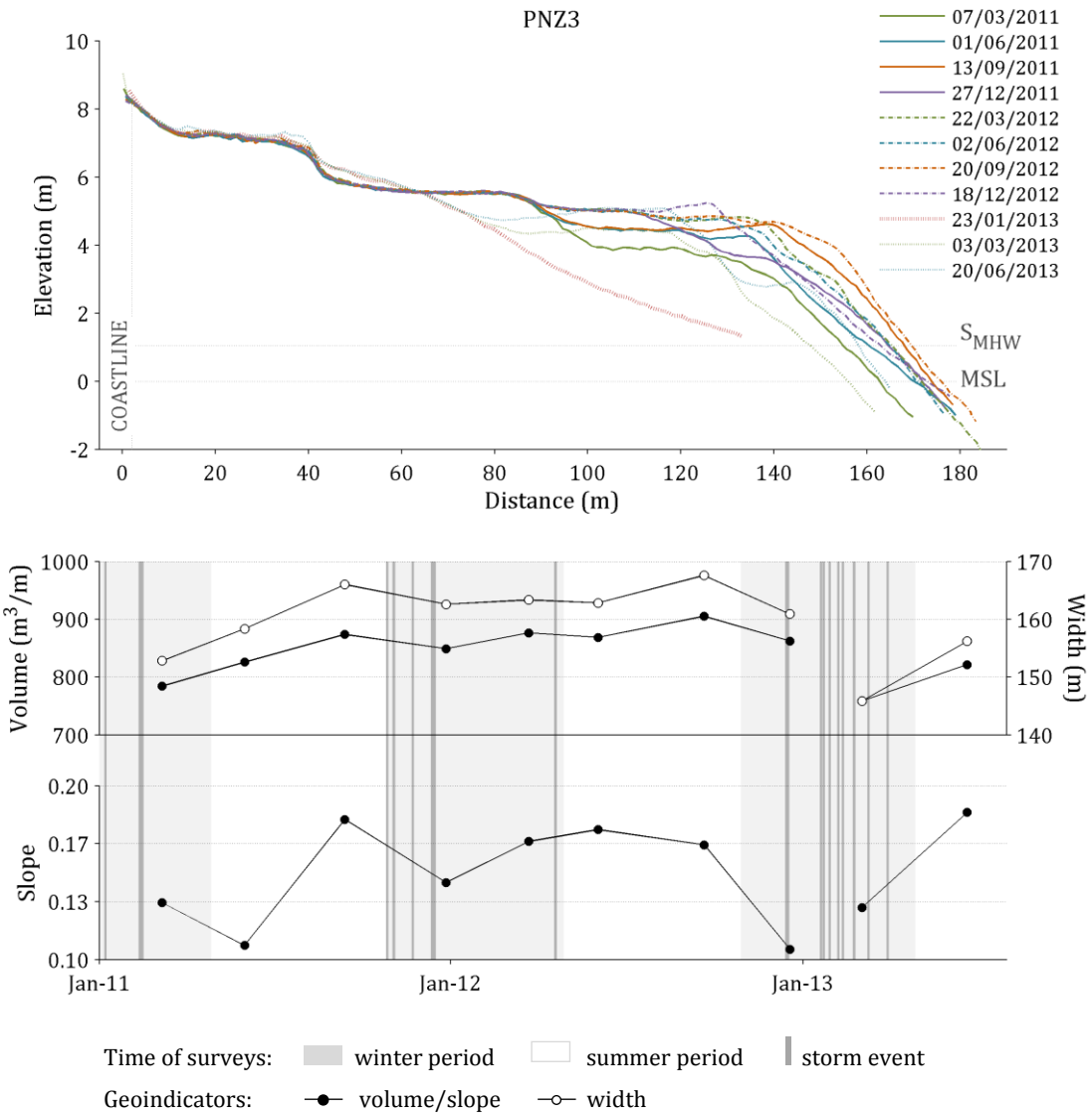

Figure 4.34. Beach profile PNZ3 (Nazaré study site) and variation of beach geoindicators (volume, width and slope) for the period between March 2011 and June 2013.

The Nazaré beach is very stable at the seasonal and annual scales, showing only significant changes when affected by storms with particular characteristics, that induce overwash of the beach berm and overtopping of the adjacent seawall (cf. Silveira et al., 2016 for description of overwash-inducing storms). The singular setting of this embayment, at the head of the Nazaré canyon, makes it particularly vulnerable to higher waves that reach the beach with small dissipation of energy in the mearshore domain. The January 2013 storm recorded very high waves and induced the most intense changes. Still, the beach recovered quickly (within a month's time) its previous ad typical configuration and width.

Figure 4.35. Upper beach area and seawall looking north towards PNZ2 profile location on January 20, 2013, following the Gong storm event.

The process of destruction and reconstruction of the second berm seems to determine the morphodynamic behavior of this beach, althoug there was no evidence of a repetitive pattern during the three years of monitoring. The three monitored sectors showed similar behavior, suggesting that there is no significant longshore transport along the bay.

The sediments of Nazaré beach vary in time and space between medium and very coarse sand (Figure 4.36). The permanency of a well-developed plunge-step, and the presence of beach cusps potentiate the accumulation of the coarser sediments that are detected in the record. The dune sediments at PNZ3 are very constant and correspond essentially to medium sand.

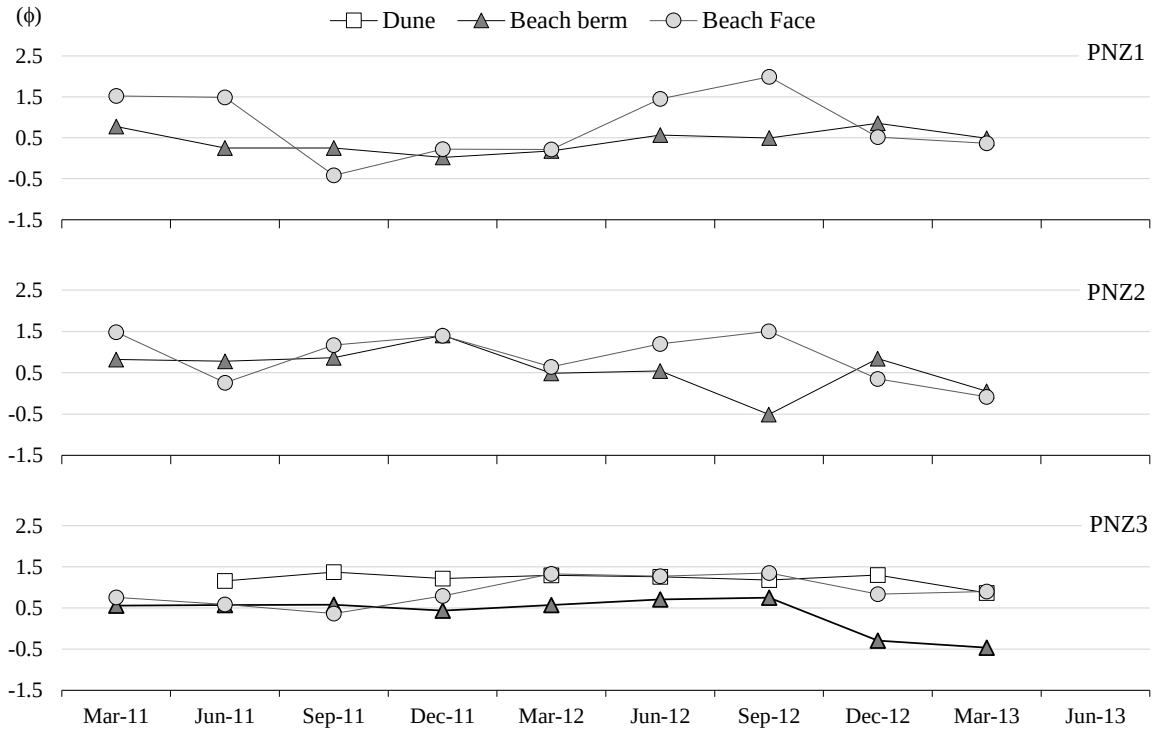

Figure 4.36. Variation of mean grain size for the period between March 2011 and June 2013, for samples taken at the beach face, beach berm and dune at Nazaré study site.

4 Lagoa de Óbidos - Baleal

Due to the weak GNSS signal closer to the cliffs that make up most of the Lagoa de Óbidos-Baleal coastal stretch, many of the surveys of the three northernmost profiles did not reach the base of the cliff. Therefore, geoindicator measurements were made taking into account the maximum landward limit common to most of the surveys, around 10 to 20 m seaward of the actual coastline.

From north to south, there is a gradient in the volumes of the beach. The volume and width increases, and the variability of the beach profile decreases from PLOB1 to PLOB4 (Figures 4.37, 4.38, 4.40 and 4.41). The northernmost half of this sector (PLOB1 and PLOB2) is characterized by slopes typical of intermediate morphodynamic stages, around 0.07, with presence of alongshore swash bars that can reach more than 50 m in length (Figure 4.39A). These bars migrate toward the shore and offshore (as seen in some cross-sections) but seldom seem to connect with, or further migrate across the subaerial beach, and berm development is rare. The typical beach section presents a constant sloping surface that scarcely reaches 4 m at PLOB1 and 5 m at PLOB2.

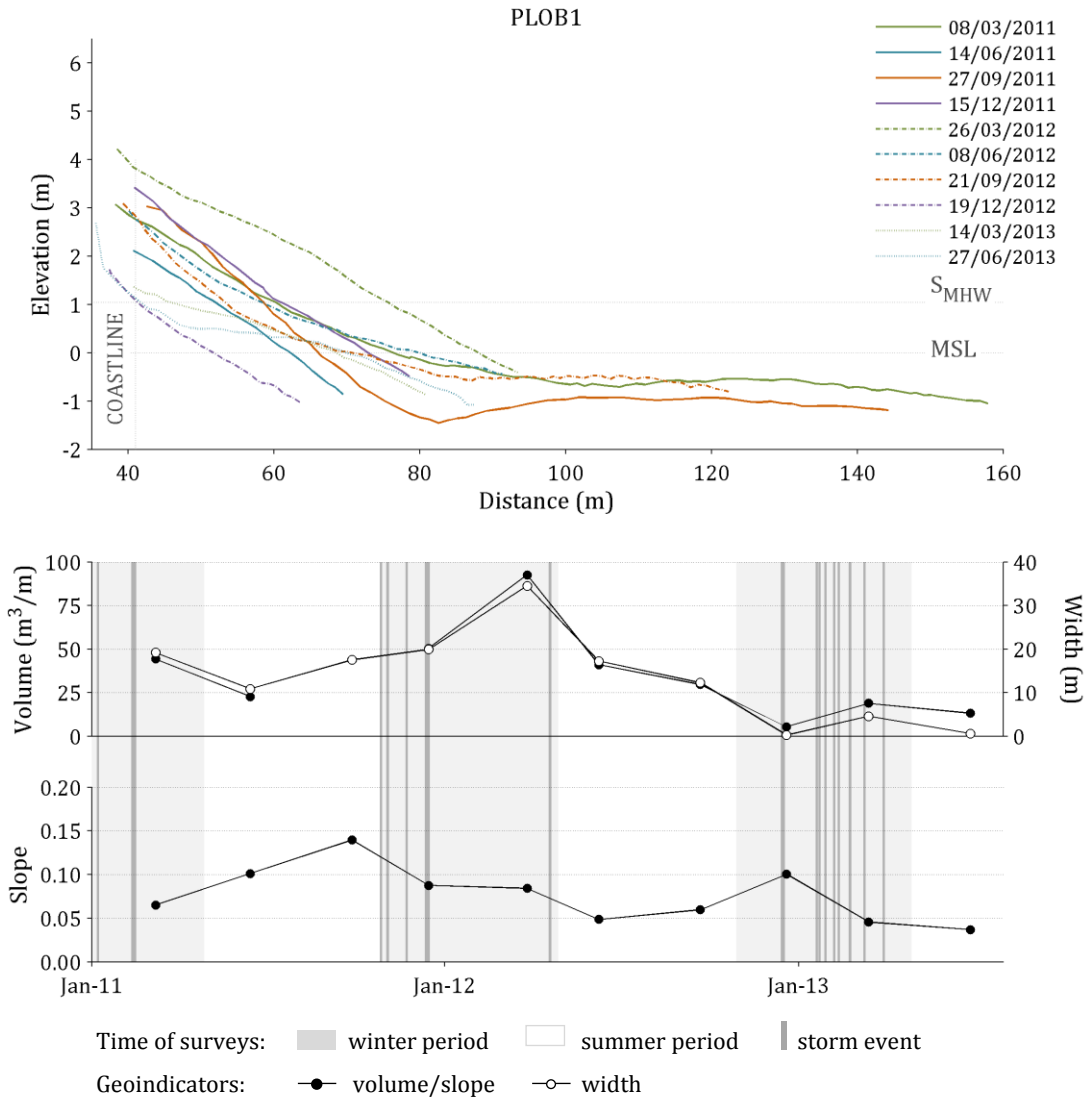

Figure 4.37. Beach profile PLOB1 (Lagoa de Óbidos-Baleal study site) and variation of beach geoindicators (volume, width and slope) for the period between March 2011 and June 2013.

The low and narrow beach surface, combined with the energetic wave regime that reaches this stretch of the coast, results in water levels easily reaching the base of the cliff, and explains frequent cliff collapse and landslides in this area (Figure 4.39B). Beaches vary considerably at the seasonal time scale, reaching minimum volumes of 5 m^3/m and 30 m^3/m at PLOB1 and PLOB2, and exhibiting differences in elevation at their landward limit of 3 m and 2.5 m, respectively. At PLOB1, the featureless and gently sloping beach widens and shrinks without developing any prominent feature, other than the beach face, and showing no apparent cyclicity or seasonality. PLOB2 however, develops higher berms in the summer, and more flattened and featureless profiles during the winter. The exception is the 2013 summer profile that is extremely low.

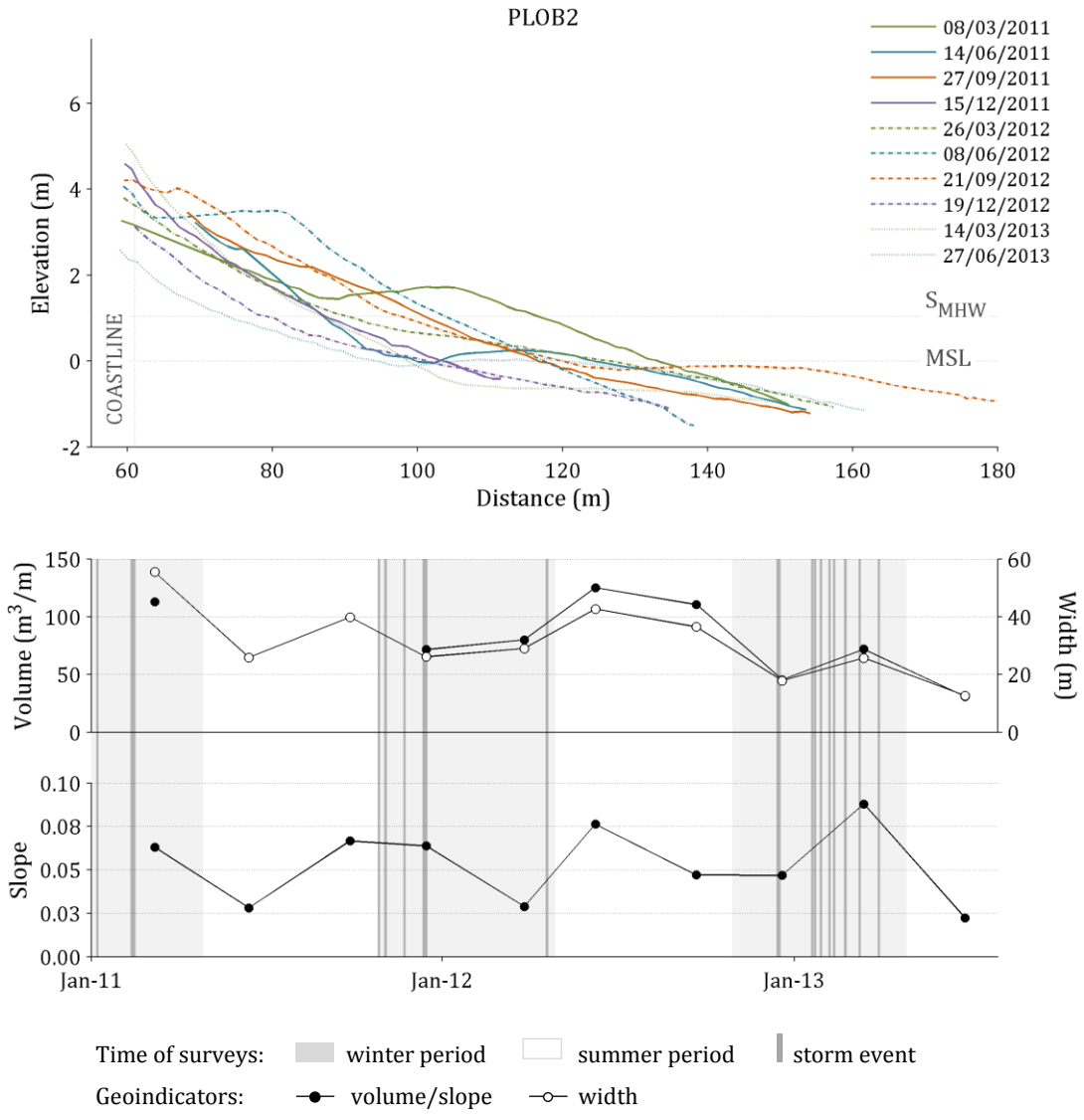

Figure 4.38. Beach profile PLOB2 (Lagoa de Óbidos-Baleal study site) and variation of beach geoindicators (volume, width and slope) for the period between March 2011 and June 2013.

The southernmost profiles, PLOB3 and PLOB4, are much more dissipative in terms of beach slope, characterized by average slopes of 0.03 and 0.02, respectively. Beaches are progressively wider southward, reaching a maximum of 64 m at PLOB3 and 100 m at PLOB4. Still, the upper beach area is low, and doesn't build above 4.3 m. Variations of the beach surface are smaller and the profiles are much more stable trough time than those from the northernmost beaches. Except for a few occurrences of a berm feature, both profiles exhibit linear cross-sections characterized by a relatively constant-sloping surface. PLOB4 lower beach face contacts with a rocky platform, normally exposed during low-tide, and therefore there are no substantial changes or morphologic features developing at the lower intertidal area of the beach profile (Figure 4.42).

Regarding PLOB3 and PLOB4, the only evidence of a season-related behavior is that berm development mainly occurs during the summer season, translating into a modest increase in volume and width of the beach profiles towards September. There are exceptions in both cases, where berm development was detected at one of the winter profiles.

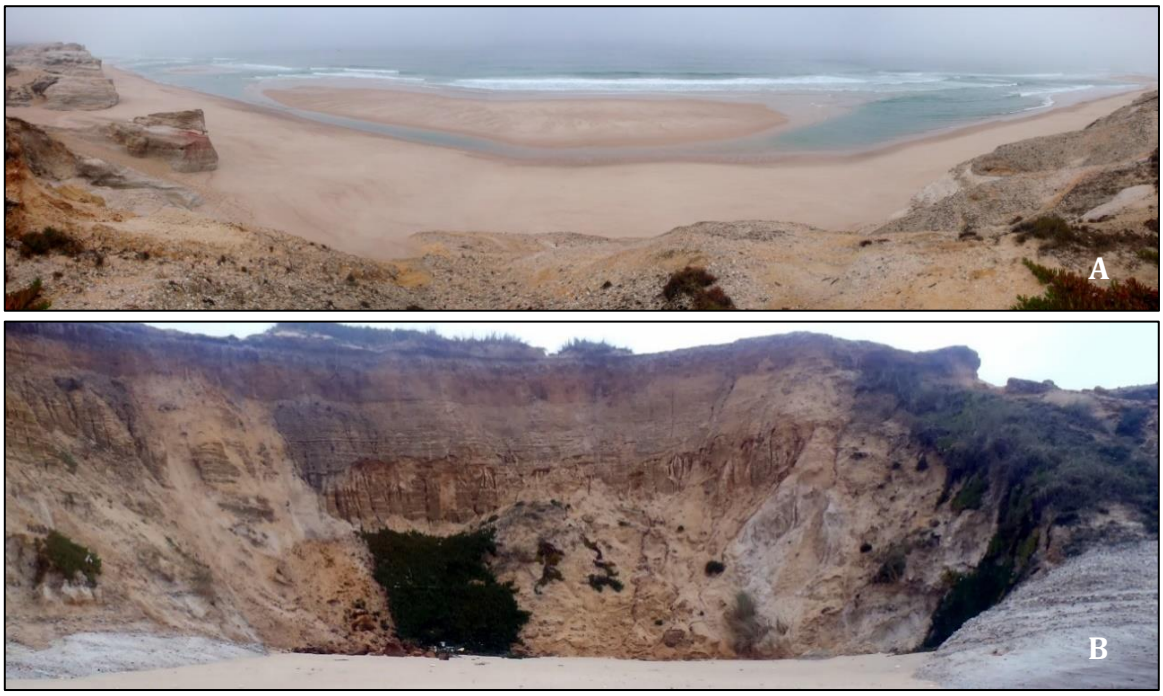

Figure 4.39. Some characteristics of the PLOB1 area (Rei do Cortiço beach): A – longshore bar disposed parallel to the coast and gaps created by rip currents (photo from September 27, 2011); and B – accumulation of cliff deposits originated from a landslide c. 25 m wide (photo from December 19, 2012).

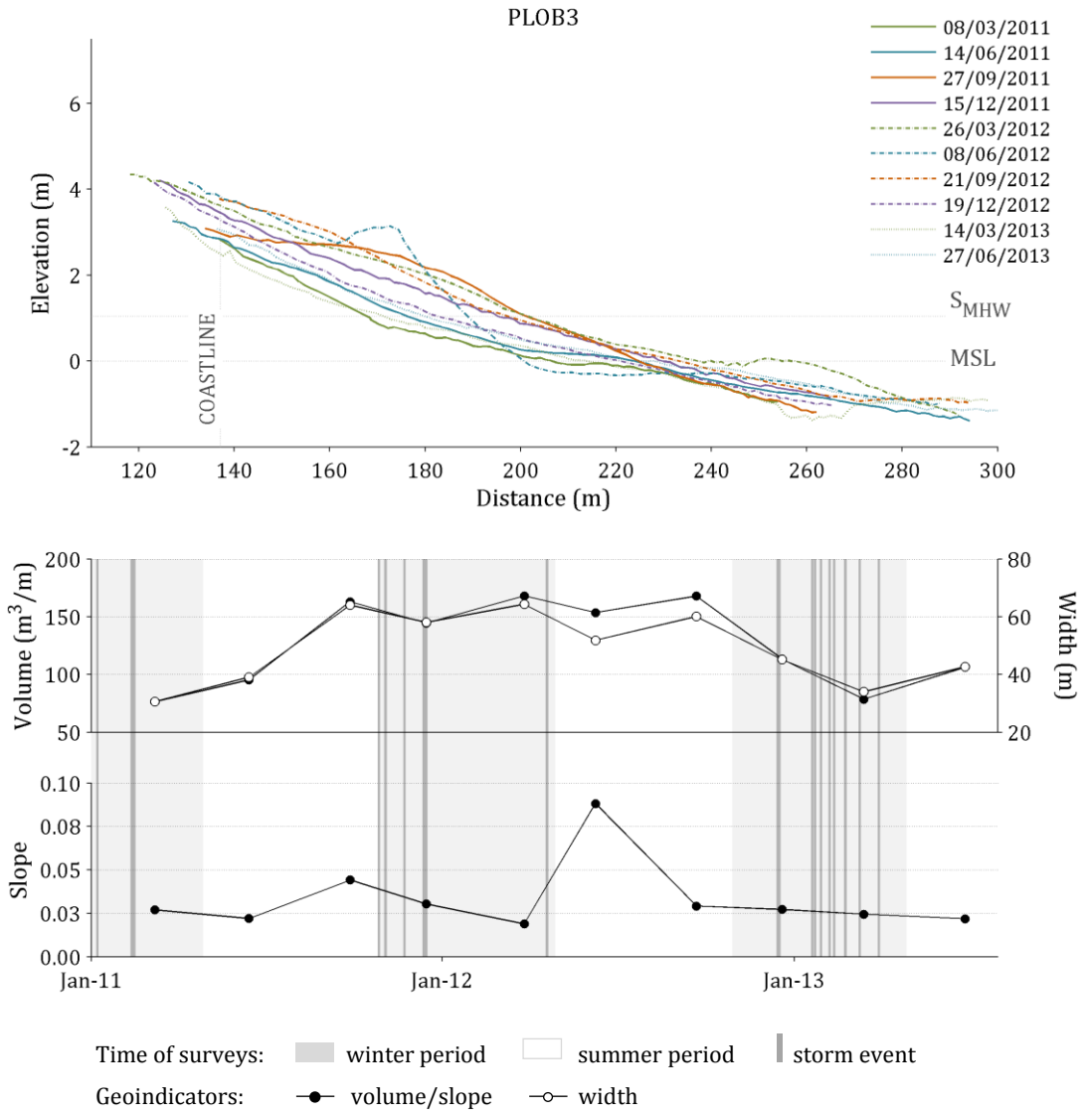

Figure 4.40. Beach profile PLOB3 (Lagoa de Óbidos-Baleal study site) and variation of beach geoindicators (volume, width and slope) for the period between March 2011 and June 2013.

All profiles of the LOB study site had a lowering of the beach surface at the end of 2012 following the early December storm and this was accompanied by volume and width decrease. In particular, PLOB1 experienced significant sediment removal that left uncovered wave-cut notches at the base of the cliff (Figure 4.43).

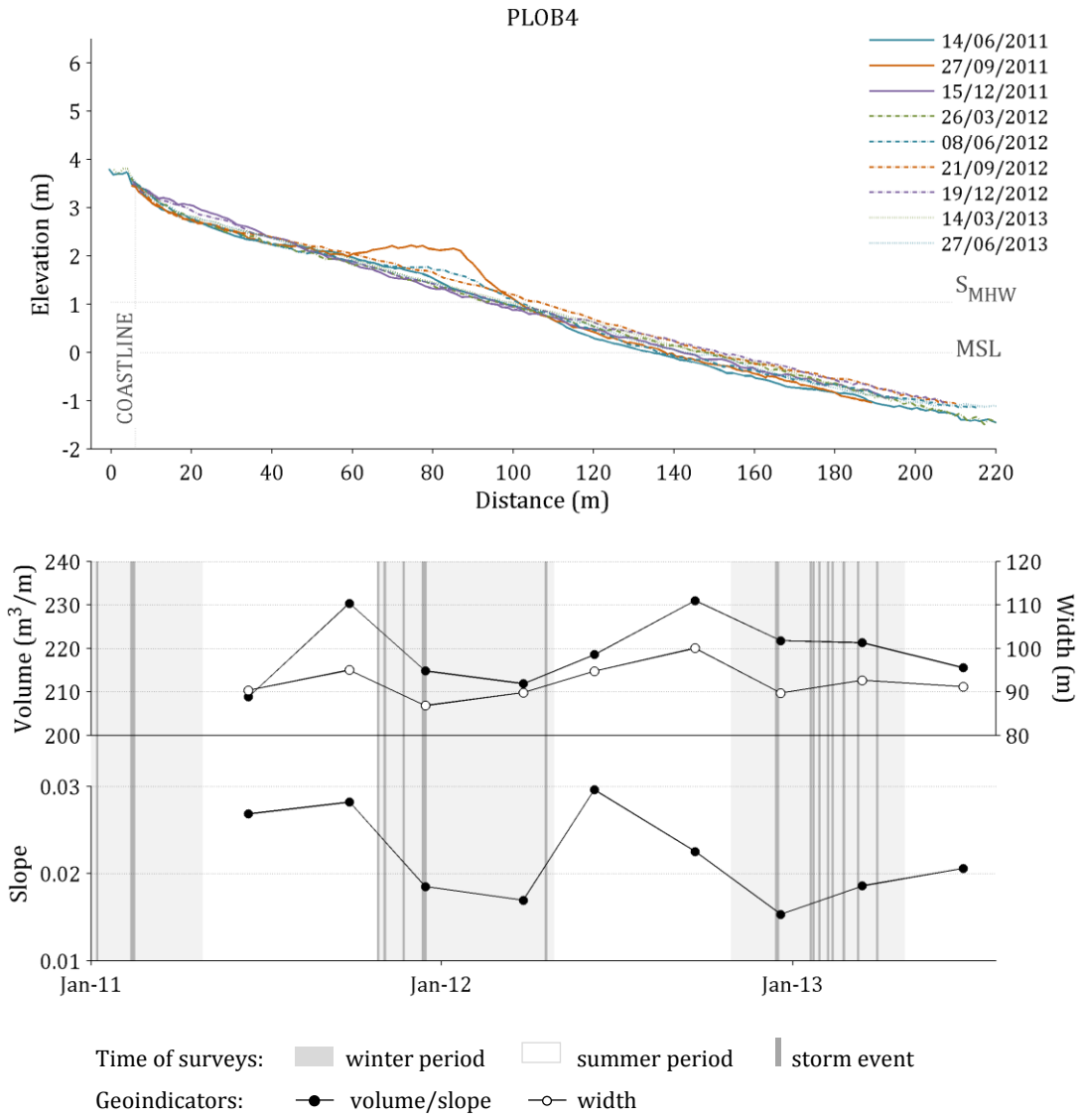

Figure 4.41. Beach profile PLOB4 (Lagoa de Óbidos-Baleal study site) and variation of beach geoindicators (volume, width and slope) for the period between March 2011 and June 2013.

The LOB study site exhibits a gradient in morphological behavior associated to the variations in geomorphological framework and wave regime reaching this area. From north to south, beaches are generally more stable and more robust, and the three years monitoring suggest a discreet seasonal pattern related to berm feature development during summer. The northernmost sector is more exposed to the incoming wave regime and thus more prone to changes caused by storms.

Figure 4.42. Aerial photograph from September 22, 2009, looking south towards the southernmost sector of the Lagoa de Óbidos-Baleal study site (the Baleal-Peniche sector in the background). PLOB4 characterizes the embayed beach making the northward façade of the Baleal tombolo. The rocky platform is exposed at low-tide. Source: SIARL, 2013.

Figure 4.43. Wave cut notches exposed at Rei do Cortiço beach (PLOB1 location).

The sediments of the Lagoa de Óbidos-Baleal coastal stretch decrease in mean diameter from north to south – average of 0.92, 0.76, 1.34, 2.03 ϕ for PLOB1, PLOB2, PLOB3 and PLOB4, respectively (Figure 4.44). The two northern profiles are more variable in terms of sediment grain size that ranges from medium sand to very coarse sand, whereas PLOB3 sediments vary about 1 phi unit centered on medium sand, and PLOB4 sediments are practically invariable, between medium and fine sand. The berm sediments, when present, are practically identical to those of the beach face. The variation in grain size is compatible with a more energetic environment to the north (also associated to more frequent dismantling of the cliffs) and more sheltered conditions to the south.

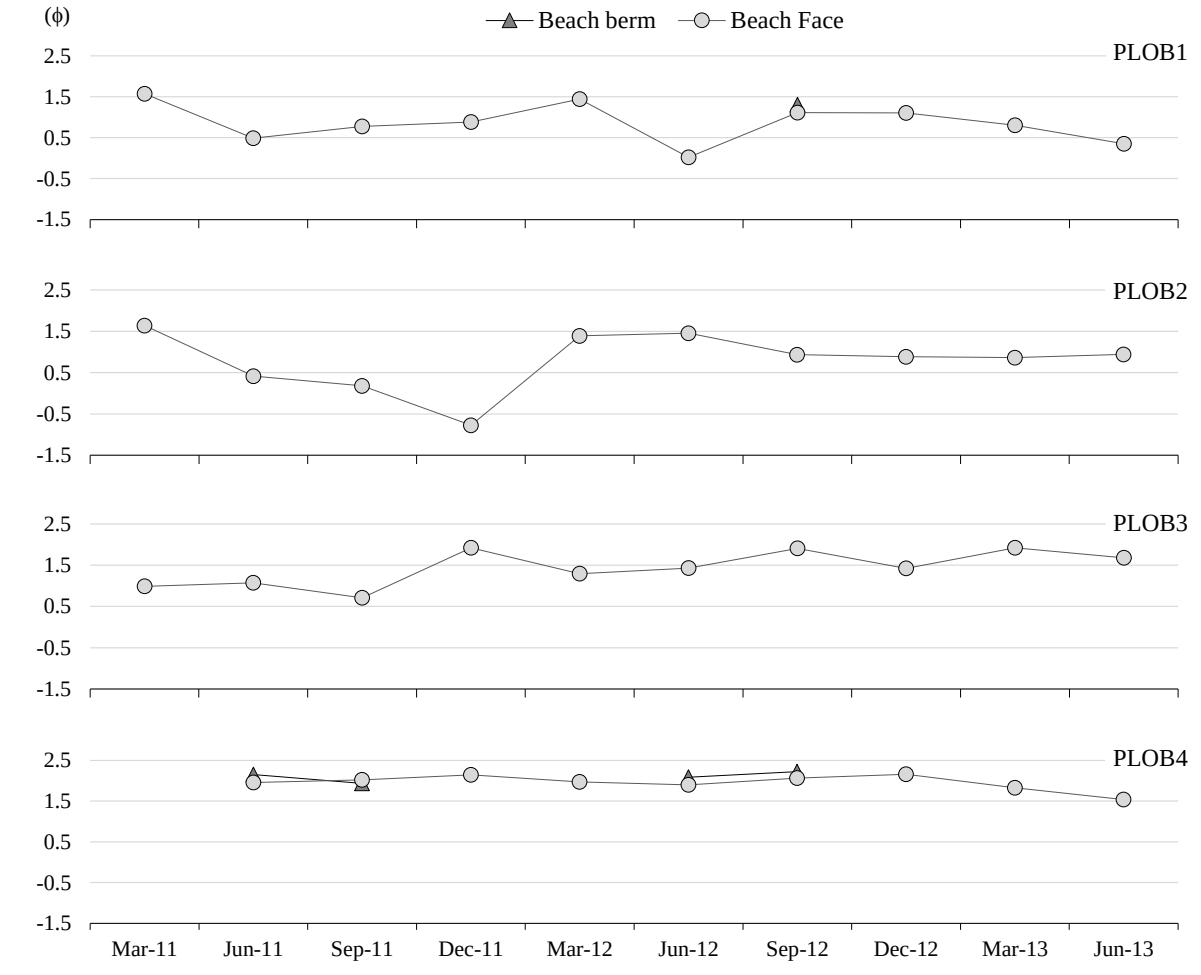

Figure 4.44. Variation of mean grain size for the period between March 2011 and June 2013, for sediment of the beach face and berm at Lagoa de Óbidos-Baleal study site.

5 Baleal - Peniche

The seasonal surveys of the Baleal-Peniche coastal stretch resulted in the creation of 10 high-resolution digital elevation models covering the period between March 2011 and June 2013, extending from the base of the dune to at least the MSL contour position at the time of each survey (Figure 4.45). The DEM reveal a narrow beach with fairly constant sloping surface. The beach is slightly wider at the easternmost sector, at the Baleal tombolo. The area covered by each DEM can be quite different in what concerns the lower part of the beach, owing to the different beach features present at the time of each survey. Whereas the peripheral areas of the embayment tend to contact directly with the underlying rocky platform, the central part of the embayment often exhibits a complex morphology of bars and rip channels, as seen in some of the DEM and in Figure 4.46. The presence/absence of these features doesn't seem to follow any temporal pattern, probably because they respond to events that occur at a shorter time scale (storm and post-storm recovery) than the seasonal surveys.

Nonetheless, this is considered a stable sector given the small volumetric variation that was measured between surveys (Figure 4.47). Except for the 13% loss after the 2012/2013 winter, all volumetric changes were within 10% of the total beach volume (average of 404 000 m^3). Sediment budget analysis reveals a seasonal pattern related to beach volume gain during the summer period (between March and September) and beach volume loss during the winter (October to February, after the impact of storms) as depicted in Figure 4.48. Maps of differences in elevation obtained by subtracting consecutive DEM portray the locations of sediment removal and accumulation between surveys (Figure 4.49). The most intense net sediment loss is well evidenced in the figure portraying the differences between the December 2012 and March 2013 surveys. There is generalized loss of sediment from the upper beach and base of the dune, and little sediment accumulation in the lower beach area.

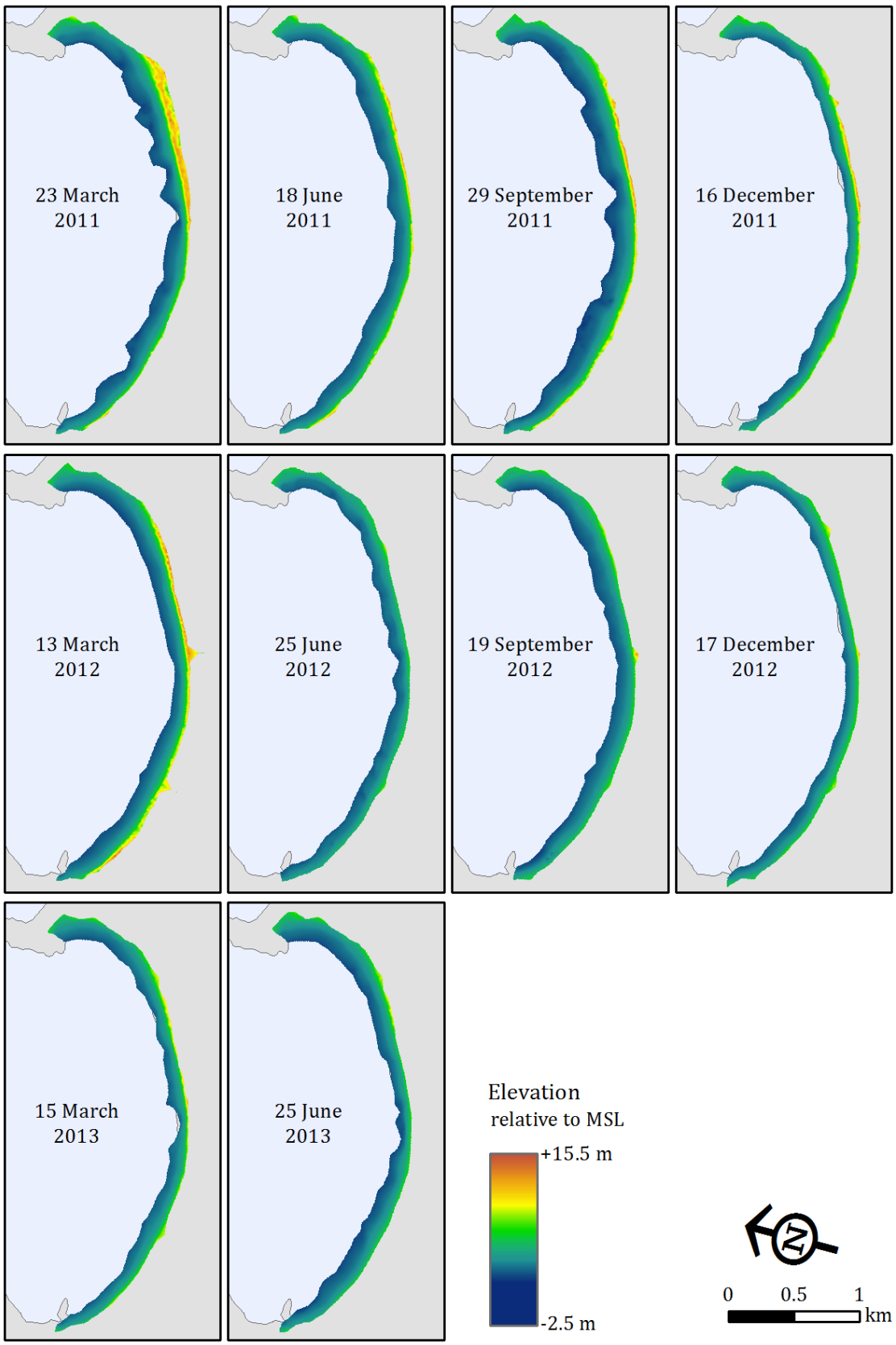

Figure 4.45. Digital elevation models of the Baleal-Peniche study site covering the period between March 2011 and June 2013.

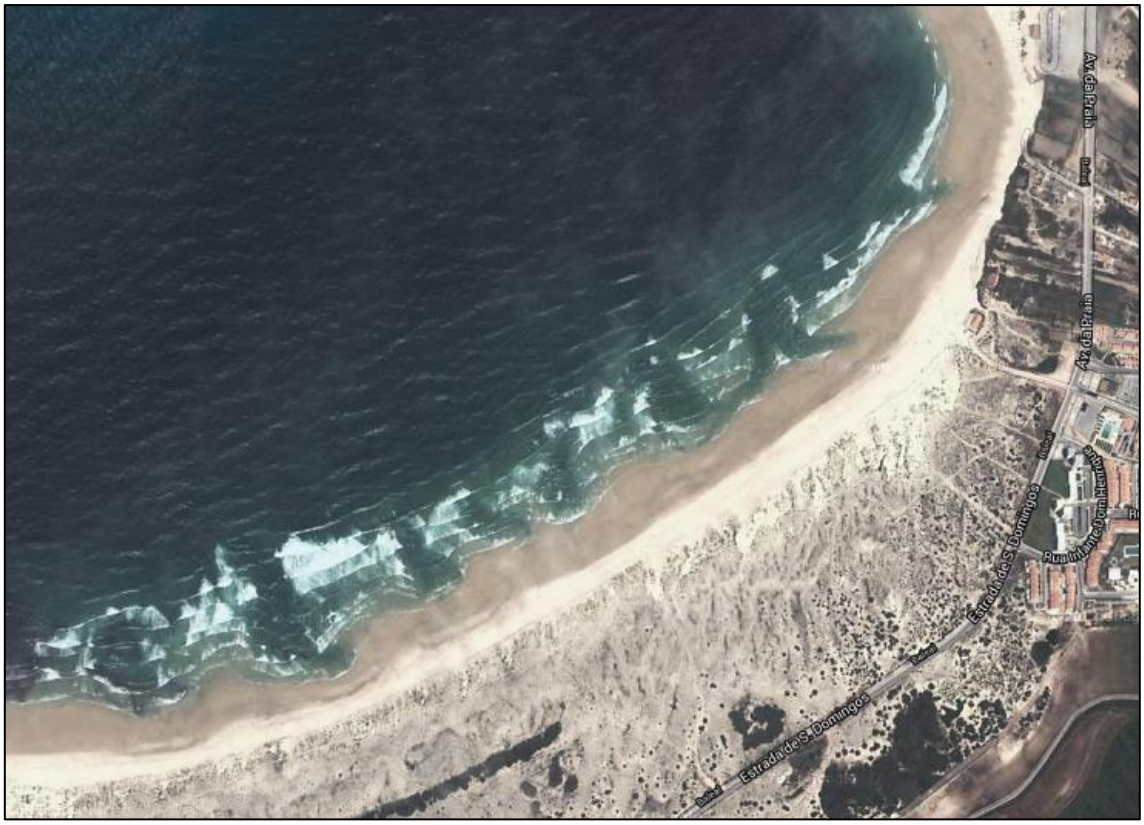

Figure 4.46. Satellite image of the central-eastern sector of the Baleal-Peniche study site, showing the bar and rip channels system.

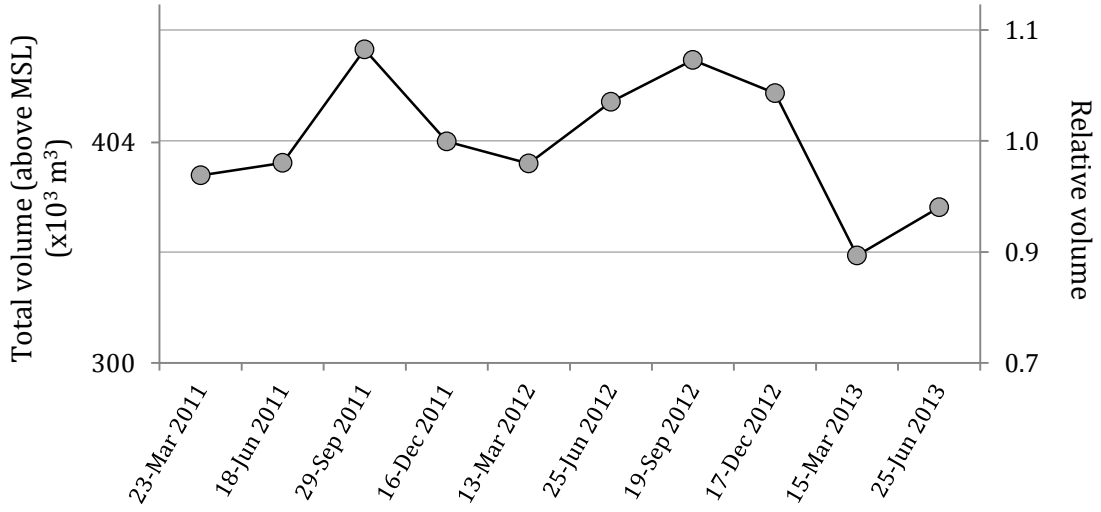

Figure 4.47. Beach volume measured from each survey of the Baleal-Peniche study site. Left axes: absolute volume (x10³ m³) and right axes: volume relative to average.

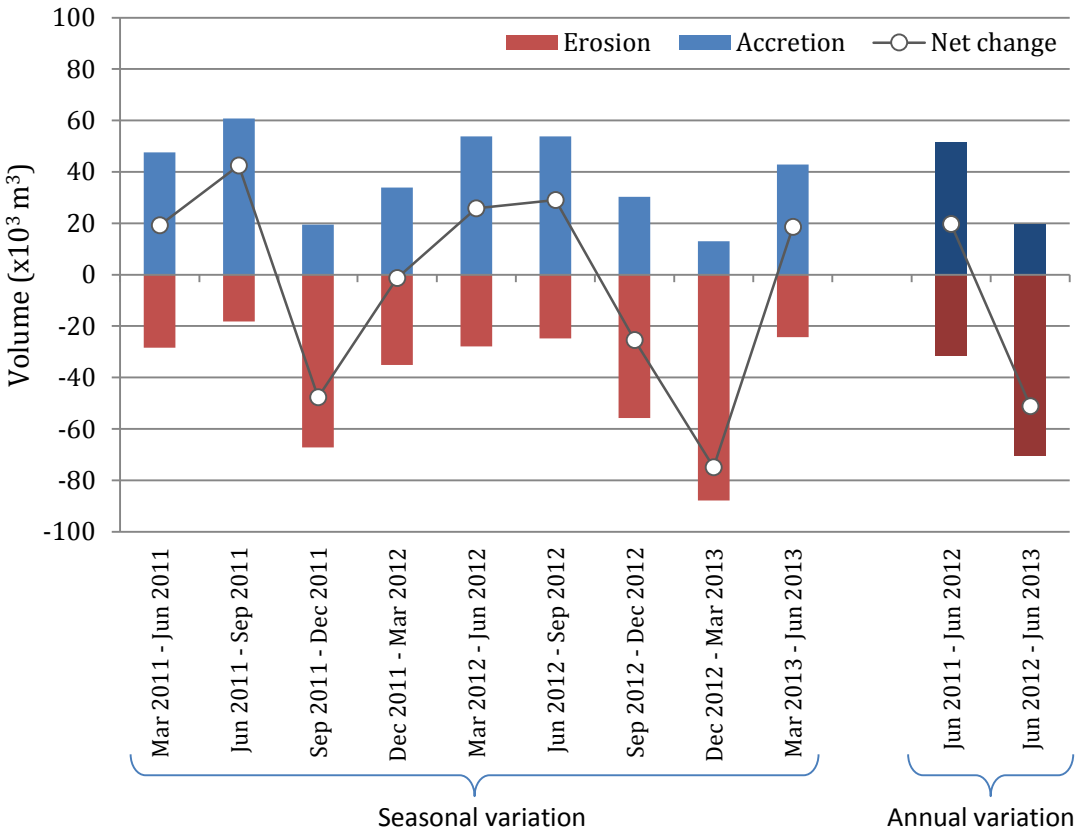

Figure 4.48. Seasonal and annual sediment budget for the Baleal-Peniche study site. Total accretion (blue bars), erosion (red bars) and net volume change (circle markers) between consecutive surveys and between the months of June of each year of the survey period.

The pattern of sediment transfers is variable along the study period. Spots of erosion and accretion occur either as limited and focused sites along the embayment, or as alongshore areas that extend for much of the embayment. Both cross and longshore sediment transport seem to occur, probably associated to the migration of the bar system that develops adjacent to the beach face.

Changes at the annual scale are of the same order of the seasonal ones (Figure 4.48 and 4.50), and reflect the net changes that occur along the year. Three years, however, are not enough to detect long-term beach changes.

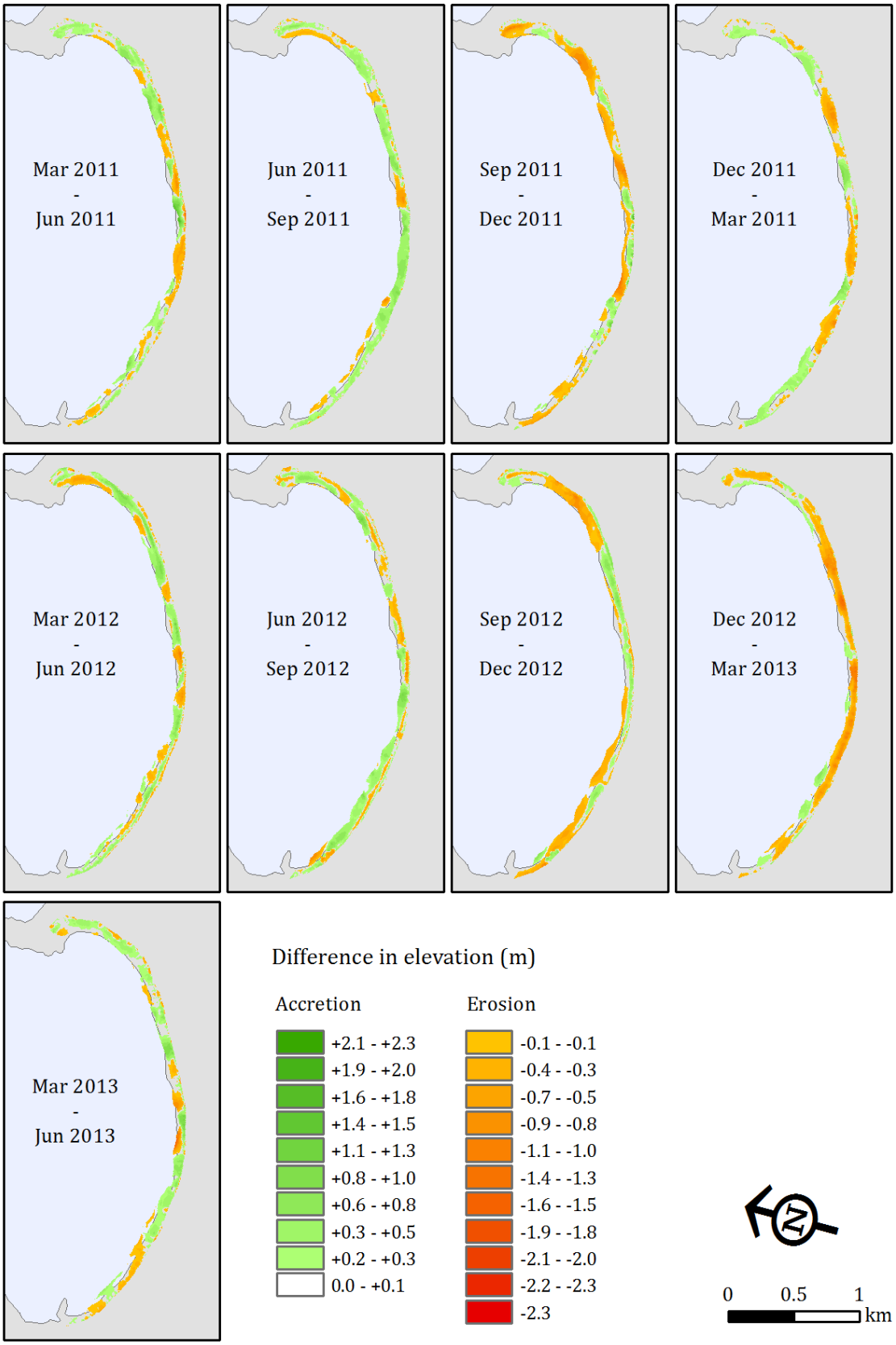

Figure 4.49. Map of elevation differences portraying the altimetric changes between consecutive surveys. Locations of sediment loss are highlighted in orange-red color scale and locations of sediment gains in green color scale.

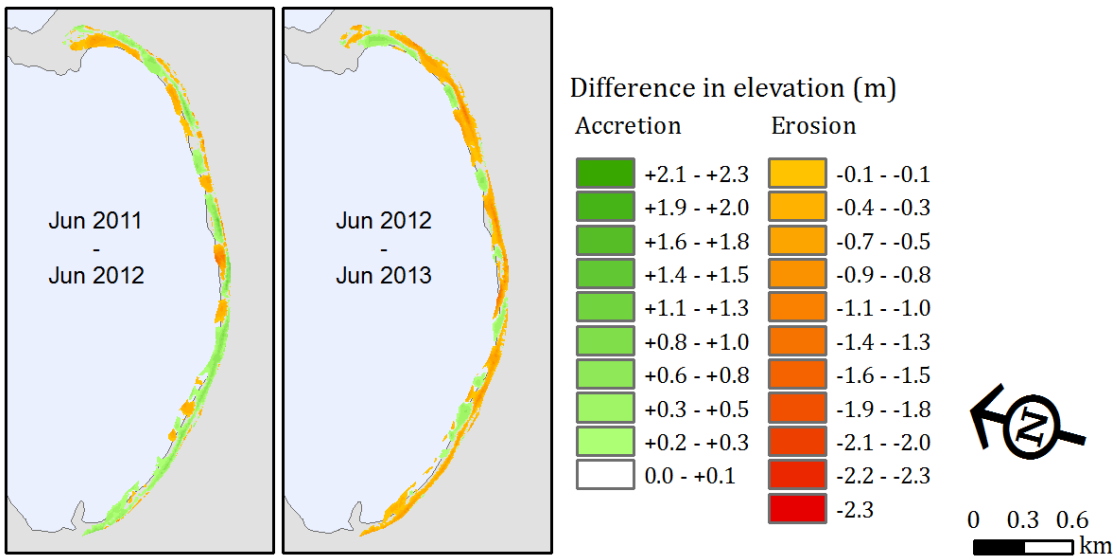

Figure 4.50. Difference in elevation maps portraying the annual altimetric changes between the June surveys. Locations of sediment loss are highlighted in orange -red color scale; and locations of sediment gains in green color scale.

The cross-sections of the Baleal–Peniche study site, corresponding to PBP1 to PBP4 beach profiles, reveal the same general pattern of behavior as detected in the DEM analysis (Figures 4.51 to 4.54). Beach profiles depict narrow and dissipative beaches, concave-shaped and usually lacking berms, and landward limited by high dunes (except for PBP1), that reach 8 and 12 m above MSL. From PBP3 to PBP1, along the eastern half of the embayment, there is a gradual increase in beach width and volume, and, inversely, a decrease in the average slope. PBP4 in the westernmost sector behaves similarly to PBP2. A small berm develops during the summer, detectable in the June and September surveys, just above 2-3 m (MSL), more frequently at PBP1 and seldom in the remaining profiles. There is an exchange of sediment between the upper and lower beach, and the area between MSL and the mean high water (S_{MHW}) lines corresponds to the rotation point of the profiles. Still, the beach is generally featureless and most changes occur mainly by the alternate lowering and raising of the beach surface, and thus the fairly constant slopes. PBP3 seems to be an exception and the entire beach surface is lowered or raised in its whole width up until the coastline, where it contacts a high dune with its seaward slope usually scarped.

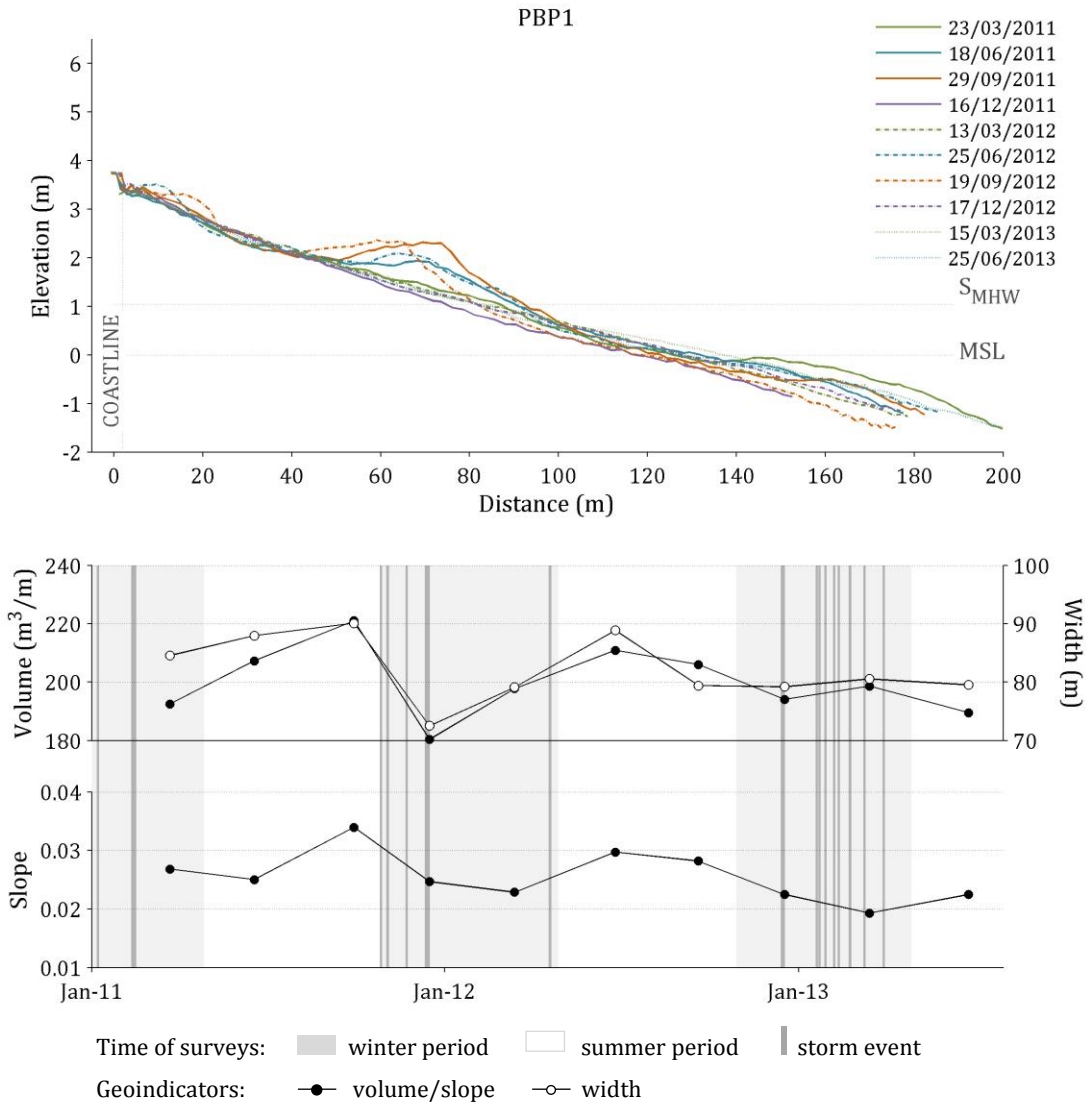

Figure 4.51. Beach profile PBP1 (Baleal-Peniche study site) and variation of beach geoindicators (volume, width and slope) for the period between March 2011 and June 2013.

Volumes tend to increase in the summer season, and decrease in winter. However, contrast between summer and winter periods is not as evident in profiles as in the DEM volumetric analysis. PBP3 shows a different behavior, whereby volume increases following a storm season. This might be explained by the transfer of sediment from the dunes to the beach during storm events.

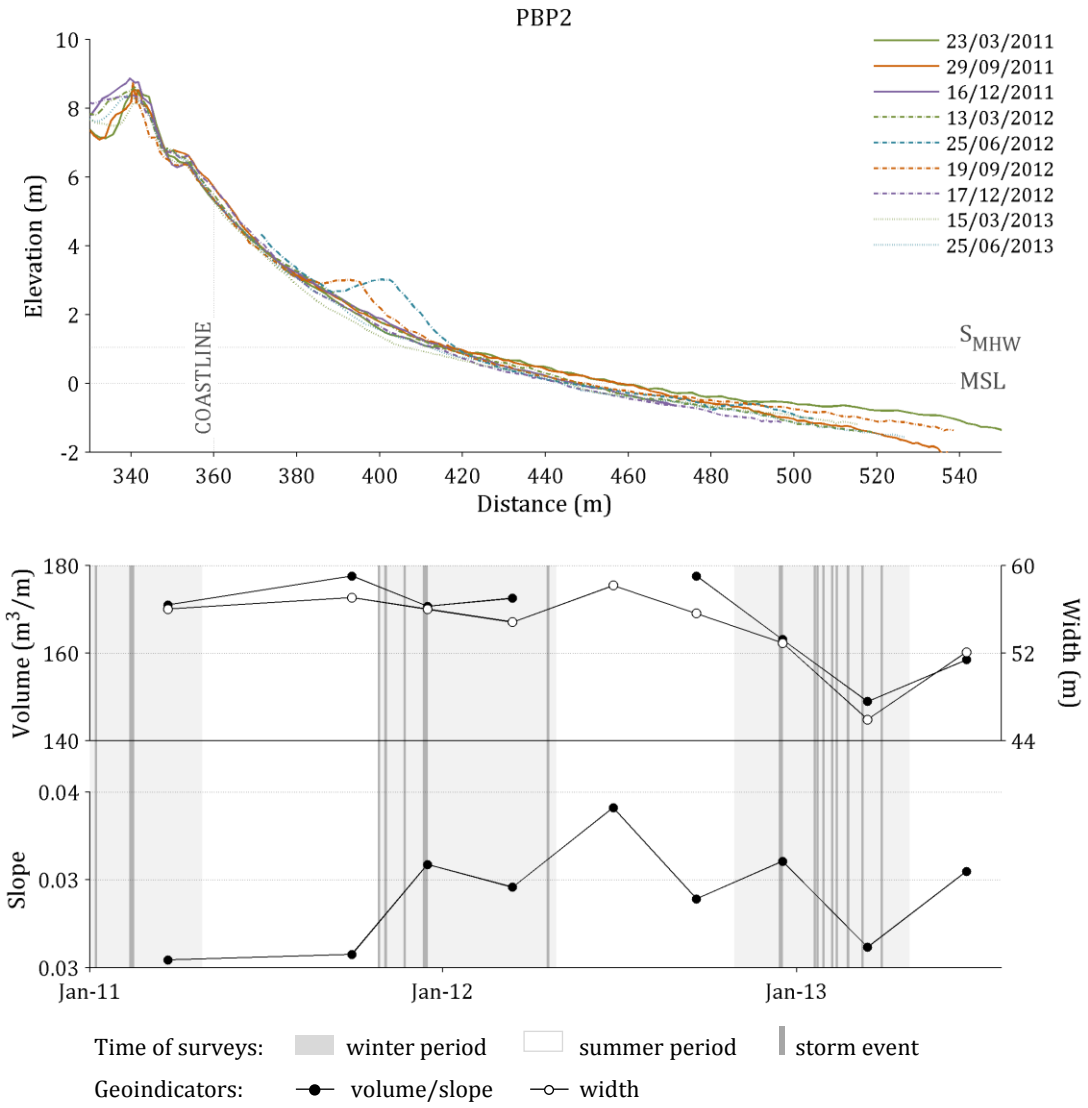

Figure 4.52. Beach profile PBP2 (Baleal-Peniche study site) and variation of beach geoindicators (volume, width and slope) for the period between March 2011 and June 2013.

Storm effects frequently correspond to the collapse and erosion of the foredunes that are easily reached and occasionally overtopped by storm waves during higher water levels (Figure 4.55 – upper and middle panels). Conversely, dune build-up is favored during low water levels when the beach surface provides the source and configuration for onshore winds to transport sand across the beach-dune system (Figure 4.55 – lower panel). Still, changes in the profiles and corresponding geoindicators are small and the result is a fairly stable coastal stretch in line with the findings of the DEM analyses.

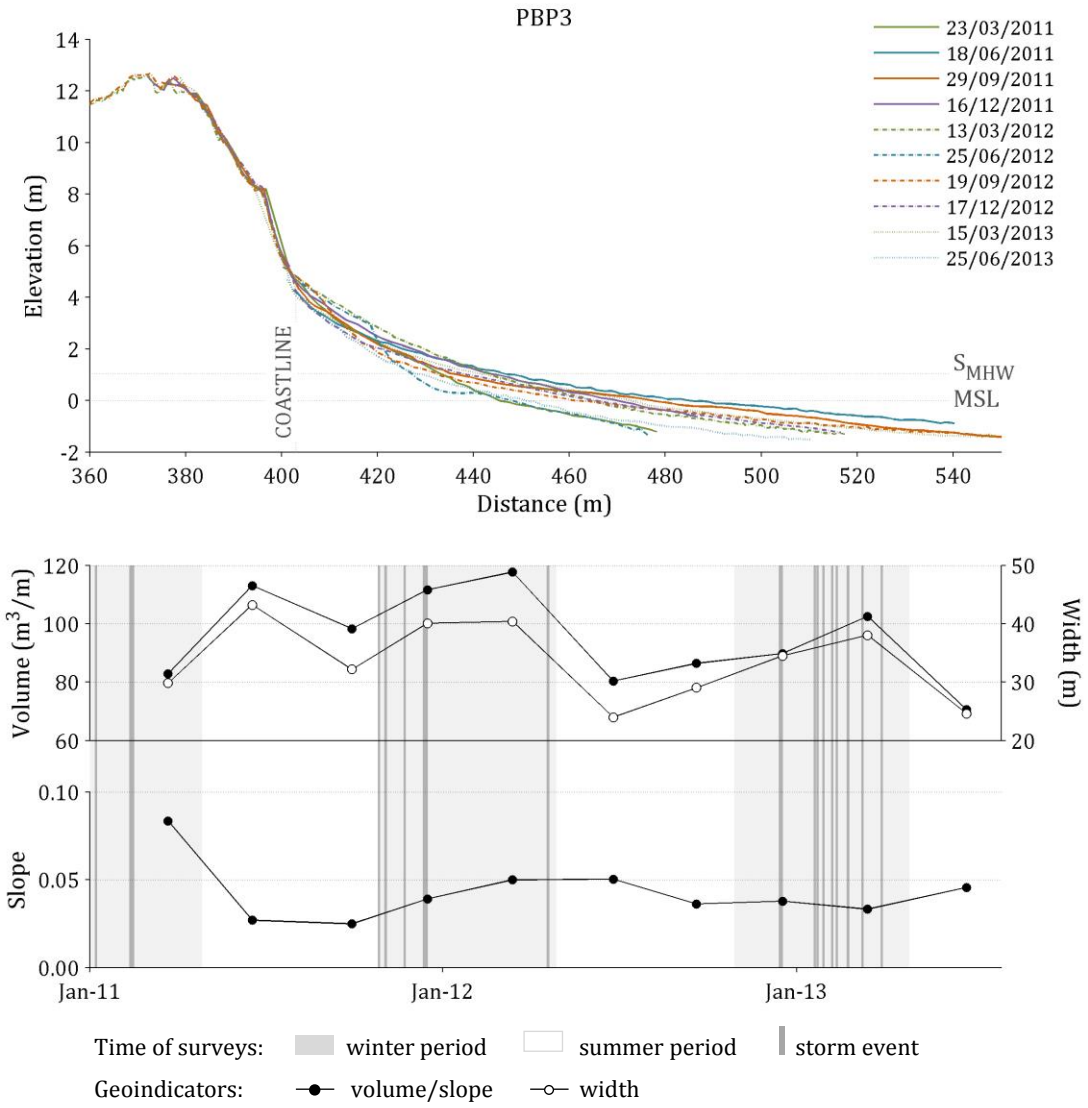

Figure 4.53. Beach profile PBP3 (Baleal-Peniche study site) and variation of beach geoindicators (volume, width and slope) for the period between March 2011 and June 2013.

The morphological analysis indicates that Baleal-Peniche coastal stretch is fairly stable, experiencing small changes that are associated with the winter/summer seasonality. Sediment exchanges seem to be mostly cross-shore, including the active dune system in the central portion of the embayment (PBP3).

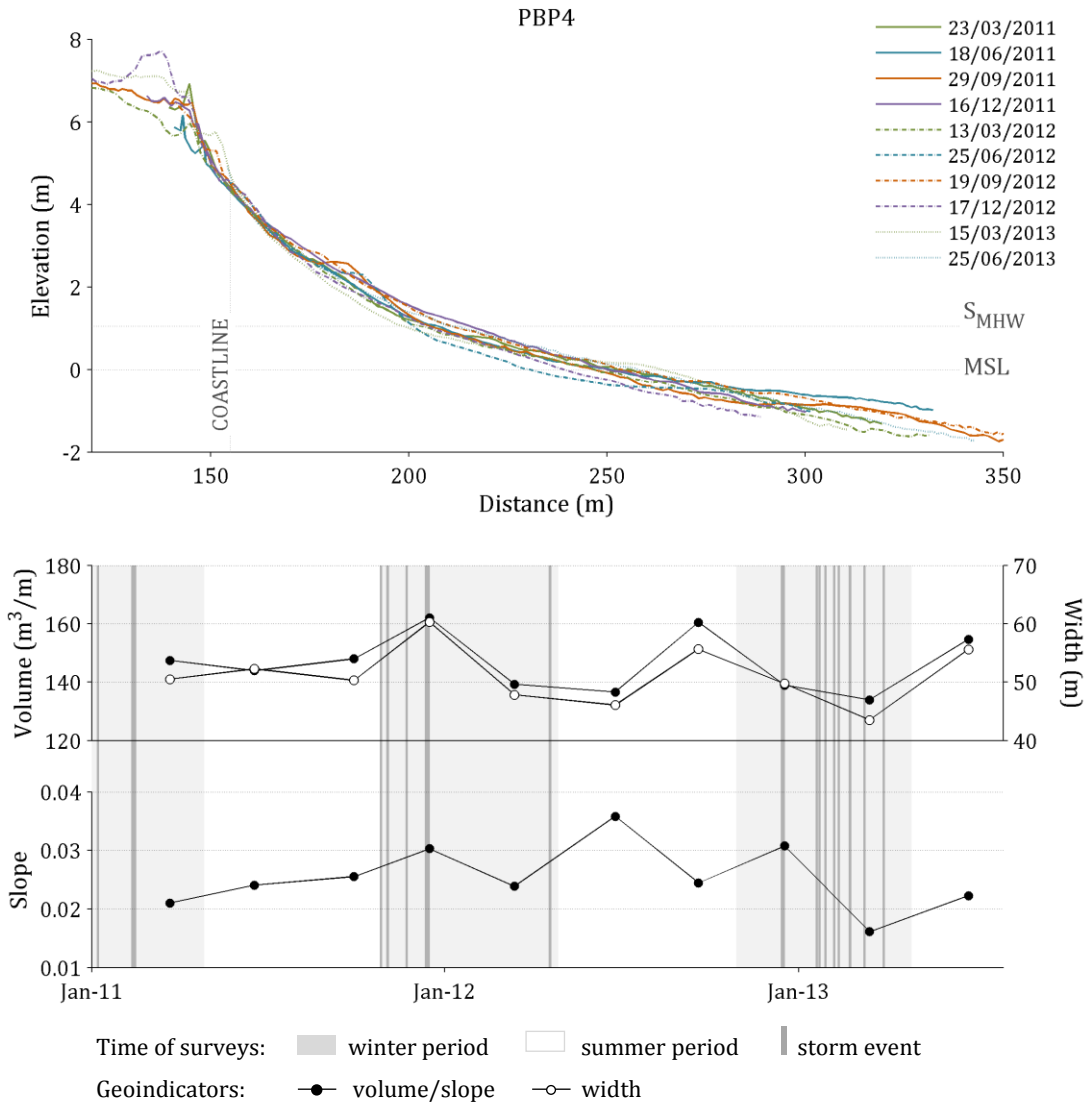

Figure 4.54. Beach profile PBP4 (Baleal-Peniche study site) and variation of beach geoindicators (volume, width and slope) for the period between March 2011 and June 2013.

The Baleal-Peniche coastal stretch is also very stable in the sedimentary content (Figure 4.56). The sediments of the beaches characterizing this section of the coast correspond essentially to fine to medium sands (≈2 ϕ), with some exceptions of coarse sand collected on the beach face at PBP2 profile during the March 2012 and 2013 surveys.

Figure 4.55. Photographs of the Baleal-Peniche study site showing prominent scarping of the foredune on March 23, 2011 (upper panel), and December 16, 2011 (middle panel), and the aspect of the beach dune-system with windblown sand accumulating against, and rebuilding the foredunes on March 15, 2013 (lower panel).

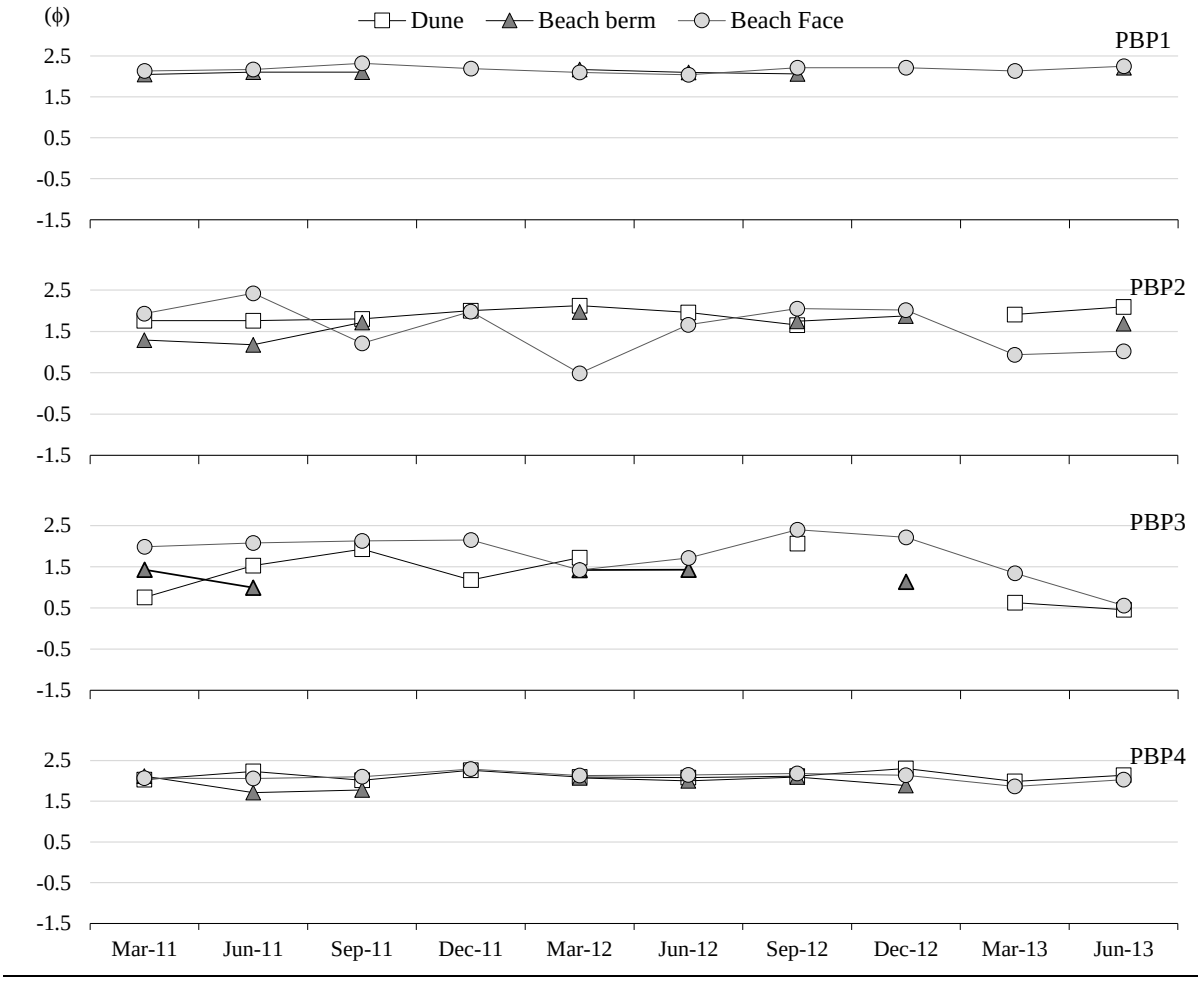

Figure 4.56. Variation of mean grain size for the period between March 2011 and June 2013, for sediment of the beach face, berm and dune at Baleal-Peniche study site.

6 Santa Cruz

The cross-shore profiles of Santa Cruz study site depict well developed and wide beaches that may present two berms (Figures 4.57 to 4.59) in summer. A permanent high berm stands between 5 and 6.5 m (MSL). In the beginning of the summer and especially following a particularly severe winter, this upper beach area may be artificially shaped by mechanical means to create a levelled and optimized area for recreational use. This is more frequent in the beach area sampled by PSC2 and PSC3.

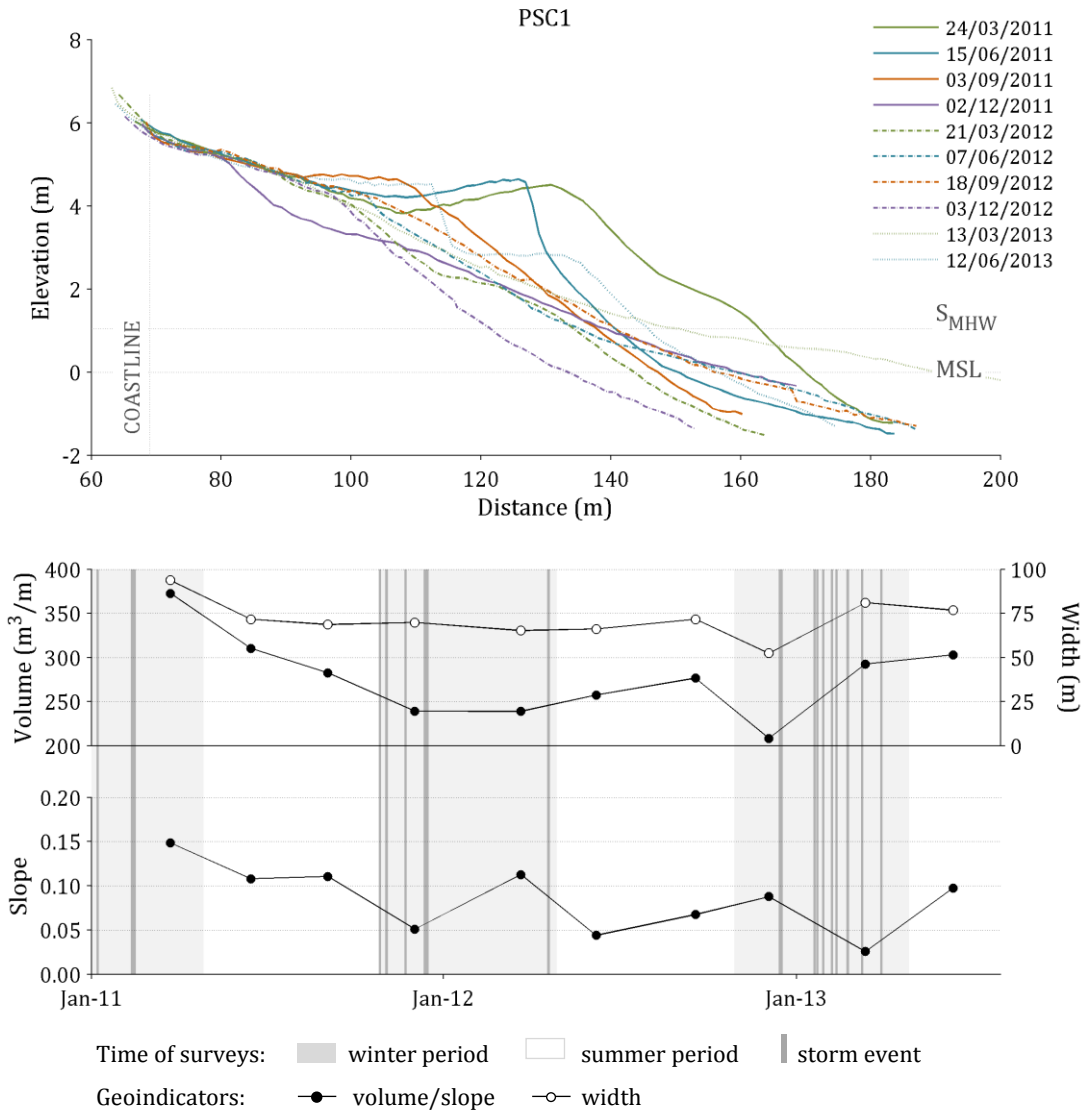

Figure 4.57. Beach profile PSC1 (Santa Cruz study site) and variation of beach geoindicators (volume, width and slope) for the period between March 2011 and June 2013.

The lower berm is ephemeral and mobile in elevation and location along the profile, its crest lying between 2.5 m and 5 m (MSL), and shifting a total of 30 m in cross-shore position during the survey period and at all profile locations. Regarding slope, beaches vary between modal intermediate and reflective stages, and may acquire a gentler slope (typical of dissipative beaches) following a storm event.

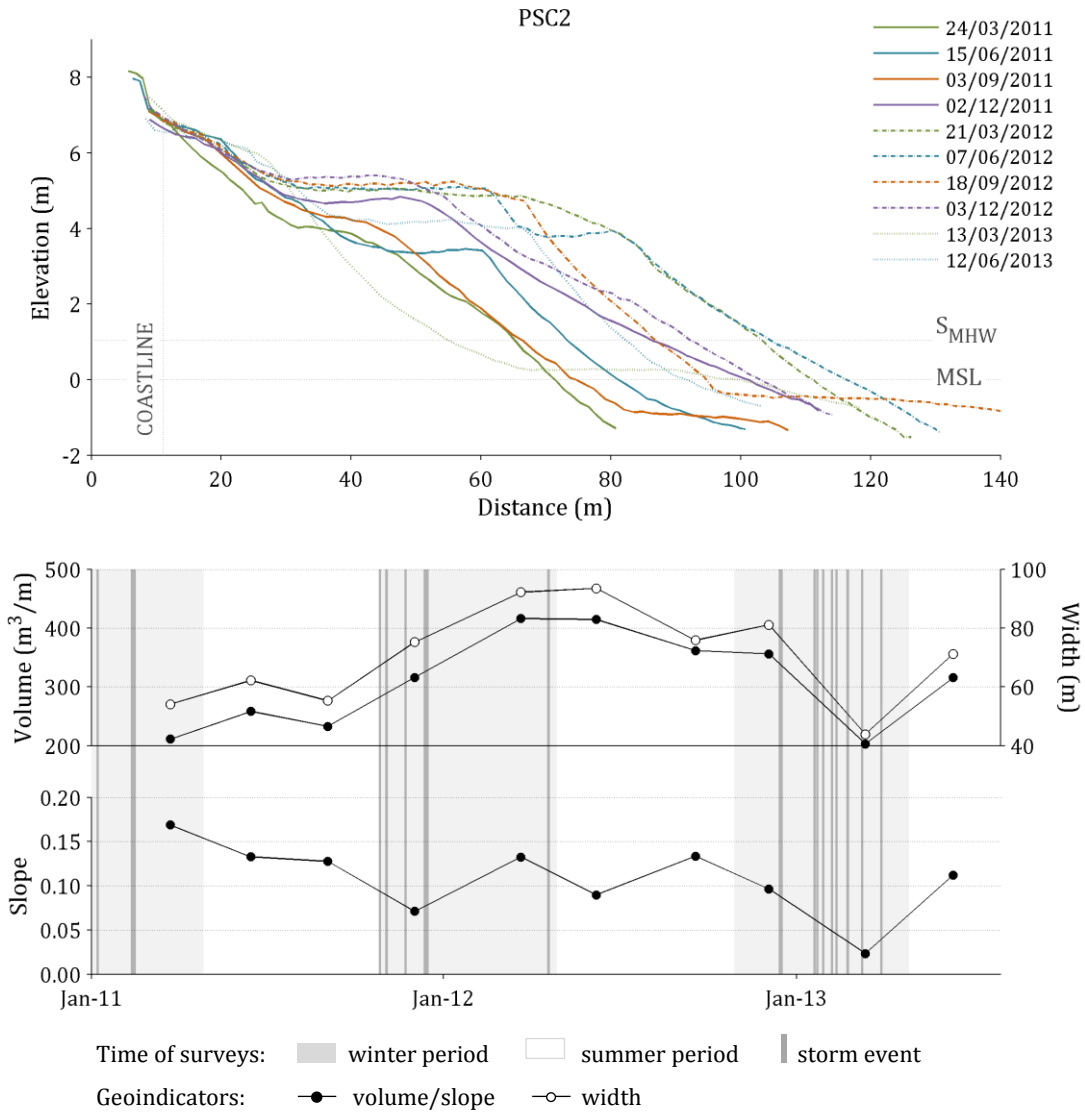

Figure 4.58. Beach profile PSC2 (Santa Cruz study site) and variation of beach geoindicators (volume, width and slope) for the period between March 2011 and June 2013.

There is a seasonal behavior associated to the beach changes. In all three profiles the beach tends to grow in summer through the building of the upper beach and berms. Except for the 2011 summer in PSC1, these changes are accompanied by an increase in volume. During winter, the beach berm retreats and beach profiles become flatter, and slope decreases. The effect of the 2011/2012 winter on PSC2 was an exception to this pattern, because there was a net increase in volume and width. Changes induced by storms included creation of scarps of metric dimensions, and depletion of the beach face sediment, to the point that the rocky platform got exposed in the southernmost sector. The effects of the early 2013 storm on profile PSC3 are depicted on the middle and lower panels of Figure 4.60.

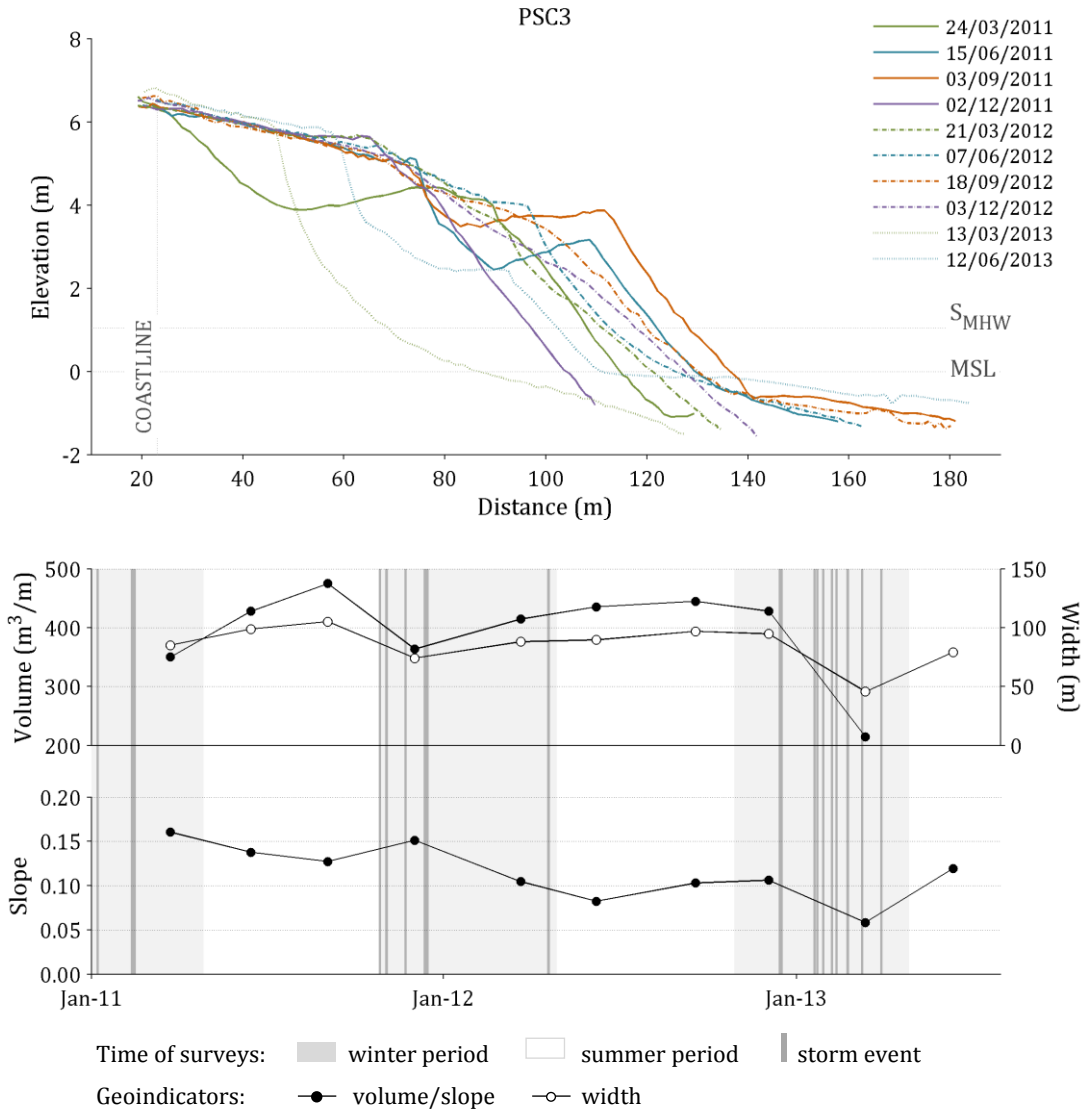

Figure 4.59. Beach profile PSC3 (Santa Cruz study site) and variation of beach geoindicators (volume, width and slope) for the period between March 2011 and June 2013.

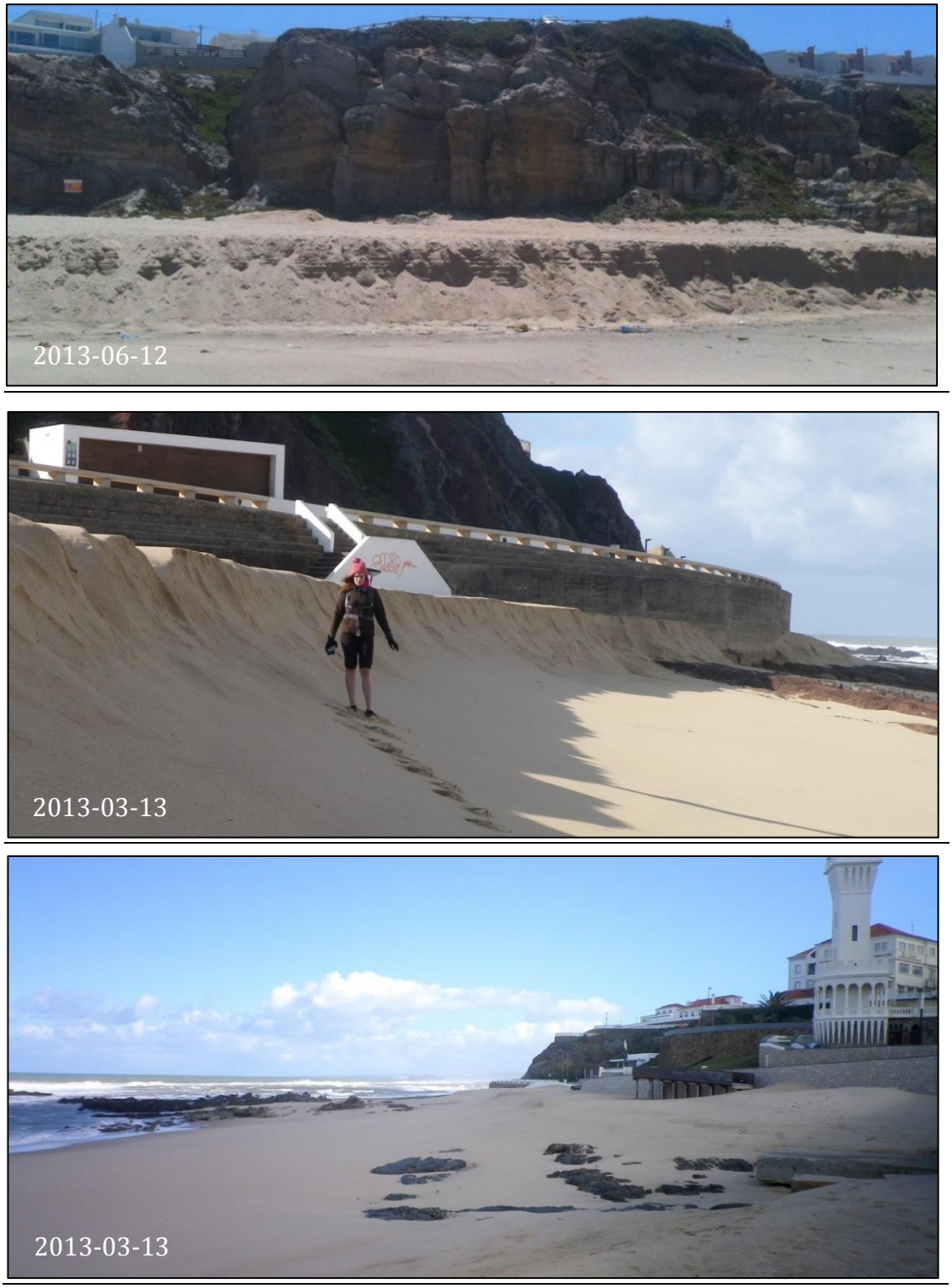

Figure 4.60. Ground photographs of the Santa Cruz study site showing a prominent scarp at PSC1 on June 12, 2013 (upper panel), and PSC3 on March 13, 2013 (middle panel), and the lowering of the beach profile leaving the rocky platform uncovered at PSC3 on March 13, 2013 (lower panel).

Santa Cruz experiences considerable changes in beach configuration, volume, area and slope. Its modal characteristics are those of a reflective beach with a high and robust landward berm and a typical steep beach face that migrates with the growth and destruction of the summer berm.

Contrary to the morphology, the sedimentary content of Santa Cruz beach (Figure 4.61) is fairly constant, characterized by medium to coarse sand at the beach face (average mean diameter around 1 ϕ), and coarse sand at the beach berm (sometimes medium sand at PSC1). There is a slight increase in mean diameter from north to south.

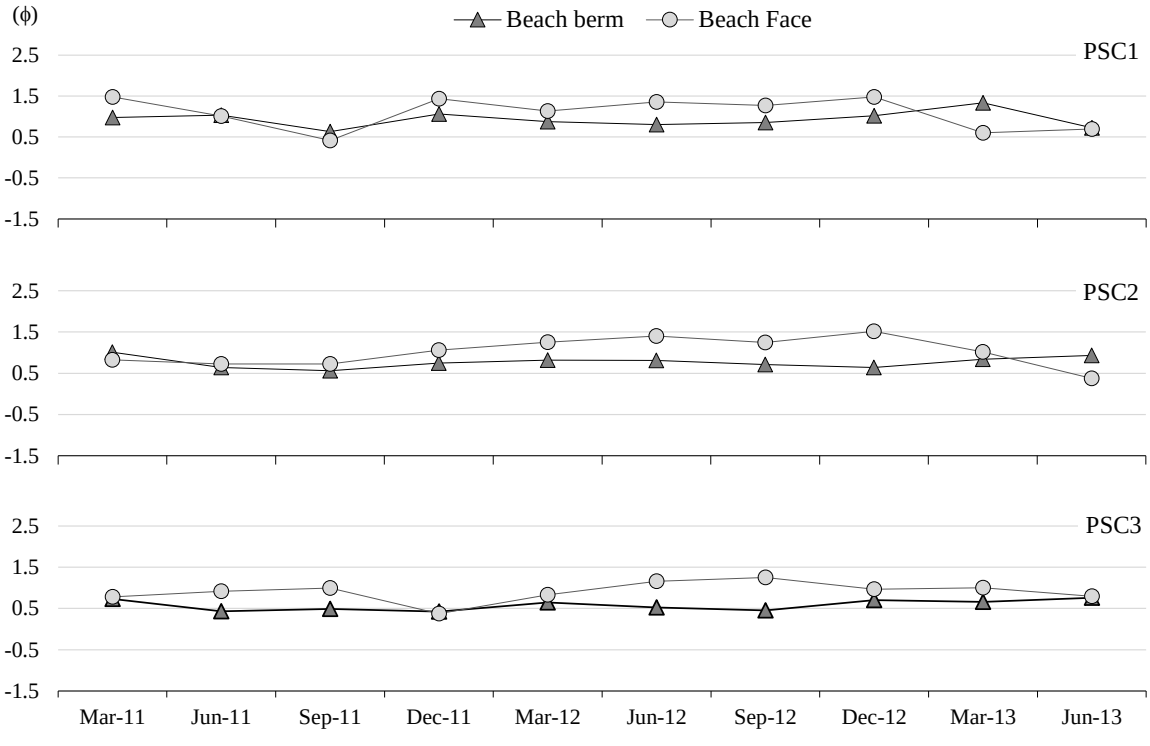

Figure 4.61. Variation of mean grain size for the period between March 2011 and June 2013, for sediment of the beach face and berm at Santa Cruz study site.

7 Coxos

The one profile that characterizes Coxos beach (PCX1), describes a typically reflective beach with a well-developed berm and steep slope (Figure 4.62).

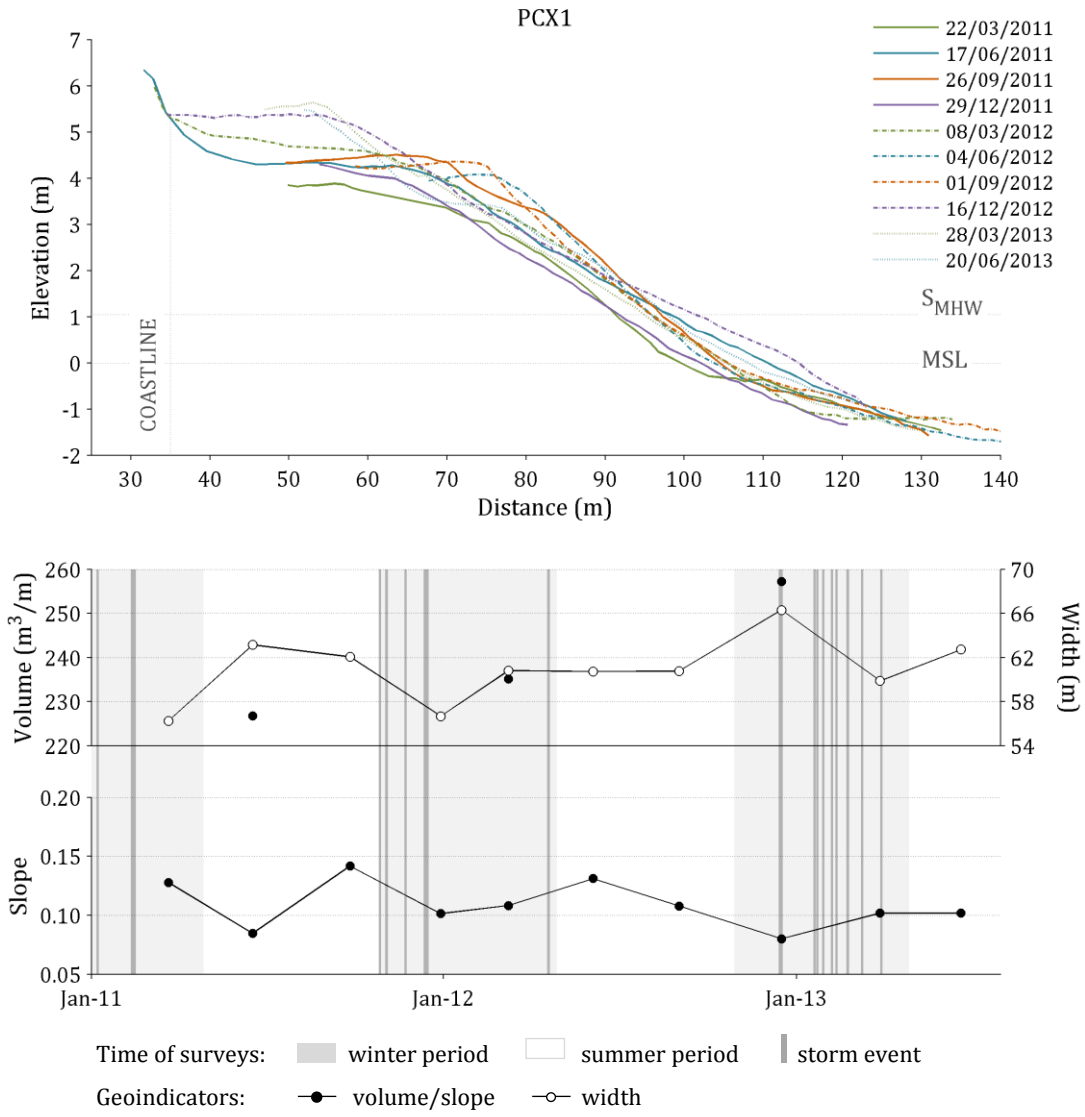

Figure 4.62. Beach profile PCX1 (Coxos study site) and variation of beach geoindicators (volume, width and slope) for the period between March 2011 and June 2013.

The cross-sections depicted in the figures above do not represent the full width of the beach, and are often incomplete because of survey limitations, and therefore some geoindicators' values are missing. Even so, the beach face corresponds to a stable feature for the entire study period, with relatively constant slope and location. The most relevant changes occur at the beach berm that oscillates in elevation between 3.8 and 5.5 m (MSL), and shifts c. 25 m in berm crest position. The berm retreats and grows in elevation during winter, and gets lower and builds seaward during summer. During the monitored period, the beach had small changes.

The embayed character of Coxos beach is also responsible for a weak variability in the sedimentary content (Figure 4.63). The beach berm is typically characterized by coarse sand, and the beach face ranges from coarse to medium sand, with an average diameter of 0.94 ϕ.

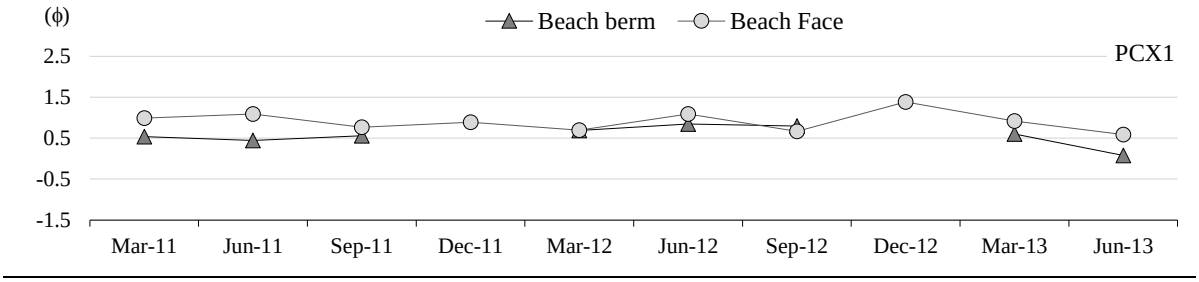

Figure 4.63. Variation of mean grain size for the period between March 2011 and June 2013, for sediment of the beach face and berm at Coxos study site.

8 Baleia/Sul

The three profiles monitored at Baleia/Sul study site describe an alongshore varying embayed beach, mainly constrained by the existing structures and human manipulation of the sediment (Figure 4.64 to 4.66). Nonetheless, the beach presents an unvarying steep beach face, typical of more reflective beaches and the lower surface contacts with the underlying rocky platform that is normally exposed and deprived of any sedimentary accumulation forms.

Beach volume and width increase from north to south, as well as their variability. Both PBS1 and PBS2 (north and central profiles) correspond to sloping surfaces extending landward of the rocky platform and culminating against the seawall, at elevations between 3 and 4.5 m (MSL). The well-developed beach berms depicted in the summer profiles of PBS2 correspond to artificial morphologies. They were built through beach scrapping in order to increase the available beach space for users, and wave action destroys this feature in the following months.

In, the southernmost sector, PBS3 presents a naturally-developing beach berm that can reach 25 m in width, and that gradually increases in elevation to 5.5 m (MSL) where it contacts with the landward limiting structure.

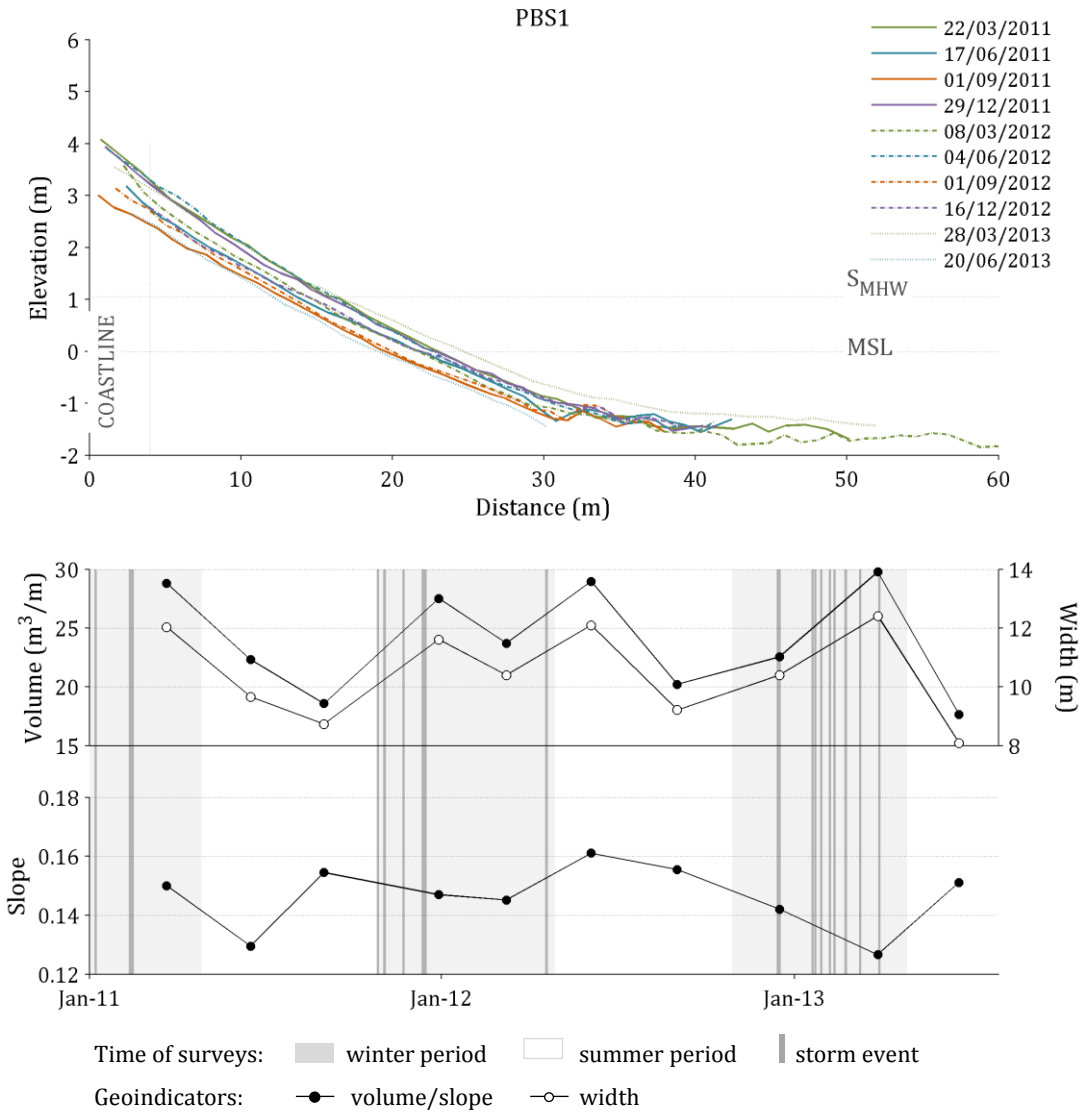

Figure 4.64. Beach profile PBS1 (Baleia/Sul study site) and variation of beach geoindicators (volume, width and slope) for the period between March 2011 and June 2013.

Storms promote lowering of the beach surface at PBS2 and PBS3 profiles, commonly resulting in more concave-shaped profiles. PBS1, on the other hand, increases in volume and area following a storm while maintaining the same linear configuration. Still, changes to the Baleia/Sul beach surface following a storm are modest. During extreme events, high water levels easily inundate the beach and rise above the structure that limits the beach, leading to overtopping and sediment transport over the seawall (Figure 4.67).

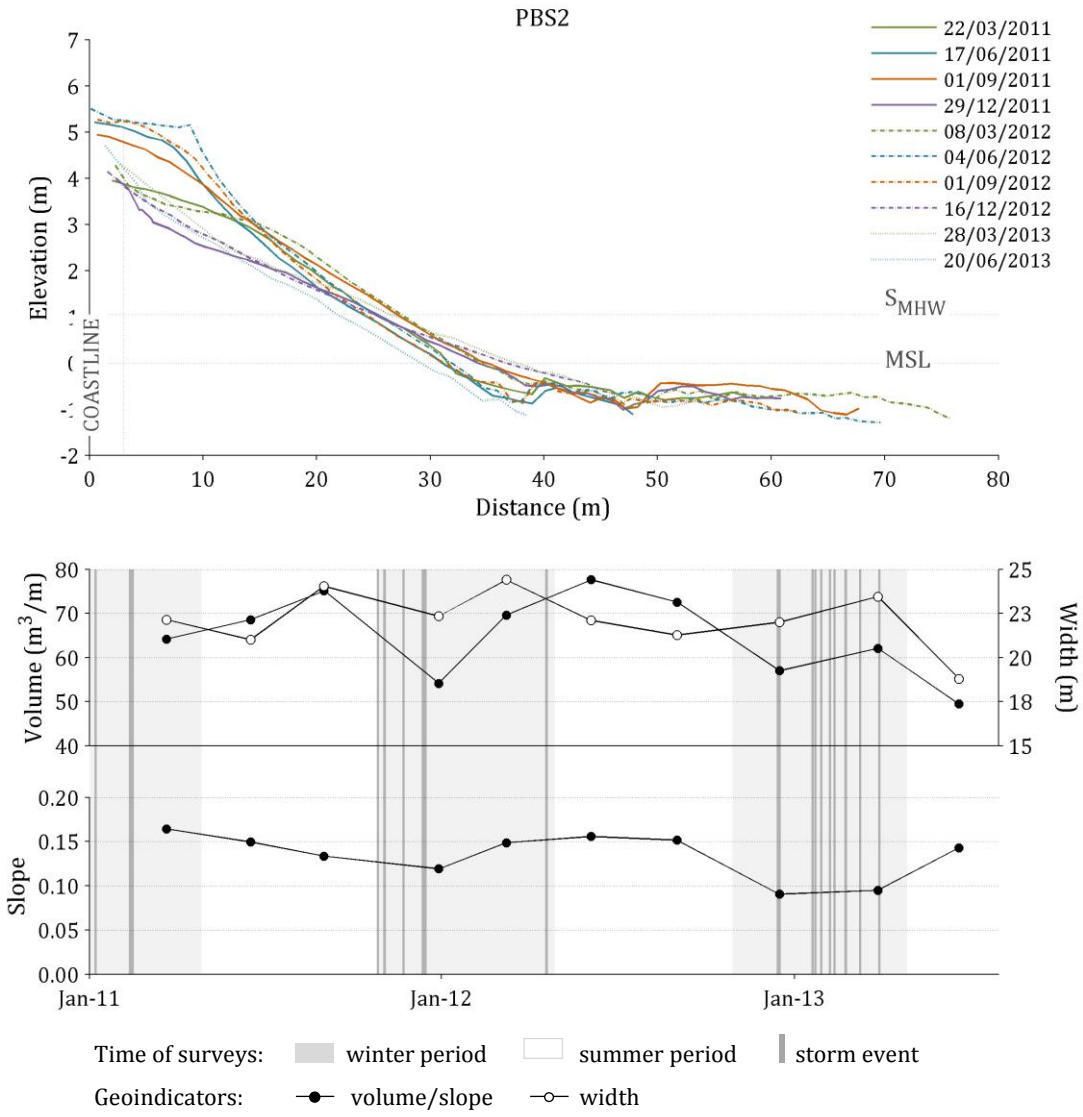

Figure 4.65. Beach profile PBS2 (Baleia/Sul study site) and variation of beach geoindicators (volume, width and slope) for the period between March 2011 and June 2013.

Overall, Baleia/Sul is a narrow beach with conditions for berm development only in its southern end, where the presence of a groin allows for sediment to accumulate. Changes to the configuration and morphology are minor, and its reduced size allows for recurrent storm-induced overwash to occur.

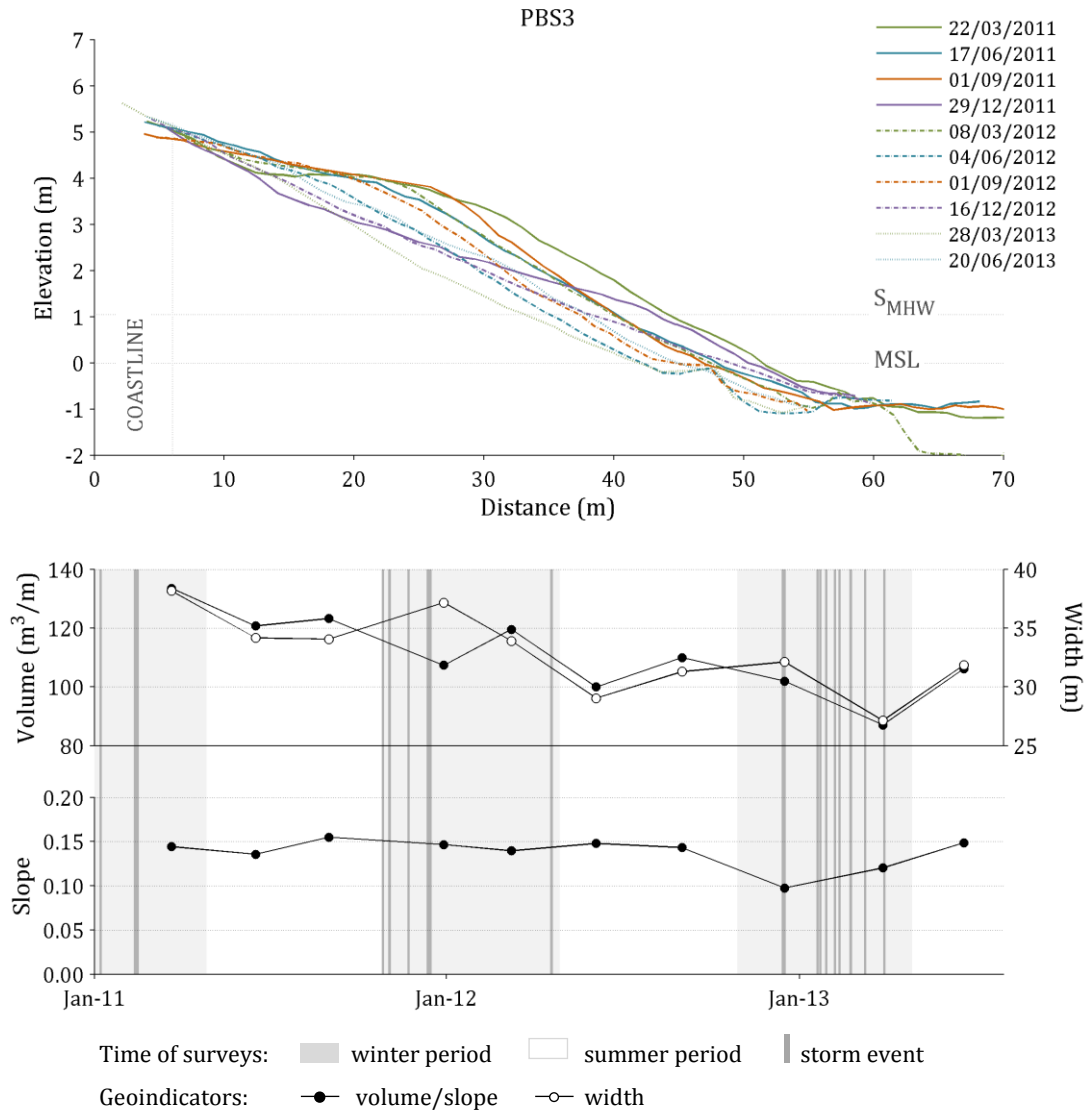

Figure 4.66. Beach profile PBS3 (Baleia/Sul study site) and variation of beach geoindicators (volume, width and slope) for the period between March 2011 and June 2013.

The sheltered and low-energy environment that characterizes this beach is also reflected in the sediment content that is practically size-invariant during the two and a half years of monitoring (Figure 4.68). The sediments of the beach face and berm correspond to coarse sand, with mean diameter of 0.40, 0.41 and 0.50 ϕ, for PBS1, PBS2 and PBS3, respectively.

Figure 4.67. Effects of storms at Baleia/Sul beach. Overwash and sediment deposition over the seawall on December 16, 2012.

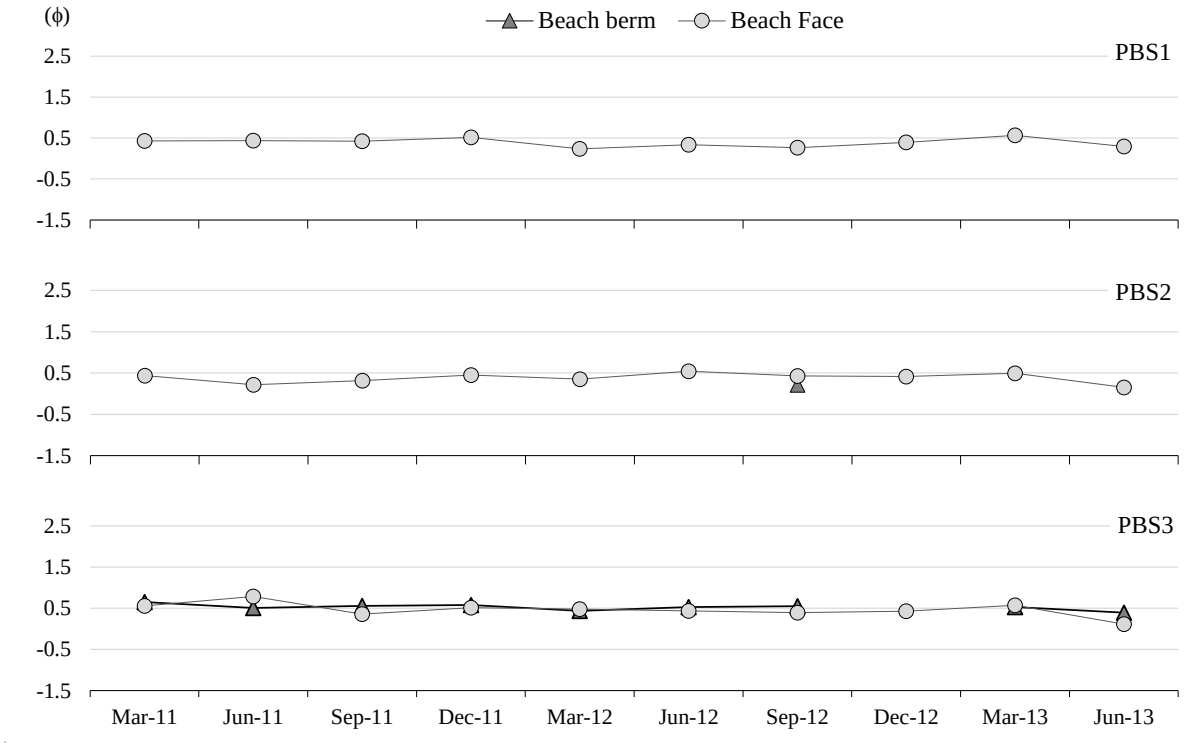

Figure 4.68. Variation of mean grain size for the period between March 2011 and June 2013, for sediment of the beach face and berm at Baleia/Sul study site.

9 Magoito

All three profiles at Magoito study site (PMG1 to PMG3) describe a typical narrow platform beach with limited sediment availability. The beach corresponds to a small volume of sediment overlying the rocky platform that is often exposed below MSL (Figures 4.69 to 4.71). Some surveys failed to fully represent the cross-sections due to GNSS equipment malfunction because of the proximity to the high cliffs, especially along PMG2 and PMG3.

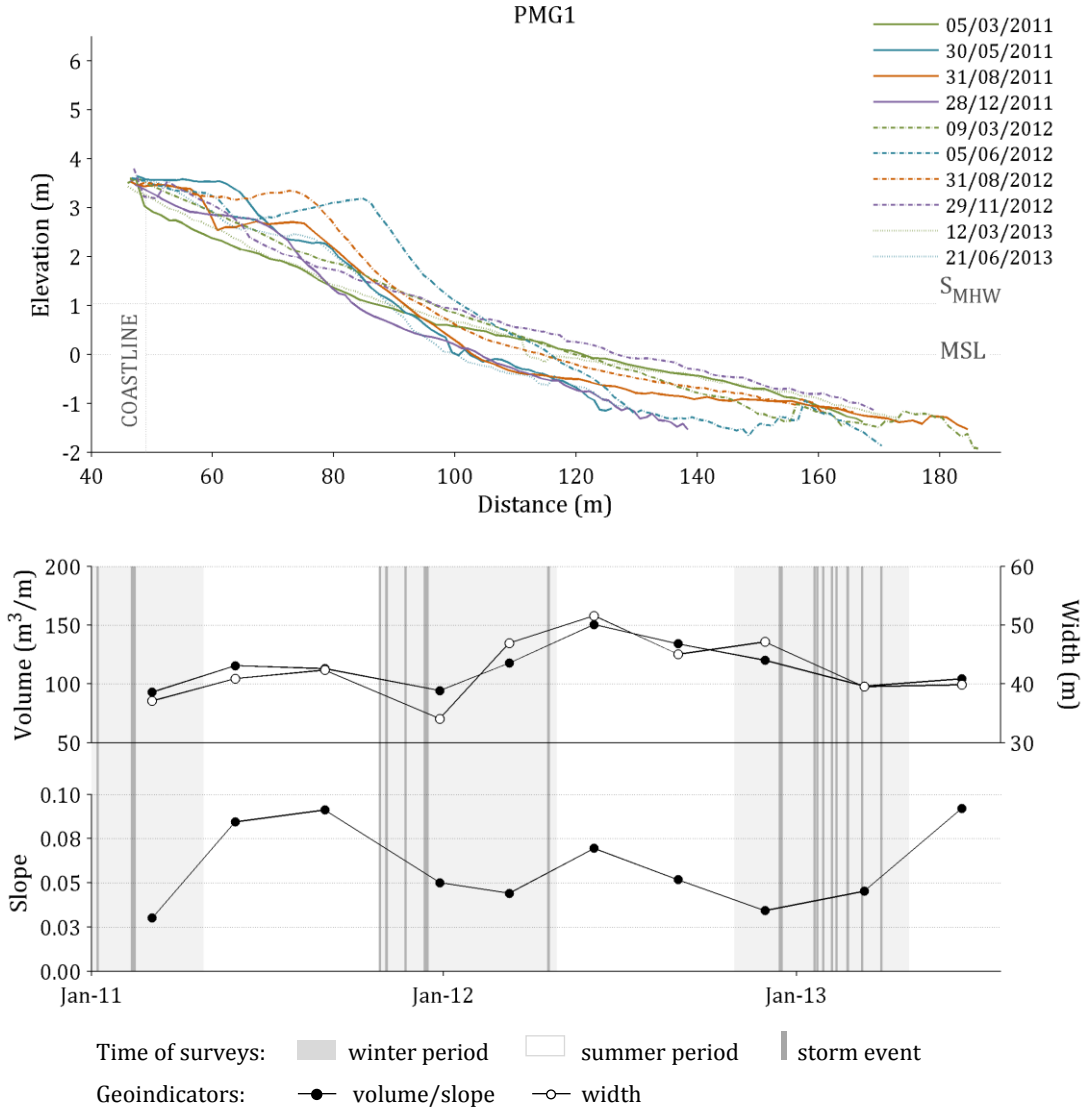

Figure 4.69. Beach profile PMG1 (Magoito study site) and variation of beach geoindicators (volume, width and slope) for the period between March 2011 and June 2013.

In general, summer profiles present a narrow and low beach berm, developing between 2.5 and 3.5 m (MSL) in elevation, growing landward and reaching 4 m (MSL), consequently creating steeper beach slopes that are characteristic of intermediate type of beach. Winter profiles are more linear and featureless, typically showing gentler slopes, characteristic of more dissipative beaches. There are exceptions to this behavior, especially at PMG3.

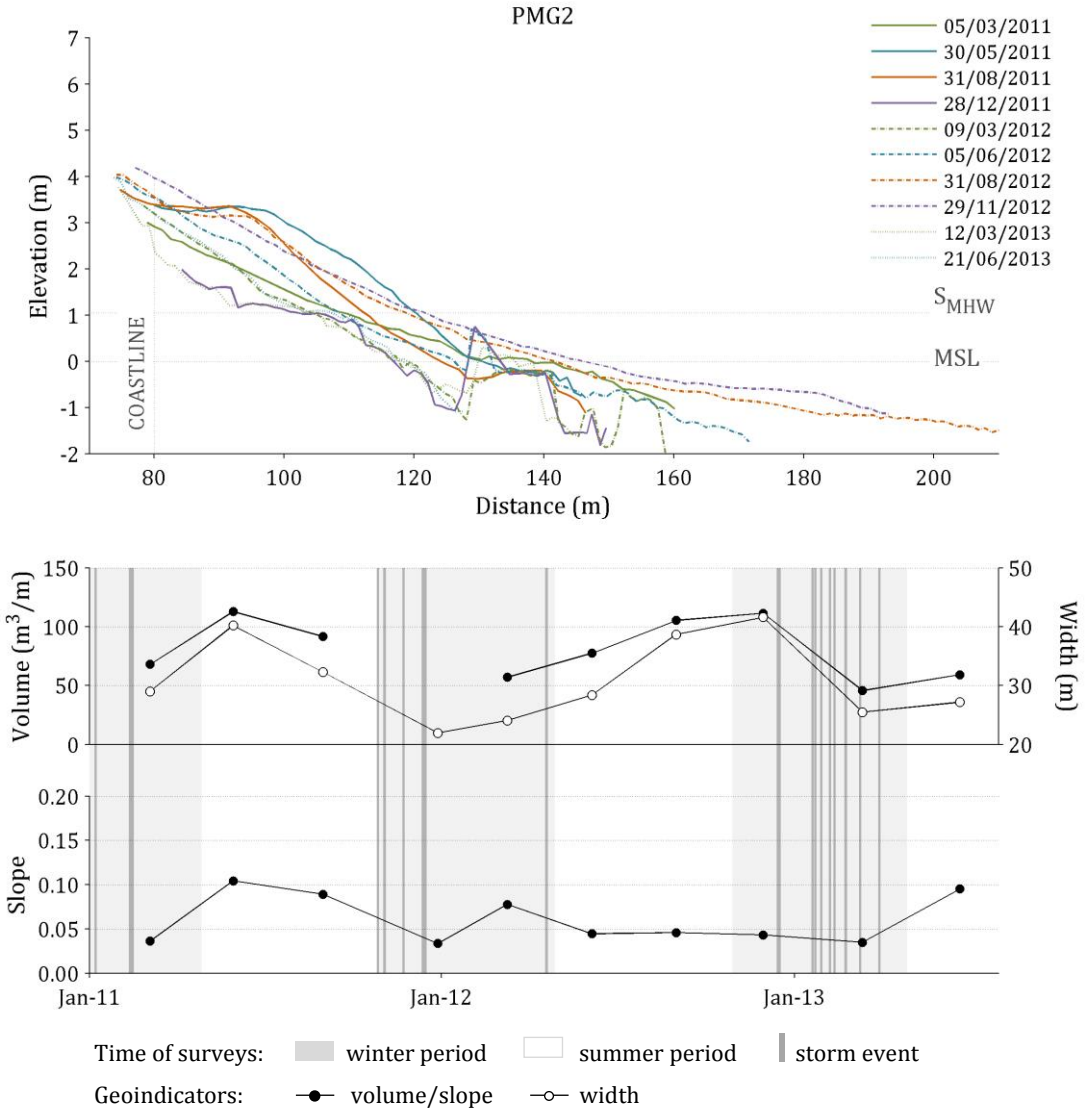

Figure 4.70. Beach profile PMG2 (Magoito study site) and variation of beach geoindicators (volume, width and slope) for the period between March 2011 and June 2013.

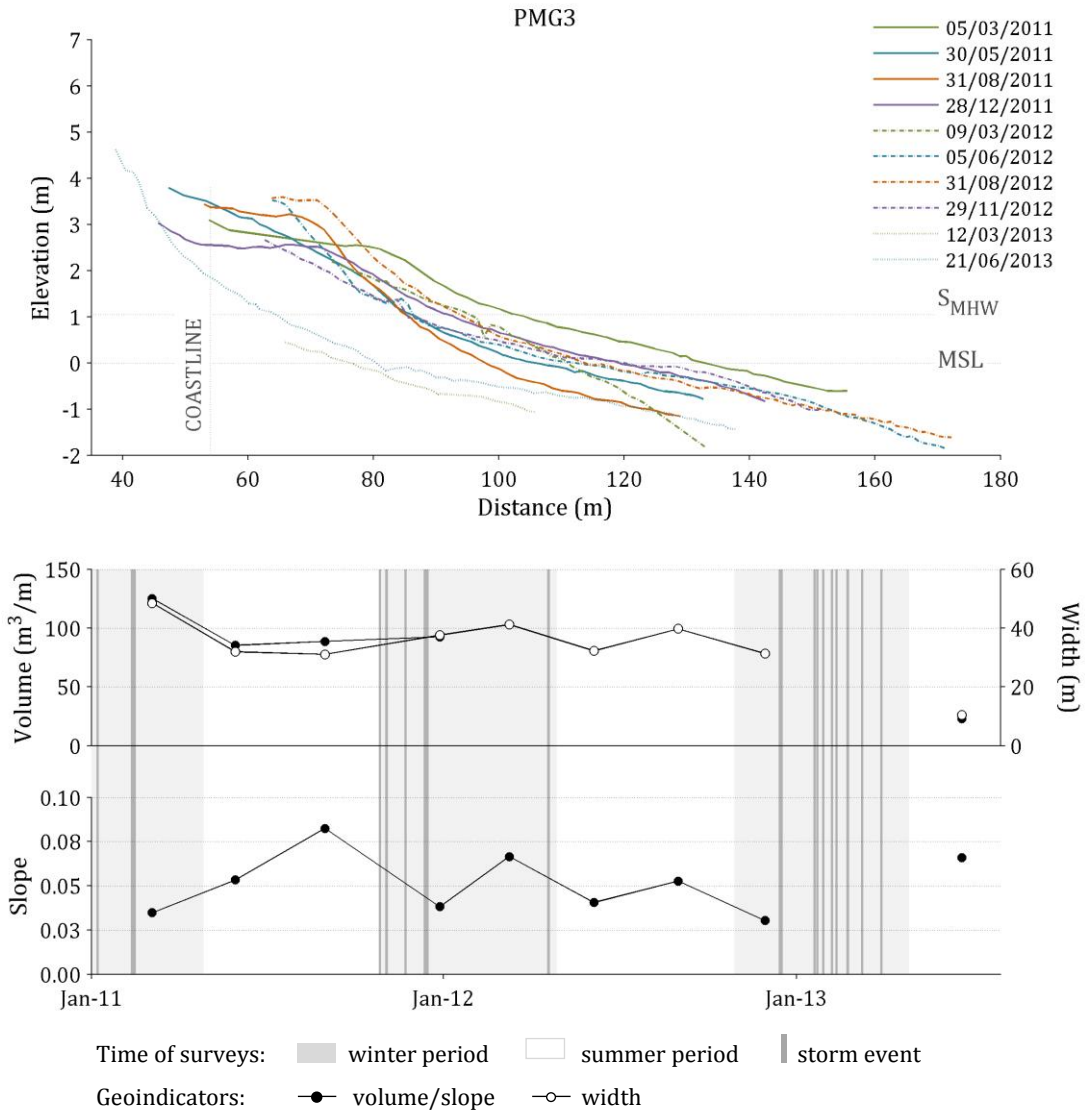

Figure 4.71. Beach profile PMG3 (Magoito study site) and variation of beach geoindicators (volume, width and slope) for the period between March 2011 and June 2013.

After a severe storm, the sediment might be almost completely removed, leaving the rocky platform exposed in its full extension up to the cliff or structure that make the beach landward limit. This pattern may persist for several weeks, as shown by the effects of the January 19, 2013 storm that stripped off all sand from Magoito beach, the whole profile still reducing to the hard substrate two months after this storm subsided (Figure 4.72).

Magoito is a typical platform beach with limited sediment availability, and therefore is characterized by a low surface with narrow berm building during the summer. Storms may result in almost complete removal of the sediment, and exposure of the underlying rocky platform.

Figure 4.72. General view of Magoito beach looking north towards PMG2, in November 29, 2012 (upper panel), and in March 12, 2013 (lower panel), showing the effect of the January 19, 2013 storm that left the rocky platform completely exposed.

Sediments vary very little, from medium to coarse sand, with mean diameters of 1.37, 1.10 and 1.21 ϕ for PMG1, PMG2 and PMG3, respectively (Figure 4.73).

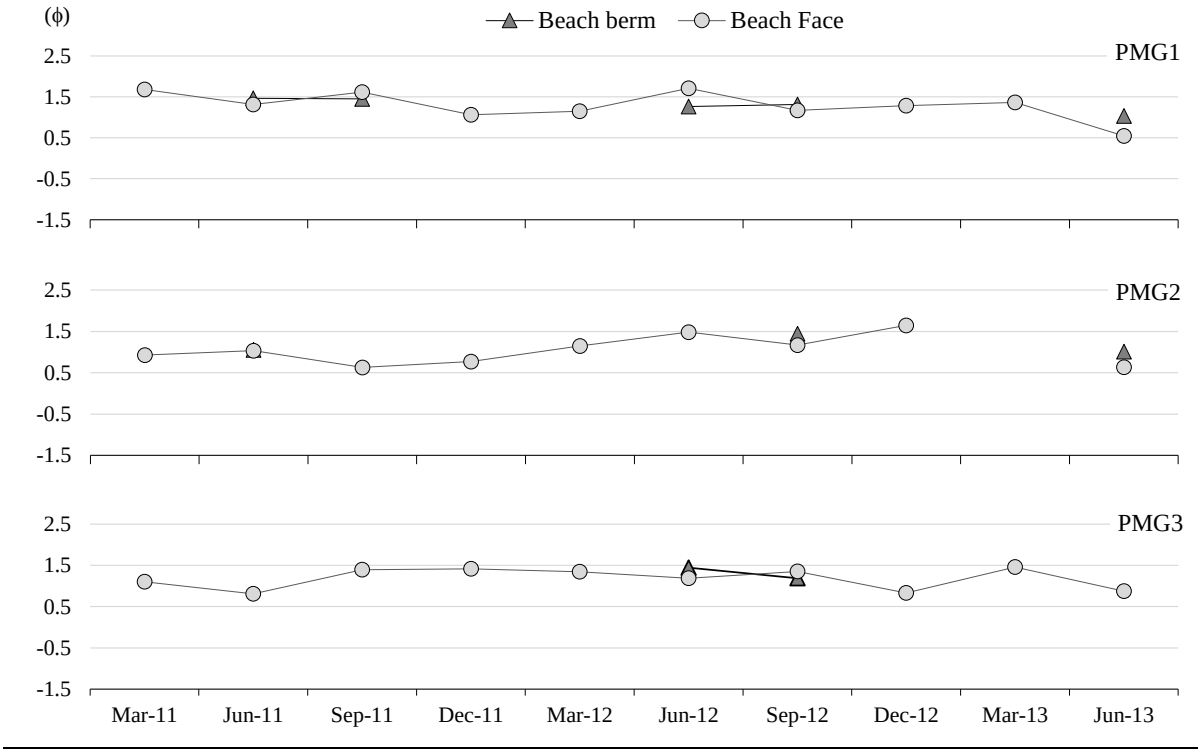

Figure 4.73. Variation of mean grain size for the period between March 2011 and June 2013, for sediment of the beach face and berm at Magoito study site.

10 Tamariz

The four Tamariz beach profiles describe the alongshore varying morphology of this embayed beach that is enclosed between structures and subjected to eastward net littoral drift, whereby the beach increases in volume and area from west to east (Figures 4.74 to 4.77, PTM1 to PTM4). PTM1, located west of the main embayment, depicts a narrow beach face with no berm, extending from the rocky platform below MSL, to the seawall structure c. 3 m above MSL. This surface has slope characteristic of reflective beaches, and is morphologically very stable. But in winter and post-storm conditions, the beach surface can be substantially lowered to a point that the entire beach surface is intertidal.

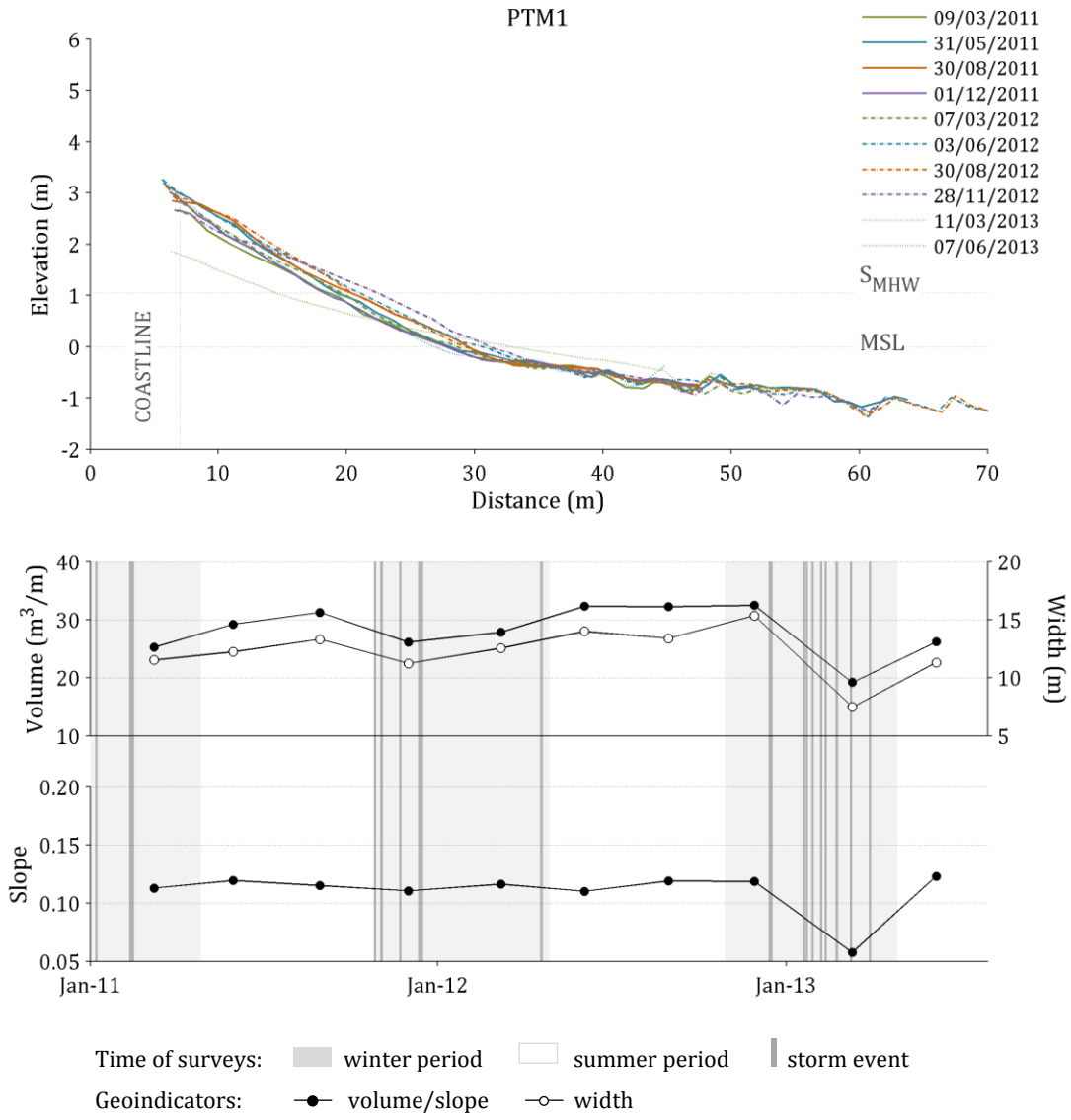

Figure 4.74. Beach profile PTM1 (Tamariz study site) and variation of beach geoindicators (volume, width and slope) for the period between March 2011 and June 2013.

The most striking characteristic of the remaining three profiles is the well-developed beach berm that occurs systematically during the summer. This is an artificial berm, built through beach scraping, to serve the recreational purpose of this urban beach. Berm width increases from PTM2 to PTM4, towards the groin that limits this embayment, and elevation is consistently low, not exceeding 3.5 m (MSL). The beach face is steep, with slope values between 0.10 and 0.11, characteristic of intermediate to reflective profiles.

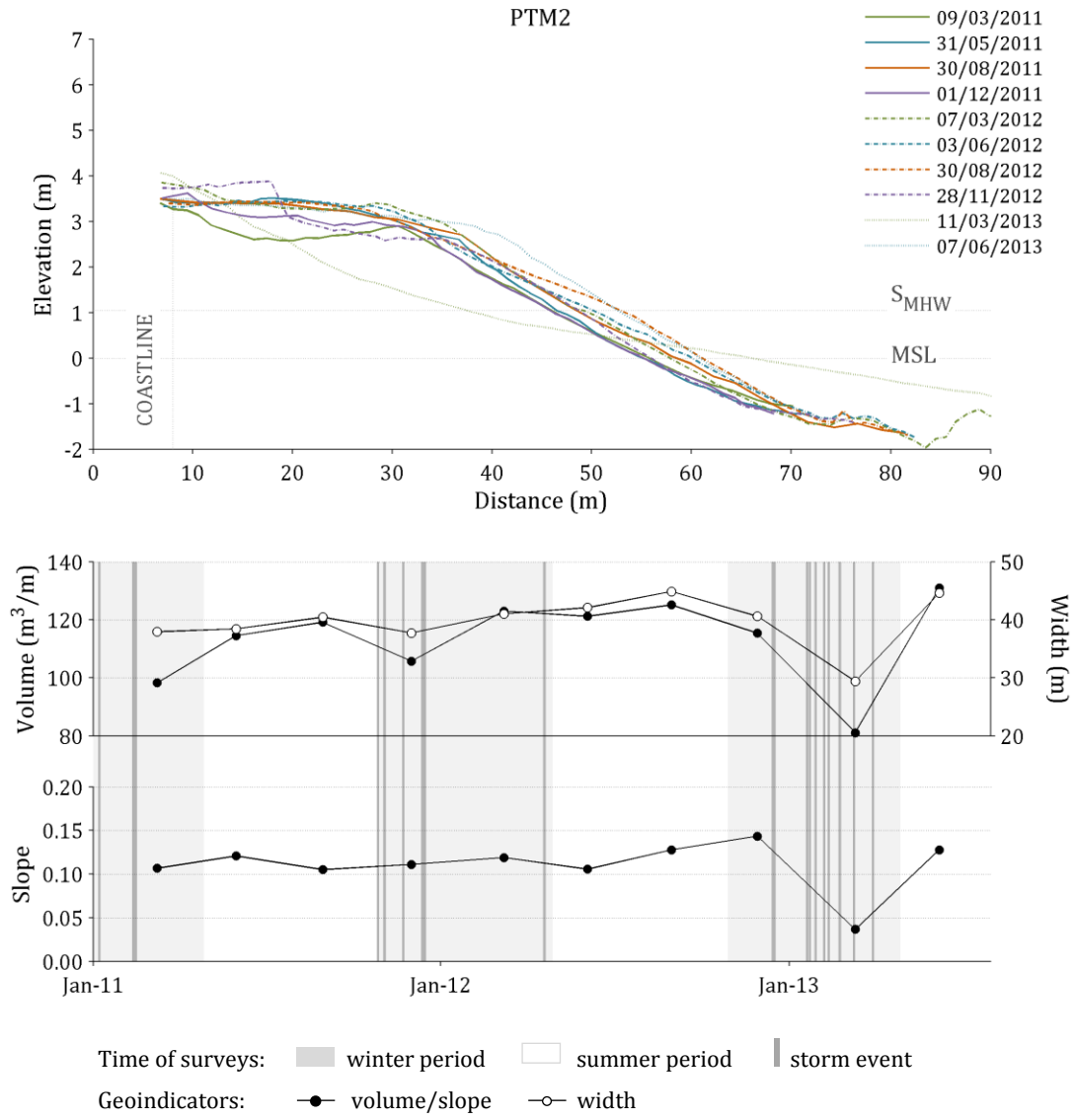

Figure 4.75. Beach profile PTM2 (Tamariz study site) and variation of beach geoindicators (volume, width and slope) for the period between March 2011 and June 2013.

Except for the surveys following the January 2013 winter storms, cross-sections differ somewhat from the summer ones. There is some lowering of the beach berm crest and a tendency to make the profile more linear, with sediment cross-shore redistribution and consequent lowering of the beach slope. However, changes are minor and the geoindicators remain fairly constant.

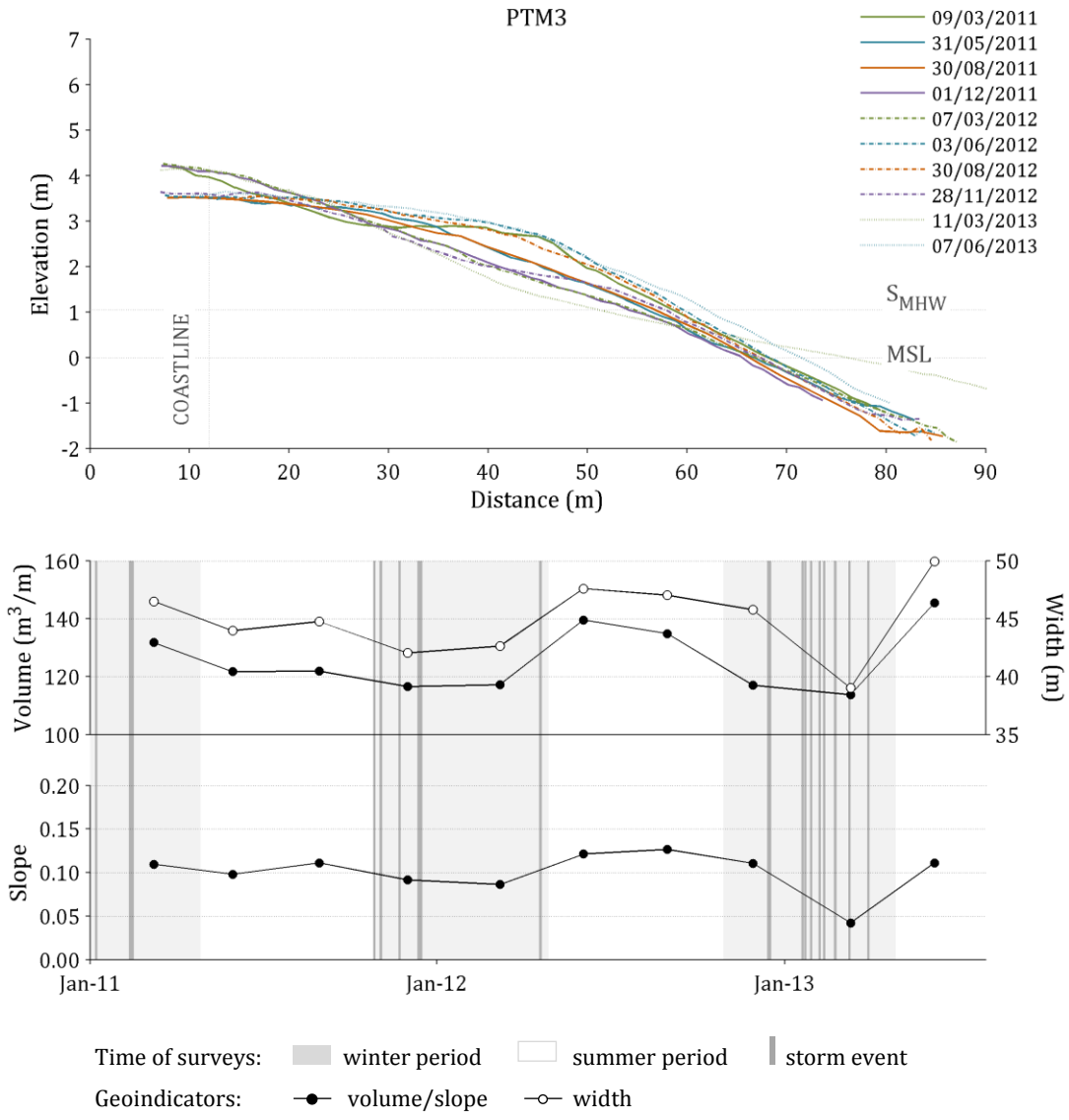

Figure 4.76. Beach profile PTM3 (Tamariz study site) and variation of beach geoindicators (volume, width and slope) for the period between March 2011 and June 2013.

The 2013 post-storm profiles are significantly different from the remaining ones, especially at PTM2, where the beach acquired a concave shape. During storm events, sediment mobilization is more intense and its redistribution across the profile, on- and off-shore, results in the destruction of the berm and in a more linear profile, with a gentler slope. The adjacent seawall is, at times, overtopped during these events, resulting in sediment transport over the seawall (Figure 4.78).

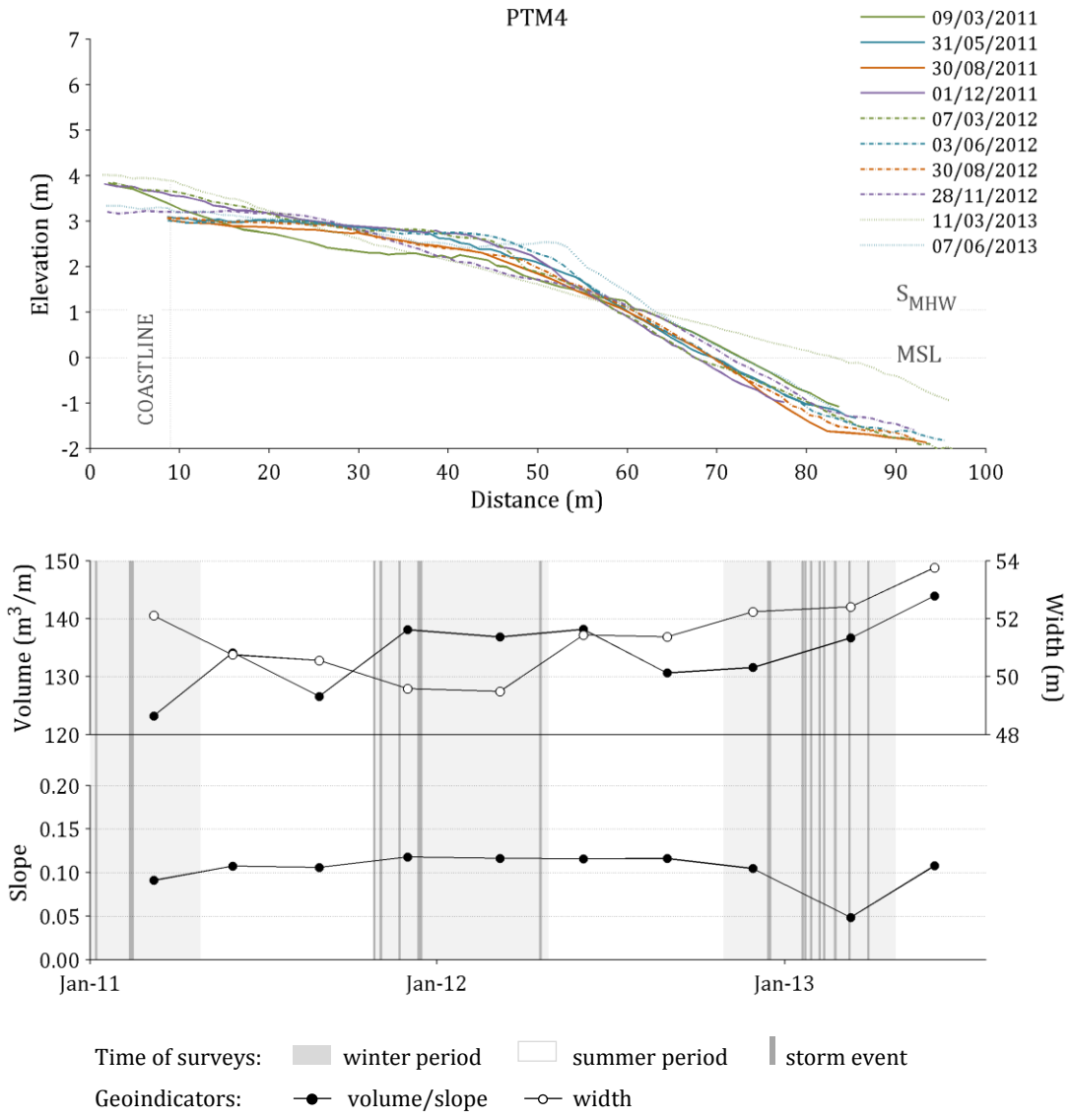

Figure 4.77. Beach profile PTM4 (Tamariz study site) and variation of beach geoindicators (volume, width and slope) for the period between March 2011 and June 2013.

Figure 4.78. Example of storm effects on Tamariz beach. Overtopping of the seawall and overwash along PTM2 and PTM3 during a storm that hit the site on October 2010.

In general, Tamariz is a fairly stable beach, artificially reshaped during the summer sand acquiring a more natural and linear shape during winter. Storms, however, impact this site by lowering of the beach surface and, more severely, by overtopping and damaging the seawall that limits the beach.

Beach sediment consists of medium sand, practically invariable over the two and a half years of monitoring (Figure 4.79). There is, however, a slight decrease in mean diameter from west to east: 1.5 ϕ in PTM1 and PTM2; 1.6 ϕ in PTM3 and 1.7 ϕ in PTM4. Samples from the beach berm show that sediments at the eastern three profiles (when present), are systematically coarser than those of the beach face (about 0.3 ϕ), although they are also classified as medium sand.

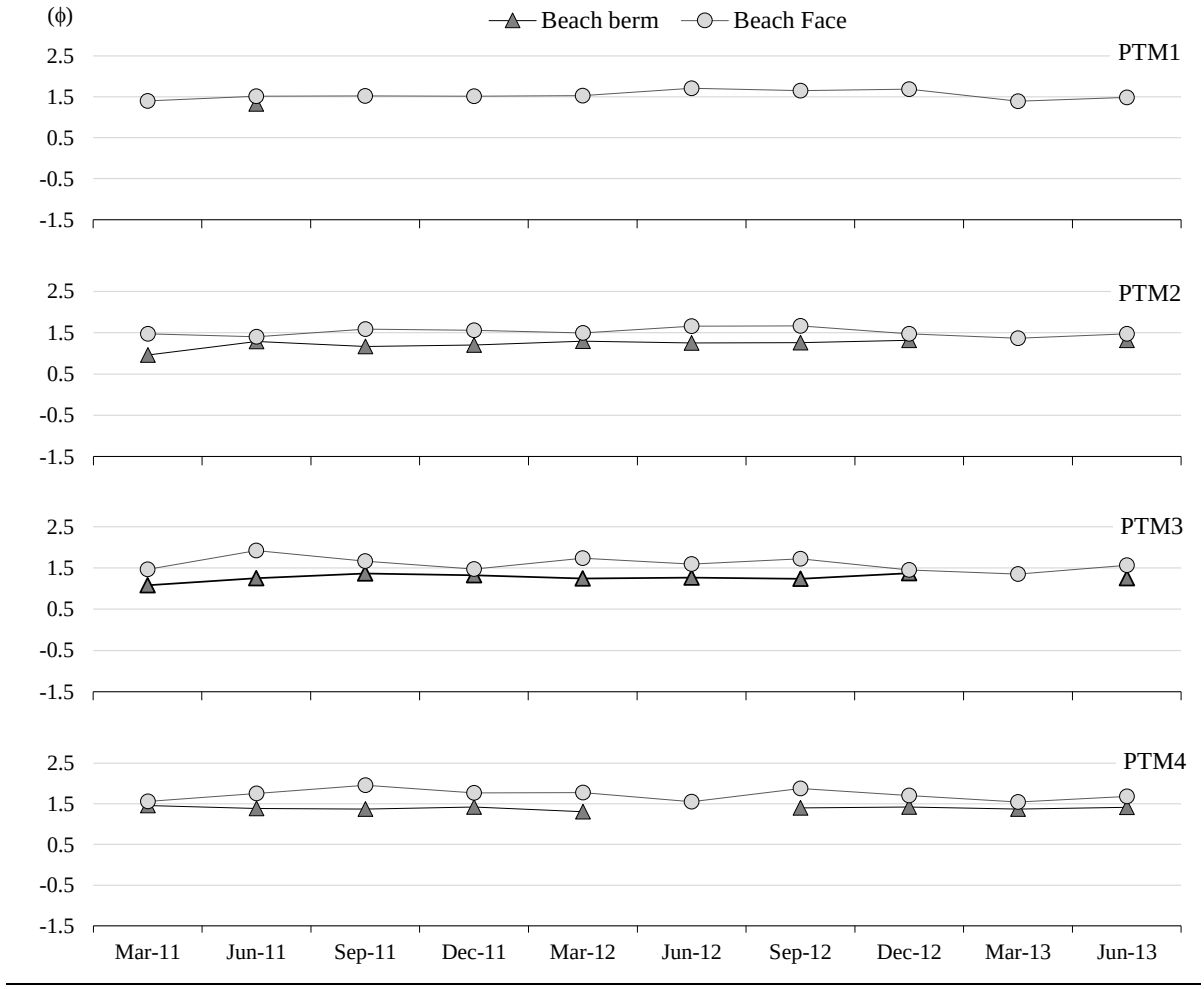

Figure 4.79. Variation of mean grain size for the period between March 2011 and June 2013, for samples taken at the beach face, beach berm and dune at Tamariz study site.

11 Costa da Caparica

Costa da Caparica study site is described in two sections, one relative to São João da Caparica and another, referred to as Groin field beaches, relative to the subsequent beaches that extend southward until, and including, Praia da Saúde.

São João da Caparica

Eleven digital elevation models were created from the high-resolution topographic surveys carried out at Sao João da Caparica (Figure 4.80). The beach is consistently wider in the northernmost sector, frequently presenting a wide berm that contacts with the adjacent dune field, and progressively narrows southward. At its southernmost region, the beach contacts the adjoining seawall structure. Here, the beach usually reduces to a low-angle beach face, only occasionally topped by a narrow and ephemeral berm.

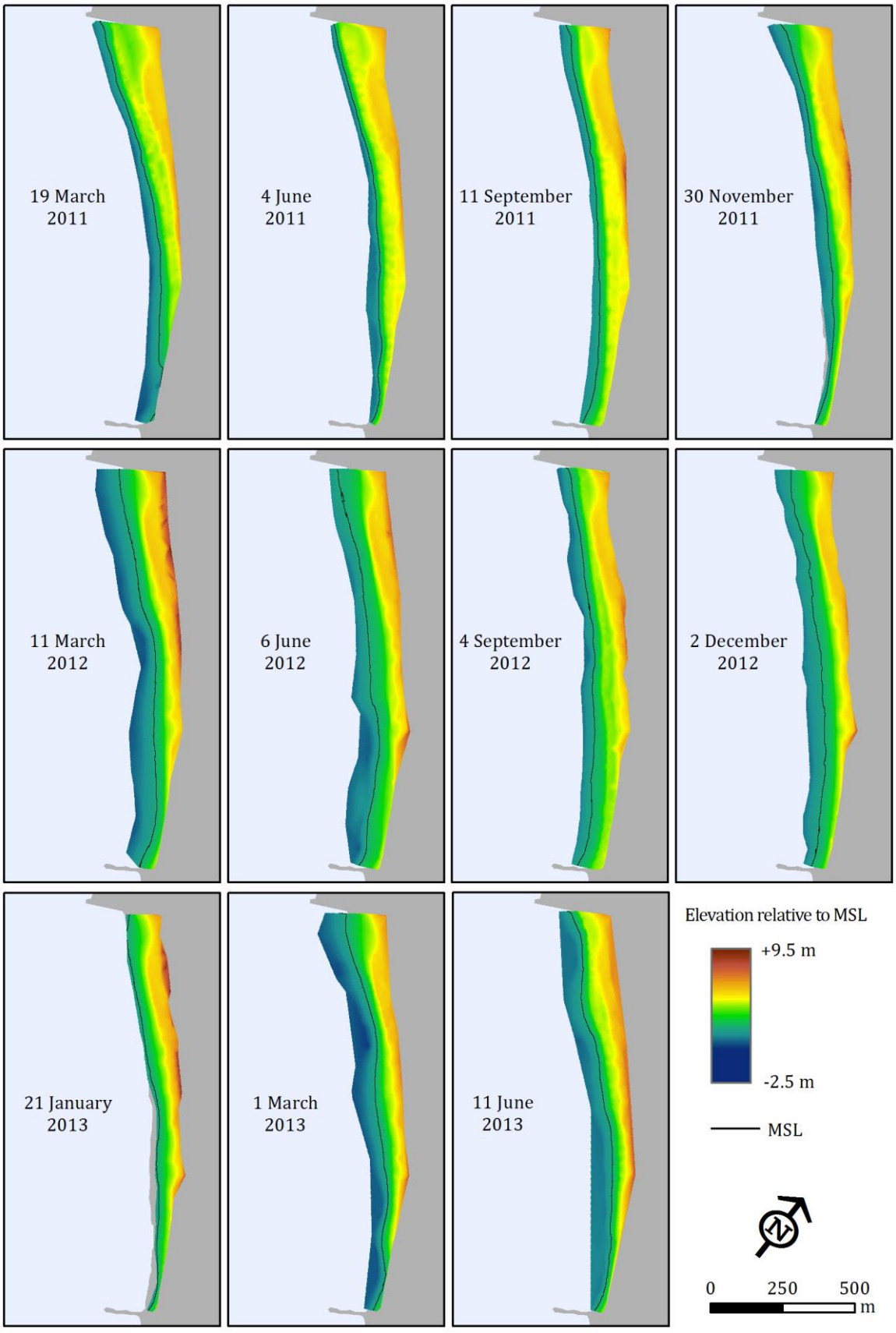

Figure 4.80. Digital elevation models of the São João da Caparica beach, part of the Costa da Caparica study site, covering the period between March 2011 and June 2013.

Changes between successive surveys reached as much as 20 % of the average beach volume (about 278x10^3 m^3), corresponding to variations of about 65 000 m^3 (Figure 4.81).

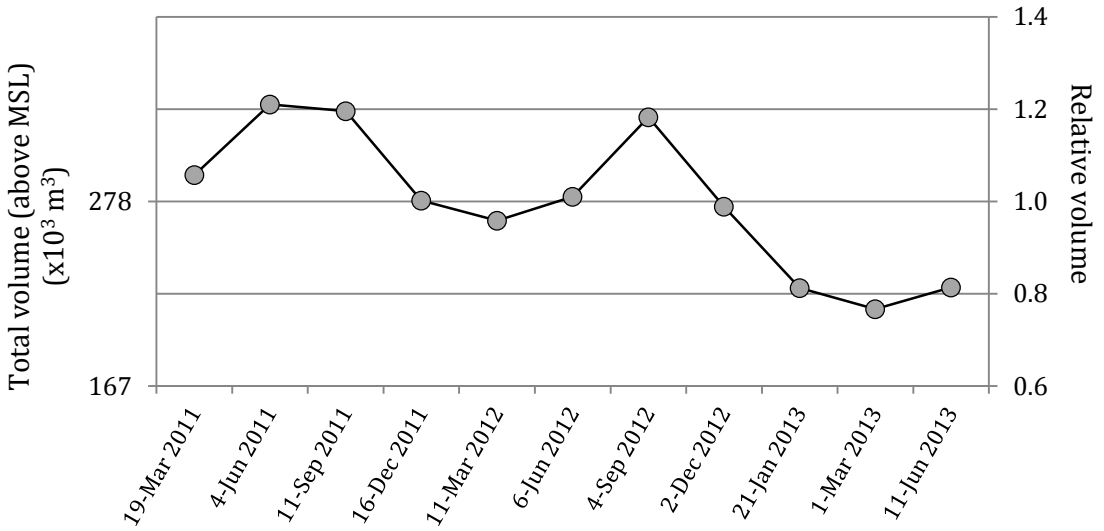

Figure 4.81. Beach volume measured from each survey of the São João da Caparica beach. Left axes: absolute volume (x10^3 m^3) and right axes: volume relative to average.

Sediment budget analysis between consecutive surveys was obtained from the difference in elevation surfaces that hold the magnitude of sediment losses and gains along the beach (Figure 4.82 and 4.83). Positive net changes occurred always in the summer season, between March and June, or June and September, whilst net sediment losses concentrated in the winter, between September and December, or December and March. Furthermore, these surfaces of altimetric change depict alternate and opposite behaviors between the northern and southern sectors, indicating that the beach rotates seasonally by growing in the south and eroding in the north during summer, and retreating in the south and accreting in the north during the winter. The analysis of the shoreline (MSL contour) variation during the survey period highlights this pattern of beach rotation (Figure 4.84).

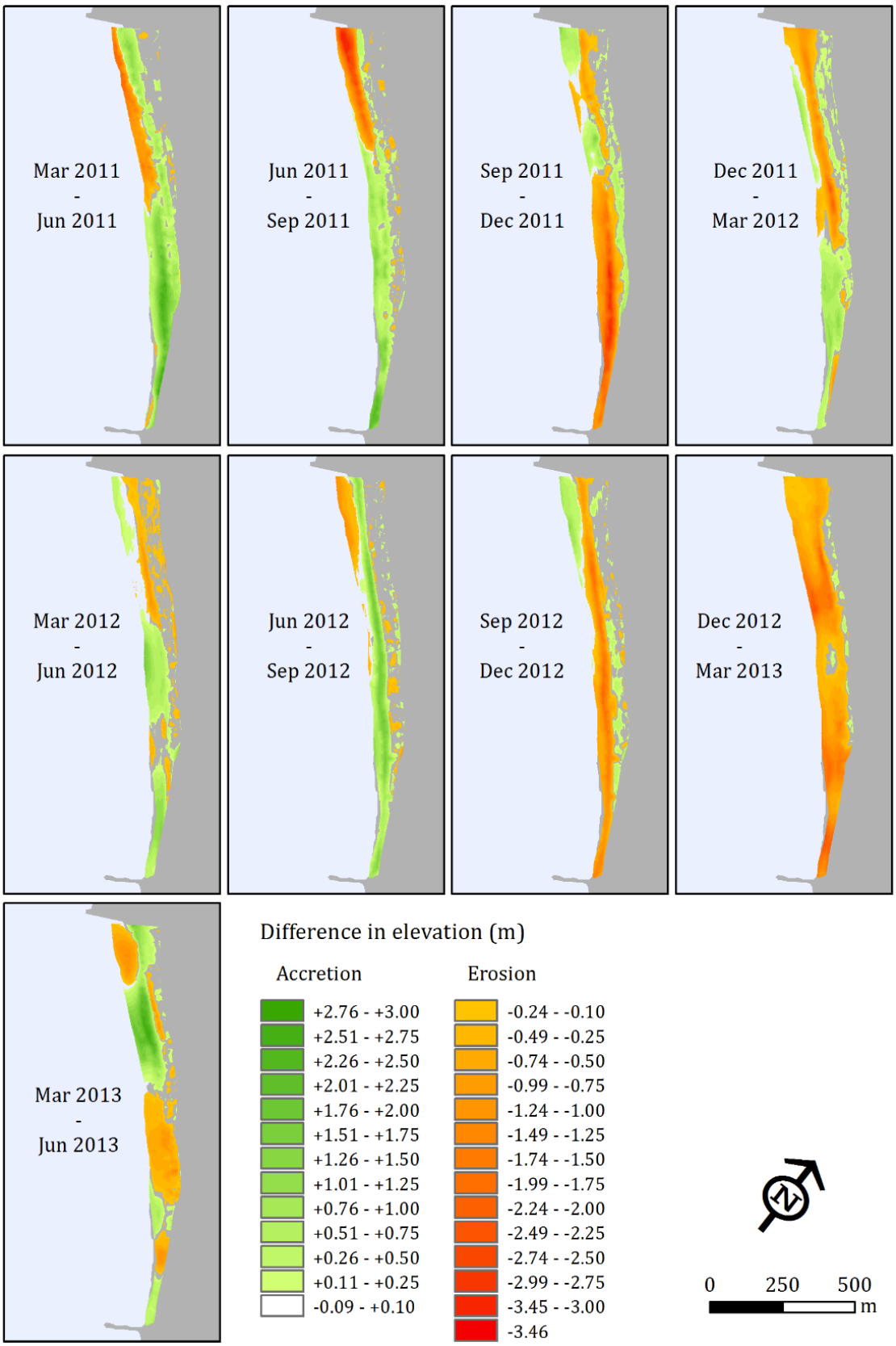

Figure 4.82. Difference in elevation surfaces portraying the altimetric changes between consecutive surveys at São João da Caparica beach. Locations of sediment loss are highlighted in orange -red color scale; and locations of sediment gains in green color scale.

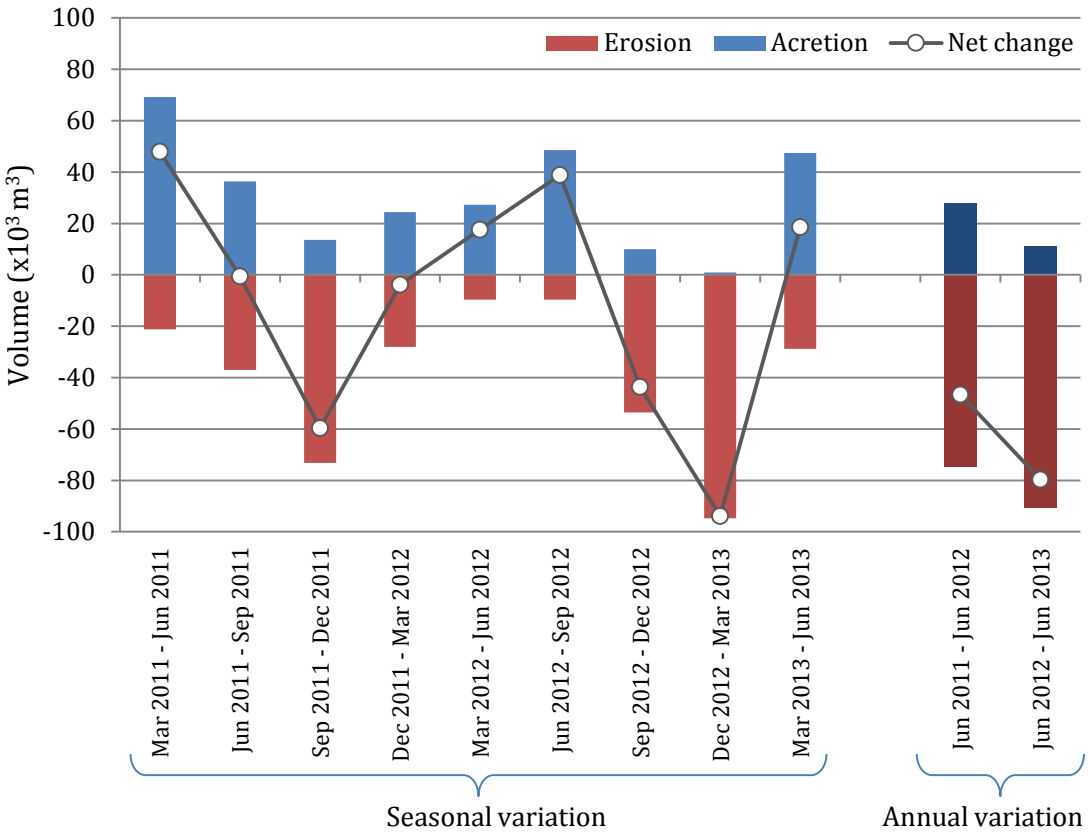

Figure 4.83. Seasonal and annual sediment budget for São João da Caparica beach. Total accretion (blue bars), erosion (red bars) and net volume change (circle markers) between consecutive surveys and between the months of June of each year of the survey period.

The surfaces and shorelines depict a segment of relative stability located between 300 and 600 m south of the northernmost groin, suggesting that this is the rotation point of the beach.

The January 2013 winter storm had considerable impacts along the entire length of the beach. Sediment transfers reached a maximum of 94000 m^3, almost exclusively related to sediment loss, between December 2012 and March 2013, and the shoreline retreated on average 20 m along its full extension and up to 41 m in the south sector. There were evidences of some sediment transfer towards the upper part of the beach and dunes, through wind-blown sand accumulation (Figure 4.85).

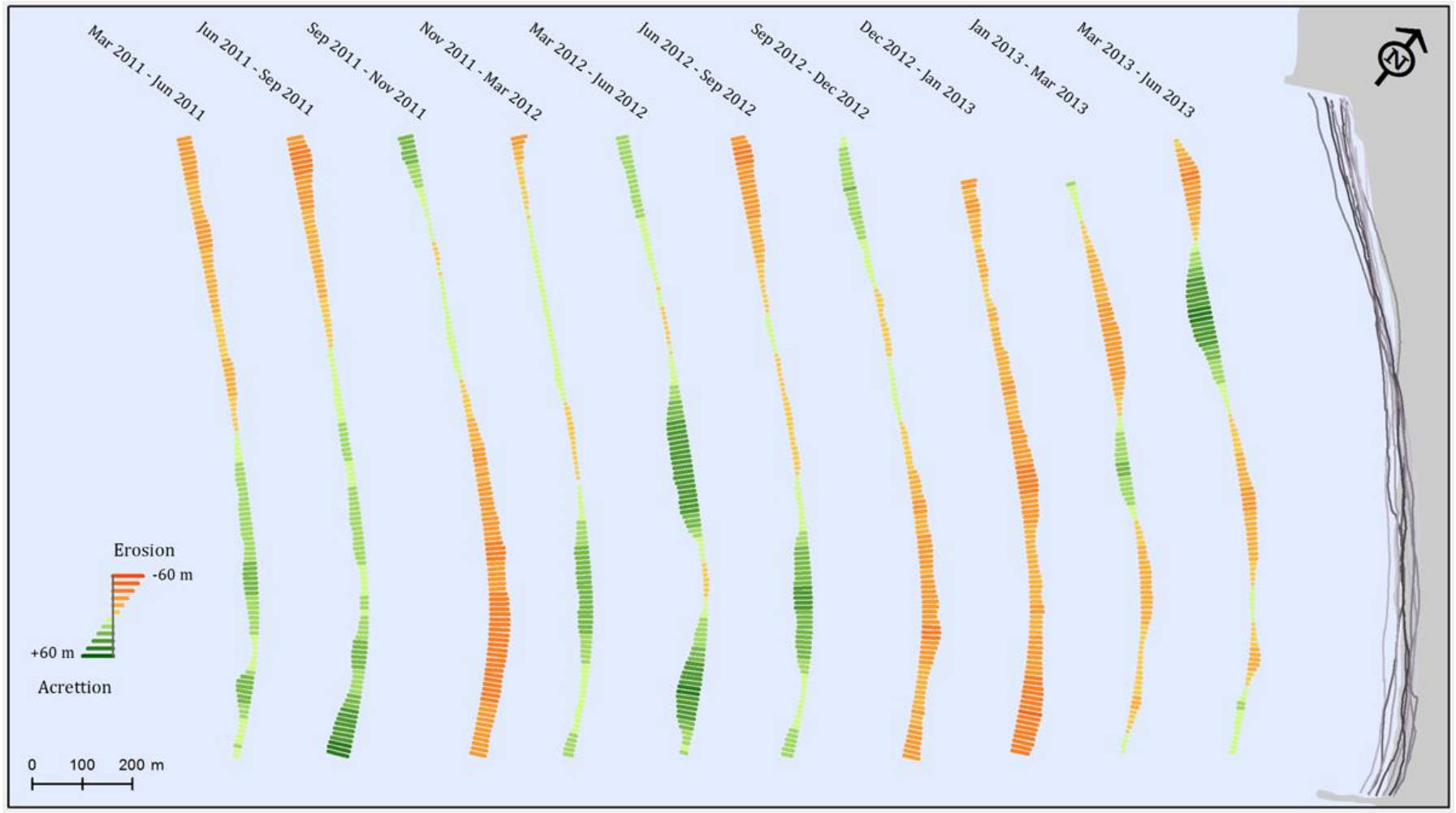

Figure 4.84. Shoreline change between consecutive surveys, March 2011 to Jun 2013, at São João da Caparica. Colored vectors depict MSL contour displacement every 10 m alongshore.

Figure 4.85. Photograph taken on January 21, 2013, of the upper beach area at São João da Caparica, showing the accumulation of wind-blown sand against sand fences and covering one of the concessionary areas.

Annual variations, obtained from the comparison between the DEM from June of each year, are comparable in magnitude and spatial distribution to those of the seasonal scale. Three years of monitoring is insufficient to detect an annual and long term behavior, and the difference in elevation models actually portray the occurrences of the preceding winter season (Figure 4.86).

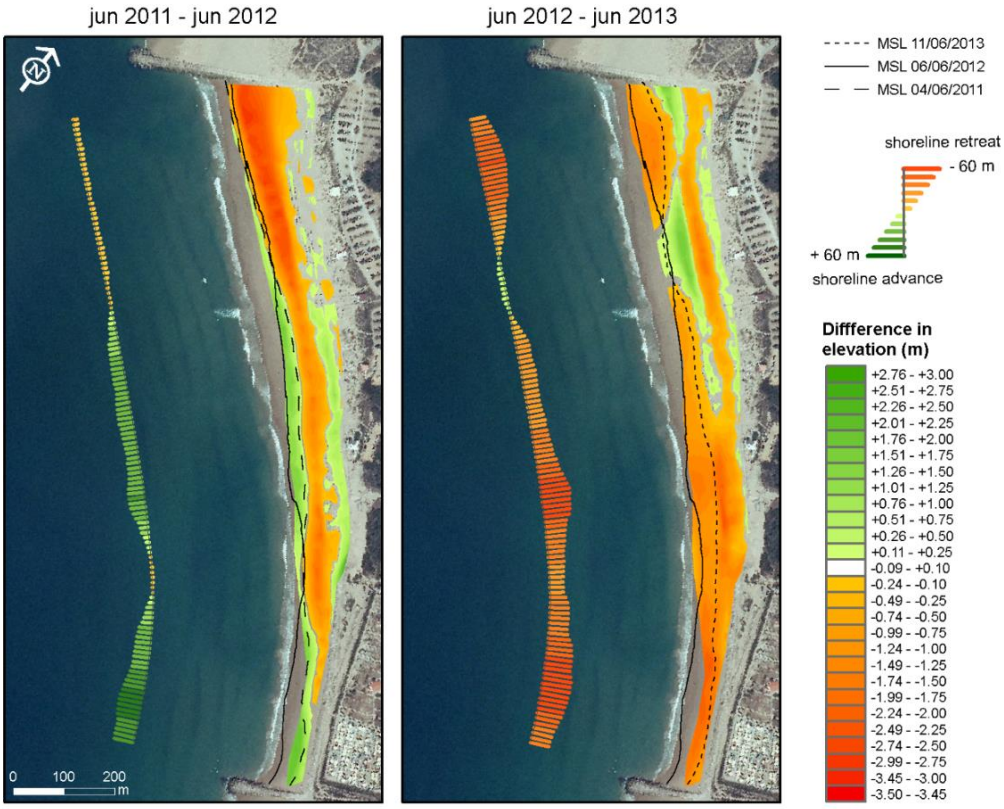

Figure 4.86. Difference in elevation maps portraying the altimetric changes between the June annual surveys at São João da Caparica beach. Locations of sediment loss are highlighted in orange -red color scale; and locations of sediment gains in green color scale.

The cross-sections pertaining to the São João da Caparica section of Costa da Caparica study site, correspondent to the PCC1 to PCC8 beach profiles (Figures 4.87 to 4.94), reveal the same general pattern of behavior as detected in the DEM and shoreline analysis, although the rotational behavior is not as evident.

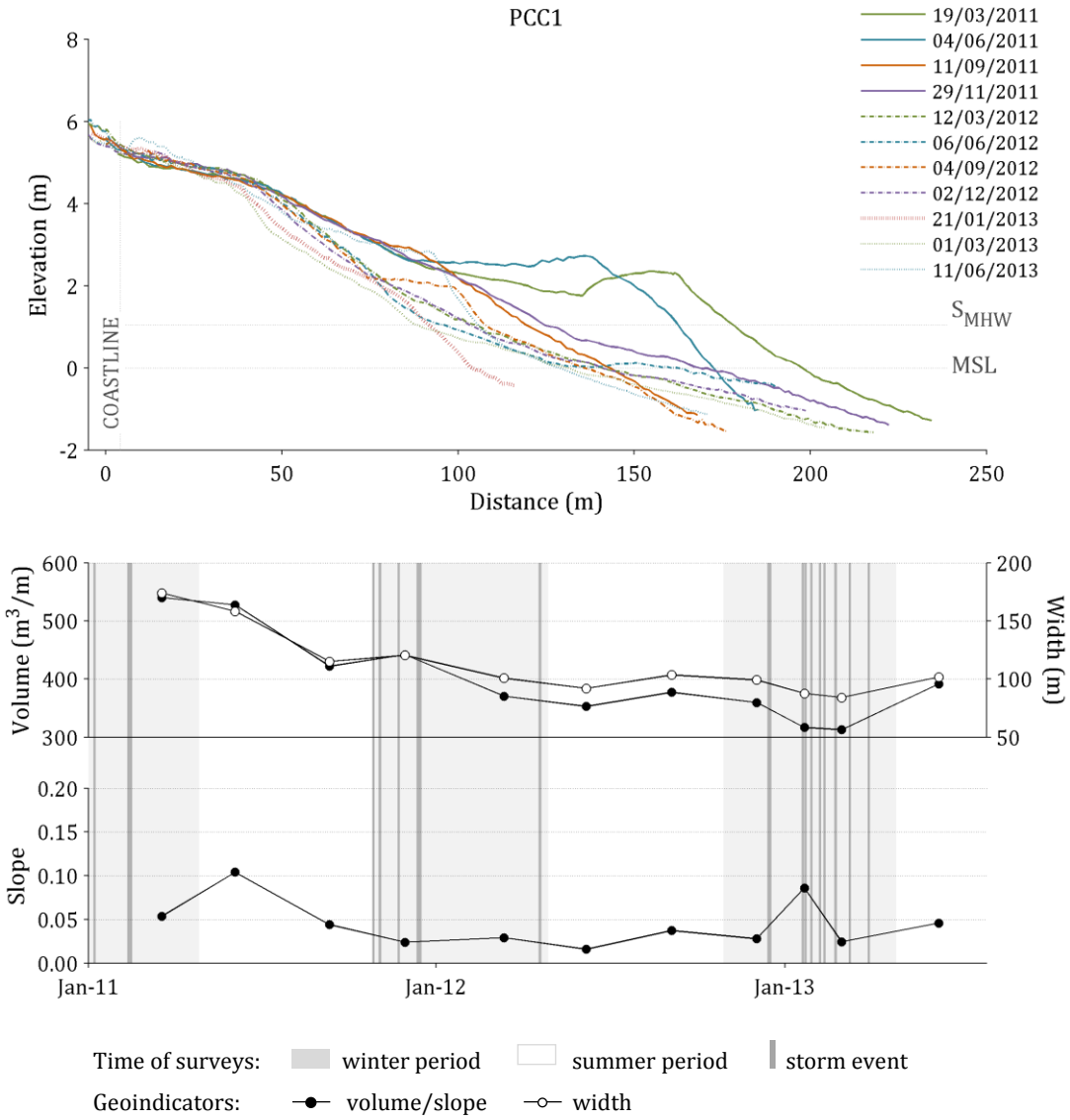

Figure 4.87. Beach profile PCC1 (Costa da Caparica study site) and variation of beach geoindicators (volume, width and slope) for the period between March 2011 and June 2013.

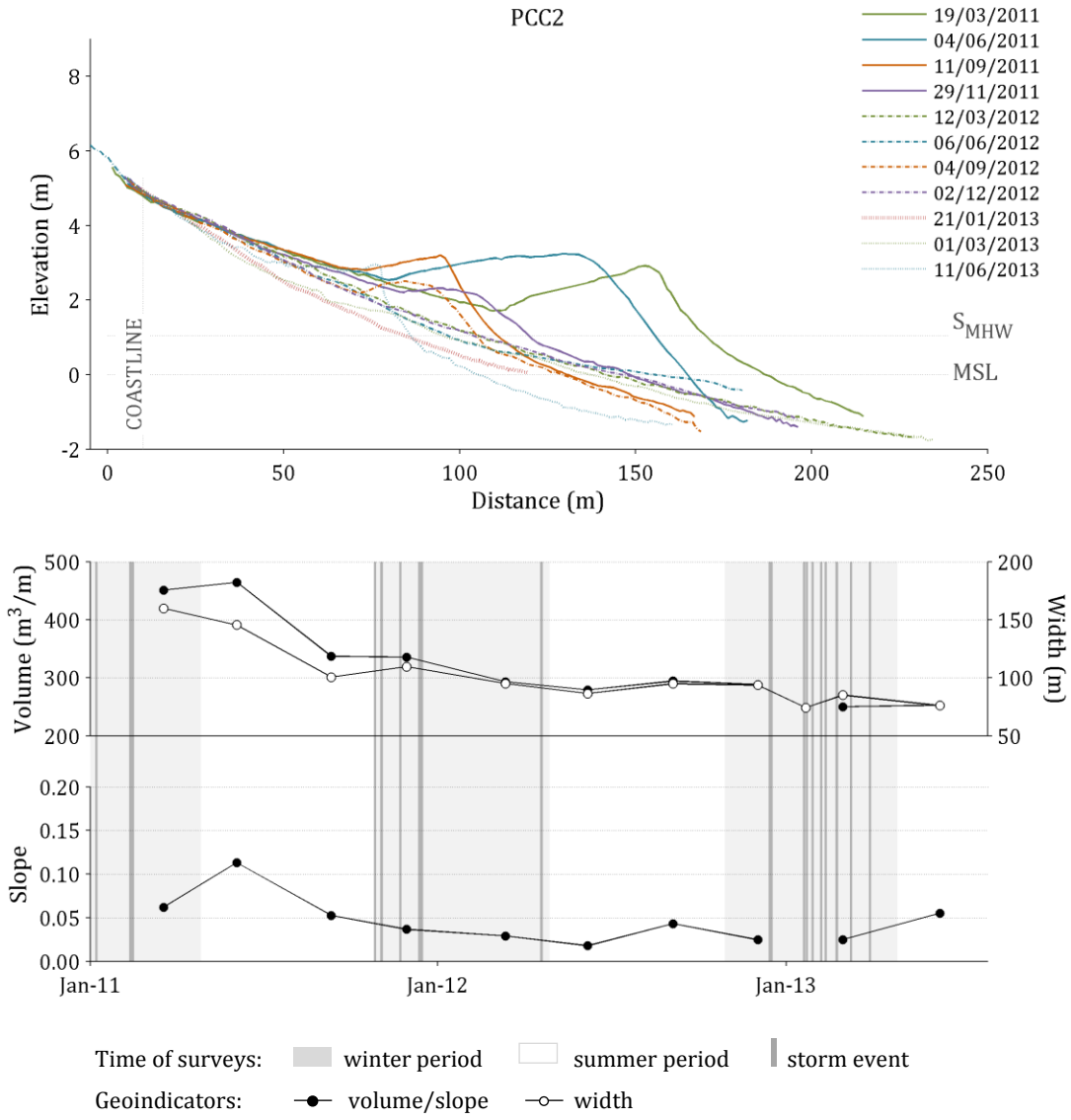

Figure 4.88. Beach profile PCC2 (Costa da Caparica study site) and variation of beach geoindicators (volume, width and slope) for the period between March 2011 and June 2013.

In general, all cross-sections reflect the high variability of São João da Caparica, changing considerably in volume, width and slope. The latter parameter, for example, varies between 0.02 (typically in the winter) and 0.10 for all profiles, corresponding to alternating morphologies with different stages of beach berm growth.

Profiles located north of the rotation point (PCC1 to PCC3) show wider berms, developing at higher elevations (4 m) than the southernmost ones (3 m). PCC7 and PCC8, in the southernmost sector of the beach, are the narrowest profiles, and seldom show berm development. This is mostly due to the limited accommodation space fronting the seawall structure that exists there, but also because of the induced reflection processes.

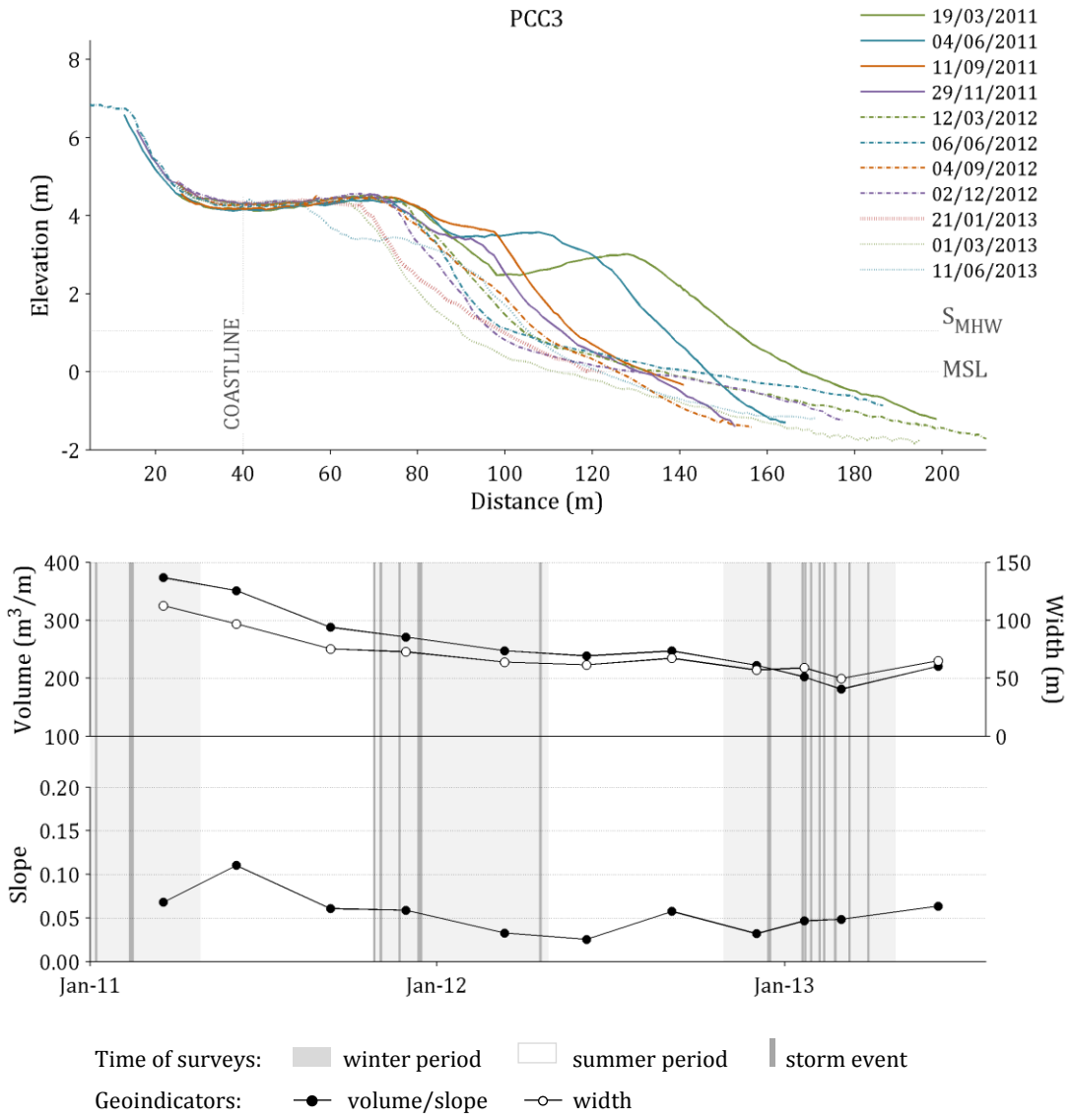

Figure 4.89. Beach profile PCC3 (Costa da Caparica study site) and variation of beach geoindicators (volume, width and slope) for the period between March 2011 and June 2013.

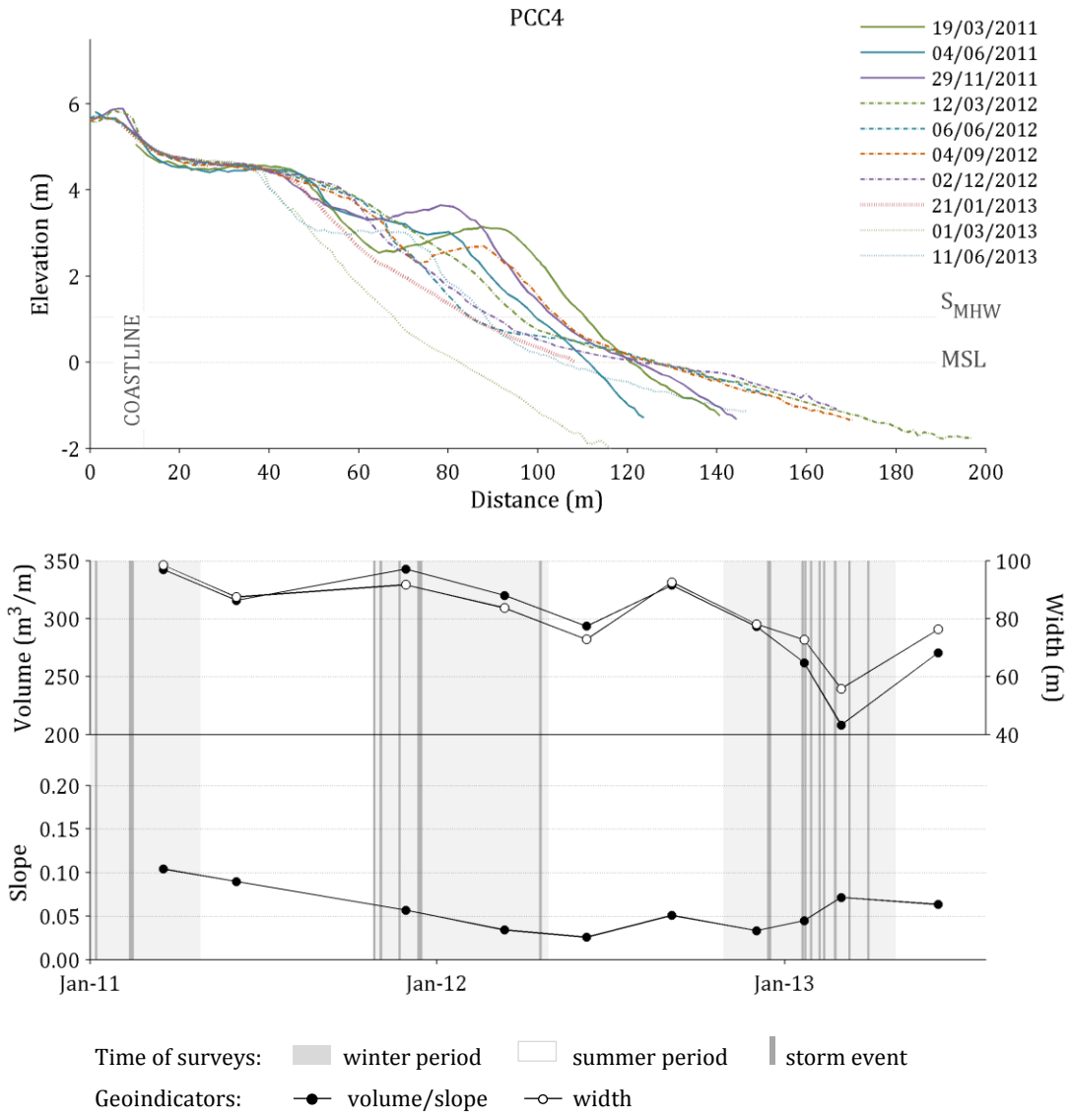

Figure 4.90. Beach profile PCC4 (Costa da Caparica study site) and variation of beach geoindicators (volume, width and slope) for the period between March 2011 and June 2013.

In general, it is possible to detect a seasonality associated to the beach configuration, where the widest and most robust configuration (with substantial berm development) occurs in summer, and the narrowest and most flattened configuration corresponds to winter or post-storm periods. Nevertheless, beach configurations in between these two peaks occur during the overall survey period, with narrower berms in some summer surveys, and occurrence of intertidal bar welding onto the beach face in some winter surveys. As a consequence of this variability, the pattern of volume and width evolution through time does not show a clear seasonality.

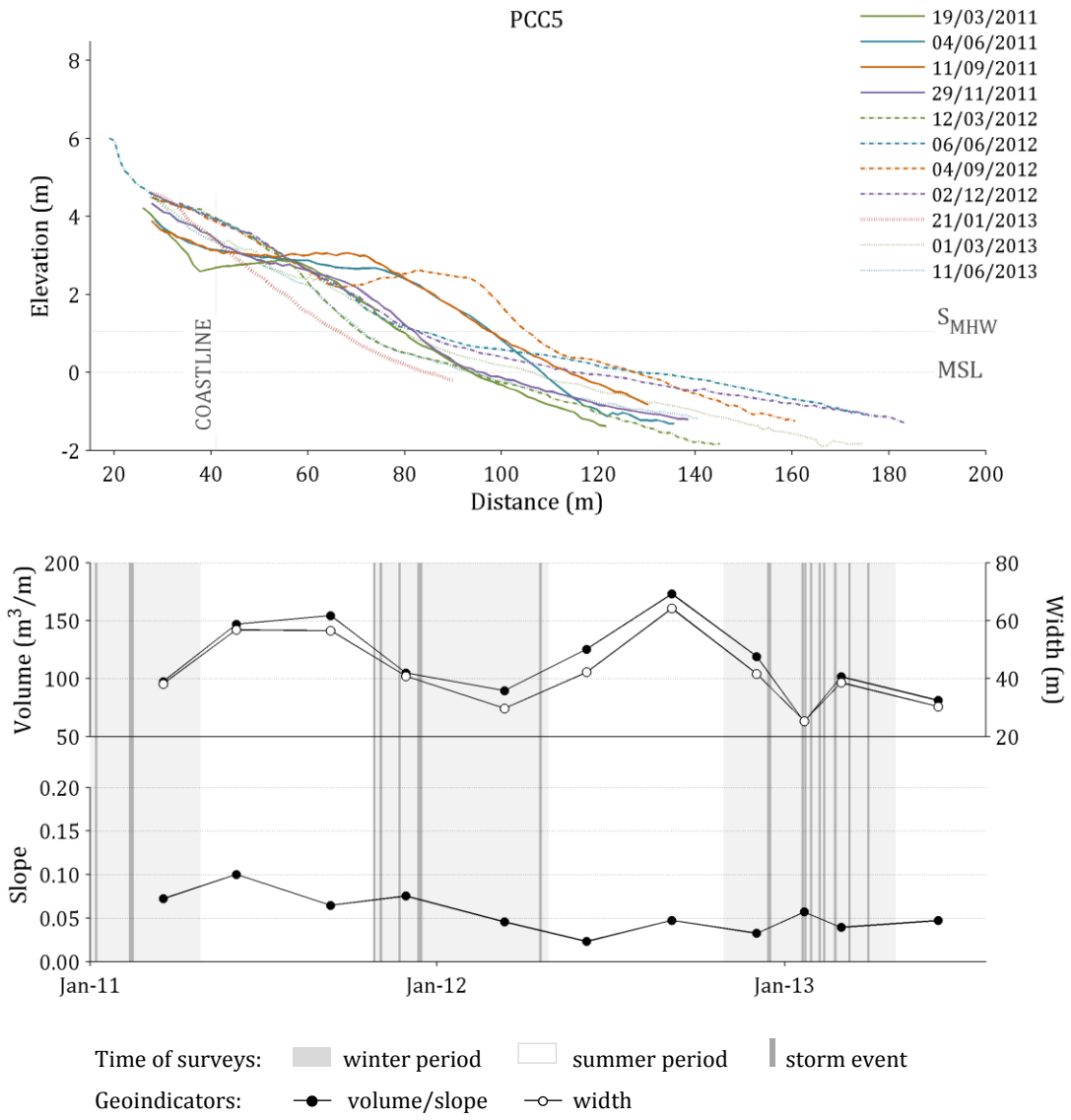

Figure 4.91. Beach profile PCC5 (Costa da Caparica study site) and variation of beach geoindicators (volume, width and slope) for the period between March 2011 and June 2013.

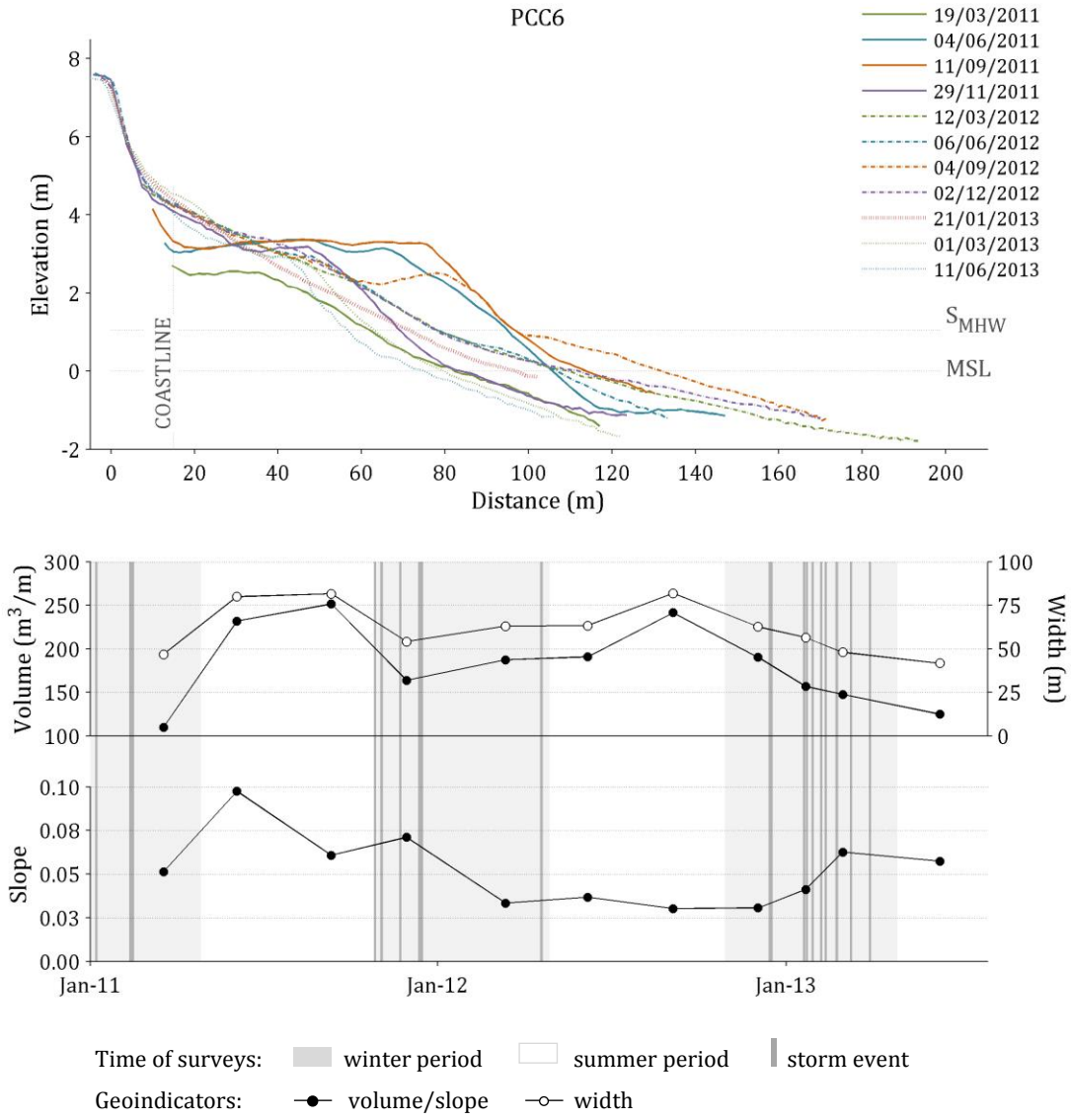

Figure 4.92. Beach profile PCC6 (Costa da Caparica study site) and variation of beach geoindicators (volume, width and slope) for the period between March 2011 and June 2013.

Overall, São João da Caparica beach undergoes considerable variation at the seasonal scale, with volumetric changes on the order of 10^4 m^3 and migration of the shoreline by tens of meters, capable of affecting the entire subaerial beach, up until its landward limit. There is a seasonal behavior related to beach rotation, with retreat of the northernmost sector and accretion in the southernmost one until September, and opposite behavior until December.

During the study period, storms reached and overtoped the dunes and structure, promoting the creation of scarps of several meters. Still, post-storm recovery took place in a few months, indicating that the beach corresponds to a resilient system.

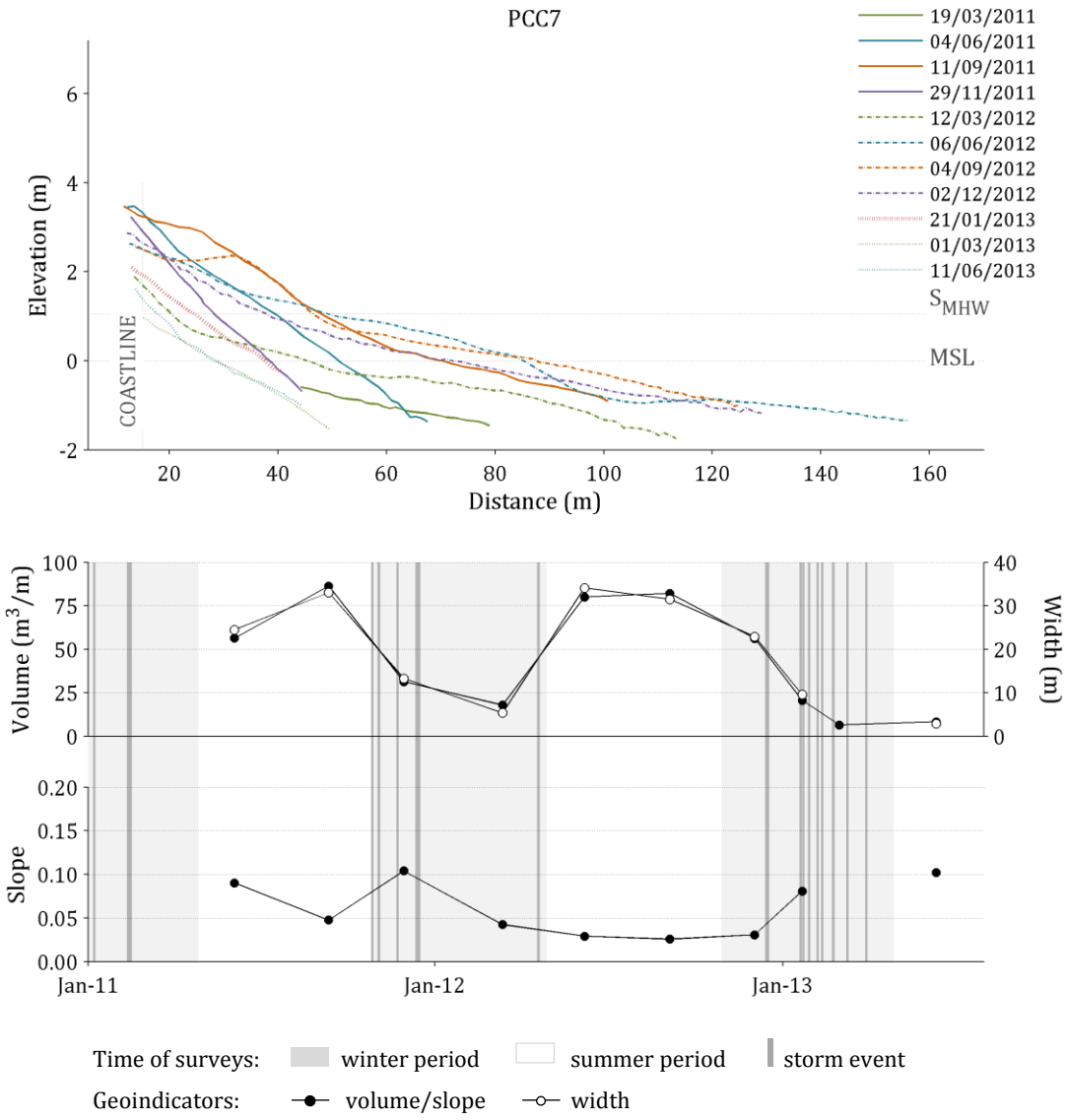

Figure 4.93. Beach profile PCC7 (Costa da Caparica study site) and variation of beach geoindicators (volume, width and slope) for the period between March 2011 and June 2013.

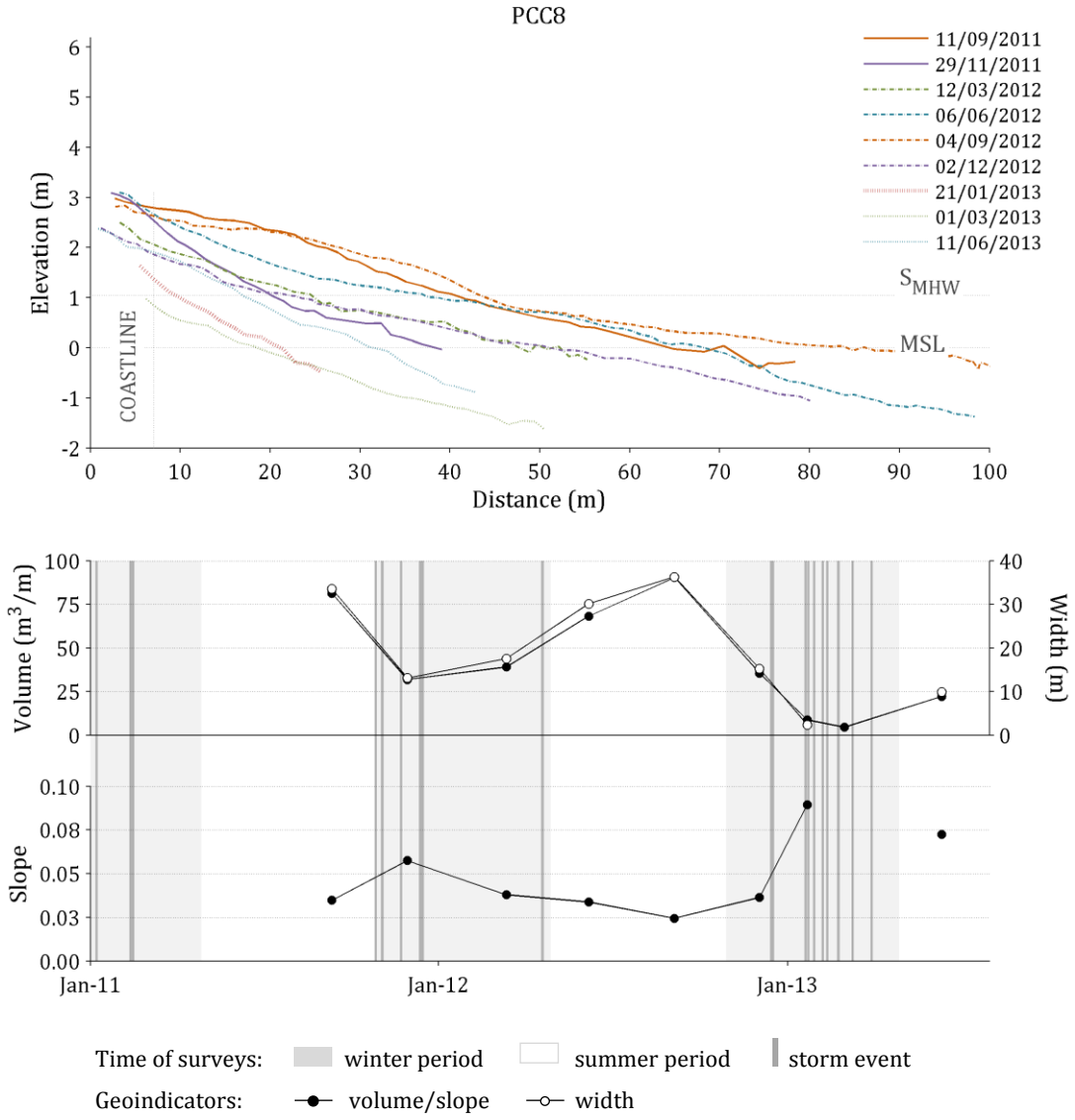

Figure 4.94. Beach profile PCC8 (Costa da Caparica study site) and variation of beach geoindicators (volume, width and slope) for the period between March 2011 and June 2013.

Sediment description for São João da Caparica is based on the samples collected at profiles PCC2 and PCC6 (Figure 4.95). Sediments are classified as fine to medium sand. PCC2 beach face, berm and dune sediments are very similar and invariant through time, with average mean grain size values of 1.8 ϕ. Sediments of the southernmost section of the beach (characterized by PCC6) are somewhat coarser and a little more variable than those of the northern section, showing an average mean diameter of 1.6 ϕ at the berm.

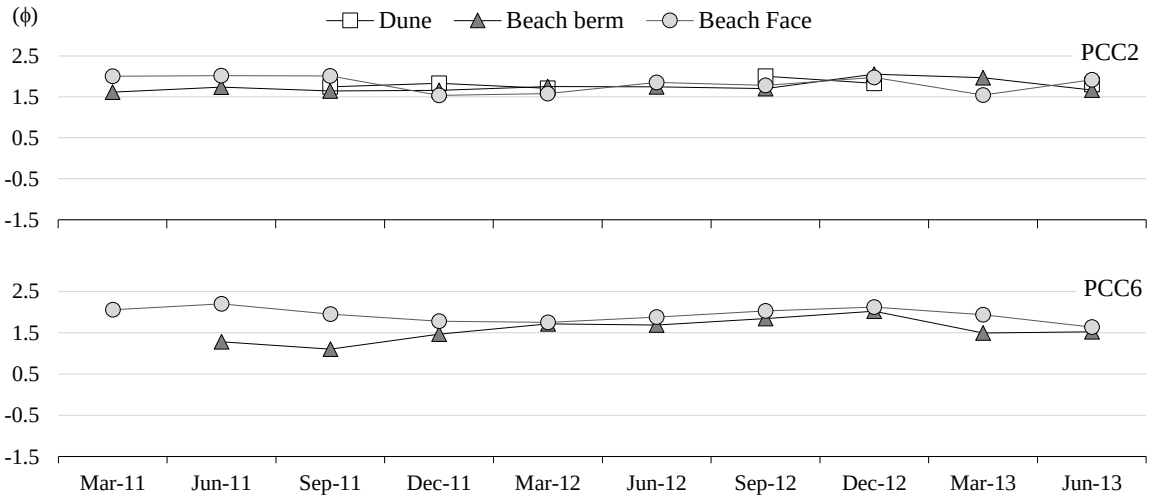

Figure 4.95. Variation of mean grain size for the period between March 2011 and June 2013, for samples taken at the beach face, beach berm and dune at São João da Caparica section of the Costa da Caparica study site.

Groin field

The Groin field section of Costa da Caparica study site corresponds to the beaches that extend southwards of São João da Caparica. Six beach profiles – PCC9 to PCC14 – describe the beaches that develop between groins (Figures 4.96 to 4.101), and three profiles are located south of the last groin – PCC15 to PCC17 – and describe the northern tip of the sand ribbon with open beaches that characterize the Caparica-Espichel coastal stretch (Figures 4.102 to 4.104). PCC15, is located adjacent to the last (southernmost) groin and is limited by the seawall in its landward side, and therefore behaves similarly to the within-groins profiles.

Beach profiles enclosed by the groins are generally concave in shape, narrow (maximum of 80 m), and with slopes typical of dissipative to intermediate morphodynamic stages (0.04-0.05 on average). PCC9 to PCC11 are narrower than the rest of the beaches and generally featureless, characterized by small volumes. From PCC12 southwards, the coastline bends inland, following the configuration of the seawall, whereas the shoreline retains its general alignment. For this reason, the southernmost beaches have more space to retain more sediment and thus more volume. These conditions allow for the development of a summer berm around the elevation of 3 m above MSL.

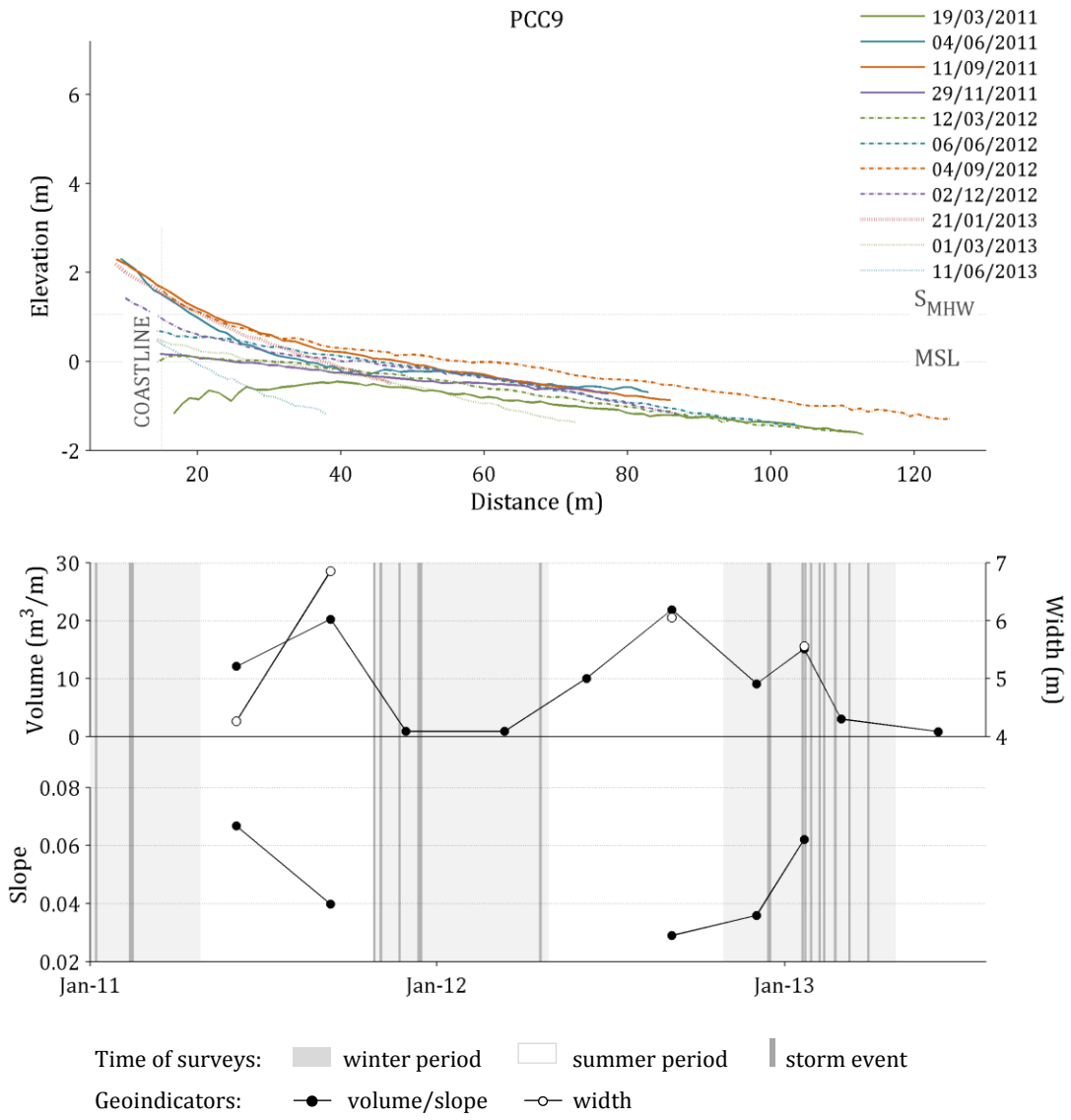

Figure 4.96. Beach profile PCC9 (Costa da Caparica study site) and variation of beach geoindicators (volume, width and slope) for the period between March 2011 and June 2013.

The full cross-section of the profiles in the groin field experiences variations up to the contact with the seawall, varying in height at the coastline on the order of 2.5-4 m. The impact of winter storms is felt along the entire length of the groin field beaches promoting decrease in volume and width.

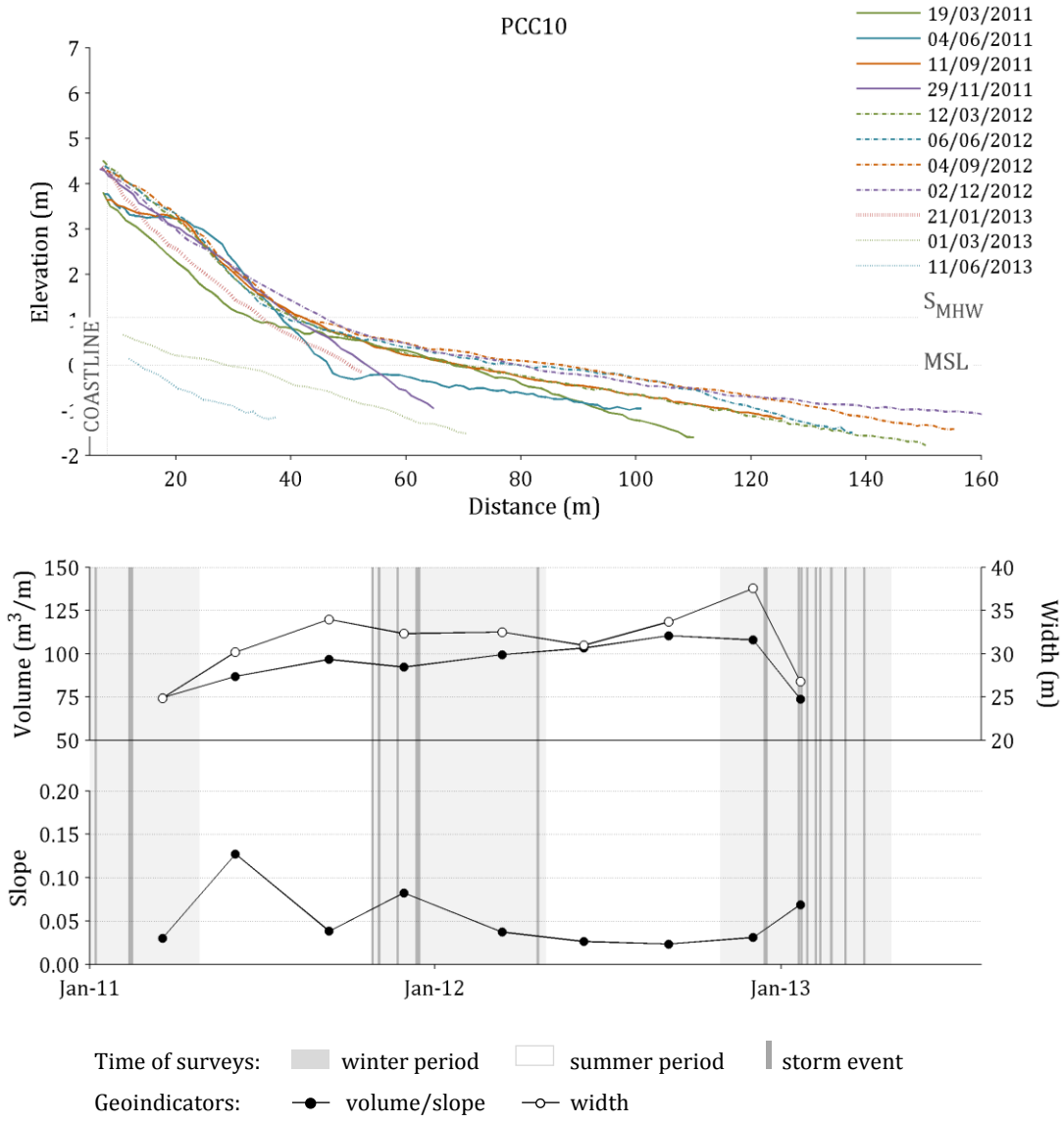

Figure 4.97. Beach profile PCC10 (Costa da Caparica study site) and variation of beach geoindicators (volume, width and slope) for the period between March 2011 and June 2013.

The beaches south of the groin field, and outside the influence of the seawall (PCC16 and PCC17), are wider (70 m on average) and present a much more stable and frequent beach berm. Variations are on the same order of magnitude as the northernmost ones, but significant vertical variation is limited to the seaward portion of the profile, and changes are very small at the coastline, at the contact with the dune. Seasonality is evident in the behavior of winter profiles that lose sediment and become more dissipative following a major storm, such as the December 2012, and January 2013 storms.

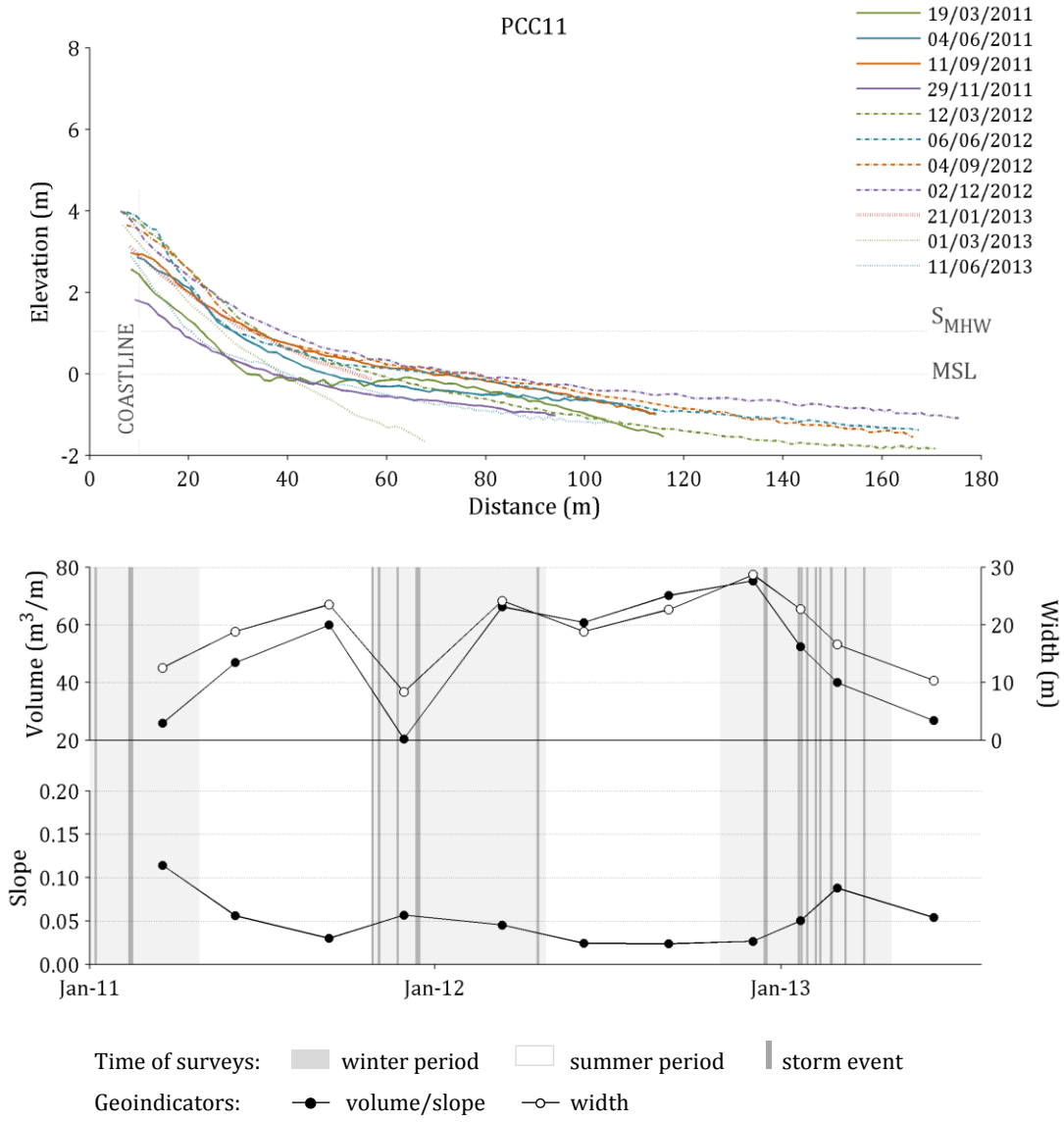

Figure 4.98. Beach profile PCC11 (Costa da Caparica study site) and variation of beach geoindicators (volume, width and slope) for the period between March 2011 and June 2013.

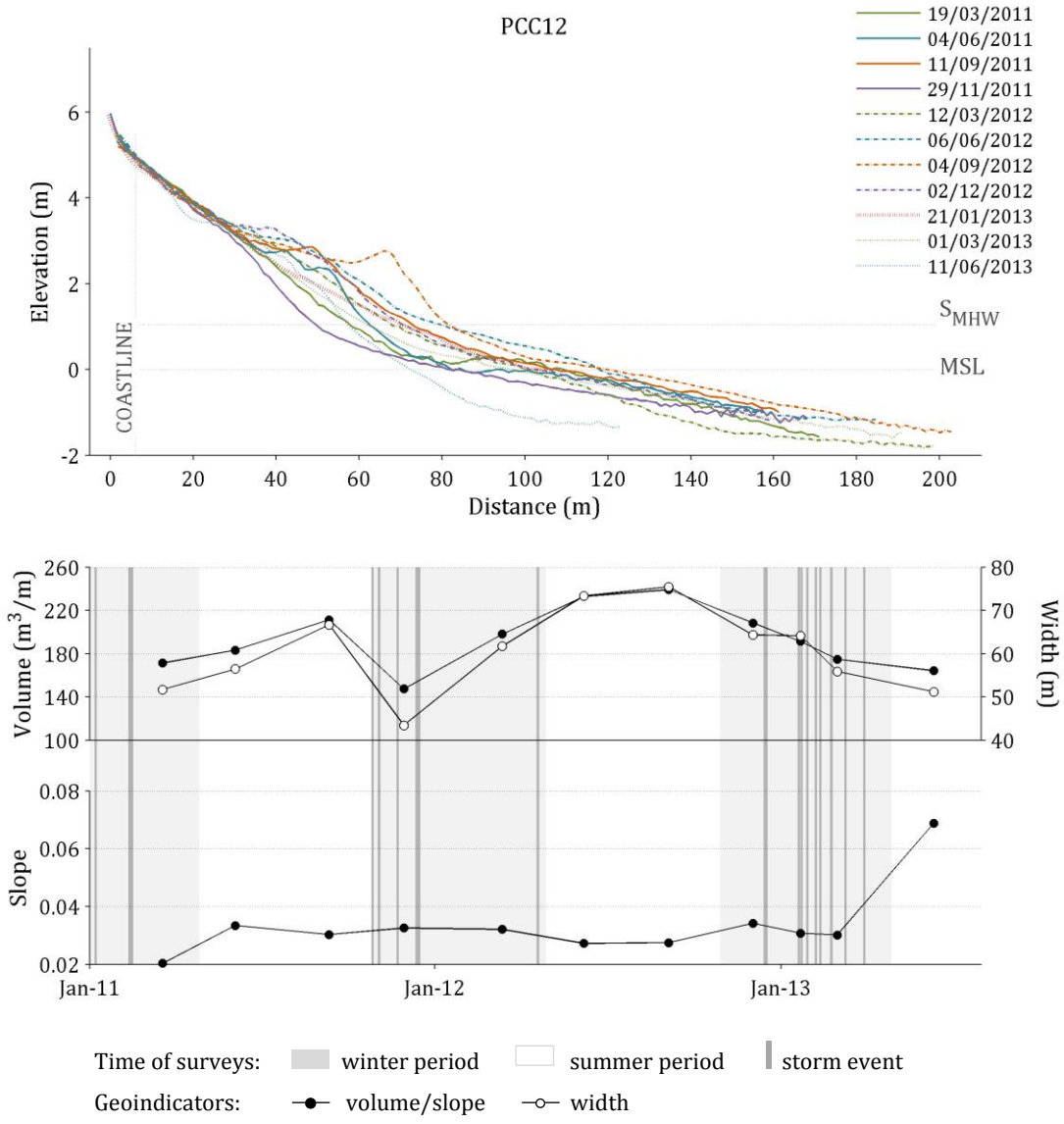

Figure 4.99. Beach profile PCC12 (Costa da Caparica study site) and variation of beach geoindicators (volume, width and slope) for the period between March 2011 and June 2013.

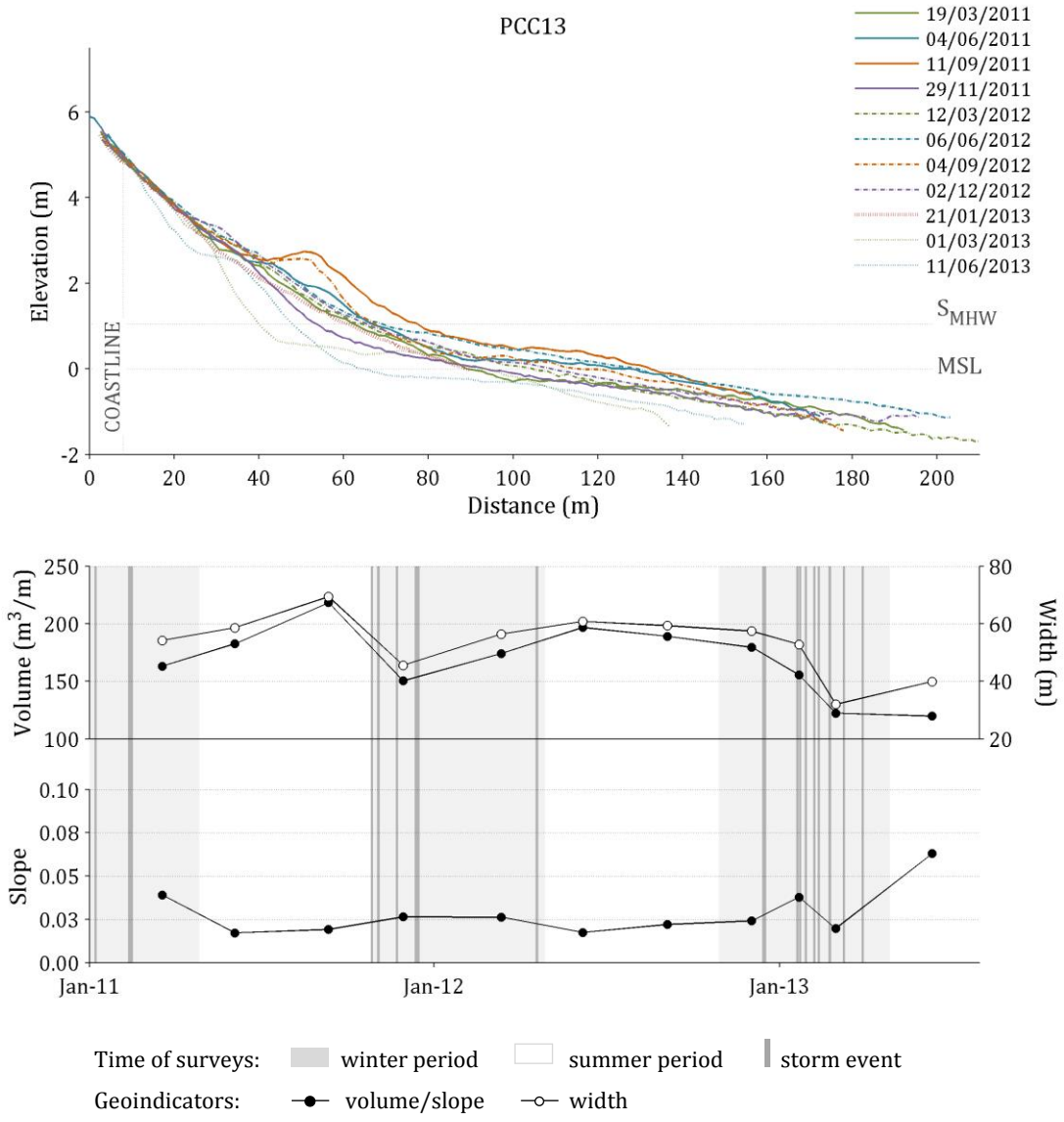

Figure 4.100. Beach profile PCC13 (Costa da Caparica study site) and variation of beach geoindicators (volume, width and slope) for the period between March 2011 and June 2013.

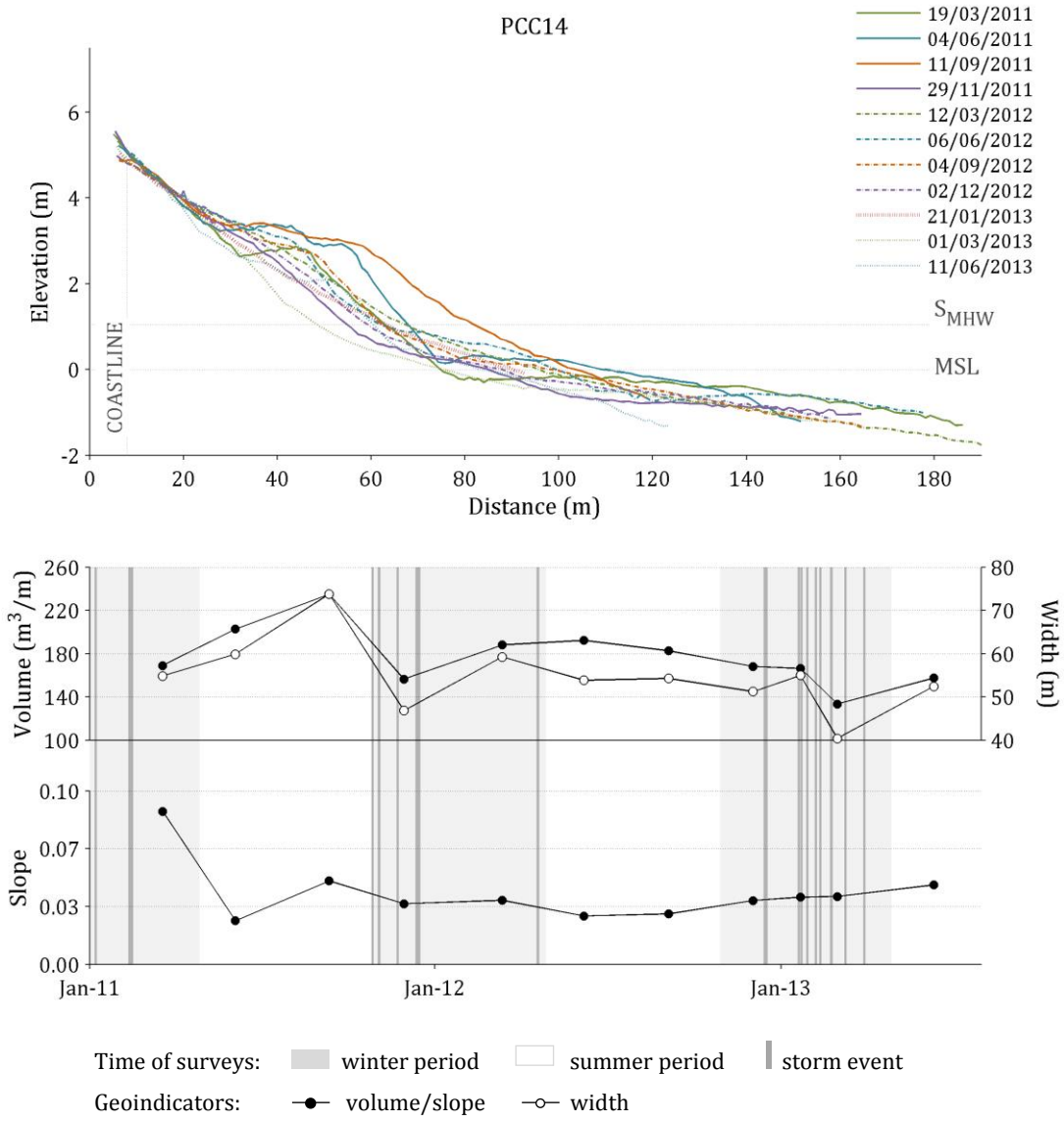

Figure 4.101. Beach profile PCC14 (Costa da Caparica study site) and variation of beach geoindicators (volume, width and slope) for the period between March 2011 and June 2013.

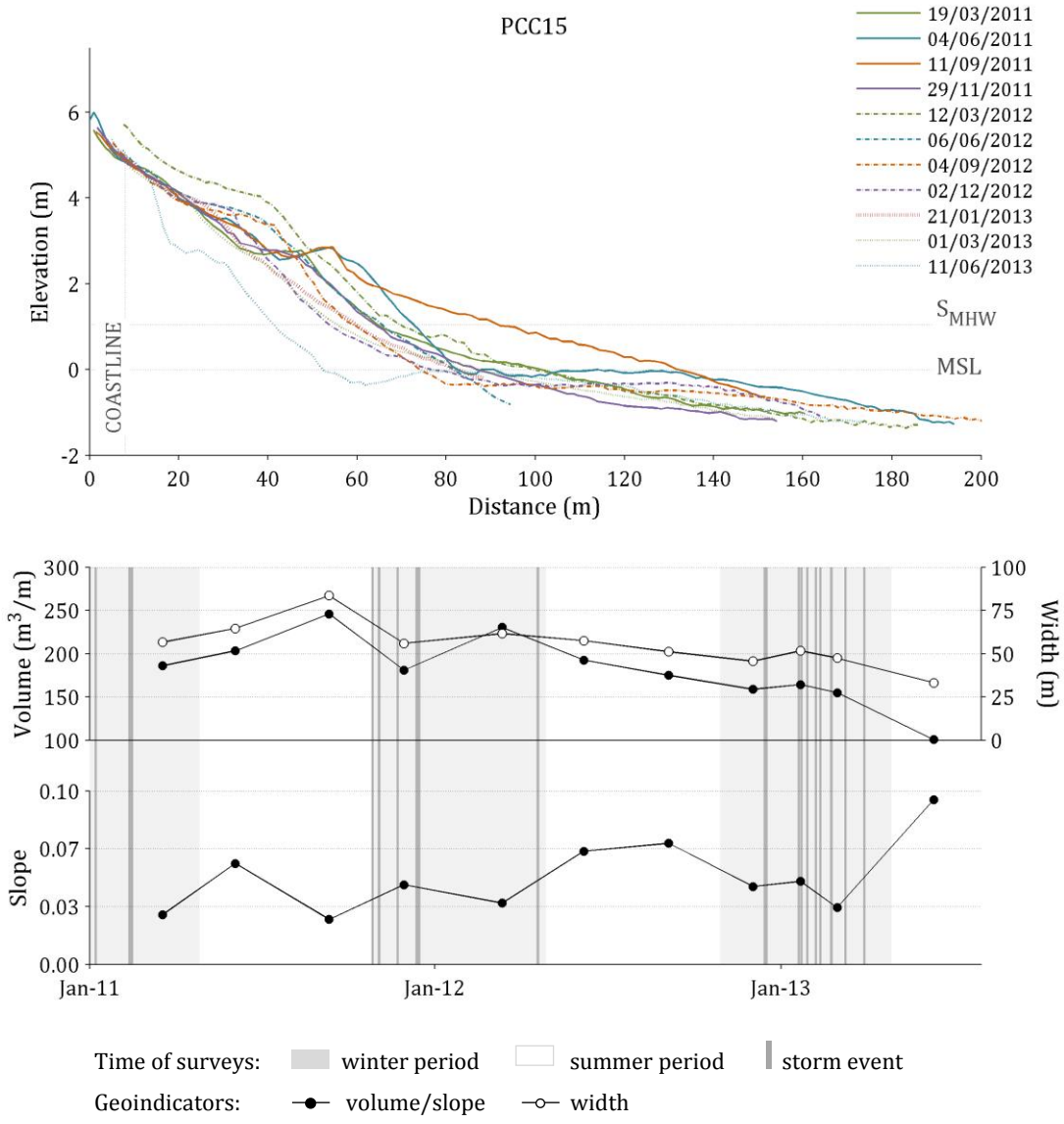

Figure 4.102. Beach profile PCC15 (Costa da Caparica study site) and variation of beach geoindicators (volume, width and slope) for the period between March 2011 and June 2013.

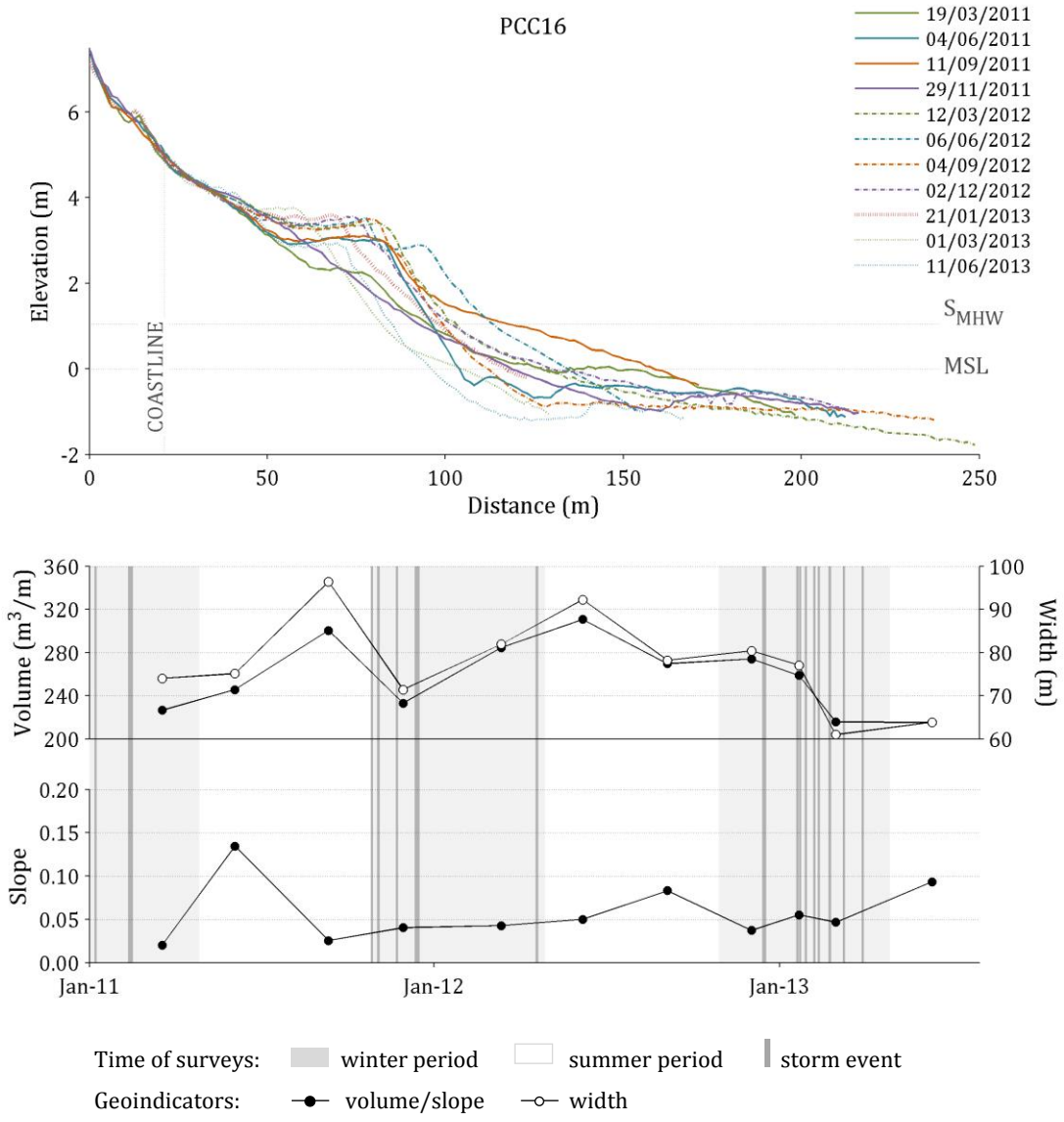

Figure 4.103. Beach profile PCC16 (Costa da Caparica study site) and variation of beach geoindicators (volume, width and slope) for the period between March 2011 and June 2013.

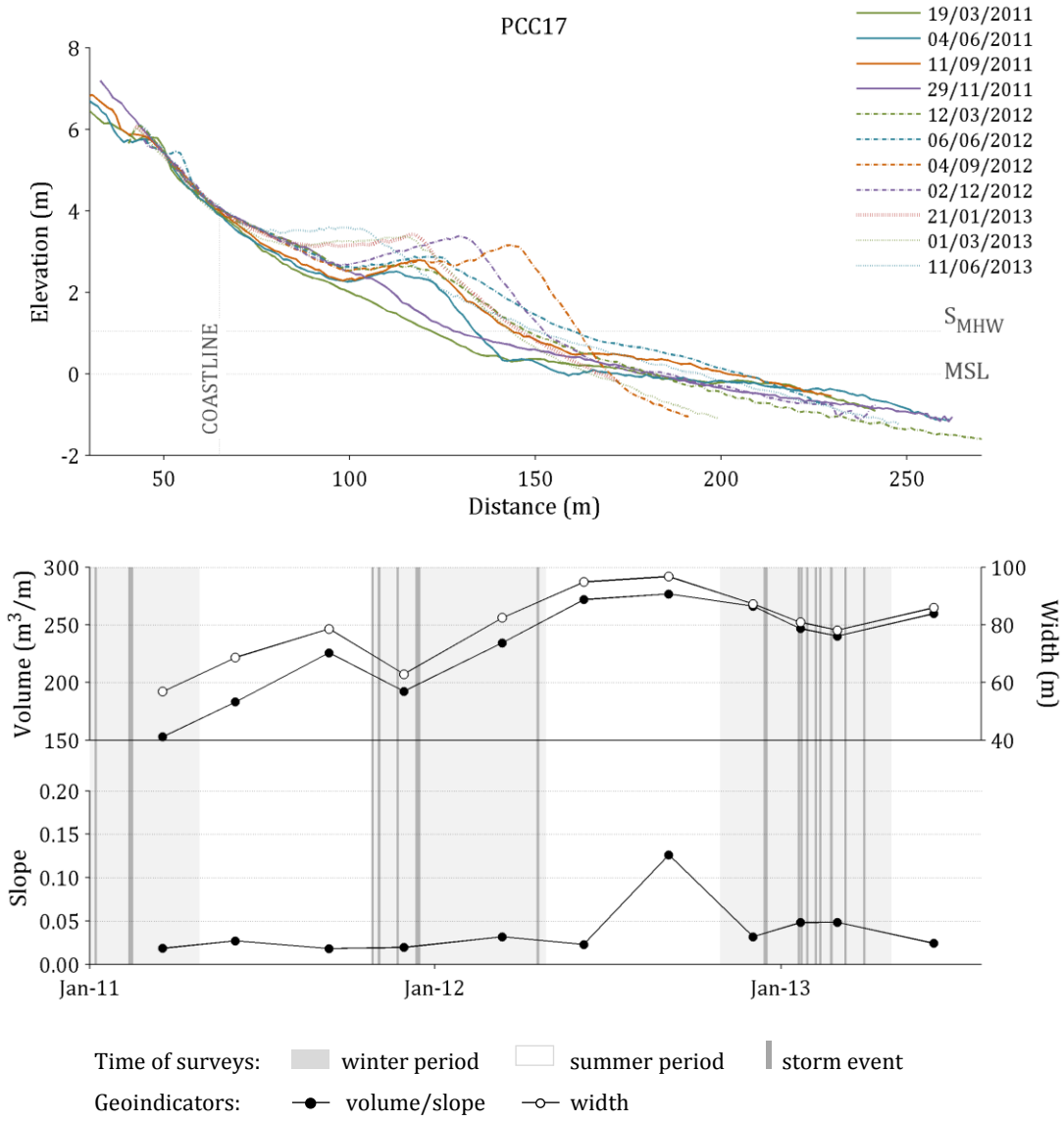

Figure 4.104. Beach profile PCC17 (Costa da Caparica study site) and variation of beach geoindicators (volume, width and slope) for the period between March 2011 and June 2013.

Sediments of the groin field beaches are similar to those of São João da Caparica, varying between fine and medium sand (Figure 4.105). PCC13 and PCC17 are very constant through time and their sediments have mean diameter between 1.6 and 1.8 ϕ. PCC10 is the most variable of the three profiles and shows slightly coarser sand at the berm.

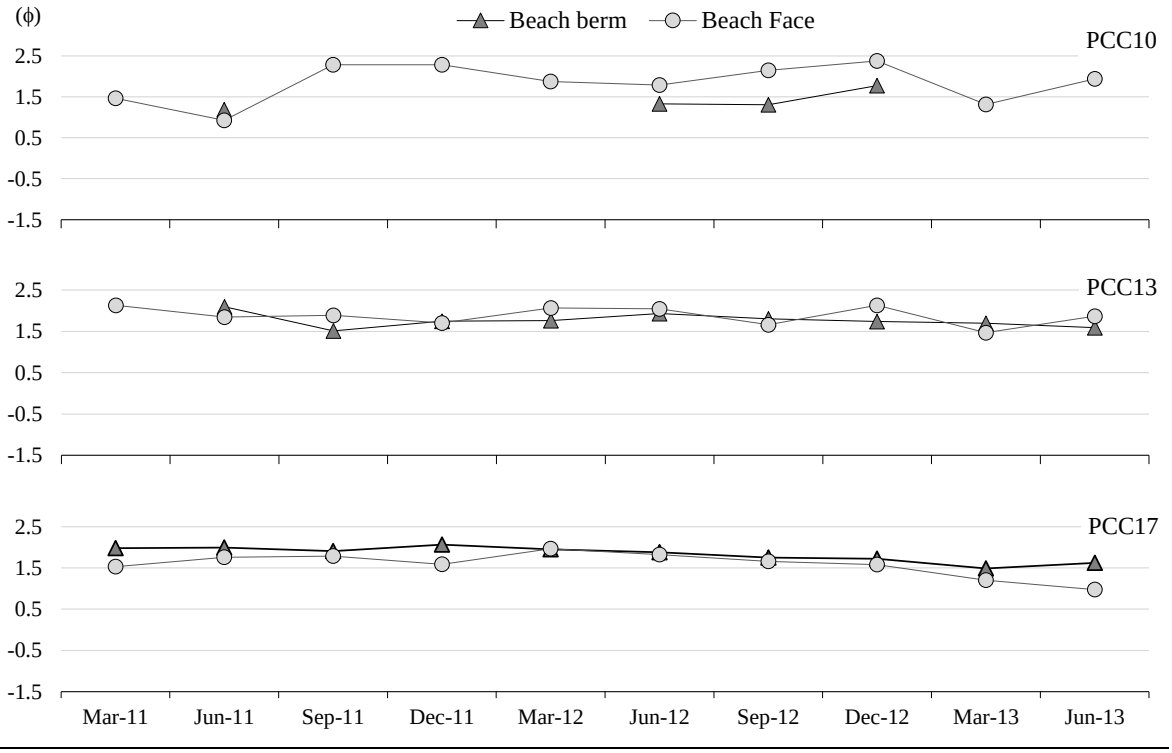

Figure 4.105. Variation of mean grain size for the period between March 2011 and June 2013, for sediment of the beach face and berm at the groin field section of the Costa da Caparica study site.

12 Rainha

Rainha beach shows a distinct morphology between summer and winter seasons (Figure 4.106). Summer profiles typically present two beach berms. The landward berm is c. 20 m wide and develops at 4.5 m (MSL), culminating against the dune that is consistently scarped and reaches 10 m (MSL). The second berm develops between 2.5 m and 3 m (MSL) and may reach 35 m in width. Winter profiles are lower and lack the second berm, and become more linear-shaped or concave. Redistribution of the sediment occurs both seaward and landward, and accumulation of sediment in the upper beach and base of the dune is also characteristic of winter profiles, especially following a storm (Figure 4.107).

The evolution of the geoindicators reflects the morphological contrast between summer and winter profiles, through the systematic decrease in volume and area in the winter, although the several storms that occurred during the study period did not inflict major changes to the beach profile.

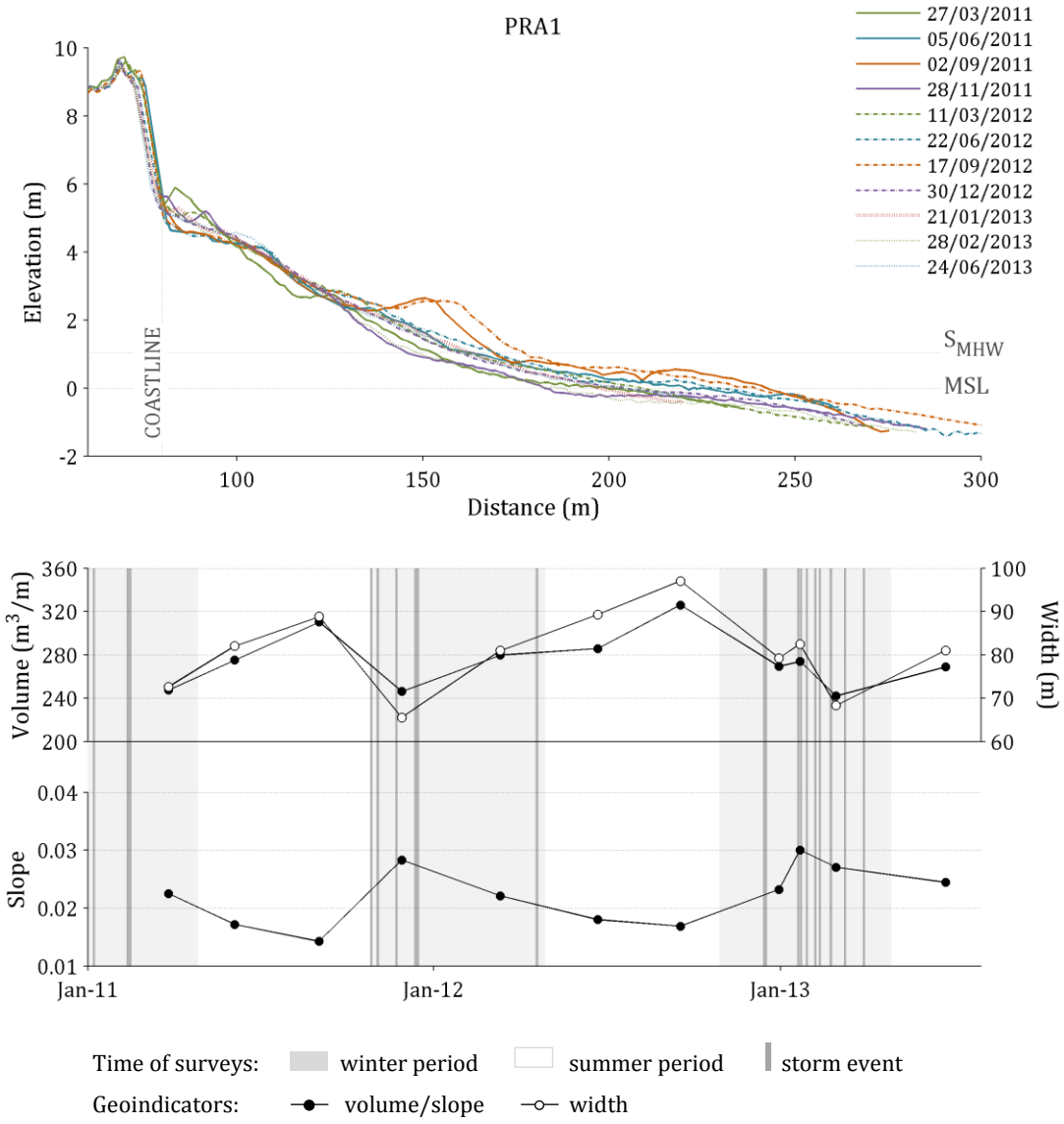

Figure 4.106. Beach profile PRA1 (Rainha study site) and variation of beach geoindicators (volume, width and slope) for the period between March 2011 and June 2013.

In the lower part of the beach, below MHW, the beach acquires a gentler slope that gradually becomes subhorizontal, progressing into a low tide terrace that is often characterized by the presence of sandy swash bars developing at around MSL or higher. Despite the variations in elevation and position of the beach face, slope varied very little throughout the 2.5 years of monitoring, lying in the dissipative range, between 0.01 and 0.04.

Figure 4.107. Sediment transported landward during storms and accumulated in the upper beach area, at the base of the dunes, and beach accesses at Rainha study site. Example from the January 2013 storm.

The monitoring at Rainha study site revealed a pattern of changing morphology between winter and summer profiles. The more seaward berm is the mobile feature that grows and retreats seasonally, whereas the landward berm persists through time, varying only in elevation.

Sediment grain size at Rainha study site is very stable in time and space (Figure 4.108). Average values of mean diameter of 1.9, 2.0 and 2.1 ϕ for the beach face, beach berm and dune samples, respectively, indicate there is a slight gradient of fining of the sediment towards land.

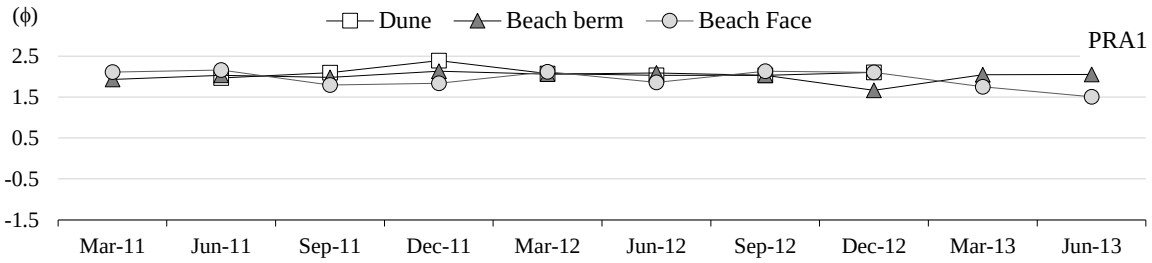

Figure 4.108. Variation of mean grain size for the period between March 2011 and June 2013, for sediment of the beach face, berm and dune at the Rainha study site.

13 Fonte da Telha

Both profiles surveyed at Fonta da Telha study site depict a beach with highly changeable morphology that contacts with a high dune (8-9 m MSL) through a pronounced sloping surface (Figures 4.109 and 4.110). This type of surface is more evident along the beach section adjacent to the developed backshore and corresponds to the effect of trampling. Away from the developed area, the contact between the dune and beach is sharp and marked either by a narrow string of embryo dunes or by the slope-break at the toe of the vegetated foredune. The geoindicators evolution indicates some seasonality in the beach behavior, with volume, area and slope decreasing during winter season. Both summer and winter profiles present berms at different stages of growth or retreat, or a flatter surface with only a short berm present. Berms develop anywhere between 2.5 m and 4 m (MSL) at both profiles, and migrate cross-shore as much as 35 m. Likewise, the occurrence of a low tide terrace is not persistent, nor characteristic of a time of the year. Still, the lowest beach surfaces do correspond to winter surveys, and, interestingly, winter and post-storm surfaces also have a constructive character and typically depict the higher berms and higher sediment accumulation in the upper beach area, as a result of the landward sediment transport, wave- and wind-driven, that occurs during a storm. The dune features however, remained fairly constant and no major changes were recorded.

Slope values were highly variable, ranging between 0.02 and 0.13, crossing the dissipative to reflective categories. Similar to Rainha, shore-parallel sand bars are also present along Fonte da Telha site, but located farther offshore, and thus with no expression on the beach profile. When the berm builds seaward and in elevation, conditions are propitious for the development of beach scarps that can reach 1.5 m (example on Figure 4.111).

Fonte da Telha varies considerably in volume, area and slope throughout the year, showing a seasonal trend of sediment decrease during winter. However, there is no clear summer or winter morphology associated with these changes and berm development can occur at different elevations and with very different widths, alternating with flat and featureless surfaces.

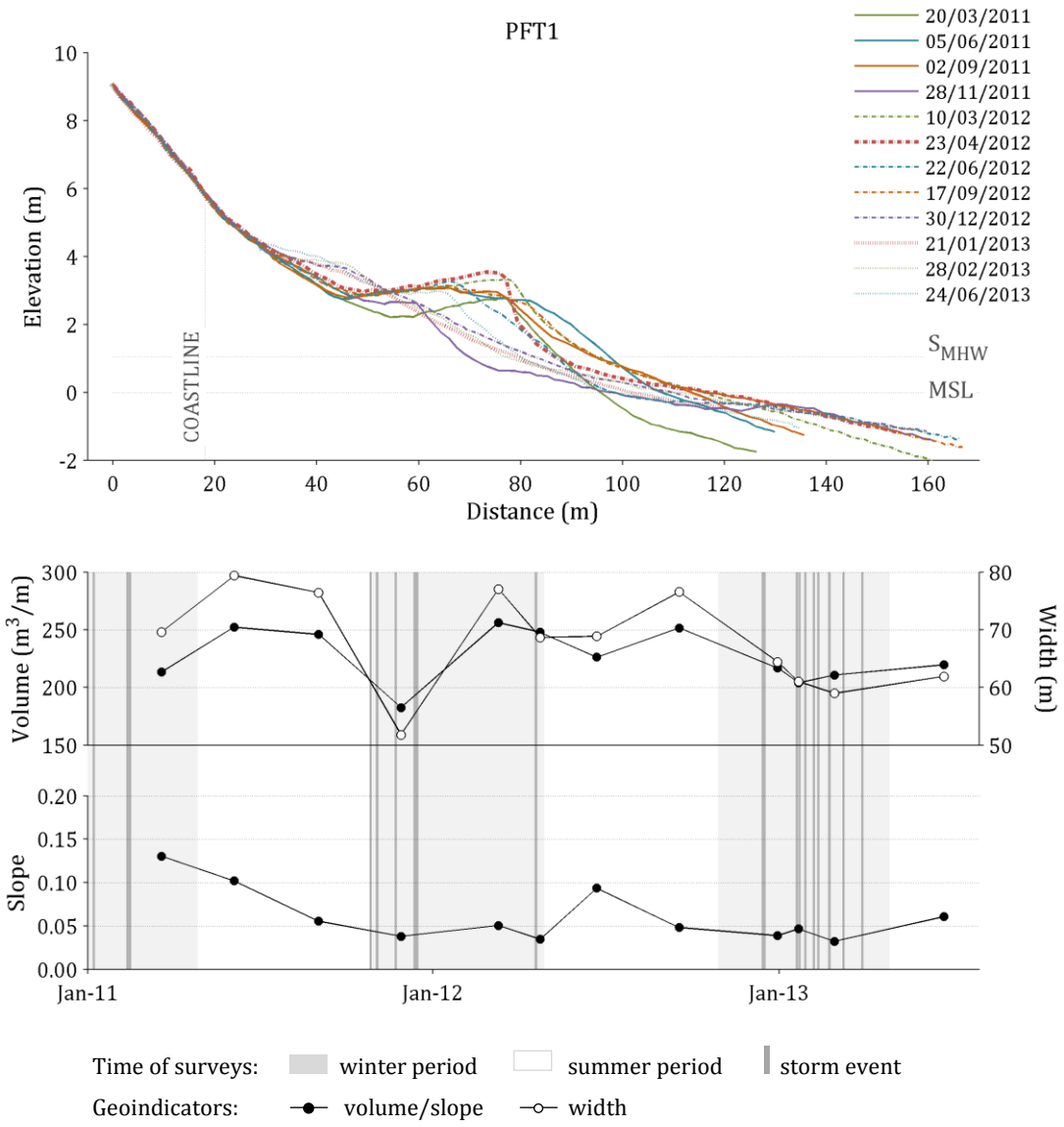

Figure 4.109. Beach profile PFT1 (Fonte da Telha study site) and variation of beach geoindicators (volume, width and slope) for the period between March 2011 and June 2013.

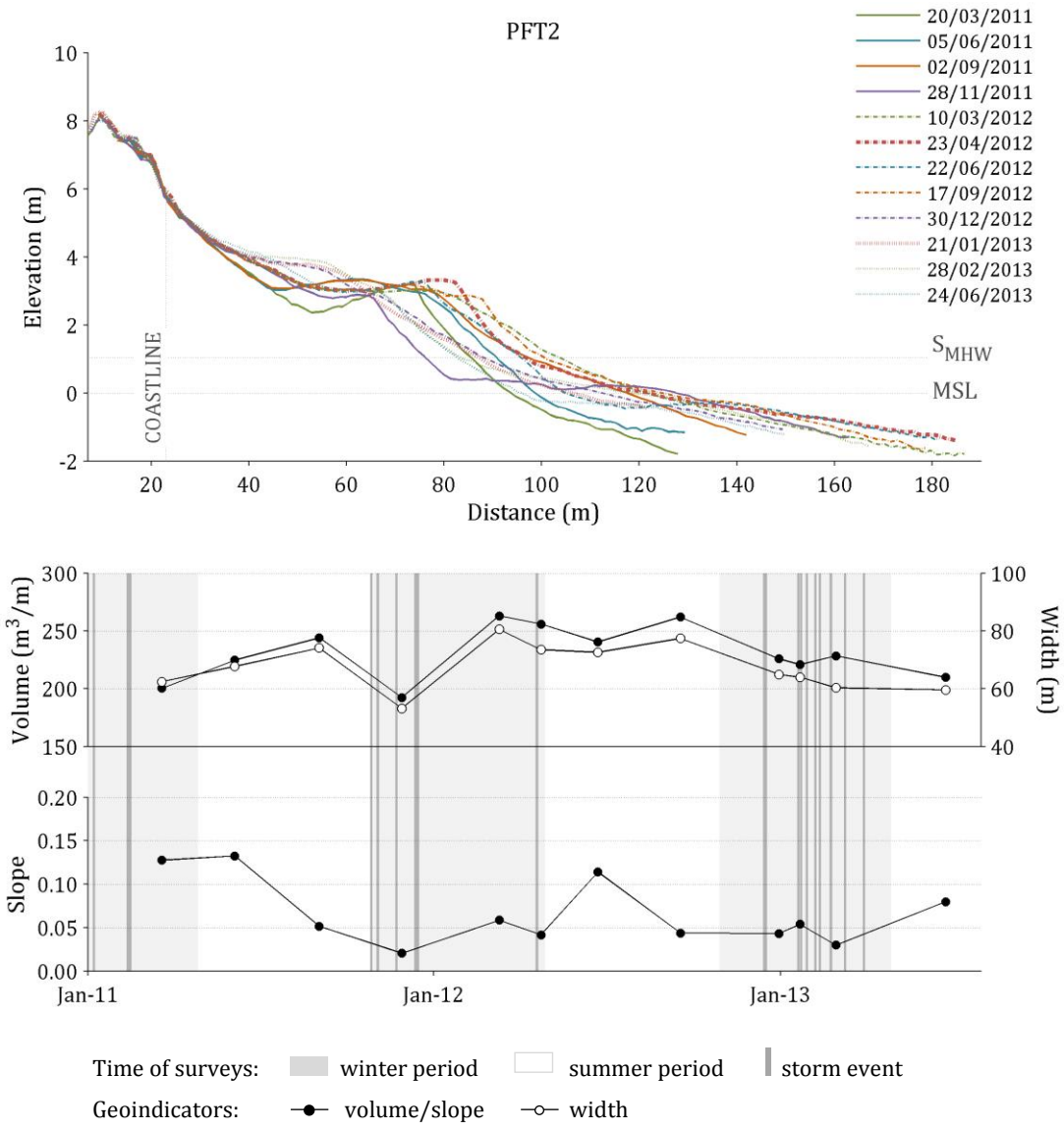

Figure 4.110. Beach profile PFT2 (Fonte da Telha study site) and variation of beach geoindicators (volume, width and slope) for the period between March 2011 and June 2013.

Fonte da Telha sediments correspond to medium sand and show no significant difference between the two profiles (Figure 4.112). Average mean diameter for both profiles is 1.7 and 1.6 ϕ for the beach face and dune samples, respectively, and the beach berm is slightly coarser, with 1.4 ϕ.

Figure 4.111. Scarp formation after a storm hitting the site, wave swash having reworked a wide and elevated berm. Photograph taken by Ivana Bosnic on April 21, 2012.

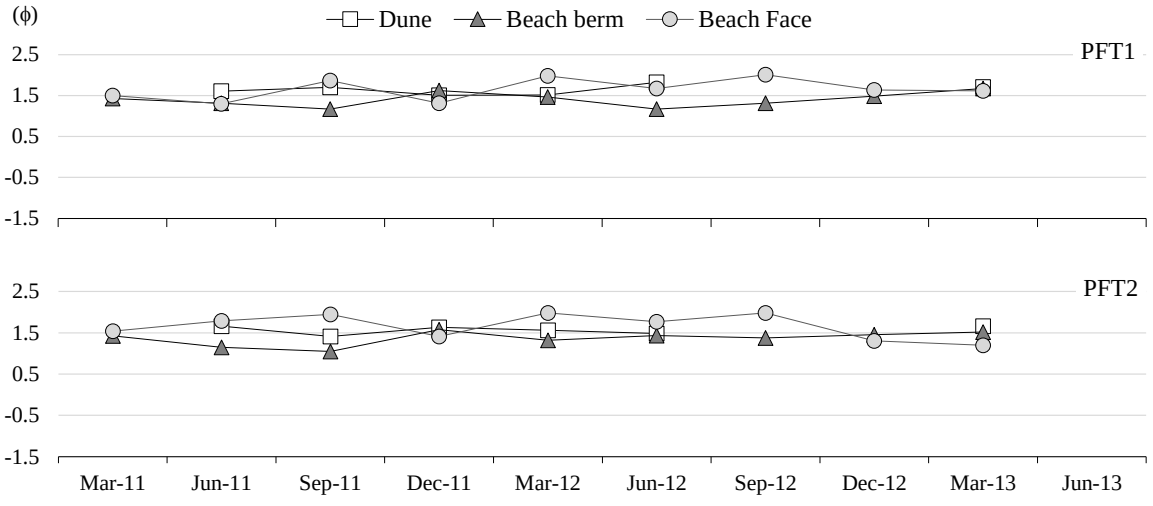

Figure 4.112. Variation of mean grain size for the period between March 2011 and June 2013, for sediments of the beach face, berm and dune at Fonte da Telha study site.

14 Lagoa de Albufeira

Lagoa de Albufeira beach profile depicts a robust beach with a wide and high single beach berm (c. 45 m wide developing at 4.5 m relative to MSL) that gradually increases in elevation towards the cliff that constitutes its landward limit (Figure 4.113). The beach face is typically steep, characteristic of intermediate and reflective morphodynamic

states sometimes growing in the summer towards development of a second berm located seaward at 3 m (MSL). Beach cusps, with decametric length, are commonly present. In the winter season, the berm retreats between 10 and 20 m. The geoindicators record this seasonality, especially the beach volume and width that consistently decrease in winter and increase in summer.

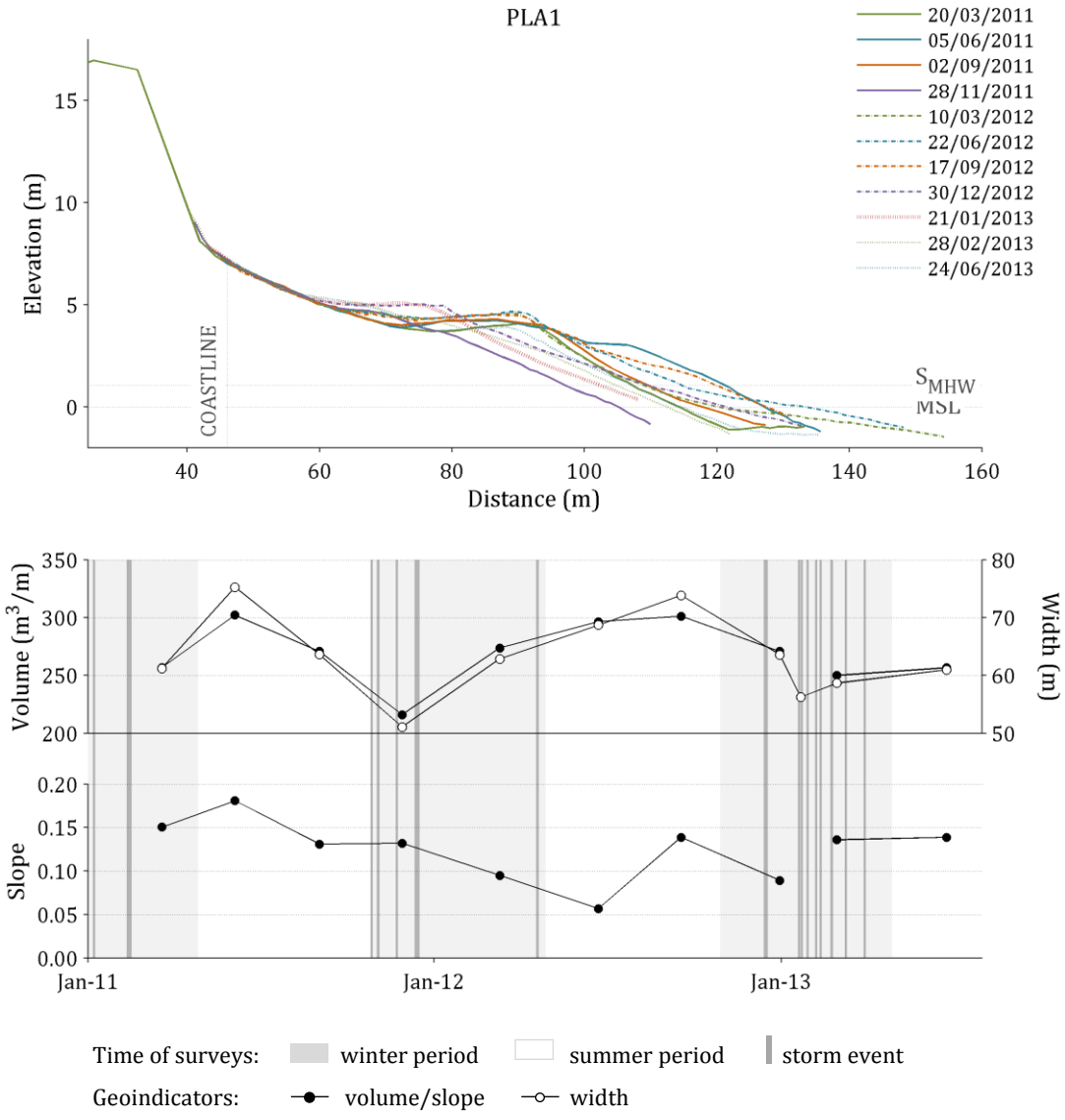

Figure 4.113. Beach profile PLA1 (Lagoa de Albufeira study site) and variation of beach geoindicators (volume, width and slope) for the period between March 2011 and June 2013.

Lagoa de Albufeira represents the southernmost sector of the Caparica-Espichel littoral arc, and is characterized by a robust beach with a typical beach berm morphology that responds to the seasonal wave climate.

Sediments correspond to coarse sand, with average mean diameter of 0.9 ϕ at the beach face, 0.6 ϕ at the beach berm, and 0.8 ϕ at the dune (Figure 4.114). Beach face sediments vary considerably (about 1 ϕ unit) throughout the year but are frequently in the range of medium sand.

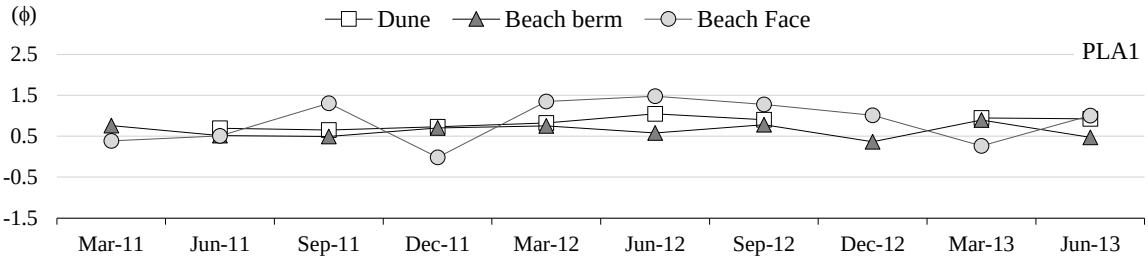

Figure 4.114. Variation of mean grain size for the period between March 2011 and June 2013, for sediments of the beach face, berm and dune at the Lagoa de Albufeira study site.

4.2.2. Overall study area

Distribution of beach geoindicator values for all the beach profiles along the study area, and for the overall surveys conducted between 2011 and 2013, is depicted in the form of boxplot diagrams in Figures 4.115 (volume), 4.116 (width) and 4.117 (slope). The full geoindicator values is presented in Appendix B.

Patterns of spatial distribution of volume and width along the study area are identical in broad terms and show the high variability both in average dimensions and in amplitude of change. Some of the alongshore variations detected within the study sites are highlighted in the diagrams. For example, the Lagoa de Óbidos-Baleal and Baleia/Sul study sites, depict increase in beach dimensions towards south, whereas at the São João da Caparica section of the Costa da Caparica study site the beach dimensions decrease towards the south. However, looking at the overall distribution of beach geoindicators, there is no clear alongshore spatial trend at the regional scale, only similarities of beach behavior between study sites.

Nazaré study site profiles clearly stand apart from the general beach volume and width values recorded along the study area, with average values on the order of 800 m^3/m and 160 m, for volume and width, respectively. These are twice the values of the PSC3 profile (at Santa Cruz study site) that presents the highest of the records for the remaining beaches.

The magnitude of change between surveys is also different along the study area, with beaches varying as much as 500% of their mean volume throughout the survey period (Paredes de Vitória), and coastal stretches experiencing volume changes as low as 10 and 20% (Tamariz and Baleal-Peniche) over the same two and a half years.

The most variable of the beaches, in volume and width, are Paredes de Vitória, Santa Cruz, and the northernmost profiles of Costa da Caparica (São João da Caparica section) that recorded ranges of volume variation higher than 200 m^3/m, reaching a maximum of 302 m^3/m at PPV1. Likewise, these sites recorded large amplitudes of width variation, higher than 60 m, and reaching 107 m at PPV2.

Some beaches stand out for the small range of variation, when compared with the rest of the study sites. The southernmost profile of Lagoa de Óbidos – Baleal, Baleal-Peniche, Baleia/Sul, Magoito, Tamariz, and the northernmost profiles of the groin field section of Costa da Caparica (PCC9 to PCC11) recorded the smallest variations during the study period. All of these sites recorded amplitudes of volume and width variation below 50 m^3/m and 20 m, respectively.

Beach slope values range from as low as 0.01 at Paredes de Vitória, to a maximum of 0.18 at Nazaré. The latter, along with Santa Cruz (southern section), Baleia/Sul, Tamariz and Lagoa de Albufeira show the highest values of slope, clearly within the reflective range. There are some sites that lie on the other side of the morphodynamic spectrum, with very low values of slope, characteristic of dissipative beaches: the southernmost profile of the Lagoa de Óbidos-Baleal stretch, Baleal-Peniche and Rainha study sites. The majority of the beach profiles, however, lie within intermediate morphodynamic range in what concerns slope characteristics.

A striking characteristic of beach slope along the study area is the large range of variation within each profile (Figure 4.117). Almost half of the overall beach profiles show values that range between the dissipative and reflective fields. This is a reflection of beach seasonal variation and the response of the study site's beaches to winter storms and following recovery, as described earlier.

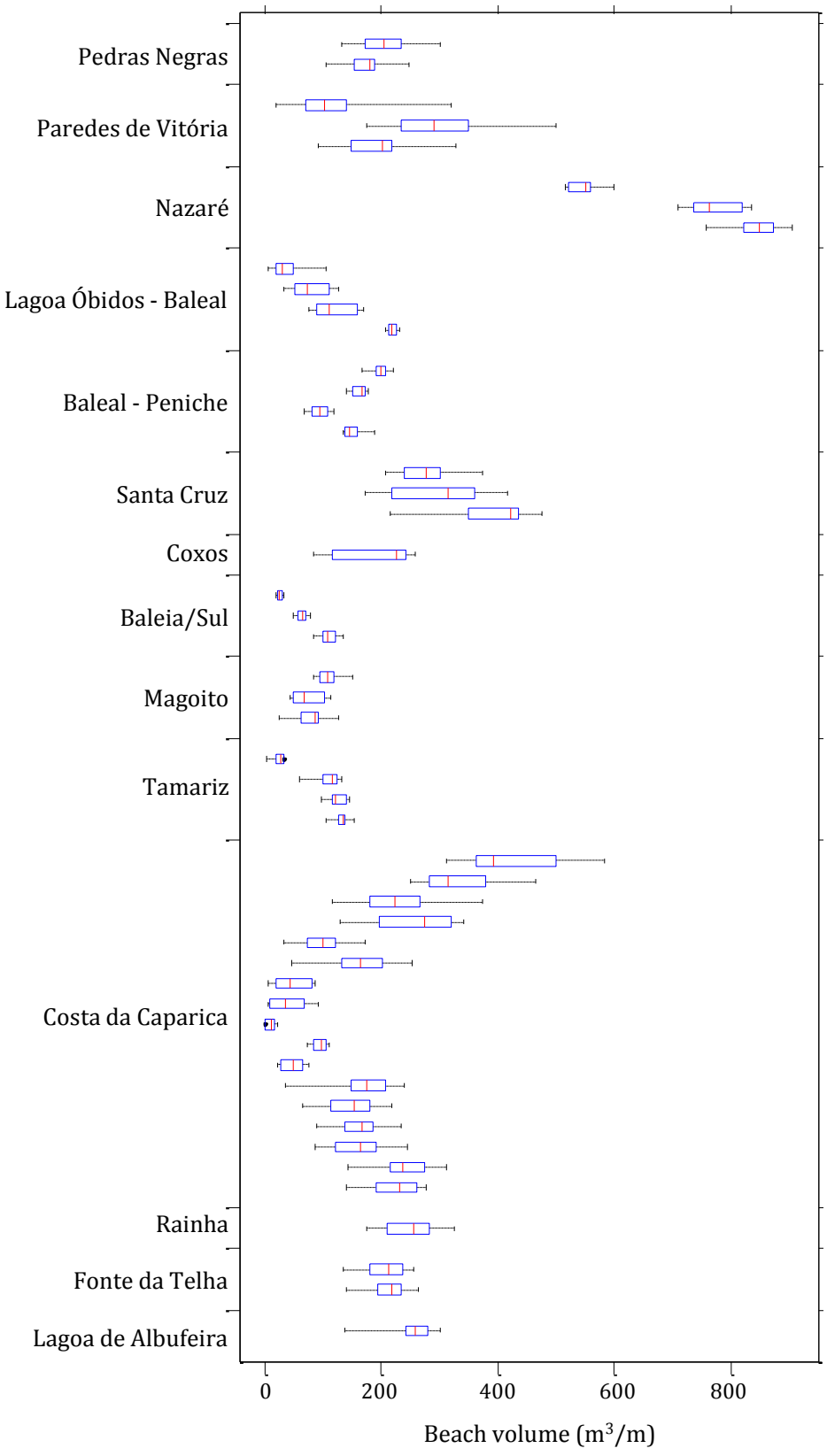

Figure 4.115. Boxplots of beach volumes (m^3/m) data for all beach profiles surveyed along the study area.

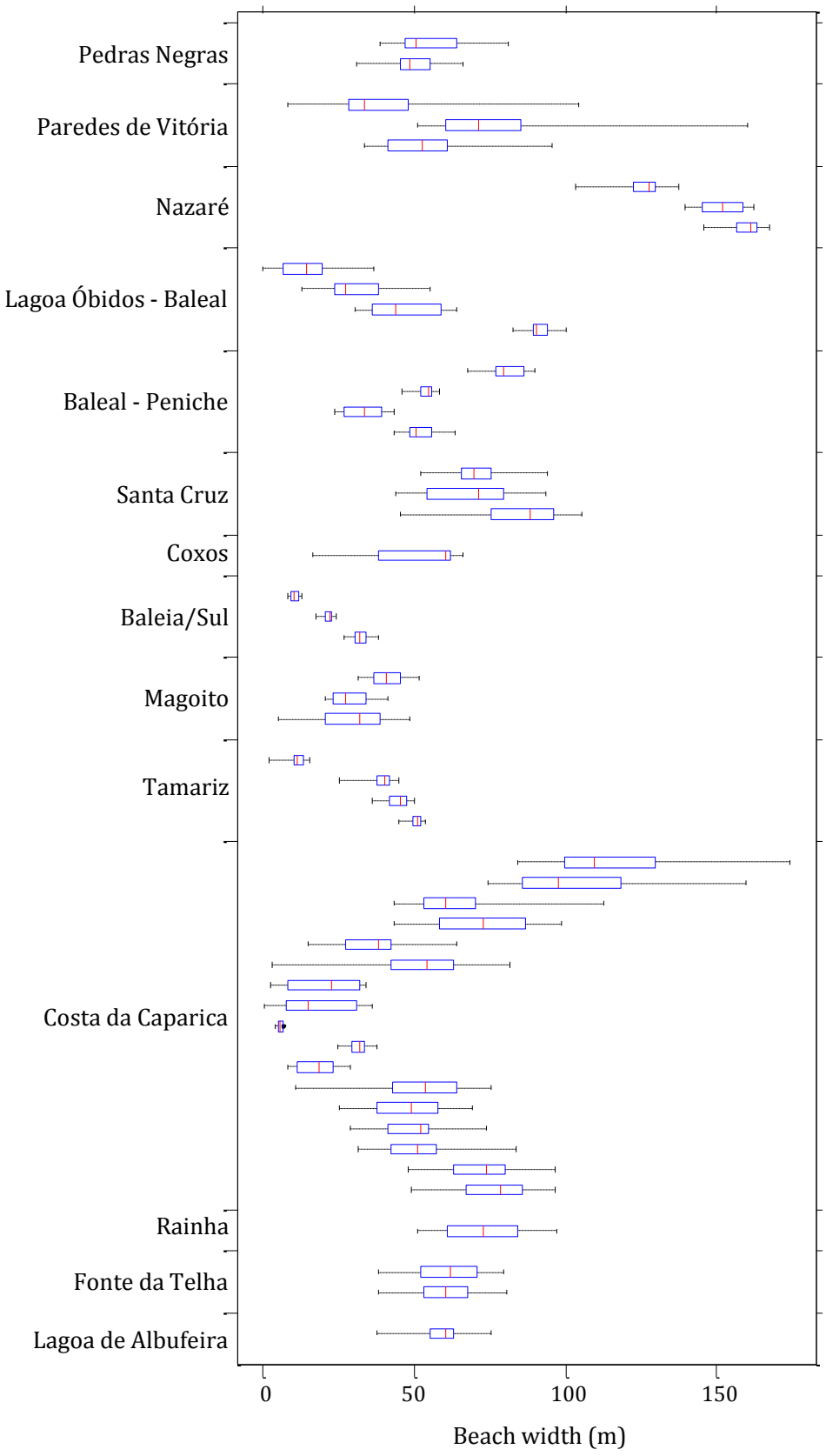

Figure 4.116. Boxplots of beach width (m) data for all beach profiles surveyed along the study area.

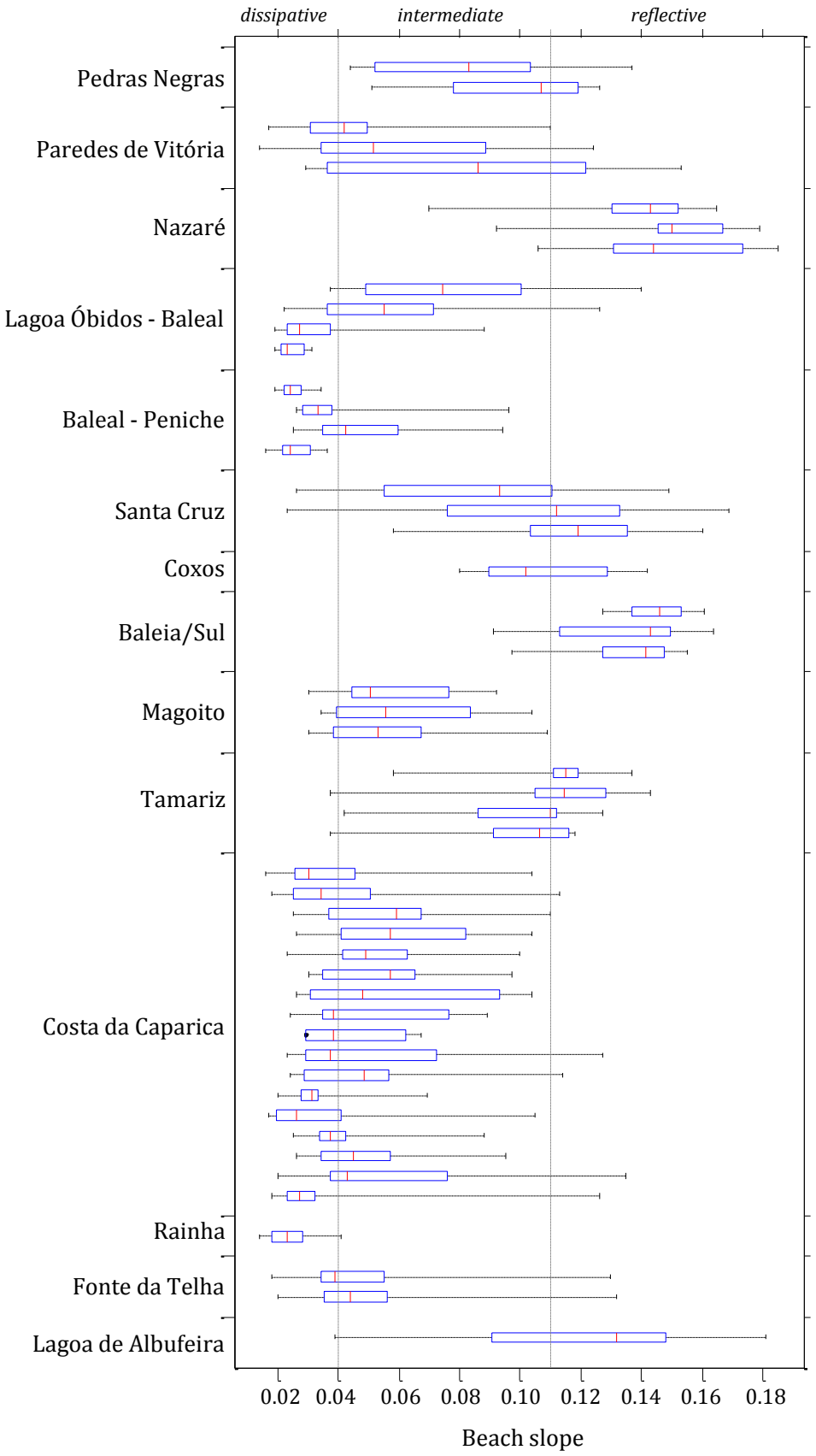

Figure 4.117. Boxplots of beach slope data for all beach profiles surveyed along the study area.

4.2.3. Morphology and sediment parameters used in the exploratory analysis

Statistical parameters pertaining to the morphology and sediments description were further used in the exploratory analysis (Chapter 5). Table 4.2 holds the statistical values used – average and standard deviation. For the purpose of the analysis, and as explained in Subchapter 4.1, two of the study sites (LOB and CC) were divided, and therefore two new locations were added to the data – BL (corresponding to beach profile PLOB4) and SJC (corresponding to beach profiles PCC1 to PCC9).

Table 4.2. Statistical values of the geoindicators pertaining to the morphology and sediment parameters of each study site used in the exploratory analysis. Average values of subaerial beach volume (Vol), beach width (Width), beach face slope (Slope) and sediment mean diameter (Mz_{Face}); and standard deviation of beach volume (Δ_{vol}) and width (Δ_{width}).

Study site		Vol (m^3/m)	Δv_{ol} (m^3/m)	Width (m)	Δ_{width} (m)	Slope	Mz_{Face} (ϕ)
01	PN	188.8	38.26	52.5	10.14	0.07	1.00
02	PV	217.7	73.78	61.9	23.60	0.05	0.66
03	NZ	720.1	36.91	147.0	6.00	0.16	0.87
04a	LOB	81.0	30.24	31.3	11.21	0.03	1.27
04b	BL	219.3	7.22	92.2	3.88	0.03	1.27
05	BP	152.3	14.98	55.3	4.96	0.04	1.99
06	SC	327.2	64.29	76.0	13.97	0.12	1.04
07	CX	239.7	12.86	60.9	2.82	0.11	0.94
08	BS	66.7	12.81	21.8	2.06	0.14	0.44
09	MG	92.6	33.15	35.7	7.19	0.06	1.23
10	TM	100.4	14.04	37.1	2.61	0.11	1.60
11a	SJC	235.8	46.55	71.5	17.18	0.06	1.83
11b	CC	202.0	32.84	56.1	9.50	0.04	1.88
12	RA	275.1	25.96	80.5	9.28	0.02	1.98
13	FT	228.3	22.61	67.9	8.49	0.06	1.65
14	LA	269.5	25.29	64.0	6.79	0.13	0.84

4.3 Hydrodynamic forcing

The hydrodynamic forcing was analyzed in terms of waves (both offshore/deepwater conditions - and nearshore regimes), tides, and their combined effect. A method was developed to estimate total water levels, including the contributions of surge and wave runup along the study sites, validated with local field data. The results describe the site-specific total water level regimes, providing frequency, magnitude and elevation reach of the free surface of the ocean driving beach morphological change.

4.3.1. Waves

4.3.1.1. Offshore wave regime

Validation results

The deepwater wave time series was compared with the available synoptic data from the oceanic wave buoy Monican01-CSA88/1, located in deep water off the coast of Nazaré (http://monican.hidrografico.pt/en) and maintained by the Instituto Hidrográfico. A total of 23262 records spanning a little over 3 years, with some gaps, were used in the comparison and there is a good agreement between the two time series (example of Hs comparison in Figure 4.118).

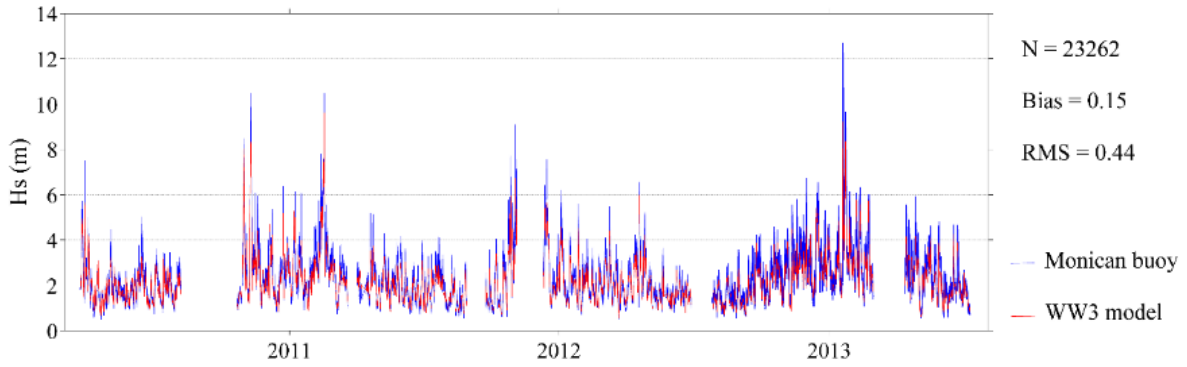

Figure 4.118. Comparison of deepwater Hs records between the WW3 modelled data and the measured data at the Monican oceanic wave buoy, for the period between March 2010 and July 2013.

Bias and root mean square error (rmse) between observed and modeled values of Hs, T and direction, for the period between March 2010 and July 2013, yielded values presented in Table 4.3. Validation results were similar to those obtained by Dodet et al. (2010) and indicate that the hindcast wave data are of acceptable quality and provide an adequate representation and quantification of reality. Differences between observed and modelled wave height data indicate that the model somewhat underestimated this parameter, particularly during storm conditions. However, the present study is more concerned with the modal conditions, and therefore the poorer representation of extreme conditions is not expected to impact the results. Differences in the deepwater wave direction are strongly attenuated as waves propagate onshore, and therefore expected deviations between modelled values at the study site outputs and field data are herein considered acceptable.

Table 4.3. Error statistics derived from the comparison between the WW3 modelled wave parameters and those measured at the Monican oceanic wave buoy, for the period between March 2010 and July 2013.

Error statistics	**Hs** (m)	**Tp** (s)	**θp** (°)
rmse	0.44	1.9	23.21
bias	0.15	-0.38	13.57
Number of records		23262	

1979-2014 wave regime

The offshore wave time series used in the present study spans the period from January 1, 1979 to August 31, 2014. It describes a high energy wave regime that propagates towards the central Portuguese west coast practically exclusively from the northwest quadrant (Figure 4.119) with mean significant wave height of 2.1 m and mean peak period of 11.1 s (Table 4.4).

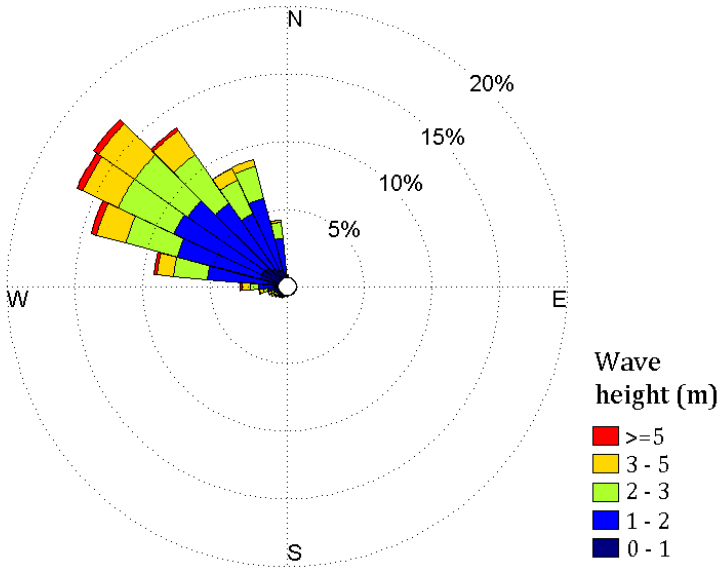

Figure 4.119. Wave rose of the offshore wave record spanning the period from 1979 to 2014, depicting the frequency of significant wave heights according to wave directions.

Table 4.4. Wave parameters statistics, derived from the 1979 to 2014 period offshore wave time series.

Hs mean (m)	Hs max (m)	Hs $P_{97.5}$ (m)	Hs P_{75} (m)	Hs P_{50} (m)	Hs P_{25} (m)	T_P mean (s)	Dir mean (°)
2.1	11.2	4.8	2.6	1.9	1.4	11.1	307

There is a clear seasonality associated with the wave regime offshore the study area, with larger wave heights and periods during winter, and smaller heights and periods in summer, as depicted in the boxplots in Figure 4.120. The typical values of both parameters show small fluctuations throughout the year, but the maximum values, especially in wave height, vary substantially. Wave direction (Figure 4.120, lower panel) also displays a seasonal pattern, shifting between more northerly incoming waves during summer, and more westerly incoming waves during winter.

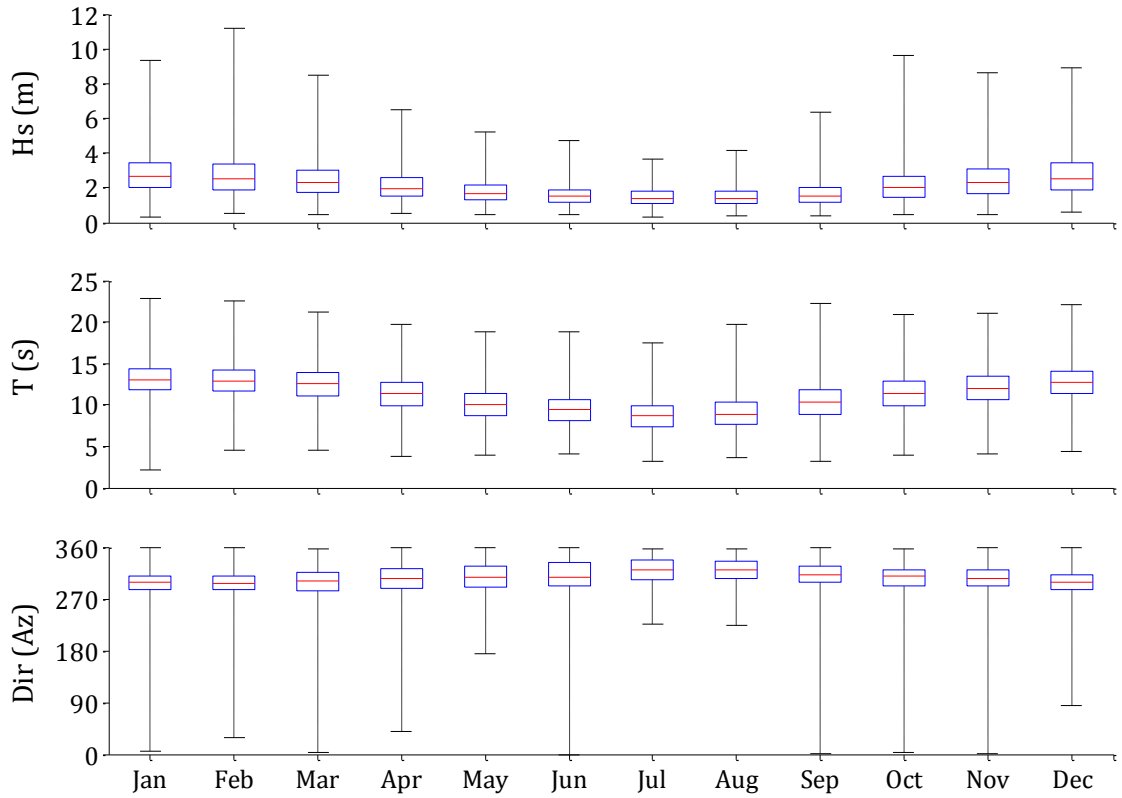

Figure 4.120. Boxplots depicting the statistics (maximum, modal, minimum and 25th and 75th percentiles) of the monthly distributions of wave height (upper panel), wave period (middle panel), and wave direction (lower panel) for the offshore wave regime for the 1979 to 2014 time period.

During the 36-year period analyzed, 282 storm events occurred (Figure 4.121). As described in Chapter 3, Storm events are herein defined as periods when offshore H_s remained consistently higher than 5 m (according to the storm threshold established by Costa and Esteves, 2009), including intervals of lower H_s shorter than 24 h (as defined by Silva and Taborda, 2014).

Storm frequency was usually higher during the months of December and January. They are typically from WNW (296°) with average H_s of 5.9 m and T_p of 15 s. 50% of the records show a duration of less than 12 hours, and 20% less than 24 hours. During the 36-yr period a total of 25 storms exceeded 8 m H_s, and maximum values reached 11 m H_s and 22 s T_p.

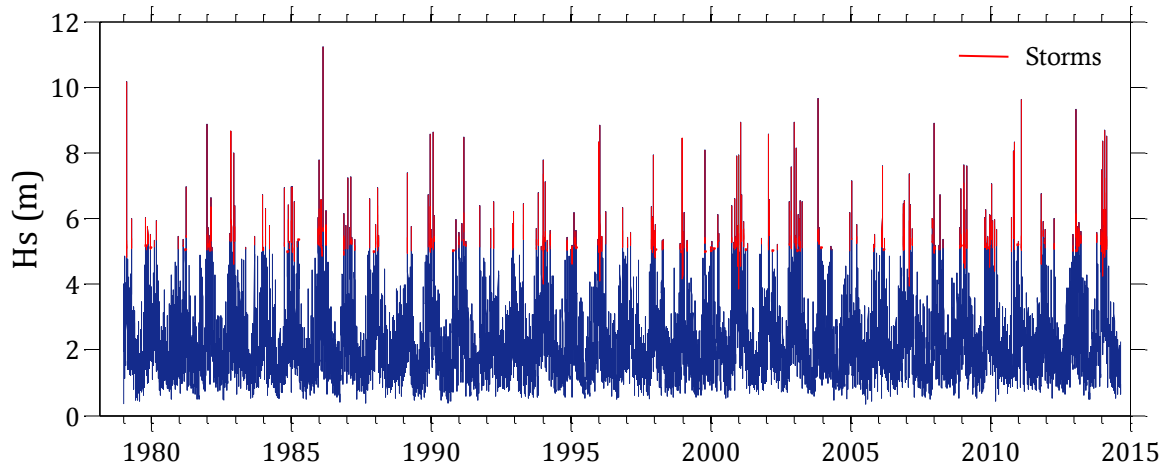

Figure 4.121. Offshore significant wave height record spanning the period from 1979 to 2014, with demarcation of storm events in red.

2011-2013 wave regime

The wave characteristics during the study period (Figure 4.122) are similar to the 36-year time series, with mean significant wave height of 2.2 m, mean wave period of 11.4 s, and mean wave direction of 305° (Table 4.5). The seasonality associated with higher energy levels in the winter and calmer conditions in the summer is evident in the time distribution of wave period and height, and the most noteworthy record are those of the 2011 and 2013 winters. Overall, there were 20 storms during the study period, similar to those described for the 36-yr period of wave data: average H_s of 5.9 m, T_p of 15 s and typically from WNW (296°).

Table 4.5. Wave parameters statistics, derived from the January 2011 to August 2013 period offshore wave time series.

Period	Hs mean (m)	Hs max (m)	Hs $P_{97.5}$ (m)	Hs P_{75} (m)	Hs P_{50} (m)	Hs P_{25} (m)	T_P mean (s)	Dir mean (º)
1979-2014	2.1	11.2	4.8	2.6	1.9	1.4	11.1	307
2011-2013	2.2	9.6	4.7	2.7	2.0	1.5	11.4	305

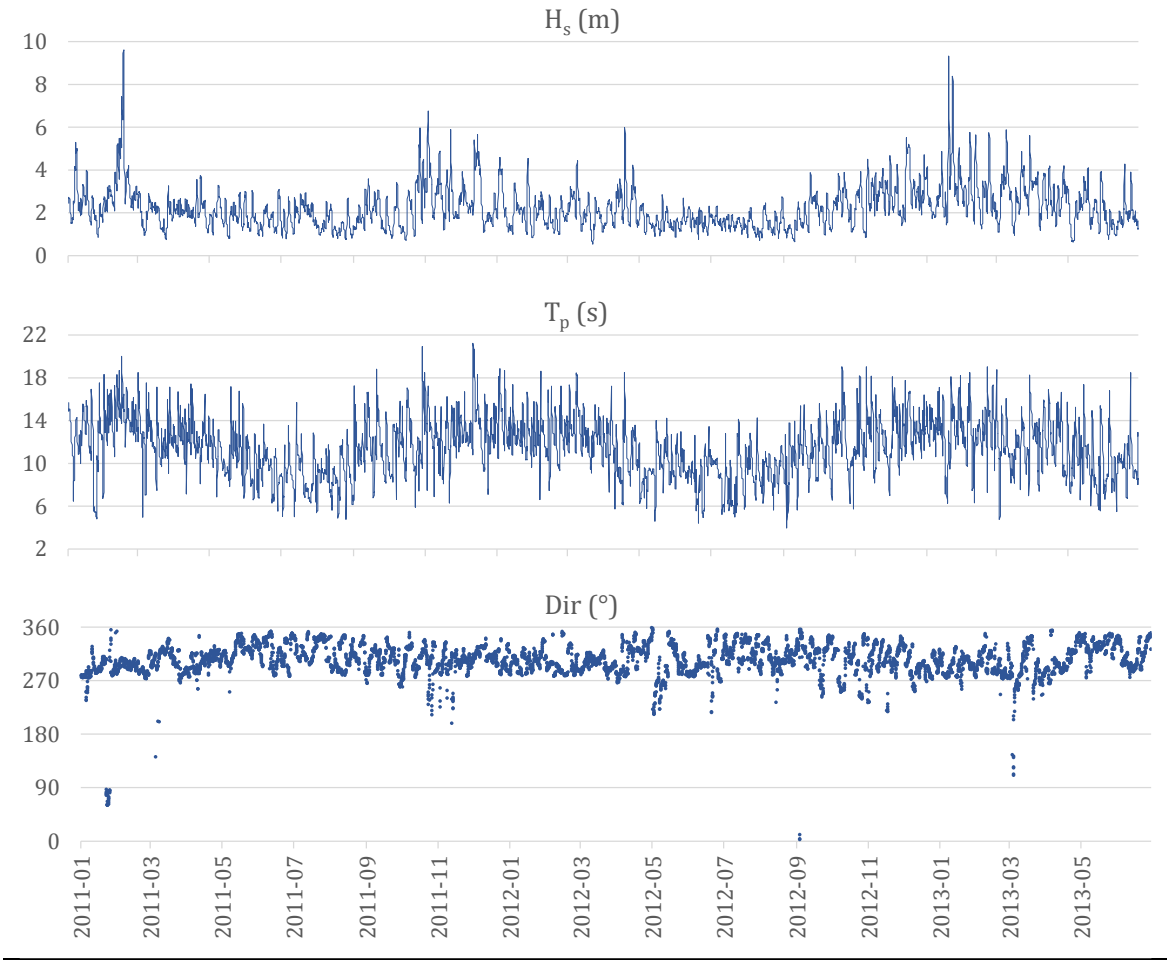

Figure 4.122. Offshore wave parameters (significant wave height in upper panel, peak period in middle panel, and mean direction in lower panel), for the study period.

The offshore wave regime during the two and a half years study period can therefore be considered representative of the general and modal conditions of the forcing climate reaching this coast, having not induced exceptional conditions to the study beaches.

4.3.1.2. Nearshore wave regime

The nearshore wave regime at each study site was obtained through modeling of wave propagation and arriving from the offshore conditions. The following section describes the results of the validation of the simulation outputs. Subsequently, the description of the simulated wave time series for each study site is presented.

Validation results

The validation results indicate that the wave propagation model produces a very satisfactory description of the nearshore wave regime. The simulated wave characteristics at both validation locations are in good agreement with the measured parameters. Table 4.6 presents the error statistics derived from the comparison between the model output and the *in situ* measurements.

Table 4.6. Results of the validation of the wave propagation model. Error statistics: bias - mean error; rmse – root mean squared error; nrmse – normalized rmse; r - correlation coefficient; N – number of observations.

Validation point	**Error statistics**	**Wave parameters**		
		Hs (m)	T (s)	Dir (°)
APL buoy Tagus south channel buoy	bias	-0.02	2.88	-4.98
	rmse	0.30	3.30	17.6
	nrmse	0.26	0.58	-
	r	0.88	0.56	-
	N	15728	15728	15728
IH ADCP * Praia de Almagreira	bias	0.00	-1.51	1.89
	rmse	0.42	2.41	9.1
	nrmse	0.23	0.22	-
	r	0.88	0.70	-
	N	2812	2812	2812

***** Source: Ribeiro (2013)

The wave height parameter shows the best fit with the observed data. Modeled values of Hs are practically unbiased and with rmse values below 0.42 m. The correlation coefficient of 0.88 for both validation points indicates a very good fit between the datasets, as shown in Figures 4.123 and 4.124 (upper panels). Wave period presents lower correlation coefficients (0.56 and 0.7), but still good rmse values, especially when model results are compared with the ADCP measurements. The larger bias derived from the comparison with the APL buoy data, indicates overestimation of the modeled wave

period, as depicted in figures 4.123 and 4.124 (middle panels). This overprediction is in part due to the modelling strategy that did not account for the higher-frequency locally-generated wind waves that are recorded by the buoy.

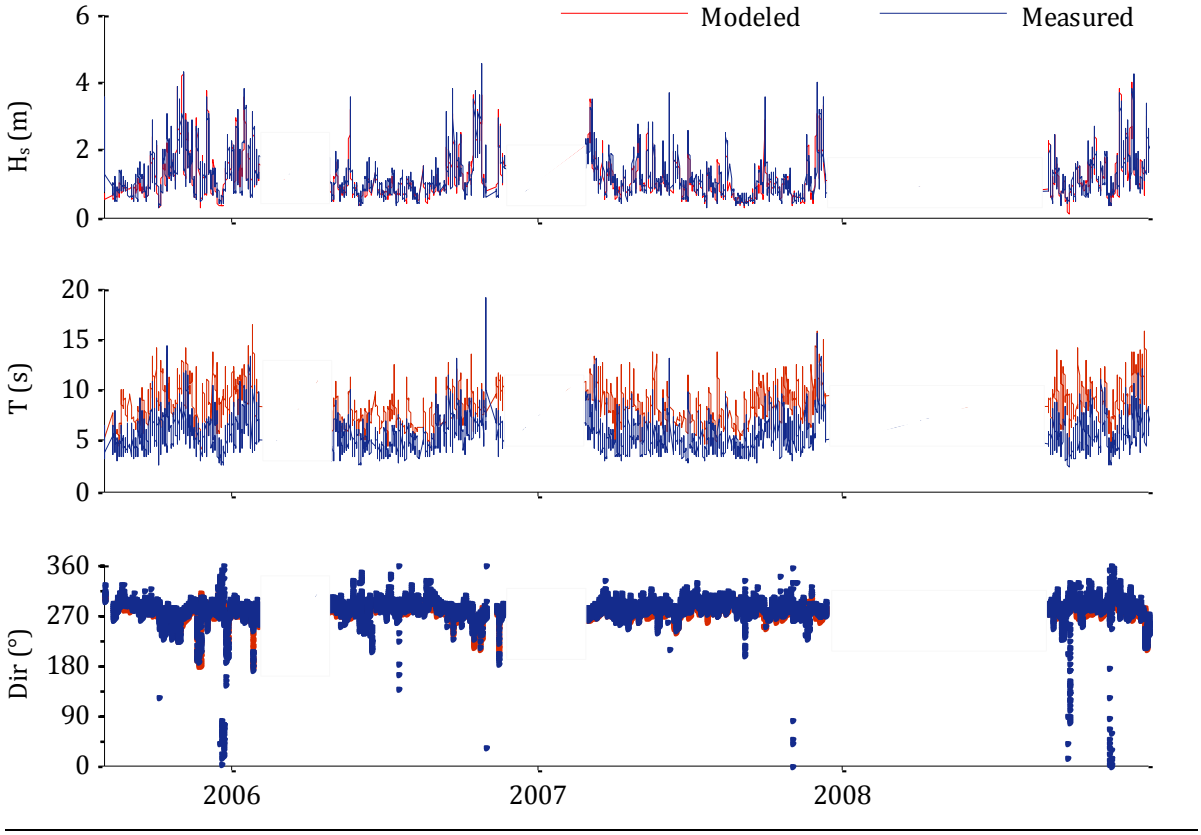

Figure 4.23. Comparison between the wave parameters measured at the APL wave buoy, and the model results, for the period between 31 July 2005 and 31 December 2008 (height in upper panel, period in middle panel, and direction in lower panel).

The validation results for the wave direction parameter differ between the two locations, presenting 17.6° and 9.1° of rmse for the APL buoy, and the IH ADCP, respectively. Bias is also not consistent, indicating underestimation in the first case, and a slight overestimation on the second location. Again, the exclusion of the wind-derived local waves can explain these differences. Moreover, there is a systematic time lag between the datasets because the model was run in stationary mode and therefore did not take into account the propagation time from offshore to the simulation point. Nonetheless, for this type of model, validation results are considered satisfactory (Dykes et al., 2002; Mazarakis et al. 2012). They are indicative of very good fit between the modeled and

observed records, and therefore the obtained model results were considered good descriptors of the nearshore wave regime along the study area.

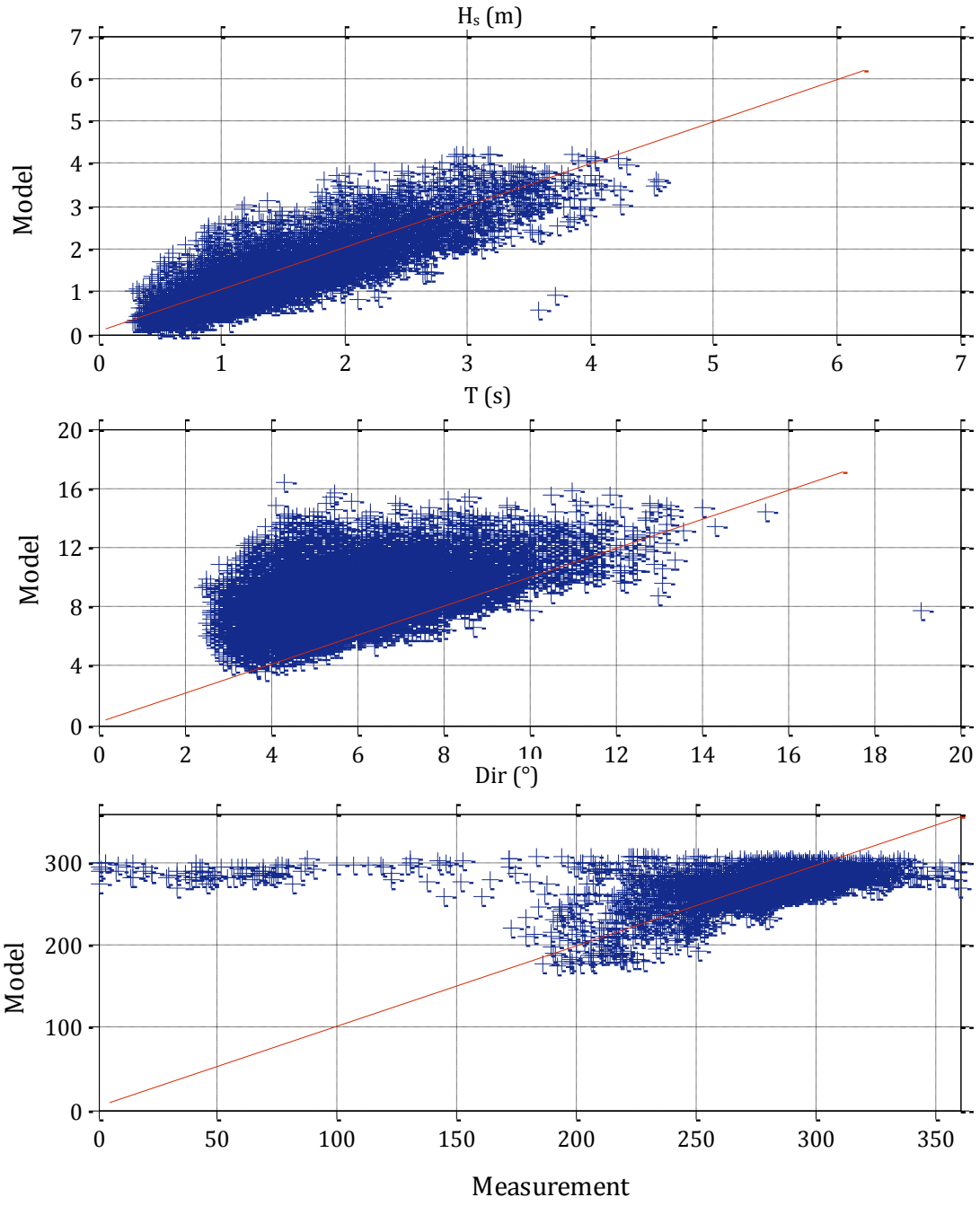

Figure 4.124. Comparison between wave parameters obtained in the wave propagation model, and the wave parameters recorded at the APL wave buoy (significant wave height in upper panel, peak period in middle panel, and mean direction in lower panel). Red line segments indicate a 1:1 relationship.

Nearshore wave regime at the study sites

Despite being exposed to the same general offshore wave regime, the study area is characterized by varying nearshore wave conditions, and the several study sites present contrasting incident wave characteristics. The continental shelf morphology and configuration presents alongshore variations that modulate the patterns of wave propagation and interaction with the sea floor as they approach the coast. These differences are reflected in the nearshore wave parameters as shown in the alongshore depiction of the average values of height, period and direction, in Figure 4.125.

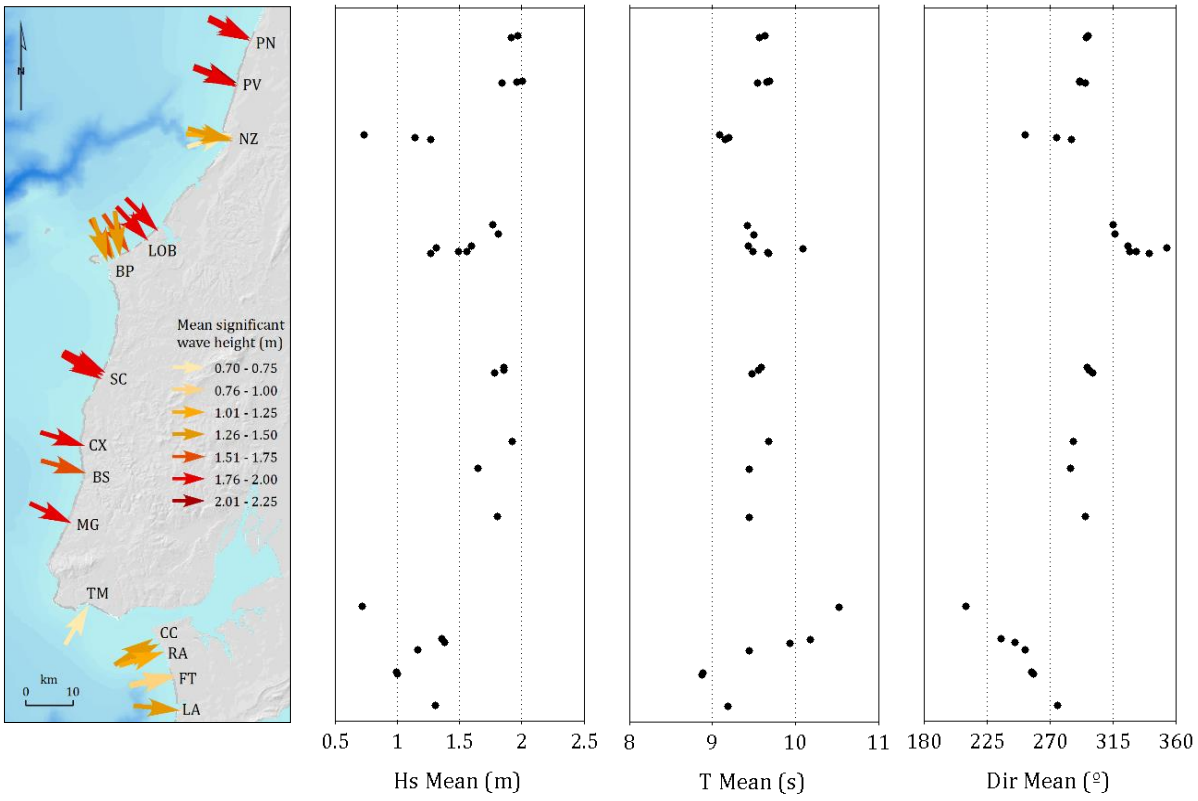

Figure 4.125. Mean wave parameters (height, period and direction) at each simulation point along the study area. In the left panel, color and orientation of the arrows indicate mean significant wave height and mean wave direction, respectively.

Mean wave height ranges between 1 and 2 m, with exception of the northernmost simulation point at Nazaré and the simulation point fronting Tamariz that present a mean wave height of 0.7 m. Mean wave period is fairly constant throughout the study area, ranging between 8.9 and 10.2 s. The only exception corresponds to the Tamariz study site

that is characterized by larger mean wave period, 10.5 s. This might be due to the sharp contrast in orientation between the coastline north of Cabo Raso (northeast-southwest), and the segment where Tamariz is located (east-west). This configuration provides an effective shelter to shorter and smaller waves, and only longer waves are refracted and reach this beach.

Mean wave direction tends to be orthogonal to the general orientation of the bathymetry at the location of the simulation point. The observed alongshore variation of this parameter reflects differences in the trend of the nearshore ocean bottom, mirrored by the shoreline orientation. The statistical parameters derived from the study sites' nearshore wave time series (36-year period) are presented in Table 4.7.

There is a clear distinction between the study sites located north of Cabo Raso (PN to MG – open symbols in Figure 4.126), and the southernmost ones (solid symbols in Figure 4.126). The former sites are exposed to a higher wave energy regime, with mean wave heights higher than 1.5 m, whilst the latter are characterized by nearshore mean wave heights lower than 1.4 m. The few exceptions correspond to the Nazaré beach, and the southernmost simulation points at Lagoa de Óbidos-Baleal and Baleal-Peniche stretch.

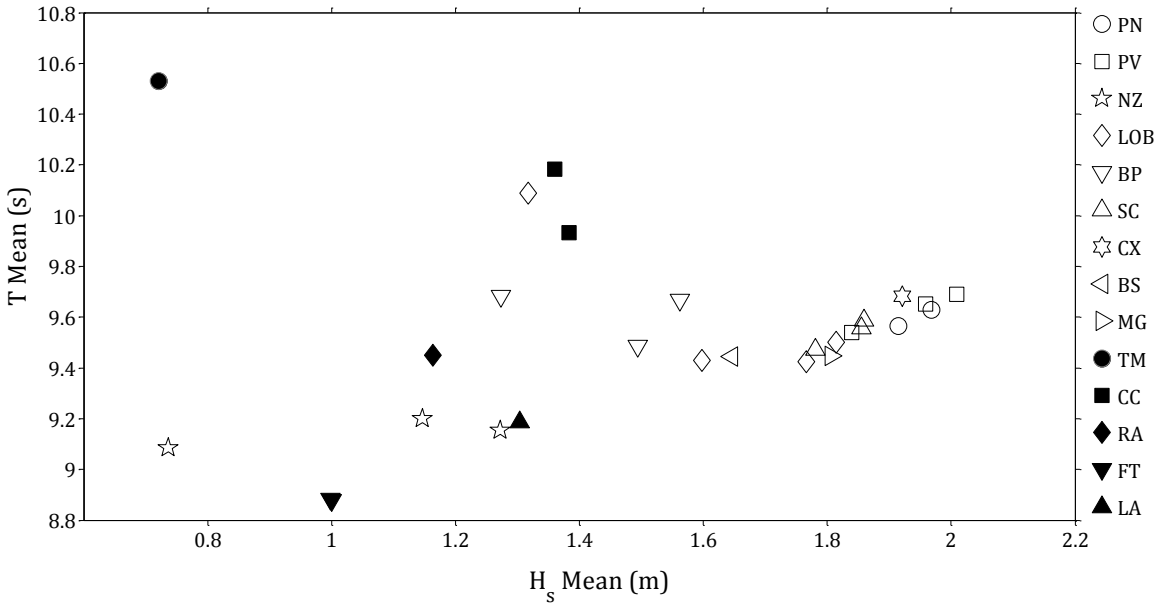

Figure 4.126. Representation and distribution of the study sites nearshore wave average conditions in terms of mean wave height and mean wave period.

The lower wave regime at NZ was probably the product of the limited exposure of this coastal segment to the incident waves – the lowest of all study sites (see chapter 2. Study area). The LOB and BP simulation points that present an exception to the observed pattern, are located near promontories that limit the coastal stretches and embayments, and therefore are under the influence of the bottom irregularities associated with these features. Cabo Raso combined with the presence of the Tagus prominent ebb delta, promote sheltering and wave refraction effects that account for the lower nearshore wave regime that characterizes the study sites located towards the south.

Figures 4.127 to 4.137 depict the nearshore significant wave height distribution along the computational grids for the study sites, obtained from the wave propagation model. The portrayed example is of an average offshore wave characterized by the mean height, period and direction values for the 36-year time series. The figures also present wave roses depicting the directional distribution of wave height for the 36-year wave time series at the simulation points used as model output to derive the nearshore wave time series.

Wave regime is, as expected, very similar within each study site, with exception of those areas that are highly embayed. In these cases, alongshore variations of the wave distribution is clear between the more exposed sectors and those that are more peripheral and generally more influenced by the lateral boundaries of the beach system. NZ and LOB are an example of this variability. Simulation points fronting the most peripheral and sheltered profile locations (the northernmost one in NZ and the southernmost one in LOB), are characterized by different distribution of depth-sensitive properties of nearshore waves (direction and height) when compared to the remaining ones.

When arriving at shallower depths, waves have already experienced some transformations. The wave directional range becomes much smaller than in the offshore domain, and confined to directions that are close to orthogonal to the shoreline. This filtering of wave directional spreading is especially evident in NZ, BP and TM sites, where the directional distribution of wave height is characterized by a single predominant mode of wave direction.

Table 4.7. Nearshore wave parameters' statistics for each study site, for the period between 1979 and 2014.

Study site	Simulation point	Wave parameters							
		$H_{s\ Mean}$ (m)	$H_{s\ Max}$ (m)	$H_s P_{97.5}$ (m)	$H_s P_{75}$ (m)	$H_s P_{50}$ (m)	$H_s P_{25}$ (m)	T_{Mean} (s)	Dir_{Mean} (º)
Pedras Negras	wPPN1	1.97	5.86	4.81	2.48	1.68	1.20	9.6	297
	wPPN2	1.92	5.77	4.67	2.40	1.65	1.18	9.6	296
Paredes de Vitória	wPPV1	2.01	6.02	4.88	2.55	1.72	1.21	9.7	291
	wPPV2	1.96	5.94	4.78	2.47	1.68	1.19	9.7	291
	wPPV3	1.84	5.77	4.51	2.30	1.58	1.13	9.5	295
Nazaré	wPNZ1	0.74	4.03	1.87	0.94	0.63	0.42	9.1	252
	wPNZ2	1.15	5.22	2.72	1.45	1.01	0.70	9.2	275
	wPNZ3	1.27	5.59	2.93	1.59	1.12	0.80	9.2	285
Lagoa de Óbidos – Baleal	wPLOB1	1.77	7.02	4.24	2.19	1.54	1.11	9.4	315
	wPLOB2	1.81	6.76	4.33	2.26	1.58	1.14	9.5	317
	wPLOB3	1.60	6.26	3.72	1.98	1.42	1.02	9.4	326
	wPLOB4	1.32	5.91	3.33	1.68	1.15	0.78	10.1	353
Baleal – Peniche	wPBP1	1.49	5.07	3.50	1.86	1.32	0.95	9.5	327
	wPBP3	1.56	5.24	3.75	1.95	1.38	0.98	9.7	332
	wPBP4	1.27	4.59	3.03	1.62	1.14	0.79	9.7	341
Santa Cruz	wPSC1	1.86	6.84	4.71	2.33	1.57	1.12	9.6	297
	wPSC2	1.85	7.28	4.66	2.31	1.58	1.12	9.6	298
	wPSC3	1.78	6.67	4.43	2.21	1.52	1.10	9.5	301
Coxos	wPCX1	1.92	7.36	4.86	2.43	1.63	1.13	9.7	287
Baleia/Sul	wPBS1	1.65	6.26	4.10	2.06	1.41	0.99	9.4	285
Magoito	wPMG1	1.81	6.78	4.41	2.25	1.55	1.12	9.4	295
Tamariz	wPTM1	0.72	4.49	2.14	0.96	0.59	0.34	10.5	210
Costa da Caparica	wPCC1	1.36	4.57	3.51	1.80	1.21	0.73	10.2	235
	wPCC2	1.38	5.42	3.46	1.83	1.21	0.77	9.9	245
Rainha	wPRA1	1.16	5.31	2.87	1.49	1.02	0.67	9.4	252
	wPFT1	1.00	5.87	2.74	1.26	0.82	0.54	8.9	257
Fonte da Telha	wPFT2	1.00	5.91	2.76	1.26	0.82	0.54	8.9	258
Lagoa de Albufeira	wPLA1	1.30	6.88	3.25	1.65	1.12	0.76	9.2	276

The wave height spatial distribution along the nearshore illustrates the rapid changes that waves experience near the coast and how they differ from site to site, depending on the bottom morphology. Wave transformation processes include wave refraction and shoaling that are represented by the alongshore and cross-shore wave height variations and most noticeable near prominent features, such as promontories. The shallower depth perturbations on the wave height distribution pattern are, in general, due to proximal features such as longshore bars, and their location and magnitude are inevitably dependent on the bathymetry used for the model. In fact, the bathymetric description used herein represents an instantaneous time frame that may or may not be the most typical configuration of the site. Although one must acknowledge this limitation of the data, it is considered that the output simulation points are located deeper than this zone of highest variability, and therefore may be considered fairly representative of the typical and modal conditions affecting the area.

In general there is a reduction in wave height from the offshore, indicative of the influence of the refraction processes as waves travel onshore. Nonetheless, the shoaling process and increase in wave height closer to shoreline is clear in the model results.

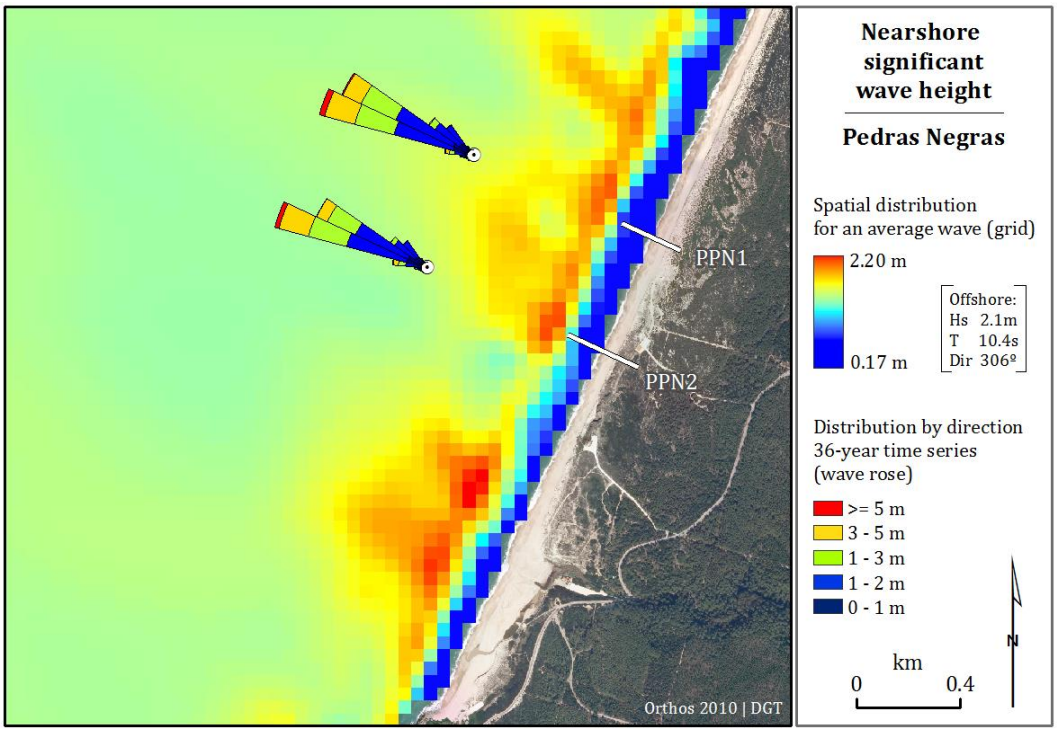

Figure 4.127. Nearshore significant wave height distribution at Pedras Negras study site, obtained from the propagation of an average offshore wave. Wave roses depict the directional distribution of H_s for the 36-year wave time series at the simulation points.

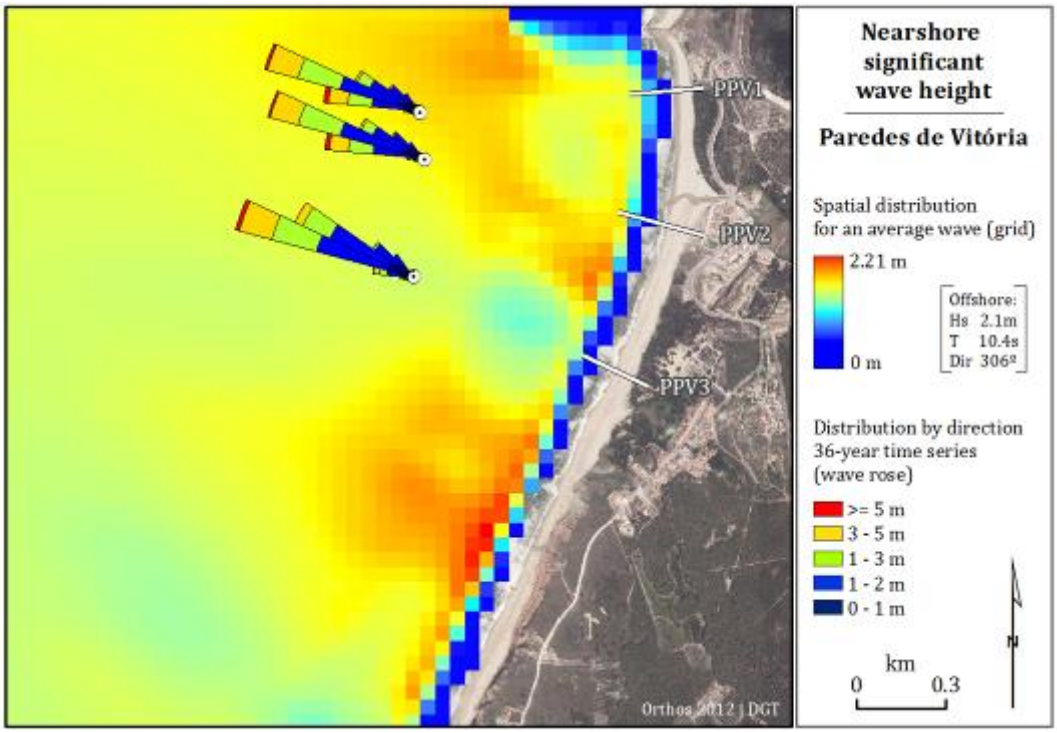

Figure 4.128. Nearshore significant wave height distribution at Paredes de Vitória study site, obtained from the propagation of an average offshore wave. Wave roses depict the directional distribution of H_s for the 36-year wave time series at the simulation points.

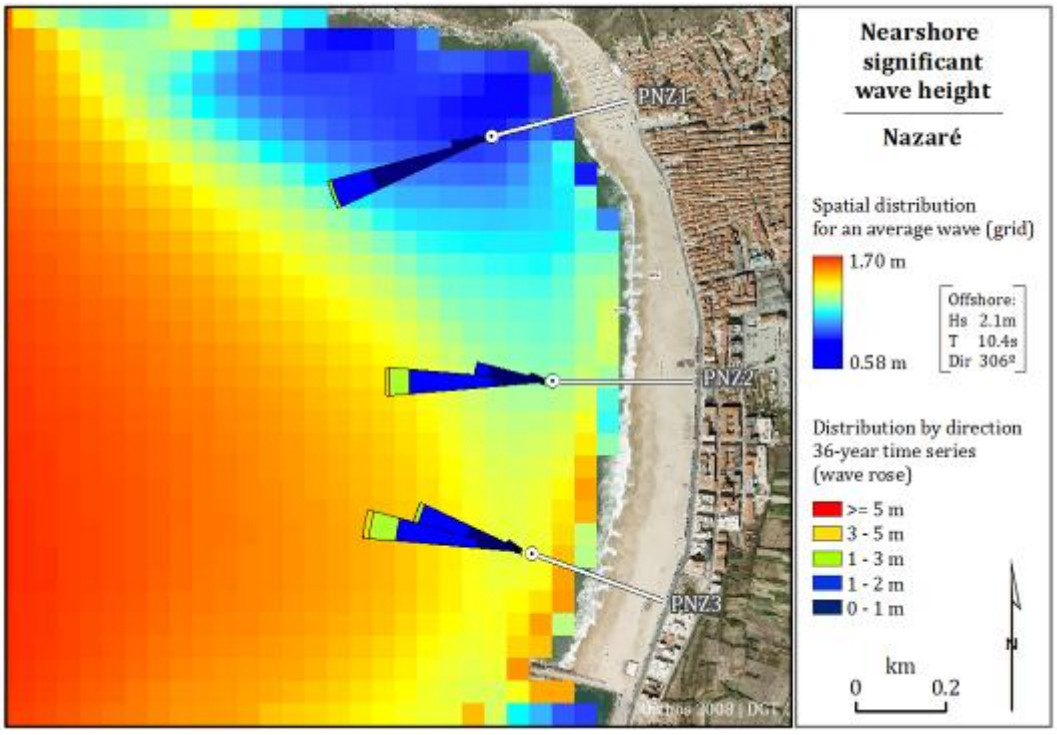

Figure 4.129. Nearshore significant wave height distribution at Nazaré study site, obtained from the propagation of an average offshore wave. Wave roses depict the directional distribution of H_s for the 36-year wave time series at the simulation points.

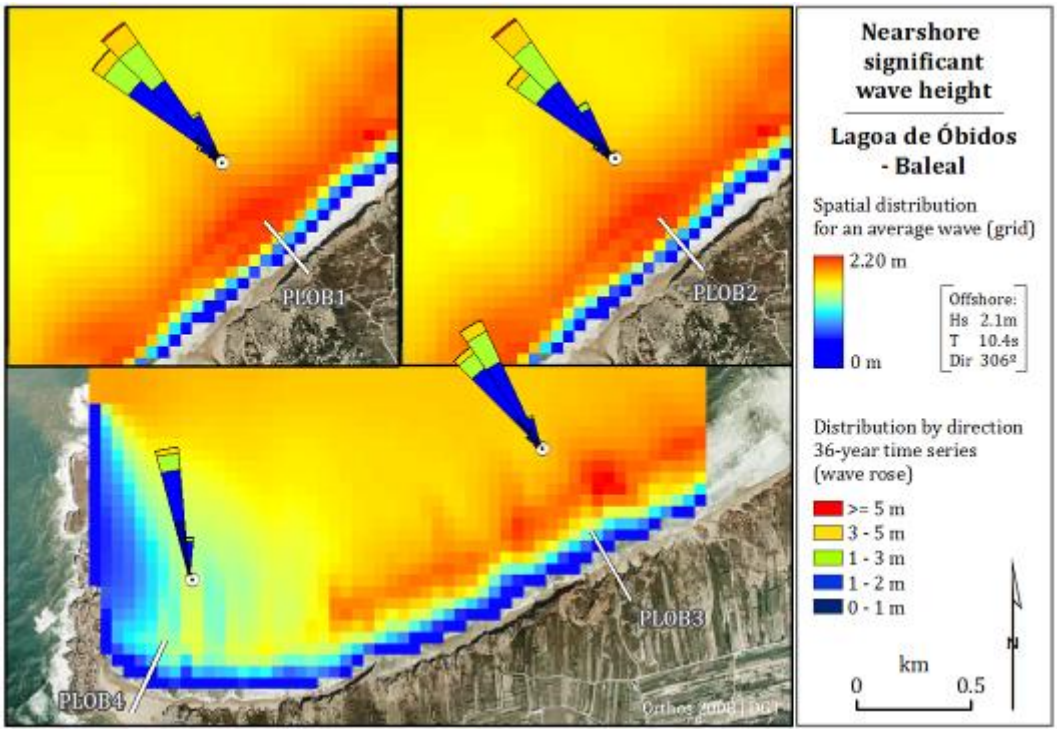

Figure 4.130. Nearshore significant wave height distribution at Lagoa de Óbidos - Baleal study site, obtained from the propagation of an average offshore wave. Wave roses depict the directional distribution of H_s for the 36-year wave time series at the simulation points.

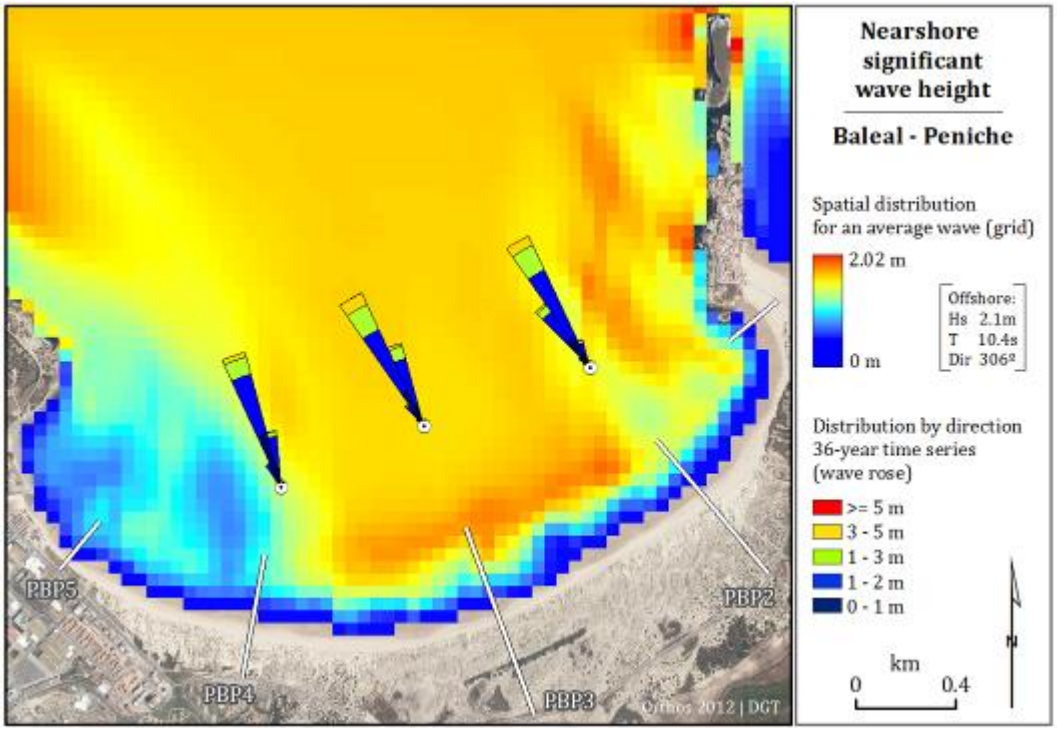

Figure 4.131. Nearshore significant wave height distribution at Baleal-Peniche study site, obtained from the propagation of an average offshore wave. Wave roses depict the directional distribution of H_s for the 36-year wave time series at the simulation points.

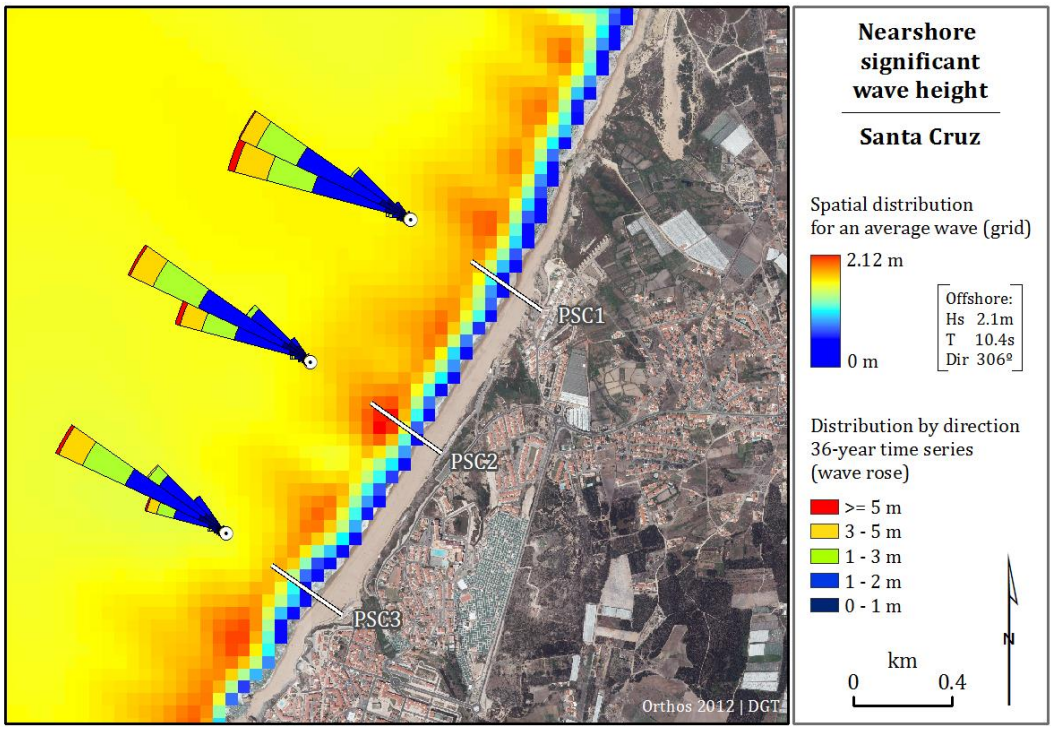

Figure 4.132. Nearshore significant wave height distribution at Santa Cruz study site, obtained from the propagation of an average offshore wave. Wave roses depict the directional distribution of H_s for the 36-year wave time series at the simulation points.

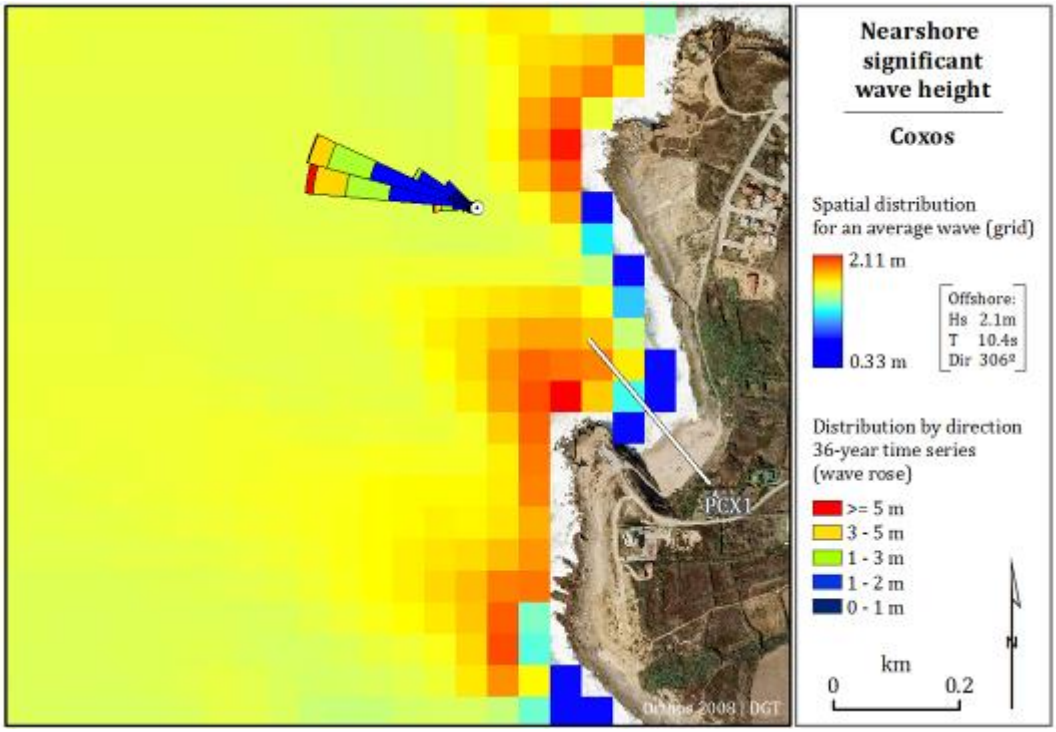

Figure 4.133. Nearshore significant wave height distribution at Coxos study site, obtained from the propagation of an average offshore wave. Wave rose depicts the directional distribution of H_s for the 36-year wave time series at the simulation point.

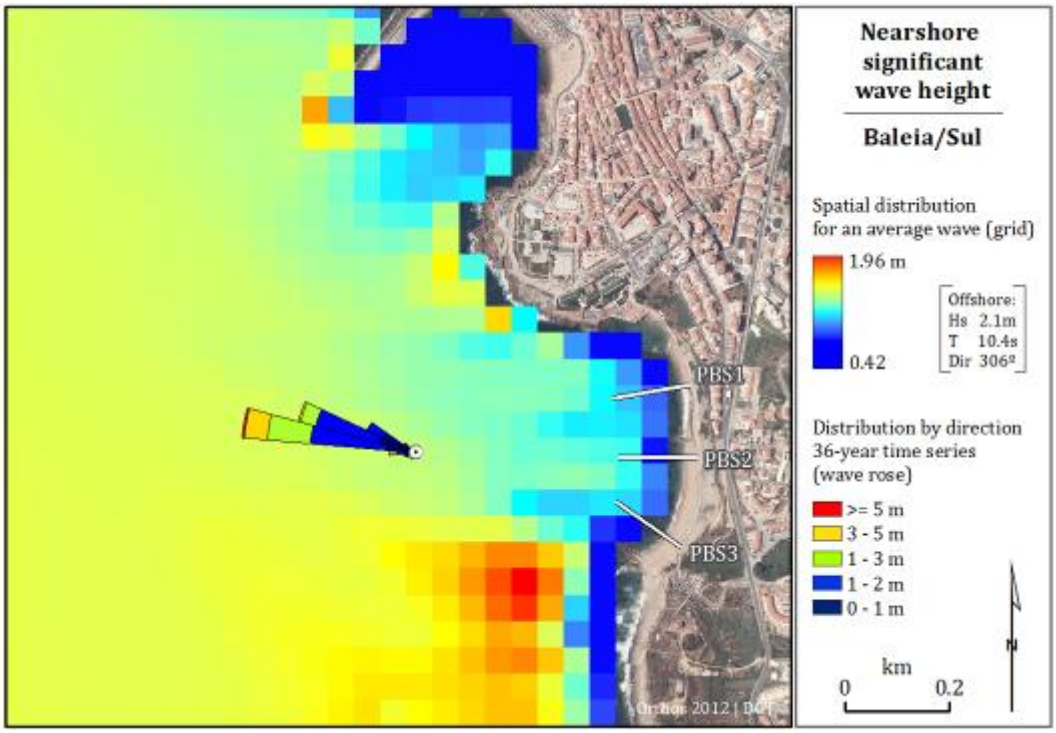

Figure 4.134. Nearshore significant wave height distribution at Baleia/Sul study site, obtained from the propagation of an average offshore wave. Wave rose depicts the directional distribution of H_s for the 36-year wave time series at the simulation point.

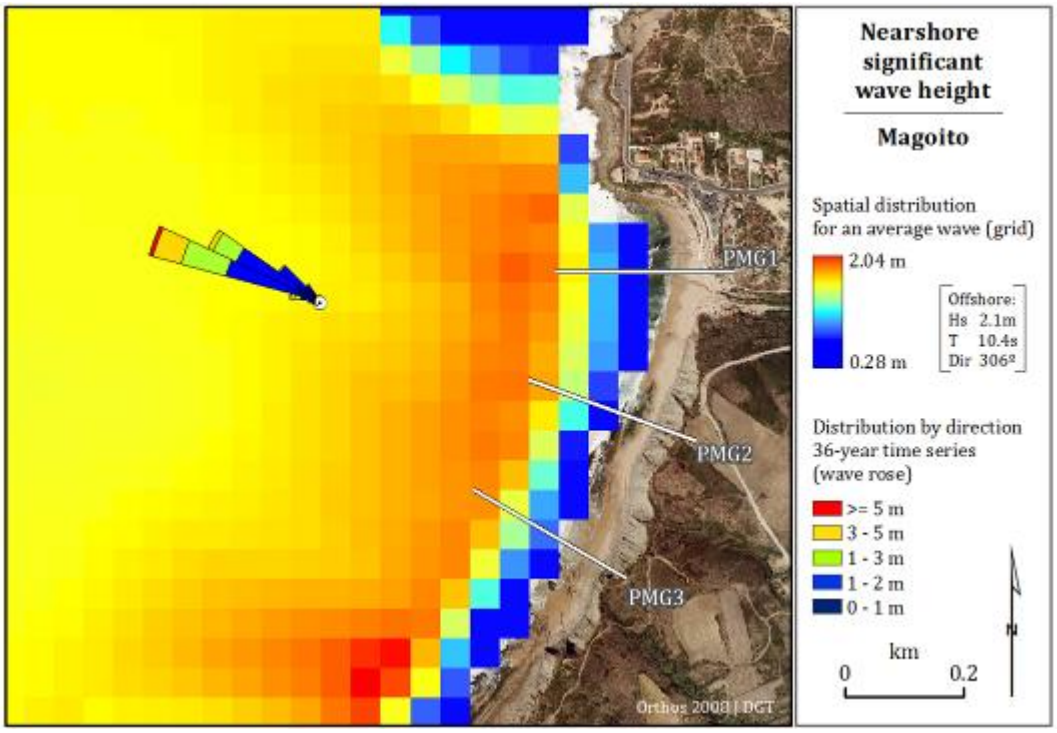

Figure 4.135. Nearshore significant wave height distribution at Magoito study site, obtained from the propagation of an average offshore wave. Wave rose depicts the directional distribution of H_s for the 36-year wave time series at the simulation point.

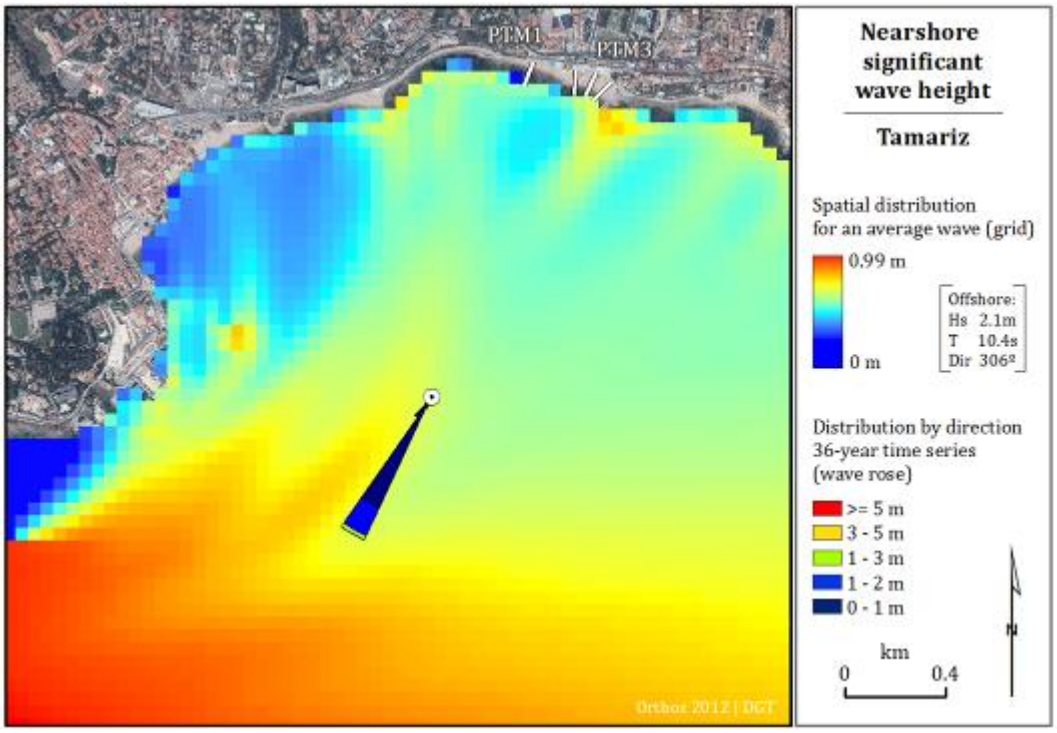

Figure 4.136. Nearshore significant wave height distribution at Tamariz study site, obtained from the propagation of an average offshore wave. Wave rose depicts the directional distribution of H_s for the 36-year wave time series at the simulation point.

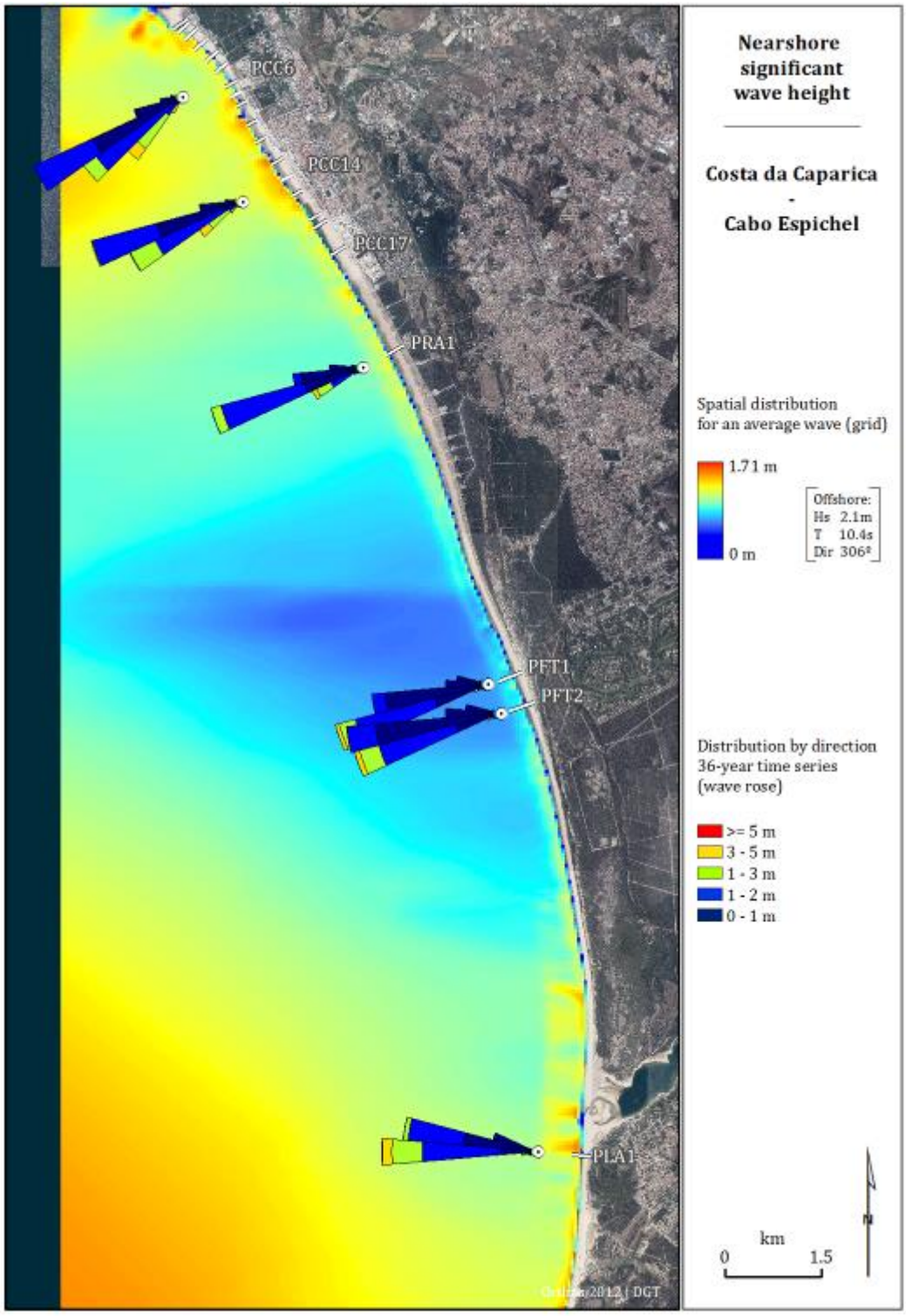

Figure 4.137. Nearshore significant wave height distribution at Costa da Caparica – Cabo Espichel stretch, that includes the Rainha, Fonte da Telha and Lagoa e Albufeira study sites, obtained from the propagation of an average offshore wave. Wave roses depict the directional distribution of H_s for the 36-year wave time series at the simulation points.

4.3.2. Tides

The water levels record at the Cascais tide gauge for the period between January 1, 1979 and August 31, 2014 is presented in the middle panel of figure 4.138, along with the predicted tide levels (upper panel) and the calculated residuals (lower panel). The segments in the residual record that correspond to zero are gaps in the measured time-series that were filled with data extracted from the astronomical tide predictions. Two records from the measured dataset (21-Nov-2007 16:00:00 and 29-Feb-2008 16:00:00) have unusually low values of low tide (-2.08 m). These two records were considered measurement errors and removed from the data series that was subsequently used in the data analysis. Table 4.8 lists the maximum and minimum values of the predicted and measured water levels, as well as of the residual values.

In both measured and predicted records, the average water levels are above 0 m: 0.11 and 0.10 m, respectively. This offset is expected and mainly due to sea level rise relative to the static datum (established in 1938) that levels are measured to at the gauge.

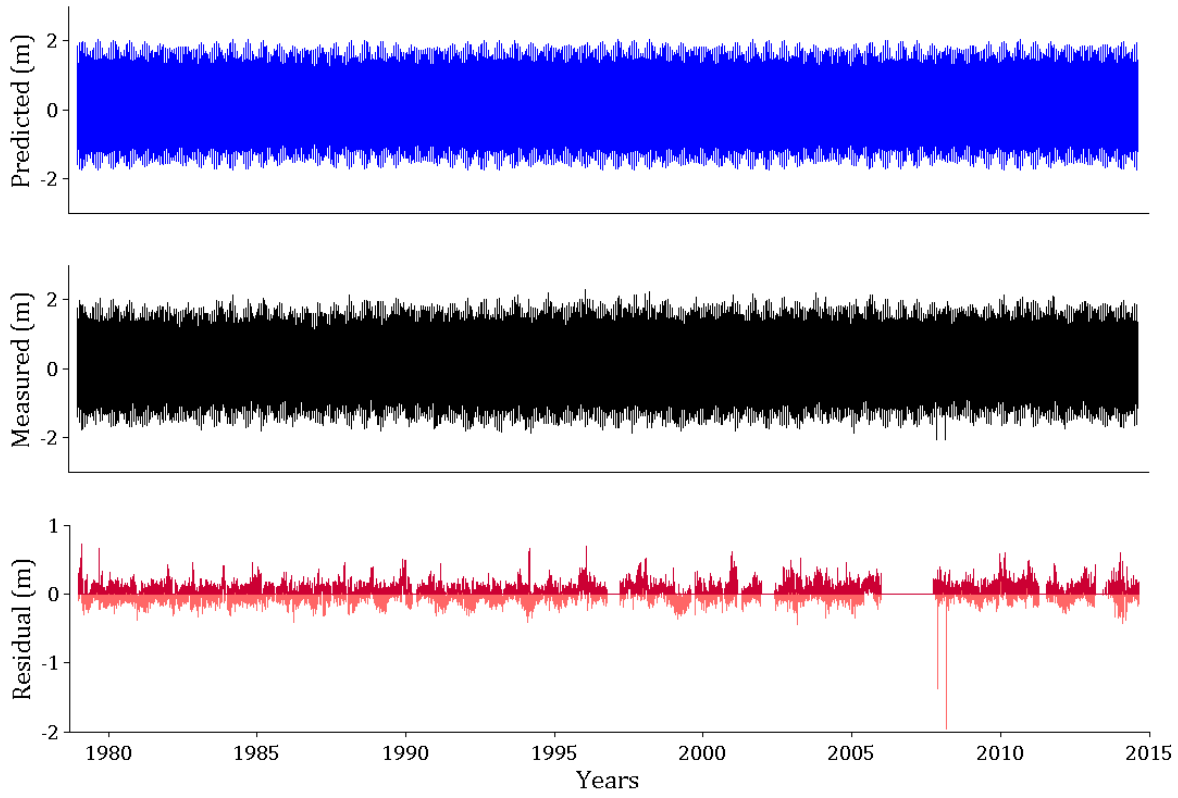

Figure 4.138. Water levels for the period between January 1, 1979 and 31 August 31, 2014, for the Cascais tide gauge. Predicted tide levels in upper panel, recorded water levels in the middle panel and residuals in the lower one. Values are relative to mean sea level.

Table 4.8. Statistics derived from the predicted and measured water levels, and the calculated residuals, for the period between 1979 and 2014.

Water levels	Max	Min
Predicted	2.03	-1.76
Measured	2.28	-1.87
Residual	0.72	-0.45

Residual values correspond to the non-tidal component of water levels, and positive residuals to the surge effect that raises water levels. The distribution of the residual values shows a small asymmetry towards positive values as shown in figure 4.139, and concentrate in the lower values range, between -0.2 and 0.2 m. The surge-related records present a mean value of 0.08 m. This value is in agreement with the findings of other analysis of water levels' time series for the same location (Andrade et al., 2006; Antunes et al., 2013). The surge component is relatively small when compared to the tidal range affecting the study area, and thus may be considered unimportant to the overall water levels affecting and imposing changes to the beach morphology.

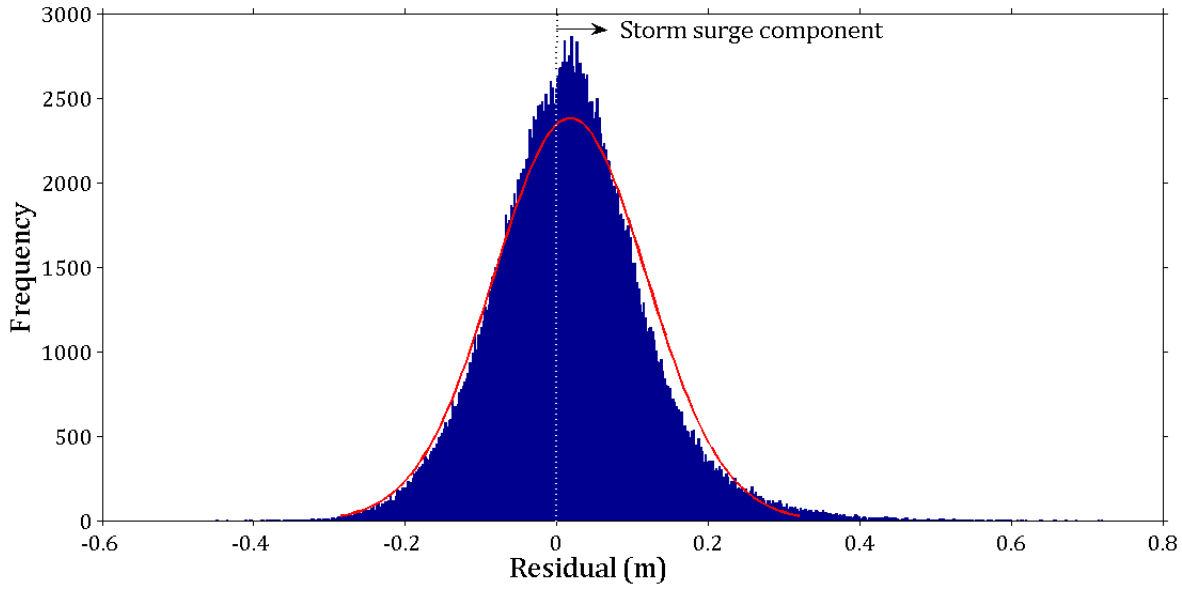

Figure 4.139. Histogram and distribution fit of the calculated residual. Positive values correspond to the storm surge component.

4.3.3. Total Water Levels

4.3.3.1. Runup model validation results

The four tested solutions for estimating the runup levels were compared with the observed field measurements of the high tide swash line (see Chapter 3. Methods). Figures 4.140 to 4.143 illustrate the relationship between the model input parameters and the runup being modeled (observed), and provide the coefficient of determination (R^2) derived from simple linear regression. This coefficient was taken as indicative of the goodness of fit between the two variables.

The runup distributions for the overall study sites are scattered and present a poor relationship between the modelled and observed values for all tested solutions (R^2 between 0.32 and 0.36). Table 4.9 presents the regression parameter derived from the linear regression analysis between the modelled and observed runup values for each solution, as well as error statistics derived from the fitted model results (bias, rmse and nrmse). The data dispersion is in part due to the differences between the study sites that may not behave in the same way in response to the modelled variables, indicating that there is not a single solution for wave runup determination for the overall study area.

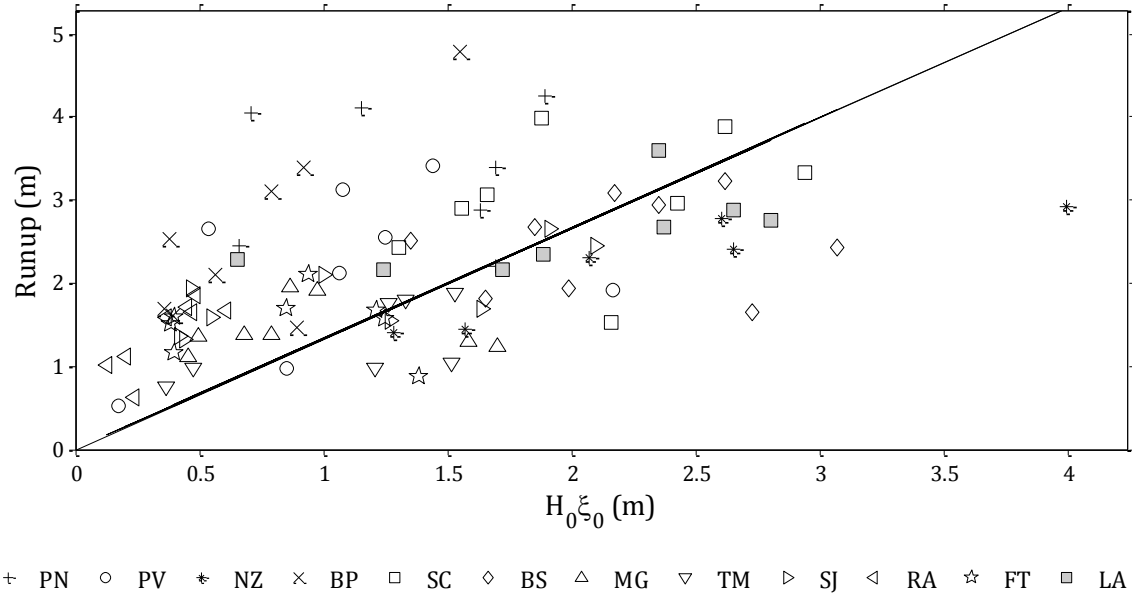

Figure 4.140. Comparison between the model input (solution #1 $R=H_0\xi$) and the observed runup.

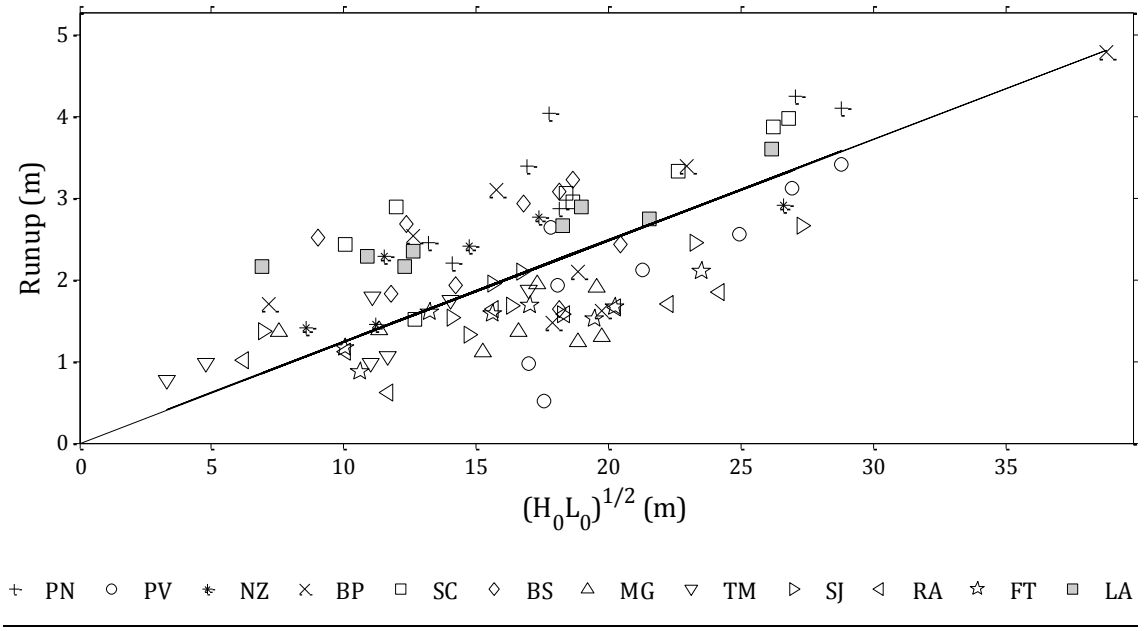

Figure 4.141. Comparison between the model input (solution #2 $R=(H_0L_0)^{1/2}$) and the observed runup.

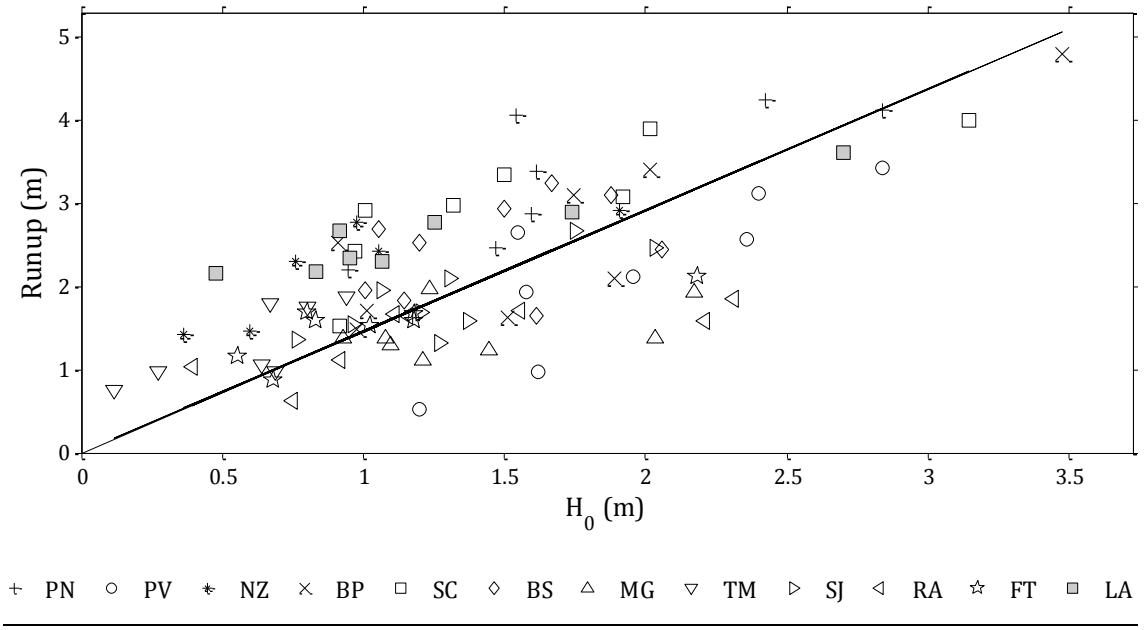

Figure 4.142. Comparison between the model input (solution #3 $R=H_0$) and the observed runup.

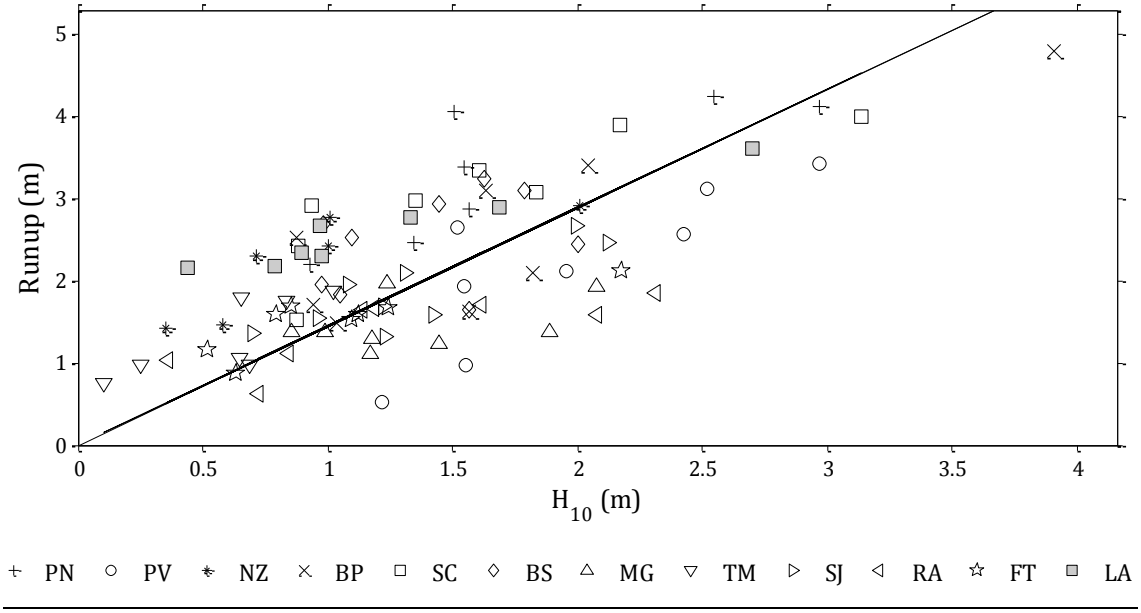

Figure 4.143. Comparison between the model input (solution #4 $R=H_{10}$) and the observed runup.

Table 4.9. Regression parameter (y-intercept) and error statistics (bias, rmse and nrmse) derived from linear regression analysis between the modelled solutions and the observed runup values for the overall study area.

	$R=H_0\xi$	$R=(H_0L_0)^{1/2}$	$R=H_0$	$R=H_{10}$
slope	1.33	0.12	1.46	1.44
bias	-0.39	-0.07	-0.16	-0.18
rmse	1.07	0.72	0.76	0.77
nrmse	0.50	0.33	0.35	0.36

The comparison and regression analysis applied separately to each study site provided better results in some cases, with R^2 values as high as 0.8 (NZ, BP and RA study sites), but also some poorer relationships. Figure 4.144 presents the error statistics in the form of graph and table for each solution. The normalized rmse shows a good fit between the modeled and observed data for the overall study sites and modelled solutions, lying mostly within 0.3, and reaching as low as 0.14 for FT study site.

As expected, the solution that best fits the observed data varies depending on the study site. However, the differences are not substantial, and the solution that offers the best

estimation of runup elevations for the overall sites is solution #2 ($R=(H_0L_0)^{1/2}$). This solution provides the higher number of sites where predictions were correlated to the observations (R^2 >0.6), and therefore where systematic errors could be corrected. BS, MG and TM are the only exceptions and present very low values of R^2. Still, after fitted, the model provides normalized errors below 0.3. Only three study sites present rmse values above 0.5 m, and they are all below 0.7 m.

Figure 4.145 shows the comparison between the observed and estimated runup values with solution #2, and the regression derived for each study site. The runup equations parameterized for each study site are presented in Table 4.10.

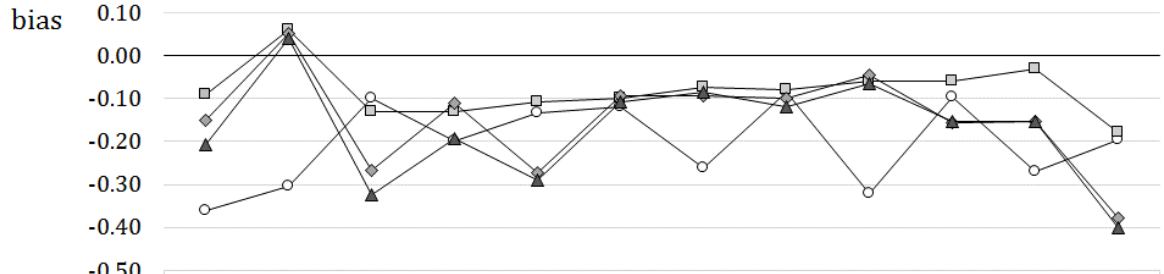

	PN	PV	NZ	BP	SC	BS	MG	TM	CC	RA	FT	LA
$R = H'_0\xi$	-0.36	-0.30	-0.10	-0.20	-0.13	-0.12	-0.26	-0.08	-0.32	-0.09	-0.27	-0.20
$R = (H'_0)^{1/2}$	-0.09	0.06	-0.13	-0.13	-0.11	-0.10	-0.07	-0.08	-0.06	-0.06	-0.03	-0.18
$R = H'_0$	-0.15	0.05	-0.27	-0.11	-0.27	-0.09	-0.09	-0.10	-0.04	-0.16	-0.15	-0.38
$R = H_{10}$	-0.21	0.04	-0.32	-0.19	-0.29	-0.11	-0.09	-0.12	-0.07	-0.15	-0.15	-0.40

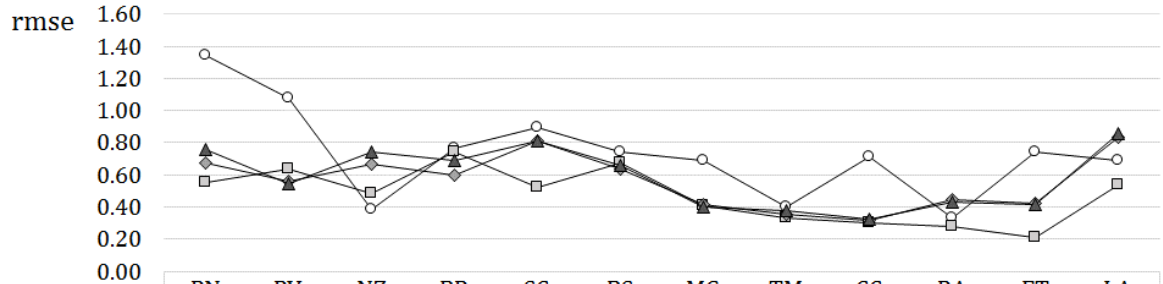

	PN	PV	NZ	BP	SC	BS	MG	TM	CC	RA	FT	LA
$R = H'_0\xi$	1.34	1.08	0.39	0.77	0.89	0.74	0.69	0.40	0.71	0.33	0.74	0.69
$R = (H'_0)^{1/2}$	0.56	0.64	0.49	0.75	0.52	0.68	0.41	0.33	0.30	0.28	0.21	0.54
$R = H'_0$	0.67	0.56	0.67	0.60	0.81	0.64	0.42	0.36	0.32	0.45	0.42	0.84
$R = H_{10}$	0.76	0.55	0.74	0.69	0.81	0.66	0.40	0.38	0.33	0.43	0.42	0.86

Figure 4.144. Error statistics (bias, rmse and nrmse) derived from linear regression analysis between the modelled and observed runup values for each solution and each study site.

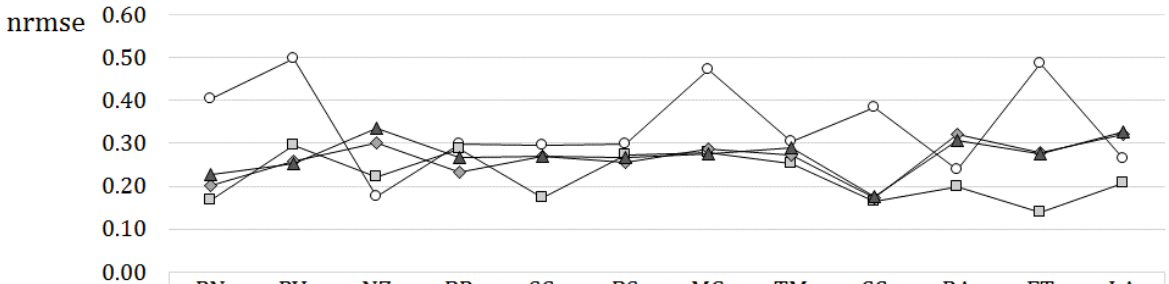

	PN	PV	NZ	BP	SC	BS	MG	TM	CC	RA	FT	LA
$R = H'_0\xi$	0.40	0.50	0.17	0.30	0.30	0.30	0.47	0.30	0.38	0.24	0.49	0.26
$R = (H'_0)^{1/2}$	0.17	0.30	0.22	0.29	0.17	0.27	0.28	0.25	0.16	0.20	0.14	0.21
$R = H'_0$	0.20	0.26	0.30	0.23	0.27	0.26	0.29	0.27	0.17	0.32	0.28	0.32
$R = H_{10}$	0.23	0.25	0.34	0.27	0.27	0.27	0.28	0.29	0.18	0.31	0.28	0.33

Figure 4.144 (continuation). Error statistics (bias, rmse and nrmse) derived from linear regression analysis between the modelled and observed runup values for each solution and each study site.

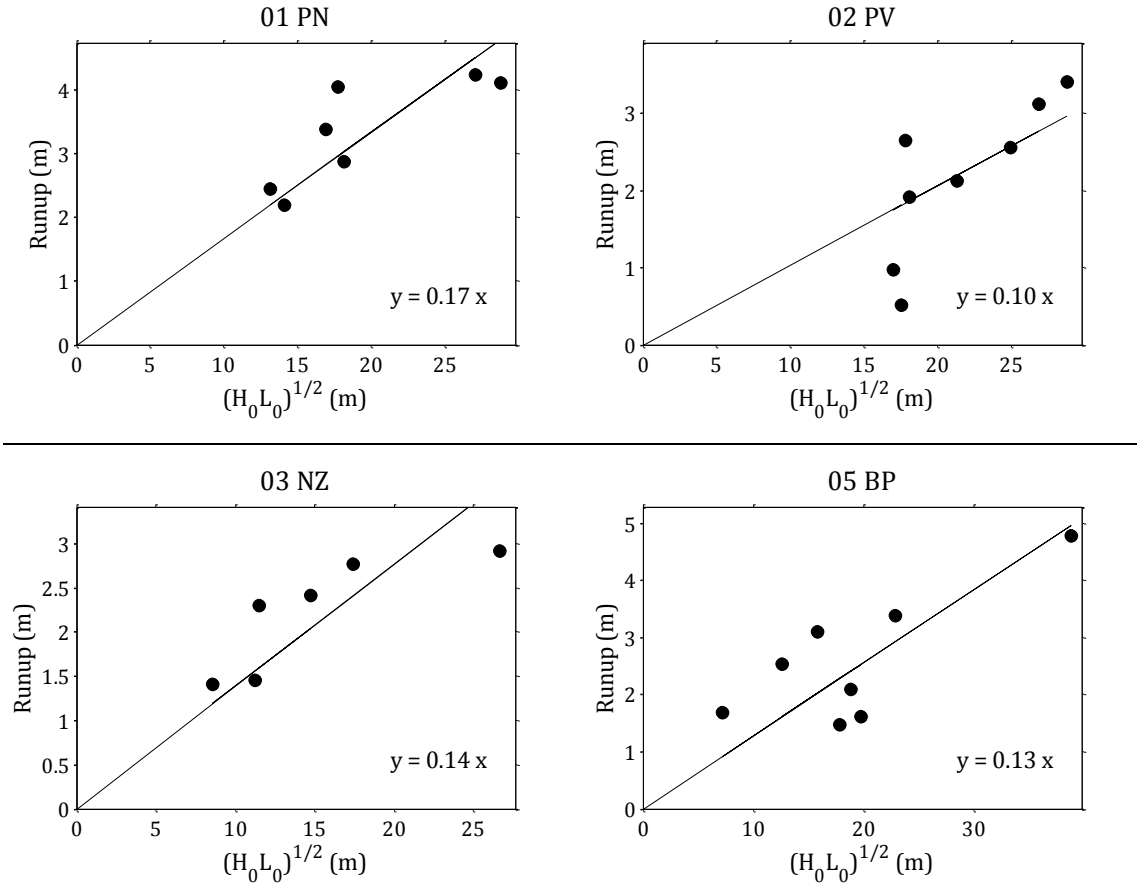

Figure 4.145. Observed and modeled (solution #2) runup and linear-regression fitting for each study site.

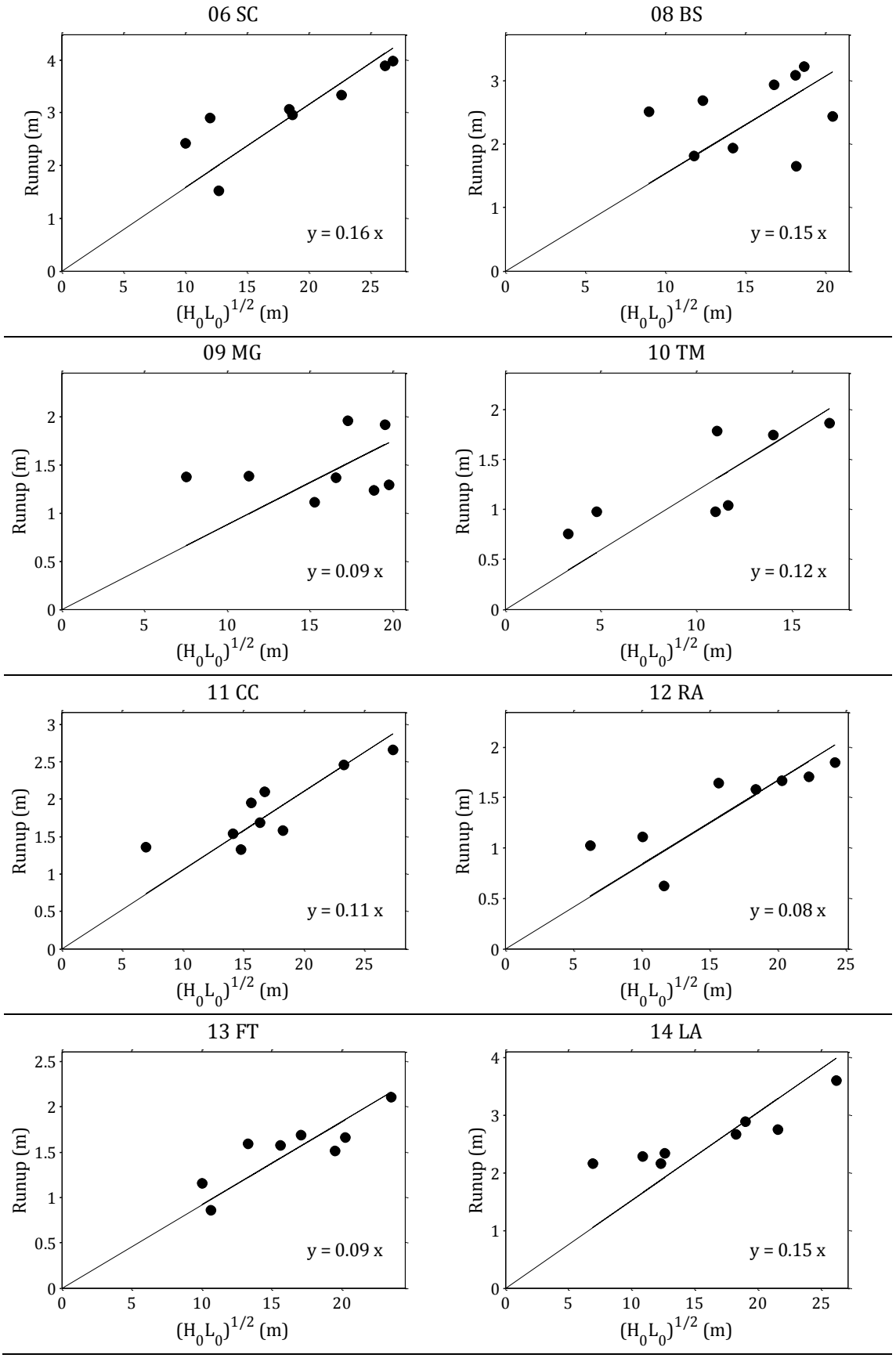

Figure 4.145 (continuation). Observed and modeled (solution #2) runup and linear-regression fitting for each study site.

Table 4.10. Runup equations parameterized for each study site.

Beach		Runup Equation $R = \beta (HL)^{1/2}$
01	PN	$R = 0.17 (HL)^{1/2}$
02	PV	$R = 0.10 (HL)^{1/2}$
03	NZ	$R = 0.14 (HL)^{1/2}$
05	BP	$R = 0.13 (HL)^{1/2}$
06	SC	$R = 0.16 (HL)^{1/2}$
08	BS	$R = 0.15 (HL)^{1/2}$
09	MG	$R = 0.09 (HL)^{1/2}$
10	TM	$R = 0.12 (HL)^{1/2}$
11	CC	$R = 0.11 (HL)^{1/2}$
12	RA	$R = 0.08 (HL)^{1/2}$
13	FT	$R = 0.09 (HL)^{1/2}$
14	LA	$R = 0.15 (HL)^{1/2}$

The validation procedure determined that runup can be predicted with sub-meter accuracy using the height and period of the offshore waves, through site-specific and locally parameterized formulas.

4.3.3.2. Total water levels at the study sites

With the selected and parameterized runup solutions and by adding the SL component, a 36-year time series of total water levels (TWL) was calculated, with a total of 104 199 records (example of RA study site in Figure 4.146).

The descriptive statistics of each study sites' TWL time series is presented in Table 4.11, through the mean, maximum and standard deviation values, as well as the 25th, 50th, 75th and 97. 5th percentiles. The latter value represents an extreme water level condition, correspondent to elevations only reached 12 hours per year, on average.

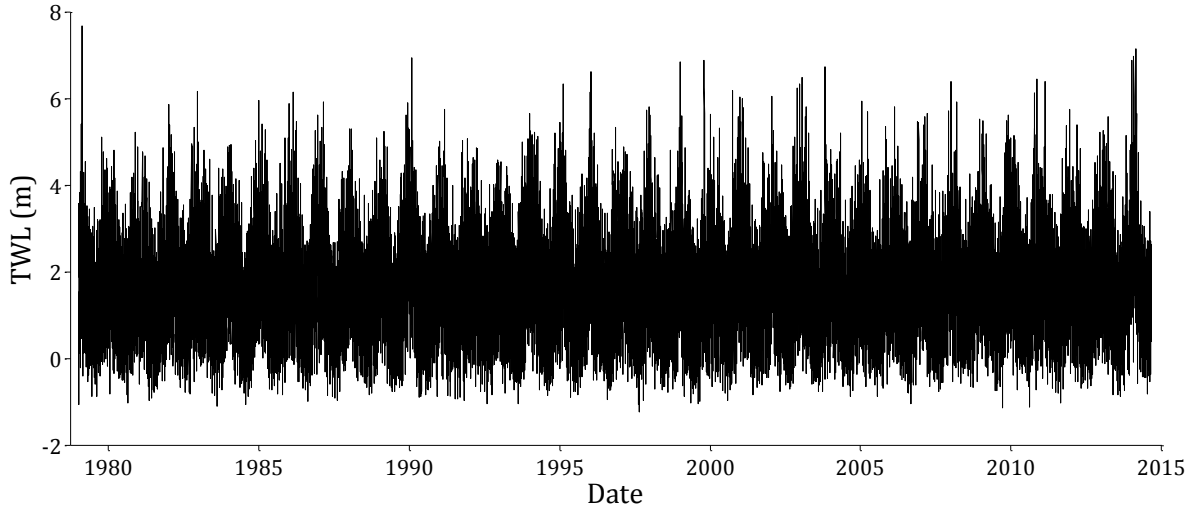

Figure 4.146. Total water level record for the 36-year time series of combined sea level and runup values for the RA study site.

Table 4.11. Total water level statistics for each study site (values in m, above MSL). Mean, Max – maximum, St.Dev - standard deviation, and percentiles (P).

Beach		Mean	St.Dev.	Max	$P_{97.5}$	P_{75}	P_{50}	P_{25}
01	PN	4.15	1.37	12.84	7.20	4.98	4.03	3.17
02	PV	2.82	1.71	14.14	6.74	3.82	2.61	1.61
03	NZ	3.35	1.20	10.59	5.94	4.09	3.28	2.48
05	BP	2.97	1.36	11.56	5.99	3.79	2.86	2.01
06	SC	4.03	1.23	11.55	6.70	4.79	3.95	3.14
08	BS	3.08	0.85	6.55	4.69	3.73	3.09	2.41
09	MG	1.35	0.82	3.73	2.82	2.02	1.34	0.71
10	TM	2.34	0.91	6.66	4.12	2.99	2.33	1.63
11	CC	2.54	1.01	8.03	4.62	3.22	2.52	1.78
12	RA	1.67	1.06	7.66	3.89	2.37	1.64	0.89
13	FT	1.85	0.84	5.08	3.41	2.50	1.86	1.18
14	LA	3.25	1.18	10.32	5.79	3.99	3.19	2.40

The highest TWL values are concentrated in the northernmost sectors of the study area. PN study site presents the highest mean value of TWL, above 4 m (above MSL), and

standard deviation of 1.37 m, whilst PV displays the highest TWL value, above 14 m (above MSL). Extreme conditions (97.5^{th} percentile) along the northernmost sites, and as far as BS, are characterized by TWL between 4.69 m (BS) and 7.20 m (PN), and maximum records along the four northernmost sites reach beyond the 10 m elevation (above MSL).

South of BS, TWL values decrease in magnitude and also in range. The lowest of all TWL time series corresponds to MG study area, with a mean value of 1.35 m (above MSL). In this southernmost sector, extreme conditions values are below 4.62 m and are as low as 2.82 m for MG study site. Variability of this parameter is also, in general, lower than that of the northernmost sector. LA study site is an exception to this alongshore spatial pattern, and presents a TWL record similar to that of the northernmost ones in magnitude and in range.

The frequency distribution of the TWL data illustrates these alongshore differences in the water levels regime (Figure 4.147). In the northernmost study sites (PN, PV, NZ, BP and SC), TWLs spread over a wider range of classes of elevations whereas in the remaining study sites, TWLs tend to concentrate on the lower elevation classes. The upper tail of the cumulative distribution is also different, and shows that the northernmost study sites have higher probabilities of occurrence of high water levels.

The TWL regime reflects the wave seasonality that affects the study area. Figure 4.148 illustrates the monthly fluctuations in mean and maximum TWL at each study site. TWLs are on average 4.16 m in the winter (for January that is the month with highest TWL values), reaching a maximum mean of 5.04 m at PN study site, and a minimum mean of 3.20 m at MG. In the summer, differences between study sites are smaller and, interestingly, for the month of July average TWLs range between a maximum of 1.54 m at MG, and a minimum of 1.11 m at PN. Seasonal fluctuations in monthly average TWL reach 3.9 m at PN, decrease towards south, reaching a minimum of 2.2 m at MG, and increasing again progressively southward, reaching a new maximum of 3.7 m at LA.

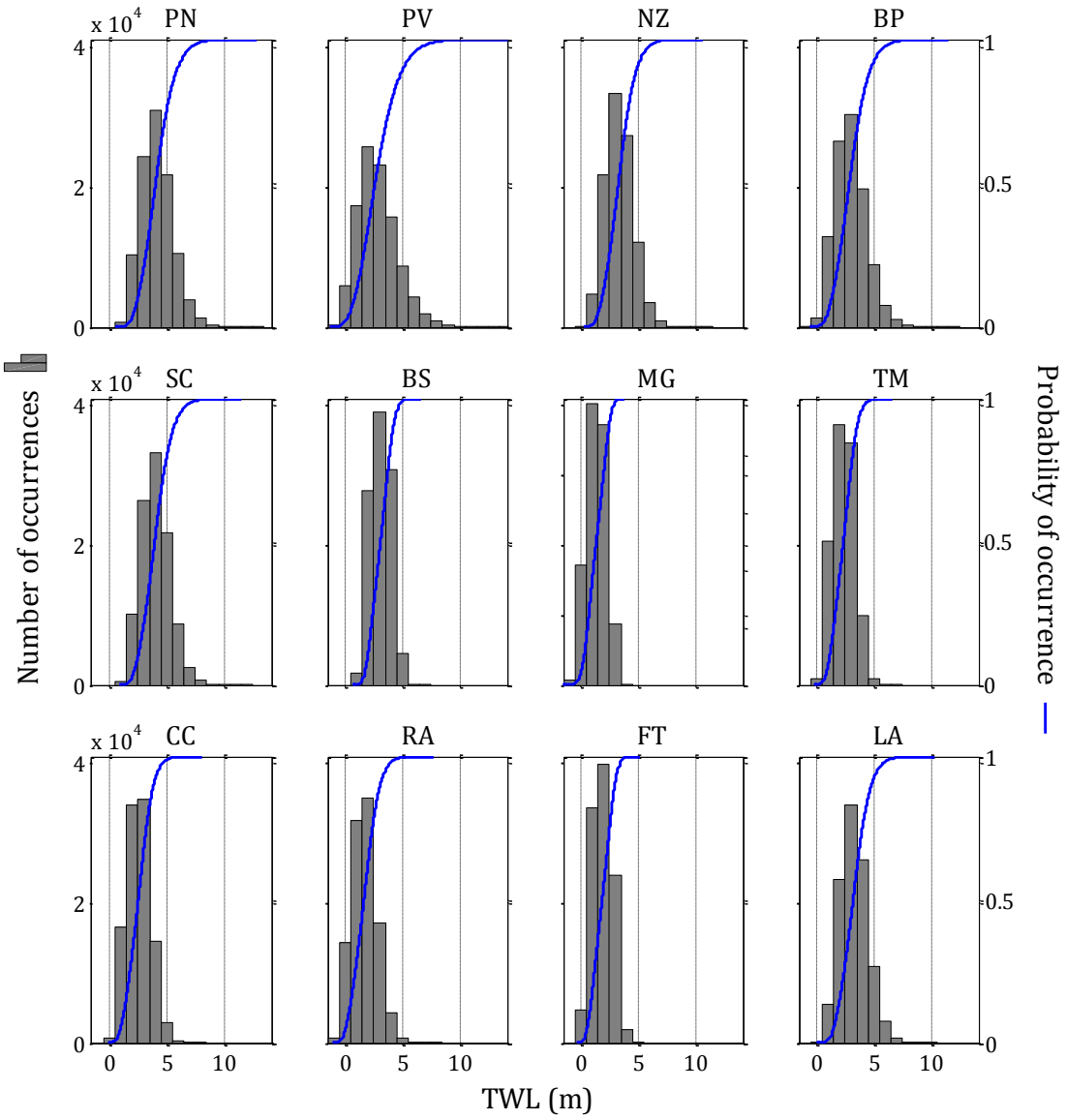

Figure 4.147. Distribution of the TWL data, described by absolute frequency (grey bar histograms) and relative cumulative frequency (blue curve), providing the probability of occurrence of water levels for each study site.

TWLs combine the effects of the sea level and wave components that affect the study area and were successfully validated and parameterized for each study site, through the measures of swash limits imprinted on the beach (runup validation). The resulting time series reflect the hydrodynamic forcing that reaches each specific study site. Through this analysis it was possible to characterize and quantify each study sites' TWL regime and, importantly, estimate typical and extreme elevation reaches of water levels that are potential triggers of beach morphological change.

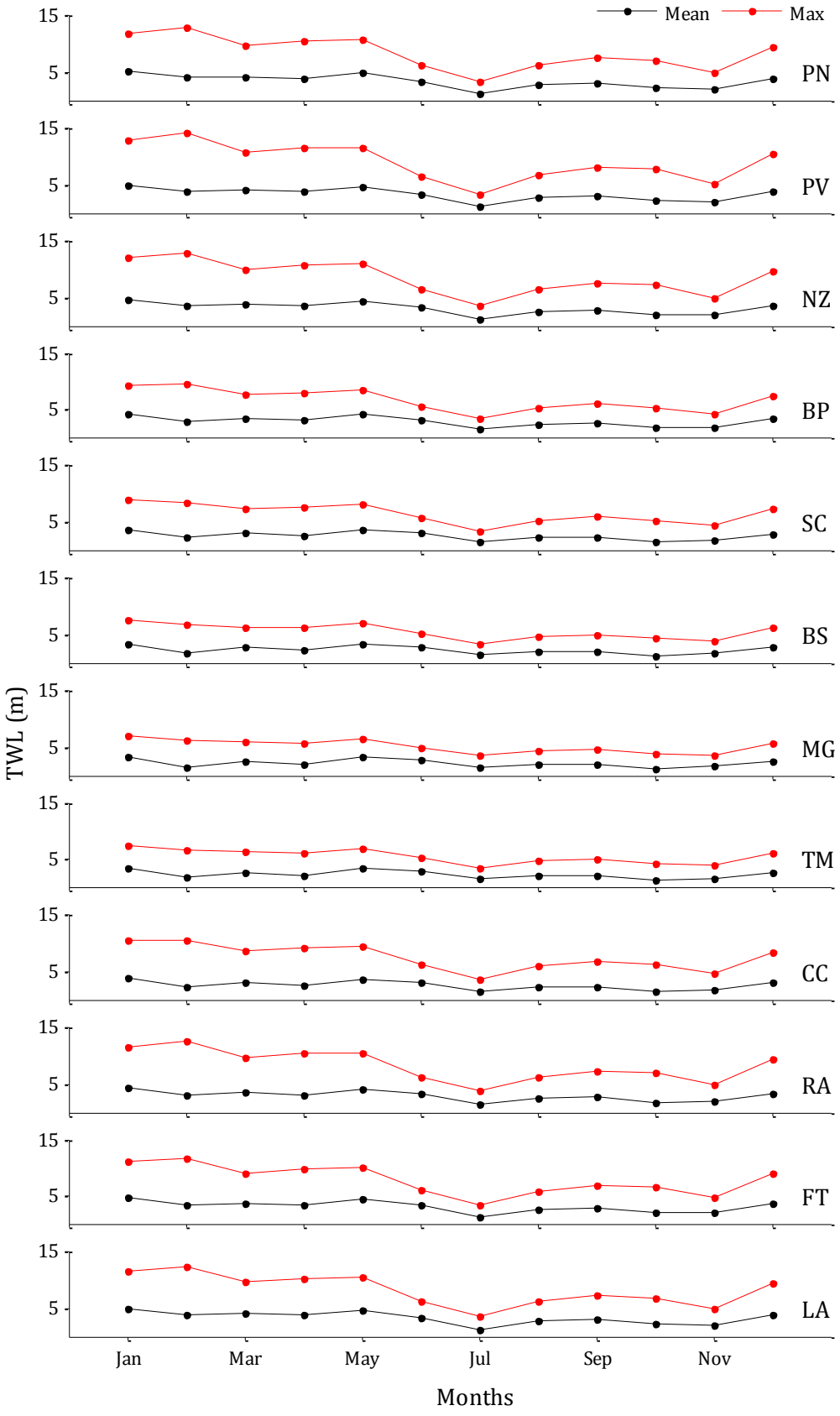

Figure 4.148. Monthly mean and maximum values of TWL (in m above MSL) for each study site.

4.3.4. Hydrodynamic forcing parameters used in the exploratory analysis

A subset of the analyzed parameters describing the hydrodynamic conditions during the study period – from January 2011 to August 2013 – were used to derive morphodynamic parameters and were used in the exploratory analysis (Chapter 5). Table 4.12 holds the average values of each parameter for each site. In addition to the parameters that were herein presented, the wave height at breaking was computed for each nearshore simulation point at the study sites. For the purpose of the analysis, and as explained in Subchapter 4.1, two of the study sites (LOB and CC) were divided, and therefore two new locations were added to the data – BL (corresponding to simulation point PLOB4) and SJC (corresponding to simulation point PCC1).

Table 4.12. Average values of the hydrodynamic parameters of each study site, for the period between January 2011 and August 2013.

Study site		H_0 (m)	H_b (m)	T (s)	TWL
01	PN	1.77	2.42	9.63	4.08
02	PV	1.81	2.41	9.65	2.72
03	NZ	0.94	1.55	9.20	3.29
04a	LOB	1.06	2.15	9.50	-
04b	BL	1.17	1.76	10.09	-
05	BP	1.69	2.00	9.67	2.90
06	SC	1.60	2.29	9.56	3.96
07	CX	1.60	2.24	9.68	-
08	BS	1.46	2.04	9.45	3.06
09	MG	1.40	2.19	9.45	1.37
10	TM	0.59	1.09	10.53	2.31
11a	SJC	1.30	1.81	10.18	2.50
11b	CC	1.42	1.82	11.18	-
12	RA	1.30	1.57	9.45	1.62
13	FT	1.05	1.37	8.88	1.83
14	LA	1.24	1.72	9.19	3.20

Chapter 5. Analysis and Discussion

Results presented in Chapter 4 are herein explored further, through investigation of the relations between the beach morphological and sedimentary response parameters, hydrodynamic forcing and geomorphological framework along the study area.

5.1. Beach state models

In order to carry out the analysis of the data and make use of all the descriptive parameters, the two beach systems identified in Subchapter 4.1 (Geomorphological Framework) - Baleal (4b BL) and São João da Caparica (11a SJC) - were considered independently in the analysis, giving rise to 16 study sites.

Most of the study sites' beaches are classified as unconstrained – type I according to the conceptual model of Jackson and Cooper (2009). As verified from the beach profile analysis in the previous chapter, the majority of envelope-lines encompassing the beach profiles measured at each location do not interact with the underlying substrate. The only exception is Magoito beach that has rocky outcrops on the intertidal area, especially in its southernmost section, causing this beach to be classified as type III – Highly constrained. The other beach systems that have a rocky platform, BL, BP, CX, BS and TM, might be classified as type II – semi-constrained. Here, the underlying substrate interacts only with the subtidal zone of the natural beach profile envelope.

The application of the data to commonly used beach state models' formulations led to the calculation of the Surf Scaling Parameter - ε, the Dimensionless Fall Velocity Parameter - Ω, and the Embayment Scaling Parameter - δ' (see Chapter 3 for description) for all the study sites. These are presented in Table 5.1, and in the following figures.

There are some differences between the Surf Scaling Parameter and the Dimensionless Fall Velocity classifications of the studied beaches (Figures 5.1 and 5.2). PN, PV, SC, CX, MG, SJC and LA are classified as intermediate in both classifications. This type of beach is characterized by the presence of low tide terraces and bar and rip systems in the surf zone. These features occur at PN, PV, SC and LA, but field observations indicate they are not present at CX nor at MG. On the contrary, both of these beaches exhibit exposed rocky platforms below low tide. LA in particular, is classified in the lower intermediate to reflective range, and this is consistent with the persistent berm and steep beach face, as well as the permanent presence of large cusps and coarser sediments at this location. TM is classified as reflective in both models, owing to the lower waves with longer periods. Accordingly, the beach presents reflective type characteristics, such as a well-developed berm and steep beach face.

Table 5.1. Surf Scaling Parameter - ε, the Dimensionless Fall Velocity Parameter – Ω, and the Embayment Scaling Parameter – δ', for all the study sites.

Beach		ε	Ω	δ'
01	PN	9.44	2.04	75.0
02	PV	19.87	2.67	10.2
03	NZ	1.42	1.51	30.5
04a	LOB	44.86	1.81	56.7
04b	BL	83.37	0.95	14.3
05	BP	27.57	1.14	54.1
06	SC	3.43	1.90	17.9
07	CX	3.73	1.96	5.6
08	BS	2.18	3.25	6.4
09	MG	12.59	1.67	5.3
10	TM	1.64	0.63	9.5
11a	SJC	8.65	1.02	17.9
11b	CC	24.02	0.91	131.6
12	RA	66.88	0.91	153.6
13	FT	10.59	0.94	176.0
14	LA	2.41	1.70	140.3

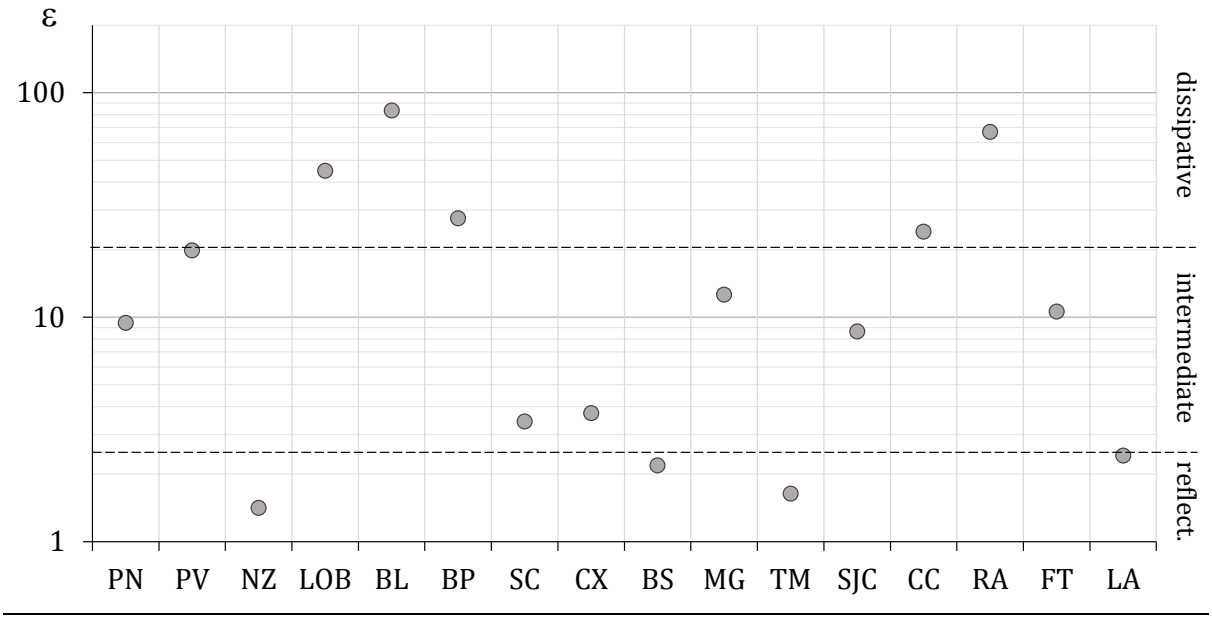

Figure 5.1. Surf Scaling Parameter - ε - distribution along the study area.

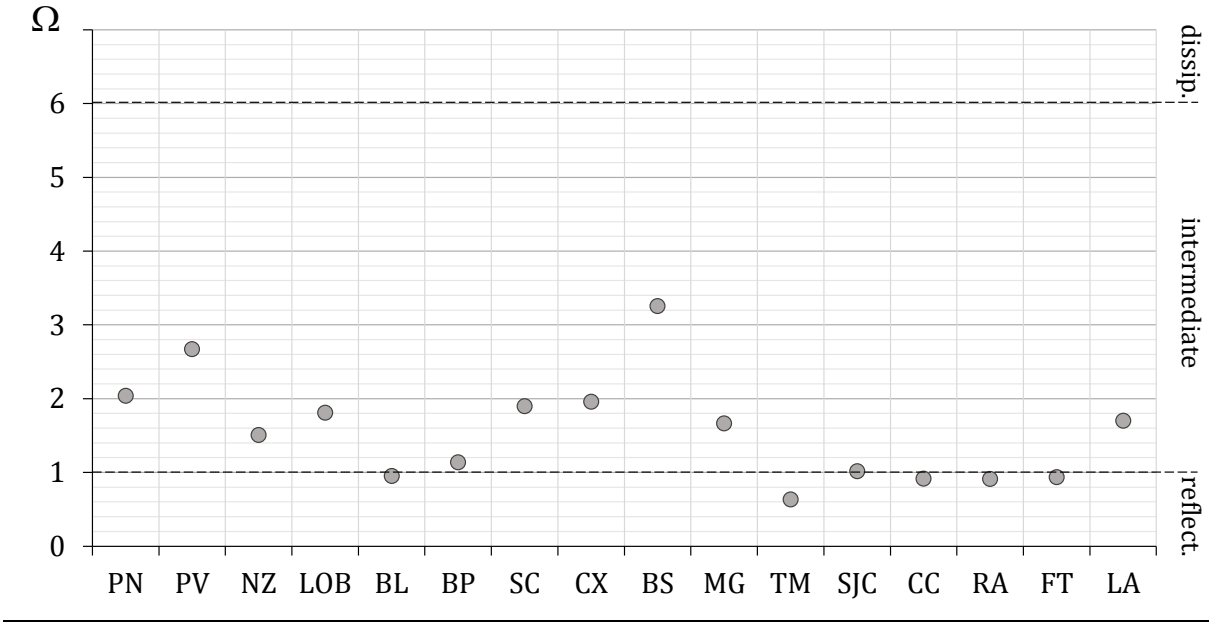

Figure 5.2. Dimensionless Fall Velocity – Ω - distribution along the study area.

NZ is classified as reflective according to the Surf Scaling Parameter, mostly due to the extremely high values of the beach slope. Classification based on the Dimensionless Fall Velocity falls in the low-intermediate range category that, according to Wright and Short (1984), shares characteristics of the more reflective beaches. This includes a steep beach face and well-defined beach cusps, both observable characteristics at NZ.

The low values of beach slope at LOB, BL, BP, CC and RA result in a classification of dissipative according to the Surf Scaling Parameter. However, they are classified as low intermediate to reflective according to the Dimensionless Fall Velocity. The former classification is in better agreement with the characteristics of the LOB-BP segment of the study area, where the wave heights are relatively large and the swash zone shows a low gradient. However, CC and RA are better described by the low intermediate to reflective types' characteristics.

FT exhibits similar characteristics to CC and RA, and is classified similarly according to the Dimensionless Fall Velocity, as low reflective. But, probably due to its steeper slope, compared to the other two sites, is classified as intermediate by the Surf Scaling Parameter.

The high beach slope at BS, results in a classification of type reflective according to the Surf Scaling Parameter. But, the Dimensionless Fall Velocity provides an intermediate classification. Despite the coarser sediments, the higher waves result in a higher energy

type of beach state. Two factors influence this particular site, making it difficult to rely on any of the two classifications: the presence of the rocky platform and the intense human interventions in the beach.

The Embayment Scaling Parameter classifies beaches based on the embayment configuration and incident wave characteristics, providing a degree of impact of the lateral boundaries on beach circulation (see Subchapter 3.4 - Exploratory Analysis) (Figure 5.3). According to this parameter, end effects are more intense at CX, BS, and MG, where occurrence of cellular beach circulation is expected. According to Short and Masselink (1999), in these situations longshore flow dominates within the embayment and seaward-flowing mega-rips occur at one or both ends.

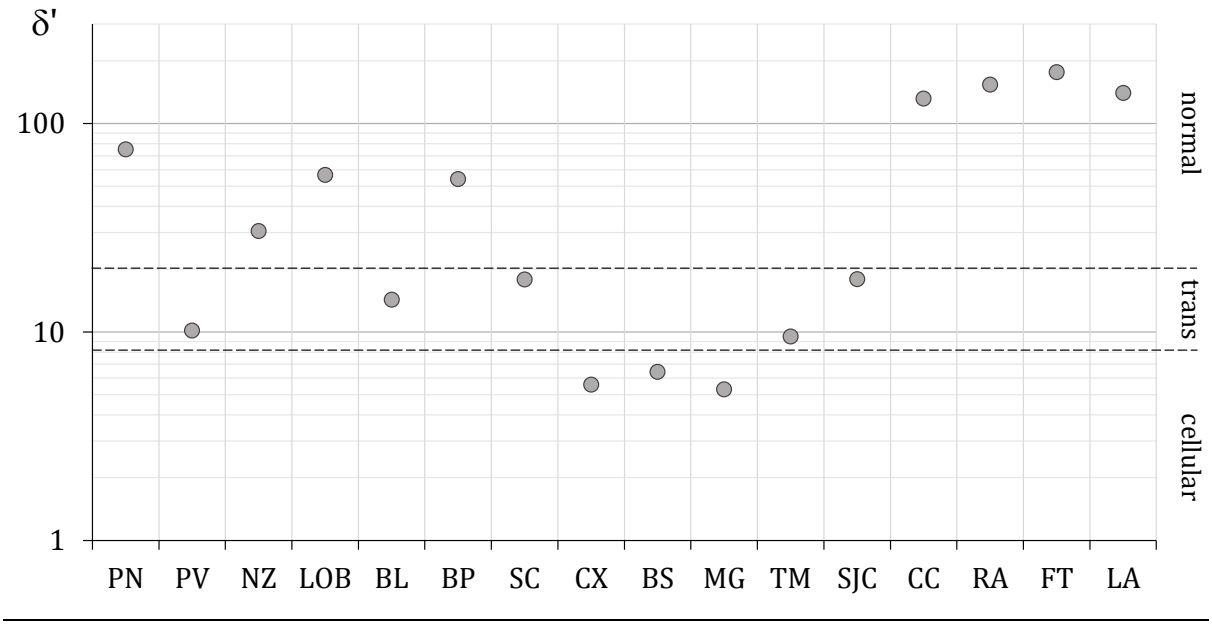

Figure 5.3. Embayment Scaling Parameter - δ' - distribution along the study area.

On the other extreme of the classification, PN, NZ, LOB, BP, and to a greater extent the southernmost sites of the study area along the Caparica-Espichel coastal segment, CC, RA, FT and LA, are considered as not impacted by the lateral boundaries of the system and experience normal beach circulation. Contrary to the other platform beaches, BP study site had nearshore bars in the central section of the embayment, suggestive of a normal circulation pattern away from the lateral boundaries and for most of the shoreline, and therefore in agreement with the classification.

Transitional beach circulation is suggested to occur at PV, BL, SC, TM and SJC. At these sites, longshore currents turning and flowing seaward near the lateral boundaries are expected, but normal beach circulation probably occurs away from the embayment ends.

From the field observations, the application of the Embayment Scaling Parameter seems to provide an adequate classification of the study sites.

Short and Masselink (1999) provide an additional model for beach state classification making use of the Embayment Scaling Parameter and the Dimensionless Fall Velocity (Figure 5.4), and therefore supportive of the previous classification.

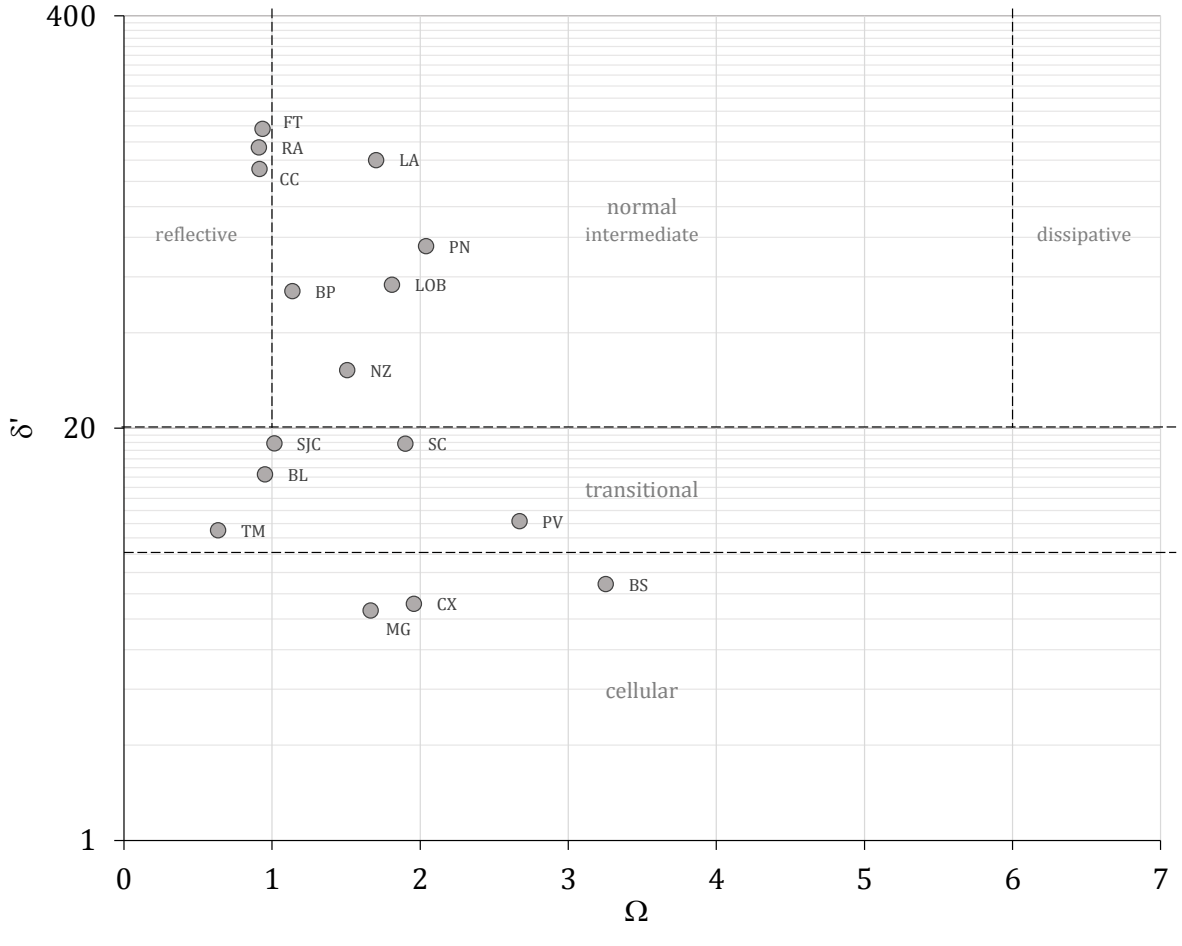

Figure 5.4. Plot of the studied beaches in the Dimensionless Fall Velocity (Ω) versus Embayment Scaling Parameter (δ') classification scheme (Short and Masselink, 1999).

Besides the wave characteristics, the beach state models described above make use of the beach slope (Surf Scaling Parameter), sediment size (Dimensionless Fall Velocity Parameter), and indentation index (Embayment Scaling Parameter). The Embayment Scaling Parameter provided a description of the beach systems that is closer to the observations. Unlike the other two parameters, the Embayment Scaling Parameter disregards the beach response characteristics (slope e sediments) and relies on the planform geometry to classify the beach state. In fact, the Embayment Scaling Parameter was introduced (Short and Masselink, 1999) to provide description of embayed and structurally controlled beaches, by quantifying relevant attributes of the geomorphological framework.

Another aspect of the commonly used beach state models is that they refer to the morphodynamic character of the nearshore environment, including the surf and swash zones. The present study, however, focuses on the description and dynamics of the subaerial beach, as well as on its dependence on the hydrodynamic forcing and, especially, on the geomorphological framework controlling factor. Thus, the following section will make use of the Embayment Scaling Parameter and explore further the relation between the forcing and the bounding characteristics and response of the subaerial beach.

5.2. Exploratory analysis

The several descriptive parameters of the geomorphological framework, hydrodynamic forcing and beach response, are herein explored together. Given the significance of the Embayment Scaling Parameter, it was also used as a descriptor of the combined effects of the geomorphological control and hydrodynamic forcing.

Figure 5.5 portrays the statistics of several parameters after normalization by the mean of the overall study area, showing the relative variation of each parameter along the study area. The Embayment Scaling Parameter (δ') stands out as the most variable of all the parameters, whilst the wave period (T_p) is the least variable. In the hydrodynamic forcing, TWL seems to be the most variable along the study sites, and slope and volume variation (Δ_{vol}) show similar range of variability in the beach response.

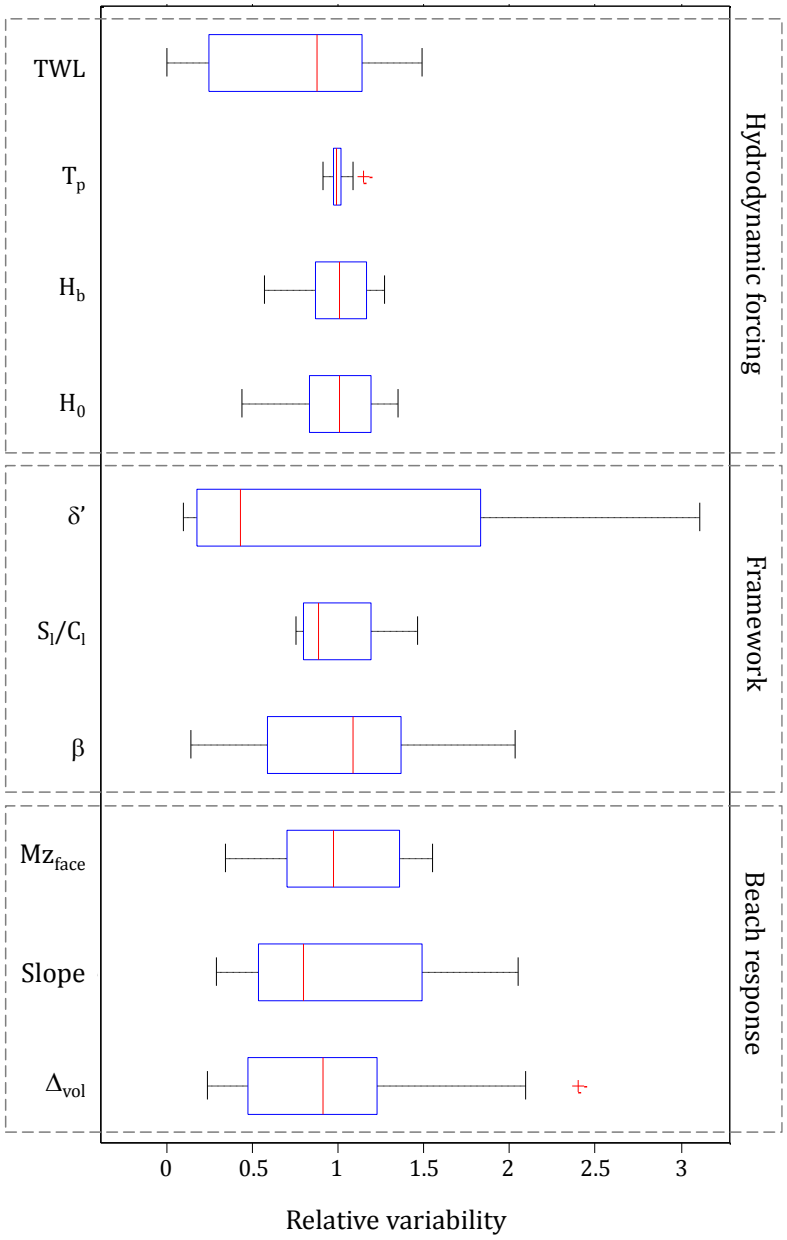

Figure 5.5. Relative variability of the several parameters descriptive of the geomorphological framework, hydrodynamic forcing, and beach response.

The correlation matrix between all parameters is provided in table 5.2. Most of the significant correlations occur between variables of the same category of descriptors, meaning that they are different measures of the same feature, or at least mutually dependent. These cells are highlighted with light grey color. Particularly, the parameters that describe the geomorphological framework have very similar behavior and therefore correlate strongly with each other. In the hydrodynamic forcing, it is the offshore and

breaker wave heights that are strongly correlated, and in the beach response, the volume and width variation co-vary, as expected.

Table 5.2. Correlation matrix between all measured variables. Darker cells indicate higher level of correlation between variables (> ±0.60).

	Beach response				**Geomorphological framework**							**Hydrodynamic forcing**			
	Δ_{Vol}	Δ_{Width}	Slope	Mz_{Face}	a	S_l	C_l	β	S_l/C_l	a/C_l	δ'	H_0	H_b	T_p	TWL
Δ_{Vol}															
Δ_{Width}	0.90														
Slope	-0.01	-0.33													
Mz_{Face}	-0.21	-0.01	**-0.64**												
a	-0.15	-0.02	-0.26	0.46											
S_l	-0.05	0.07	-0.30	0.34	0.88										
C_l	-0.03	0.08	-0.30	0.31	0.86	1.00									
β	-0.42	-0.30	0.01	0.48	0.14	-0.13	-0.16								
S_l/C_l	-0.52	-0.57	0.36	-0.11	-0.41	-0.64	-0.67	0.36							
a/C_l	-0.51	-0.57	0.36	-0.08	-0.36	-0.65	-0.69	0.54	0.94						
δ'	-0.13	0.00	-0.30	0.43	0.95	0.96	0.95	0.01	-0.53	-0.51					
H_0	0.40	0.39	-0.16	-0.23	-0.14	-0.02	-0.02	**-0.64**	-0.03	-0.20	-0.11				
H_b	0.46	0.40	-0.08	-0.46	-0.44	-0.21	-0.20	**-0.81**	-0.10	-0.28	-0.37	0.85			
T_p	-0.05	0.02	-0.25	0.40	-0.06	-0.09	-0.09	0.37	0.05	0.09	-0.16	-0.07	-0.12		
TWL	0.30	0.09	0.53	-0.51	-0.32	-0.07	-0.06	-0.37	0.04	-0.13	-0.22	0.37	0.44	0.01	

One correlation that stands out is that between beach face mean grain size and mean slope. The results show an inverse relationship between the variables, indicating that beaches with coarser sediments have steeper slopes (Figure 5.6). This is in agreement with multiple observations from several beaches worldwide, and reported in the literature about beaches and sediments (e.g., Sunamura, 1984; Komar, 1998).

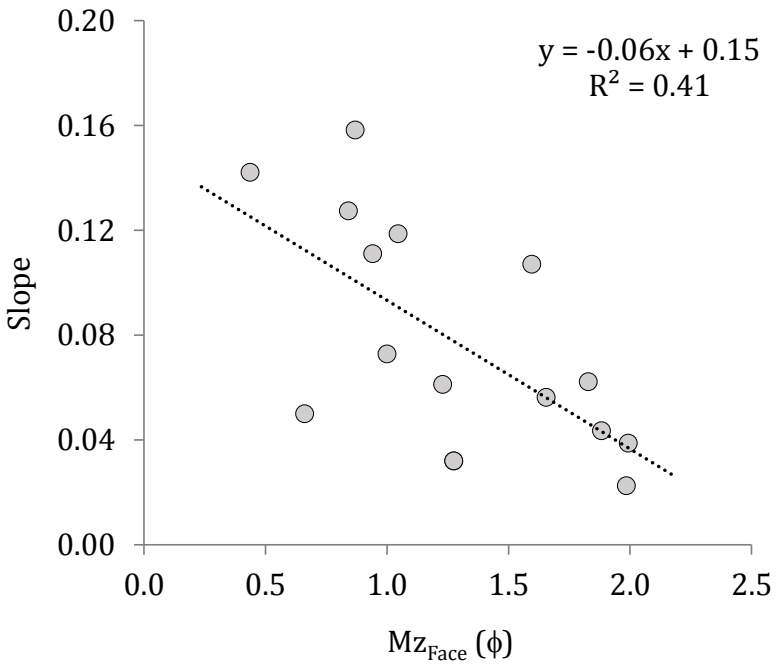

Figure 5.6. Linear regression analysis between the beach face mean slope and mean grain size, showing correlation between the parameters (R = -0.64).

Outside the "same category" descriptors comparison, the correlation matrix highlights only two meaningful relationships between variables: the wave obliquity (β) has an inverse behavior relative to the breaking wave height (H_b) and, to a lesser degree, to the offshore wave height (H_0). The variation of wave height with changing β values is shown in the scatter plot in figure 5.7. The observed pattern is expected. The lower the β, the more exposed the coast is to the dominant waves and the less the incident waves are transformed by refraction when propagating onshore. The higher the β, the more sheltered the coast is, meaning that the incoming waves will incur a higher degree of refraction before breaking at the coast, experiencing higher energy divergence along the embayments and thus lower wave heights reaching the beach.

Apart from these two particular cases, no significant correlations were detected between the several parameters. Simple linear regression analysis between the multiple parameters shows the irregular distribution of the variables (Figure 5.8). None of the combinations provided a good fit, with all coefficient of determination (R^2) lying below 0.32.

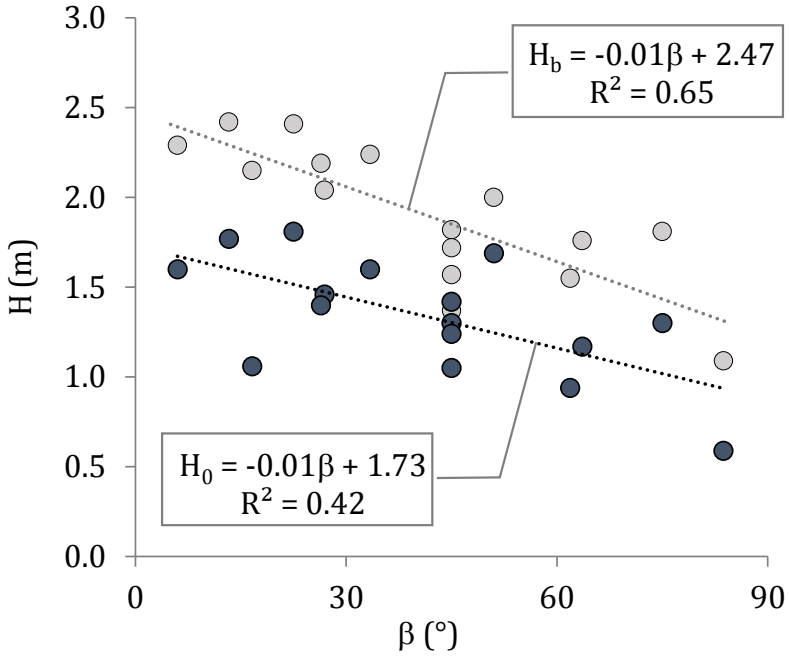

Figure 5.7. Linear regression analysis between the wave obliquity and wave height at breaking (light grey circles) (R = -0.81), and offshore (dark grey circles) (R = -0.64).

Given the non-linearity between variables, the Canonical Correspondence Analysis – CCA was used to evaluate to what extent the response data-sets (morphology and sediments) are influenced by the controlling (geomorphological framework) and forcing (hydrodynamic parameters) factors. Only some of the variables were selected to avoid redundancy (see Subchapter 3.4 – Exploratory Analysis, for explanation).

Figure 5.9 holds the CCA results, showing the study sites, the beach response variables, and the control/forcing variables plotted with respect to the first two canonical axes of the CCA. This biplot approximates the weighted averages of each of the study sites (red and grey dots) and response variables (blue dots) with respect to each of the control/forcing variables (green vectors); the grand mean is represented by the origin (0,0) of the plot.

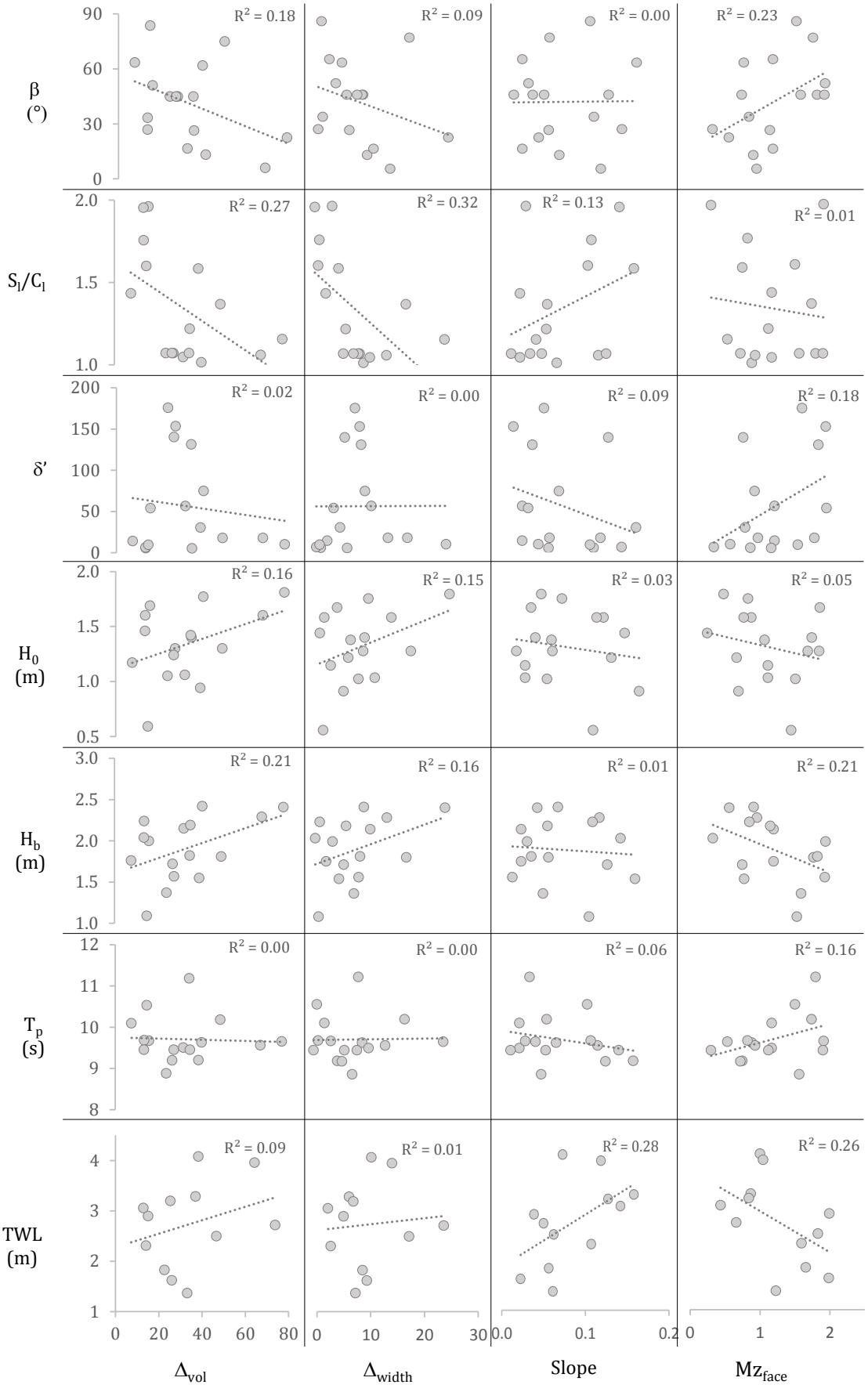

Figure 5.8. Simple bi-variate scatter plots and linear regression analysis.

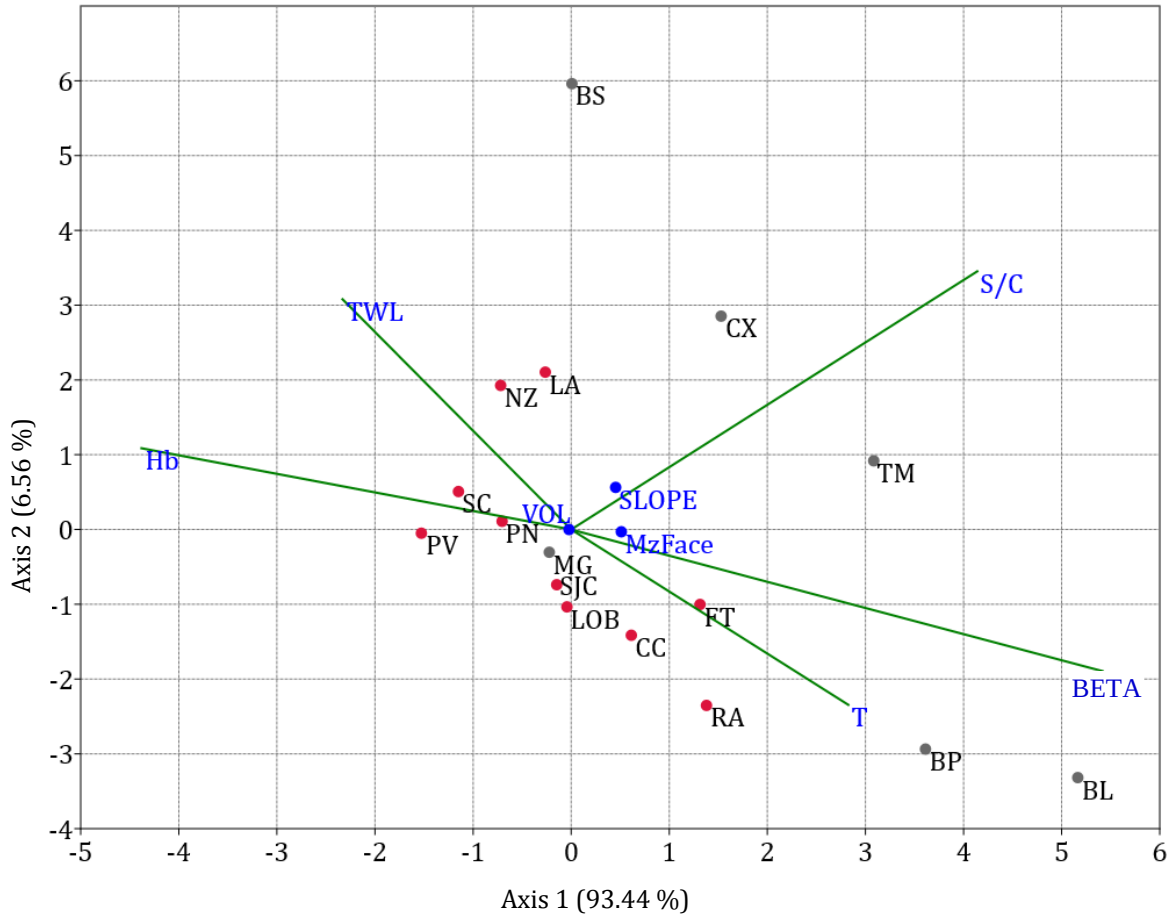

Figure 5.9. CCA biplot: filled red and grey circles represent study sites (grey represent beaches with platforms); filled blue circles represent the beach response variables (VOL – volume variation; Mz_{Face} – mean grain size; and SLOPE – mean beach face slope); and vectors represent the control/forcing variables (BETA – wave obliquity; S/C – indentation index; T – wave period; Hb – breaker wave height; and TWL – total water levels).

CCA axis 1 incorporates 93.44 % of the overall variance. TWL and H_b vectors increase in the opposite direction of the other three control/forcing variables (S_l/C_l, β and T_p), and, as verified earlier, H_b and β have inverse behaviors. Curiously, TWL and T_p also have inverse behaviors.

Regarding the study sites, those that are close together correspond to beaches that have similar behavior. The circles are somewhat scattered and no obvious clusters are detectable. Still, it is possible to see that the beaches with rocky platforms (grey circles) are all (except for MG) separated from the rest of the beaches, somewhat aligned along an imaginary line that crosses the S_l/C_l vector halfway on its increasing side, revealing a similar and high influence of this parameter on these beaches. Beaches with no-platform

(red circles), also seem more or less aligned along a direction that is perpendicular and crosses the S_l/C_l vector, but on its decreasing side (not drawn on the graph), and at a shorter distance from the origin, meaning that these beaches are more related to low indentation indexes and closer to average. NZ, LA and FT are an exception amongst the no-platform beaches, lying on the increasing side of the S_l/C_l vector, but still very close to the axes' origin and therefore under a small influence of this parameter.

BP, BL, and to a lesser degree TM are projected onto the farthest increasing segment of vectors β and T_p, and inversely onto the decreasing side of vectors H_b and TWL. This indicates that the high wave obliquity (BP=51°, BL=64°, TM=84°) that relates to small local waves (as verified earlier) and TWL regimes, is actually a preponderant factor controlling these beaches' behavior. CX is also located on the increasing side of vector β, but much closer to the origin, and therefore closer to the average values, and projecting onto the increasing side of the TWL vector.

SJC, LOB, CC, FT and RA are also located on the increasing side of vectors T_p and β, but closer to average (ordered in increasing distance along the vector). PN, PV, SC, LA and NZ are on the opposite side of these vectors, showing a relation with increasing H_b and TWL. NZ and LA actually have high values of β (NZ=62°, LA=45°), indicating that the wave and TWL regime must have a larger influence than β, on these particular beaches.

BS stands out for projecting onto the control/forcing vectors on their decreasing side, relating to an opposite behavior in relation to the other platform beaches. It correlates highly with TWL and H_b, and inversely with T_p and β. MG is the only platform beach located very close to the origin of the control/forcing vectors, showing a small influence of the S_l/C_l vector. This indicates that there is no dominant control/forcing factor influencing this beach's behavior.

Regarding the response variables, the volume variation parameter is centered on the plot and indicates that there is no preponderant relation with any of the control/forcing variables. Mz_{Face} and Slope, on the other hand are each aligned with one of the vectors. Slope is aligned with the S_l/C_l vector, and Mz_{Face} is more related with the β vector.

Again, there are no obvious clusters, but there is a pattern given by the platform and no-platform beaches general alignments that relate to the indentation index. Platform beaches are highly correlated with high indentation indexes, and no-platform beaches are less related to this controlling factor, lying at the average to lower values of S_l/C_l. These results are in line and reflect the conclusions forwarded at the end of Subchapter 4.1 -

Geomorphological framework analysis: more indented beach systems are those that have an exposed rocky platform, and no-platform beaches have smaller values of the indentation index.

The plot of study sites scatter around the other control/forcing vectors showing several combinations and degrees of influence between them. This is not surprising given that the selection of the beach sites aimed at describing the full range of forcing and controlling variables.

Following the CCA analysis, and exploring further the observed pattern between platform and no-platform beaches, the beach response variables were again analyzed using all the profile data instead of one value per study site. Beach face slope and sediment size were plotted together, given their close correlation (Figure 5.10), and beach volume variation was plotted against beach width variation (Figure 5.11).

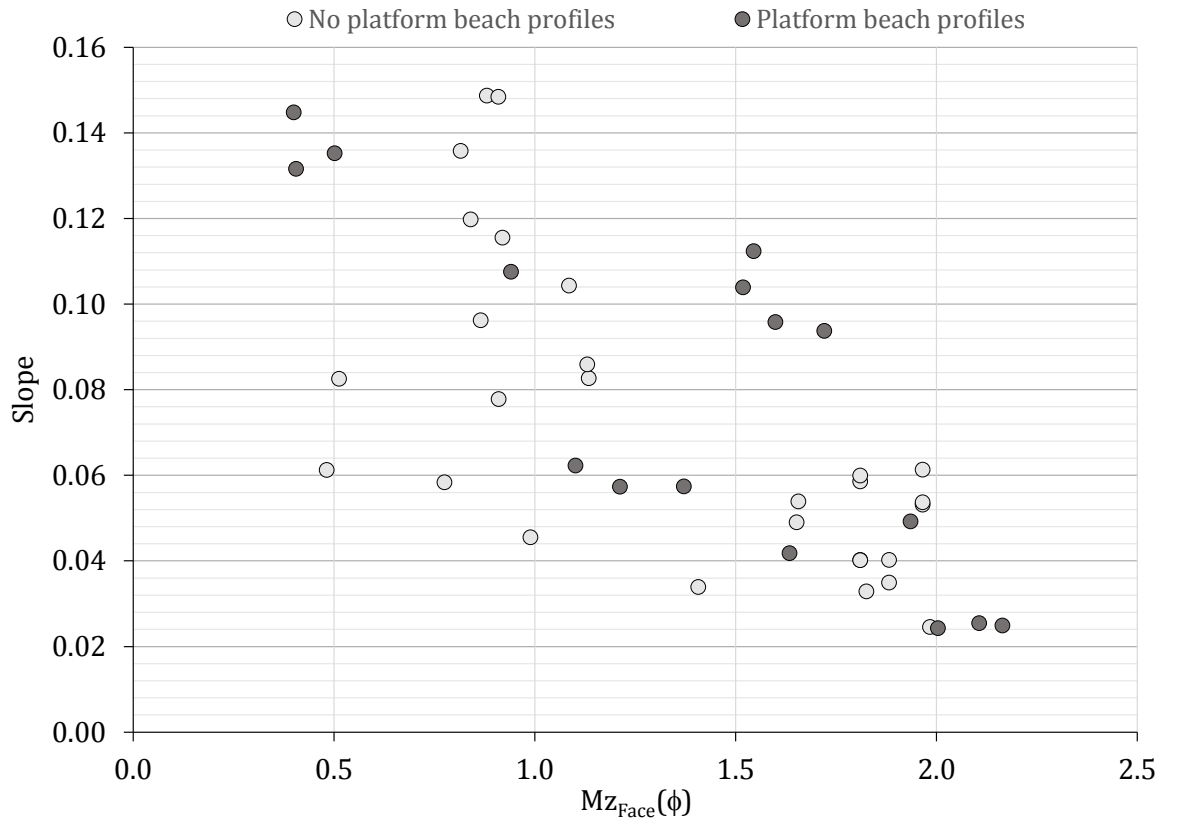

Figure 5.10. Scatter plot of beach face sediment size and slope for all the study sites' beach profiles, highlighting the study sites that have rocky platform (dark circles).

Regarding the slope and sediment size, the previously detected correlation between variables is still visible, but there are no apparent differences between platform and no-platform beaches. Profiles from both types of beaches spread out through the entire range of sediment size and slope values. However, when looking at the volume variation vs width variation scatter plot (Figure 5.11), besides the obvious good fit between the two variables, there is a clear distinction between platform and no-platform beach profiles. The platform beaches are concentrated in the lower part of the range of variation, detached from the remaining profiles. The exception are two profiles that show higher variations, similar to those of the no-platform beaches.

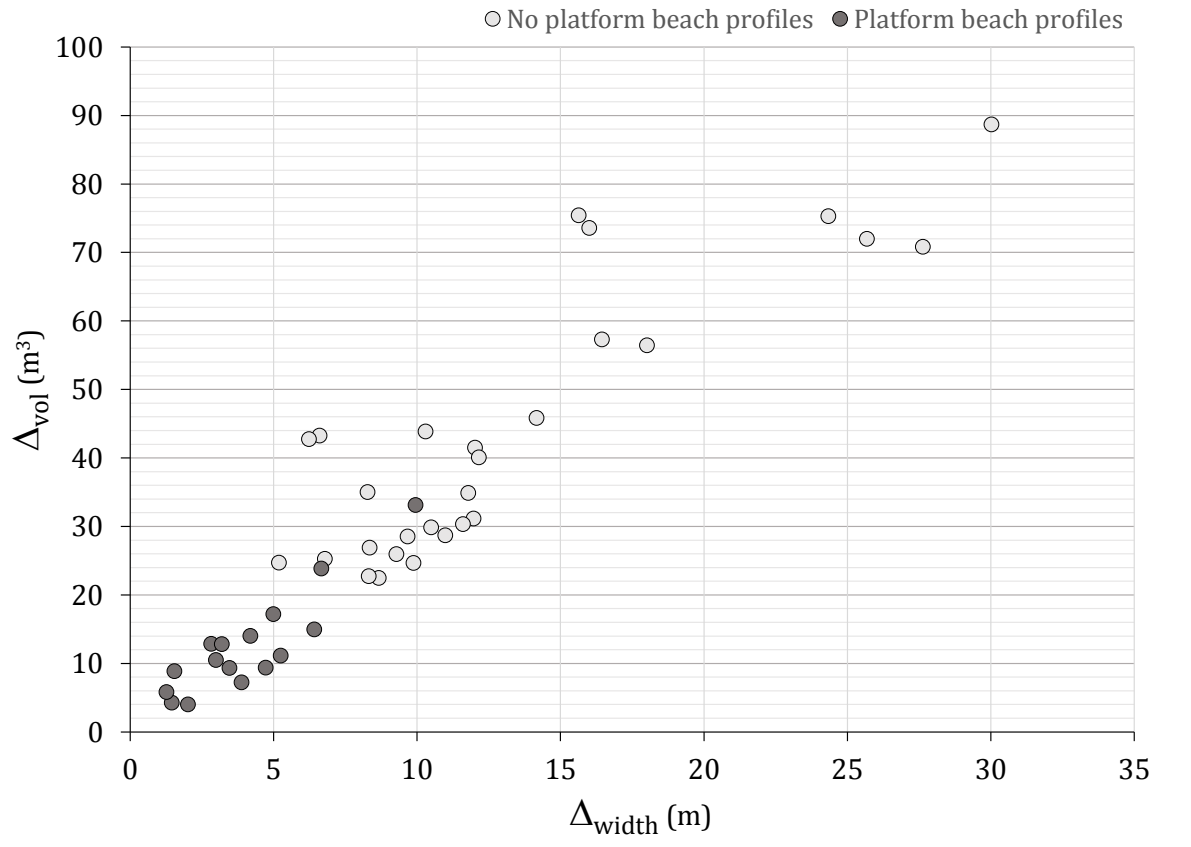

Figure 5.11. Scatter plot of beach volume and beach width variation for all the study sites' beach profiles, discriminating platform (dark circles) from no-platform beaches (light circles).

Furthermore, there are eight profiles from the no-platform beaches that stand out from the rest, with higher values of volume variation (>50 m^3) and width variation (>15 m). When the profiles are grouped into beaches, the plot of the mean values for each beach shows the same general display (Figure 5.12). Platform beaches concentrate in the lower

range of beach variation, clearly separated from the no-platform beaches, with one exception (MG) that gets closer to the no-platform beaches, but still with low values.

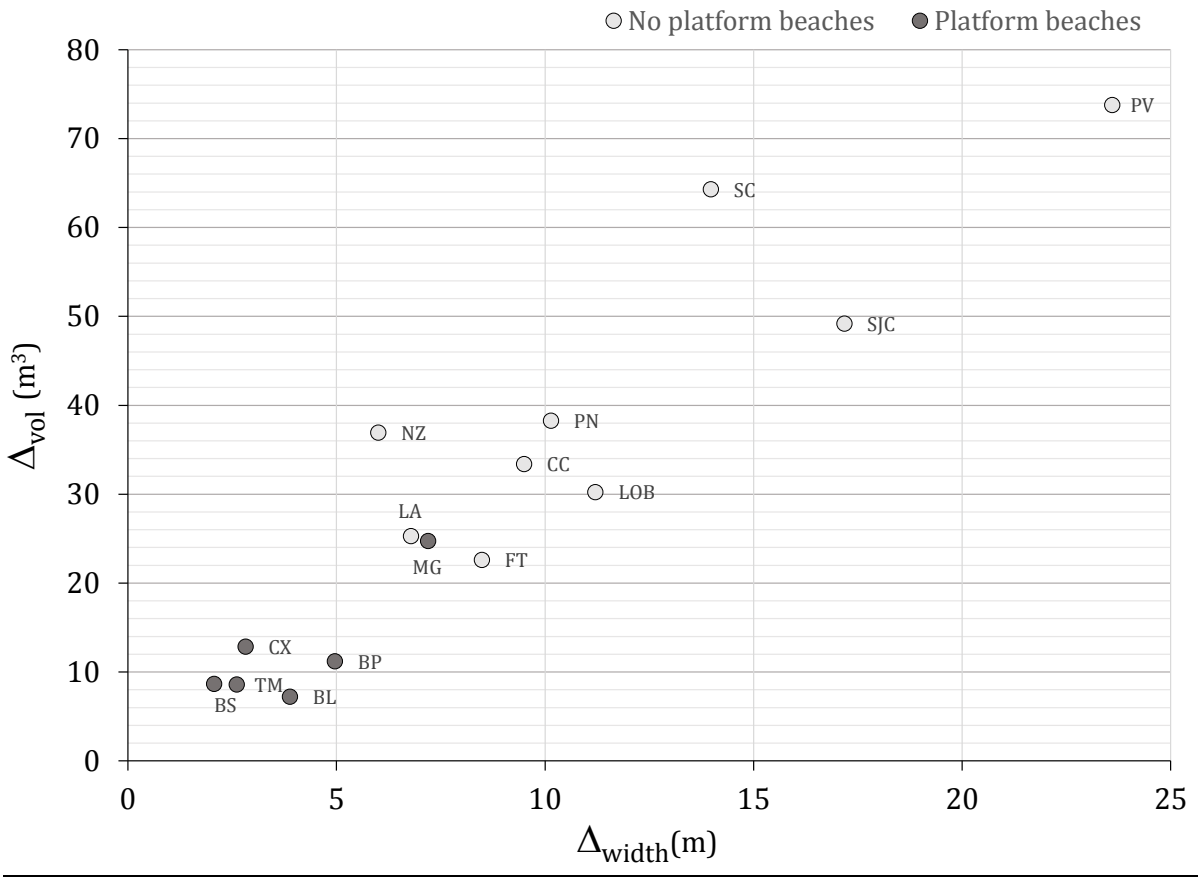

Figure 5. 12. Scatter plot of beach volume and beach width variation for the study sites.

The higher variation profiles that were detected in Figure 5.11 are now convened as three beaches – PV, SC and SJC, creating a gap from the rest. These three beach systems are located in very different segments of the study area – PV in the northern part, SC in the middle section, and SJC in the southern Caparica-Espichel coastal stretch. They display different geomorphological frameworks and also experience different wave and total water levels regimes, as verified in the Results chapter (Chapter 4) and from the CCA analysis. The only similarity between the three sites is that they have the lowest Embayment Scaling Parameter value of the no-platform beaches, being the only classified as having a transitional type of circulation according to this parameter (Figure 5.3). Actually, this is also suggested by the results of the CCA analysis, because the plot of these sites along the S_I/C_I vector is their only common attribute. This suggests that beach

variability may be controlled by the embayment configuration and relative incident wave conditions.

Figure 5.13 presents the comparison between beach profile volume variation and the Embayment Scaling Parameter for all the profiles. Again, the plot of platform beach profiles cluster around the lowest values of Δ_{vol} and also lower δ'. This confirms interpretations from CCA analysis that indicated a large dependency of these beaches on the degree of indentation. Regarding no-platform beaches, in spite of a general tendency of increasing Δ_{vol} towards lower values of δ', they concentrate on the higher values of Δ_{vol} (above 20 m^3) and scatter along the δ' axis.

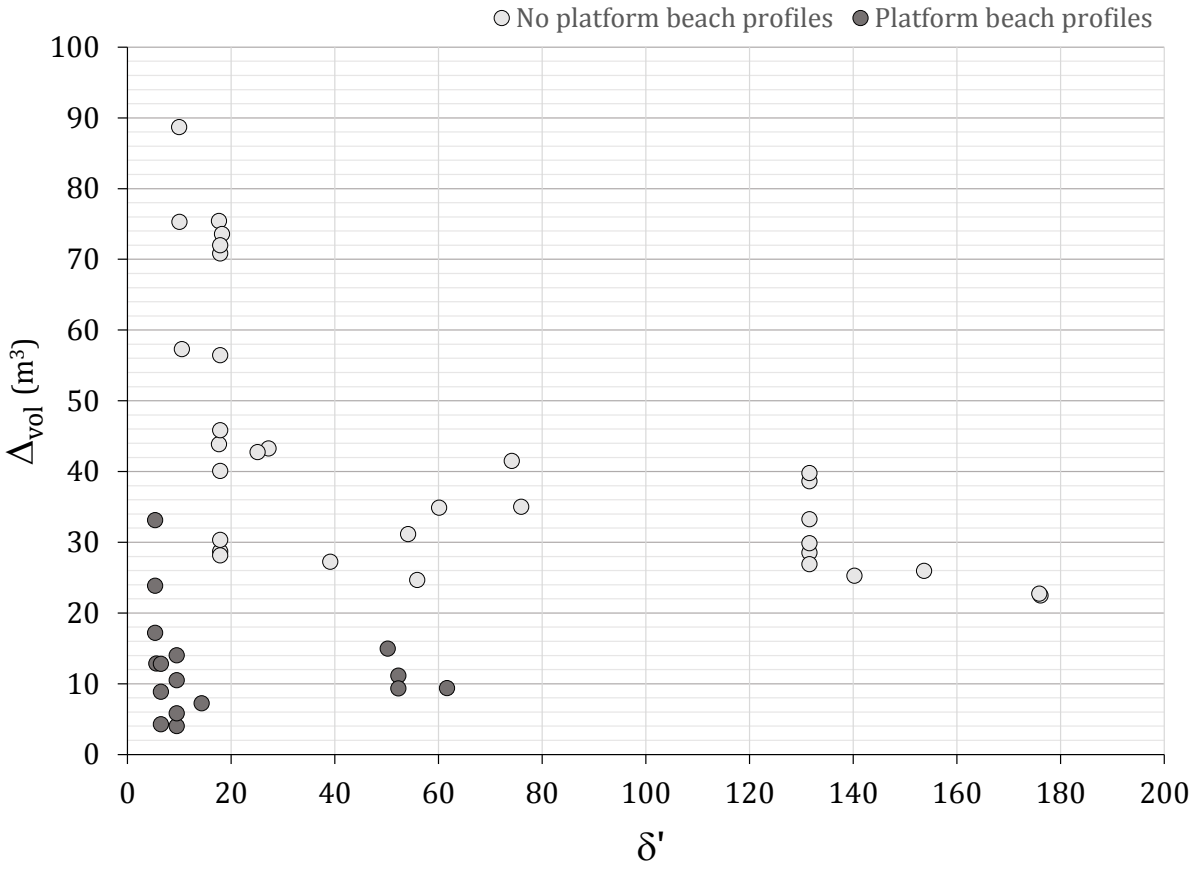

Figure 5.13. Scatter plot of beach volume variation (standard deviation) and the Embayment Scaling Parameter for all the study sites' beach profiles.

When grouped into beaches, the pattern described above becomes more clear (Figure 5.14). The platform beaches cluster in the lower Δ_{vol} and δ' values. Exceptions are MG, that shows some deviation in Δ_{vol} (higher values) as verified previously, and BP, that is located towards higher values of δ'. BP is the only platform beach classified as having a normal circulation according to the δ' and Ω parameters (Figure 5.4), suggesting that BP behaves as an unconstrained beach. The findings from the Results chapter (Chapter 4) also emphasized that this site, despite occurring over a rocky platform, displayed characteristics of no-platform beaches, especially in its central section.

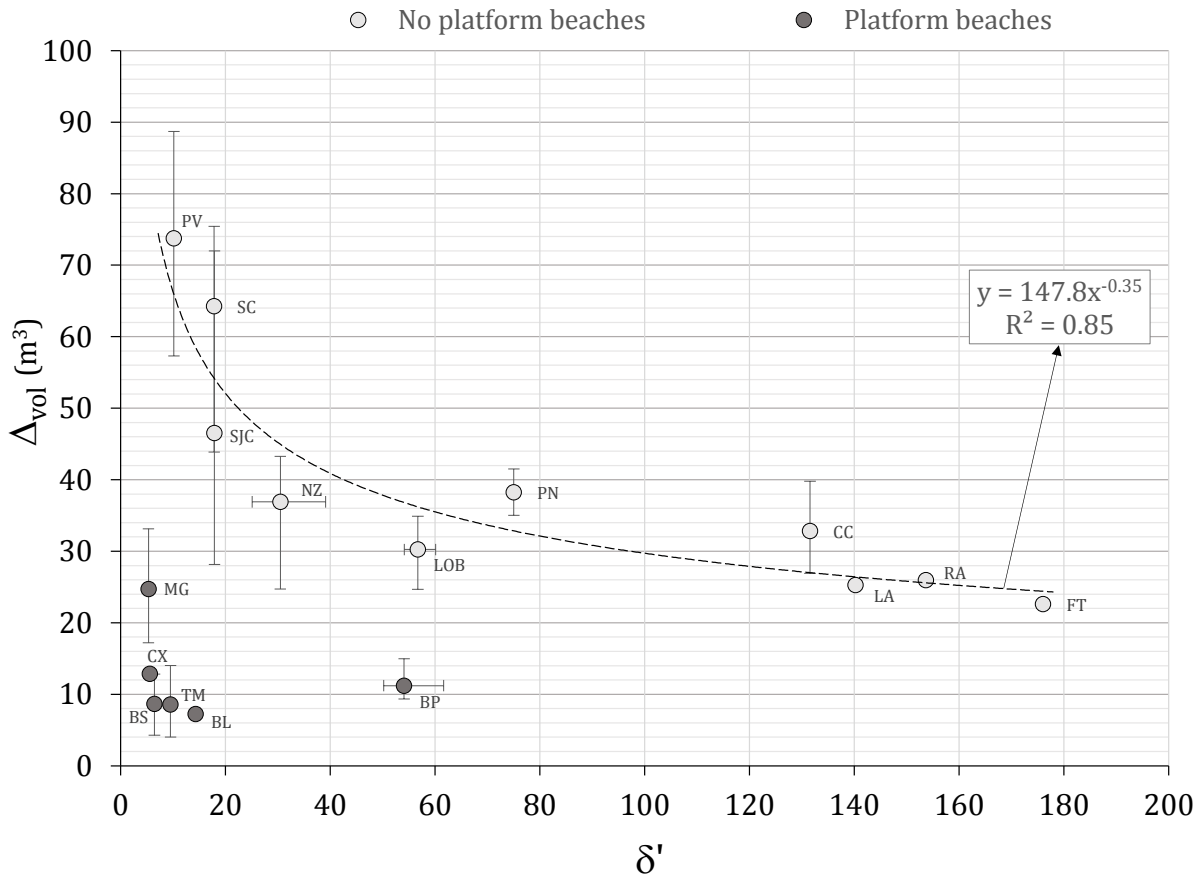

Figure 5.14. Scatter plot of beach volume variation and Embayment Scaling Parameter for all the study sites, with indication of the range of values for both variables in the form of vertical and horizontal bars for each site. Dashed line indicates best fit for the no-platform beaches data.

The general trend of increasing Δ_{vol} towards lower values of δ' amongst the no-platform beaches is evident in the plot in Figure 5.14, and further demonstrated by the line of best fit that shows a R^2 of 0.85 (dashed line). The fitted curve demonstrates the non-linearity

of the relation between parameters, and the good fit to a power regression model for no-platform beaches. Notice that PV, SC and SJC study sites that were previously detached from the remaining no-platform beaches, now fit the curve effectively. The observations that lie more distant from the rest of the no-platform beaches are the ones from the Caparica-Espichel coastal stretch (CC, LA, RA and FT), showing much higher δ' values, reflecting their unconstrained character. In Figure 5.15 these four beaches are grouped together, because they were considered part of the same beach system (see Chapter 4.1. Geomorphological Framework). The new regrouped data for the no-platform beaches continue to show a good fit with R^2=0.81.

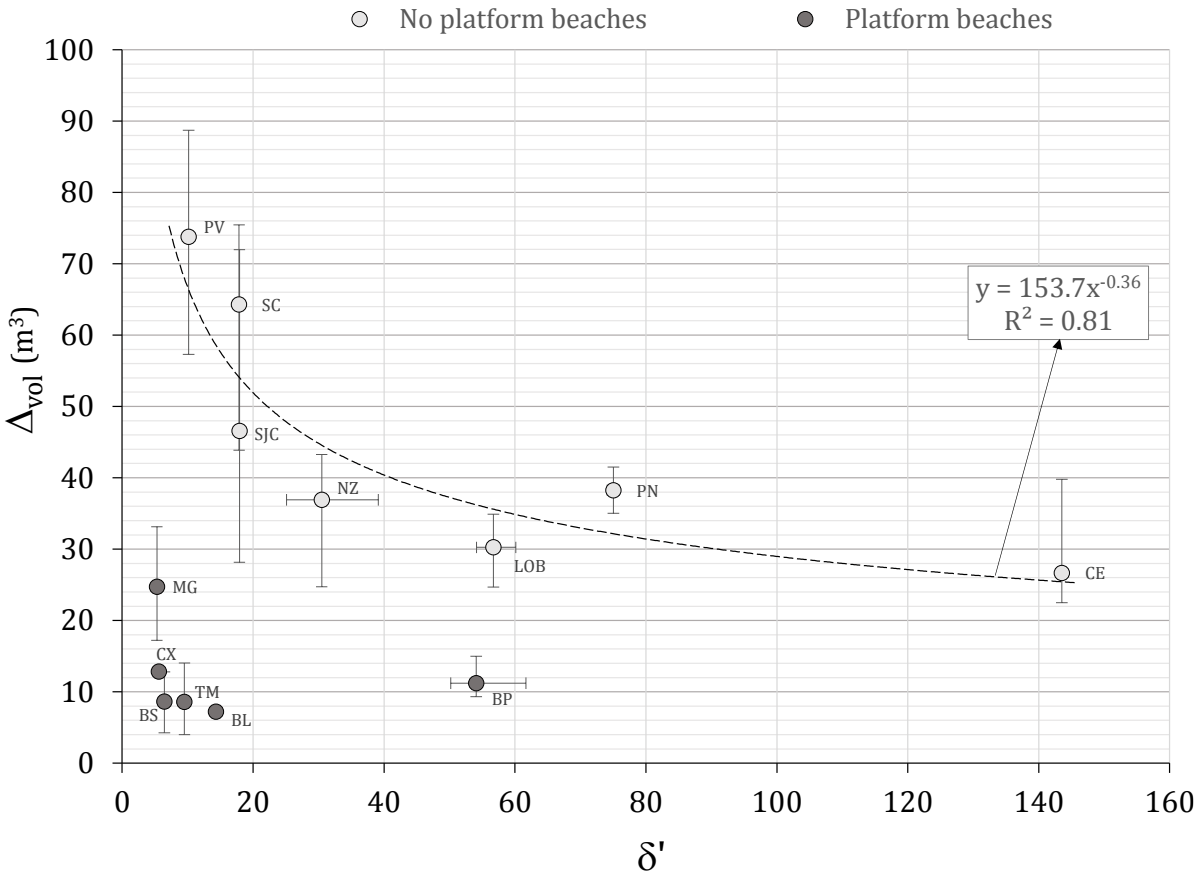

Figure 5.15. Scatter plot of beach volume variation (standard deviation) and Embayment Scaling Parameter for all the study sites, grouped in beach systems with indication of the range of values for both variables in the form of vertical and horizontal bars for each site. Dashed line indicates best fit for the no-platform beaches' data.

These results emphasize the high variability of volumetric change among the study sites, and relates it to the type of physical boundaries that are present: rocky platform and lateral boundaries.

The presence of a platform may control the available space for the beach to migrate vertically, and limit the maximum volume losses. But in the time-frame of the present study none of the platform beaches had their sand cover totally removed and the underlying platforms fully exposed. The beach surface shifted within the profile envelope, regardless of the underlying platform. The only exception was the southernmost beach profile at Magoito.

On the other hand, the presence of a platform may affect the incoming waves, and influence the working ability of waves over the full extent of the beach. Results presented herein show that the TWL regime was not a differentiating factor between platform and no-platform beaches. However, this study simplified the wave propagation from the nearshore simulation point, at 15 m depth, until breaking and the transformations experienced by broken waves and bores propagating over the platform have not been addressed at all. This constitutes an obstacle for further exploration or discussion on the subject.

Still, one might anticipate that the presence of a permanent and rigid obstacle in the surf zone, such as a rocky platform, limits the range of wave characteristics reaching the subaerial beach. On the other hand, beaches characterized by a mobile substrate (no-platform beaches) that can assume a variety of different morphologies in the surf zone, will necessarily lead to a wider range of wave breaking conditions and subsequent effects on the subaerial beach. This accounts for the fact that beaches with no platform varied consistently more than beaches with platforms. To what extent the "filtering effect" of the platform is absolute, regardless the wave characteristics in deep water or, in some way, proportional to both the morphological expression of the platform and incoming wave pattern, remains to be explained.

Within the no-platform beaches, those regarded as unconstrained beaches, such as RA, FT and LA along the Caparica-Espichel coastal stretch, or PN, varied the least, whilst beaches with the higher degree of embaymentization (lower δ') varied the most.

Volume variation (Δ_{vol}) at each beach system represents the mean of the standard deviation in volume measured from the overall beach profiles. Therefore, it reflects the sediment exchanges within the beach system where the source-profiles were measured

and any particular profile can change in response to cross-shore or alongshore sediment transfer across the system.

In order to evaluate the alongshore component of the morphological variability in beach response, the longshore variation index - LVI, was assessed and compared with the embaymentization parameter (Figure 5.16). The application of this index is strongly limited by the number of profiles monitored at each site (two in some cases and as a minimum) and interpretations must take this limitation into account. Still, it is a measure of the variability between the several profiles monitored at each beach system, and given their spacing, it can provide insights into the dominancy of cross- or longshore processes.

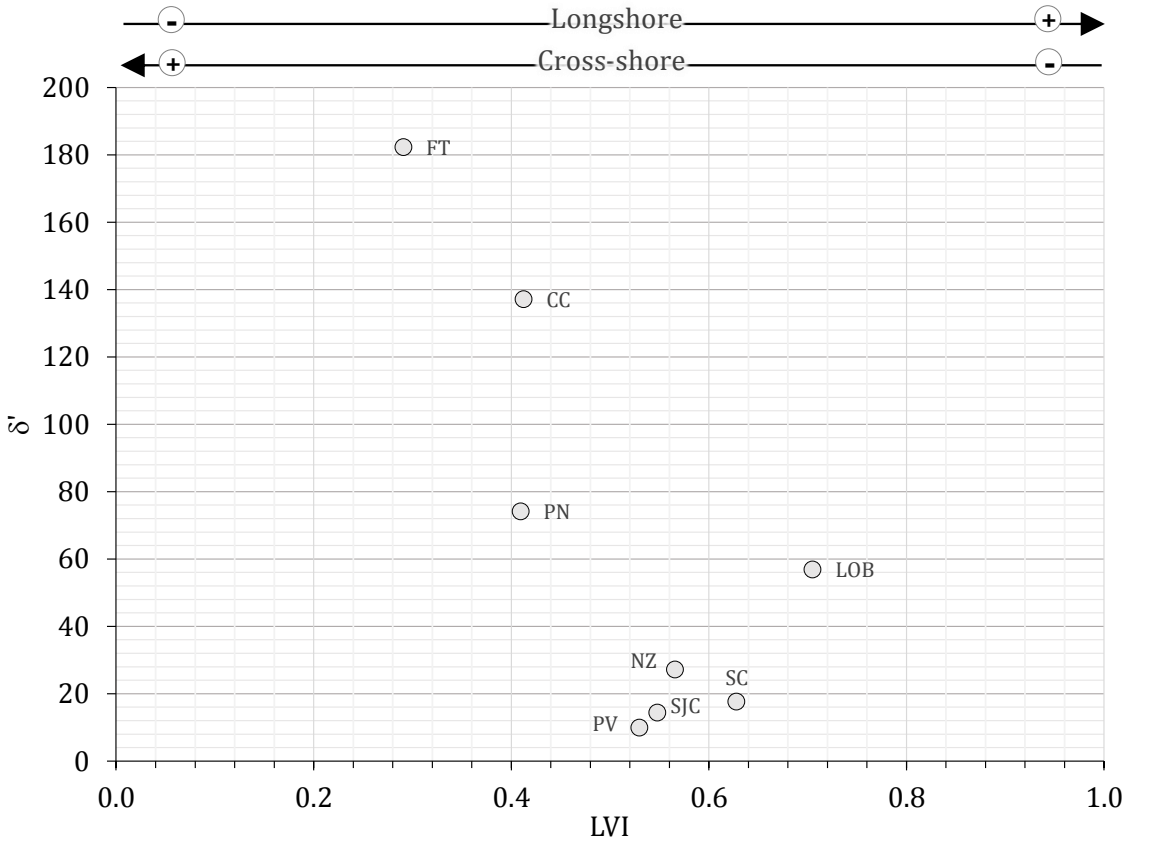

Figure 5.16. Scatter plot of the Longshore Variability Index and the Embayment Scaling Parameter for the no-platform study sites with at least two monitored profiles.

LVI varies between 0 and 1 with higher values representing greater longshore variability in beach response. With due caution in the interpretation, the scatter plot in Figure 5.16 shows that the beaches with lower degree of embaymentization (higher δ',

correspondent to essentially unconstrained beaches), plot on the left side of the graph (LVI<0.5). This indicates predominance of cross-shore processes, whilst the rest of the beaches, with higher degree of embaymentization (lower δ') plot in the middle and higher values of LVI, suggesting predominance of alongshore processes.

Results suggest that the beach profile variations that are being detected at the unconstrained beaches are mostly due to cross-shore sediment exchange, rather than the alongshore sediment movement that probably leaves the beach profile unaltered. The constrained beaches, on the other hand, vary in response to the alongshore sediment transport processes that, in the presence of lateral constraints, promote beach accumulation on the downdrift end of the beach system, making the beach profile change differently between both extremities of the embayment. This behavior was detected at PV, SC and SJC (see Chapter 4.2). At SJC in particular, seasonal beach rotation was evident in the DEM and shoreline change analysis. In modal conditions, the above considerations translate in higher beach volume variability along constrained beach systems when compared to unconstrained ones.

The results and interpretation above suggest that beaches with no-platform distribute along a continuum and their cross-shore morphology and volume vary in response to either cross-shore or longshore processes and sediment transport. Unconstrained beaches have open lateral boundaries, therefore, see their cross-shore morphology and volume vary mostly with the cross-shore sediment exchanges. These exchanges occur with more intensity under extreme oceanographic conditions, and less under modal conditions. The constrained beaches on the other hand, are bounded laterally and therefore are prone to beach rotation processes promoted by the longshore sediment transport that occurs under modal conditions. This explains why constrained beaches are more variable than the unconstrained beaches. The detected behavior and patterns exist regardless of the backshore features or type of lateral boundaries.

These results are in agreement with those by Ribeiro (2017) who studied the embayed beaches between Peniche and Cabo Raso - a coastal stretch characterized by embayed beaches within the present study area. She found a high correlation between beach rotation and beach length, concluding that beach rotation increases with the decrease of the beach length, and that longer beaches (>1 km), have low-degree of embayment. Likewise, results by Loureiro et al. (2012) emphasize the role of beach rotation as a prevailing mode of alongshore variability in embayed beaches.

Results from the exploratory analysis indicated that the degree of embayment is a preponderant parameter in differentiating between platform and no-platform beaches. Platform beaches have a restricted range of degree of embayment and typically show small embayment widths and accommodation space. Under these circumstances the subaerial beach experiences small variations in its volumetric content. Beaches with no platform present a wider range of embaymentization conditions, varying between unconstrained and constrained beaches, but are always highly exposed to the permanent wave regime. On these beaches, subaerial volume variations are expected to be always higher than in platform beaches, and to increase with the degree of embayment.

5.3. Conceptual model

It can be inferred from the results and exploratory analysis that the magnitude of beach variation along the study sites is controlled by 1) the presence of a rocky platform; and, 2) in no-platform beaches, by the degree of embayment and its impact on the beach circulation. Figure 5.17 provides a conceptual model of the subaerial beach dynamics (given by the volumetric variability) as a function of the geomorphological framework (given by the degree of embaymentization and boundaries). Platform beaches typically occur as small constrained beaches and experience small volume variations. On the other hand, no-platform beaches may vary between unconstrained and constrained beach types with different degrees of embaymentization. Subaerial volume variations in no-platform beaches are expected to be always higher than in platform beaches, and increase with the degree of embaymentization and its impact on beach circulation. It is suggested that the magnitude of volume variation in no-platform beaches can be approximated by the following equation:

$$\Delta_{vol} = 154\delta'^{-0.36} \qquad \text{Eq. 5.1}$$

The proposed regression model describes a continuum between unconstrained and constrained systems in which beaches vary in response to cross-shore or longshore predominant transport, respectively.

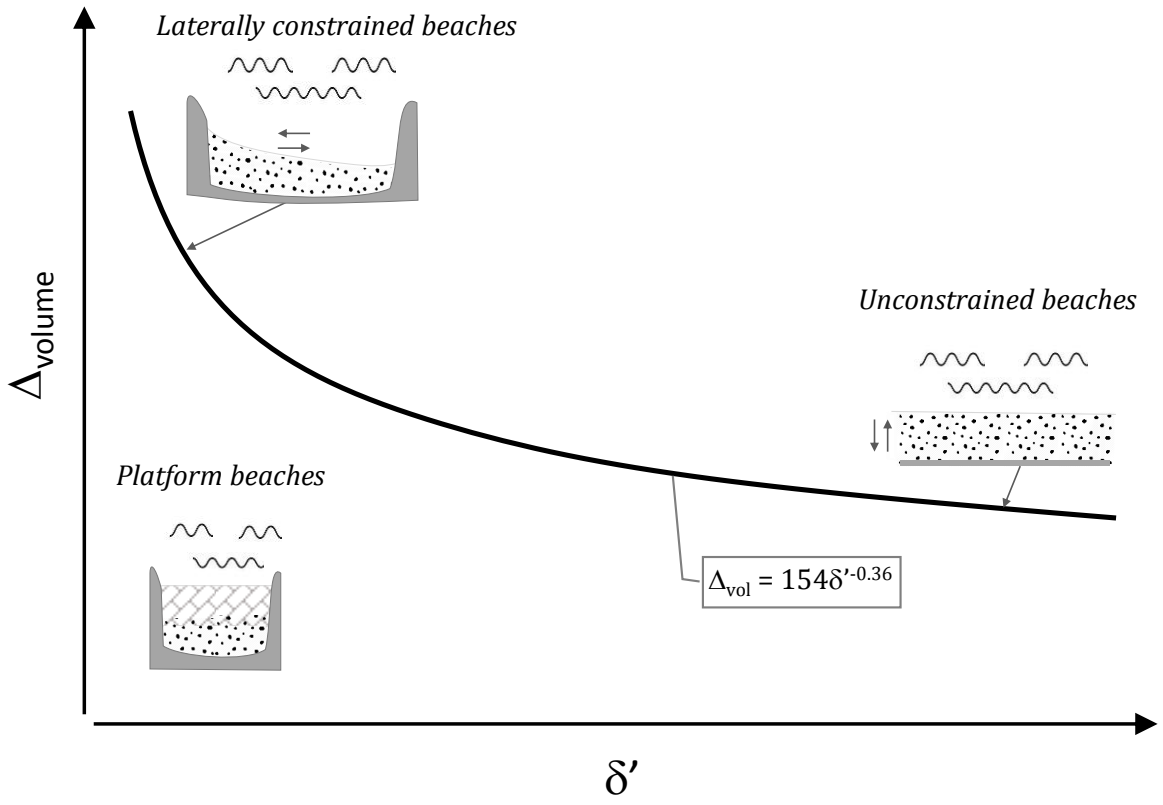

Figure 5.17. Conceptual model of the subaerial beach dynamics (given by the volumetric variability) as a function of the geomorphological framework (degree of embaymentization and boundaries).

Chapter 6. Conclusions

This chapter provides the concluding remarks. A summary of the main findings is presented in subchapter 6.1 and suggestions for future research are provided in subchapter 6.2.

6.1. Summary

This thesis focused on the hypothesis that the geomorphological framework interacts with the available coastal sediments and controls the beach configuration and behavior. The work was carried out at the seasonal scale and over a two and a half year period, along 14 selected sites, representative of a 200 km-long coastal stretch under a meso-tidal and wave dominated regime.

The investigation departed from the knowledge that the geomorphological framework determines the accommodation space in which the beach develops. It also defines the boundaries that condition the migration of beach forms, and thus beach variability. Moreover, topographical features such as headlands, submerged sand bars, shoals or submarine canyons are known to change the incoming wave characteristics as they propagate through progressively shallower waters, inducing large changes in wave height and direction of travel, that, in turn, are responsible for differentiated beach morphodynamics along the same coast.

There was also the understanding that the detection of patterns of change and evolution of beach sediments and morphology is a difficult task in a context of multiple and varying geomorphological settings and forcing factors. Thus, the methodology was specifically designed and data were gathered on three major components that regulate beach morphodynamics: 1) geomorphological framework, 2) subaerial beach response, and 3) hydrodynamic forcing. The datasets were thoroughly analyzed and described to provide understanding of each of the components affecting the beach systems, focusing on the subaerial portion of the beach, under model process-response conditions. The products of the analyses were further quantified to derive metrics and detect an existing spatial organization related to the geomorphological settings.

Chapter 2 provides some of the information that supported the outline and conduct of the work. It summarizes the geological and geomorphological setting, including the coastal processes and landforms present along the study area. Importantly, it retrieves information on the recent historical shoreline change, providing background on the balanced sediment budget scenario for the study period. A general description of the study sites is made attesting to the myriad of conditions being investigated along a high-energy coastal stretch that is under the influence of the same general deepwater wave regime.

The geomorphological framework is described in Subchapter 4.1 and addresses each study site in terms of planform geometry and physical boundaries, as well as type of nearshore and backshore features. It is shown how variable the geomorphological framework is along the study area and how the selected sites are representative of this variability. It stands out that beaches with rocky platforms have smaller embayment widths and higher degree of indentation.

In Subchapter 4.2, the analysis of the beach morphology and sediments is presented, and geoindicators are used to evaluate and describe the study sites' seasonal behavior. The pattern of change along the quarterly surveys showed that survey timing and resolution was appropriate to detect beach morphological and sedimentary variations at the seasonal scale. It stood out from the analysis that the magnitude of seasonal change was very different between study sites; some beaches varied as much as 500% of their average volume over the two and a half years of study (e.g. Paredes de Vitória), whereas other beaches experienced volume changes as low as 10 and 20% (e.g. Tamariz and Baleal-Peniche) throughout the same period.

Detailed analysis of oceanographic data was undertaken to describe the hydrodynamic forcing affecting the study area. Subchapter 4.3 presents the description of deep water wave conditions and provides the results of the wave propagation model used to simulate nearshore waves at each study site. The analysis of wave patterns in modal and storm conditions of both a 36 year-long series (adequate to describe the wave climate) and a shorter, two and a half years-long series (contemporaneous of the field surveys) attested that the duration of the monitoring program was appropriate to characterize the modal process-response conditions, descriptive of a period with no extreme events. Results show that there is a distinction between study sites located north of Cabo Raso (from Pedras Negras to Magoito) and the southernmost ones, the former sites being exposed to a higher wave-energy regime. Total water levels were calculated and validated with local field data. Likewise, results showed that there is an alongshore difference in the total water levels regime and that the northernmost study sites have higher probabilities of occurrence of higher water levels.

The exploratory analysis presented in Chapter 5 includes the application of the commonly used beach morphodynamic models, and statistical analysis of the overall data. The Embayment Scaling Parameter provided the better results in what concerns quantitative description and categorization of beach morphodynamic behavior, consistent with the field data and observations. Correlation analysis and Canonical

Correspondence Analysis results provided no evident relationships between the several controlling, forcing and beach response variables. The latter methodology, however, hinted at the disjunction between platform beaches and no-platform beaches that was related to the degree of indentation. Further exploration of this pattern revealed distinct behaviors in terms of volumetric changes, with platform beaches varying much less than the no-platform counterparts. Moreover, the volumetric variability within no-platform beaches was shown to be strongly correlated, although non-linearly, with the degree of embayment, given by the Embayment scaling parameter.

A conceptual model of the subaerial beach dynamics as a function of the geomorphological framework is put forth, in which the magnitude of beach variation is controlled by: 1) the presence of a rocky platform; and 2) in no-platform beaches, by the degree of embayment and its impact on beach circulation.

Platform beaches typically show small embayment widths and accommodation space, and experience small subaerial beach volume variations. Beaches with no platform vary between the unconstrained and constrained beach types, and are typically highly exposed to the permanent wave regime. No-platform beaches undergo subaerial volume variations that are consistently higher than in platform beaches, and these variations are expected to increase with the degree of embaymentization. A regression model is proposed that describes a continuum between unconstrained and constrained systems in which no-platform beaches vary in response to cross-shore or longshore predominant transport, respectively.

The conclusions of this thesis have been far reaching. The thesis outline is, by itself, a significant effort in the context of the study of beaches because it was set up to evaluate the magnitude and patterns of the beach response among contrasting environments that are usually treated and studied separately.

The present work grows on the existing literature that suggested that other controls, such as the inherited geological framework, are important determinants of beach morphodynamics. Still, the general literature lacks on field testing of this proposition, in part owing to the difficulty in covering a comprehensive description of the variables involved. The hypothesis that the geomorphological framework of beaches is a primary driver of the morphological beach responses was herein tested and verified, allowing for the grouping of beaches according to this criterion. The conceptual model herein proposed departs from existing morphodynamic models (that apply only to unconstrained beaches) by incorporating both unconstrained and constrained, platform

and no-platform beaches. The model relates the constraining boundaries (both lateral and vertical) to the beach subaerial dynamics, a descriptor seldom used in the literature, but of foremost importance for coastal management.

6.2. Future research

Field data are essential to describe beach systems and to support empirical and numerical models that adequately simulate beach processes and responses through time and space. The current research was well supported by a consistent and coherent database on beach morphology and sediments, at a seasonal to annual scale, covering a comprehensive and regional-scale coastal stretch. It verifies and demonstrates the hypothesis that beaches located along a coastal stretch exposed to the same offshore forcing conditions experience very different behavior as a result of the control of the geomorphological framework. On this note, it is expected that other controls and forcing mechanisms remain to be adequately described. For example, the processes responsible for the smaller magnitude of subaerial beach dynamics detected on platform beaches remain largely unknown. It is suggested that the rocky platforms function as permanent and static natural breakwaters, promoting early dissipation of the wave energy and limiting the range of wave bore characteristics reaching and inducing changes to the subaerial beach. This remains to be tested and demonstrated, ideally by further studying the transformation processes that occur in the surf zone in platform and no-platform beaches.

Furthermore, the present work was conducted over a period of modal process-response conditions. It would be desirable to test the proposed hypothesis under the occurrence of extreme events.

The conceptual model discriminates between platform and no-platform beaches, but, as stated in the introductory section of this work, one must be aware that beaches probably fall along a continuum of characteristics that reflect several combinations of similarities and differences between them. Including selected beaches from other parts of the coast (and the world) in a monitoring program would probably fill the gap between these two extreme types of beaches (platform and no-platform), thus increasing the scope of the model to fully address the continuity between environments, geomorphological framework and beach response, in line with how the coast functions.

x

The process of data gathering and analysis was long and, I now see, accompanied by an intense process of learning and maturing of ideas. The output of this work certainly does not answer all the questions that were put forth in the beginning of the endeavor (and that continued to come up along the way), but hopefully will contribute to the growing understanding of beaches and help trigger new hypotheses. It is indeed a matter of scale, and one can easily feel overwhelmed by the myriad of elements influencing beaches form and behavior. Still, studying these magnificent environments is an endless but rewarding adventure.

References

Aleman N, Robin N, Certain R, Anthony EJ, Barusseau J-P, 2015. Longshore variability of beach states and bar types in a microtidal, storm-influenced, low-energy environment. Geomorphology, 241:175-191.

Andrade C, Freitas MC, Cachado C, Cardoso AC, Monteiro JH, Brito P, Rebelo L, 2002. Coastal Zones. In, Santos, F. D.; Forbes, K. & Moita, R. (Eds). Climate Change in Portugal. Scenarios, Impacts and Adaptation Measures. SIAM Project, Gradiva, pp. 173-219.

Andrade C, Marques FMSF, Freitas MC (coords), 2013a. Final Report, Projeto Criação e implementação de um sistema de monitorização no litoral abrangido pela área de jurisdição da Administração da Região Hidrográfica do Tejo. FFCUL/APA, I.P, Lisbon, June 2013, 47p. + appendixes (Unpublished results).

Andrade C, Pires HO, Silva P, Taborda R, Freitas MC, 2006. Zonas Costeiras. In: Santos, F.D, Miranda, P. (eds.) Alterações Climáticas em Portugal: Cenários, Impactos e Medidas de Adaptação – Projecto SIAM II. Gradiva Publicações, Lisboa, 169-208.

Andrade C, Taborda R, Oliveira MA, Alves M, Carapuço AM. 2013b. Entregável 1.1.7.a Caracterização do clima de agitação ao largo. Relatório Técnico, Projeto Criação e implementação de um sistema de monitorização no litoral abrangido pela área de jurisdição da Administração da Região Hidrográfica do Tejo. FFCUL/APA, I.P, Lisboa, junho 2013, 14p. (não publicado).

Anfuso G, Martínez del Pozo JÁ, Gracia FJ, López-Aguayo F, 2003. Long-shore distribution of morphodynamic beach states along an apparently homogeneous coast in SW Spain. Journal of Coastal Conservation, 9:49-56.

Antunes C, 2007. Previsão de Marés dos Portos Principais de Portugal. FCUL Webpage, http://webpages.fc.ul.pt/~cmantunes/hidrografia/hidro_mares.html.

Antunes C, Vieira R, Andrade C, Taborda R, 2013. Entregável 1.1.5.a Caracterização da sobre-elevação meteorológica. Relatório Técnico, Projeto Criação e implementação de um sistema de monitorização no litoral abrangido pela área de jurisdição da Administração da Região Hidrográfica do Tejo. FFCUL/APA, I.P, Lisboa, junho 2013, 17p. (não publicado).

Backstrom JT, Jackson DWT, Cooper JAG, 2009. Shoreface morphodynamics of a high-energy, steep and geologically constrained shoreline segment in Northern Ireland. Marine Geology, 257(1):94-106.

Badiei P, Kamphuis JW, Hamilton DG, 1994. Physical Experiments on the Effects of Groins on Shore Morphology. In: Coastal Engineering, pp. 1782–1796.

Battjes JA. 1974. Surf Similarity. Proceedings of the 14th Coastal Engineering Conference, American Society of Civil Engineers, pp. 569-587.

Belknap DF, Kraft JC, 1985. Influence of antecedent geology on stratigraphic preservation potential and evolution of Delaware's barrier systems. Marine Geology, 63:235-262.

Bertin X, Prouteau E, Letetrel C, 2013. A significant increase in wave height in the North Atlantic Ocean over the 20th century. Global and Planetary Change, 106:77-83.

Bird ECF, 2000. Coastal Geomorphology: An Introduction. Wiley, Chichester, 332p.

Blott SJ, Pye K, 2001. GRADISTAT: a grain size distribution and statistics package for the analysis of unconsolidated sediments. Earth Surface Processes and Landforms, 26:1237-1248.

Booij N, Ris R, Holthuijsen L, 1999. A third-generation wave model for coastal regions. I-Model description and validation. Journal of Geophysical Research, 104:7649-7666.

Bowman D, Guillén J, López L, Pellegrino V, 2009. Planview Geometry and morphological characteristics of pocket beaches on the Catalan coast (Spain). Geomorphology, 108(3):191-199

Bowman D, Rosas V, Pranzini E, 2014. Pocket beaches of Elba Island (Italy) – Planview geometry, depth of closure and sediment dispersal. Estuarine, Coastal and Shelf Science, 138:37-46.

Browder AG, McNinch JE, 2006. Linking framework geology and nearshore morphology: Correlation of paleo-channels with shore-oblique sandbars and gravel outcrops. Marine Geology, 231:141-162.

Burvingt O, Masselink G, Russell P, Scott T, 2017 (Accepted Manuscript). Classification of beach response to extreme storms. Geomorphology.

Carapuço MM, Taborda R, Silveira TM, Psuty NP, Andrade C, Freitas MC, 2016. Coastal geoindicators: Towards the establishment of a common framework for sandy coastal environments. Earth-Science Reviews, 154:183-190.

Carrasco AR, Ferreira Ó, Matias A, Freire P, 2012. Natural and human-induced coastal dynamics at a back-barrier beach. Geomorphology, 159:30-36.

CERC (Coastal Engineering Research Center), 1995. Irregular wave runup on beaches. CETA No. I-60 (3/95), U.S. Army Corps of Engineers, Coastal Engineering Research Center, Fort Belvoir, VA. 5p.

Cleary WJ, Riggs SR, Marcy DC, Snyder SW, 1996. The influence of inherited geological framework upon a hardbottom-dominated shoreface on a high-energy shelf: Onslow Bay, North Carolina, USA. Geological Society, London, Special Publications 117:249–266.

Codiga DL, 2011. Unified Tidal Analysis and Prediction Using the UTide Matlab Functions. Technical Report 2011-01. Graduate School of Oceanography, University of Rhode Island, Narragansett, RI. 59p.

Cooper JAG, Jackson DWT, Dawson AG, Dawson S, Bates CR, Ritchie W, 2012. Barrier islands on bedrock: A new landform type demonstrating the role of antecedent topography on barrier form and evolution. Geology, 40(10):923–926.

Costa M, Esteves R, 2009. Clima de agitação marítima na costa oeste de Portugal Continental. Comunicações das XI Jornadas Técnicas de Engenharia Naval, Instituto Superior Técnico, Lisboa, 15p.

Daly C, Bryan KR, Roelvink JA, Klein AHF, Hebbeln D, Winter C, 2011. Morphodynamics of Embayed Beaches: The Effect of Wave Conditions. Journal of Coastal Research, SI 64: 1003-1007.

Davidson MA, Turner IL, 2009. A behavioral template beach profile model for predicting seasonal to interannual shoreline evolution. Journal of Geophysical Research, 114: F01020, 21p.

Dee DP, Uppala SM, Simmons AJ, Berrisford P, Poli P, Kobayashi S, Andrae U, Balmaseda MA, Balsamo G, Bauer P, Bechtold P, Beljaars ACM, van de Berg L, Bidlot J, Bormann N, Delsol C, Dragani R, Fuentes M, Geer AJ, Haimberger L, Healy SB, Hersbach H, Hólm EV, Isaksen L, Kållberg P, Köhler M, Matricardi M, McNally AP, Monge-Sanz BM, Morcrette J-J, Park B-K, Peubey C, de Rosnay P, Tavolato C, Thépaut J-N, Vitart F, 2011. The ERA-Interim reanalysis: configuration and performance of the data assimilation system. Quarterly Journal of the Royal Meteorological Society, 137:553–597.

Demarest J, Biggs R, Kraft J, 1981. Time-stratigraphic aspects of a formation: Interpretation of surficial Pleistocene deposits by analogy with Holocene paralic deposits, southeastern Delaware. Geology, 9:360–365.

Dias JMA, Boski T, Rodrigues A, Magalhães F, 2000. Coast line evolution in Portugal since the Last Glacial Maximum until present - a synthesis. Marine Geology, 170(1-2):177-186.

Diogo Z, Bastos A, Lira C, Taborda R, Andrade C, Silveira TM, Ribeiro M, Silva AN, Carapuço MM, Pinto CA, Freitas MC, 2014. Morphological impacts of Christina storm on the beaches of the central western Portuguese coast. Comunicações Geológicas, 101(III):1445-1448.

Dodet G, Bertin X, Taborda R, 2010. Wave climate variability in the North-East Atlantic Ocean over the last six decades. Ocean Modelling, 31(3-4):120-131.

Dubois A, Sedrati M, Menier D, 2011. Morphologic response of four pocket beaches to high energy conditions: including the Xynthia storm (South Brittany, France). Journal of Coastal Research, Special Issue 64:1845-1849.

Dykes JD, Hsu YL, Rogers WE, 2002. SWAN Evaluation in the Northern Gulf of Mexico, submitted to the 7th International Workshop on Wave Hindcasting and Forecasting, Banff, Alberta, Canada, 13p.

Ferreira Ó, Garcia T, Matias A, Taborda R, Dias JA, 2006. An integrated method for the determination of set-back lines for coastal erosion hazards on sandy shores. Continental Shelf Research, 26:1030-1044.

Folk RL, Ward WC, 1957. Brazos River Bar: a study in the significance of grain size parameters. Journal of Sedimentary Petrology, 27(1):3-26.

Gallop SL, Bosserelle C, Eliot I, Pattiaratchi C, 2012. The influence of limestone reefs on storm erosion and recovery of a perched beach. Continental Shelf Research, 47:16-27.

Gallop SL, Bosserelle C, Pattiaratchi C, Eliot I, 2011. Rock topography causes spatial variation in the wave, current and beach response to sea breeze activity. Marine Geology, 290:29-40.

Gama C, Coelho C, Baptista P, Albardeiro L, 2011. Equilibrium configuration of sandy embayed beaches from the Southwest Portuguese rocky coast. Journal of Coastal Research, SI64:2037–2041.

Gama C, Dias JA, Ferreira Ó, Taborda R, 1994. Analysis of storm surge in Portugal, between June 1986 and May 1988. Proceedings of Littoral´94, 381-387, EUROCOAST. Lisboa, Portugal.

Gourlay MR, 1968. Beach and dune erosion tests. Delft Hydraulics Laboratory, Report No. M935/M936, May 1968.

Grune J, Wang Z, 2000. Wave run-up on sloping seadykes and revetments Proc. 27th International Conference on Coastal Engineering (ICCE 2000). Sydney, Australia.

Guza RT, Inman DL, 1975. Edge waves and beach cusps. Journal of Geophysical Research, 80(21):2997-3012.

Guza RT, Thornton EB.1982. Swash Oscillations on a Natural Beach. Journal of Geophysical Research, 87(C1):483-491.

Hammer Ø, Harper DAT, Ryan PD, 2001. PAST: Paleontological Statistics Software Package for Education and Data Analysis. Palaeontologia Electronica, 4(1):9p.

Harley MD, Turner IL, Short AD, Ranasinghe R, 2011. A reevaluation of coastal embayment rotation: The dominance of cross-shore versus alongshore sediment transport processes, Collaroy-Narrabeen Beach, southeast Australia. Journal of Geophysical Research, 116:F04033.

Harris M, Gayes P, Kindinger J, Flocks JG, Krantz DE, Donovan P, 2005. Quaternary geomorphology and modern coastal development in response to an inherent geologic framework: an example from Charleston, South Carolina. Journal of Coastal Research, 21(1):49-64.

Hegge B, Eliot IG, Hsu J, 1996. Sheltered sandy beaches of southwestern Australia. Journal of Coastal Research, 12(3):748-760.

Holman RA, 1986. Extreme value statistics for wave-run-up on a natural beach. Coastal Engineering, 9:527-544.

Honeycutt M, Krantz D, 2003. Influence of the Geologic Framework on Spatial Variability in Long-Term Shoreline Change, Cape Henlopen to Rehoboth Beach, Delaware. Journal of Coastal Research, SI38:147-167.

Hsu JRC, Silvester R, Xia YM, 1987. New characteristics of equilibrium shaped bays. In: ASCE (Ed.), 8th International Conference on Coastal Engineering, 140-144.

Hsu JRC, Silvester R, Xia YM, 1989a. Generalities on static equilibrium bays. Coastal Engineering, 12:353-369.

Hsu JRC, Silvester R, Xia YM, 1989b. Application of Headland control. Journal of Waterway, Port, Coastal, and Ocean Engineering, 115(3):298-310.

Inman DL, 2003. Littoral cells. In: Schwartz, M. (Ed.), Encyclopedia of Coastal Science. The Earth Sciences Encyclopedia Online. Kluwer Academic Publishers, Dordrecht, Netherlands, 19p.

Jackson DWT, Cooper JAG, 2009. Geological control on beach form: accommodation space and contemporary dynamics. Journal of Coastal Research, SI56:69–72.

Jackson DWT, Cooper JAG, Del Rio L, 2005. Geological control of beach morphodynamic state. Marine Geology, 216:297-314.

Jackson NL, Nordstrom KF, 1992. Site-specific controls on wind and wave processes and beach mobility on estuarine beaches. Journal of Coastal Research, 8:88-98.

Jeanson M, Anthony EJ, Dolique F, Aubry A, 2013. Wave characteristics and morphological variations of pocket beaches in a coral reef–lagoon setting, Mayotte Island, Indian Ocean. Geomorphology, 182:190-209.

Karunarathna H, Horrillo-Caraballo J, Kuriyama Y, Mase H, Ranasinghe R, Reeve DE, 2016. Linkages between sediment composition, wave climate and beach profile variability at multiple timescales, Marine Geology, 381:194-208.

Kennedy DM, Milkins J, 2014. The formation of beaches on shore platforms in microtidal environments. Earth Surface Processes and Landforms, 40:34-46.

Khalil SM, Finkl CW, 2007. Submarine geomorphology and coastal process zones: morphodynamics of the inner continental shelf off southeast Florida. Journal of Coastal Research, SI50:480-485.

King CAM, 1959. Beaches and coasts. Edward Arnold, London, 403p.

Klein AHF, Filho LB, Schumacher DH, 2002. Short-Term Beach Rotation Processes in Distinct Headland Bay Beach Systems. Journal of Coastal Research, 18(3):442-458.

Klein HF, Menezes JT, 2001. Beach morphodynamics and profile sequence for a headland bay coast. Journal of Coastal Research, 17:812-835.

Komar PD, 1998. Beach Processes and Sedimentation. 2nd Edition, Prentice Hall, 544p.

Kroon A, Larson M, Möller I, Yokoki H, Rozynski G, Cox J, Larroude P, 2008. Statistical analysis of coastal morphological data sets over seasonal to decadal time scales. Coastal Engineering, 55(7):581-600.

Krumbein WC, 1944. Shore processes and beach characteristics. Beach Erosion Board, Technical Memorandum, No. 3, U.S. Army Corps of Engineers, 47p.

Larson M, Capobianco M, Jansen H, Rozynski G, Southgate HN, Stive M, Wijnberg KM, Hulscher S, 2003. Analysis and modeling of field data on coastal morphological evolution over yearly and decadal time scales. Part 1: Background and linear techniques. Journal of Coastal Research, 19(4):760–775.

Larson M, Hoan LX, Hanson H, 2010. Direct formula to compute wave height and angle at incipient breaking. Journal of Waterway, Port, Coastal and Ocean Engineering, 136:119-122.

Larson M, Kraus N, 2000. Representation of Non-Erodible (Hard) Bottoms in Beach Profile Change Modeling. Journal of Coastal Research, 16(1), 1-14.

Larson M, Kubota S, Erikson L, 2004. Swash-zone sediment transport and foreshore evolution: field experiments and mathematical modeling. Marine Geology, 212:61-79.

Larson M, Rosati JD, Kraus NC, 2002. Overview of Regional Coastal Sediment Processes and Controls. ERDC/CHL CHETN-XIV-4, 22p.

Lasagna R, Montefalcone M, Albertelli G, Corradi N, Ferrari M, Morri C, Bianchi CN, 2011. Much damage for little advantage: Field studies and morphodynamic modelling highlight the environmental impact of an apparently minor coastal mismanagement. Estuarine, Coastal and Shelf Science, 94(3):255-262.

Lentz EE, Hapke CJ, 2011. Geologic framework influences on the geomorphology of an anthropogenically modified barrier island: Assessment of dune/beach changes at Fire Island, New York. Geomorphology, 126(1):82-96.

Lira C, Silva AN, Taborda R, Andrade CF, 2016. Coastline evolution of Portuguese low-lying sandy coast in the last 50 years: an integrated approach, Earth System Science Data, 8(1):265-278.

Loureiro C, Ferreira Ó, Andrew JAG, 2013. Applicability of parametric beach morphodynamic state classification on embayed beaches. Marine Geology, 346:153-164.

Loureiro C, Ferreira Ó, Cooper JAG, 2009. Contrasting Morphologic Behaviour at Embayed Beaches in Southern Portugal. Journal of Coastal Research, SI56:83-87.

Loureiro C, Ferreira Ó, Cooper JAG, 2012. Geologically constrained morphological variability and boundary effects on embayed beaches. Marine Geology, 329:1-15.

Marques FMSF, 2009. Sea cliff instability hazard prevention and planning: examples of practice in Portugal. Journal of Coastal Research, SI56:856-860.

Marques FMSF, Penacho N, Queiroz S, Sousa H, Silveira TM, Gouveia L, Matildes R, Redweik P, Garzón V, Bastos AP, Diogo ZS, Taborda R, Andrade C, Freitas MC, 2013. Entregável 1.2.1.a Caracterização das principais unidades geológicas e da organização geomorfológica da faixa costeira. Relatório Técnico, Projeto Criação e implementação de um sistema de monitorização no litoral abrangido pela área de jurisdição da Administração da Região Hidrográfica do Tejo. FFCUL/APA, I.P, Lisboa, junho 2013, 36 p. + anexos (não publicado)

Marshall R, Stephenson W, 2011. The morphodynamics of shore platforms in a micro-tidal setting: Interactions between waves and morphology. Marine Geology, 288(1):18-31.

Mase H, 1989. Random wave run-up height on gentle slope. Journal of Waterway, Port, Coastal and Ocean Engineering, 115:649-661.

Masselink G, Pattiaratchi CB, 2001. Seasonal changes in beach morphology along the sheltered coastline of Perth, Western Australia. Marine Geology, 172:243-263.

Masselink G, Short AD, 1993. The effect of tide range on beach morphodynamics and morphology: a conceptual beach model. Journal of Coastal Research, 9(3):785–800.

Mastronuzzi G, Palmentola G, Sanso` P, 1992. Esempi di caratterizzazione morfometrica di tratti di litorale rocciose della Puglia. In: Proceedings of the XXVI Congresso Geografico Italiano, Genova, Italy, pp.372-377.

Mather A, Stretch D, Garland G, 2011. Predicting Extreme Wave Run-Up on Natural Beaches for Coastal Planning and Management. Coastal Engineering Journal, 53:87-109.

Matildes R, 2016. Técnicas de teledeteção de alta resolução aplicadas à monitorização 3D de arribas litorais: adequabilidade, modelação da informação e resultados. Tese de Doutoramento. Universidade de Lisboa, 210p.

Mazarakis N, Kotroni V, Lagouvardos K, Bertotti L, 2012. High-resolution wave model validation over the Greek maritime areas. Natural Hazards and Earth System Sciences, 12:3433-3440.

McNinch JE, 2004. Geologic control in the nearshore: shore-oblique sandbars and shoreline erosional hotspots, Mid-Atlantic Bight, USA. Marine Geology, 211(1):121-141.

Muñoz-Perez JJ, Medina R, 2010. Comparison of long-, medium- and short-term variations of beach profiles with and without submerged geological control. Coastal Engineering, 57(3):241-251.

Nielsen P, Hanslow D. 1991. Wave run-up distributions on natural beaches. Journal of Coastal Research, 7(4):1139-1152.

Ojeda E, Guillén J, 2008. Shoreline dynamics and beach rotation of artificial embayed beaches. Marine Geology, 253(1):51-62.

Penacho N, 2012. Caracterização, evolução e análise de suscetibilidade à ocorrência de instabilidades das arribas do arco Baleal - Bom Sucesso (Peniche-Óbidos). Dissertação de mestrado em Geologia Aplicada, Universidade de Lisboa, 205p.

Pilkey OH, Young RS, Riggs SR, Smith AWS, Wu H, Pilkey WD, 1993. The Concept of Shoreface Profile of Equilibrium: A Critical Review. Journal of Coastal Research, 9:255-278.

Pinto C, Silveira T, Taborda R, 2015. Alimentação artificial das praias da Costa da Caparica: síntese dos resultados de monitorização (2007 a 2014). 3ª Conferência sobre morfodinâmica estuarina e costeira, 47-48. Universidade do Algarve, 14-15 Maio, Faro.

Pinto CA, Taborda R, Andrade C, Teixeira SB, 2009. Seasonal and Mesoscale Variations at an Embayed Beach (Armação de Pera, Portugal). Journal of Coastal Research, SI56:118-122.

Pranzini E, Rosas V, Jackson NL, Nordstrom KF, 2013. Beach changes from sediment delivered by streams to pocket beaches during a major flood. Geomorphology, 199:36-47.

Psuty NP, Duffy M, Pace JF, Skidds DE, Silveira TM, 2010. Northeast Coastal and Barrier Network geomorphological monitoring protocol: Part I – ocean shoreline position. Natural Resource Report NPS/NCBN/NRR – 2010/185. National Park Service, Fort Collins, Colorado

Psuty NP, Schmelz WJ, Spahn A, Greenberg J, 2016. Geotemporal vectors of coastal geomorphological change interacting with National Park Service management policy at Great Kills Park, Gateway National Recreation Area, USA. Geomorphology, 252:5-16.

Ribeiro M, Taborda R, Rodrigues A, Silveira T, 2014. Insights on sediment bypassing at headland-bay beaches: an example at the Portuguese west coast. Actas das 3as Jornadas de Engenharia Hidrográfica, Lisboa, Portugal, pp. 301-304.

Ribeiro M. 2017. Headland sediment bypassing processes. PhD Dissertation. University of Lisbon, 229p.

Riggs SR, Cleary WJ, Snyder SW, 1995. Influence of inherited geologic framework on barrier shoreface morphology and dynamics. Marine Geology, 126:213-234.

Santos F, Lopes A, Moniz G, Ramos L, Taborda R, 2014. Gestão da Zona Costeira - O Desafio da Mudança. Relatório do Grupo de Trabalho do Litoral, 237p.

Schupp CA, McNinch JE, List JH, 2006. Nearshore shore-oblique bars, gravel outcrops, and their correlation to shoreline change. Marine Geology, 233(1):63-79.

Schwab WC, Thieler ER, Allen JR, Foster DS, Swift BA, Denny JF, 2000. Influence of Inner-Continental Shelf Geologic Framework on the Evolution and Behavior of the Barrier-Island System between Fire Island Inlet and Shinnecock Inlet, Long Island, New York. Journal of Coastal Research, 16:408-422.

Scott T, Masselink G, Russell P, 2011. Morphodynamic characteristics and classification of beaches in England and Wales. Marine Geology, 286(1):1-20.

Short AD (Editor), 1999. Handbook of beach and shoreface morphodynamics. John Wiley, 379p.

Short AD, 2006. Australian Beach Systems - Nature and Distribution. Journal of Coastal Research, 22(1):11-27.

Short AD, 2010. Role of geological inheritance in Australian beach morphodynamics. Coastal Engineering, 57(2):92-97.

Short AD, 2016. The Coastal Studies Unit and development of the Australian beach models. Journal of Coastal Research, SI75:1–7.

Short AD, Masselink G, 1999. Embayed and structurally controlled beaches. In: Short, A.D. (Ed.), Handbook of Beach and Shoreface Morphodynamics. John Wiley & Sons, pp. 230–250.

Silva AN, Lira C, Andrade C, Taborda R, Freitas MC, 2013a. Entregável 1.2.2.2.a Análise da evolução da linha de costa em litoral baixo arenoso nos últimos 50 anos. Relatório Técnico, Projeto Criação e implementação de um sistema de monitorização no litoral abrangido pela área de jurisdição da Administração da Região Hidrográfica do Tejo. FFCUL/APA, I.P, Lisboa, junho 2013, 37 p. + anexos (não publicado).

Silva AN, Lira C, Sousa H, Silveira TM, Andrade C, Taborda R, Freitas MC, 2013b. Entregável 1.2.2.2.b Análise da evolução da linha de costa nos últimos 50 anos – caso especial da Costa da Caparica. Relatório Técnico, Projeto Criação e implementação de um sistema de monitorização no litoral abrangido pela área de jurisdição da Administração da Região Hidrográfica do Tejo. FFCUL/APA, I.P, Lisboa, junho 2013, 27 p. + anexos (não publicado).

Silva R, Coelho C, Veloso-Gomes F, Taveira-Pinto F, 2007. Dynamic numerical simulation of medium term coastal evolution of the west coast of Portugal. Journal of Coastal Research, SI50:263–267.

Silveira LF, Klein AHF, Tessler MG, 2010. Headland-bay beach planform stability of Santa Catarina State and of the Northern Coast of São Paulo State. Brazilian Journal of Oceanography, 58(2):101-122.

Silveira TM, Taborda R, Carapuço AM, Andrade C, Freitas MC, Duarte JF, Psuty NP, 2016. Assessing the extreme overwash regime along an embayed urban beach. Geomorphology, 274:64-77.

Silvester R, 1960. Stabilization of Sedimentary Coastlines. Nature, 188:467-469.

Silvester R, Hsu JR-C, 1993. Coastal stabilization: Innovative concepts. Englewood Cliffs: Prentice-Hall, 578p.

Silvester R, Hsu JRC, 1997. Coastal stabilization. Advanced series on ocean engineering, Vol. 14, World Scientific, Singapore, 578 pp.

Smith AW, 2001. Headland Bypassing. Coasts & Ports 2001: Proceedings of the 15th Australasian Coastal and Ocean Engineering Conference and the 8th Australasian Port and Harbour Conference. Institution of Engineers Australia, Barton, A.C.T, 214-216.

Soulsby R, 1997. Dynamics of Marine Sands: A Manual for Practical Applications. Thomas Telford, London.

Southgate HN, Wijnberg KM, Larson M, Capobianco M, Jansen H, 2003. Analysis of Field Data of Coastal Morphological Evolution over Yearly and Decadal Timescales. Part 2: Non-Linear Techniques. Journal of Coastal Research, 19(4):776-789.

Spagnolo M, Llopis IA, Pappalardo M, Federici PR, 2008. A new approach for the study of the coast indentation index. Journal of Coastal Research, 24(6):1459-1468.

Stokes CH, Russell P, Conley D, Beaumont E, Greaves D, 2013. Exploring Monthly To Seasonal Beach Morphodynamics Using Empirical Orthogonal Functions. Journal of Coastal Research, SI65(2):1868-1873.

Sunamura T, 1984. Quantitative predictions of beach-face slopes. Geological Society of America Bulletin, 95:242-245.

Taborda R, Andrade C, 2014. Morfodinâmica do Estuário Exterior do Tejo e Intervenção na Região da Caparica – v1. Grupo de Trabalho do Litoral (Doc.de trabalho), 21p.

Taborda R, Ribeiro MA, 2015. A simple model to estimate the impact of sea-level rise on platform beaches. Geomorphology, 234:204-210.

Teixeira NJS, 2014. Estudo do Limite de Espraiamento das Ondas. Dissertação de Mestrado em Engenharia Civil. Departamento de Engenharia Civil, Universidade de Aveiro. Aveiro, 156p.

ter Braak CJF, Verdonschot PFM. 1995. Canonical correspondence analysis and related multivariate methods in aquatic ecology. Aquatic Sciences, 57:255–289.

ter Braak CJF. 1986. Canonical correspondence analysis: a new eigenvector technique for multivariate direct gradient analysis. Ecology, 67:1167-1179.

Thieler ER, Brill AL, Cleary WJ, Hobbs CH, Gammisch RA, 1995. Geology of the Wrightsville Beach, North Carolina shoreface: Implications for the concept of shoreface profile of equilibrium. Marine Geology, 126:271-287.

Thieler ER, Himmelstoss EA, Zichichi JL, Ergul A, 2009. Digital Shoreline Analysis System (DSAS) version 4.0— An ArcGIS extension for calculating shoreline change: U.S. Geological Survey Open-File Report 2008-1278.

Thomas T, Phillips MR, Williams AT, 2010. Mesoscale evolution of a headland bay: Beach rotation processes. Geomorphology, 123(1):129-141.

Thomas T, Phillips MR, Williams AT, Jenkins RE, 2012. Medium time-scale behaviour of adjacent embayed beaches: Influence of low energy external forcing. Applied Geography, 32(2):265-280.

Trenhaile AS, 2004. Modeling the accumulation and dynamics of beaches on shore platforms. Marine Geology, 206:55–72.

Trenhaile AS, 2016. Rocky coasts — their role as depositional environments. Earth-Science Reviews, 159:1-13.

Valvo LM, Murray AB, Ashton A, 2006. How does underlying geology affect coastline change? An initial modeling investigation. Journal of Geophysical Research, 111, F02025, 18p.

Van der Meer JW, Stam CJ, 1992. Wave runup on smooth and rock slopes of coastal structures. American Society of Civil Engineers, Journal of Waterway, Port, Coastal, and Ocean Engineering, 118(5):534-550.

Wright LD, Short AD, 1984. Morphodynamic variability of surf zones and beaches: a synthesis. Marine Geology, 56(1–4):93-118.

Yasso WE, 1965. Plan Geometry of Headland-Bay Beaches. The Journal of Geology, 73:702-714.

Appendix A. Field Booklets

Available at:

http://sniamb.apambiente.pt/infos/geoportaldocs/Politicas/Agua/Ordenamento/SistemasMonitorizacaoLitoral/E_1.2.3.b_LivroCampoI_Litoral.pdf

http://sniamb.apambiente.pt/infos/geoportaldocs/Politicas/Agua/Ordenamento/SistemasMonitorizacaoLitoral/E_2.1.a_LivroCampoII_Caparica.pdf

Criação e implementação de um sistema de monitorização no litoral abrangido pela área de jurisdição da Administração da Região Hidrográfica do Tejo, I.P.

Livro de Campo

REDE ESPACIAL DE PONTOS DE REFERÊNCIA E CABEÇAS DE PERFIL PARA O LITORAL ABRANGIDO PELA ÁREA DE JURISDIÇÃO DA ADMINISTRAÇÃO DA REGIÃO HIDROGRÁFICA DO TEJO, I.P.

I. PRAIA DA VIEIRA – SÃO JULIÃO DA BARRA

Versão 1, Junho 2011

ÍNDICE

INTRODUÇÃO

OBJECTIVO DO LIVRO DE CAMPO

Este "Livro de Campo" tem como objectivo caracterizar a rede de pontos de referência definidos no litoral abrangido pela área de jurisdição da Administração da Região Hidrográfica (ARH) do Tejo, I.P, entre a Praia da Vieira (limite sul) e São Julião da Barra, para apoio à realização de levantamentos topográficos, nomeadamente perfis de praia. Identificam-se também as localizações e rumos de perfis de praia, objecto de monitorização de projectos desenvolvidos pelo Departamento de Geologia da Faculdade de Ciências e Centro de Geologia da Universidade de Lisboa (GeoFCUL e CeGUL), em colaboração com a ARH do Tejo, I.P.. Contém ainda um guia de nomenclatura e códigos de identificação de praias, perfis e objectos notáveis para utilização em trabalho de campo, contribuindo para a uniformização de futuras bases de dados.

As coordenadas cartográficas dos pontos de referência, bem como dos pontos iniciais dos perfis de praia (cabeças de perfil), são apresentados num quadro síntese no final do livro de campo, no sistema PT-TM06 (Quadro V). A informação acerca dos pontos de referência e perfis de praia está também disponível em formato *shapefile* (ESRI) com metadados associados, como anexo a este documento. O presente livro e anexos estão sujeitos a revisões e actualizações. O número da versão é identificado no nome dos ficheiros (e na capa e rodapé das páginas do livro) e todas as alterações feitas são documentadas, sob a forma de um histórico, no Quadro IV.

PONTOS DE REFERÊNCIA

O livro é constituído por um conjunto de fichas. Cada ficha caracteriza um ponto de referência – pontos fixos e materializados no terreno por objectos específicos, naturais ou implantados, com coordenadas planimétricas e altimétrica muito bem conhecidas. Cada ficha inclui no seu título (barra superior), o nome do troço das praias onde o ponto de referência se localiza, e um código único de identificação. No caso da praia do Tamariz indica-se ainda a designação adoptada em projectos anteriores. Os outros elementos constituintes da ficha são:

- Fonte dos dados: corresponde ao nome da instituição (GeoFCUL ou DEGGE - Departamento de Engenharia Geográfica, Geofísica e Energia) e, quando possível, dos operadores que estabeleceram o ponto de referência;
- Data do estabelecimento do ponto de referência;
- Qualidade do ponto de referência, relativamente à planimetria (M e P), posição altimétrica (H) e monumentação ou materialização (ver Quadro I);
- Objectivo do ponto: ponto de referência e quando aplicável, cabeça de perfil;
- Descrição da localização e das características do ponto de referência;
- Tabela com as coordenadas planimétricas (M e P) e elevação (H) do ponto (em unidades métricas);
- Informação iconográfica:
  - ✓ Imagem de conjunto orientada, com recurso a ortofotografias ou outras bases cartográficas recentes, que permite a visualização da localização espacial dos pontos de referência e, quando aplicável, apresenta a(s) linha(s) de perfil de praia;
  - ✓ Registo fotográfico, que inclui duas fotografias terrestres mostrando a área envolvente e uma imagem de pormenor da materialização do ponto.

INTRODUÇÃO

A qualidade do ponto de referência é definida segundo o seu posicionamento absoluto (M, P e H) e a sua monumentação ou materialização. Os pontos foram estabelecidos com recurso a equipamento de sistema e posicionamento global (GPS). Assim, a classificação planimétrica e altimétrica depende do modo de observação (modo estático ou modo cinemático) e do processamento dos dados (em pós-processamento ou em tempo real). Na determinação da qualidade da monumentação, considera-se a sua estabilidade, durabilidade e acessibilidade. O quadro I resume essas classificações.

Quadro I: Qualidade do ponto de referência.

Qualidade		Classe	Precisão	Descrição
Posicionamento	planimétrica	I	1 a 2 cm	• ponto medido em modo estático com pós-processamento • observações > 20 minutos
		II	2 a 5 cm	• ponto medido em tempo real (DGPS/ RTK)
	altimétrica	I	≈ 5 cm	• ponto medido em modo estático com pós-processamento • com recurso a marcas com altimetria de precisão nas proximidades da medição do ponto
		II	7 a 10 cm	• ponto medido em tempo real (DGPS/ RTK)
Monumentação		I	Alta	• marcas permanentes ao nível do solo ou sobre construções estáveis • elementos proeminentes sobre construções estáveis • pontos em locais de fácil acesso
		II	Média	• marcas provisórias no solo • pontos em locais menos protegidos
		III	Baixa	• marcas materializadas em estruturas não permanentes ou de estabilidade duvidosa

GUIA DE NOMENCLATURA NO TRABALHO DE CAMPO

O guia de nomenclatura inclui uma lista de códigos aplicáveis ao nome do trabalho, que permitem identificar a data do levantamento, o servidor utilizado em modo "tempo real", o operador e o nome da praia (Quadro II), e uma lista de códigos associados às medições, que permitem identificar o perfil de praia e os pontos medidos (por exemplo: topografia, local de recolha de sedimentos, local de aquisição de fotografias, etc.), bem como os limites ou elementos lineares medidos (por exemplo: crista de berma, limite do espraio ou da vegetação, etc.) (Quadro III).

Quadro II: Guia de nomenclatura dos trabalhos e medições.

		Código	Exemplo
Trabalho		*Código de praia | data (aaaammdd) | servidor | operador*	TM20110306Rpa
Medição	Perfil de praia	*Código de perfil*	PTM3
	Limite ou ponto	*Código de leitura*	UESP

INTRODUÇÃO

Quadro III: Lista de códigos de medição.

Grupo de Código	Código	Descrição do código
Geral	TOPO	Levantamento topográfico indiferenciado
	CBER	Crista da berma
	VEG	Limite da vegetação
	BDUN	Base da duna primária
	CDUN	Crista da duna primária
	BARR	Base da arriba
	UESP	Limite do espraio das ondas referente à preia-mar precedente (última)
	MESP	Limite máximo do espraio das ondas
	SED	Localização de recolha de amostra de sedimentos
	FOTO	Localização de aquisição de fotografia
	TEST	Topo de estrutura
	BEST	Base de estrutura
Exemplos (os códigos de cada praia, pontos de referência e perfis de praia encontram-se nas fichas seguintes):		
Praia A	PA1	Ponto de Referência 1 da Praia A
	PA2	Ponto de Referência 2 da Praia A
	PPA1	Perfil de praia 1 da Praia A
Praia B	PB1	Ponto de Referência 1 da Praia B
	PB2	Ponto de Referência 2 da Praia B
	PPB1	Perfil de praia 1 da Praia B

INTRODUÇÃO

Quadro IV: Lista das versões e alterações ao Livro de Campo.

Versão	Data	Comentários
V1	Junho 2011	1º livro de campo após colocação e georreferenciação dos pontos de referência.

ENQUADRAMENTO GERAL

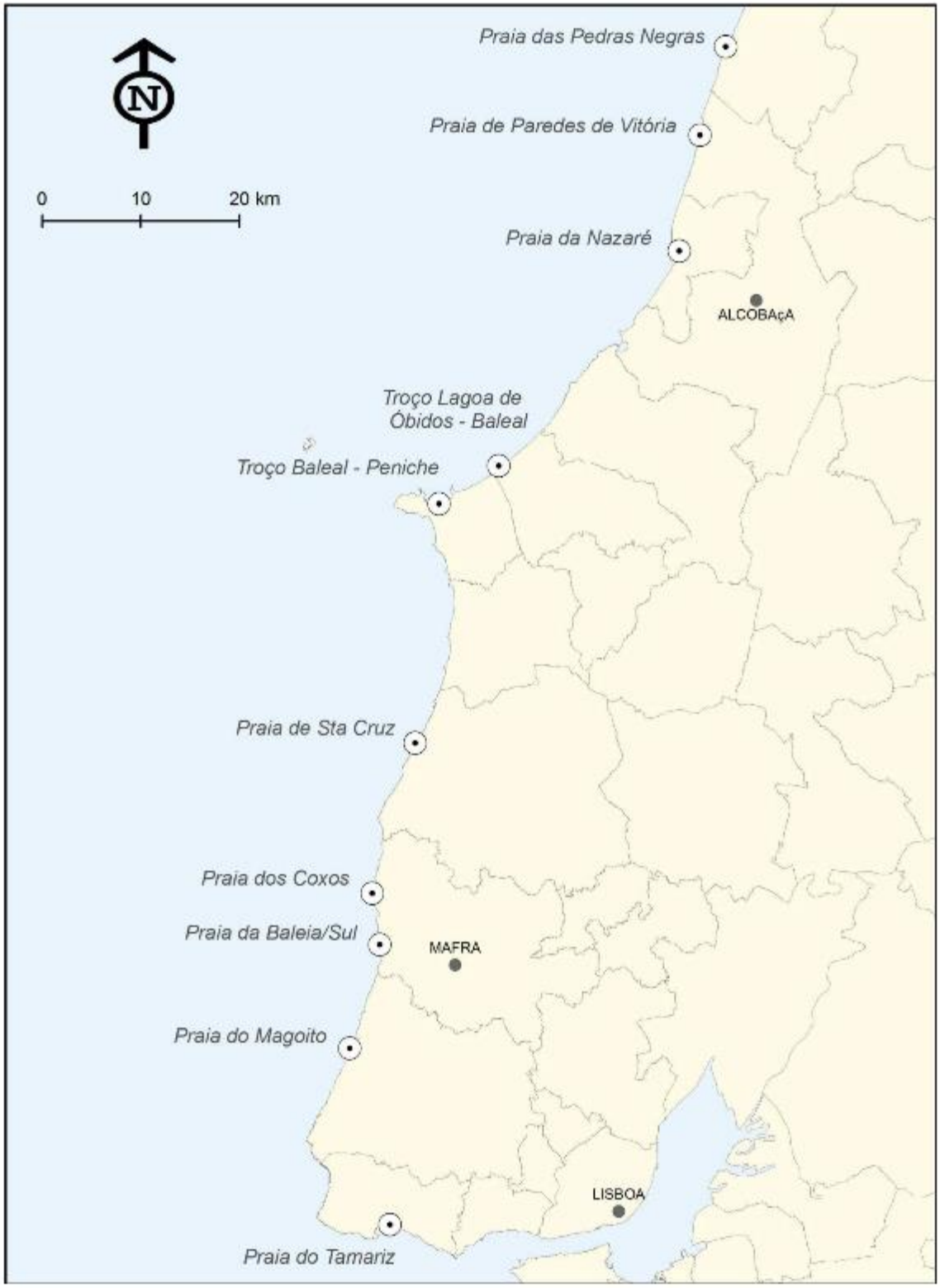

Versão 1, Junho 2011 7

PEDRAS NEGRAS - PN

Versão 1, Junho 2011 8

PEDRAS NEGRAS - PN	PN1

Estabelecido por: GeoFCUL (Tanya Silveira e Pedro Costa) **Data:** 2011/02/02

Qualidade: Planimetria – II, Altimetria – II, Monumentação – I

Objectivo: Ponto de Referência + Cabeça de Perfil (PPN1)

Descrição: Cabeça de prego no topo de um tubo de PVC preenchido com argamassa; localizado no campo dunar a cerca de 400 m a norte do parque de estacionamento norte da praia das Pedras Negras.

M	P	H
-75755.884	13501.599	14.576

Sistema Coordenadas: PT-TM06 | Datum Vertical: NMM Cascais 1938 | medido em: 2011/02/02

Versão 1, Junho 2011 9

PEDRAS NEGRAS - PN	PN2

Estabelecido por: Instituto Hidrográfico **Data:** n.d.

Qualidade: Planimetria – I, Altimetria – I, Monumentação – I

Objectivo: Ponto de Referência + Cabeça de Perfil (PPN2)

Descrição: Chapa metálica com inscrição do Instituto Hidrográfico (IH) no topo do cilindro de betão; localizado no topo da duna a cerca de 50 m a sul do parque de estacionamento norte da praia das Pedras Negras.

M	P	H
-75921.220	13046.418	24.838

Sistema Coordenadas: PT-TM06 | Datum Vertical: NMM Cascais 1938 | medido em: 2011/02/02

Versão 1, Junho 2011 10

PEDRAS NEGRAS - PN	PN3

Estabelecido por: GeoFCUL (Tanya Silveira e Pedro Costa) **Data:** 2011/02/02

Qualidade: Planimetria – II, Altimetria – II, Monumentação – I

Objectivo: Ponto de Referência

Descrição: Spit no topo de um dos pilares de madeira que delimitam o passadiço longitudinal à praia. Localiza-se no parque de estacionamento norte da praia das Pedras Negras, e corresponde ao terceiro pilar a contar das escadas de acesso à praia.

M	P	H
-75918.365	13128.166	18.111

Sistema Coordenadas: PT-TM06 | Datum Vertical: NMM Cascais 1938 | medido em: 2011/02/02

Versão 1, Junho 2011 11

PEDRAS NEGRAS - PN	PN4

Estabelecido por: GeoFCUL (Tanya Silveira e Pedro Costa) **Data:** 2011/02/02

Qualidade: Planimetria – II, Altimetria – II, Monumentação – I

Objectivo: Ponto de Referência

Descrição: Spit no topo de um dos pilares de madeira que delimitam o passadiço longitudinal à praia. Localiza-se no parque de estacionamento norte da praia das Pedras Negras, e corresponde ao segundo pilar a contar do extremo sul do parque.

M	P	H
-75927.843	13116.644	18.053

Sistema Coordenadas: PT-TM06 | Datum Vertical: NMM Cascais 1938 | medido em: 2011/02/02

Versão 1, Junho 2011 12

PAREDES DE VITÓRIA - PV

Versão 1, Junho 2011

13

PAREDES DE VITÓRIA - PV	PV1

Estabelecido por: GeoFCUL (Tanya Silveira e Pedro Costa) **Data:** 2011/02/02

Qualidade: Planimetria – II, Altimetria – II, Monumentação – I

Objectivo: Ponto de Referência

Descrição: Spit na junção das lajes da calçada; localizado em frente ao Restaurante "Oceano Branco" e na direcção das escadas de acesso à praia.

M	P	H
-78568.872	4105.070	8.606

Sistema Coordenadas: PT-TM06 | Datum Vertical: NMM Cascais 1938 | medido em: 2011/02/02

Versão 1, Junho 2011 14

PAREDES DE VITÓRIA - PV	PV2

Estabelecido por: GeoFCUL (Tanya Silveira e Pedro Costa) **Data:** 2011/02/02

Qualidade: Planimetria – I, Altimetria – I, Monumentação – I

Objectivo: Ponto de Referência + Cabeça de Perfil (PPV2)

Descrição: Spit na base de cimento junto à tampa de saneamento quadrada; localizado em frente ao edifício novo localizado no extremo sul do paredão da praia.

M	P	H
-78589.622	4024.858	10.023

Sistema Coordenadas: PT-TM06 | Datum Vertical: NMM Cascais 1938 | medido em: 2011/02/02

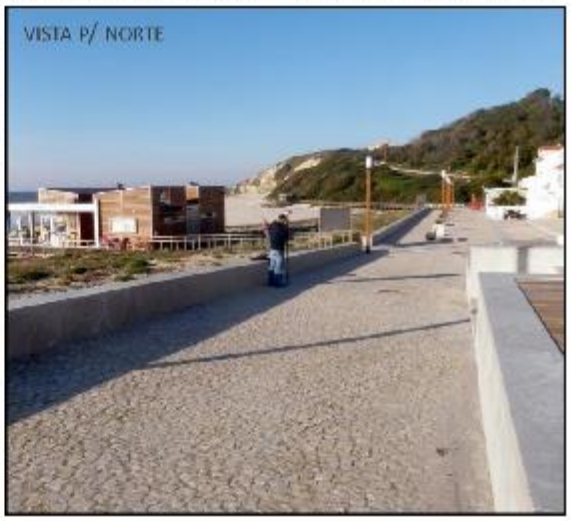

Versão 1, Junho 2011 15

PAREDES DE VITÓRIA - PV	PV3

Estabelecido por: GeoFCUL (Tanya Silveira e Pedro Costa) **Data:** 2011/02/02

Qualidade: Planimetria – II, Altimetria – II, Monumentação – I

Objectivo: Ponto de Referência

Descrição: Centro da marca (forma de pás de moinho) em alto relevo correspondente ao símbolo das "Águas do Oeste" na tampa de saneamento; localizada em frente ao caminho de acesso ao paredão.

M	P	H
-78573.471	4071.862	8.847

Sistema Coordenadas: PT-TM06 | Datum Vertical: NMM Cascais 1938 | medido em: 2011/02/02

Versão 1, Junho 2011 16

NAZARÉ - NZ

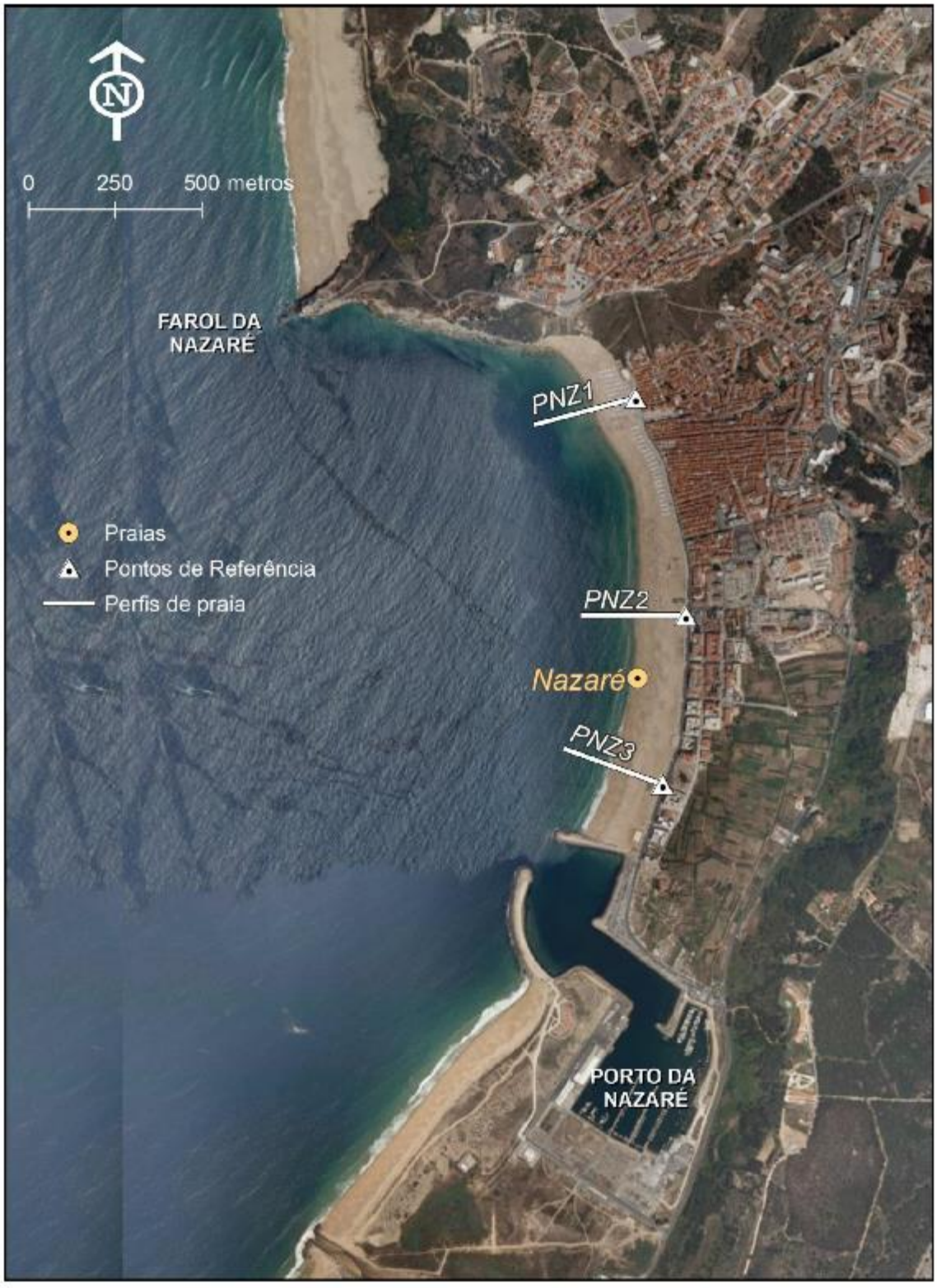

Versão 1, Junho 2011

17

NAZARÉ - NZ	NZ1

Estabelecido por: GeoFCUL (Tanya Silveira e Anabela Dias) **Data:** 2011/01/26

Qualidade: Planimetria – II, Altimetria – II, Monumentação – I

Objectivo: Ponto de Referência + Cabeça de Perfil (PNZ1)

Descrição: Spit entre lajes no lancil do paredão da praia; localizado em frente ao edifício da Capitania, entre porta azul e escadas de acesso à praia.

M	P	H
-80832.021	-6909.602	5.994

Sistema Coordenadas: PT-TM06 | Datum Vertical: NMM Cascais 1938 | medido em: 2011/02/02

Versão 1, Junho 2011 18

NAZARÉ - NZ	NZ2

Estabelecido por: GeoFCUL (Tanya Silveira e Pedro Costa) **Data:** 2011/02/02

Qualidade: Planimetria – II, Altimetria – II, Monumentação – I

Objectivo: Ponto de Referência + Cabeça de Perfil (PNZ2)

Descrição: Spit no lancil do paredão da praia; localizado entre dois cafés de praia, em frente ao Centro Cultural da Nazaré.

M	P	H
-80686.738	-7536.057	8.359

Sistema Coordenadas: PT-TM06 | Datum Vertical: NMM Cascais 1938 | medido em: 2011/02/02

Versão 1, Junho 2011 19

NAZARÉ - NZ	NZ3

Estabelecido por: GeoFCUL (Tanya Silveira e Pedro Costa) **Data:** 2011/02/02

Qualidade: Planimetria – I, Altimetria – I, Monumentação – I

Objectivo: Ponto de Referência + Cabeça de Perfil (PNZ3)

Descrição: Spit no lancil do paredão da praia; localizado entre dois cafés de praia, em frente à esquina norte do edifício "Dom Fuas", e a cerca de 200 m do esporão sul da Nazaré.

M	P	H
-80754.566	-8022.244	9.017

Sistema Coordenadas: PT-TM06 | Datum Vertical: NMM Cascais 1938 | medido em: 2011/02/02

Versão 1, Junho 2011 20

LAGOA DE ÓBIDOS - BALEAL – LOB

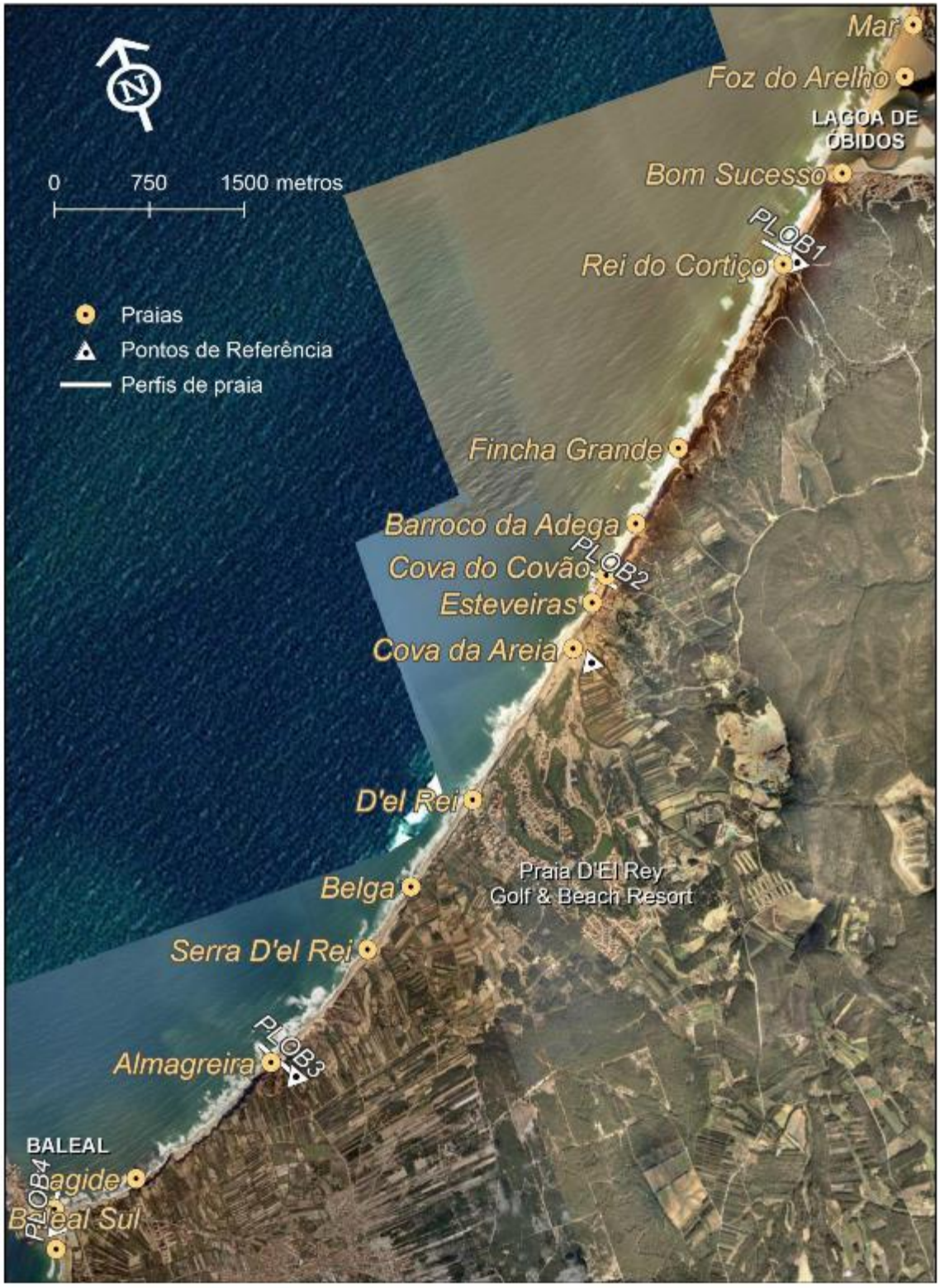

Versão 1, Junho 2011 21

LAGOA DE ÓBIDOS - BALEAL – LOB	RC1

Estabelecido por: GeoFCUL (Tanya Silveira e Rodrigo Ceia) **Data:** 2011/01/31

Qualidade: Planimetria – II, Altimetria – II, Monumentação – I

Objectivo: Ponto de Referência + Cabeça de Perfil (PLOB1)

Descrição: Cabeça de prego no topo de um tubo de PVC preenchido com argamassa; localizado no topo da arriba a cerca de 50 m para nordeste do acesso à praia do Rei do Cortiço.

M	P	H
-95799.123	-26851.971	21.341

Sistema Coordenadas: PT-TM06 | Datum Vertical: NMM Cascais 1938 | medido em: 2011/06/14

Versão 1, Junho 2011 22

LAGOA DE ÓBIDOS - BALEAL – LOB	CA1

Estabelecido por: GeoFCUL (Tanya Silveira e Rodrigo Ceia) **Data:** 2011/01/31

Qualidade: Planimetria – I, Altimetria – I, Monumentação – I

Objectivo: Ponto de Referência

Descrição: Cabeça de prego no topo de um dos postes de madeira que delimitam o parque de estacionamento; localizado no canto noroeste do parque de estacionamento da praia da Cova da Areia na Urbanização "Praia D'el Rei".

M	P	H
-98385.811	-29301.041	5.996

Sistema Coordenadas: PT-TM06 | Datum Vertical: NMM Cascais 1938 | medido em: 2011/01/31

Versão 1, Junho 2011 23

LAGOA DE ÓBIDOS - BALEAL – LOB	ALM2

Estabelecido por: GeoFCUL (Tanya Silveira e Rodrigo Ceia) **Data:** 2011/01/31

Qualidade: Planimetria – I, Altimetria – I, Monumentação – I

Objectivo: Ponto de Referência + Cabeça de Perfil (PLOB3)

Descrição: Cabeça de prego no topo de estaca de madeira; localizada perto de um caminho de terra à direita do acesso principal à praia da Almagreira.

M	P	H
-101679.187	-31611.820	31.622

Sistema Coordenadas: PT-TM06 | Datum Vertical: NMM Cascais 1938 | medido em: 2011/01/31

Versão 1, Junho 2011 24

BALEAL - PENICHE – BP

Versão 1, Junho 2011 25

BALEAL - PENICHE – BP	BP1

Estabelecido por: GeoFCUL (Tanya Silveira e Tiago Silva) **Data:** 2011/02/09

Qualidade: Planimetria – II, Altimetria – II, Monumentação – I

Objectivo: Ponto de Referência + Cabeça de Perfil (PBP1) + Cabeça de Perfil (PLOB4)

Descrição: Spit no lancil de dentro na estrada que atravessa a praia do Baleal, fazendo a ligação entre Casais do Baleal e Baleal (Rua Francisco Silvestre); localizado perto do 2º poste de iluminação e da 2ª tampa de saneamento a contar de este.

M	P	H
-103863.726	-32102.105	3.783

Sistema Coordenadas: PT-TM06 | Datum Vertical: NMM Cascais 1938 | medido em: 2011/02/09

Versão 1, Junho 2011 26

BALEAL - PENICHE – BP	BP2

Estabelecido por: GeoFCUL (Tanya Silveira e Tiago Silva) **Data:** 2011/02/09

Qualidade: Planimetria – I, Altimetria – I, Monumentação – I

Objectivo: Ponto de Referência

Descrição: Prego entre pedras da calçada no canto norte do parque de estacionamento da praia do Baleal junto ao Restaurante "Algamar" e perto das escadas de acesso à praia.

M	P	H
-103794.640	-32191.303	8.224

Sistema Coordenadas: PT-TM06 | Datum Vertical: NMM Cascais 1938 | medido em: 2011/02/09

Versão 1, Junho 2011 27

BALEAL - PENICHE – BP	BP3

Estabelecido por: GeoFCUL (Tanya Silveira e Tiago Silva) **Data:** 2011/02/09

Qualidade: Planimetria – I, Altimetria – I, Monumentação – I

Objectivo: Ponto de Referência

Descrição: Cabeça de prego no topo da estaca de madeira que delimita o acesso ao parque de estacionamento do bar da praia da Gambôa; 2º poste a contar do bar, na fiada oeste de postes.

M	P	H
-106838.356	-33080.596	4.259

Sistema Coordenadas: PT-TM06 | Datum Vertical: NMM Cascais 1938 | medido em: 2011/02/09

Versão 1, Junho 2011 28

BALEAL - PENICHE – BP	BP4

Estabelecido por: GeoFCUL (Tanya Silveira e Tiago Silva) **Data:** 2011/02/09

Qualidade: Planimetria – II, Altimetria – II, Monumentação – I

Objectivo: Ponto de Referência

Descrição: Spit no terraço do edifício amarelo da Marinha, localizado a sul do Forte de Peniche, na praia da Gambôa.

M	P	H
-106876.884	-32948.331	3.598

Sistema Coordenadas: PT-TM06 | Datum Vertical: NMM Cascais 1938 | medido em: 2011/02/09

Versão 1, Junho 2011 29


STA. CRUZ - SC
N
0
250
500 metros
Praias
Pontos de Referência
Perfis de praia
Seixo
Mexeloeira
Amanhã/Vigia
PSC1
Navio
Mirante
PSC2
Pisão
Física
Centro
PSC3
Parque de Campismo
Santa Helena
Guincho
Sul
SANTA CRUZ
Formosa
Amoeiras
Versão 1, Junho 2011
30

STA. CRUZ - SC	SC1

Estabelecido por: GeoFCUL (Tanya Silveira e Tiago Silva) **Data:** 2011/02/09

Qualidade: Planimetria – I, Altimetria – I, Monumentação – I

Objectivo: Ponto de Referência

Descrição: Spit no 1º lancil das escadas que ligam a povoação no topo da arriba à praia do Mirante; imediatamente a norte da escola de surf "35".

M	P	H
-107506.156	-57682.713	10.756

Sistema Coordenadas: PT-TM06 | Datum Vertical: NMM Cascais 1938 | medido em: 2011/02/09

Versão 1, Junho 2011 31

STA. CRUZ - SC	SC2

Estabelecido por: GeoFCUL (Tanya Silveira e Tiago Silva) **Data:** 2011/02/09

Qualidade: Planimetria – II, Altimetria – II, Monumentação – I

Objectivo: Ponto de Referência + Cabeça de Perfil (PSC2)

Descrição: Cabeça de prego no topo da estaca de madeira (com topo metálico), localizado na cerca que limita o parque de estacionamento da praia do Mirante; 3º poste para sul a contar do 1º passadiço de madeira a norte da escola de surf "35".

M	P	H
-107476.004	-57626.850	11.944

Sistema Coordenadas: PT-TM06 | Datum Vertical: NMM Cascais 1938 | medido em: 2011/05/19

Versão 1, Junho 2011 32

Coxos - CX

Versão 1, Junho 2011 33

Coxos - CX	CX1

Estabelecido por: GeoFCUL (Tanya Silveira e Alexandra Oliveira) **Data:** 2011/01/28

Qualidade: Planimetria – I, Altimetria – I, Monumentação – I

Objectivo: Ponto de Referência

Descrição: Cabeça de prego no topo de estaca de madeira que faz parte da cerca que delimita o parque de estacionamento da praia dos Coxos; localiza-se no canto norte do parque, no 1º poste a este da lacuna na cerca, perto do caixote do lixo.

M	P	H
-112063.386	-72899.981	19.789

Sistema Coordenadas: PT-TM06 | Datum Vertical: NMM Cascais 1938 | medido em: 2011/01/28

Versão 1, Junho 2011 34

Coxos - CX	CX2

Estabelecido por: GeoFCUL (Tanya Silveira e Alexandra Oliveira) **Data:** 2011/01/28

Qualidade: Planimetria – II, Altimetria – II, Monumentação – I

Objectivo: Ponto de Referência

Descrição: Spit na base de cimento junto a tampa metálica localizada à entrada da estrada que faz o acesso do parque de estacionamento à praia.

M	P	H
-112030.773	-72934.640	18.058

Sistema Coordenadas: PT-TM06 | Datum Vertical: NMM Cascais 1938 | medido em: 2011/05/19

Versão 1, Junho 2011 35

BALEIA/SUL - BS

Versão 1, Junho 2011

36

BALEIA/SUL - BS	BS1

Estabelecido por: GeoFCUL (Tanya Silveira e Alexandra Oliveira) **Data:** 2011/01/28

Qualidade: Planimetria – II, Altimetria – II, Monumentação – I

Objectivo: Ponto de Referência + Cabeça de Perfil (PBS1)

Descrição: Spit no muro que delimita o paredão da praia; localizado em frente ao segundo restaurante/bar a contar de norte.

M	P	H
-111159.323	-77998.731	6.668

Sistema Coordenadas: PT-TM06 | Datum Vertical: NMM Cascais 1938 | medido em: 2011/01/28

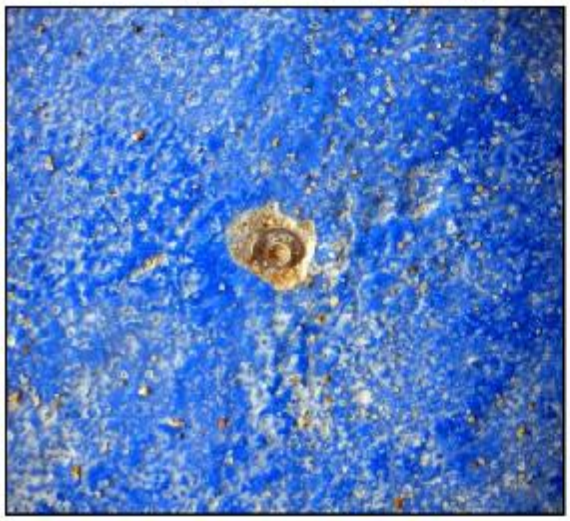

Versão 1, Junho 2011 37

BALEIA/SUL - BS	BS2

Estabelecido por: GeoFCUL (Tanya Silveira e Alexandra Oliveira) **Data:** 2011/01/28

Qualidade: Planimetria – II, Altimetria – II, Monumentação – I

Objectivo: Ponto de Referência + Cabeça de Perfil (PBS2)

Descrição: Spit no muro que delimita o paredão da praia; localizado cerca de 40 m a sul do esporão central da praia e imediatamente a norte do antigo duche forrado a pedra na base da escarpa.

M	P	H
-111144.520	-78138.761	6.816

Sistema Coordenadas: PT-TM06 | Datum Vertical: NMM Cascais 1938 | medido em: 2011/01/28

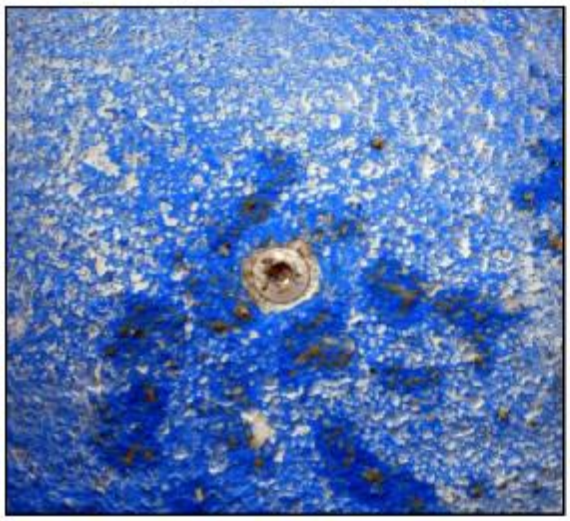

Versão 1, Junho 2011 38

BALEIA/SUL - BS	BS3

Estabelecido por: GeoFCUL (Tanya Silveira e Alexandra Oliveira) **Data:** 2011/01/28

Qualidade: Planimetria – I, Altimetria – I, Monumentação – I

Objectivo: Ponto de Referência + Cabeça de Perfil (PBS3)

Descrição: Spit no lancil de um dos degraus da escadaria que ladeia o acesso sul à praia; localizado perto da curva, a cerca de 30 m da base da escadaria.

M	P	H
-111176.859	-78307.692	10.128

Sistema Coordenadas: PT-TM06 | Datum Vertical: NMM Cascais 1938 | medido em: 2011/01/28

Versão 1, Junho 2011 39

MAGOITO - MG

Versão 1, Junho 2011

40

MAGOITO - MG	MG1

Estabelecido por: GeoFCUL (Tanya Silveira e Bárbara Proença) **Data:** 2011/02/07

Qualidade: Planimetria – I, Altimetria – I, Monumentação – I

Objectivo: Ponto de Referência

Descrição: Spit no lancil do passeio; localizado na curva junto ao acesso norte à praia, perto do bar da praia.

M	P	H
-114271.196	-88326.318	29.292

Sistema Coordenadas: PT-TM06 | Datum Vertical: NMM Cascais 1938 | medido em: 2011/02/07

Versão 1, Junho 2011 41

MAGOITO - MG	MG2

Estabelecido por: GeoFCUL (Tanya Silveira e Bárbara Proença) **Data:** 2011/02/07

Qualidade: Planimetria – II, Altimetria – II, Monumentação – I

Objectivo: Ponto de Referência

Descrição: Spit no topo de poste de madeira; 2º poste a contar de norte da fiada que ladeia o passeio no parque de estacionamento sul da praia do Magoito.

M	P	H
-114202.457	-88382.633	35.425

Sistema Coordenadas: PT-TM06 | Datum Vertical: NMM Cascais 1938 | medido em: 2011/02/07

Versão 1, Junho 2011 42

MAGOITO - MG	MG3

Estabelecido por: GeoFCUL (Tanya Silveira e Bárbara Proença) **Data:** 2011/02/07

Qualidade: Planimetria – II, Altimetria – II, Monumentação – I

Objectivo: Ponto de Referência

Descrição: Spit no lancil do passeio; localizado na esquina sul do parque de estacionamento sul da praia do Magoito, junto ao acesso à praia.

M	P	H
-114192.277	-88427.158	32.114

Sistema Coordenadas: PT-TM06 | Datum Vertical: NMM Cascais 1938 | medido em: 2011/02/07

Versão 1, Junho 2011 43

TAMARIZ - TM

Versão 1, Junho 2011

44

TAMARIZ - TM	TM1

Estabelecido por: n.d. **Data:** n.d.

Qualidade: Planimetria – II, Altimetria – II, Monumentação – I

Objectivo: Ponto de Referência

Descrição: Chapa metálica no lancil do paredão da praia; localizada em frente ao restaurante "La Villa", a cerca de 5 m para este das escadas de acesso à praia .

M	P	H
-110250.363	-106406.868	5.057

Sistema Coordenadas: PT-TM06 | Datum Vertical: NMM Cascais 1938 | medido em: 2011/02/07

Versão 1, Junho 2011 45

TAMARIZ - TM	TM2 (=TM00)

Estabelecido por: GeoFCUL (Tanya Silveira e Bárbara Proença) **Data:** 2011/02/07

Qualidade: Planimetria – I, Altimetria – I, Monumentação – I

Objectivo: Ponto de Referência

Descrição: Spit na pedra da calçada do esporão no extremo este da praia, a cerca de 70 m do paredão da praia.

M	P	H
-110073.823	-106522.655	3.614

Sistema Coordenadas: PT-TM06 | Datum Vertical: NMM Cascais 1938 | medido em: 2011/02/07

Versão 1, Junho 2011 46

QUADRO SÍNTESE

Quadro V: Coordenadas planimétricas (M e P) e elevação (H) dos pontos de referência (PR) e, cabeças de perfis (CP) e respectivos rumos geográficos (Az). (PT-TM06 | NMM Cascais 1938)

Ponto	Tipo	Perfil	Az	M	P	H
Pedras Negras – PN						
PN1	PR | CP	PPN1	295	-75755.884	13501.599	14.576
PN2	PR | CP	PPN2	295	-75921.220	13046.418	24.838
PN3	PR |	-	-	-75918.365	13128.166	18.111
PN4	PR |	-	-	-75927.843	13116.644	18.053
Paredes de Vitória – PV						
PV1	PR |	-	-	-78568.872	4105.070	8.606
-	| CP	PPV1	265	-78591.556	4523.039	-
PV2	PR | CP	PPV2	285	-78589.622	4024.858	10.023
PV3	PR |	-	-	-78573.471	4071.862	8.847
-	| CP	PPV3	295	-78777.223	3512.981	-
Nazaré – NZ						
NZ1	PR | CP	PNZ1	255	-80832.021	-6909.602	5.994
NZ2	PR | CP	PNZ2	270	-80686.738	-7536.057	8.359
NZ3	PR | CP	PNZ3	290	-80754.566	-8022.244	9.017
Lagoa de Óbidos-Baleal – LOB						
RC1	PR | CP	PLOB1	320	-95799.123	-26851.971	21.341
CA1	PR |	-	-	-98385.811	-29301.041	5.996
-	| CP	PLOB2	320	-97990.940	-28832.684	-
ALM2	PR | CP	PLOB3		-101679.187	-31611.820	31.622
-	| CP	PLOB4	25	-103863.772	-32102.093	3.783
Baleal-Peniche – BP						
BP1	PR | CP	PBP1	230	-103863.726	-32102.105	3.783
BP2	PR |	-	-	-103794.640	-32191.303	8.224
-	| CP	PBP2	320	-103900.851	-33200.232	-
-	| CP	PBP3	340	-104841.921	-33767.972	-
-	| CP	PBP4	10	-106014.011	-33618.308	-
-	| CP	PBP5	40	-106749.809	-33183.761	-
BP3	PR |	-	-	-106838.356	-33080.596	4.259
BP4	PR |	-	-	-106876.884	-32948.331	3.598

QUADRO SÍNTESE

Quadro V (cont.): Coordenadas planimétricas (M e P) e elevação (H) dos pontos de referência (PR) e, cabeças de perfis (CP) e respectivos rumos geográficos (Az). (PT-TM06 | NMM Cascais 1938)

Ponto	Tipo	Perfil	Az	M	P	H
Sta. Cruz – SC						
-	| CP	PSC1	305	-107071.158	-57051.786	-
SC1	PR |	-	-	-107506.156	-57682.713	10.756
SC2	PR | CP	PSC2	305	-107476.004	-57626.850	11.944
-	| CP	PSC3	305	-107876.843	-58280.405	-
Coxos – CX						
CX1	PR |	-	-	-112063.386	-72899.981	19.789
CX2	PR |	-	-	-112030.773	-72934.640	18.058
-	| CP	PCX1	320	-111895.967	-72963.583	-
Baleia/Sul – BS						
BS1	PR | CP	PBS1	260	-111159.323	-77998.731	6.668
BS2	PR | CP	PBS2	270	-111144.520	-78138.761	6.816
BS3	PR | CP	PBS3	305	-111176.859	-78307.692	10.128
Magoito – MG						
MG1	PR |	-	-	-114271.196	-88326.318	29.292
MG2	PR |	-	-	-114202.457	-88382.633	35.425
MG3	PR |	-	-	-114192.277	-88427.158	32.114
-	| CP	PMG1	270	-114154.937	-88481.537	-
-	| CP	PMG2	290	-114219.248	-88766.367	-
-	| CP	PMG3	300	-114335.373	-88998.597	-
Tamariz – TM						
TM1	PR |	-	-	-110250.363	-106406.868	5.057
TM2 (=TM00)	PR |	-	-	-110073.823	-106522.655	3.614
-	| CP	PTM1	200	-110359.167	-106360.378	-
-	| CP	PTM2	185	-110189.747	-106395.398	-
-	| CP	PTM3	205	-110111.883	-106403.700	-
-	| CP	PTM4	225	-110049.559	-106442.212	-

Criação e implementação de um sistema de monitorização no litoral abrangido pela área de jurisdição da Administração da Região Hidrográfica do Tejo, I.P.

Livro de Campo

Rede Espacial de Pontos de Referência e Cabeças de Perfil para o Litoral abrangido pela área de jurisdição da Administração da Região Hidrográfica do Tejo, I.P.

II. Cova do Vapor - Cabo Espichel

Versão 1, Junho 2011

ÍNDICE

INTRODUÇÃO

OBJECTIVO DO LIVRO DE CAMPO

Este "Livro de Campo" tem como objectivo caracterizar a rede de pontos de referência definidos no litoral abrangido pela área de jurisdição da Administração da Região Hidrográfica (ARH) do Tejo, I.P, entre a Cova do Vapor e o Cabo Espichel, para apoio à realização de levantamentos topográficos, nomeadamente perfis de praia, e áreas de levantamento topográfico total no caso da praia de São João da Caparica. Identificam-se também as localizações e rumos de perfis de praia, objecto de monitorização de projectos desenvolvidos pelo Departamento de Geologia da Faculdade de Ciências e Centro de Geologia da Universidade de Lisboa (GeoFCUL e CeGUL), em colaboração com a ARH do Tejo, I.P.. Contém ainda um guia de nomenclatura e códigos de identificação de praias, perfis e objectos notáveis para utilização em trabalho de campo, contribuindo para a uniformização de futuras bases de dados.

As coordenadas cartográficas dos pontos de referência, bem como dos pontos iniciais dos perfis de praia (cabeças de perfil), são apresentados num quadro síntese no final do livro de campo, no sistema PT-TM06 (Quadro V). A informação acerca dos pontos de referência e perfis de praia está também disponível em formato *shapefile* (ESRI) com metadados associados, como anexo a este documento. O presente livro e anexos estão sujeitos a revisões e actualizações. O número da versão é identificado no nome dos ficheiros (e na capa e rodapé das páginas do livro) e todas as alterações feitas são documentadas, sob a forma de um histórico, no Quadro IV.

PONTOS DE REFERÊNCIA

O livro é constituído por um conjunto de fichas. Cada ficha caracteriza um ponto de referência – pontos fixos e materializados no terreno por objectos específicos, naturais ou implantados, com coordenadas planimétricas e altimétrica muito bem conhecidas. Cada ficha inclui no seu título (barra superior), o nome do troço das praias onde o ponto de referência se localiza, e um código único de identificação. No caso da praia de São João da Caparica, troço da Costa da Caparica e praia da Lagoa de Albufeira, indica-se ainda as designações adoptadas em projectos anteriores. Os outros elementos constituintes da ficha são:

- Fonte dos dados: corresponde ao nome da instituição (GeoFCUL ou DEGGE - Departamento de Engenharia Geográfica, Geofísica e Energia) e, quando possível, dos operadores que estabeleceram o ponto de referência;
- Data do estabelecimento do ponto de referência;
- Qualidade do ponto de referência, relativamente à planimetria (M e P), posição altimétrica (H) e monumentação ou materialização (ver Quadro I);
- Objectivo do ponto: ponto de referência e quando aplicável, cabeça de perfil;
- Descrição da localização e das características do ponto de referência;
- Tabela com as coordenadas planimétricas (M e P) e elevação (H) do ponto (em unidades métricas);
- Informação iconográfica:
  - ✓ Imagem de conjunto orientada, com recurso a ortofotografias ou outras bases cartográficas recentes, que permite a visualização da localização espacial dos pontos de referência e, quando aplicável, apresenta a(s) linha(s) de perfil de praia;
  - ✓ Registo fotográfico, que inclui duas fotografias terrestres mostrando a área envolvente e uma imagem de pormenor da materialização do ponto.

INTRODUÇÃO

A qualidade do ponto de referência é definida segundo o seu posicionamento absoluto (M, P e H) e a sua monumentação ou materialização. Os pontos foram estabelecidos com recurso a equipamento de sistema e posicionamento global (GPS). Assim, a classificação planimétrica e altimétrica depende do modo de observação (modo estático ou modo cinemático) e do processamento dos dados (em pós-processamento ou em tempo real). Na determinação da qualidade da monumentação, considera-se a sua estabilidade, durabilidade e acessibilidade. O quadro I resume essas classificações.

Quadro I: Qualidade do ponto de referência.

Qualidade		Classe	Precisão	Descrição
Posicionamento	planimétrica	I	1 a 2 cm	• ponto medido em modo estático com pós-processamento • observações > 20 minutos
		II	2 a 5 cm	• ponto medido em tempo real (DGPS/ RTK)
	altimétrica	I	≈ 5 cm	• ponto medido em modo estático com pós-processamento • com recurso a marcas com altimetria de precisão nas proximidades da medição do ponto
		II	7 a 10 cm	• ponto medido em tempo real (DGPS/ RTK)
Monumentação		I	Alta	• marcas permanentes ao nível do solo ou sobre construções estáveis • elementos proeminentes sobre construções estáveis • pontos em locais de fácil acesso
		II	Média	• marcas provisórias no solo • pontos em locais menos protegidos
		III	Baixa	• marcas materializadas em estruturas não permanentes ou de estabilidade duvidosa

GUIA DE NOMENCLATURA NO TRABALHO DE CAMPO

O guia de nomenclatura inclui uma lista de códigos aplicáveis ao nome do trabalho, que permitem identificar a data do levantamento, o servidor utilizado em modo "tempo real", o operador e o nome da praia (Quadro II), e uma lista de códigos associados às medições, que permitem identificar o perfil de praia e os pontos medidos (por exemplo: topografia, local de recolha de sedimentos, local de aquisição de fotografias, etc.), bem como os limites ou elementos lineares medidos (por exemplo: crista de berma, limite do espraio ou da vegetação, etc.) (Quadro III).

Quadro II: Guia de nomenclatura dos trabalhos e medições.

		Código	Exemplo
Trabalho		*Código de praia | data (aaaammdd) | servidor | operador*	RA20110306Rpa
Medição	Perfil de praia	*Código de perfil*	PRA1
	Limite ou ponto	*Código de leitura*	UESP

INTRODUÇÃO

Quadro III: Lista de códigos de medição.

Grupo de Código	Código	Descrição do código
Geral	TOPO	Levantamento topográfico indiferenciado
	CBER	Crista da berma
	VEG	Limite da vegetação
	BDUN	Base da duna primária
	CDUN	Crista da duna primária
	BARR	Base da arriba
	UESP	Limite do espraio das ondas referente à preia-mar precedente (última)
	MESP	Limite máximo do espraio das ondas
	SED	Localização de recolha de amostra de sedimentos
	FOTO	Localização de aquisição de fotografia
	TEST	Topo de estrutura
	BEST	Base de estrutura
Exemplos (os códigos de cada praia, pontos de referência e perfis de praia encontram-se nas fichas seguintes):		
Praia A	PA1	Ponto de Referência 1 da Praia A
	PA2	Ponto de Referência 2 da Praia A
	PPA1	Perfil de praia 1 da Praia A
Praia B	PB1	Ponto de Referência 1 da Praia B
	PB2	Ponto de Referência 2 da Praia B
	PPB1	Perfil de praia 1 da Praia B

INTRODUÇÃO

Quadro IV: Lista das versões e alterações ao Livro de Campo.

Versão	Data	Comentários
V1	Junho 2011	1º livro de campo após colocação e georreferenciação dos pontos de referência.

ENQUADRAMENTO GERAL

Versão 1, Junho 2011

7

COSTA DA CAPARICA - CC

Versão 1, Junho 2011

8

COSTA DA CAPARICA	SÃO JOÃO DA CAPARICA (SJC)

Versão 1, Junho 2011 9

COSTA DA CAPARICA	**CC1** (= PT01)

Estabelecido por: DEGGE FCUL (Carlos Antunes) **Data:** 2010/01/18

Qualidade: Planimetria – II, Altimetria – I, Monumentação – I

Objectivo: Ponto de Referência

Descrição: Spit no bloco de calcário, salpicado de tinta verde, no início e berma do esporão que limita a norte a praia de São João da Caparica.

M	P	H
-97757.9342	-111173.9482	6.025

Sistema Coordenadas: PT-TM06 | Datum Vertical: NMM Cascais 1938 | medido em: 2010/11/30

Versão 1, Junho 2011 10

COSTA DA CAPARICA	CC2 (= SP7)

Estabelecido por: DEGGE FCUL (Carlos Antunes) **Data:** 2010/01/18

Qualidade: Planimetria – II, Altimetria – I, Monumentação – I

Objectivo: Ponto de Referência

Descrição: Spit no final do esporão 7, que limita a sul a praia de São João da Caparica.

M	P	H
-97004.9348	-112340.8730	3.489

Sistema Coordenadas: PT-TM06 | Datum Vertical: NMM Cascais 1938 | medido em: 2010/11/30

Versão 1, Junho 2011 11

COSTA DA CAPARICA	CC3 (=SP6)

Estabelecido por: DEGGE FCUL (Carlos Antunes) **Data:** 2010/01/18

Qualidade: Planimetria – II, Altimetria – I, Monumentação – I

Objectivo: Ponto de Referência

Descrição: Spit no esporão 6, aproximadamente na secção central do mesmo, em frente ao bar "Sentido do Mar".

M	P	H
-96850.0367	-112640.9367	3.049

Sistema Coordenadas: PT-TM06 | Datum Vertical: NMM Cascais 1938 | medido em: 2010/11/30

COSTA DA CAPARICA	CC4 (=SP1)

Estabelecido por: DEGGE FCUL (Carlos Antunes) **Data:** 2010/01/18

Qualidade: Planimetria – II, Altimetria – I, Monumentação – I

Objectivo: Ponto de Referência

Descrição: Spit no esporão 1, aproximadamente na secção central do mesmo, em frente à pizzaria "Da Wave".

M	P	H
-95929.1212	-114022.1041	3.374

Sistema Coordenadas: PT-TM06 | Datum Vertical: NMM Cascais 1938 | medido em: 2010/11/30

COSTA DA CAPARICA	CC9 (= SP67)

Estabelecido por: DEGGE FCUL (Carlos Antunes) **Data:** 2010/01/18

Qualidade: Planimetria – II, Altimetria – I, Monumentação – I

Objectivo: Ponto de Referência + Cabeça de Perfil (PCC9)

Descrição: Spit num dos blocos de pedra do molhe aderente, entre o esporão 7 e o esporão 6, em frente do bar "Tasca do Leandro".

M	P	H
-96817.2461	-112426.5832	6.361

Sistema Coordenadas: PT-TM06 | Datum Vertical: NMM Cascais 1938 | medido em: 2010/11/30

Versão 1, Junho 2011 14

COSTA DA CAPARICA	**CC10** (= SP56)

Estabelecido por: DEGGE FCUL (Carlos Antunes) **Data:** 2010/01/18

Qualidade: Planimetria – II, Altimetria – I, Monumentação – I

Objectivo: Ponto de Referência + Cabeça de Perfil (PCC10)

Descrição: Spit num dos blocos do molhe aderente, entre o esporão 6 e o esporão 5, próximo das escadas de acesso ao areal e em frente ao restaurante-bar "Costa Nova".

M	P	H
-96661.3122	-112720.5111	6.396

Sistema Coordenadas: PT-TM06 | Datum Vertical: NMM Cascais 1938 | medido em: 2010/11/30

COSTA DA CAPARICA	CC11 (= SP45)

Estabelecido por: DEGGE FCUL (Carlos Antunes) **Data:** 2010/01/18

Qualidade: Planimetria – II, Altimetria – I, Monumentação – I

Objectivo: Ponto de Referência + Cabeça de Perfil (PCC11)

Descrição: Spit num dos blocos do molhe aderente, entre o esporão 5 e o esporão 4, próximo da entrada das escadas de acesso ao areal e do bar "O Barbas".

M	P	H
-96519.9716	-112985.7927	6.313

Sistema Coordenadas: PT-TM06 | Datum Vertical: NMM Cascais 1938 | medido em: 2010/11/18

Versão 1, Junho 2011 16

COSTA DA CAPARICA	CC12 (= SP34)

Estabelecido por: DEGGE FCUL (Carlos Antunes) **Data:** 2010/01/18

Qualidade: Planimetria – II, Altimetria – I, Monumentação – I

Objectivo: Ponto de Referência + Cabeça de Perfil (PCC12)

Descrição: Spit num dos blocos do molho aderente, entre o esporão 4 e o esporão 3, próximo das escadas de acesso ao areal e do restaurante-bar "Tarquínio".

M	P	H
-96265.2537	-113311.9021	5.973

Sistema Coordenadas: PT-TM06 | Datum Vertical: NMM Cascais 1938 | medido em: 2010/11/30

COSTA DA CAPARICA	CC13 (= SP23)

Estabelecido por: DEGGE FCUL (Carlos Antunes) **Data:** 2010/01/18

Qualidade: Planimetria – II, Altimetria – I, Monumentação – I

Objectivo: Ponto de Referência + Cabeça de Perfil (PCC13)

Descrição: Spit num dos blocos do molhe aderente, entre o esporão 3 e o esporão 2, próximo das escadas de acesso à praia.

M	P	H
-96111.4791	-113570.0182	5.958

Sistema Coordenadas: PT-TM06 | Datum Vertical: NMM Cascais 1938 | medido em: 2010/11/30

Versão 1, Junho 2011 18

RAINHA - RA

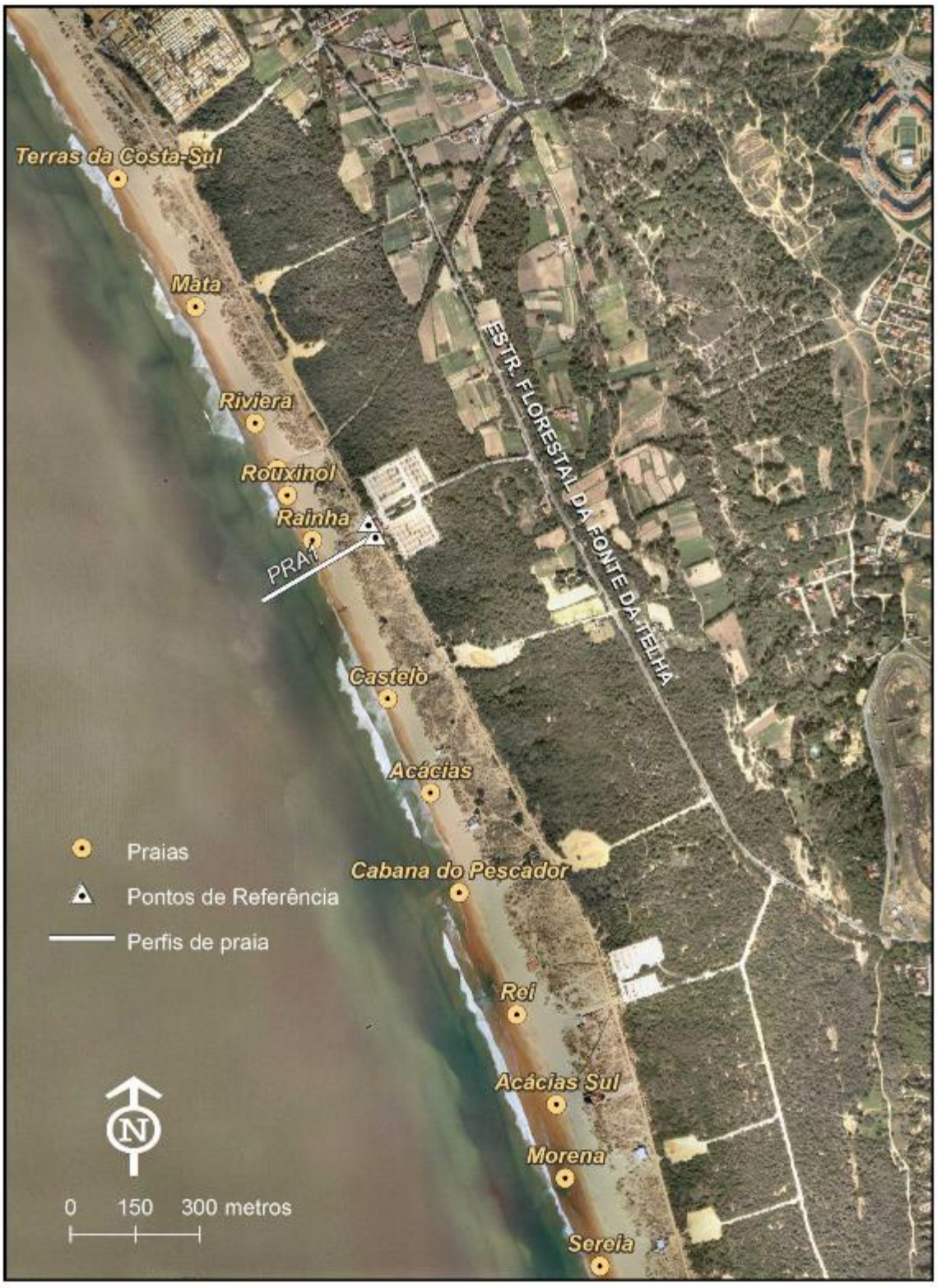

Versão 1, Junho 2011 19

RAINHA	RA1

Estabelecido por: GeoFCUL (Tanya Silveira e Mafalda Carapuço) **Data:** 2011/02/11

Qualidade: Planimetria – II, Altimetria – II, Monumentação – I

Objectivo: Ponto de Referência + Cabeça de Perfil (PRA1)

Descrição: Cabeça do prego no topo da estaca de madeira, junto à linha férrea e próximo do canto sul do restaurante "Queen's Beach Club".

M	P	H
-94392.6800	-116207.5077	5.345

Sistema Coordenadas: PT-TM06 | Datum Vertical: NMM Cascais 1938 | medido em: 2011/02/11

Versão 1, Junho 2011 20

RAINHA	RA2

Estabelecido por: DEGGE FCUL (Carlos Antunes) **Data:** 2008/01/11

Qualidade: Planimetria – II, Altimetria – II, Monumentação – I

Objectivo: Ponto de Referência

Descrição: Spit na intersecção das lajes de mosaico no caminho de acesso à praia pelo restaurante "Queen's Beach Club", próximo da passagem da linha férrea.

M	P	H
-94409.1778	-116179.0566	5.209

Sistema Coordenadas: PT-TM06 | Datum Vertical: NMM Cascais 1938 | medido em: 2011/02/11

Versão 1, Junho 2011 21

FONTE DA TELHA - FT

Versão 1, Junho 2011

22

FONTE DA TELHA	FT1

Estabelecido por: GeoFCUL (Tanya Silveira e Mafalda Carapuço) **Data:** 2011/02/11

Qualidade: Planimetria – II, Altimetria – II, Monumentação – II

Objectivo: Ponto de Referência + Cabeça de Perfil (PFT1)

Descrição: Cabeça do prego no topo da estaca de madeira localizada na duna, a sul do restaurante "Cabana Beach Bar".

M	P	H
-92556.3384	-121283.7045	9.639

Sistema Coordenadas: PT-TM06 | Datum Vertical: NMM Cascais 1938 | medido em: 2011/02/11

Versão 1, Junho 2011 23

FONTE DA TELHA	FT2

Estabelecido por: GeoFCUL (Tanya Silveira e Mafalda Carapuço) **Data:** 2011/02/11

Qualidade: Planimetria – II, Altimetria – II, Monumentação – I

Objectivo: Ponto de Referência

Descrição: Cabeça do prego no topo de estaca de madeira, localizado junto ao lado noroeste do bar "Ineditu's Klub".

M	P	H
-92447.5362	-121512.4800	9.880

Sistema Coordenadas: PT-TM06 | Datum Vertical: NMM Cascais 1938 | medido em: 2011/02/11

Versão 1, Junho 2011 24

FONTE DA TELHA	FT3

Estabelecido por: GeoFCUL (Tanya Silveira e Mafalda Carapuço) **Data:** 2011/02/11

Qualidade: Planimetria – II, Altimetria – II, Monumentação – I

Objectivo: Ponto de Referência

Descrição: Cabeça do prego no topo de estaca de madeira, junto ao poste de bandeira e a cerca de 30 metros para norte de FT2, do lado oposto da estrada.

M	P	H
-92436.0698	-121489.5307	10.575

Sistema Coordenadas: PT-TM06 | Datum Vertical: NMM Cascais 1938 | medido em: 2011/02/11

Versão 1, Junho 2011 25

LAGOA DE ALBUFEIRA - LA

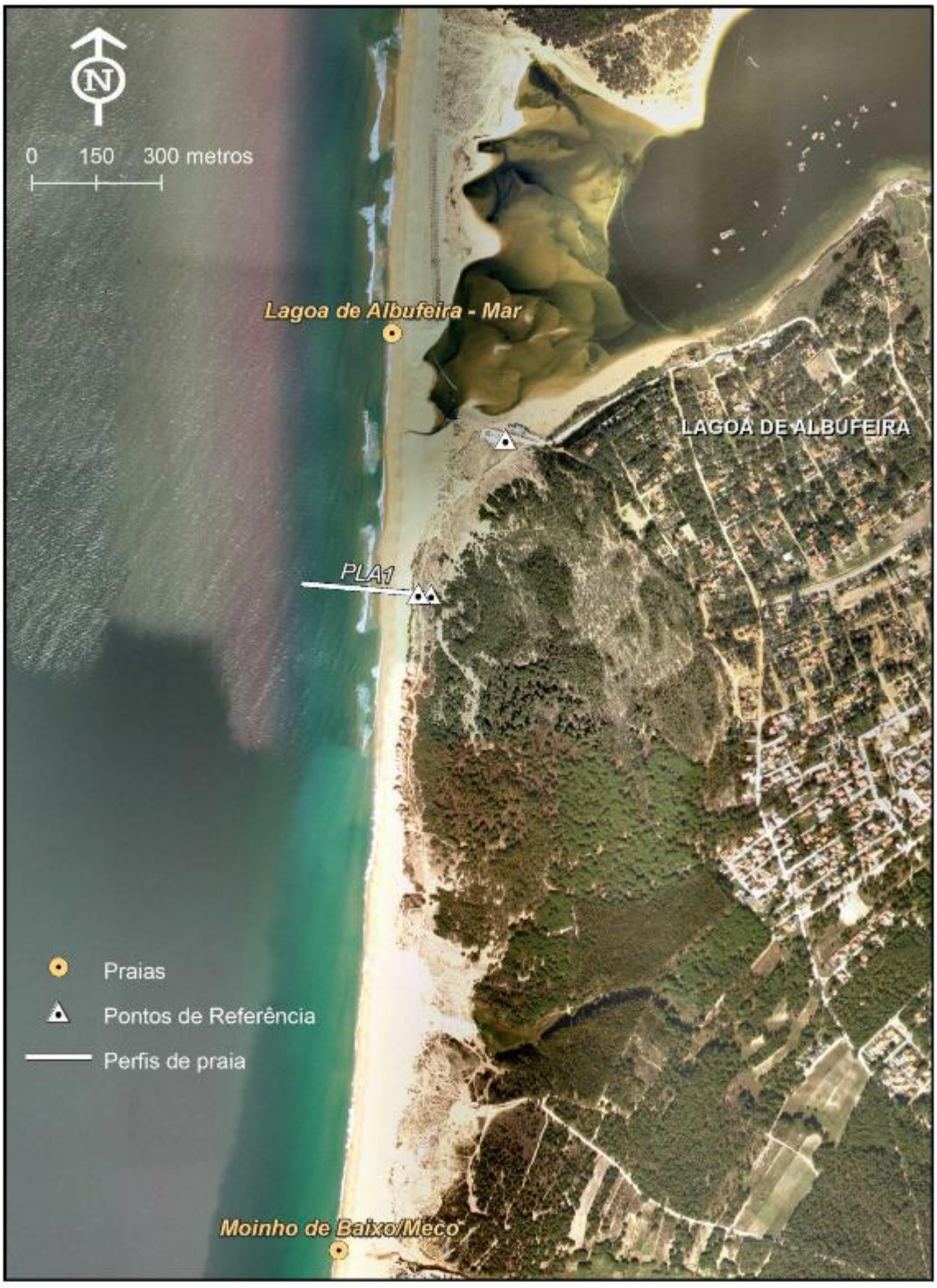

Versão 1, Junho 2011 26

LAGOA DE ALBUFEIRA	LA1

Estabelecido por: GeoFCUL (Tanya Silveira e Pedro Costa) **Data:** 2011/01/21

Qualidade: Planimetria – II, Altimetria – II, Monumentação – I

Objectivo: Ponto de Referência + Cabeça de Perfil (PLA1)

Descrição: Cabeça do prego no topo de um tubo de PVC preenchido com argamassa, no topo da arriba, a cerca de 40 m da crista da mesma e a 400 m a sul do parque de estacionamento da praia da Lagoa de Albufeira.

M	P	H
-91493.7819	-128778.1721	17.647

Sistema Coordenadas: PT-TM06 | Datum Vertical: NMM Cascais 1938 | medido em: 2011/01/21

Versão 1, Junho 2011 27

LAGOA DE ALBUFEIRA	LA2

Estabelecido por: Instituto Hidrográfico **Data:** n.d.

Qualidade: Planimetria – II, Altimetria – II, Monumentação – I

Objectivo: Ponto de Referência

Descrição: Chapa metálica com inscrição "Albufeira" no topo do cilindro de betão; localizado no topo da arriba, a cerca de 10 m da crista da mesma e a cerca de 400 m a sul do parque de estacionamento da praia da Lagoa de Albufeira.

M	P	H
-91523.5283	-128775.8978	17.054

Sistema Coordenadas: PT-TM06 | Datum Vertical: NMM Cascais 1938 | medido em: 2011/01/21

Versão 1, Junho 2011 28

LAGOA DE ALBUFEIRA	LA3 (=PA02)

Estabelecido por: DEGGE (Carlos Antunes) **Data:** 2006/12/15

Qualidade: Planimetria – II, Altimetria – II, Monumentação – I

Objectivo: Ponto de Referência

Descrição: Spit no lancil no canto este do parque de estacionamento da praia da Lagoa de Albufeira.

M	P	H
-91321.6344	-128417.0239	7.105

Sistema Coordenadas: PT-TM06 | Datum Vertical: NMM Cascais 1938 | medido em: 2011/01/21

Versão 1, Junho 2011 29

QUADRO SÍNTESE

Quadro V: Coordenadas planimétricas (M e P) e elevação (H) dos pontos de referência (PR) e, cabeças de perfis (CP) e respectivos rumos geográficos (Az) e referência a amostragem de sedimentos (Sed). (PT-TM06 | NMM Cascais 1938)

Ponto	Tipo	Perfil	Az	Sed	M	P	H
Costa da Caparica – CC							
CC1 (= PT01)	PR |	-	-	-	-97757.9342	-111173.9482	6.025
-	| CP	PCC1	240	-	-97746.2899	-111171.1213	-
-	| CP	PCC2	230	SED	-97707.8793	-111211.6802	-
-	| CP	PCC3	230	-	-97592.1978	-111319.6071	-
-	| CP	PCC4	230	-	-97439.4257	-111473.4629	-
-	| CP	PCC5	230	-	-97265.0432	-111656.388	-
-	| CP	PCC6	230	SED	-97120.5207	-111830.9137	-
-	| CP	PCC7	240	-	-96972.2063	-112114.908	-
-	| CP	PCC8	240	-	-96906.8736	-112278.4251	-
CC2 (= SP7)	PR |	-	-	-	-97004.9348	-112340.8730	3.489
CC3 (= SP6)	PR |	-	-	-	-96850.0367	-112640.9367	3.049
CC4 (= SP1)	PR |	-	-	-	-95929.1212	-114022.1041	3.374
CC9 (= SP67)	PR | CP	PCC9	240	-	-96817.2461	-112426.5832	6.361
CC10 (= SP56)	PR | CP	PCC10	240	SED	-96661.3122	-112720.5111	6.396
CC11 (= SP45)	PR | CP	PCC11	240	-	-96519.9716	-112985.7927	6.313
CC12 (= SP34)	PR | CP	PCC12	240	-	-96265.2537	-113311.9021	5.973
CC13 (= SP23)	PR | CP	PCC13	240	SED	-96111.4791	-113570.0182	5.958
-	| CP	PCC14	240	-	-95957.5114	-113806.5014	-
-	| CP	PCC15	240	-	-95683.1835	-114178.7522	-
-	| CP	PCC16	240	-	-95583.9243	-114279.9223	-
-	| CP	PCC17	240	SED	-95294.1501	-114684.1495	-
Rainha – RA							
RA1	PR | CP	PRA1	240	SED	-94392.6800	-116207.5077	5.345
RA2	PR	-	-	-	-94409.1778	-116179.0566	5.209
Fonte da Telha – FT							
FT1	PR |CP	PTF1	250	SED	-92556.3384	-121283.7045	9.639
FT2	PR |	-		-	-92447.5362	-121512.4800	9.880
FT3	PR |	-		-	-92436.0698	-121489.5307	10.575
-	| CP	PFT2	250	SED	-92377.237	-121743.991	-
Lagoa de Albufeira – LA							
LA1	PR |CP	PLA1	275	SED	-91493.7819	-128778.1721	17.647
LA2	PR |	-	-	-	-91523.5283	-128775.8978	17.054
LA3 (= PA02)	PR |	-	-	-	-91321.6344	-128417.0239	7.105

Appendix B. Beach geoindicators

Appendix B.1. Beach volume (m^3/m) geoindicator for all surveys and beach profiles.

Beach Profile		Mar 2011	Jun 2011	Sep 2011	Dec 2011	Mar 2012	Jun 2012	Sep 2012	Dec 2012	Jan 2013	Mar 2013	Jun 2013
PN	PPN1	246.58	209.75	150.86	198.74	178.16	223.36	169.34	174.20	-	300.19	218.94
	PPN2	154.48	180.32	103.89	153.02	187.97	180.74	188.23	154.40	-	247.63	154.89
PV	PPV1	157.59	319.87	156.82	108.71	95.41	134.92	102.06	65.12	-	18.25	133.56
	PPV2	390.48	498.97	461.86	275.96	252.76	310.96	306.68	206.98	-	269.44	306.45
	PPV3	207.62	223.77	326.77	201.73	169.39	150.40	208.72	102.64	-	221.16	145.83
NZ	PNZ1	515.43	515.09	517.21	529.82	598.49	552.20	555.38	555.86	-	543.53	559.31
	PNZ2	729.03	709.07	758.20	776.03	819.80	828.45	836.55	-	-	767.75	737.40
	PNZ3	784.08	825.76	873.82	848.86	876.56	868.69	905.10	862.39	-	759.00	821.57
LOB	PLOB1	44.35	22.76	-	50.46	92.63	40.99	29.70	5.37	-	18.85	13.17
	PLOB2	112.81	-	-	71.48	80.10	125.19	110.49	45.48	-	71.95	31.00
	PLOB3	76.39	95.29	162.95	144.45	168.09	153.49	167.84	113.37	-	78.54	106.32
	PLOB4	-	208.81	230.36	214.78	211.86	218.55	230.98	221.73	-	221.27	215.54
BP	PBP1	192.55	207.26	221.00	180.34	197.75	210.87	206.01	194.13	-	198.66	189.52
	PBP2	170.96	-	177.57	170.68	172.50	-	177.54	163.04	-	148.92	158.45
	PBP3	82.86	113.02	98.30	111.66	117.69	80.34	86.43	89.78	-	102.56	70.58
	PBP4	147.44	143.91	147.98	162.05	139.30	136.59	160.49	138.99	-	133.97	154.69
SC	PSC1	372.75	310.32	282.50	239.13	238.88	257.44	276.50	208.07	-	292.46	303.09
	PSC2	211.34	258.30	232.89	316.04	416.05	414.76	361.46	356.17	-	202.75	315.52
	PSC3	350.23	427.86	474.99	363.55	414.56	435.24	444.72	427.81	-	214.21	-
CX	PCX1	-	226.73	-	-	235.12	-	-	257.22	-	-	-
BS	PBS1	28.80	22.31	18.58	27.51	23.71	28.97	20.21	22.55	-	29.78	17.64
	PBS2	64.17	68.56	75.13	54.13	69.60	77.63	72.52	57.00	-	62.07	49.44
	PBS3	133.51	120.74	123.27	107.37	119.51	99.97	109.97	101.95	-	87.03	106.16
MG	PMG1	92.99	115.53	112.87	94.24	117.73	150.47	134.04	120.05	-	98.07	104.33
	PMG2	67.94	112.84	91.51	-	57.02	77.48	105.24	111.42	-	45.69	59.25
	PMG3	125.07	85.37	88.71	92.56	-	-	-	-	-	-	23.04

Appendix B.1. (continuation). Beach volume (m^3/m) geoindicator for all surveys and beach profiles.

Beach Profile		Mar 2011	Jun 2011	Sep 2011	Dec 2011	Mar 2012	Jun 2012	Sep 2012	Dec 2012	Jan 2013	Mar 2013	Jun 2013
TM	PTM1	25.25	29.24	31.25	26.14	27.84	32.31	32.23	32.49	-	19.19	26.20
	PTM2	98.23	114.52	119.18	105.69	122.96	121.18	125.10	115.38	-	81.08	130.96
	PTM3	131.80	121.74	121.85	116.52	117.19	139.51	134.81	117.02	-	113.73	145.43
	PTM4	123.17	134.12	126.56	138.09	136.82	138.15	130.61	131.55	-	136.67	143.94
CC	PCC1	540.13	527.68	422.03	441.84	370.32	352.86	377.07	359.37	316.67	312.91	391.81
	PCC2	450.97	464.61	336.84	335.57	293.11	279.04	294.47	288.38	-	250.06	252.96
	PCC3	373.54	351.09	287.98	271.00	247.63	238.43	247.18	222.13	202.12	181.19	220.89
	PCC4	342.38	315.73	-	342.75	319.98	293.57	328.93	293.11	261.99	208.19	270.63
	PCC5	97.50	146.83	154.32	104.78	89.49	125.21	173.01	118.98	62.60	101.63	81.12
	PCC6	109.54	231.71	251.41	163.72	187.24	190.70	241.49	190.20	156.72	147.55	124.68
	PCC7	-	56.29	86.32	31.41	17.84	80.08	82.17	56.15	20.58	6.50	8.32
	PCC8	-	-	81.19	31.86	39.06	68.18	90.35	35.56	8.71	4.54	22.24
	PCC9	-	12.09	20.25	0.89	0.88	10.05	21.86	9.09	15.13	3.00	0.86
	PCC10	74.49	86.86	96.71	92.22	99.43	103.16	110.35	107.96	73.80	-	-
	PCC11	25.83	46.88	59.95	20.32	66.18	60.77	70.17	75.25	52.49	39.96	26.80
	PCC12	171.27	183.22	211.30	147.38	198.05	232.96	239.26	208.34	191.46	174.80	164.10
	PCC13	163.14	182.62	218.34	150.30	174.14	196.67	189.09	179.51	155.53	122.20	119.73
	PCC14	169.06	202.80	234.91	156.54	188.11	192.25	182.53	168.17	166.35	133.30	157.43
	PCC15	185.90	203.18	245.84	180.89	230.46	192.46	174.94	158.67	164.19	154.77	100.72
	PCC16	226.55	245.53	300.47	233.08	284.54	310.72	269.57	274.11	258.74	215.67	215.14
	PCC17	152.81	183.10	225.66	192.21	234.33	271.90	276.67	266.07	246.68	240.29	259.57
RA	PRA1	247.45	274.98	310.31	246.21	279.68	285.82	326.04	269.25	273.89	242.02	268.74
FT	PFT1	213.30	252.29	245.98	182.35	256.16	226.18	251.62	216.93	203.96	210.78	219.65
	PFT2	200.38	224.64	244.03	192.19	263.02	240.35	262.04	225.93	220.84	228.37	209.81
LA	PLA1	256.76	302.14	270.69	215.99	273.79	296.59	301.21	270.86	-	250.02	256.67

Appendix B.2. Beach width (m) geoindicator for all surveys and beach profiles.

Beach Profile		Mar 2011	Jun 2011	Sep 2011	Dec 2011	Mar 2012	Jun 2012	Sep 2012	Dec 2012	Jan 2013	Mar 2013	Jun 2013
PN	PPN1	64.01	48.63	45.94	57.19	47.13	64.33	43.55	48.51	-	81.31	71.42
	PPN2	44.80	47.59	31.09	45.83	51.24	49.55	51.91	46.43	-	66.08	42.91
PV	PPV1	50.12	104.07	47.56	35.15	31.99	45.74	29.70	25.65	-	8.54	59.47
	PPV2	94.92	160.26	114.61	65.57	60.96	81.72	75.56	53.30	-	71.30	73.63
	PPV3	59.83	67.55	95.44	61.17	49.88	43.95	55.29	34.25	-	60.73	38.72
NZ	PNZ1	128.41	123.25	120.36	119.54	137.39	129.10	126.20	132.55	103.12	130.20	127.84
	PNZ2	148.95	142.17	151.30	158.74	157.62	162.10	160.31	158.68	-	151.88	144.17
	PNZ3	152.82	158.37	166.01	162.59	163.34	162.84	167.59	160.92	-	145.85	156.19
LOB	PLOB1	19.17	10.86	17.53	19.90	34.53	17.23	12.27	0.23	-	4.60	0.61
	PLOB2	55.45	25.89	39.87	26.12	29.03	42.66	36.46	17.86	-	25.73	12.68
	PLOB3	30.62	39.02	64.01	58.04	64.33	51.84	60.06	45.15	-	34.03	42.68
	PLOB4	90.32	95.00	86.82	89.83	94.73	100.02	89.71	-	92.64	91.18	-
BP	PBP1	84.55	87.97	90.08	72.53	79.14	88.86	79.42	79.21	-	80.56	79.51
	PBP2	56.01	-	57.06	55.98	54.83	58.16	55.62	52.92	-	45.91	52.07
	PBP3	29.84	43.22	32.18	40.08	40.39	23.98	29.04	34.49	-	38.04	24.63
	PBP4	50.52	52.26	50.30	60.29	47.83	46.07	55.65	49.76	-	43.51	55.62
SC	PSC1	93.82	71.61	68.70	69.89	65.19	66.13	71.65	52.40	-	81.02	76.71
	PSC2	54.13	62.20	55.24	75.22	92.20	93.51	75.83	81.08	-	43.84	71.20
	PSC3	85.08	98.89	105.20	74.05	88.06	89.69	96.83	94.65	-	45.67	79.25
CX	PCX1	56.26	63.14	62.05	56.68	60.80	60.73	60.76	66.30	-	59.88	62.73
BS	PBS1	12.03	9.66	8.74	11.61	10.40	12.10	9.22	10.40	-	12.41	8.09
	PBS2	22.15	21.01	24.04	22.34	24.40	22.10	21.27	22.00	-	23.45	18.78
	PBS3	38.15	34.17	34.06	37.16	33.90	29.04	31.30	32.11	-	27.14	31.86
MG	PMG1	37.10	40.89	42.36	34.07	46.92	51.57	45.04	47.13	-	39.53	39.82
	PMG2	29.01	40.21	32.29	21.96	24.08	28.39	38.68	41.60	-	25.48	27.17
	PMG3	48.50	31.95	31.05	37.60	41.22	32.25	39.74	31.28	-	-	10.37

Appendix B.2. (continuation). Beach width (m) geoindicator for all surveys and beach profiles.

Beach Profile		Mar 2011	Jun 2011	Sep 2011	Dec 2011	Mar 2012	Jun 2012	Sep 2012	Dec 2012	Jan 2013	Mar 2013	Jun 2013
TM	PTM1	11.52	12.23	13.31	11.23	12.55	14.00	13.39	15.35	-	7.49	11.31
	PTM2	37.91	38.42	40.44	37.74	41.03	42.10	44.86	40.61	-	29.36	44.59
	PTM3	46.50	43.96	44.76	42.04	42.63	47.59	47.02	45.76	-	39.01	49.94
	PTM4	52.10	50.75	50.56	49.58	49.49	51.43	51.38	52.24	-	52.41	53.76
CC	PCC1	173.94	158.36	115.18	120.33	100.78	91.90	103.55	99.11	87.56	84.10	101.67
	PCC2	159.82	145.43	100.60	109.57	95.14	86.39	94.79	93.75	74.27	84.99	75.95
	PCC3	112.66	96.86	75.39	72.80	63.99	61.54	67.34	57.00	58.98	49.76	65.13
	PCC4	98.50	87.48	-	91.68	83.73	72.84	92.56	78.09	72.67	55.78	76.29
	PCC5	38.17	56.82	56.55	40.87	29.66	42.15	64.17	41.59	25.26	38.55	30.29
	PCC6	46.85	79.94	81.64	54.10	63.06	63.29	81.83	62.69	56.41	47.96	41.62
	PCC7	-	24.48	33.03	13.29	5.37	34.13	31.48	22.91	9.58	-	2.84
	PCC8	-	-	33.54	13.09	17.56	30.10	36.31	15.23	2.40	-	9.89
	PCC9	-	4.26	6.86	-	-	-	6.05	-	5.56	-	-
	PCC10	24.87	30.18	33.95	32.32	32.49	30.95	33.69	37.55	26.77	-	-
	PCC11	12.53	18.85	23.50	8.33	24.16	18.85	22.64	28.69	22.70	16.60	10.34
	PCC12	51.70	56.44	66.67	43.44	61.72	73.33	75.48	64.30	64.15	55.91	51.16
	PCC13	54.21	58.60	69.37	45.54	56.40	60.78	59.30	57.43	52.82	31.99	39.87
	PCC14	54.86	59.85	73.76	46.83	59.27	53.84	54.28	51.21	55.01	40.38	52.41
	PCC15	56.55	64.65	83.52	55.94	61.52	57.48	51.09	45.64	51.67	47.39	33.21
	PCC16	73.98	75.10	96.37	71.37	81.94	92.21	78.21	80.41	77.02	60.95	63.86
	PCC17	56.87	68.63	78.62	62.86	82.42	94.86	96.74	87.22	80.87	78.14	85.92
RA	PRA1	72.58	82.01	88.83	65.53	80.96	89.31	97.06	79.26	82.48	68.28	81.04
FT	PFT1	69.61	79.38	76.44	51.80	77.05	68.85	76.55	64.45	61.01	58.98	61.91
	PFT2	62.41	67.68	74.09	53.11	80.53	72.58	77.42	64.90	63.95	60.33	59.58
LA	PLA1	61.21	75.28	63.60	51.07	62.88	68.69	73.86	63.58	56.24	58.66	60.99

Appendix B.3. Beach slope geoindicator for all surveys and beach profiles.

Beach Profile		Mar 2011	Jun 2011	Sep 2011	Dec 2011	Mar 2012	Jun 2012	Sep 2012	Dec 2012	Jan 2013	Mar 2013	Jun 2013
PN	PPN1	0.12	0.10	0.05	0.08	0.07	0.09	0.04	0.04	-	0.14	0.05
	PPN2	0.11	0.12	0.12	0.08	0.11	0.12	0.05	0.05	-	0.13	0.08
PV	PPV1	0.03	0.08	0.03	0.05	0.05	0.05	0.03	0.04	-	0.11	0.02
	PPV2	0.01	0.05	0.05	0.05	0.04	0.12	0.03	0.05	-	0.12	0.12
	PPV3	0.03	0.03	0.06	0.04	0.04	0.12	0.15	0.11	-	0.12	0.09
NZ	PNZ1	0.14	0.13	0.15	0.15	0.14	0.13	0.11	0.07	-	0.14	0.16
	PNZ2	0.14	0.12	0.15	0.15	0.15	0.18	0.17	0.09	-	0.18	0.15
	PNZ3	0.13	0.11	0.18	0.14	0.17	0.17	0.17	0.11	-	0.13	0.18
LOB	PLOB1	0.07	0.10	0.14	0.09	0.08	0.05	0.06	0.10	-	0.05	0.04
	PLOB2	0.06	0.03	0.07	0.06	0.03	0.08	0.05	0.05	-	0.09	0.02
	PLOB3	0.03	0.02	0.04	0.03	0.02	0.09	0.03	0.03	-	0.02	0.02
	PLOB4	0.03	0.03	0.02	0.02	0.03	0.02	0.02	-	0.02	0.02	-
BP	PBP1	0.03	0.03	0.03	0.02	0.02	0.03	0.03	0.02	-	0.02	0.02
	PBP2	0.03	-	0.03	0.03	0.03	0.04	0.03	0.03	-	0.03	0.03
	PBP3	0.08	0.03	0.02	0.04	0.05	0.05	0.04	0.04	-	0.03	0.05
	PBP4	0.02	0.02	0.03	0.03	0.02	0.04	0.02	0.03	-	0.02	0.02
SC	PSC1	0.15	0.11	0.11	0.05	0.11	0.04	0.07	0.09	-	0.03	0.10
	PSC2	0.17	0.13	0.13	0.07	0.13	0.09	0.13	0.10	-	0.02	0.11
	PSC3	0.16	0.14	0.13	0.15	0.10	0.08	0.10	0.11	-	0.06	0.12
CX	PCX1	0.13	0.08	0.14	0.10	0.11	0.13	0.11	0.08	-	0.10	0.10
BS	PBS1	0.15	0.13	0.15	0.15	0.15	0.16	0.16	0.14	-	0.13	0.15
	PBS2	0.16	0.15	0.13	0.12	0.15	0.16	0.15	0.09	-	0.09	0.14
	PBS3	0.14	0.14	0.15	0.15	0.14	0.15	0.14	0.10	-	0.12	0.15
MG	PMG1	0.03	0.08	0.09	0.05	0.04	0.07	0.05	0.03	-	0.05	0.09
	PMG2	0.04	0.10	0.09	0.03	0.08	0.04	0.05	0.04	-	0.03	0.10
	PMG3	0.03	0.05	0.08	0.04	0.07	0.04	0.05	0.03	-	-	0.07

Appendix B.3. (continuation). Beach slope geoindicator for all surveys and beach profiles.

Beach Profile		Mar 2011	Jun 2011	Sep 2011	Dec 2011	Mar 2012	Jun 2012	Sep 2012	Dec 2012	Jan 2013	Mar 2013	Jun 2013
TM	PTM1	0.11	0.12	0.12	0.11	0.12	0.11	0.12	0.12	-	0.06	0.12
	PTM2	0.11	0.12	0.11	0.11	0.12	0.11	0.13	0.14	-	0.04	0.13
	PTM3	0.11	0.10	0.11	0.09	0.09	0.12	0.13	0.11	-	0.04	0.11
	PTM4	0.09	0.11	0.11	0.12	0.12	0.12	0.12	0.10	-	0.05	0.11
CC	PCC1	0.05	0.10	0.04	0.02	0.03	0.02	0.04	0.03	0.09	0.02	0.05
	PCC2	0.06	0.11	0.05	0.04	0.03	0.02	0.04	0.02	-	0.03	0.06
	PCC3	0.07	0.11	0.06	0.06	0.03	0.03	0.06	0.03	0.05	0.05	0.06
	PCC4	0.10	0.09	-	0.06	0.03	0.03	0.05	0.03	0.04	0.07	0.06
	PCC5	0.07	0.10	0.06	0.08	0.05	0.02	0.05	0.03	0.06	0.04	0.05
	PCC6	0.05	0.10	0.06	0.07	0.03	0.04	0.03	0.03	0.04	0.06	0.06
	PCC7	-	0.09	0.05	0.10	0.04	0.03	0.03	0.03	0.08	-	0.10
	PCC8	-	-	0.03	0.06	0.04	0.03	0.02	0.04	0.09	-	0.07
	PCC9	-	0.07	0.04	-	-	-	0.03	0.04	0.06	-	-
	PCC10	0.03	0.13	0.04	0.08	0.04	0.03	0.02	0.03	0.07	-	-
	PCC11	0.11	0.06	0.03	0.06	0.05	0.02	0.02	0.03	0.05	0.09	0.05
	PCC12	0.02	0.03	0.03	0.03	0.03	0.03	0.03	0.03	0.03	0.03	0.07
	PCC13	0.04	0.02	0.02	0.03	0.03	0.02	0.02	0.02	0.04	0.02	0.06
	PCC14	0.09	0.03	0.05	0.03	0.04	0.03	0.03	0.04	0.04	0.04	0.05
	PCC15	0.03	0.06	0.03	0.05	0.04	0.07	0.07	0.04	0.05	0.03	0.09
	PCC16	0.02	0.13	0.03	0.04	0.04	0.05	0.08	0.04	0.06	0.05	0.09
	PCC17	0.02	0.03	0.02	0.02	0.03	0.02	0.13	0.03	0.05	0.05	0.02
RA	PRA1	0.02	0.02	0.01	0.03	0.02	0.02	0.02	0.02	0.03	0.03	0.02
FT	PFT1	0.13	0.10	0.06	0.04	0.05	0.09	0.05	0.04	0.05	0.03	0.06
	PFT2	0.13	0.13	0.05	0.02	0.06	0.11	0.04	0.04	0.05	0.03	0.08
LA	PLA1	0.15	0.18	0.13	0.13	0.09	0.06	0.14	0.09	-	0.14	0.14